ENGINEERING MECHANICS 2015

21st INTERNATIONAL CONFERENCE

MAY 11-14, 2015, SVRATKA, CZECH REPUBLIC

EXTENDED ABSTRACTS

Editors: Jiří NÁPRSTEK and Cyril FISCHER

ENGINEERING MECHANICS 2015

21st INTERNATIONAL CONFERENCE

MAY 11–14, 2015, SVRATKA, CZECH REPUBLIC

EXTENDED ABSTRACTS

Editors: Jiří Náprstek and Cyril Fischer

Institute of Theoretical and Applied Mechanics,
Academy of Sciences of the Czech Republic, v.v.i.

Institute of Solid Mechanics, Mechatronics and Biomechanics,
Faculty of Mechanical Engineering, Brno University of Technology

Institute of Thermomechanics,
Academy of Sciences of the Czech Republic, v.v.i.

ŽĎAS, a.s., Žďár nad Sázavou

IFTOMM Member Committee of the Czech Republic

Czech Society for Mechanics

Text and facts may be copied and used freely, but credit should be given to these Proceedings.

All papers were reviewed by members of the scientific committee.

Corresponding authors are indicated with stars in the individual papers.

First edition, 2015

Cover figure: Visualized airflow around the section model of the Kao Pin Hsi bridge (Taiwan).
Photo courtesy of S. Kuznetsov, ITAM AS CR, Telč.

ISBN 978-80-86246-42-0
ISSN 1805-8248

The Conference is hosted by the hotel ŽĎAS at Svratka

Honorary committee:

Miroslav Šabart, MSc — **Managing Director of the ŽĎAS, a.s.**

František Mládek — **Mayor of Svratka**

Scientific committee:

Jiří Náprstek, DSc (chairman)
ITAM AS CR, Prague, CZ

Prof. Ján Benčat, PhD.
University of Žilina, SK

Prof. Tomáš Březina, PhD.
Brno University of Technology, CZ

Prof. Jiří Burša, PhD.
Brno University of Technology, Brno, CZ

Assoc. Prof. Vladimír Čech, PhD.
OPROX, a.s., Brno, CZ

Prof. Miloš Drdácký, DSc.
ITAM AS CR, Prague, CZ

Prof. Paola Forte
University of Pisa, IT

Assoc. Prof. Vladimír Fuis, PhD.
Brno Univ. of Technology & IT AS CR, Brno, CZ

Prof. Ardeshir Guran, PhD.
Institute of Structronics, Ottawa, CA

Prof. Ivo Herle
TU Dresden, DE

Jaromír Horáček, DSc.
Institute of Thermomechanics AS CR, Prague, CZ

Assoc. Prof. Lidia Ilieva-Mitutsova, PhD.
Bulgarian Academy of Sciences, Sofia, BG

Prof. Milan Jirásek, DSc.
Czech Technical University in Prague, CZ

Prof. Zdeněk Kala, PhD.
Brno University of Technology, CZ

Prof. Zbyněk Keršner, PhD.
Brno University of Technology, CZ

Prof. Anne-Maria Laukkanen, PhD.
University of Tampere, FI

Prof. Dušan Maga, PhD.
Czech Technical University in Prague, CZ

Prof. František Maršík, DSc.
Institute of Thermomechanics AS CR, Prague, CZ

Prof. dr. Damijan Miljavec
University of Ljubljana, Ljubljana, SI

Jiří Minster, DSc.
ITAM AS CR, Prague, CZ

Prof. Bořek Patzák, PhD.
Czech Technical University in Prague, CZ

Prof. Michail Pavlenko
National University of Science and Technology MIS&S, Moscow, RU

Prof. Jindřich Petruška, PhD.
Brno University of Technology, CZ

Jiří Plešek, PhD.
Institute of Thermomechanics AS CR, Prague, CZ

Assoc. Prof. Stanislav Pospíšil, PhD.
ITAM AS CR, Prague, CZ

Prof. Jaromír Příhoda, PhD.
Institute of Thermomechanics AS CR, Prague, CZ

Ladislav Půst, DSc.
Institute of Thermomechanics AS CR, Prague, CZ

Prof. Michal Šejnoha, DSc.
Czech Technical University in Prague, CZ

Prof. Ján Sládek, DSc.
ICA, SAS, Bratislava, SK

Prof. Vladimír Sládek, DSc.
ICA, SAS, Bratislava, SK

Prof. Alexander Tesár, DSc.
ICA, SAS, Bratislava, SK

Prof. Václav Tesař, PhD.
Institute of Thermomechanics AS CR, Prague, CZ

Prof. Pavel Vlasák, DSc.
Institute of Hydrodynamics AS CR, Prague, CZ

Prof. Yuri Sergeevich Vorobiev
NAS of Ukraine, Kharkov, UA

Radek Votrubec, PhD.
Technical University of Liberec, CZ

Prof. Jaroslav Zapoměl, DSc.
Institute of Thermomechanics AS CR, Ostrava, CZ

Prof. Vladimír Zeman, DSc.
University of West Bohemia in Pilsen, CZ

Prof. Anatoly P. Zinkovskii, DSc.
National Academy of Sciences of Ukraine, Kiev, UA

Igor Zolotarev, PhD.
Institute of Thermomechanics AS CR, Prague, CZ

Prof. Rudolf Žitný, PhD.
Czech Technical University in Prague, CZ

Prof. Milan Žmindák, PhD.
University of Žilina, SK

Main Headings

List of sections:

Table of contents

(alphabetic order according to the name of the first author)

KEYNOTE LECTURES

PAPERS

Table of contents

(grouped by sections)

KEY – Keynote Lectures

BIO – Biomechanics

CSW – Computational Software

DYN – Dynamics

FLU – Fluid Mechanics

FRA – Fracture Mechanics

HIS – Historical Structures

MCT – Mechatronics

REL – Reliability

SOL – Mechanics of Solids

TER – Thermodynamics

KEYNOTE LECTURES

21st International Conference **ENGINEERING MECHANICS 2015**
Svratka, Czech Republic, May 11 –14, 2015
Paper **#084, pp. 2–5**

Application of the DOProC Method in Solving Reliability Problems

Martin Krejsa[a*], Petr Janas[b], Vlastimil Krejsa[c]

VSB–Technical University of Ostrava, Faculty of Civil Engineering, Department of Structural Mechanics, Ludvika Podeste 1875/17, 708 33 Ostrava–Poruba, Czech Republic
[a]martin.krejsa@vsb.cz, [b]petr.janas@vsb.cz, [c]vlast.krejsa@seznam.cz

Keywords: Direct Optimized Probabilistic Calculation, DOProC, probabilistic method, random variable, reliability assessment, probability of failure, bolt reinforcement, fatigue crack propagation, ProbCalc, anchor, FCProbCalc

Abstract: The Direct Optimized Probabilistic Calculation (DOProC) is originally developed as one way of solving probabilistic problems which don't use any simulation technique. DOProC is based on general terms and procedures used in probabilistic theories. Input random quantities (such as the load, geometry, material properties, or imperfections) are in DOProC method expressed by the parametric or empirical distribution in histograms. DOProC applications are processed in ProbCalc software, in which the calculation model under analysis can be expressed analytically as a sign arithmetic expression or can be expressed using code from the dynamic library. The method requires high-performing information systems for complex tasks. Therefore, efforts have been made to optimize calculations in order to reduce the number of operations, keeping, at the same time, reliable calculation results. The paper will also focus on other special software applications that are able to assess the reliability of bearing structures with respect to fatigue damage or underground works with anchors.

Introduction

Calculation model can be defined in probabilistic tasks in general as the function of n random variables $X_1, X_2 \ldots X_n$, which can be mutually statistically dependent and independent. Resulting variable Z, expressed generally as:

$$Z = f(X_1, X_2 \ldots X_n) \,, \tag{1}$$

is also random variable, which may be expressed as statistical moments, parametric probability distribution or empirical probability distribution in form of nonparametrically defined histogram.

The structure must be designed so that the resistance of the structure R is greater than the load effect S. Taking into account all randomness in loads, manufacturing and assembly imperfections and the environment properties in which designed structure performs its function, resistance R and load effect S is to be considered as random variables. In the case of probabilistic assessment of the structure is the function of the random variables under analysis Eq. 1 safety margin, defined e.g. as:

$$Z = R - S \,. \tag{2}$$

Common notation of the estimated failure probability p_f, relative to the criterion of reliability, is defined as:

$$p_f = P(R < S) = \int_{D_f} f(X_1,\, X_2 \ldots X_n)\, \mathrm{d}X_1,\, \mathrm{d}X_2 \ldots \mathrm{d}X_n \,, \tag{3}$$

where D_f is failure area of the safety margin $Z(\mathbf{X}) < 0$, a $f(X_1,\, X_2 \ldots X_n)$ as the function of joint probability density of random variables $\mathbf{X} = X_1,\, X_2 \ldots X_n$.

Determination of failure probability p_f based on the explicit calculation of the integral Eq. 3 is generally unmanageable. For solutions have been developed and continues to develop a series of stochastic methods (simulation, approximate - see [1]). The proposed method: Direct Optimized Probabilistic

Calculation - DOProC, which is developed since 2002, solves the integral Eq. 3 pure numerical way that is based on basis of probability theory and does not require any simulation technique. This is highly effective way of probabilistic calculation in terms of computation time and accuracy of the solution. The novelty of the proposed method lies in an optimized numerical integration. In summary was published in [2].

DOProC Method - theory

Similar to many other probabilistic methods, the non-parametric (empirical) distribution of input random quantities in DOProC, such as the load, geometry, material properties, or imperfections, are expressed by means of histograms. It is also possible to use parametric distributions, typically based on observations, often of long-term data [3].

In probabilistic tasks are input random variables often statistically dependent - for example xross-section properties, strength and stiffness characteristics of the materials. In the calculations carried out by DOProC method can be statistically dependent input random variable expressed by the so-called multidimensional histograms (double, triple) [4].

Mathematical description of the basic computational algorithm of the DOProC method is based on a calculation of the probability $b^{(i)}$ of resulting random variable B, which is discretized to $i = 1 \ldots n$ intervals:

$$p_b^{(i)} = \sum_{l=1}^{l} p_{bl}^{(i)} = \sum_{l=1}^{l} \left(p_{aj}^{(i1)} \cdot p_{aj}^{(i2)} \cdot p_{aj}^{(i3)} \cdot \ \ldots \ \cdot p_{aj}^{(ij)} \cdot \ \ldots \ \cdot p_{aj}^{(in)} \right) \ , \tag{4}$$

where value $b^{(i)}$ is resultant probability $\left(a_1^{i1}, a_2^{i2} \ \ldots \ a_j^{ij} \ \ldots \ a_n^{in}\right)_l$ of function f with input random variables A_j of i_j intervals. The procedure above was comprehensively published, e.g. in [5].

Number of intervals i_j of each histogram A_j can be different as well as the number of intervals i of histogram B. The number of intervals N with the total number of input random variables n is for the number of necessary arithmetic operations and necessary calculation time the most decisive factor. It also significantly affects the accuracy of probabilistic calculation. If there are too many random quantities, the tasks require too much time even if advanced computational facilities are available. Therefore, efforts have been made to optimize calculations in order to reduce the number of operations, while retaining reliable calculation results:

The grouping of variables. This procedure can be used e.g. in situations where the random variable input or output variables can be expressed using one joint histogram. This leads to a large reduction of computational operations.

Parallelization. The calculation algorithm of DOProC method is advantageous for use on machines with two or more CPUs or their cores. The basic computational algorithm of DOProC Eq. 4 can be divided the number of computational operations up to as many parts as there are available execution units, and after partial calculations can be put together from partial results into the histogram of resulting variable, e.g. histogram of safety margin Z.

Interval optimizing. The purpose of this computational procedure is to reduce the intervals of each variables involved in the calculation. Input random variables don't affect the outcome of the probabilistic calculation as well - are differently sensitive. For input variables that affect the outcome probability less, therefore the number of classes can be reduced. Custom probabilistic calculation is then carried out with the minimum number of intervals for each input random variables.

Zone optimizing. The intervals of each individual histogram are clearly defined during the calculation using one to three types of zones, depending on influence on resulting probability of failure (contribute always, may or may not contribute, contribute never). The calculation then will be limited only on intervals of input random variables which clearly don't contribute the resulting value of failure probability.

Trend optimizing. This optimization of probabilistic calculation follow the zonal optimizing. This optimization of probabilistic calculation determines the trends of changes in the histograms of input variables when defining individual zones.

Such procedures can be combined, thereby achieving an even stronger acceleration of the calculation. Computational procedures have been described were comprehensively published in [6, 7, 8].

DOProC Method - applications

The algorithm of DOProC method has been implemented in several software applications, and has been used several times in probabilistic tasks and probabilistic reliability assessments. For the application of the DOProC method can be used programming system ProbCalc, in which it is relatively easy to implement analytical and numerical transformation probabilistic model of solved tasks [9, 10]. The program system ProbCalc is extensively usefull in solving of probabilistic tasks of engineering practice, especially on probabilistic reliability assessment according to the current standards [11].

Probabilistic calculation of fatigue cracks in steel structures under cyclical loads. In [12, 13, 14] was published in detail the methodology for probabilistic assessment of structures exposed to fatigue, focusing on the determination of acceptable size of fatigue crack and definition of the regular inspection system. This relatively advanced probabilistic task was solved using ProbCalc, but also using new application under development titled FCProbCalc [15], which allows in a user friendly environment to calculate the probability of fatigue crack progression.

Probabilistic reliability analysis of anchor reinforcement. The comprehensively methodology for probabilistic design and reliability assessment of anchor reinforcement in long mining and underground works was utilized. It was also established a program Anchor, with which is possible to realize the probabilistic calculation very flexibly [16].

Summary

The paper introduces the development of probabilistic methods with particular attention to a new method, DOProC, which is still under development. DOProC appears to be a very efficient method and the solution suffers only from numerical errors and those errors resulting from discretizing of input and output quantities. One shortcoming of DOProC is the considerable increase in the required computer time for probabilistic operations with many random variables in the model. The maximum number of random variables depends on the complexity of this model, and importantly whether it is possible to use any of the described optimization steps. Also the developed program tools implementing the DOProC method were stated and which are at present able to solve many challenges in probabilistic calculations.

Acknowledgement: This project has been completed with the financial support provided to VSB–Technical University of Ostrava by the Czech Ministry of Education, Youth and Sports from the budget for conceptual development of science, research and innovations for the year 2015.

References

[1] R. E. Melchers, Structural Reliability Analysis and Prediction, Second edition, John Wiley & Sons Ltd., England (1999) 437 p, ISBN: 0-471-98324-1.

[2] P. Janas, M. Krejsa, V. Krejsa, J. Sejnoha, Direct Optimized Probabilistic Calculation — DOProC, submitted to Probabilistic Engineering Mechanics (2014).

[3] R. Cajka, M. Krejsa, Measured data processing in civil structure using the DOProC method, Advanced Materials Research, 859 (2014) 114–121, DOI: 10.4028/www.scientific.net/AMR.859.114.

[4] P. Janas, M. Krejsa, Statistical Dependence of Input Variables in DOProc Method, Transactions of the VSB – Technical University of Ostrava, Civil Engineering Series, 12 (2012) 48–58, ISSN: 1804-4824, DOI: 10.2478/v10160-012-0017-3.

[5] P. Janas, M. Krejsa, I. Kolos, Reliability assessment of structure expressed to impact, in: Proceedings of conference Engineering Mechanics 2003, The Institute of Theoretical and Applied Mechanics AS CR (2003) ISBN: 80-86246-18-3. (In Czech)

[6] P. Janas, M. Krejsa, V. Krejsa, Contemporary Capability of Direct Determined Probabilistic Calculation, in: Proceedings of conference Engineering Mechanics 2006, The Institute of Theoretical and Applied Mechanics AS CR (2006) p 132–33, ISBN: 80-86246-27-2.

[7] P. Janas, M. Krejsa, V. Krejsa, Structural reliability assessment using a Direct Determined Probabilistic Calculation, in: Proceedings of the 12th Conference on Civil, Structural and Environmental Engineering Computing, Civil-Comp Press (2009) DOI: 10.4203/ccp.91.72.

[8] P. Janas, M. Krejsa, V. Krejsa, Using the Direct Determined Fully Probabilistic Method for determination of failure, in: European Safety and Reliability Conference ESREL 2009, Reliability, Risk and Safety: Theory and Applications. Taylor & Francis Group, London (2010) p 1467–1474, ISBN: 978-0-415-55509-8, DOI: 10.1201/9780203859759.ch203.

[9] M. Krejsa, P. Janas, V. Krejsa, Software Application of the DOProC Method, International Journal of Mathematics and Computers in Simulation, 8 (2014) 121–126, ISSN: 1998-0159.

[10] M. Krejsa, P. Janas, V. Krejsa, ProbCalc - An efficient tool for probabilistic calculations, Advanced Materials Research, 969 (2014) 302–307, DOI: 10.4028/www.scientific.net/AMR.969.302.

[11] M. Krejsa, P. Janas, R. Cajka, Using DOProC Method in Structural Reliability Assessment, Applied Mechanics and Materials, 300–301 (2013) 860–869, DOI:10.4028/www.scientific.net/AMM.300-301.860.

[12] Krejsa, M., Stochastic Modelling of Fatigue Crack Progression using the DOProC Method, in: Proceedings of the 11th International Conference on Computational Structures Technology, Civil-Comp Press (2012) DOI: 10.4203/ccp.99.113.

[13] M. Krejsa, Probabilistic failure analysis of steel structures exposed to fatigue, Key Engineering Materials, 577–578 (2013) 101–104, DOI: 10.4028/www.scientific.net/KEM.577-578.101.

[14] M. Krejsa, Probabilistic reliability assessment of steel structures exposed to fatigue, Safety, Reliability and Risk Analysis: Beyond the Horizon, CRC Press-Taylor & Francis Group (2014) 2671–2679, ISBN: 978-1-315-81559-6; 978-1-138-00123-7, DOI: 10.1201/b15938-404.

[15] M. Krejsa, The Probabilistic Calculating of Fatigue Crack Propagation Using FCProbCalc Program, in: Proceedings of 18th International Conference Engineering Mechanics 2012, The Institute of Theoretical and Applied Mechanics AS CR (2012) p 745–754, ISBN: 978-80-86246-39-0.

[16] M. Krejsa, P. Janas, I. Yilmaz, M. Marschalko, T. Bouchal, The Use of the Direct Optimized Probabilistic Calculation Method in Design of Bolt Reinforcement for Underground and Mining Workings, Scientific World Journal, Vol. 2013 (2013) DOI: 10.1155/2013/267593.

21st International Conference **ENGINEERING MECHANICS 2015**
Svratka, Czech Republic, May 11 –14, 2015
Paper **#213, pp. 6–7**

Solution of Large Engineering Problems on Parallel Computers

Jaroslav Kruis

Department of Mechanics, Faculty of Civil Engineering, Czech Technical University in Prague,
Thákurova 7, 166 29, Prague, Czech Republic

jk@cml.fsv.cvut.cz

Keywords: parallel computing, domain decomposition method, FETI method, Schur complement method, multi-scale problems.

Abstract: This contribution reviews utilization of parallel computers in engineering problems. Solution of systems of algebraic equations is usually the most demanding part of an analysis which could be accelerated by domain decomposition methods. Other application of parallel computers in engineering simulations contains multi-scale problems where different processors solve different levels of the problems.

Introduction

Although hardware is permanently being developed, requirements on computer power and memory arising from engineering practice exceed usually its possibility. Single processor computers are definitely unable to solve large problems. Therefore parallel computers are becoming very popular and they are used not only in academic institutions but also in engineering practice.

Parallel computers could be sorted out with respect to their memory. The computers with shared memory are called massively parallel computers. All processors have access to all data. On the contrary, a cluster of single-processor computers connected via suitable network is a parallel computer with distributed memory. Each processor has an access only to data stored in its memory. If a processor A needs data stored in memory of processor B, the data has to be sent. The massive parallel computers are significantly more expensive in comparison with clusters. The biggest parallel computers at this time are clusters of multi-processor nodes and the memory is distributed while in nodes is shared.

Classification of problems

There are four basic groups of demanding computations. First group contains problems with many unknowns (more than million) which are solved only once. Such problems can be split into smaller subproblems which are distributed to processors of a parallel computer and they are solved independently there. At the end, the original continuity on subproblem interfaces is enforced. This is the principle of domain decomposition methods [1, 2, 3]. Their parallelization requires data transfer among processors, synchronization of operations and load balancing.

Second group contains problems with moderate number of unknowns (tens of thousands) which are solved repeatedly and the order of solution is not important or it is important only partially. The Monte Carlo simulations, various optimization tasks or multi-scale analysis [4], where a problem defined on the lower level is solved for every finite element of the upper level can serve as examples. Parallelization of such computations can lead to the ideal speedup because the master processor sends and receives only small amount of data. The same number of operations executed on the slave processors leads to the ideal load balancing which is another advantage.

Third group contains problems with a moderate number of unknowns which are solved repeatedly and the order of solution is important. As an example can serve a numerical time integration. Parallelization of such problems is questionable. The only solution is simultaneous space-temporal

discretization where the number of unknowns grows significantly in comparison with the classical approach but the resulting system of equations is solved only once. Methods of the first group mentioned in this contribution can be used.

Fourth group contains problems with many unknowns which should be solved repeatedly. These are not solvable at this time.

Examples

Two domain decomposition methods will be described in detail, namely the Schur complement method [5] and the FETI (Finite Element Tearing and Interconnecting) method [6, 7]. Behaviour of the methods will be documented on several examples solved. Second group of problems will be represented by a two-level analysis of coupled heat and moisture transport in a masonry bridge structure [4]. The coupled transport is described by the Künzel model. The bridge is described by two and three dimensional models and two different meso-scale levels are used because of heterogeneous masonry.

References

[1] A.Toselli, O. Widlund, Domain Decomposition Methods--Algorithms and Theory, Springer-Verlag, Berlin, 2005.

[2] A. Quarteroni, A. Valli, Domain Decomposition Methods for Partial Differential Equations, Clarendon Press, Oxford, 2005.

[3] J. Kruis, Domain Decomposition Methods for Distributed Computing, Saxe-Coburg Publications, Kippen, Stirling, 2006.

[4] J. Sýkora, T. Krejčí, J. Kruis, M. Šejnoha, Computational homogenization of non-stationary transport processes in masonry structures, Journal of Computational and Applied Mathematics, 236 (2012) 4745–4755.

[5] J. Kruis, Domain Decomposition Methods on Parallel Computers, in: B.H.V. Topping, C.A. Mota Soares (Eds.), Progress in Engineering Computational Technology, Saxe-Coburg Publications, 2004, 299–322.

[6] Z. Dostál, Optimal Quadratic Programming Algorithms With Applications to Variational Inequalities, Springer Verlag, 2009.

[7] J. Kruis, The FETI Method and its Applications: A Review, in: B.H.V. Topping, P. Iványi (Eds.), Parallel, Distributed and Grid Computing for Engineering, Saxe-Coburg Publications, 2009, 199–216.

PAPERS

21st International Conference **ENGINEERING MECHANICS 2015**
Svratka, Czech Republic, May 11 –14, 2015
Paper **#090, pp. 10–11**

Model Based Design of Fuel Pump Control

Ondrej Andrs[a]*, Jan Vetiska[b], Michal Holub[c], Jiri Kovar[d]

Faculty of Mechanical Engineering, Brno University of Technology,
Technická 2896/2, 616 69 Brno, Czech Republic

[a]andrs@fme.vutbr.cz, [b]vetiska@fme.vutbr.cz, [c]holub@fme.vutbr.cz, [d]kovar@fme.vutbr.cz

Keywords: model based design, fuel pump, control

Abstract: This paper presents a co-simulation method to design of speed controller for turbojet fuel pump. Expected fuel pump is used for small turbine engine concept with reducer driven by free turbine. The amount of injected fuel into the combustion chamber is based on the speed of the fuel pump which is controlled by the engine control unit. The final flow of fuel into the combustion chamber is restricted by fuel bypass which constricts the return fuel according to pressure in the nozzles. This back fuel bypass has nonlinear and fixed characteristic determined by its structure. The only way how to control the amount of incoming fuel to the engine is the pump speed control. Effect of the bypass represents a variable component in the fuel pump load and from the view of the speed controller it is a disturbance variable. This paper describes the co-simulation model based on the use of MATLAB/Simulink and MSC Adams environment. This simulation uses interconnection of Simulink controller design and simplified model of the fuel pump dynamics in Adams (without hydraulic modeling).

Introduction

The fuel - oil pump supplies the fuel to combustion chamber and also the oil for motor lubricating. The pump is driven by a couple of three-phase motor with permanent magnets supplied from the engine control unit. The fuel - oil pump consists of three main segments – the oil pump, the high pressure and the low pressure fuel parts. Block diagram of mentioned pump is shown in Fig. 1. The fuel pump is equipped with a pair of electronically commutated motors (EC, BLDC) located on a common shaft. It represents full mechatronic system [1, 2].

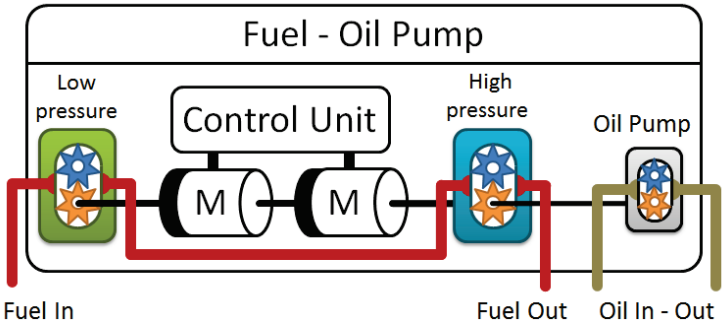

Fig. 1: Block diagram of the motor fuel – oil pump

Creating of co-simulation model

According to the model-based design methodology [3] the simulation model was developed. Proposed control design is based on co-simulation model which connects controller design in MATLAB/Simulink environment with simplified model of the fuel pump dynamics in Adams, Fig. 2. According to [4, 5], EC motor model can be approximated by a DC motor model with a corrected design parameters (constructional constants of the motor). The presented design is based on a simulation model of a pair of BLDC motors mounted on a common shaft with oil and fuel pump in MSC Adams environment. BLDC motors have been approximated by modified DC motors

models. Commutation of BLDC motors is handled by lower layer control system. In simulation scheme, there are also power components and sensors which were approximated by models of the first order dynamic systems. There was implemented discrete speed controller with subordinate current/torque controllers for each motor with the ability to switch between them according to prescribed distribution of performance.

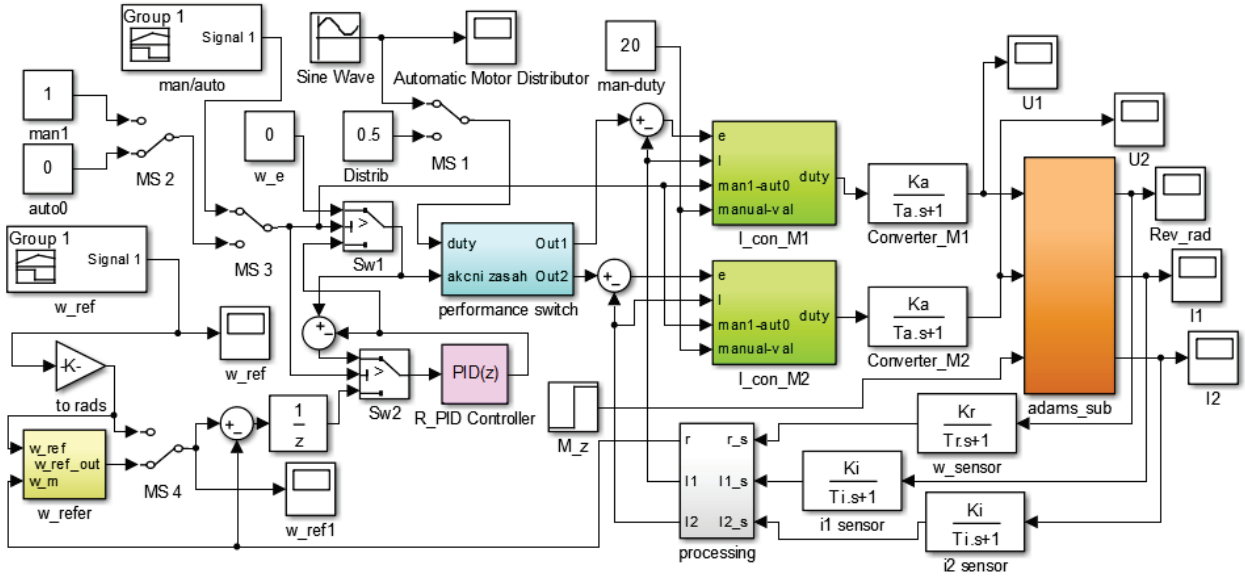

Fig. 2: Simulation model of the co-simulation control structure

Summary

Simulation results verify the functionality of the proposed control design. The proposed scheme can be used as the upper layer for the layer providing of measuring process, generating control signals and providing self-commutation of motors.

References

[1] O. Andrs, Z. Hadas, J. Kovar, J. Vetiška, V. Singule, Model-Based Design of Mobile Platform with Integrated Actuator – Design with Respect to Mechatronic Education. Mechatronics 2013 Recent Technological and Scientific Advances, Springer International Publishing, 2014, pp. 891–898, ISBN: 978-3-319-02293- 2.

[2] Z. Hadas, V. Vetiska, V. Singule, O. Andrs, J. Kovar, J. Vetiska, Energy Harvesting from Mechanical Shocks Using a Sensitive Vibration Energy Harvester, International Journal of Advanced Robotic Systems, 9 (2012) 1–7. ISSN: 1729-8806.

[3] J. Kovar, O. Andrs, Particle swarm optimization technique applied to image recognition using delta robot, in Mendel 2011 - 17th international conference on soft computing, 2011, pp. 67–72. ISBN: 978-1-4673-1300-1.

[4] V. Hubik, M. Sveda, V. Singule, Mathematical model of a sensorless BLDC motor for aerospace actuators, in Proceedings of the 19th IASTED International Conference on Modelling and Simulation, 2008, pp. 158–162.

[5] O. Andrs, J. Kovar, Z. Hadaš, Introduction to Design of Speed Controller for Fuel Pump, In: Proceedings of the 16th International Conference on Mechatronics – Mechatronika 2014, Brno, VUT v Brně, 2014, p. 672–676, ISBN: 978-80-214-4817-9.

21st International Conference **ENGINEERING MECHANICS 2015**
Svratka, Czech Republic, May 11 –14, 2015
Paper **#230, pp. 12–13**

Safety Factors γ_{M0} and γ_{M1} in Metal Eurocodes

Ivan Baláž[1,a] *, Yvona Koleková[2,b]

[1]KKDK Stavebná fakulta STU v Bratislave, Radlinského 11, 810 05 Bratislava, Slovakia

[2]KSM Stavebná fakulta STU v Bratislave, Radlinského 11, 810 05 Bratislava, Slovakia

[a]ivan.balaz@stuba.sk, [b]yvona.kolekova@stuba.sk

Keywords: partial safety factors, recommended values, definitions, applications, Eurocodes.

Abstract: Overview of values and definitions of γ_{M0} and γ_{M1} safety factors used in all 20 parts of Eurocodes EN 1993 Design of steel structures [1] and in all 5 parts of EN 1999 Design of aluminium structures [2]. Applications of the γ_{M0} and γ_{M1} safety factors values and definitions in all clauses of EN 1993. Comparison of safety levels of former Czechoslovak standards with current Eurocodes. Proposals for correction of definitions and applications of γ_{M0} and γ_{M1} safety factors in all clauses of EN 1993. The overview and corrections enable to do better choice from several official options aiming to change current value $\gamma_{M1} = 1,0$ valid in EN 1993-1-1 for buildings, which were presented at CEN/TC250 SC3 meetings in October 24th 2014 and in March 19th 2015 in Berlin

Analysis of safety factors recommended values and definitions

20 parts of Eurocode 1993 Design of steel structures may be divided into two groups: a) servants (containing theoretical procedures), b) masters (application parts). Part 1 EN 1993-1 consists from twelve subparts: EN 1993-1-1 to EN 1993-1-12. They are all servants except EN 1993-1-1 which contains general rules and rules for design of buildings as well. The group of masters consists from 6 application parts: EN 1993-2 bridges, EN 1993-3 tall structures, EN 1993-4 storage structures, EN 1993-5 pilings, EN 1993-6 crane runway girders. Overview of recommended numerical values of partial safety factors γ_{M0} and γ_{M1} in all 20 parts of EN 1993 is given in the Table 1.

Tab. 1: Recommended values of partial safety factors γ_{M0} and γ_{M1} in all 20 parts of EN 1993

EN 1993	-1-1	-1-2	-1-3	-1-4	-1-5	-1-6
γ_{M0}	1,0	ref. to -1-1	1,0	1,1	A.P.	A.P.
γ_{M1}	1,0	ref. to -1-1	1,0	1,1	A.P.	A.P.
EN 1993	-1-7	-1-8	-1-9	-1-10	-1-11	-1-12
γ_{M0}	A.P.	ref. to -1-1	-	-	-	-
γ_{M1}	A.P.	ref. to -1-1	-	-	-	-
EN 1993	-2	-3-1	-3-2	-4-1	-4-2	-4-3
γ_{M0}	1,0	1,0	1,0	1,0	1,0	-
γ_{M1}	1,1	1,0	1,1	1,1	1,1	-
EN 1993	-5	-6	Key:			
γ_{M0}	ref. to -1-1	1,0	ref. to -1-1 = refers to EN 1993-1-1			
γ_{M1}	ref. to -1-1	1,0	A.P. = as in relevant application part of EN 1993			

Overview of safety factors definitions and their applications in all clauses containing partial safety factors γ_{M1} and γ_{M1} in all 20 parts of EN 1993 is given in the Table 2.

In the prestandard ENV 1999 and standard EN 1999 for design of aluminium structures there is only one recommended value $\gamma_{M1} = 1,1$. Partial safety factor γ_{M0} is not used in these Eurocodes.

In prestandard ENV 1993 there are recommended values $\gamma_{M0} = \gamma_{M1} = 1,1$.

Tab. 2: Definitions of partial safety factors γ_{M0} and γ_{M1} in all 20 parts of EN 1993

EN 1993-1-1:	γ_{M0}: resistance of cross-sections whatever the class is γ_{M1}: resistance of members to instability assessed by member checks
EN 1993-1-2:	No γ_{Mi} definitions. Only γ_{M0} is used in part -1-2, which refers only to 1993-1-1
EN 1993-1-3:	γ_{M0}: resistance of cross-sections to excessive yielding including local and distortional buckling γ_{M1}: resistance of members and sheeting where failure is caused by global buckling
EN 1993-1-4:	γ_{M0}: resistance of cross-sections to excessive yielding including local buckling γ_{M1}: resistance of members to instability assessed by member checks
EN 1993-1-5:	No γ_{Mi} definitions.
EN 1993-1-6:	No γ_{Mi} definitions. This part is intended for use in conjunction with EN 1993-1-1,-1-3, -1-4, -1-9 and the relevant application parts of EN 1993, which include -3-1 for towers and masts, -3-2 for chimneys, -4-4 for silos, -4-2 for tanks, -4-3 for pipelines
EN 1993-1-7:	No γ_{Mi} definitions. Recommended γ_{M0} and γ_{M1} values are given in the relevant application standards
EN 1993-1-8:	No γ_{Mi} definitions. γ_{Mi} for resistance of members and cross-sections see in -1-1
EN 1993-1-9, -1-10, -1-11, -1-12:	γ_{M0} and γ_{M1} are not used in these standards
EN 1993-2:	γ_{M0}: resistance of cross-sections to excessive yielding including local buckling γ_{M1}: resistance of members to instability assessed by member checks
EN 1993-3-1:	γ_{M0}: resistance of member to yielding γ_{M1}: resistance of member buckling
EN 1993-3-2:	γ_{M0}: resistance of structural elements or members related to the yield strength f_y, when no global or local buckling occurs γ_{M1}: resistance of structural elements or members related to the yield strength f_y, where global or local buckling is considered
EN 1993-4-1:	γ_{M0}: resistance of welded or bolted shell wall to plastic limit state γ_{M1}: resistance of shell wall to stability
EN 1993-4-2:	γ_{M0}: resistance of welded or bolted shell wall to plastic limit state, cross-sectional resistance γ_{M1}: resistance of shell wall to stability
EN 1993-4-3:	γ_{M0} and γ_{M1} are not used in this standard
EN 1993-5:	No γ_{Mi} definitions. For the partial factors to be applied to resistance see EN 1993-1-1
EN 1993-6:	γ_{M0}: resistance of cross-sections to excessive yielding including local buckling γ_{M1}: resistance of members to instability assessed by member checks

In prestandard ENV 1993 there are different safety factors definitions comparing with EN 1993.

Summary

The definitions of safety factors used in EN 1993 should be unified, the cross-references among its parts improved and applications of safety factors in some clauses corrected. These measurements enable to make change of recommended value $\gamma_{M1} = 1,0$ used in EN 1993-1-1 easier.

Acknowledgement: Project No. 1/0748/13 was supported by the Slovak Grant Agency VEGA.

References

[1] EN 1993 Eurocode 3. Design of steel structures. Set of 20 standards. CEN Brussels. 2005-2007.

[2] EN 1999 Eurocode 9. Design of aluminium structures. Set of 5 standards. CEN Brussels. 2007.

21st International Conference **ENGINEERING MECHANICS 2015**
Svratka, Czech Republic, May 11 –14, 2015
Paper **#240, pp. 14–15**

Bending, Torsion and Distortion of Thin-Walled Beams

Ivan Baláž[1,a]*, Yvona Koleková[2,b]

[1]KKDK Stavebná fakulta STU v Bratislave, Radlinského 11, 810 05 Bratislava, Slovakia

[2]KSM Stavebná fakulta STU v Bratislave, Radlinského 11, 810 05 Bratislava, Slovakia

[a]ivan.balaz@stuba.sk, [b]yvona.kolekova@stuba.sk

Keywords: thin-walled beams, bending, torsion, distortion, influence of shear, analogies

Abstract: Analysis of thin-walled beams using modified Generalised Beam Theory (GBT) developed by R. Schardt [1, 2] for calculation of cross-section properties. Numerical examples show in details the calculation of internal forces, deformations and stresses due to torsion and distortion with the help of: (i) exact formulae, (ii) computer program IQ 100 using analogies with beams in bending on elastic foundations loaded by transverse load and tension force. Formulae for open and closed profiles. Influence of shear is analysed too [5].

Introduction

The theory of thin-walled structures was developed by Vasilij Zacharovič Vlasov, who published basic publications in 1931, 1935, 1936, 1940 and seven monographs in 1933, 1936, 1940, 1949, 1949 and 1958. Generalized Beam Theory (GBT), which describes the mechanical behaviour of prismatic structures in the 1st order theory by ordinary differential equations

$$E.{}^{\mathrm{k}}C.{}^{\mathrm{k}}V^{IV}(x) - G.{}^{\mathrm{k}}D.{}^{\mathrm{k}}V^{II}(x) + {}^{\mathrm{k}}B.{}^{\mathrm{k}}V(x) = {}^{\mathrm{k}}q(x) \tag{1}$$

for each mode k, which are not coupled and can be solved independently, was developed in Germany by Richard Schardt in 1966 [1] and by Gerhard Sedlacek in 1968 [3]. G. Sedlacek gave to this theory its name. R. Schardt published the bible of GBT in 1989 [2]. Details and list of all references may be found in [4, 5]. Eq. 1 does not take into account influence of shear. Influence of shear is investigated in numerical examples.

Cross-sectional functions, stiffnesses, internal forces, deformations and stresses

A unifying feature of the GBT is the concept of warping functions whereby each mode k of deformation is associated with a distribution of axial strain ${}^{\mathrm{k}}u(s)$. The first mode (k = 1) of deformation is a uniform distribution of axial strain over cross-section. The second and third modes (k = 2, 3) are bending modes and the associated warping functions are linear distributions strain about the two principal axes. The fourth mode (k = 4) is torsion and here the term warping has its conventional meaning as the warping function is the sectorial coordinate which reflects the distribution of axial strain due to a bimoment. The fifth (k = 5) and further modes (k > 5) are the modes of cross-sectional distortions. It is important to realize at the outset that all these warping functions are orthogonal. Practically, this means that in any first-order analysis they can be considered quite independently and their effects combined by simple superposition. The cross-sectional functions of C-profile (k = 1 to 6) are calculated in numerical example and illustrated graphically in tables. The C-profile has 5 plane elements (n = 5) and 6 main nodes (n + 1 = 6). Nodes numbering is r = 0; 1; 2; 3; 4; 5. It should be noted that all the quantities tabulated for modes k = 1 to k = 4 are already obtainable from standard procedures of structural mechanics which are given in basic texts on the subject. The details of the calculation of the warping functions ${}^{\mathrm{k}}u(s)$ [or $-{}^{\mathrm{k}}u(s) = 1,\ y(s),\ z(s),\ \omega(s),\ \omega_{\mathrm{D1}}(s),\ \omega_{\mathrm{D2}}(s)$] may be found also in [4, 5].

The values ${}^{\mathrm{k}}Q_{\mathrm{r}}$ may be calculated from the first moments of area using the following formulae

$$ {}^{\mathrm{k}}Q_{\mathrm{i\text{-}j}} = \left({}^{\mathrm{k}}S_{\mathrm{i}} + {}^{\mathrm{k}}S_{\mathrm{j}} + \frac{\left({}^{\mathrm{k}}u_{\mathrm{j}} - {}^{\mathrm{k}}u_{\mathrm{i}} \right) t_{\mathrm{i\text{-}j}} L_{\mathrm{i\text{-}j}}}{6} \right) \frac{L_{\mathrm{i\text{-}j}}}{2} = \left({}^{\mathrm{k}}S_{\mathrm{i}} + {}^{\mathrm{k}}S_{\mathrm{j}} + \frac{{}^{k}f_{s,\mathrm{i\text{-}j}} t_{\mathrm{i\text{-}j}} L_{\mathrm{i\text{-}j}}^2}{6} \right) \frac{L_{\mathrm{i\text{-}j}}}{2} \tag{2} $$

The ${}^{\mathrm{k}}C^{\mathrm{M}}$ warping constants, which include also the cross-sectional area ${}^{1}C^{\mathrm{M}} = A$, the second moments of area about the principal axes ${}^{2}C^{\mathrm{M}} = I_{\mathrm{z}}$, ${}^{2}C^{\mathrm{M}} = I_{\mathrm{y}}$ and the warping constant ${}^{4}C^{\mathrm{M}} = I_{\mathrm{w}}$, may be calculated from the following formulae

$$ {}^{\mathrm{k}}C^{\mathrm{M}} = \int_0^{\mathrm{n}} \left[{}^{\mathrm{k}}u(s) \right]^2 ds = \int_0^{\mathrm{n}} - \frac{d\left[{}^{\mathrm{k}}u(s) \right]}{ds} {}^{\mathrm{k}}S(s) ds = \sum_{\mathrm{r=1}}^{\mathrm{n=5}} - \frac{d\left[{}^{\mathrm{k}}u(s) \right]}{ds} {}^{\mathrm{k}}Q_{\mathrm{r}} = \sum_{\mathrm{r=1}}^{\mathrm{n=5}} - {}^{\mathrm{k}}f_{\mathrm{s,r}} \, {}^{\mathrm{k}}Q_{\mathrm{r}} \tag{3} $$

The "torsion" constants may be calculated from the formulae

$$ {}^{\mathrm{k}}D = \frac{1}{3} \sum_{\mathrm{r=1}}^{\mathrm{n=5}} {}^{\mathrm{k}}f_{v,\mathrm{r}}^2 L_{\mathrm{r}} t_{\mathrm{r}}^3 \quad \text{for} \quad k = 4,5,6, \qquad {}^{\mathrm{k}}D = 0 \ \text{(it does not exist)} \ \text{for} \quad k = 1,2,3 \tag{4} $$

The transverse bending stiffnesses ${}^{k}B$ may be calculated from the formulae

$$ {}^{\mathrm{k}}B = \sum_{\mathrm{i=0}}^{\mathrm{n=5}} {}^{\mathrm{k}}m_{\mathrm{s,i}} \, {}^{\mathrm{k}}V_{\mathrm{i}} \quad \text{for} \quad k = 5,6, \qquad {}^{\mathrm{k}}B = 0 \quad \text{(it does not exist)} \ \text{for} \quad k = 1,2,3,4 \tag{5} $$

Summary

Numerical example shows in details the calculation of all cross-sectional functions and stiffnesses. Internal forces and deformations of torsion and distortion are obtained by computer program enabling to calculate beam in bending on elastic foundation loaded by transverse and tension forces.

Acknowledgement: Project No. 1/0748/13 was supported by the Slovak Grant Agency VEGA.

References

[1] R. Schardt, Eine Erweiterung der technischen Biegelehre für die Berechnung biegesteifer-prismatischer Faltwerke. Der Stahlbau, 35, 161-171, 1966.

[2] R. Schardt, Verallgemeinerte Technische Biegetheorie. Lineare Probleme. Springer-Verlag 1989.

[3] G. Sedlacek, Systematische Darstellung des Biege- und Verdrehvorganges für Stäbe mit dünnwandigem, prismatischem Querschnitt unter Berücksichtigung der Profilverformung. Dissertation, TU Berlin, 1968. Forschritt-Berichte. VDI-Zeitschrift Reihe 4, Nr. 8, September 1968.

[4] I. Baláž, Dünnwandige Stäbe mit öffenem oder geschlossenem deformierbarem Querschnitt. Stahlbau, 68, H.1, Ernst & Sohn, A Wiley Company, Berlin, 1999, s.70-77.

[5] I. Baláž, Tenkostenné oceľové konštrukcie. Vplyv krútenia pri tenkostenných mostných sústavách. ES STU Bratislava, 1. vydanie, 1984, s.1-168. 5. rozšírené vydanie. 2004, s.1-295.

21st International Conference **ENGINEERING MECHANICS 2015**
Svratka, Czech Republic, May 11 –14, 2015
Paper **#070, pp. 16–17**

Determination of Mechanical Properties of Magnesium Alloys and Composites by Small Punch Testing

Denisa Bártková[1,a] *, Jiří Langer[1,c] , Petr Dymáček[2,c] , Libor Válka[1,d]

[1]Brno University of Technology, Faculty of Mechanical Engineering,
Technická 2896/2, 616 69 Brno, Czech Republic

[2]Institute of Physics of Materials, ASCR, Žižkova 22, 616 62 Brno, Czech Republic

[a]bartkova@ipm.cz, [b]longerj@seznam.cz, [c]pdymacek@ipm.cz, [d]valka@fme.vutbr.cz

Keywords: small punch test, magnesium alloys, thin disc

Abstract: Tests on miniature samples are increasingly used for the testing of mechanical properties of materials available in small volumes (non-destructive or semi-destructive approach). Small punch testing at constant deflection rate (SPT-CDR) of selected magnesium alloys and composites was performed at room temperature. Mechanical properties (yield strength, ultimate strength and ductility) were evaluated from SPT and correlated with results of uniaxial tensile tests (UTT). SPT characteristics were converted to uniaxial tensile properties by empirical formulas available in the literature. New formulas more appropriate for magnesium alloys were suggested.

Introduction

Principle of the method is a penetration of small puncher through thin disc (thickness up to 0.5 mm, diameter up to 10 mm) placed on a ring until the disc bursts (see Fig. 1). There are two main SPT approaches i) Constant Displacement Rate (CDR) – puncher moves with constant rate. This is an analogy of UTT. ii) Constant Force (CF) - puncher penetrates under a constant force *F*. This test is an analogy to conventional constant load creep tests.

Certain weakness of this method presents complicated clarification of the relations between SPT and UTT. Most of previous correlation formulas were based on testing steel specimens; therefore confirmation of these empirical formulas on different materials is appropriate.

Five magnesium alloys (AZ31, AZ61, AZ91, WE54, MgZnMn) and one composite with magnesium alloy matrix (AZ91 + 20% saffil) were chosen as an experimental material for the study.

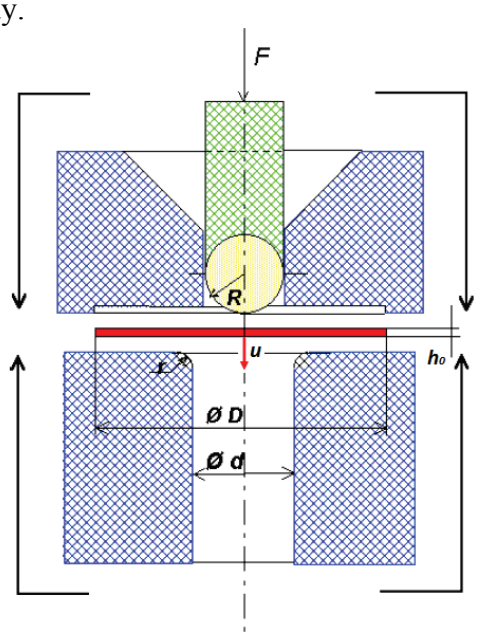

Fig. 1: Scheme of a test arrangement for SPT.

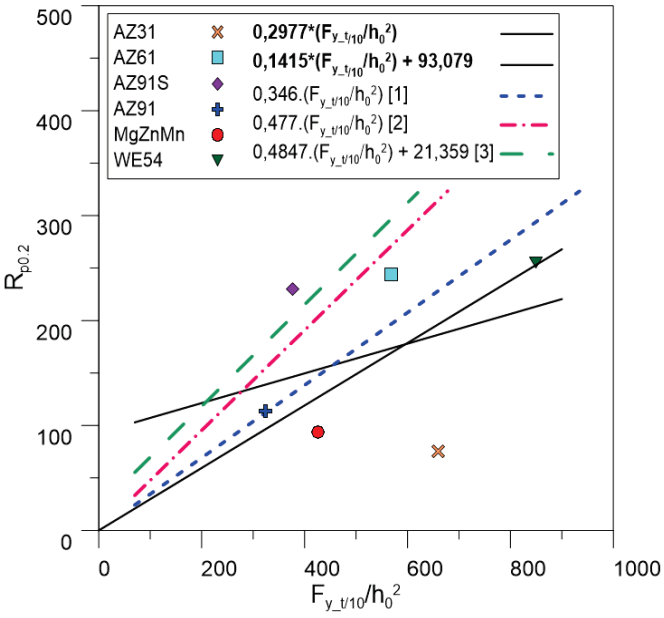

Fig. 2 Dependence of UTT yield strength on SPT yield strength.

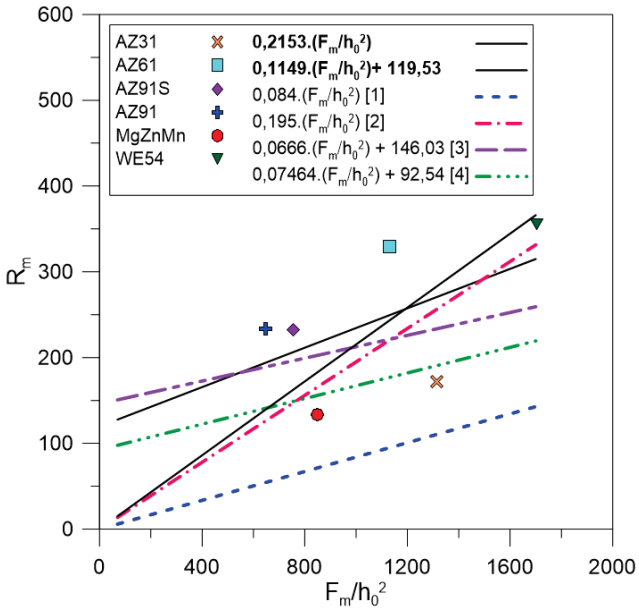

Fig. 3: Dependence of UTT ultimate strength on SPT yield strength with h_0^2 parameter.

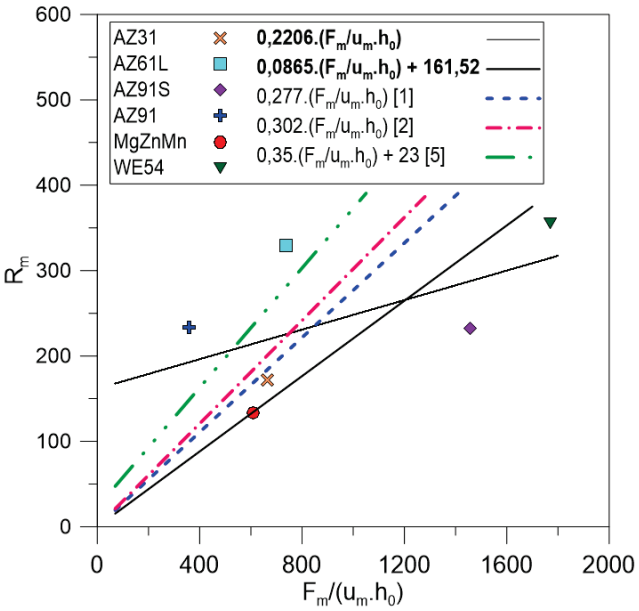

Fig. 4: Dependence of UTT yield strength on SPT yield strength with $h_0.u_m$ parameter

Discussion

Dependence of UTT strength on strength acquired from SPT tests for studied Mg alloys is shown in Figs. 2 - 4. Large scatter of data is apparent. Measured data were fitted by empirical formulas from literature [1-5] and by new linear regression with both zero and non-zero intersection with Y axis. Non-zero intersection is in contrary to physical presumption of zero strength R_m at zero SPT force F, nevertheless these formulas are suitable approximation at some test results range.

The macroscopic appearance of fracture surfaces exhibited two main phenomena – "star" fracture and "cap" fracture, which reflects brittle resp. ductile character of the material. Materials with "cap" fracture lie in Figs. 2 - 3 below regression lines, conversely those with "star" fracture lie above regression lines. In Fig. 4 it can be seen that deflection u_m at maximum force F_m is shifting ductile alloys (e.g. MgZnMn, AZ31) closer to regression lines in contrary brittle composite (AZ91 + 20% saffil) was shifted significantly farther. These can be reasons why it is unrealistic to define universal empirical formula. Therefore a more advanced approach to define correlation between UTT and SPT data might be to sort materials by ratio of "star" to "cap" fracture, eventually according to microscopical evaluation of brittle/ductile ratio of fracture appearance.

References

[1] T.E. García, C. Rodríguez, F.J. Belzunce, C. Suárez, Estimation of the mechanical properties of metallic materials by means of the small punch test. J. Alloy Compd. 582 (2014) 708–717.

[2] J. Langer, Stanovení mechanických vlastností lehkých kovů a jejich slitin a kompozitů pomocí protlačovacích zkoušek na miniaturních discích. Brno: VUT v Brně, FSI, 2014. 71 s.

[3] K. Guan, Z. Wang, SPT code of tensile test, Int. Conf. SSTT, (2010).

[4] M. Song, K. Guan, W. Qin, J. A. Szpunar, Comparison of mechanical properties in conventional and small punch tests of fractured anisotropic A350 alloy forging flange. Nucl Eng Des. 247 (2012) 58–65.

[5] J. Purmenský, K. Matocha, Small Sample Testing in Physical Metallurgy, in: Metal 2001.

21st International Conference **ENGINEERING MECHANICS 2015**
Svratka, Czech Republic, May 11 –14, 2015
Paper **#196, pp. 18–19**

Changes of Dynamic Properties of a Timber Frame Due to Simulated Seismic Load: A Case Study

Jan Bayer[1,a]*, Stanislav Pospíšil[1], Shota Urushadze[1], Bohumil Kasal[2]

[1] ITAM AS CR, v. v. i., Prosecká 809/76, 190 00 Praha 9, Czech Republic

[2] Fraunhofer Wilhelm-Klauditz Institut, Bienroder Weg 54E, 38108 Braunschweig, Germany

[a] bayer@itam.cas.cz

Keywords: modal analysis, frequency response function, structural health monitoring, timber frame, stiffened joints

Abstract: The data from a laboratory seismic resistance test of a three-story timber frame stiffened with steel joints were used to compare sweep and random excitation techniques on the platform of experimental modal analysis. The changes of mechanical properties due to increasing seismic load of the timber structure are demonstrated on corresponding changes of vibration modes and on changes of averaged frequency response functions. The comparison of averaged frequency response functions turned out to be at least as efficient tool for damage indication as the comparison of modal properties in this case. The experiences obtained in this case study are aimed at increasing the efficiency of dynamic tests and methods of Structural Health Monitoring.

Evaluation of experiments

In the scope of the research project Seventh Framework Program of EU [FP7/2007-2013] for access to the dynamic testing facility of the University of Bristol, UK, under grant agreement No.227887 [1], the acquired data from a seismic loading test were used for subsequent analysis. X-modal-III software of the University of Cincinnati was applied for the evaluation [2].

The "Output-only" measurements, as it is the usual case in the practice, using sweep excitation and random excitation of the intact structure were available for the evaluation. Fourteen modes could be extracted from the sweep test and only 7 from the random test. There are differences of identified natural frequencies between the two tests from +0,54 to -2,01 % with the average difference of approximately 1,3% which is explainable through the nonlinear behavior of the timber frame, because the intensity of loading was higher in the case of the random test.

The wooden frame was anchored on the vibration table which simulated the seismic load in four subsequent cycles with the intensity of 0.1g, 0.3g, 0.5g, 1.0g, and 2.0g. During the last test (2.0 g) the structure failed. Experimental modal analysis using random excitation test was carried out after each loading step in order to monitor the progressive damage. The results are summarized in the Table 1.

If we assume the uncertainty of identified modal frequencies about ±1% we can see that clearly apparent changes occurred just after the application of the seismic load with the intensity of 1g (N7). The evaluation of damping for the purposes of damage detection did not seem to be promising. Attention was also dedicated to damage indication from averaged frequency response functions, which seems to be simpler and not less reliable than the modal analysis. However, it is possible to find measured special quantities like frequency response functions of measured strains at particular locations that reflect the progressing damage since the first load step (see Fig.1).

Tab. 1: Identified vibration modes and their changes along with loading history

N4- 0.1 g		N5- 0.3 g		N6- 0.5 g		N7- 1.0 g		Frequency: difference [%]			Damping: difference [%]		
[Hz]	ν [%]	[Hz]	ν [%]	[Hz]	ν [%]	[Hz]	ν [%]	N5	N6	N7	N5	N6	N7
4,29	*16,97*	4,21	*17,18*	4,24	*13,23*	3,49	*12,76*	-1,93	-1,23	-18,71	*1,20*	*-22,04*	*-24,81*
5,39	*2,98*	5,37	*3,30*	5,30	*3,47*	4,74	*6,51*	-0,43	-1,61	-12,01	*10,72*	*16,50*	*118,78*
15,67	*3,87*	15,70	*3,55*	15,67	*2,86*	14,50	*5,32*	0,22	0,01	-7,44	*-8,31*	*-26,30*	*37,22*
16,59	*3,16*	16,50	*3,59*	16,39	*3,32*			-0,58	-1,21		*13,56*	*4,93*	*-64,22*
18,99	*3,23*												
21,36	*1,05*	21,38	*0,91*	21,42	*1,09*	21,15	*1,13*	0,10	0,25	-0,99	*-13,36*	*4,01*	*22,04*
21,82	*1,44*	21,79	*1,46*	21,72	*1,31*			-0,13	-0,44		*0,97*	*-9,02*	
25,29	*1,00*	25,17	*1,05*	25,14	*1,15*	25,25	*1,28*	-0,50	-0,61	-0,15	*4,91*	*15,53*	*69,64*
27,60	*1,74*			27,59	*2,17*				-0,04			*24,56*	
28,86	*2,04*	28,79	*1,84*	28,88	*1,44*	28,50	*1,69*	-0,25	0,07	-1,26	*-9,75*	*-29,40*	
31,37	*1,20*												*-53,88*
33,44	*1,36*	33,54	*1,20*	33,06	*0,56*			0,31	-1,12		*-11,41*	*-58,76*	
34,07	*1,39*			33,86	*2,70*	32,89	*0,55*		-0,64	-3,47		*93,96*	*63,17*
38,07	*2,04*	38,31	*1,74*	38,28	*1,28*			0,63	0,55		*-14,91*	*-37,27*	
39,70	*2,59*	39,72	*2,40*	39,93	*1,88*	39,61	*2,27*	0,07	0,59	-0,22	*-7,11*	*-27,32*	
Average changes:								**-0,23**	**-0,42**	**-5,53**	***-3,05***	***-3,89***	***20,99***

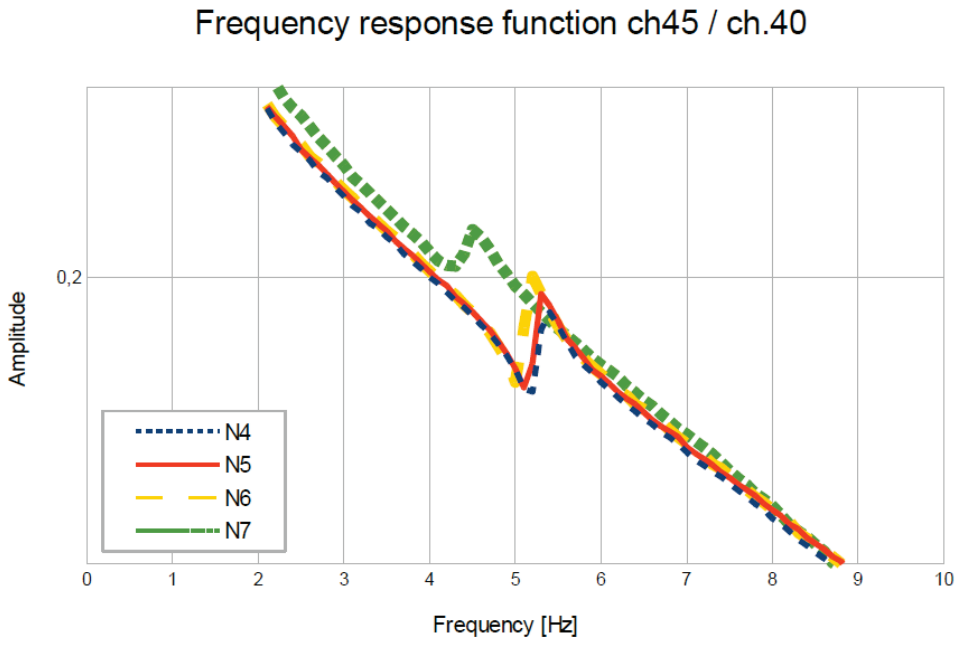

Fig. 1: Frequency response function between the strains of the first column and the accelerations of the third floor in the direction X.

References

[1] Bohumil Kasal, Andreas Heiduschke, Stanislav Pospíšil, Shota Urushadze, Shake table tests of a three-storey spatial timber frame with moment connections, World conference on timber engineering, Riva del Garda, Italy, 2010

[2] R.J. Allemang, The Modal Assurance Criterion – Twenty Years of Use and Abuse, Sound and Vibration, Aug. 2003, 14 – 21.

21st International Conference **ENGINEERING MECHANICS 2015**
Svratka, Czech Republic, May 11 –14, 2015
Paper **#105, pp. 20–21**

Stone in Historical Architecture in Slovakia

Martin Bednarik[a]*, Rudolf Holzer, Rudolf Tornyai

Comenius University in Bratislava, Faculty of Natural Sciences, Dept. of Engineering Geology, Mlynská dolina; 842 15, Bratislava; SK

[a]mbednarik@fns.uniba.sk

Keywords: Leitha limestone, travertine, volcanites, physical and mechanical properties

Abstract: Most of the historical monuments and buildings in Slovakia are built of natural, generous stone. The use of natural rock material in the area of the Western Carpathians is always bound on specifics of the regional - geological development of Slovakia. Different rock formation conditions and subsequent geological evolution caused considerable regional differentiation of rock masses. Major faulting of rocks during the folded-fault tectonics caused rather poor deposits on building and decorative stone in Slovakia. The rock masses of Western Carpathians provide stones which are of different natural and technical characteristics and different manner of utilization.

Introduction

The aim of this paper is to give an overview of most used rocks with the examples of their application on historical monuments of Slovakia. Another part of the contribution is to demonstrate petrophysical and material-technical characteristics of selected types of mentioned rocks.

Rocks used in various forms of building and decoration stone can be divided into 5 basic groups:

A. Consolidated clastic (granular) sediments – sandstone, conglomerate, breccia, quartzite, arkose, graywacke.
B. Carbonate rocks - travertine, limestone, marble.
C. Effusive volcanic rocks – rhyolite, andesite, basalt, quartz porphyre, melaphyre, diabase and their tuffs.
D. Intrusive rocks - granites, granodiorites, diorites, syenites, gabbros.
E. Metamorphic rocks – slate, serpentinite, ophicalcite, gneiss, migmatite, amphibolite.

Rocks as a building and decoration stone

Each rock group is characterised by basic properties (strength, porosity and water absorption) which are determining for the stone behaviour and resistance at its building utilization.

A. Consolidated clastic sediments. From this rock group the most used as building and decoration stone were the Carpathian Creataceous and Paleogene sandstones, and the Neogene sandstones from Vienna basin, as well.

A.1 Porous Cretaceous, Eocene and Neogene sandstones and conglomerates served as ashlars for the building of churches and palaces in Banská Bystrica and in Sádok, in monastery on Kláštorisko, etc. Worked stone blocks of sandstone were found in the historic site of Myšia hôrka from the Bronze Age near to Spišský Štvrtok. Sandstone and conglomerate from the Dobrá Voda quarry were used in the city of Trnava in the interior and on the portal of the St. Nicolaus basilica. The plates from Dobrá Voda or Chtelnica-Trianova rocks served by the renovation of the portal of Klarissa church, pedestal of the St. Trinity statue and entrance stairs into the Trnava archdiocese. Stone from Chtelnica-Trianova replaced the old entrance of the St. Jacob church and used for the renovation of the statue of St. Joseph on the St. Nicolaus square. The lithotype from Dobrá Voda has been in Bratislava used for staircases and basal window parapets of the former Erdödy palace, from the same material was laid the pavement in the entrance hall of the former Mindszenty atelier.

The Leitha limestone („Leithakalk“) - petrographically calcareous sandstone, conglomerate or biodetritic or algae limestone (Badenian) were exploited since the Roman Empire. Leitha limestone ashlars from Mannersdorf were with a high probability used in the Bratislava town hall. On the slopes of Devíska Kobyla (Small Carpathians) was exploited the Badenian calcareous sandstone and used in structures of Bratislava town hall, St. Martin´s basilica and Gothic church in the village Devín.

A.2 Compact sandstones of Paleogene and Neogene. In the Váh region, in Kysuca, Orava and Liptov regions these sandstones were used (parish churches in Žilina, Liptovský Mikuláš and in Gothic churches of the Spiš and Šariš regions). Tertiary sandstones create ashlars in the Great Moravian church in Kopčany. The quarry in Oravský Biely Potok provided a good-class sandstone for the Orava castle. Siliceous sandstone (Sarmatian) from the quarry in Sokolovce was exploited for the restoration of the St. Martin´s Cathedral in Bratislava in 60-ties and 70-ties of the last century. The same stone was found on the St. Emeram church in the Nitra castle. Roman churches in Bernolákovo, Boldog and Štvrtok n/Ostrove are built from the Neogene sandstone (Pannonian/Pontian).

B. Carbonate rocks. The Spiš travertine (quarry Dreveník) served since the medieval Ages material for structures of the Spiš castle and churches. The white or white-gray travertine represents the most significant decoration stone. It was used as facing and decoration stone in Bratislava and in several buildings in Prague and whole Czechoslovakia. The most importance belongs to the travertine from the Liptov basin, first of all from Bešeňová quarry, Ludrová and Lúčky. This material was for its particular texture and soft yellow-brown colour and good properties used on many significant historic objects (in Budapest, Comenius University in Bratislava, Palace of Nations in Geneva). The exploitation site of the most original decorative travertine („onyx d´or“) was the hill Šiklóš near Levice, which was used for decorations, mostly for interiors and stone bijouterie. Tuhár marble quarry served facing stones, pavements, window parapets, stairs, etc. Beside it, in many manor-houses occur decorations and products (since 18th century) of varicoloured marbles from Germany, Poland, Dalmatia, Italy, France, Belgium.

C. Effusive volcanic rocks.

C.1 Solid volcanites. To the most attractive building and decorative stone belongs the pink-red and porous rhyolite from Hliník n/Hronom. Since medieval Ages the rock has been used for individual decorative or building elements or as building ashlars on several buildings in Banská Štiavnica and Kremnica Mts., the tunnel below the Bratislava castle. From andesites were prevailingly used pyroxene and pyroxene-amphibolite andesites, and considering the appearance, extremely fair amphibole-biotite (AB) andesite, brownish-red or dark gray coloured. The AB andesite was historically exploited in underground gallery near Banská Štiavnica. This stone was used on significant buildings as Kammerhof, Old castle, Rubigall house, town hall and many other buildings on St. Trinity square in Banská Štiavnica, and on bridge piers in Budapest. Basalt was as building stone less used, a special disposal of it show sacred buildings of Calvary hill in Banská Štiavnica.

C.2 Semi solid volcanic rocks. The easy workable pyroclastic and epiclastic rocks were largely used as building stone in Central and Eastern Slovakia since the medieval Ages. Ashlars of easy workable material were used on medieval churches in Kalinčiakovo, Hronský Beňadik, on castles in Zvolen, Bojnice and Banská Štiavnica. Many rural buildings in villages near to Banská Štiavnica (eg. Prenčov) were built from this beautiful stone. So called “Obyce tuff” (Pohronský Inovec Mts., quarry Obyce served an appropriate building material since medieval Ages in buildings in Zlaté Moravce, Topoľčianky, Kostoľany p/Tríbečom, Nitra, Sádok and Klížske Hradište.

Rocks of the groups D. and E. are for the utilization as a building stone of no functional importance, occasionally were from granite and granodiorite manufactured cobble-stones and edge-stones. In case of suitable blockiness there were produced ashlars as for example a monument and gates in Devín, in Bratislava granite ashlars constitute the piers of the Červený most and the Calvinist church, as well. Granite from Mauthausen (Austria) was imported too. Piers of the Old Bridge over Danube and the Blumental church walls consist of this granite.

21st International Conference **ENGINEERING MECHANICS 2015**
Svratka, Czech Republic, May 11 –14, 2015
Paper **#139, pp. 22–23**

Comparison of Hybrid Metal-Composite Micropin Joints with Conventional Ones in Terms of Fatigue Life

Ganna Beketova[1,a], Marina Shevtsova[1,b], Volodymyr Symonov[2,c] *

[1]National aerospace university - "Kharkiv Aviation Institute",
17 Chkalova str, Kharkiv 61070, Ukraine

[2] Brno University of Technology, Faculty of Mechanical Engineering,
Technicka 2896/2, Brno 61669, Czech Republic

[a]a.c.beketova@gmail.com, [b]shevmar@d4.khai.edu, [c]symonov@fme.vutbr.cz

Keywords: metal-composite joint, reinforcing micro-pin elements, pull-off tests, fatigue strength

Abstract: The current research deals with special hybrid metal-composite joints which use thin sheet-metal reinforcement with small die-fixed pins (2-3 mm) imbedded into the composite part of the joint. This technological trick significantly and positively influences strength of the metal-composite bolted joints loaded in out-of-plane direction. This fact was proved by comparison of pull-off fatigue tests results of metal-composite joints with and without reinforcement.

Introduction

The conventional laminates based on polymer matrixes show low delamination resistance in consequence of very weak interlaminar strength. In order to increase the efficiency of composite structures and prevent the crack propagation in interlaminar and intralaminar directions, micro-pin elements are imbedded into laminates in out-of-plane direction (hereafter z-direction). Investigations of static and fatigue strength of composite specimens reinforced with thin metal pins [1-3] showed up prospects for implementation of such reinforcements to composite structures.

Very wide and longstanding experience in theoretical investigations and implementation of mechanical (bolted, riveted, etc.) joints showed up not enough efficiency for thin-walled composite structures. Therefore, the described hybridization of composite structures could be a good solution for increasing the efficiency of composite-composite and metal-composite joints. The hybridization and modification of the joints area is usually done by through-thickness cross-stitching elements (different kinds of clamps, wires, welded, pressed-in or milled metal micropin elements) [4-6].

The current research is devoted to fatigue life definition of a hybrid metal-composite joint (hereafter MCJ) loaded in z-direction. The fatigue life of the investigated joint is compared to the fatigue life of the same joint without hybridization.

Description of specimens and experiment set-up

The specimens consist of a composite basement and a metal fitting joined to the basement by 2 steel bolts 5 mm in diameter (see Fig. 1). The composite basement of the specimens was made of fiberglass twill-woven fabric 03BG225LD (the producer is Lange-Ritter, Germany) and epoxy resin LH-275 cured at 3.5 atm. pressure and 50°C temperature. Two types (type I and type II) of specimens were tested. The type I specimens (see Fig. 1a) represent the conventional bolted MCJ loaded in z-direction without any modifications. The type II specimens represent hybrid MCJ. The hybridization is provided by 0.5 mm thick metal reinforcement with die-fixed micropin elements imbedded into the lower side of the composite basement before curing (see Fig. 1b). Both the surface of the reinforcement facing the composite and micropins were covered with gluing compound VK-25. The fatigue tests were performed on a hydraulic test machine with asymmetrical loading cycle (R = 0.1) at 5 Hz frequency. The specimens were fixed in the machine grips with help of a special jig. The jig assembled with a specimen is shown in the Fig. 1c.

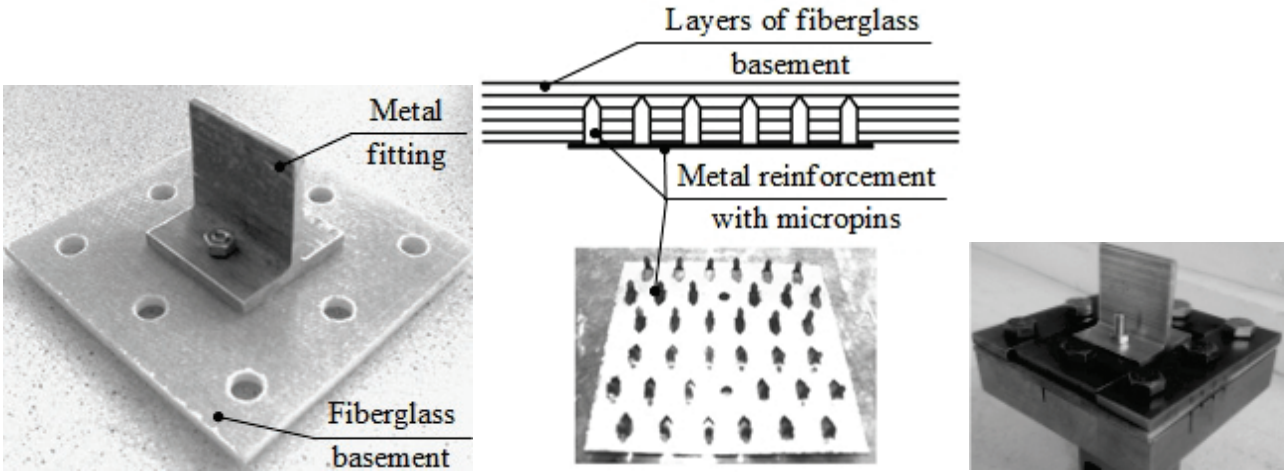

a) b) c)

Fig. 1: Tested specimens: a) conventional, b) reinforced, c) the test jig assembled with a specimen

Tests results

The results of the tests were analyzed according to ASTM E739 and are summarized in the linearized fatigue life curves shown in Fig. 2.

It can be seen from the curves the implementation of thin metal reinforcement with micropins is very efficient and allow increasing the load carrying capacity of such joints more than 1.5 times without remarkable weight increasing.

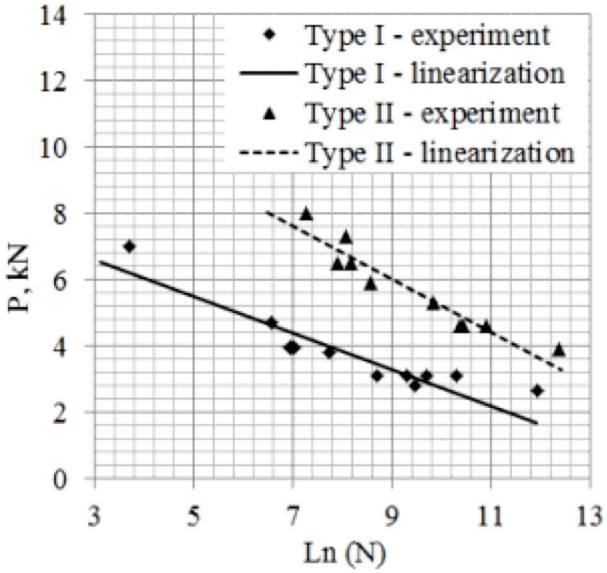

Fig. 2: Tests results

References

[1] A.P. Mouritz, Review of z-pinned composite laminates, Composites Part A: Applied Science and Manufacturing. – 12 (2007) 2383–2397.

[2] T.M. Koh, Experimental determination of the structural properties and strengthening mechanisms of z-pinned composite T-joints, Composite Structures. 9 (2011) 2222–2230.

[3] T.M. Koh, Strengthening mechanics of thin and thick composite T-joints reinforced with z-pins, Composites Part A: Applied Science and Manufacturing. 8 (2012) 1308–1317.

[4] B. Kolesnikov, CFRP/titanium hybrid material for improving composite bolted joints, Composite Structures. 83 (2008) 368–380.

[5] T. Löbel, Enhanced tensile strength of composite joints by using staple-like pins: Working principles and experimental validation, Composite Structures. 106 (2013) 453–460.

[6] M. Pacchione, D. Furfari, U.S. Patent 2013/0149,501 A1. (2013).

Dedication: Current research was done with the financial support of the international European project FP7-INCO-2011-6 “Integrating the National Aerospace University "KhAI" into ERA” and NETME Centre, regional R&D centre built with the financial support from the Operational Programme Research and Development for Innovations within the project NETME Centre (New Technologies for Mechanical Engineering), Reg. No. CZ.1.05/2.1.00/01.0002.

21st International Conference **ENGINEERING MECHANICS 2015**
Svratka, Czech Republic, May 11 –14, 2015
Paper **#219, pp. 24–25**

Full – Scale Testing of the Highway Arch Viaduct

Jan Benčat

University of Žilina, Research Centre of UZ, Univerzitna 1, 010 26 Žilina, Slovak Republic

jan.bencat@gmail.com

Keywords: bridge structures, railway viaducts, modal identification, full - scale dynamic testing, static and dynamic, loading tests, spectral analysis

Abstract: Full–scale dynamic testing of structures can provide valuable information on the service behavior and performance of structures. With the growing interest in the structural condition of highway bridges, dynamic testing can be used as a tool for assessing the integrity of bridges. From the measured dynamic response, induced by instructed passing trucks, modal parameters (natural frequencies, mode shapes and modal damping values) and system parameters (stiffness, mass and damping matrices) are obtained. These identified parameters can then be used to characterize and monitor the performance of the structure in the future. Analytical models of the structure can also be validated using these parameters [1,2].

Introduction

This paper refers the assessment of dynamic tests parameters of the highway viaduct [3] that were performed shortly after the end of its construction as part of standard requiring tests that include also static load tests. The *dynamic tests* consisted in the measurement of heavy lorries induced vibrations. Excitation of the bridge was performed by 25 tons testing lorries crossing the bridge with scheduled runs and known variable speeds. Further details of instrumentation layout, test and data processing procedures adopted are given in [1,2].

The paper presents, therefore, the results obtained in those tests, both in terms of levels of vibration measured during the passage lories (e.g. dynamic load factor – DLF) and also in what concerns the identified dynamic properties. For the experimental modal parameters identification the spectral procedures via software package *NI LabView* were used [4]. The identified bridge dynamic characteristics were also compared with the frequencies computed with finite element models and a good agreement was obtained between the experimental and FEM results.

Description of the Highway Viaduct and FEM

Highway viaduct description. The steel arch highway *Viaduct Structure 205* (*BS 205*) constructed on Highway D1 in the northern part of Slovakia (*Spiš region*) crosses part of this region. The viaduct bridge consists of two independent bridges (left and right bridge – LB and RB) with two traffic lanes, on each bridge for one direction only and sidewalks on both sides. The *Viaduct Structure 205* (*BS 205*) has a long length in total 670 m, but is composed by 9 dilatation modules (DM) that are structurally independent with common transition piers. Seven arch steel structure modules (DM2 – DM8) have a total length of 500 m, with spans 60 + 70 + 80 + 80 + 80 + 70 + 60 m. The remaining two modules (DM1 and DM9) with total length of 2 x 84,3 m are bridge junctions from both sides of viaduct.

FEM Calculation. Finite element models were developed in order to help in the preparation of the static and dynamic tests and in the interpretation of their results. The software FEM – IDA NEXIS 32 [5] was used for that purpose. Different models were developed for the tested modules since there is a slight difference in their geometry. Since there are several structural and material parameters that would affect the modal behavior of the viaduct bridge, such as the mass, the vertical and transverse bending stiffness of the deck etc., the calibration of the FE model was performed using the results of field vibration measurements.

Dynamic Tests. The dynamic tests of the *BS 205 – Right Bridge* were carried out in May 2010 and dynamic tests of the *BS 205 – Left Bridge* in November 2012, [1,2].

Conclusions

The dynamic tests of the viaduct *Bridge Structure 205 – Right Bridge*, allowed measuring the vibrations in the structure induced by a total of 17 runs of different crossing the viaduct with speeds from 4.95 km/h to 50.6 km/h. From the analysis of the levels of vibration, expressed in the *maximum* and *RMS* values of both accelerations and displacements, the following conclusions were taken:

i) The experimental analysis of the bridge dynamic response caused by moving load it possible to identify 10 basic natural frequencies of bridge vibration. These frequencies have been received by analysis of small amplitude vibration and so the analysis corresponds to linear vibration.

ii) In relation to the natural frequencies of vibration, the results obtained by spectral analysis are also in good agreement with the frequencies computed with finite element models.

iii) The experimentally achieved values of dynamic load factor $\delta_{EXP}(v)$ shows the real stiffness of structure is fully comparable with the corresponding standard value of the dynamic load factor δ (DLF) used by the designer for the bridge structures according to relevant standards [6,7].

iv) The logarithmic decrement corresponding to the first mode of the bridge vibrations varies in the range $0.16 \div 0.25$, then the damping ratios of the steel bridge structure were found to be $0.025\ \% \div 0.040\ \%$ of critical damping, respectively. It was possible to evaluate the damping characteristics of the bridge structure only from limited number of measurements. They are therefore only indicative.

v) The comparison of the numerical and experimental results of the bridge parameters shows good agreement of theoretical and experimental values of natural frequencies and DLF respectively. The required criteria of all loading states by the Slovak standards have been also fulfilled. It should be noted that the recorded levels of vibration and the identified dynamic characteristics are an important contribution for the characterization of the global behavior and condition of the viaduct *Bridge Structure 205* and of the dynamic effects of future highway traffic [8,9].

Acknowledgments: We kindly acknowledge the project "Research Centre of University of Zilina", ITMS 26220220183, supported by European regional development fund and Slovak state budget.

References

[1] J. Bencat, et al, Static and dynamic test results of the viaduct Bridge Structure 205 on D1/DC1–9, Right Bridge, Technical Report: No. 6 – 3 – 14/SvF/12, ZU Zilina, (in Slovak), 2012.

[2] J. Bencat, et al, Static and dynamic test results of the viaduct Bridge Structure 205 on D1/DC1–9, Left Bridge, Technical Report: No. 6 – 3 – 48/SvF/09, ZU Zilina, (in Slovak), 2010.

[3] L. Baca, et al, Project of the viaduct Bridge Structure 205 on D1/DC1–9, Right and Left Bridge, Project documentation, Geoconsult, s.r.o., Bratislava, (in Slovak), 2009.

[4] NI LabVIEW 8.20, Software package, National Instruments Corporation, USA, 11500 N Mopac Expy, Austin, TX 78759, 2006.

[5] IDA NEXIS 3.2, Free Software Foundation, Inc., Boston, MA 02110–1301 USA, 2009.

[6] Slovak Standard STN 736203, Loading of Bridges, SUTN, Bratislava, (in Slovak), 1993.

[7] Slovak Standard STN 736209, Loading Tests of Bridges, SUTN, Bratislava, (in Slovak), 1993.

[8] J. Rodrigues, M. Ledesma, Dynamic Tests of a Railway Viaduct Proceedings of the 8th International Conference on Structural Dynamics, EURODYN 2011, Leuven, Belgium, 4–6 July, 2011.

[9] C. Gentile, A. Saisi, F. Busatta, Dynamic testing and permanent monitoring of an historic iron arch bridge, EURODYN 2011, Leuven, Belgium, 4–6 July, 2011.

21st International Conference **ENGINEERING MECHANICS 2015**
Svratka, Czech Republic, May 11 –14, 2015
Paper **#152, pp. 26–27**

Experimental and Numerical Analysis of Concrete Slender Columns by Stability Failure

Vladimír Benko[a]*, Ľudovít Fillo[b], Peter Kendický[c], Veronika Dvoranová[d]

Faculty of Civil Engineering at SUT in Bratislava,
Radlinského 11, SK-810 05 Bratislava, Slovak Republic

[a]vladimir.benko@stuba.sk, [b]ludovit.fillo@stuba.sk, [c]peter.kendicky@stuba.sk,
[d]veronika.dvoranova@stuba.sk

Keywords: slender columns, stability, experiment, failure, buckling, resistance, analysis, reliability.

Abstract: The European Standard [1] for design of concrete compressed slender members shows a significant deficit in global reliability. The contribution present the results of experimental and numerical verification of slender concrete columns made of different concrete strength classes - C45/55 and C100/115. A basic aim of the analysis was to design concrete columns subjected to bending moment and axial force where the stability failure proceeds at the compression strain 1.5 ‰. In the contribution will be presented the first of three series of experimental and numerical analyzed columns with the verification of global reliability. The experiments were realized at the Faculty of Civil Engineering SUT in Bratislava with cooperation of ZIPP Bratislava Company.

Introduction

Semi-probabilistic method of reliability of structural members and structures according the Eurocodes is based on the use of partial coefficients of reliability. The required reliability index and therefore the probability of failure, is ensured by partial coefficients of reliability. In ULS the effect of loads is increased by partial coefficient of reliability γ_F and the resistance of materials is reduced by partial coefficients of materials γ_M. Increasing of compressive normal force by slender concrete columns leads to raise of deformation and then to increase of total eccentricity of normal force in critical section. The raise of the eccentricity of the second order can be so significant that the stability failure can precede the material failure of critical cross-section.

Application of non-linear analysis is defined in [1] chap. 5.7 (4)P: *„The use of material characteristics which represent the stiffness in a realistic way but take account of the uncertainties of failure shall be used when using non-linear analysis...“*. The partial safety factor for stability failure of the concrete columns is not defined. Practical usage of the non-linear general method is available according [1] chap. 5.8.6 (3) with using of design values of the materials. In this case is questionable if the total reliability of the compressed structural member is sufficient.

Experimental verification

The task of the upcoming experiment was to design material and geometric characteristics and initial eccentricity of the normal force applied on reinforced concrete column that the value of strain of compressed concrete fibers in the critical cross section would reach approximately ε_{c1} = 1,5 ‰ by the stability failure of the column. The columns were made of concrete C45/55 and reinforced by steel bars B500B. The experimental samples - columns were realized in the Prefa plant Sereď with support and cooperation ZIPP Bratislava s.r.o.

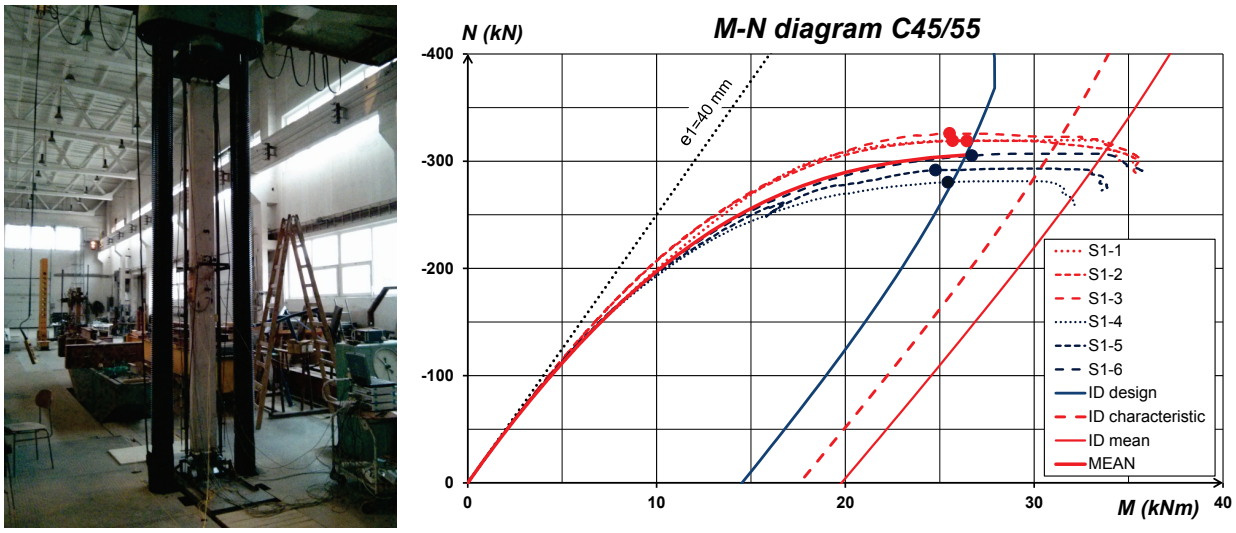

Fig. 1: Setting of the tests and M-N diagrams of the experimental columns S1 - 1 to S1 - 6

Summary

The planned experimental tests confirmed the predicted results of the authors and the nature of the behaviour of the slender columns during the tests. The columns failed by stability loss before design resistance was reached, i.e. the stability failure occurred in the domain of the interaction diagram M-N of the column cross section when strain of the compressed part of critical cross section was above 1.5 ‰ (Fig.1). According the authors, it is necessary to define the partial safety factor for stability failure of slender compressed member for such cases.

The importance of correct definition of the partial reliability coefficient for stability failure of compressed members is increased by the fact that this type of failure is sudden without warning and significant deformation. That is why by this type of the stability failure we need enhanced global reliability in comparison with classical ductile failure.

The recommended partial reliability coefficient of stability failure is not included in Eurocodes especially EN 1992-1-1, but only in Austrian National Annex [2]. EN 1992-1-1 [1] didn't treated this significant deficit of global reliability by stability failure of concrete columns even after years of experimental results proving the above mentioned fact [3, 4].

References

[1] EN 1992-1-1:2004 Eurocode 2: Design of concrete structures - Part 1-1: General rules and rules for buildings, (2004).

[2] ÖNORM B 1992-1-1:2011 Eurocode 2: Bemessung und Konstruktion von Stahlbeton- und Spannbetontragwerken Teil 1-1: Grundlagen und Anwendungsregeln für den Hochbau, (2011).

[3] M. Moravčík, M. Brodňan, P. Koteš, P. Kotula, Experience with bridges of the older types of precast (Skúsenosti s mostami zo starších typov prefabrikátov), in: Betonárske dni 2012, zborník prednášok, STU v Bratislave, 2012, ISBN 978-80-8076-104-2, pp. 439-444.

[4] S.L. Burtscher, G. Rinnhofer, V. Benko, J. Kollegger, Destructive large-scale tests on highly reinforced spun concrete columns. (Zerstörende Großversuche an hochbewehrten Schleuderbetonstützen). Bauingenieur, Band 78, April 2003, pp.. 187-193.

21st International Conference **ENGINEERING MECHANICS 2015**
Svratka, Czech Republic, May 11 –14, 2015
Paper **#159, pp. 28–29**

On Choice of Lagrange Multipliers for Fictitious Domain Method for the Numerical Simulation of Incompressible Viscous Flow around Rigid Bodies

Matej Beňo[a], Bořek Patzák[b]

Faculty of Civil Engineering, Czech Technical University, Thákurova 7, 166 29, Prague CZ

[a]matej.beno@fsv.cvut.cz, [b]borek.patzak@fsv.cvut.cz

Keywords: Lagrange multiplier, finite element method, fictitious domain method, incompressible Newtonian fluid

Abstract: The aim of this article is to present the results of flow around rigid obstacles. The finite element implementation is based on the incompressible Navier-Stokes equation on structured, two dimensional triangular meshes using operator splitting for time discretization. To model rigid particles, the fictitious domain method is used. The article compares different approaches for selection of Lagrange multipliers used to enforce rigid body constrains.

Introduction

The fictitious domain method represents useful and powerful tool for modeling of fluid flows with obstacles. The principle of this method is to extend a problem domain to include not only the fluid, but also the particles. This lead to so called "fictitious" domain. This domain is geometrically simpler, which allows to use more regular meshes. The advantage of this approach is that specific fast solvers can be developed. The second main advantage is that there is no need to compute the hydrodynamics forces and torques.

Method

The fictitious domain method used in this article follows the work of Glowinsky [1]. The use of a combined weak formulation for fluid-structure system leads to cancelation of the forces and moments between the obstacles and fluid. Then the fluid flow is solved from weak formulation everywhere in the domain, including the fictitious domain parts inside the obstacles. To enforce the rigid-body constraints on obstacles, the Lagrange multipliers are used. The multipliers represents the additional body force needed to maintain the rigid body motion inside the obstacles.

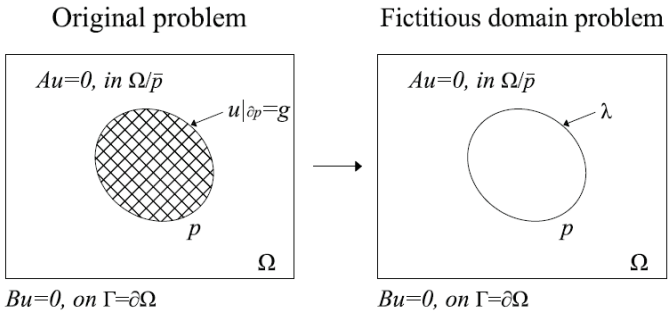

Fig. 1: Original and fictitious domain problem.

Numerical results

The numerical simulation of flow around rigid object is performed on model shown in Fig.2. The domain has been divided into 4256 elements. The perfect friction on both plates (zero velocity) has been assumed. The following parameters have been used: mass density $\rho = 1.0\, kg/m^3$, viscosity $\eta = 10^{-2} Pa\, s$, and time step $\Delta t = 0.05$. These results are presented in steady state.

To enforce no movement inside the rigid particle, the rigid movement condition is enforced using Lagrange multipliers on selected sampling points. Various strategies are tested on how to select different sampling points on the particle boundary and volume. Profiles of velocities in vertical sections at different positions are compared in Fig 3. The results are also compared using the results obtained by traditional approach, where only fluid part has been discretized.

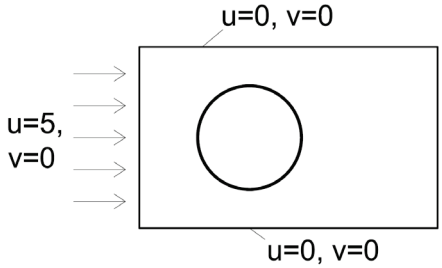

Fig. 2: The geometry and the boundary conditions of flow in tube with obstacle.

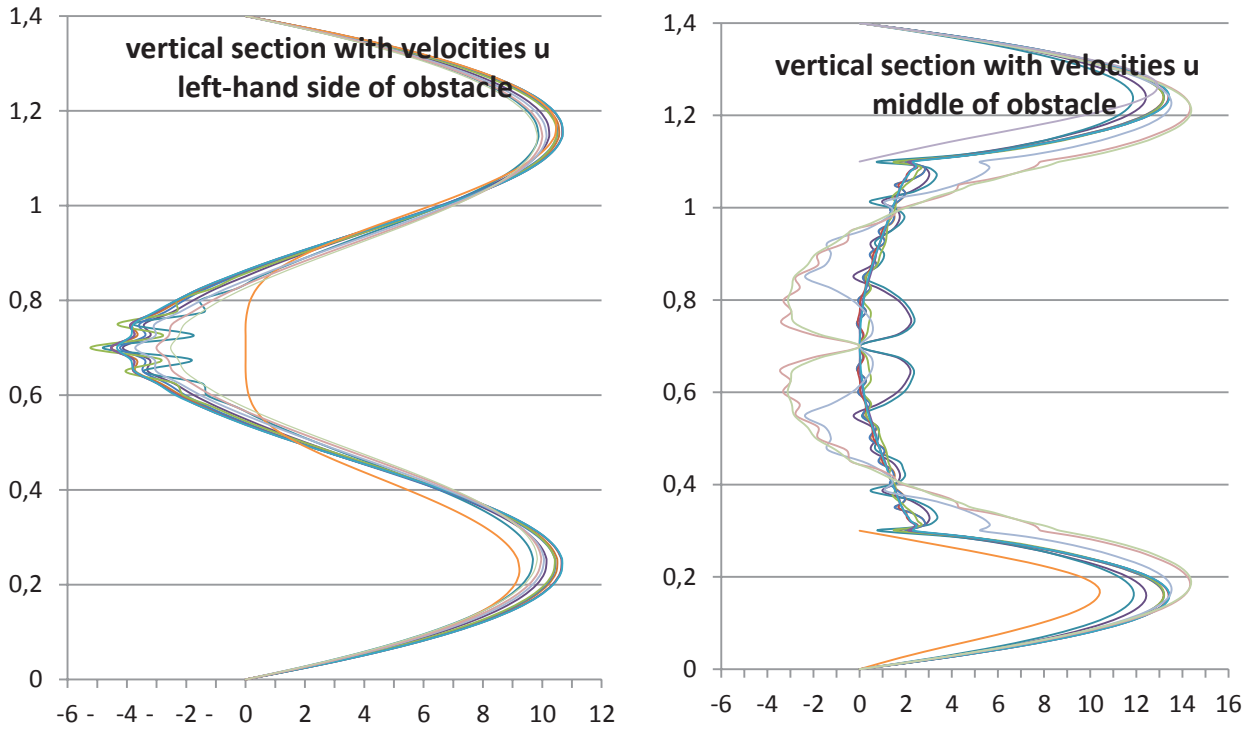

Fig. 3: Velocity profiles in front of and through obstacle.

Conclusion

Presented results show that the fictitious domain approach is capable to accurately predict the flow profiles, however, the quality strongly depends on selected strategy of sampling point selection. The optimal results have been obtained for strategy based on fifteen and more Lagrange multipliers uniformly selected throughout the obstacle.

Acknowledgment: The authors would like to acknowledge the support by the Czech Science Foundation under the project 13-23584S.

References

[1] R. Glowinski, T.-W. Pan, T.I. Hesla, D.D. Joseph, A distributed Lagrange multiplier/fictitious domain method for particulate flows, Int. Journal of Multiphase Flow, 25 (1999) 755-794.

Fatigue Testing of Polymeric Hollow Fibre Heat Transfer Surfaces by Pulsating Pressure Loads

T. Brožová[a], T. Luks[b], I. Astrouski[c], M. Raudenský[d]

[1]Brno University of Technology, Faculty of Mechanical Engineering, Heat Transfer and Fluid Flow Laboratory, Technická 2896/2, 616 69 Brno Czech Republic

[a]brozova@LPTaP.fme.vutbr.cz, [b]luks@fme.vutbr.cz, [c]astrouski@LPTaP.fme.vutbr.cz, [d]raudensky@fme.vutbr.cz

Keywords: fatigue test, pulsating pressure load, hollow fibres, heat exchanger, heat transfer surfaces

Abstract: This article deals with the fatigue tests of polymeric hollow fibre heat transfer surfaces. Hollow fibres have an outer diameter around 0.5-0.8 mm and thickness of the wall is 10 % of the outer diameter. These heat transfer surfaces made from plastics have some limitations but also a lot of benefits. One of the limitations is durability of plastic under fatigue loading. The heat transfer surfaces were subjected to pulsating pressure loads under different conditions (level of pressure, ambient temperature, number of cycles). Firstly, just the pulsating load was applied and the behaviour of hollow fibres was observed paying special attention to the presence of a leaking, rupture, etc.

Then some other conditions of operations were added. The heat transfer surfaces were immersed in a hot bath and loaded by pulsating pressure and high temperature simultaneously. Testing under the different temperature is important because the temperature significantly affects the material properties. The presence of the leaking, rupture and other possible damage was monitored as for previous tests.

Introduction

Service life is a very debated topic nowadays. It is necessary to guarantee a lifetime of every technological device. The prototypes of polymer heat exchangers consisting of many polypropylene hollow fibres are under development for hot-water applications. The working conditions will be: temperature around 80 °C and gauge pressure 0.35 MPa. Prototypes of polymeric heat exchanger developed in our laboratory need such kind of tests too. For more details see [1,2].

Stress in the wall

The aim of fatigue tests is simulation of operation conditions. In this particular case the hollow fibres were loaded by the internal pressure $p = 0.35$ MPa and the period of the pulse was $T = 1.4$ s. The parameters of fibres were the outer diameter $d = 0.5$ mm (respectively 0.8 mm), and wall-thickness was 10 % of the outer diameter, thus $w = 0.05$ mm (respectively 0.08 mm).

The important factor is the strain inside the wall of the fibres. There are two types of strain in the fibre, the hoop stress, and the axial stress. The hoop stress is obtainable from the following relation $\sigma_\theta = pd/2w$. In the case when two ends of the fibre are constrained the axial stress is obtained as $\sigma_z = pd/4w$.

From the previous equations it is obvious that the stress depends on the internal pressure p and the ratio of the parameters of fibre d/w. The dependence of the ratio σ/p on the ratio d/w is possible to see in Fig. 1.

In the measured cases was the ratio always $d/w = 10$. Hence, the hoop stress was $\sigma_\theta = 1.75$ MPa and the axial stress was $\sigma_z = 0.875$ MPa under the corresponding pressure $p = 0.35$ MPa.

Fatigue tests

Tests with prototypes of heat exchangers were run for both outer diameters, 0.5 mm and 0.8 mm under the above specified conditions (p, T, w, d). The connection method was constructed as follows: the

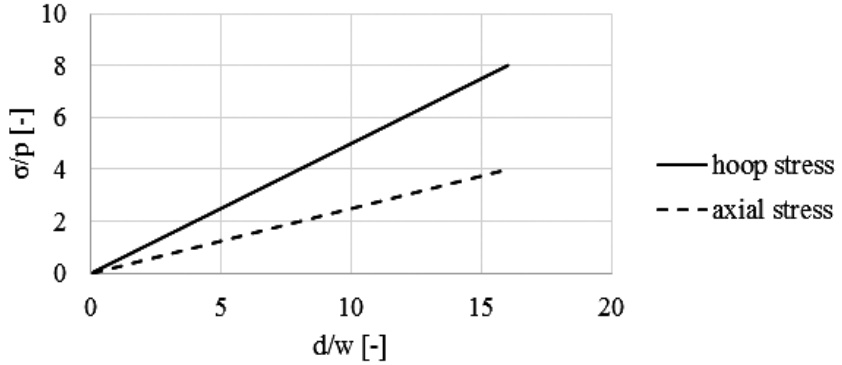

Fig. 1: The dependence of the ratio stress in the wall σ and pressure p on the ratio of the diameter d and wall thickness w of the fibre.

pressure reduction valve at the input, the water filter followed and then the system of two electromagnetic valves between which were the hollow fibres. Behind the second valve was the output to the drain. The test was done at room temperature. The system of valves was controlled in the following sequences: the input valve was open and the output valve was closed. The pressure inside the fibres reached the level of 0.35 MPa and the input valve was closed. When the pressure has stabilized, the output valve was opened and the pressure inside the system dropped. After that the output valve was closed and the input valve was again opened and then the whole process was repeated. Typical results are shown in Fig. 2. The test was stopped after more than 1.5 millions of successful cycles. Fibres showed no signs of damage. The next step are tests in a hot bath.

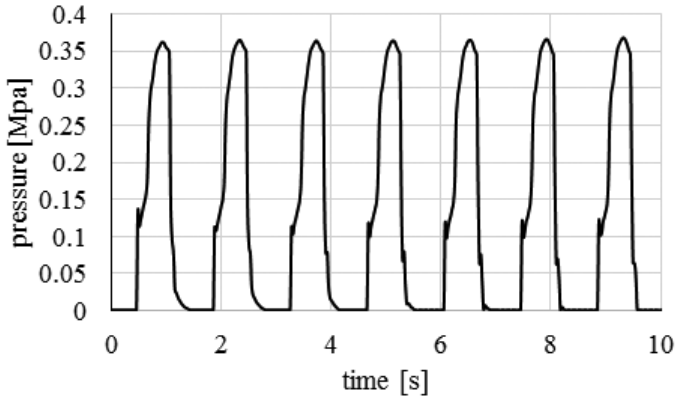

Fig. 2: The pressure profile during the test.

Conclusion

The tensile stress (yield) for the used material of hollow fibres is 35 MPa. The hoop stress reached in the wall of fibre is 1.75 MPa which is only 5 % of the yield stress. Hence, fibres are working in a safety zone but a creep can occur in a long time loading. This is why more tests has to be done.

Acknowledgement: This work is an output of research and scientific activities of this project LO1202 and the project No. CZ.1.07/2.3.00/20.0188, HEATEAM - Multidisciplinary Team for Research and Development of Heat Processes with financial support of the MEYS under the programme NPU I.

References

[1] C. Wu,S. C. Mantell, J. H. Davidson, T. Miyake, A method for measuring the creep behavior of pressurized polymer tubing. Experimental Mechanics. Vol. 41 (2001), pp. 368-374.

[2] I. Astrouski, M. Raudenský, The Study of Polymeric Hollow Fiber Heat Exchangers. In Engineering Mechanics 2012. Svratka: 2012. p. 47-57. ISBN: 978-80-86246-40- 6.

21st International Conference **ENGINEERING MECHANICS 2015**
Svratka, Czech Republic, May 11 –14, 2015
Paper **#166, pp. 32–33**

Modelling of Rotating Twisted Blades as 1D Continuum

Jan Brůha[a] *, Drahomír Rychecký[b]

Department of Mechanics, University of West Bohemia, Univerzitní 22, 306 14 Plzeň, Czech Republic

[a]bruhaj@kme.zcu.cz, [b]rychecky@kme.zcu.cz

Keywords: vibration, turbine blade, finite element method, optimization

Abstract: Presented paper deals with modelling of a twisted blade with rhombic shroud as one-dimensional continuum by using beam finite elements with linearly varying cross-sectional parameters. The blade is clamped into a rotating rigid disk and the shroud is considered as a rigid body. Besides, in consequence of eigenfrequencies comparison with a 3D finite element model of the identical blade, material properties tuning is performed.

Introduction

In some publications dealing with modelling of turbine bladed disks, the disk is modelled by using 3D finite elements, but the blades are considered as 1D continuum modelled by using Rayleigh beam elements [1, 2]. This method can be perceived as a basic tool for investigation of dynamic behaviour of the bladed disks and an alternative to more complex 3D finite element models of the blades [3]. Due to lower number of degrees of freedom, this approach can be advantageously used, for example, for geometric properties optimization because of less time-consuming computation.

However, due to Bernoulli-Navier hypothesis considering (that says: during deflection, the plane normal cross-sections of the blade remain plane and normal to the deflected longitudinal axis of the blade), the turbine blades modelled by using 1D beam elements are stiffer than the 3D finite element models. This phenomenon is pronounced especially in case of so-called “short blades”. Therefore, material properties tuning of the 1D blade model is one of the options to attenuate this handicap.

The aim of this work is modelling of rotating twisted blade as 1D continuum using material properties tuning as a result of eigenfrequencies comparison with a 3D finite element model.

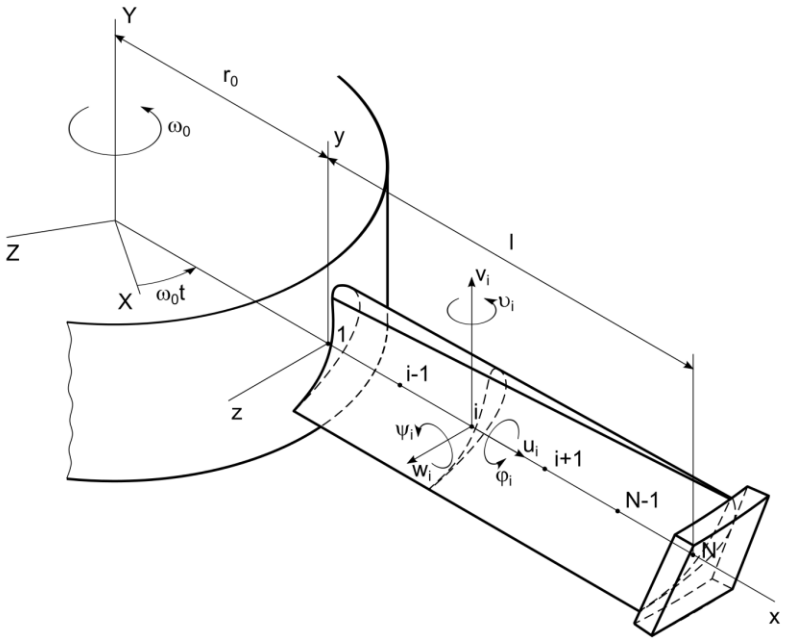

Fig. 1: Rotating twisted blade clamped into a rigid disk

Blade modelling and optimization

The computational model of a twisted blade with rhombic shroud (that is considered as rigid) and variable cross-sections along the blade is shown in Fig. 1 [4]. This blade is clamped into a rigid disk rotating with constant angular velocity ω_0. According to introduction, the blade is divided into N beam finite elements with linearly varying cross-sectional parameters and six degrees of freedom in every node [5]. Then, the equations of motion of the blade can be expressed in generalized coordinates

$$\boldsymbol{q_B} = [\ldots u_i, v_i, w_i, \varphi_i, \vartheta_i, \psi_i, \ldots]^T, \quad i = 1, \ldots, N \tag{1}$$

in following form

$$\boldsymbol{M_B}\ddot{\boldsymbol{q}}_{\boldsymbol{B}} + (\boldsymbol{B_B} + \omega_0 \boldsymbol{G_B})\dot{\boldsymbol{q}}_{\boldsymbol{B}} + \left[\boldsymbol{K_{s,B}} + \omega_0^2\left(\boldsymbol{K_{stiff,B}} - \boldsymbol{K_{\omega,B}}\right)\right]\boldsymbol{q_B} = \boldsymbol{0}, \tag{2}$$

where symmetric matrices $\boldsymbol{M_B}$, $\boldsymbol{B_B}$, $\boldsymbol{K_{s,B}}$, ${\omega_0}^2\boldsymbol{K_{stiff,B}}$, ${\omega_0}^2\boldsymbol{K_{\omega,B}}$ are mass, material damping, static stiffness, centrifugal stiffening under rotation and softening because of modelling in a rotating coordinate system, respectively. The skew symmetric matrix $\omega_0\boldsymbol{G_B}$ represents gyroscopic effects.

Due to higher stiffness as a result of Bernoulli-Navier hypothesis considering, parameters E (Young's modulus), ν (Poisson's ratio) and J_k (torsion resistance) of every beam finite element were being tuned. The objective function has the form

$$\psi(\boldsymbol{p}) = \sum_{j=1}^{m}\left[(m+1-j)^2.\left(\frac{\Omega_j(\boldsymbol{p})-\Omega_j^*}{\Omega_j^*}\right)^2\right], \tag{3}$$

where $\boldsymbol{p}$ is vector of optimization parameters, $\Omega_j(\boldsymbol{p})$ are eigenfrequencies of the 1D finite element model and Ω_j^* are eigenfrequencies of the 3D finite element model of the identical blade.

Summary

Modelling of turbine twisted blades by using 1D beam finite elements with variable cross-sectional parameters can be an alternative to large 3D finite element models, especially in cases of parameter optimization or contact problems of bladed disks. However, the blades modelled by this method based on Bernoulli-Navier hypothesis are stiffer. Parameter tuning is a suitable tool to attenuate this handicap.

Acknowledgement: This work was supported by TE01020068 project "Centre of research and experimental development of reliable energy production" of Technology Agency of the Czech Republic.

References

[1] J. Šašek, V. Zeman, J. Kellner, Modal Condensation of Bladed Disk, Engineering Mechanics, 19 (2012) 351.

[2] J. Kellner, Vibrations of Turbine Blades and Bladed Disks, PhD Thesis, University of West Bohemia, Pilsen, 2009 (in Czech).

[3] M. Hajžman, M. Byrtus, V. Zeman, Solution of the Mutual Contact in the Finite Element Analysis of Twisted Blades, Colloquium Dynamics of Machines 2012, Prague, pp. 51-58.

[4] Z. Kubín, J. Hlous, Measurement of Rhombic Bladed Disk, Research report, Doosan Škoda Power, 2012.

[5] M. Byrtus, M. Hajžman, V. Zeman, Dynamics of Rotating Systems, University of West Bohemia, Pilsen, 2010 (in Czech).

21st International Conference **ENGINEERING MECHANICS 2015**
Svratka, Czech Republic, May 11 –14, 2015
Paper **#072, pp. 34–35**

Assessment of Cast-Iron Structures

Ivan Brych[a]*, Miroslav Sýkora[b]

CTU in Prague, Klokner Institute, Šolínova 7, Prague 6, 166 08, Czech Republic

[a] ivan.brych@klok.cvut.cz, [b] miroslav.sykora@klok.cvut.cz,

Keywords: cast-iron columns, material characteristics, cross-section characteristics, imperfections, ultimate strength, slenderness, brittleness in tension, model uncertainty

Abstract: The paper focuses on the assessment of cast-iron columns in industrial heritage structures. For cast-iron structures it is difficult to verify metallurgical composition and processing technology, which directly affect the geometry of cross-sections. The crucial issue of reliability of cast-iron structures is their brittle fracture in tension at higher slenderness ratios. The load carrying capacity of columns is determined by their stability and cast-iron strengths in compression and tension. Outcomes of several computational methods, including the procedure recommended in ČSN ISO 13822, are compared with extensive experimental data and model uncertainty is identified. Unknown input parameters for the model proposed by Rondal and Rassmussen [1] that fits best to the data are then validated. The validated model is in a good agreement with experimental data and provides conservative estimates of load carrying capacity. The study provides suggestions to complete the calculation of buckling coefficient contained in ČSN ISO 13822.

Introduction

The study is focused on reliability assessment of cast-iron columns that were in the 19th and 20th century used in industrial structures including textile factories, railway stations, shelters of platforms and bridges. Eurocodes provide no methodology that would reflect specific characteristics of cast iron - a non-linear stress-strain diagram without obvious yield stress and significant differences between compressive and tensile strengths. Behaviour of cast iron is close to aluminium or stainless steel. A simplified procedure indicated in ČSN 73 0038:2014 (Czech national annexes to ISO 13822:2010 for assessment of existing structures) and analytical models proposed in [1,2] for the assessment of cast-iron columns are compared.

Considered models

Assessment of existing structures should be based on real geometrical properties of structural members. For cast-iron structures it is difficult to identify metallurgical composition and technological process that directly affect the geometry of structural members. The primary issue in determining the resistance of cast-iron structures in compression is their brittle fracture without plastic deformation for higher slenderness ratios. Stability affected by geometrical imperfections and compressive and tensile strengths determines the load-bearing capacity of cast-iron columns. The imperfections result from a commonly unknown process of casting such as hand casting or forging. That is why cross-sections often have inner eccentricities and different wall thicknesses due to casting in a horizontal position. Moreover, axis of cast-iron columns is typically deviated.
The study critically compares the following models for estimating load-bearing capacity of cast-iron columns centrically loaded in compression:

- *Approach 1* [1] determines the ultimate strength σ_{ult} for a column susceptible to buckling as a minimum value of ultimate compressive strength $\sigma_{ult,c}$ and ultimate tensile strength $\sigma_{ult,t}$ (tension strength playing a role for slender columns); $\sigma_{ult} = \min(\sigma_{ult,c}; \sigma_{ult,t})$.
- *Approach 2* [2] is similar to the design method for columns exposed to buckling according to EN 1993-1-1:2006. The ultimate compressive strength $\sigma_{ult,c}$ takes into account buckling by a coefficient χ_c dependent on slenderness ratio and specified buckling curves, and eccentricities of cross-sections; $\sigma_{ult} = \sigma_{ult,c}$.

- *Approach 3* is based on the recommendations of ČSN 73 0038. The ultimate strength σ_{ult} is obtained considering a modified buckling coefficient χ_c covering effects of slenderness ratio and recommended strength of cast iron σ_u, and the procedure indicated in EN 1993-1-1 for steel structures; $\sigma_{ult} = \chi_c \times \sigma_u$.

Model uncertainty

The considered models are compared using model uncertainly θ. Its individual values are obtained as the ratio of test and model values, $\theta_i = \sigma_{ult,\ test,\ i} / \sigma_{ult,\ model,\ i}$. Basic information on the available database of tests and model uncertainty characteristics for *approach 1* is provided in Tab. 1 [1].

Tab. 1: Test database [1] and model uncertainty characteristics for *approach 1*

Cross-section	Sample size	Slenderness ratio	Column strength [MPa]	Model uncertainty - mean	Coefficient of variation
Solid cylindrical	50	26 – 242	14.8-537	1.09 - 1.2	0.05 - 0.14
Hollow cylindrical	18	50.8 - 242	31.9-186	1.12	0.11
Square	4	153.8 - 204	24.2-43.6	1.43	0.08

Model outcome based on *approach 2* is compared with an individual test result - hollow cylindrical column with complete cross-section characteristics and effective length of 3050 mm; model uncertainty is $\theta_i \approx 1.18$. *Approach 3* is compared against a test result of a column shown in Fig. 1. The column consists of four parts with different cross-sections; the effective length is 6650 mm. For the middle part of the column (hollow cylindrical cross-sections) the model uncertainty is $\theta_i \approx 0.648$; for the upper part (square cross-sections) a conservative estimate is obtained, $\theta_i \approx 1.47$.

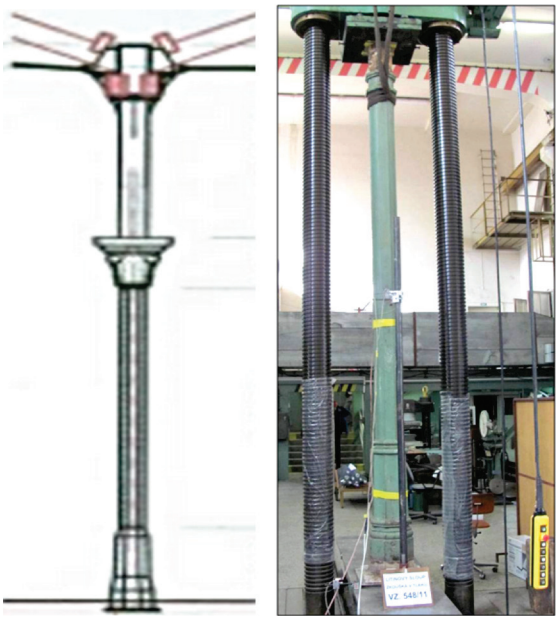

Fig. 1: Example of cast-iron column - scheme and test assembly

Conclusions

The ultimate strength σ_{ult} of cast-iron columns is significantly affected by the slenderness ratio. Critical comparison of the selected models reveals that the *approach 1* is in a good agreement with the experimental data. *Approach 2* also provides a good estimate, however comparison with more test results is needed. *Approach 3* is overly conservative due to overestimation of buckling effects. The study will be extended to provide background information for improving the technique recommended in ČSN 73 0038.

Acknowledgement: The study is a part of the research project NAKI DF12P01OVV040 supported by the Ministry of Culture of the Czech Republic.

References

[1] J. Rondal, K.J.R. Rasmussen, On the Strength of Cast Iron Columns. Journal of Constructional Steel Research 60 (2004) 1257–1270.

[2] S. Heyde, J. Lindner, Investigations on Historic Grey Cast-Iron Columns. Technical University Berlin, Department for Steel Structures, Berlin, Germany (2008).

Comparison of Flutter Derivatives for Kao Pin Hsi Bridge and Flat Plate

Andrija Buljac[1,a]*, Stanislav Pospíšil[2,b], Hrvoje Kozmar[1,c], Sergey Kuznetsov[2,d], Radomil Král[2,e]

[1] Faculty of Mechanical Engineering and Naval Architecture, University of Zagreb, Ivana Lučića 5, 10000 Zagreb, Croatia

[2] Institute of Theoretical and Applied Mechanics, Academy of Sciences of the Czech Republic, Prosecká 76, Prague 9, Czech Republic

[a] andrija.buljac@fsb.hr, [b] pospisil@itam.cas.cz, [c] hrvoje.kozmar@fsb.hr, [d] kuznetsov@itam.cas.cz, [e] kral@itam.cas.cz

Keywords: bridge-deck section, vibrations, aeroelasticity, flutter derivatives, wind-tunnel experiments

Abstract: Focus of this work is put on evaluation of dimensionless aeroelastic coefficients, i.e. flutter derivatives, which are considered to be indicators of the aeroelastic stability of bridges. A comprehensive experimental study on dynamic wind-induced behavior of the Kao-Pin-Hsi bridge in Taiwan is described. The results are compared to those of the thin flat plate with high width to height ratio, which previously proved to be aeroelastically stable.

Introduction

In the last few decades, significant development in building technology has been achieved, which allows for a major increase in span length of cable-stayed and suspension bridges. However, these structures characterized with low natural frequencies and mechanical damping are particularly sensitive to wind effects. It is therefore required to carefully analyze their aeroelastic behavior of during construction and exploitation. Scanlan and Tomko [1] proposed an original method for extracting the eight dimensionless flutter derivatives (FD), which can be thought as the contributions to the structural matrices and are considered to be the indicators of aeroelastic stability of bridges. Efforts are made to simplify this procedure recently, see [2]. In most cases, short bridge-deck section is suitable for the determination of aeroelastic behavior of a prototype bridge, see [3]. Even though some new methods for the determination of flutter derivatives are developed, [4], the wind-tunnel experiments and subsequent FD extraction methods are still the most utilized tools. In the present work, a comprehensive experimental study on dynamic behavior of Kao Pin Hsi bridge-deck section exposed to wind is carried out by using the multipurpose experimental setup for advanced aeroelastic tests. Obtained flutter derivatives are compared with those of the thin flat plate which is aeroelastically stable with respect to flutter phenomenon.

Description of the experiments

The wind tunnel experiments were carried out in the Climatic Wind Engineering Laboratory of the Centre of Excellence Telč, Czech Republic. The aerodynamic section of the tunnel is rectangular cross-section 1.9 m wide and 1.8 m high with an airflow velocity range from 1 m/s to 33 m/s. The flutter susceptibility is studied for the Kao-Pin-Hsi Bridge in Taiwan. This bridge has the main span length of 330 m. The wind-tunnel model of this bridge section is a 1:100 scaled-down model, with a width of 350 mm and length of 560 mm. This model is tested using an original and multipurpose experimental setup developed in the Centre of Excellence Telč, see [5]. The setup is designed and constructed for the purposes of quick measurements of both linear and nonlinear aeroelastic phenomena, as it enables quick and precise frequency tuning, where the heave motion is independent of pitch. Wind velocity is measured using the Pitot tube located upstream from the model and inside the plexiglass casing covering the frame of the stand and providing the 2D flow around the model. Flutter derivatives are obtained by using the free vibration method for the

double-degree-of-freedom (DDOF) system, therefore initial excitation in both the heave and torsional motion is made and free decay oscillations are recorded. The bridge-deck section and flat plate dynamic response for a given velocity is obtained and analyzed by using the Unified Least-Square (ULS) method in order to derive effective damping and frequency, [6].

Results and discussion

Eight flutter derivatives, four generalized stiffness and four generalized damping coefficients, are obtained by the means of the DDOF coupled dynamic response of the bridge-deck section. Flutter derivatives obtained for the bridge-deck section are compared with the experiments on the flat plate, which represents an aerodynamically stable profile not susceptible to flutter, Fig. 1. Derivative H_1^* is associated with aerodynamic damping in heave motion, while A_2^* derivative is related with aerodynamic damping in torsional motion.

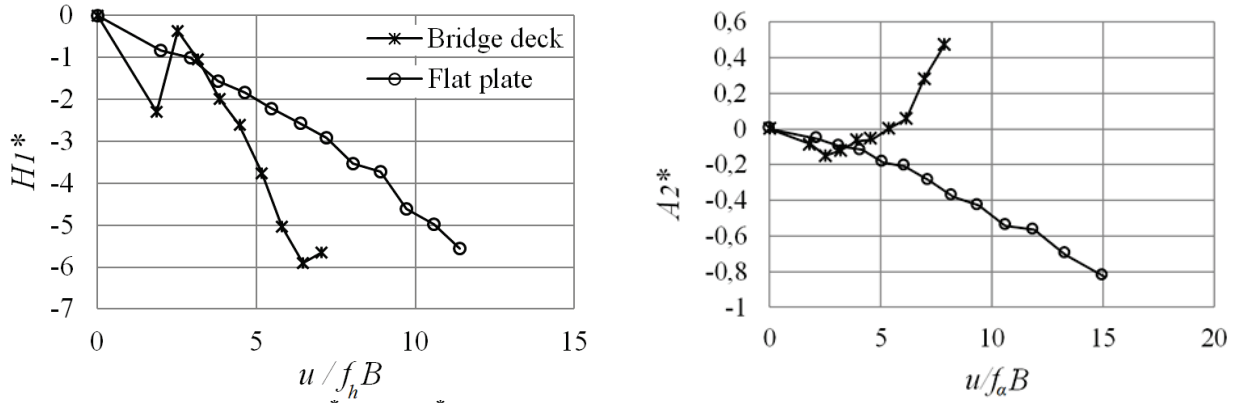

Fig. 1: Comparison of H_1^* and A_2^* derivatives for the bridge-deck section and flat plate, u is flow velocity in m/s, f_h and f_α are frequencies of oscillation for heave and pitch motion in Hz, B is the model width in m.

Even though the trends observed indicate that the investigated bridge-deck section has a stronger aerodynamic damping in the heave direction, it can be observed that the torsional instability characteristic (derivatives A_2^* crossing zero) for the bridge does not occur for the flat plate. In addition, the bridge-deck section experiences stronger shifts in the natural frequency of the pitch motion.

Acknowledgments: The authors acknowledge support of the Croatian Science Foundation, the University of Zagreb grant 05206-2, the Czech Science Foundation grant 13-34405J.

References

[1] R.H. Scanlan, J.J. Tomko, Airfoil and bridge deck flutter derivatives, J. Eng. Mech-ASCE (1971) 1717-1733.

[2] M. Shinozuka, C.B. Yun, H. Imai, Identification of linear structural dynamic system, J. Eng. Mech-ASCE 108 (1981) 1371-1390.

[3] R.H. Scanlan, et al., Comparison of the taut-strip and section-model-based approaches in long-span bridge aerodynamics, J. Wind Eng. Ind. Aerodyn. 72 (1997) 275-287.

[4] S. de Miranda, et al., On the identification of flutter derivatives of bridge decks via RANS turbulence models: Benchmarking on rectangular prisms, Eng. Struc. 76 (2014) 359-370.

[5] R. Král, S. Pospíšil, J. Náprstek, Experimental set-up for advanced aeroelastic tests on sectional models, Experimental Techniques. (2013) doi: 10.1111/ext. 12056.

[6] M. Gu, R. Zhang, H. Xiang, Identification of the flutter derivatives of bridge decks, J. Wind Eng. Ind. Aerodyn. 84 (2000) 151-162.

21st International Conference **ENGINEERING MECHANICS 2015**
Svratka, Czech Republic, May 11 –14, 2015
Paper **#087, pp. 38–39**

Influence of Vortex Excitation on the U-Tube Bundle

Jiří Buzík[a] *, Tomáš Létal[b]

Institute of Process and Environmental Engineering UPEI-VUT, Faculty of Mechanical Engineering, Brno University of Technology, Technická 2, 616 69 Brno, Czech Republic

[a]buzik@upei.fme.vutbr.cz, [b]letal@upei.fme.vutbr.cz

Keywords: fluid induced vibration, vortex excitation, vortex resonations, cyclic fatigue, cyclic stress, U-tube bundle deflection, CFD, FEA

Abstract: This contribution is devoted to causes of damaging tube bundle by fluid flow between tubes with U-bends inside a process boiler. Tube bundles are commonly used in process industry for heat transfer. Use of U-bends allows efficient space utilization and thermal dilatations of the bundle are compensated. Design of a tube bundle is strictly controlled by thermal-hydraulic design and strength design. Strength design includes flow induced vibration evaluation, which is done using simplified methods and cannot substitute fatigue assessment. This contribution studies influence of the fluid flow on the cyclic fatigue of the U-tube bundles.

Introduction

The U-tube bundles are mainly used in process heat transfer equipment such as heat exchangers, process boilers, coolers. These devices are designed by thermal-hydraulic calculations and stress calculations, however, usually only a static analysis is used for fatigue prediction. With good design and operation such devices can operate without major problems for many decades. However, there are many failures which are caused by fluid forces induced by vortex shedding.

One from many causes of cyclic fatigue of tube bundles is cross-flow of fluid around tubes. This flow distribution leads to terminal layer separation from each tube and creation of local reversed flow. A reversed flow generates vortices behind areas of terminal layer separation. As a result, there are many dynamic forces acting on tubes, which leads to fatigue. Described process is influenced mainly by following factors; U-tube bundle geometry, thermal-physics fluid parameters and fluid flow velocity. On the other side turbulent flow from the point of view of thermal-hydraulic design is considered positively, because laminar sub-layer separation intensifies heat transfer around the tubes.

Large influence on the generation of vortex has geometrical disposition of tubes in U-tube bundle. The tube arrangement according to schema 45° and 90° leads to low vortex generation in fluid flow. This disposition does not terminal layer separation on the all perimeter of tube and lead to smaller intensively heat transfer. On the other side tube arrangement according to schema 30° and 60° leads to higher vortex generation in fluid flow on the almost all perimeter. This disposition leads to terminal layer separation and consequently to intensive heat transfer. Vortices caused by intensive fluid flow lead to force responses on the tubes. These excitations lead to vibrations of tubes in the tube bundle and further to intensive stress on the tube bundle structure. In worst cases, tube excitation leads to resonation, which intensifies fatigue due to great inertia forces acting on the tube.

Flow induced vibrations of the tube bundle are also significantly influenced by the geometry of the bundle and supports. Inlets and outlets of U-tube bundle are commonly fixed to a membrane wall or a tubesheet. Usually, tube bundle is also supported in more areas, using simple supports (performed by anchoring of tube bundle) or pseudo-simply supports with clearance (performed by perforated plate, such as tubesheet or baffle). Generally, using more supports leads to more rigid state of the system, which is more convenient for reducing vibrations, but it also leads to greater thermal stresses.

Thorough evaluation of flow induced vibration fatigue is possible using coupled flow and structural transient analyses. This approach is computationally demanding, therefore it is used only

in special cases, mostly for failure assessment. For design purposes, there are simplified methods that evaluate design using allowed frequencies and amplitudes, which do not lead to significant vibrations.

Proposed evaluation procedure

Proposed evaluation procedure uses CFD and FEM analyses. In order to get adequate results, it is necessary to use relatively detailed model in the CFD analysis. On the other hand, the tubes in the tube bundle for structural analyses can be sufficiently represented by beam (pipe) elements. The main disadvantage is that these CFD and FEM meshes are incompatible and it is necessary to create a procedure for boundary condition transfer between the models. This paper deals with boundary conditions from CFD to FEM models.

In the first part it is necessary to process the results from CFD analysis. Important results describe the dynamic pressure of fluid flow acting on the U-tube bundle surface. The suitable variable describing the response of fluid flow is force in node on the surface of geometry. This variable is represented by magnitude and direction. The above procedure is recording forces from fluid flow and forces from vortices at space between tubes. Generally, this procedure is supposed to describe duration, intensity and place of vortices. These variables can specify the measurement of variables force response on the other tubes. The values from these variables can be delayed due to distance between tubes and position of vortex.

Main part of this contribution is creation of software for processing force responses on the tube surfaces caused by vortices. This program performs evaluation of force responses and from these responses define duration, intensity and position and orientation of vortices. This information is necessary for fatigue assessment using cyclic stress cumulation, respectively damaging of U-tube bundle in supported areas.

Summary

Main goal of this contribution is to find important parameters influencing cyclic stress from vortex excitations on the U-tube bundle. That is necessary for complex design and assessment of U-tube bundles. Main part is creation of software which filters responses to common forces and finds only the important vortices. These vortices lead to damage cumulation on the U-tube bundle.

Acknowledgement: The results of this project NETME CENTRE PLUS (LO1202) were co-funded by the Ministry of Education, Youth and Sports within the support programme „National Sustainability Programme I“.

References

[1] ANSYS® Academic Research, Release 14.5, Help System, Coupled Field Analysis Guide, ANSYS, Inc.

[2] Buzík, J., Nováček, F., Lošák, P., CFD and FEA Boiler Collector Analysis. In Proceedings of the 17th Conference on Process Integration, Modelling and Optimisation for Energy Saving and Pollution Reduction PRES 2014. CHEMICAL ENGINEERING TRANSACTIONS. Milan, Italy: Aidic Servizi S.r.l., 2014. pp. 847-852. ISBN: 978-88-95608-30-3. ISSN: 2283-9216.

21st International Conference **ENGINEERING MECHANICS 2015**
Svratka, Czech Republic, May 11 –14, 2015
Paper **#151, pp. 40–41**

Simulation of the Motor Power of Line-of-Sight Stabilized Devices by Passing the Test Bump

Vladimir Cech[1,a]*, Jiri Jevicky[2,b], Milan Jus[3,c]

[1]Oprox, Inc., Kulkova 8, 615 00 Brno, Czech Republic

[2]University of Defence, Kounicova 65, 662 10 Brno, Czech Republic

[3]Trencin University of A. Dubcek, Studentska 2, 911 50 Trencin, Slovak Republic

[a]cech-vladimir@volny.cz, [b]jiri.jevicky@centrum.cz, [c]milan.jus@gmail.com

Keywords: Aberdeen Proving Ground, Gun (Elevation) Stabilization Bump Course, servos of the line-of-sight (LOS) stabilized devices, vibration of vehicle suspended parts, Matlab model

Abstract: The Gun (Elevation) Stabilization Bump Course (GSBC) of the Aberdeen Proving Ground (APG) is a special road test track which is used for quality testing of the line-of-sight (LOS) stabilized devices which are mounted into military vehicles. There are optical devices, antennas and guns which are components of the fire control systems for example. The methodology for the quality testing of the LOS stabilized devices using the design of the GSBC is the basic standard for appropriate devices testing in all NATO countries. We present a simulation model of the vehicle passing the GSBC in our contribution. The Matlab model generates vibrations of suspended parts of the vehicle. These vibrations can be used as the inputs in simulators of the suspended parts movement or as the input in simulation models of the servos of the LOS stabilized devices. The spectral parameters of these vibrations are estimated, too. We present simulations of the motor power component which is required for keeping quality of LOS stabilization process.

Introduction

Authors (Cech, V., Jevicky, J.) deal in the long term with research of Intelligent Optical Tracking System (IOTS), especially of Two Survey Points Range-Finding System (TSPRFS) [2, 3].

These systems can be placed on varied ground platforms – vehicles. It is required that these mobile versions of IOTS must be able to work in motion of platforms [2]. This requirement necessitates the usage of a quality stabilization of the line-of-sight (LOS).

Ones of the most important tests of operability and measurement accuracy of IOTS are tests performed during rides on the Gun (Elevation) Stabilization Bump Course (GSBC) of the Aberdeen Proving Ground (APG), i.e. GSBC– APG [1, 2]. At the present time the GSBC as a general standard is configurable in accordance with International Test Operation Procedure (ITOP) 03-2-836 (1.3.2.2). Modified GSBC-APG according the German standard [2] was built at Military Technical and Testing Institute (MTTI) in Zahorie, the Slovak Republic (www.vtsu.sk) – Fig. 1a. Its length is only c. 100 m. This implementation was used for our model of the GSBC – APG [2].

To save money and time, it is necessary to replace experiments using the real GSBC by simulations of the vehicle traverseing the GSBC. We can build special simulators or use the computer simulations only. In both cases we need the computational model of the vehicle traverse of the GSBC – APG. Therefore, we decided to create appropriate simulation models. Their basis is the model of a vehicle motion on GBSC–APG. We presented its essential characteristics and some results of performed simulations in our paper [2].

Without this model it is impossible to properly project the control loops of the servos and the other subsystems of the LOS-stabilized devices.

Summary

One of very hard problems is a proper choice of servomotors. Especially, a motor with the sufficient power needs to be chosen. It is valid for the motor power

$$P(t) = M \cdot p_{s1}(t) + \Delta P_{los}(t) \ , \tag{1}$$

where

M [kg resp. kg/m2] – the reduced mass of the rotor resp. the moment of inertia of the motor load,
$\Delta P_{los}(t)$ [W] – the instantaneous power dissipation,
$p_{s1}(t)$ [W/(kg resp. kg/m2)] – effective specific power consumed for the acceleration or deceleration of movement of the controlled object together with next bound matters.

The specific power $p_{s1}(t)$ comprises two main components. The first component ensures the target tracking [3]. The second component allows the elimination of impacts of frame motions of the vehicle – the LOS stabilization. Our model allows to compute its course [2]. The example of computed courses is in the Fig. 1b.

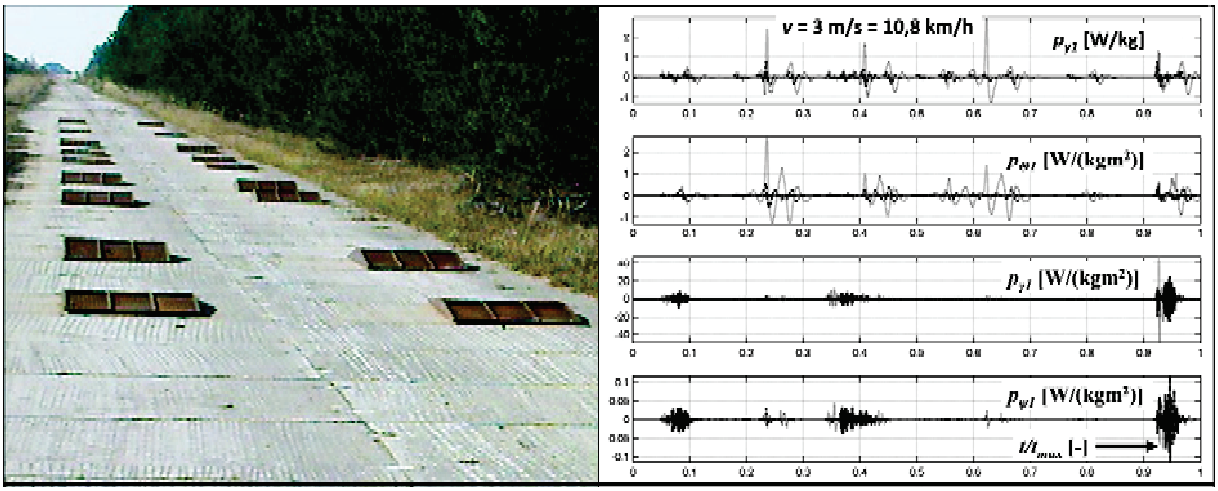

Fig. 1: a) Photo – general view on GSBC – APG built-up at MTTI in Zahorie, b) The motor power component p_{s1}, $s = y, \Theta, \gamma, \psi$ – deviations of the center of mass of vehicle suspended parts from position static equilibrium – tramp, pitch, roll and yaw. The vehicle speed is 10.8 km/h.

Acknowledgment: This work originated under the support of financial means from the industrial research project of the Ministry of the Interior of the Czech Republic - project code G20122015076: "Two survey points range-finding system utilization for perimeter security (screen)".

References

[1] Test Operations Procedure (TOP) 01-1-011A, Vehicle Test Facilities at Aberdeen Test Center and Yuma Test Center. Automotive Directorate (TEDT-AT-AD), US Army Aberdeen Test Center, 27 February 2012, p. 147.

[2] V. Cech, J. Jevicky, J. Jus, Simulation of the Vehicle Passing the Gun Stabilization Bump Course of the Aberdeen Proving Ground, in: Proceedings of the 16th International Conference on Mechatronics - Mechatronika 2014, Brno, December 3 – 5, 2014, p. 331–337.

[3] V. Cech, J. Jevicky, Generator of Command Signals for Testing Servomechanisms of Pan and Tilt Devices. In Engineering Mechanics – International Journal for Theoretical and Applied Mechanics, 18 (2011) 331–340.

Simulation of Nonlinear Characteristic of Aileron Attachment on Aeroelastic Demonstrator Using Active Electromagnetic Spring Concept

Jiří Čečrdle[a]*, Jaromír Maleček[b], Václav Hlavatý[c], Petr Malínek[d]

Aeronautical Research and Test Institute, Beranových 130, 199 05 Prague, Czech Republic

[a]cecrdle@vzlu.cz, [b]malecek@vzlu.cz, [c]hlavaty@vzlu.cz, [d]malinek@vzlu.cz

Keywords: aeroelastic experiment, active control, active electromagnetic spring

Abstract: The paper is focused on the design and development of the system simulating nonlinear attachment of the aileron actuation on the aeroelastic demonstrator. The system is based on the concept of the digitally controlled additional stiffness, activated by the real time control law system controlling the required ratio of the force and deformation. The solution is based on the electromagnetic exciter. The nonlinear force is simulated by means of the system of an exciter and the deformation sensor. The active control system is independent of the excitation system. It adds the force ensuring the required characteristics and it allows to simulate the additional stiffness, damping or mass. Doing this, it is possible to adjust the selected vibration mode by controlling the force and obtain the required nonlinear characteristics. In the second order, there is also a constant influence of the exciter mass, stiffness and damping. The simulation of the linear, quadratic and cubic additional stiffness were verified.

Introduction

The intention for the nonlinear aeroelastic demonstrator development arose in connection with the research of methods for ground vibration testing including nonlinearities. Modal characteristics of aircraft structures are always more or less nonlinear. Provided the nonlinear effect is small, the structure response to the harmonic excitation is quasi-harmonic and can be expressed by the equation including amplitude dependent damping and stiffness term. Nonlinear stiffness causes the asymmetric resonance peak, whereas nonlinear damping influences amplitude-phase curve.

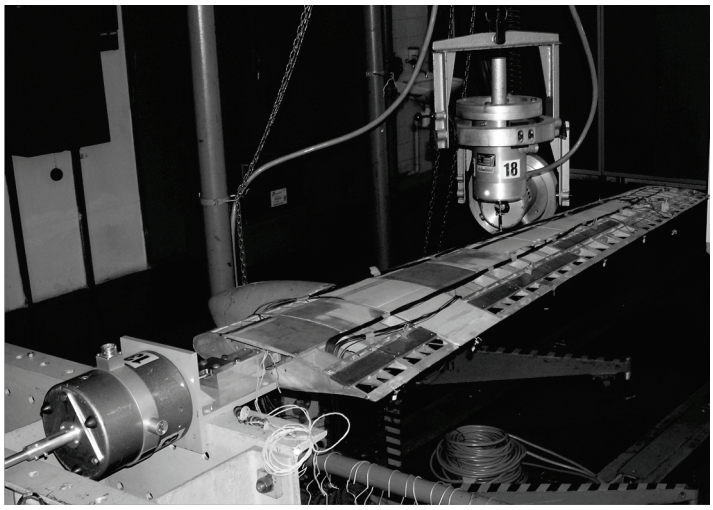

Fig. 1: NOLWING Aeroelastic Research Demonstrator

A typical nonlinear behavior of riveted aircraft structure is decreasing of a natural frequency and approaching the asymptotic value with increase of the amplitude. This is caused by the contact surfaces of rivets (or bolts) and the structure. The effect is small and the structure response can be expressed by the linear model. Much more complicated problems may be caused by the large nonlinearities caused by dry friction or backlash inside bearings or pin joints, e.g., in the control surfaces actuation systems. The natural frequency may vary significantly (by 10 - 20%) and the structure response must be described by fully nonlinear equation [1]. This is a typical behavior of the control surface flapping modes. The identification of modal parameters is complicated and the specific methods [2] for the nonlinear parameters identification must be employed. The research of such appropriate processes and methods is necessary. The aeroelastic demonstrator "NOLWING" [3], [4] was developed as a research test bed for the research of the methods for the nonlinear parameters identification.

Active electromagnetic spring concept for nonlinear aileron actuation

This concept is based on the active control of dynamic characteristics of the vibrating system by means of force generated by an electromagnetic shaker. The general control system may be capable of adding any type of force to the system, namely inertia, damping or elastic force. Our work was particularly aimed at the simulation of nonlinear stiffness of the aileron actuation system.

The regulator software is based on the LabVIEW Real-Time environment. The system also includes an independent generator of excitation signal (static force, impulse, harmonic constant frequency, harmonic frequency sweep) which was exploited for the demonstrator testing. The practical application of discrete-time regulation is based on the 3rd order (cubic) polynomial approximation of the regulation force function. It allows simulating the typical aileron stiffness, viscous damping and additional mass characteristics. Another variant facilitates the inclusion of freeplay. Fig. 2 shows the amplitude - frequency curves of the aileron flapping mode without and with active control. The former (Fig. 2a) can be considered as a symmetric behavior while the latter (Fig. 2b) shows the nonlinear effect. The parameter of active control is represented by the cubic coefficient (coefficient "a").

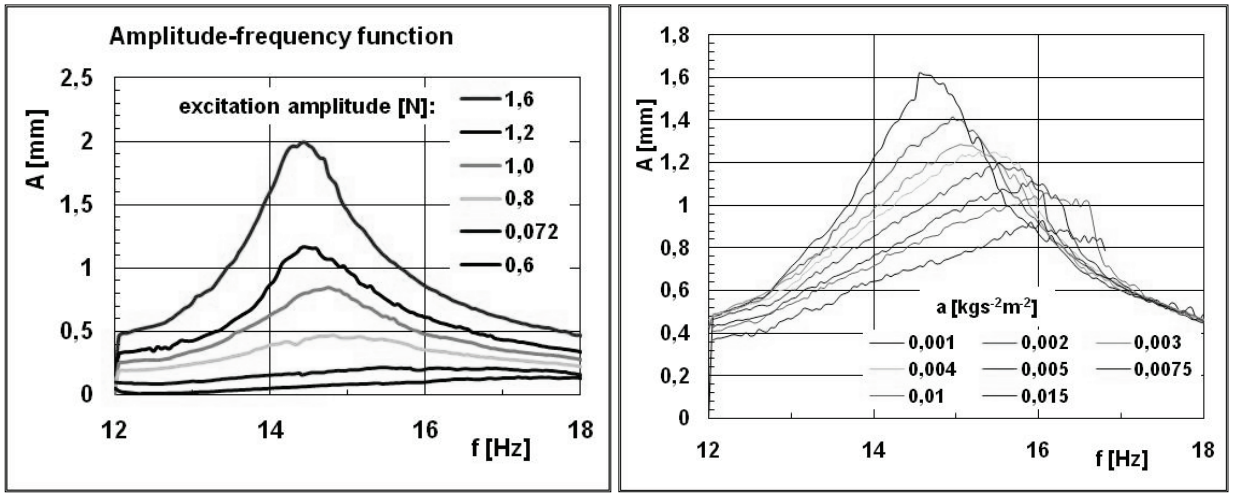

Fig. 2: Amplitude - frequency curves without (a) and with (b) active stiffness regulation

A negative linear coefficient may be used to eliminate the shaker stiffness. The additional mass equation may be used to eliminate the shaker mass effect. The system may be also stabilized by means of a damping force introduced into the additional damping equation.

References

[1] M. F. Platten, J. R. Wright, J. E. Cooper, G. Dimitriadis, Identification of a Nonlinear Wing Structure Using an Extended Modal Model, Journal of Aircraft, 46 (2009) 1614–1626.

[2] O. Černý, Experimental Analysis of Aircraft Control Surfaces Vibration Influenced by Free-plays, Czech Aerospace Proceedings, 4 (2005) 20–24.

[3] J. Maleček, V. Hlavatý, P. Malínek, J. Čečrdle, Development of Wing / Engine Component Non-linear Aeroelastic Demonstrator, International Forum on Aeroelasticity and Structural Dynamics (IFASD 2011), Paris, July 2011.

[4] J. Maleček, J. Čečrdle, V. Hlavatý, P. Malínek, Mechanical Concepts for Simulation of Nonlinearities on Aeroelastic Demonstrator, Journal of Aircraft, 50 (2013) 651–658. DOI: 10.2514/1.C031760

21st International Conference **ENGINEERING MECHANICS 2015**
Svratka, Czech Republic, May 11 –14, 2015
Paper **#057, pp. 44–45**

Experimental Studies of Heat Flow Through the Radiator of Electric Motor in a Multi-Purpose Hybrid Vehicle (WIPH)

Wojciech Danek[a]*, Rafal Lawniczek[b]

Silesian University of Technology, Faculty of Mechanical Engineering, Department of Theoretical and Applied Mechanics, 44-100 Gliwice, Konarskiego 18A, Poland

[a]Wojciech.Danek@polsl.pl, [b]Rafal.Lawniczek@polsl.pl

Keywords: cooling system, fluid mechanics, hybrid vehicle, WIPH

Abstract: This article presents research process of the heat flow through the radiator of an electric motor in cooling system, which is used in the newly designed multi-purpose hybrid vehicle. Motivation of the research is to verify that the selected components included in the cooling system provide optimum working condition for the engine. For this purpose, a specialized test stand was designed for simulation of the actual conditions of the running.

In order to ensure the most accurate determination of temperatures occurring in each section of the cooling system the temperature was read both via contact sensors (RTD) and contactless (infrared camera).

Introduction

The proper temperature of the coolant circulating in the cooling system has a high importance for smooth operation of the engine. The hybrid vehicle WIPH is driven by two electric motors with a capacity of125kW each with efficiency at approx.90%. Maximum operating temperature specified by the manufacturer is 55 °C. The both engines emit a large amount of heat which has to be discharged from the system in order to allow work with the parameters recommended by the manufacturer.

Experimental studies

The study was conducted in the OBRUM Research Department in Gliwice. The study aimed to verify that the selected components of the cooling system will allow to provide optimum working condition for the engines. The test bench consisted of the following elements:

- UQM 125 motor,
- UQM 125 motor inverter,
- alternating current dynamometer,
- radiator of the electric motor,
- measurement systems developed for testing of the cooling system.

The complete test stand and measuring equipment is shown in Fig. 1.

Fig. 1: Test stand

The test stand was subjected to a series of tests to verify proper operation of the cooling system. During each test, the temperature in the system was measured with six sensors, whose arrangement is shown in Table1, and using an infrared camera measuring temperature at three spots.

Table1: Measured parameters in the system

No.	Sensor No.	measurement
1.	2	Coolant temperature behind the radiator [° C]
2.	3	Ambient temperature [° C]
3.	4	Coolant temperature before the radiator [° C]
4.	5	The air temperature behind the radiator [° C]
5.	6	The air temperature before the radiator [° C]
6.	7	Coolant temperature before engine UQM125 [° C]
7	HYDAC flowmeter	Coolant temperature behind the radiator [° C] Coolant temperature before the radiator [° C] Cooling fluid pressure [bar] Coolant flow [l / min]

Results

The measurement confirmed that the selected components of the cooling system ensure the uninterrupted operation of the engine. The maximal temperatures obtained in our case were 37°C where the maximum temperature at which motor can work (given by the manufacturer) is 55°C. Examples of results of the measurements using IR camera are shown in Fig. 2. Fig. 3 presents the temperature value obtained during the entire test in spots described in Table 1.

Fig. 2: Images taken by FLIR infrared camera

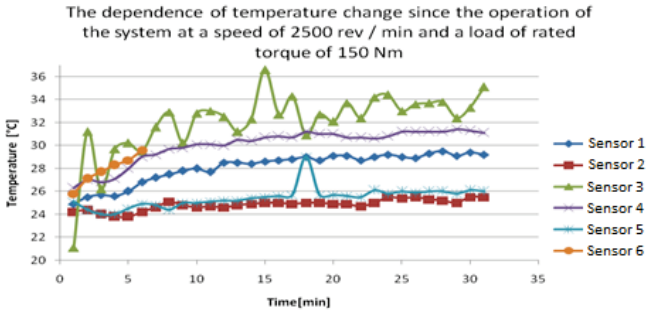

Fig. 3:Results from measurement system

Summary

On the basis of experimental studies of the cooling system of the engine UQM125 it was stated that the components of the cooling system(ie. the radiator and axial fans) were selected correctly. The selected components ensure operation of the engine with the greatest efficiency and protect UQM125 system from overheating.

Acknowledgement: The study within the project Contract No.PBS1/A6/15/2013 conducted within the 4th Applied Tests Contest

References

[1] W. Danek, R. Ławniczek, W. Klein, D. Gąsiorek, Analiza przepływu powietrza w układzie chłodzenia pojazdu gąsienicowego, Model. Inż. 50 (2014) 13-18.

[2] P. Zając, Silniki pojazdów samochodowych. Część 2. Układy zasilania, chłodzenia, smarowania, dolotowe i wylotowe, WKŁ, Warszawa 2010 (in Polish).

21st International Conference **ENGINEERING MECHANICS 2015**
Svratka, Czech Republic, May 11 –14, 2015
Paper **#058, pp. 46–47**

Experimental Study of Heat Flow through the Cooling System of the Internal Combustion Engine in a Hybrid Vehicle WIPH

Wojciech Danek[a], Rafal Lawniczek[b]

[1]Silesian University of Technology, Faculty of Mechanical Engineering, Department of Theoretical and Applied Mechanics, 44-100 Gliwice, Konarskiego 18A, Poland

[a]Wojciech.Danek@polsl.pl, [b]Rafal.Lawniczek@polsl.pl*

Keywords: cooling system, fluid mechanics, hybrid vehicle, WIPH

Abstract: In this paper authors present results of experimental studies of heat flow through the cooling system of the internal combustion VM MOTORI engine, which is used in the newly projected multi-purpose engineering hybrid vehicle (abbreviated as WIPH).

In order to determine the temperatures in each section of the cooling system, the temperature measurement was carried out in the engine control unit (ECU), via the contact sensor (RTD) and contactless (infrared FLIR camera).

Introduction

The study was conducted in the OBRUM Research Department in Gliwice. The study aimed to verify the operation of the internal combustion engine cooling system under different load on the developed test bench which included the following elements:

- VM MOTORI combustion engine with accessories,
- Cooler for an internal combustion engine VM MOTORI,
- Intercooler for an internal combustion engine VM MOTORI
- Radial fan driven by a hydraulic motor,
- The stand to testing and control of the engine,
- The measurement systems (HYDAC and FLIR infrared camera)
- Dynamometer.

Constructed stand and elements necessary for the test is shown in the picture below (Fig. 1).

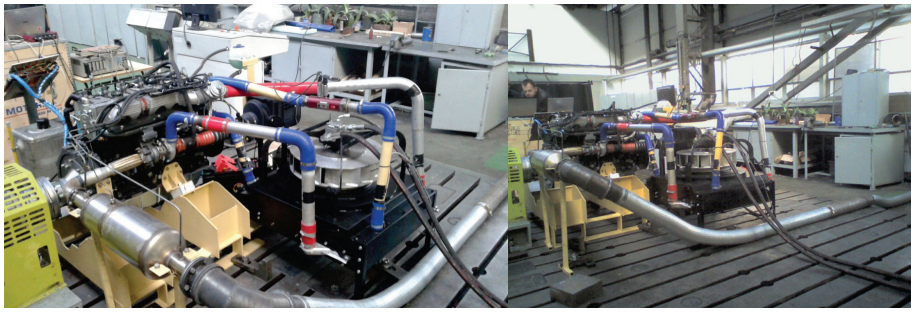

Fig. 1: Test stand

Experimental studies

The test stand described in the previous section was subjected to a series of tests to verify proper operation of the cooling system. Description of the tests and variations of engine parameters that were used is given in Table 1.

Changes of six parameters were recorded during each test, using a diagnostic interface of ECU.

The measured values were used to verify the correct operation of the cooling system and to verify the operation of the engine itself. The recorded parameters are shown in Table 2.

Tab. 1: Values of parameters during tests

No.	Engine speed [rpm]	Load of dynamometer [Nm]	Power supply of fan motor [l/min]*
1.	1500	400	16
2.	1500	400	32
3.	1500	400	48
4.	3000	330	64
5.	2300	400	70

*Fan motor was powered by hydraulic motor.

Tab. 2: Recorded parameters

No.	Parameter	Unit
1.	Engine speed	[rpm]
2.	Fuel consumption	[l/h]
3.	Engine coolant temperature	[°C]
4.	Engine load factor	[%]
5.	Torque of drive train	[Nm]
6.	Fuel rail pressure	[bar]

Results

The temperature measured during the test is shown in Fig. 3. However, to verify the changes in temperature of the cooling system authors used FLIR infrared camera. Sample images taken by the infrared camera are presented in Fig. 2.

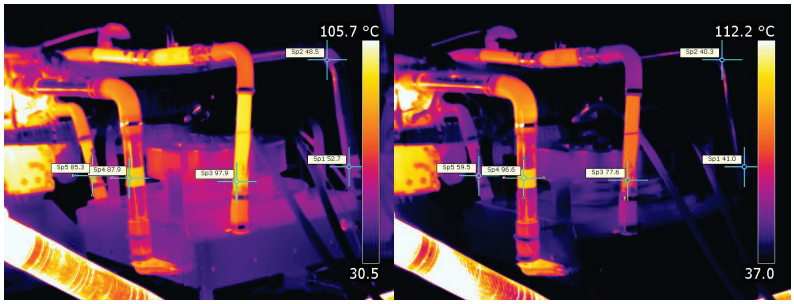

Fig. 2: Images taken by FLIR infrared camera

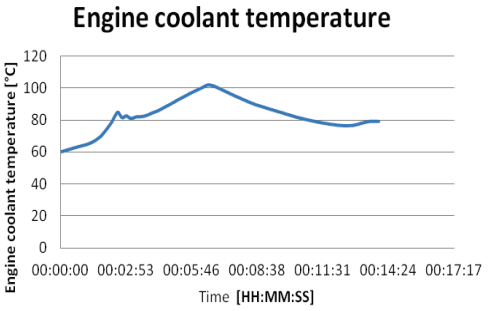

Fig. 3: Results from ECU

Summary

The effect of the variable and inflicted load on the combustion engine was studied. Results of the study were used to maximize the efficiency of the internal cooling system of the engine.

The measured data show that the necessary condition for proper operation of the system is to increase efficiency of the supply of hydraulic radial motor of the radiator fan.

When the flow rate was set at 70 l/min, the temperature ranged from 82 to 84 °C.

Acknowledgement: The study within the project Contract No.PBS1/A6/15/2013 conducted within the 4th Applied Tests Contest.

References

[1] W. Danek, R. Ławniczek, W. Klein, D. Gąsiorek, Analiza przepływu powietrza w układzie chłodzenia pojazdu gąsienicowego, Model. Inż. 50 (2014) 13-18.

[2] P. Zając, Silniki pojazdów samochodowych. Część 2. Układy zasilania, chłodzenia, smarowania, dolotowe i wylotowe, WKŁ, Warszawa 2010 (in Polish).

21st International Conference **ENGINEERING MECHANICS 2015**
Svratka, Czech Republic, May 11 –14, 2015
Paper **#100, pp. 48–49**

Advanced Computational Analysis of Connecting Rod of an Aircraft Engine

Jozef Dlugoš[a]*, Pavel Novotný[b], Peter Raffai[c]

Faculty of Mechanical Engineering, Brno University of Technology,
Technická 2896/2, 616 69 Brno, Czech Republic

[a]dlugos@iae.fme.vutbr.cz, [b]novotny.pa@fme.vutbr.cz, [c]raffai@iae.fme.vutbr.cz

Keywords: contact pressure, elastohydrodynamic lubrication, slide bearing

Abstract: Development of internal combustion engine's components is based on the use of the advanced computational models in order to compare and verify the individual design proposals. Connecting rod, which performs a general planar motion, is exposed to the gas pressure forces, inertia, contacts and hydrodynamic pressure during the engine operation cycle. To incorporate all these aspects, Finite Element Method (FEM) is extended by Finite Difference Method (FDM) simulating a slide bearing of connecting rod's eye. It includes different properties of lubricating oil (pressure and temperature dependent viscosity and density) and elastic deformations, so the pressure distribution in an oil film can be evaluated. The computational process finishes with an estimation of the endurance safety factor of the connecting rod. The four-cylinder inverted aircraft engine is used as an example.

Introduction

Countless number of structural analyses of connecting rods are available among the engineers. Widely popular commercial software usually provide the life prediction tools for mechanically loaded parts, e.g., by the force, acceleration, rotary speed, etc. But only few are able to compute pressure distribution in the lubricant oil film with or without elastic influences – elastohydrodynamic (EHD) or hydrodynamic (HD) theory.

Theoretical background and numerical methods

In many cases oil film thickness shape is determined exclusively by the rigid geometry of the running surfaces. Other situation occurs when hydrodynamic pressure is causing the active surfaces to deform, changing the oil film thickness shape and affecting the pressure distribution reversely. It happens by means of high hydrodynamic pressure (gear teeth, roller bearings, etc.) or by means of high flexibility of contact regions (connecting rod's eyes).

Oil film thickness in EHD theory is calculated as follows:

$$\boldsymbol{h}(x,z) = \boldsymbol{h}_{rigid} + \boldsymbol{K}_{eye}^{-1}\left(\boldsymbol{p}_{hydro} + \boldsymbol{p}_{rough}\right) + \boldsymbol{K}_{pin}^{-1}\left(\boldsymbol{p}_{hydro} + \boldsymbol{p}_{rough}\right) \tag{1}$$

where $\boldsymbol{h}_{rigid}$ is the external deformation e.g. due to the bolt pretension, $\boldsymbol{K}_{eye}$ and $\boldsymbol{K}_{pin}$ are the stiffness matrices of the connecting rod and the pin, respectively, $\boldsymbol{p}_{hydro}$ is the hydrodynamic pressure and $\boldsymbol{p}_{rough}$ is the pressure caused by the contact of the surface solids. The asperity contact is simulated with Greenwood and Trip [1].

Since EHD lubrication is a Fluid-Structure-Interaction (FSI) problem, Reynolds differential equation is used. It is rewritten using dimensionless variables to improve the stability properties of numerical solution. This equation is non-linear due to several phenomena like cavitation, density and viscosity dependence on the oil pressure and temperature. Viscosity-pressure relation can be expressed by Barun, or more accurate Roeland [2] as an exponential – oil viscosity η can vary very widely in the contact region (from 10 to 10^{15} times higher than the nominal viscosity η_0 [3]). This is the cause of one of the main problems in the simultaneous numerical solution of discretized

Reynolds equation and discretized oil film thickness equation. Therefore, Gauss-Seidel solver enhanced by the Successive Over Relaxation (SOR) method with underrelaxation parameter is used.

The last mandatory equation, that needs to be solved, is the force balance condition – the integral over the pressure in the oil film and the asperity pressure balance the externally applied load. In this case, Newton-Raphson Algorithm (NRA) is used:

$$\overline{\boldsymbol{X}} = \widetilde{\boldsymbol{X}} - \omega_F \boldsymbol{J}^{-1} \boldsymbol{F}(\widetilde{\boldsymbol{X}}) \tag{2}$$

where $\boldsymbol{X}$ is matrix of coordinates (overline and tilde stand for current and previous iteration, respectively), ω_F is line search parameter, $\boldsymbol{F(X)}$ is force equilibrium function and $\boldsymbol{J}$ is Jacobian.

Methods and procedures

Two computational models were used, both simulating the connecting rod quasistaticly (no damping). In first, *conventional FEA*, oil film pressure was replaced by the compression-only link elements with parabolic stiffness distribution. The crank and the piston pin were considered as rigid. Second, *FEA augmented by EHD solution*, included only a half model constrained in a cut. Fluid-structure interaction was modelled by EHD pressure applied. EHD pressure distribution was an output from algorithm described in the previous section.

Results and conclusion

Endurance safety factor serves for the results comparison, since it takes the whole time-history loading into account. The major differences are in the connecting rod's bearing as expected (Fig. 1) – the EHD oil film pressure distribution leads to the lower value of the safety factor. EHD solution is mandatory for an adequate stress distribution in the connecting rod's bearings.

Other areas show difference up to 5 % (except the regions close to the constraint boundary condition according to Saint-Venant's principle). Hence, the *conventional FEA* model can be used to accurately investigate regions different than bearings.

The *FEA augmented by EHD solution* replaces displacement constraints in the pin centers by the precomputed oil film pressure. The simulation of the whole connecting rod assembly, including EHD solution of both bearings, requires the Weak spring boundary conditions to enforce the numerical stability.

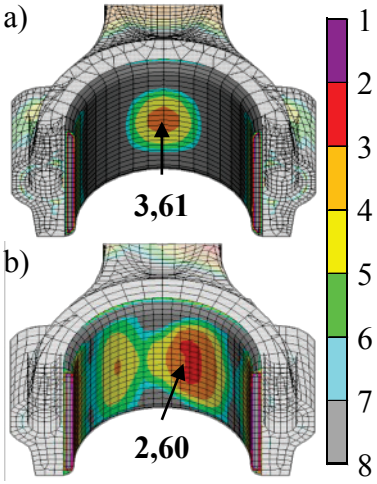

Fig. 1: Endurance safety factor: a) conventional FEA; b) FEA augmented by EHD solution.

Acknowledgement: This work is an output of NETME CENTRE PLUS research activities (project no. LO1202) and is funded by the Ministry of Education, Youth and Sports under the *National Sustainability Programme I.*

References

[1] J. A. Greenwood, J.H. Tripp, The Contact of two Nominally Flat Rough Surfaces, in: Proc. Instn. Mech. Engrs., pp. 625-633. ISSN 0954-4100. (1970)

[2] J.C.A. Roelands, Correlational Aspects of the Viscosity-Temperature-Pressure Relationship of Lubricating Oils. PhD. Thesis, Delf: Technical University Delft, The Netherlands. (1966)

[3] Venner, C. H. Multilevel Solution of the EHL Line and Point Contact Problems. PhD. Thesis, Enschede: University of Twente, The Netherlands. ISBN 90-9003974-0. (1991)

21st International Conference **ENGINEERING MECHANICS 2015**
Svratka, Czech Republic, May 11 –14, 2015
Paper **#142, pp. 50–51**

Wang Tilings in Numerical Homogenization

Martin Doškář[1,a], Jan Novák[1,2,b]

[1]Department of Mechanics, Faculty of Civil Engineering, Czech Technical University in Prague, Thákurova 7/2077, 166 29 Prague, Czech Republic

[2]Institute of Structural Mechanics, Faculty of Civil Engineering, Brno University of Technology, Veveří 331/95, 602 00 Brno, Czech Republic

[a]martin.doskar@fsv.cvut.cz, [b]novakj@cml.fsv.cvut.cz

Keywords: Wang tilings, heterogeneous materials, numerical homogenization, RVE determination

Abstract: Wang tilings have been recently shown to bring novel insights to microstructure representation efforts generalizing the conventional unit-cell approach. It allows to reconstruct stochastic realizations of the compressed medium without prior periodic assumptions on microstructural patterns. Moreover, once the microstructure is compressed, realizations of various sizes can be generated at almost negligible cost. We follow the standard numerical homogenization procedure and utilize the Wang tiles-based microstructure representation to generate computational domains. In order to alleviate computational cost, ideas of domain decomposition are adopted benefiting from the repetitive patterns in the computational domains.

Introduction

Homogenization is a standard method of incorporating knowledge of microstructure composition into macro-scale models providing that the characteristic lengths of the microstructure, l, and the macroscopic model, L, are well separated, i.e. $l/L \to 0$. For standard microstructure geometries, analytical homogenization methods provide accurate estimates of the effective properties. However, in the case of high contrast in microstructure constituents' properties, the influence of actual microstructure geometry is significantly pronounced. As a result, the general guaranteed bounds on the effective properties become unacceptably loose and a numerical homogenization technique is usually employed to determine the sought overall parameters. Besides, the latter enables to determine the size of the Representative Volume Element (RVE) and thus to validate the condition of scale-separation.

Modelling heterogeneous materials with Wang tilings

The abstract concept of Wang tilings, originally introduced in [1] in 1961 as a mean of proving certain logical statements, eventually drew attention of researchers from various branches of science, see e.g. [2] and references therein. The concept itself resembles a game of jigsaw puzzle up to some distinctions. The basic element of the concept is a square cell, a Wang tile, with codes attributed to its edges. The codes take a role of constraints during an assembly of tiles in a larger patch, a tiling, since only the tiles with the corresponding codes on the congruent edges can be placed side by side. However, unlike in jigsaw puzzles, there are infinitely many copies of each tile in the tile set allowing so generating arbitrarily large and random tilings.

First shown in Computer Graphics [3], once a visual pattern is attributed to the interior of each tile such that the pattern remains continuous across the edges sharing the same code, one can produce naturally looking patterns without visible periodicity. Benefiting from this features, Novák et al. demonstrated that the Wang tiling-based representation of material microstructure surpasses the conventional Periodic Unit Cell (PUC) approach to modelling of heterogeneous materials, namely in reducing long range order artefacts [2].They also showed that the standard procedures developed for generating PUC, e.g. optimization-based approaches, can be straightforwardly altered to account for the edge continuity requirement. As an alternative, a method making use of reference microstruc-

ture samples has been introduced in [3] and augmented with spatial statistics for purposes of material modelling in [4]. Once the tiles are designed to incorporate a part of microstructural information continuous across the corresponding edge, stochastic microstructure realizations of any size can be instantaneously generated using the stochastic tiling algorithm [3].

Numerical homogenization and RVE determination

One of the main concerns in numerical homogenization is the issue of representativeness of the computational domain. In order to render the effective properties, the domain is required to be large enough to incorporate all the microstructural features and yet remain small to be considered a material point from the perspective of the macro-scale task. Such a domain is referred to as Representative Volume Element [5]. In the standard numerical homogenization analysis, computational domains, called Statistical Volume Elements (SVE), of increasing size are generated with multiple realizations for each size. For each realisation two boundary value problems are solved rendering so the apparent properties [6]. Using the Partition theorem [7], we construct confidence intervals of the upper and lower bounds on the sought effective property for each SVE size. Taking advantage of nearly no additional cost related to generating microstructure realizations with Wang tilings, the number of realizations of each SVE size is not given a priori and adapts on-the-fly in order to accurately determine the bounds. Ideally, the SVE size is kept sequentially increasing until the bounds coincide defining so the effective property and the size of RVE. However, this holds only for an infinitely large domain. Therefore we stop the procedure when a given threshold for the bounds proximity is reached.

The above described approach leads to many calculations. Due to the tiling-based microstructure representation, computational domains are composed of non-periodic yet repeating patterns. thus, we advantageously adopt ideas of domain decomposition, the Schur complements method in particular, to mitigate the computational cost. For linear problems, each tile can be converted to a macro-element by eliminating the internal degrees of freedom (DOFs). As a result, a significantly reduced number of DOFs is necessary for each SVE's calculation.

Acknowledgements: The support by the Czech Science Foundation through project No. 1324027S is gratefully acknowledged. We would also like to thank the Grant Agency of the Czech Technical University in Prague, grant No. SGS15/030/OHK1/1T/11, and the European Social Fund endowment under Grant No. CZ.1.07/2.3.00/30.0005 of Brno University of Technology (Support for the creation of excellent interdisciplinary research teams at Brno University of Technology).

References

[1] H. Wang, Proving Theorems by Pattern Recognition — II, Bell Syst. Tech. J. 40 (1961) 1–41.

[2] J. Novák, A. Kučerová, J. Zeman, Compressing random microstructures via stochastic Wang tilings, Phys. Rev. E 84 (2012), p. 040104.

[3] M. F. Cohen, J. Shade, S. Hiller, O. Deussen, Wang Tiles for image and texture generation, ACM T. Graphic. 22 (2003) 287–294.

[4] M. Doškář, J. Novák, J. Zeman, Aperiodic compression and reconstruction of real-world material systems based on Wang tiles, Phys. Rev. E 90 (2014), p. 062118.

[5] R. Hill, Elastic properties of reinforced solids: Some theoretical principles, J. Mech. Phys. Solids 11 (1963) 357–372.

[6] T. Kanit, S. Forest, I. Galliet, V. Mounoury, D. Jeulin, Determination of the size of the representative volume element for random composites: statistical and numerical approach, Acta Mater. 58 (2010) 3647–3679.

[7] C. Huet, Application of variational concepts to size effects in elastic heterogeneous bodies, J. Mech. Phys. Solids 38 (1990) 813–841.

21st International Conference **ENGINEERING MECHANICS 2015**
Svratka, Czech Republic, May 11 –14, 2015
Paper **#146, pp. 52–53**

Validation Task for Solution of Optimal Slotted Flap Position Using FLUENT Software

Petr Doupník[a], Tomáš Koutník[b]*

Institute of Aerospace Engineering, Faculty of Mechanical Engineering,
Brno University of Technology, Technická 2, 619 69 Brno, CZ

[a]doupnik@fme.vutbr.cz, [b]koutnik@fme.vutbr.cz

Keywords: CFD validation, high-lift, slotted flap, optimization, Fluent

Abstract: CFD solvers are commonly used in optimization problems in aerodynamics. Typical task is the search for optimal position of slotted flap. It is shown on the example that the optimum predicted by CFD software can differ significantly from that found in the wind tunnel. The paper presents results of the validation task with different meshing grids and turbulent models. In conclusion, the authors suggest topics for further investigation in this field.

Recently, more complex and sophisticated optimization methods are coming into use in the field of aerodynamics. These mathematical algorithms are usually coupled with CFD solver generating the input for the optimization. Hence, the accuracy of whole process strongly depends on error of results obtained from CFD caused by low quality of computational mesh, inappropriate turbulence model, wrong settings of initial and boundary conditions, etc. Therefore only the code validated for the task should be used, otherwise the result of the optimization will not match the real optimum and traditional design methods based on engineer's experience could give better solution for much lower cost.

Detailed review of published validation cases with high-lift configuration was made by Rumsey and Ying [1]. It is summary of the data comparison of measurements and computations on 2D and 3D multielement airfoils with general recommendations on computational domain size, mesh density or compressibility corrections. Unfortunately, common practice is to examine the flow only for one geometrical configuration, which helps to increase the accuracy of the stand-alone analysis, but can be insufficient for a complex aerodynamic optimization.

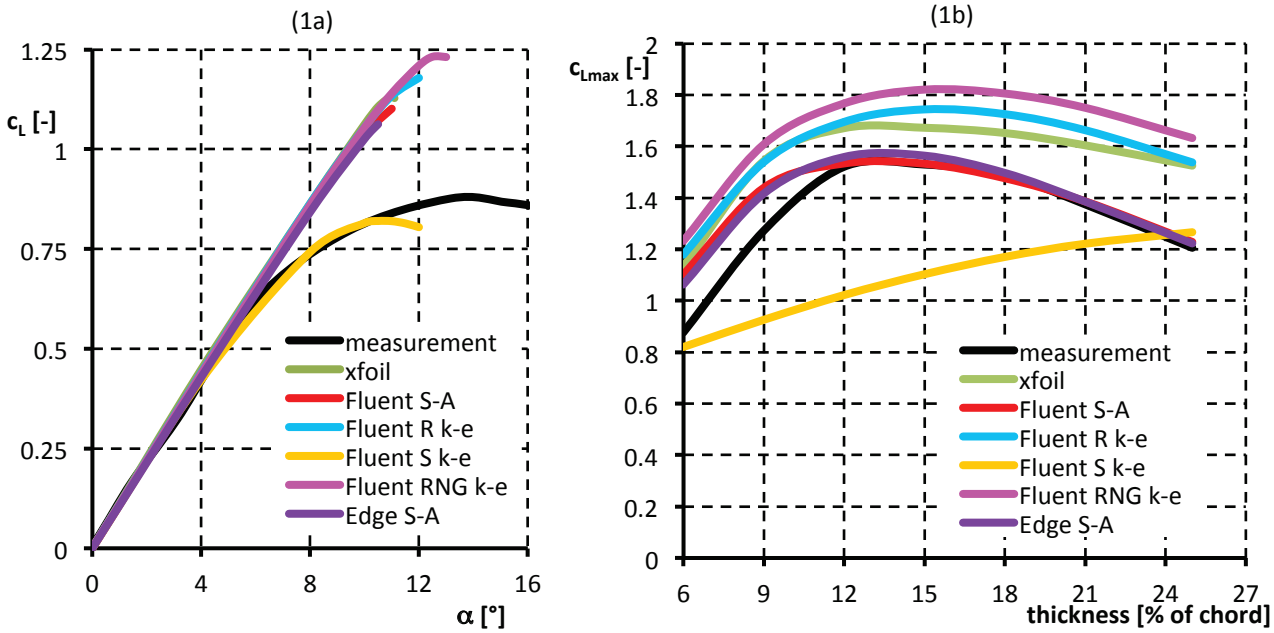

Fig. 1: Comparison of results from computations and measurement: (1a) lift curves at one design point, (1b) maximum lift coefficient through entire design space

It is shown in Fig. 1 that the best agreement with measurement at one point does not necessarily mean the best agreement in the entire design space. It is a very simple example of search for a symmetrical airfoil from NACA four-digit family with the highest lift coefficient. Aerodynamic characteristics were calculated using panel method solver Xfoil and CFD codes Fluent and Edge with different turbulence models. If the selection of the solver is based on just one of possible geometries (NACA 0006), Fluent with standard k-ε model of turbulence would be chosen, which predicts the optimum which is far from that obtained from tunnel measurements.

This is a basic validation task with only one variable changing and it is obvious that a turbulence model with results corresponding closely with measurement through the major part of the design space can be found. But further topics to be discussed arise, like whether or not it can be found also for design spaces with more variables and about applicability of such simple validation tasks to solution of more advanced problems.

Typical two-dimensional task, as a next step in validation, is positioning of slotted flap. Many engineers are satisfied with simple calibration of the most common solver they use, but they do not check its overall capability to solve the problem correctly. This was the motivation for authors to investigate and compare computed and measured data for wide range of flap settings. Airfoils were selected according to availability of measurement results needed. In this paper, current state of the work is presented and topics for further study are discussed.

References

[1] Ch.L. Rumsey, S. X. Ying, Prediction of high lift: review of present CFD capability, Progress in Aerospace Sciences 38 (2002) 145 – 180.

[2] J. Wild, Validation of Numerical Optimization of High-Lift Multi-Element Airfoils based on Navier-Stokes-Equations, in: 20th Applied Aerodynamics Conference, St. Louis (USA), 24.-26.06.2002, AIAA, 2002.

[3] R.W. Holtzclaw, Y. Weisman, Wind-tunnel investigation of the effects of slot shape and flap location on the characteristics of a low-drag airfoil equipped with a 0.25-chord slotted flap, NACA-MR-A4L28, 1944.

[4] J.N. Eastman, Tests of six symmetrical airfoils in the variable density wind tunnel, NACA-TN-385, 1931

[5] A Selection of Experimental Test Cases for the Validation of CFD Codes, AGARD AR 303, 1994

[6] ANSYS Fluent User's Guide, Release 15.0, ANSYS, Inc., 2013

21st International Conference **ENGINEERING MECHANICS 2015**
Svratka, Czech Republic, May 11 –14, 2015
Paper **#063, pp. 54–55**

Dependence of the Discrete Model on the Internal Parameters Considering Grain Crushing

Radek Dubina[a], Jan Eliáš[b]

Institute of Structural Mechanics, Faculty of Civil Engineering, Brno University of Technology, Veveří 331/95, 602 00, Brno, Czech Republic

[a]dubina.r@fce.vutbr.cz, [b]elias.j@fce.vutbr.cz

Keywords: discrete element method (DEM), grain crushing, internal control parameters, spherical elements

Abstract: For a correct representation of the ballast material behaviour in discrete element method (DEM) it is necessary to take into account crushing of grains. The representation of crushing phenomenon is based on the replacement of the original grain by a clump of 4, 6 or 14 spheres. The replacement occurs when the equivalent stress exceeds the size dependent material strength. The crushing model depends on the material parameters such as sphere radius, reference material stregth, friction angle, etc. From the simulated experiments it is clear that the behaviour of the presented approach depends also on the non-material parameters. The inluence of these parameters, namely the loading frequency and the time period of crushing condition check, is studied in the paper.

Introduction

The model under investigation is the DEM simulation of the oedometric test which was performed at Nottingham university by Lim [1]. The dimensions of the tested cylindrical specimen are 300 mm in diameter and 150 mm in height. The cylinder is fully filled with spheres which represent the ballast grains. The size of grains is 32.5 mm in diameter. The specimen is vibrated and then loaded by a compressive force in a cycle. The loading cycle proceeds according to a sine function. The loading starts at force 0.0 N and reaches in the maximal compressive force of 1.5 MN. During the loading the sphere crushing is allowed. The crushing occurs when some equivalent stress in the grain, σ_e [2] (here determined as von Mises stress computed from fabric stress tensor [3,4]) exceeds the material strength f_t. The grain is then replaced by several smaller spheres [5].

Effect of internal non-material parameters

The results of the simulated oedometric test are affected by both the speed of loading (frequency) and the time period after which the crushing condition is repetitively checked (we call this parameter *period of crushing*). Several initial configurations of spherical grains in the oedometer were prepared. Each of them was then repetitively used for simulations using all considered combinations of studied parameters. For evaluation of effect of the internal non-material parameters low value of the reference strength f_{t0} = 3000 MPa is chosen to get a large amount of crushed grains.

The first investigated parameter is the influence of the loading frequency F. The study is performed by changing of the load increment in time step. The applied loading frequencies are F = 0.25, 0.5, 1.0, 2.0, 4.0 and 8.0 Hz. Ten simulations for each frequency are calculated, but for a clarity only the results of 5 selected simulations are shown in Fig. 1a. From the graph in Fig. 1a we conclude that average behaviour of the simulation is not influenced by loading frequency. This statement is limited only to the studied range of frequencies, we expect change of the behaviour when the frequency becomes significantly larger.

The next investigated parameter is the influence of the period of crushing. This parameter should not have any effect on the results because it does not have any physical meaning. In the simulation, the

crushing condition is checked in the discrete virtual time intervals (periods). These periods range from 0.04 s to $2 \cdot 10^{-5}$ s, and also the simulation when crushing is checked every time step is considered. 60 simulations are computed for each period. The graph in Fig. 1b shows the dependence on the period of crushing. The results have a huge variability, but the mean values, represented by blue circles, are almost constant for all periods $t < 0.005$ s.

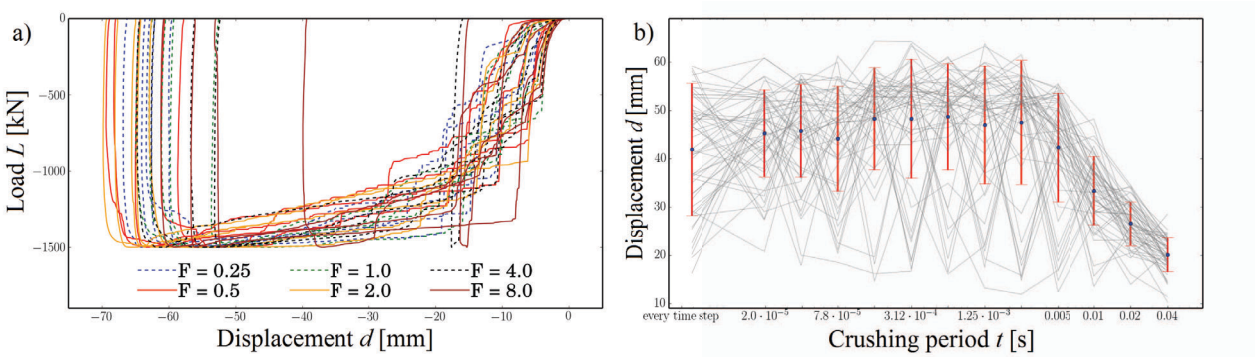

Fig. 1: Graphs of investigated non-material parameters: a) dependence of L-D diagram on the loading frequency, b) dependence of the displacement at the maximal force on the period of crushing.

Summary

Two performed studies imply that the results of a system (oedometric test) which contains large amount of crushing discrete elements are not dependent on the loading frequency. On the other hand the study of dependence on period of a crushing condition shows the undesirable dependence when the period is large. It is necessary to set the period small enough to reach such a state for which the dependence on the period is supressed.

Ackowledgement: This outcome has been achieved with the financial support under project No. FAST-J-15-2849. The support is gratefully acknowledged.

References

[1] W.L. Lim, G.R. McDowell, Discrete element modelling of railway ballast, Granular Matter. 7 (2005) 19-29.

[2] S. Lobo-Guerrero, L.E. Vallejo, Discrete element method analysis of railtrack ballast degradation during cyclic loading, Granular Matter. 8 (2006) 195-204.

[3] K. Bagi, Stress and strain in granular asseblies, Elsevier. (1996).

[4] J. Eliáš, Simulation of railway ballast using crushable polyhedral particles, Powder Technology. 264 (2014) 458-465.

[5] R. Dubina, J. Eliáš, Representation of crushing phenomenon in DEM model of railway ballast, 30th conference with international participation Computational Mechanics 2014. (2014).

21st International Conference **ENGINEERING MECHANICS 2015**
Svratka, Czech Republic, May 11 –14, 2015
Paper **#049, pp. 56–57**

Bifurcations in Mathematical Model of Nonlinear Vibration of the Nuclear Fuel Rod

Štěpán Dyk[a], Vladimír Zeman[b]

[1]Faculty of Applied Sciences, University of West Bohemia,
Univerzitní 22, 306 14, Plzeň, Czech Republic

[a]sdyk@ntis.zcu.cz, [b]zemanv@kme.zcu.cz

Keywords: bifurcation, vibration, nonlinear dynamics, nuclear fuel rods

Abstract: The paper deals with nonlinear phenomena occurring during vibration of nuclear fuel rod (FR). The FR is considered as a system consisting of two impact-interacting subsystems - FR cladding (zircalloy tube) and fuel pellets stack placed inside FR cladding. Between both subsystems, there is a small clearance. The FR is bottom-end fixed, and at eight equidistant levels, the FR cladding is supported by spacer grids (SG). Both subsystems are modelled by means of finite element method for one-dimensional Euler-Bernoulli continua. During fuel assembly (FA) motion caused by pressure pulsations of the coolant, the FR vibrates and impacts can possibly occur between FR cladding and fuel pellets stack. The paper focuses on qualitative change of vibration with change of bifurcation parameters - clearance between FR cladding and fuel pellets stack, stiffness of spacer grids cells and excitation frequency. The change of vibration quality is shown using extremes of relative radial displacements of both tubes in discretization nodes, and phase trajectories.

Introduction

Nuclear fuel rods (FR) are key part of the nuclear power plants (NPP). FRs are arranged into fuel assemblies (FA), which are submerged into coolant and fit into lower piece. Because of coolant pressure pulsations caused by main circulation pumps, vibration of the lower piece is induced and that is the cause of FA (and every FR included) kinematical excitation. Every FR consists of two parts - long thin-walled zircalloy tube (C) and UO_2 fuel pellets stack (P) fit inside (see Fig. 1). Between these two subsystems, there is a clearance which varies during reactor operational cycle. The FR cladding is supported by spacer grid cells at eight levels. The concept of FA components modelling for hexagonal type FA is borrowed from [1].

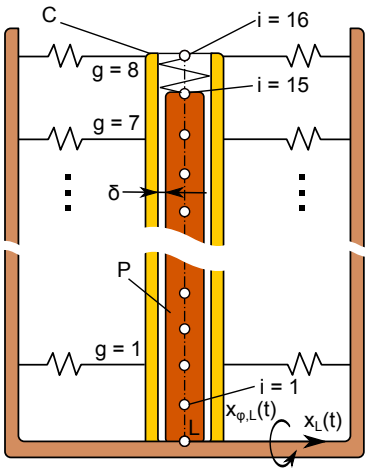

Fig. 1: Schematic diagram of the FR consisting of fuel pellets stack (P) and FR cladding (C) coupled by spacer grids cells to rigid skeleton

Mathematical model and bifurcations

Both subsystems P and C were modelled using finite element method (FEM) for Euler-Bernoulli continua [2] and only flexural vibration was considered. Lower nodes L of both subsystems are fixed into lower piece whose motion is supposed to be harmonic. FA skeleton is considered as rigid and its motion is given by L point motion. Subsystem P is divided into 15 elements and subsystem C into 16 elements. Upper nodes of both subsystems are coupled by fixation spring. Denoting vector $\boldsymbol{q}_F^{(Y)}$ of generalized coordinates of the free nodes of the subsystem $Y = P, C$, the mathematical model of the system consisting of two subsystems can be written in the

form

$$\begin{bmatrix} \boldsymbol{M}_F^{(C)} & \mathbf{0} \\ \mathbf{0} & \boldsymbol{M}_F^{(P)} \end{bmatrix} \begin{bmatrix} \ddot{\boldsymbol{q}}_F^{(C)} \\ \ddot{\boldsymbol{q}}_F^{(P)} \end{bmatrix} + \begin{bmatrix} \boldsymbol{B}_F^{(C)} & \mathbf{0} \\ \mathbf{0} & \boldsymbol{B}_F^{(P)} \end{bmatrix} \begin{bmatrix} \dot{\boldsymbol{q}}_F^{(C)} \\ \dot{\boldsymbol{q}}_F^{(P)} \end{bmatrix} + \left(\begin{bmatrix} \boldsymbol{K}_F^{(C)} & \mathbf{0} \\ \mathbf{0} & \boldsymbol{K}_F^{(P)} \end{bmatrix} + \boldsymbol{K}_{fix} \right) \begin{bmatrix} \boldsymbol{q}_F^{(C)} \\ \boldsymbol{q}_F^{(P)} \end{bmatrix} = \\ = \begin{bmatrix} \boldsymbol{f}_L^{(C)}(t) \\ \boldsymbol{f}_L^{(P)}(t) \end{bmatrix} + \begin{bmatrix} \boldsymbol{f}_{SG,C}(t) \\ \mathbf{0} \end{bmatrix} + \begin{bmatrix} \boldsymbol{f}_{P,C}(\boldsymbol{q}_F^{(C)}, \boldsymbol{q}_F^{(P)}) \\ \boldsymbol{f}_{C,P}(\boldsymbol{q}_F^{(C)}, \boldsymbol{q}_F^{(P)}) \end{bmatrix}, \quad (1)$$

where $\boldsymbol{X}_F^{(Y)}, \boldsymbol{X} = \boldsymbol{M}, \boldsymbol{B}, \boldsymbol{K}$ are mass, damping and stiffness matrices corresponding to free nodes of subsystems $Y = P, C$, matrix $\boldsymbol{K}_{fix}$ expresses coupling of fixation spring, vectors $\boldsymbol{f}_{P,C}(\boldsymbol{q}_F^{(C)}, \boldsymbol{q}_F^{(P)}), \boldsymbol{f}_{C,P}(\boldsymbol{q}_F^{(C)}, \boldsymbol{q}_F^{(P)})$ represent impact forces between P and C, vector $\boldsymbol{f}_{SG,C}(t)$ represents excitation caused by motion of the skeleton and $\boldsymbol{f}_L^{(C)}, \boldsymbol{f}_L^{(P)}$ represent kinematical excitation of lower nodes of both subsystems.

Time solution of the system described by Eq. 1 is obtained performing numerical integration in time domain using fourth order Runge-Kutta method. As bifurcation parameters, the clearance δ, spacer grid cells stiffness and excitation frequency were chosen. The qualitative change of vibration is studied using bifurcation diagrams for extremes $\hat{e}_i$ of relative radial displacements $e_i(t)$ of both subsystems in nodes $i = 1, \ldots 15$. As an example, Fig. 2 shows bifurcation diagram for clearance δ in nodes $i = 7, 11$. Equivalent diagrams were constructed for stiffnesses $k_g, g = 1, \ldots 8$ of spacer grids cells and excitation frequency ω as bifurcation parameters.

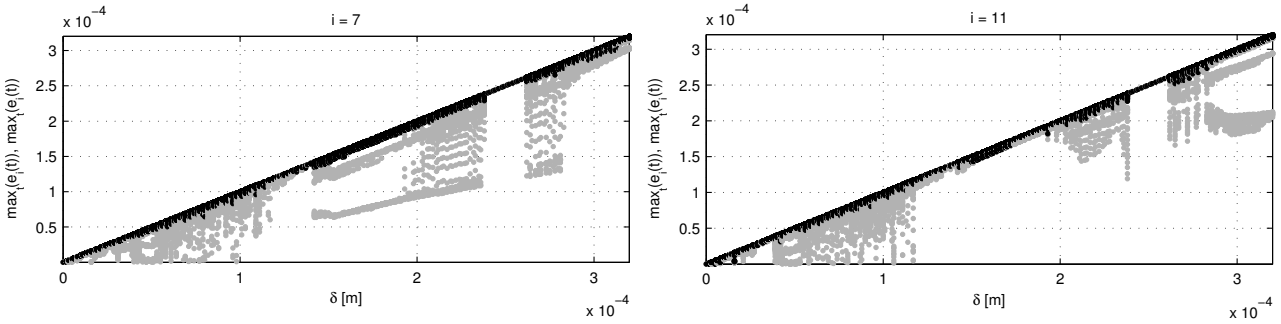

Fig. 2: Bifurcation diagram for maxima and minima of relative displacements $e_i(t)$ in node $i = 7, 11$ dependent on radial clearance between P and C

Conclusion

As described above, simplified mathematical model of a FR was formulated to describe quantitative change of FR vibration. The change is studied using bifurcation diagrams which enables to distinguish between bands with smooth operation and bands with chaotic motion which is often characterized by possible undesirable phenomena such as noise emission and wear.

Acknowledgement: This work was supported by the European Regional Development Fund (ERDF), project "NTIS" - New Technologies for the Information Society", European Centre of Excellence, CZ.1.05/1.1.00/02.0090 and the grant SGS-2013-036.

References

[1] Z. Hlaváč, V. Zeman, Vibration of Nuclear Fuel Assemblies, Lap Lambert Academic Publishing, Saarbrücken, 2013.

[2] M. Byrtus, M. Hajžman and V. Zeman, Dynamika rotujících soustav, ápadočeská univerzita v Plzni, 2010 (in Czech only).

21st International Conference **ENGINEERING MECHANICS 2015**
Svratka, Czech Republic, May 11 –14, 2015
Paper **#061, pp. 58–59**

Adaptive Remeshing Technique in Discrete Models of Random Geometry

Jan Eliáš

Institute of Structural Mechanics, Faculty of Civil Engineering
Brno University of Technology
Veveří 331/95, Brno, 602 00, Czech Republic

elias.j@fce.vutbr.cz

Keywords: discrete model, random geometry, Voronoi cell, adaptive remeshing, fracture

Abstract: The adaptive discretization technique for static discrete models of random geometry based on Voronoi cells is developed here. It is based on adding randomly located nodes into the highly stressed regions and updating the discretization based on those nodes before the crack may initiate in or propagate through the regions.

Introduction

Discrete representation of materials is a natural alternative to continuous approaches. A collection of springs and rigid cells organized into a net structure is often called a discrete or lattice model. The first attempts to model crack propagation through such discrete assemblies were made by physicists in '80s. Since that time, many types of discrete models have been developed [1, 2, 3, 4].

The extremely fine discretization of lattice models leads to extreme computational demands, however it is often necessary. Especially when the discretization is related to meso-scale structure of the simulated material. The paper introduces a technique to adaptively refine model discretization during the simulation run in the area where the crack initiates and propagates.

Without this tool, it is necessary to densely discretize the whole domain and therefore to create computationally demanding model. Some computational time can be saved by selecting a-priory areas where the crack shall not occur and use e.g. linear elastic finite elements there instead of the finely discretized discrete model [5, 3]. However even with such remedy, the area with fine discretization might be still unreasonable large because the location of crack is not known in advance.

Availability of adaptive remeshing will allow to start simulation with rough discretization and refine it adaptively as the crack initiates and propagates. Some attempts to introduce this important feature exists [6, 7]. They are based on adaptive replacement of some continuous model with the discrete one, but problematic interface between continuum and discrete model is involved and the discrete model has to have regular geometry (that produces directional bias).

Description of the algorithm

Another approach is proposed here. The adaptive remeshing is performed within the the discrete lattice model only and allows to use irregular geometry based on Voronoi tessellation. The algorithm works as follows. Initially, the whole domain is roughly discretized. Whenever any bond of the rough model exceeds some chosen limit (of equivalent strain), discretization in its vicinity is replaced by finer one and some transitional area connecting the rough and fine discretization is added as well.

The discrete model use here is a modified version of [3] from which the constitutive relations were adopted. Model geometry and connectivity is generated by Voronoi tessellation on randomly located nuclei with restricted minimal mutual distance, $l_{\min}$. The value of $l_{\min}$ may vary, whenever the discretization needs to be refined, the $l_{\min}$ is decreased over the region of interest.

The tricky part of replacing the discretization can be simply solved by adding new nuclei into region and updating the Voronoi tessellation. The rest of the domain tessellation will remain the same. 2D sketch of the proposed technique is shown in Fig. 1.

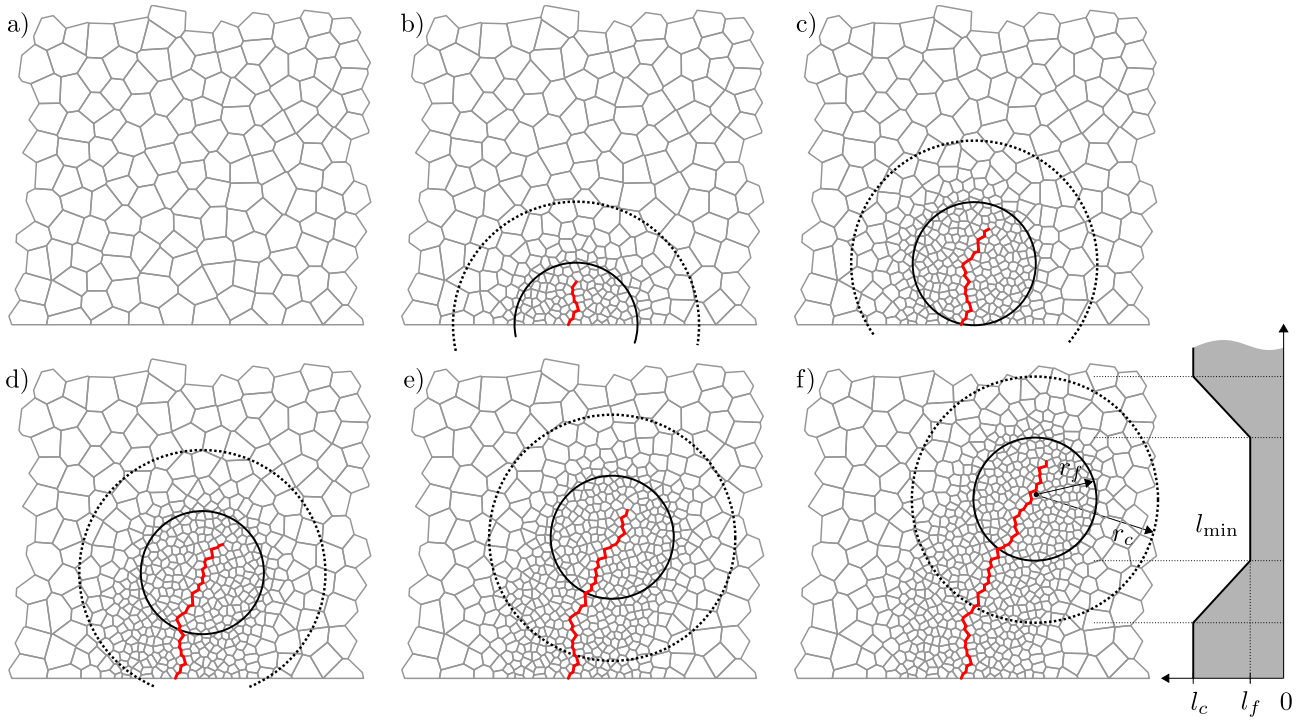

Fig. 1: Adaptive discretization refinement

Summary

Simple algorithm that allows for refinement of discretization of static discrete models of fracture adaptively during the simulation is presented. The refinement technique is tested on initiation and propagation of a crack during simulation of three-point-bending test. Results from densely discretized models are compared to results obtained from models with adaptively updated discretization.

Acknowledgement The financial support provided by the Czech Science Foundation under project No. 15-19865Y and BUT under project No. FAST-S-14-2343 is gratefully acknowledged.

References

[1] H.-K. Man, J.G.M. van Mier, Damage distribution and size effect in numerical concrete from lattice analyses, Cement Concrete Comp. 33 (2011) 867–880.

[2] J. Eliáš, H. Stang, Lattice modeling of aggregate interlocking in concrete, Int. J. Fracture 175 (2012) 1–11.

[3] G. Cusatis, L. Cedolin, Two-scale study of concrete fracturing behavior, Eng. Fract. Mech. 74 (2007) 3–17.

[4] J. Eliáš, M. Vořechovský, J. Skoček, Z. P. Bažant, Stochastic discrete meso-scale simulations of concrete fracture: comparison to experimental data, Eng. Fract. Mech. 135 (2015) 1–16.

[5] J. Eliáš, Z. P. Bažant, Fracturing in concrete via lattice-particle model, in E. Oñate, D.R.J. Owen, Particle-based methods II, Fundamentals and Applications, CIMNE, Barcelona, Spain, 2011.

[6] J.E. Bolander, T. Shiraishi, Y. Isogawa, An adaptive procedure for fracture simulation in extensive lattice networks, Eng. Fract. Mech. 54 (1996) 325–334.

[7] A. Sorg and M. Bishoff, Adaptive Modelling of Evolving Discontinuities With Smooth Transition Between Discrete and Continuous Methods., in: M. Bischoff, et al. (Eds), Particle-based methods III, Fundamentals and Applications, CIMNE, Stuttgart, Germany, 2013.

21st International Conference **ENGINEERING MECHANICS 2015**
Svratka, Czech Republic, May 11 –14, 2015
Paper **#221, pp. 60–61**

Discontinuous Galerkin Simulation of Dynamic Elasticity and Application to Fluid-Structure Interaction

Miloslav Feistauer[1,2,a], Martin Hadrava[1,b], Jaromír Horáček[2,c], Adam Kosík[1,3,d]

[1]Charles University in Prague, Faculty of Mathematics and Physics,
Sokolovská 83, 186 75 Praha 8, Czech Republic

[2]Institute of Thermomechanics, The Academy of Sciences of the Czech Republic, v. v. i.,
Dolejškova 1402/5, 182 00 Praha 8, Czech Republic

[3]University of Dortmund, Department of Mathematics, Cauerstr. 11, Dortmund, Germany

[a]feist@karlin.mff.cuni.cz, [b]martin@hadrava.eu, [c]jaromirh@it.cas.cz, [d]adam.kosik@atlas.cz

Keywords: dynamic linear and nonlinear elasticity, St. Venant-Kirchhoff model, compressible flow, ALE method, discontinuous Galerkin method

Abstract: This paper is concerned with the numerical simulation of the interaction of compressible viscous flow with a nonlinear elastic structure. The flow is described by the compressible Navier-Stokes equations written in the arbitrary Lagrangian-Eulerian (ALE) form. For the elastic deformation linear model or nonlinear St. Venant-Kirchhoff model is used. In the discretization the discontinuous Galerkin (DG) finite element method is applied both for the flow problem in a time-dependent domain and for the dynamic elasticity system. We show that the DG method is applicable to the discretization of both problems.

Introduction

Fluid-structure interaction (FSI) problems are solved in various aerospace, civil and mechanical engineering applications. Recently the methods for solution of such problems have also been quickly developed in the field of biomechanics. We are particularly interested in biomechanics of voice, where the methods of numerical simulation of human vocal folds self-oscillation are currently in an intensive development. These self-oscillations, which originate in the interaction of airflow coming from the human lungs with the compliant biological tissue of the vocal folds, produce primary sound enabling voicing (phonation, speech, singing). The numerical simulation of this problem requires the solution of dynamic elasticity equations coupled with the solution of the compressible Navier-Stokes equations in a time-dependent domain. Here we apply the DG method to the solution of both problems.

DG discretization of dynamic elasticity problem and the compressible Navier-Stokes equations

The numerical simulation of fluid-structure interaction requires the solution of dynamic elasticity equations coupled with the solution of the compressible Navier-Stokes equations in a time-dependent domain. It appears that a sufficiently robust and accurate method for the solution of both elasticity and flow problems is the discontinuous Galerkin method using piecewise polynomial approximations over a finite element mesh without any requirement on the continuity of approximate solutions.

In [3] and [4], the dynamic linear elasticity initial-boundary value problem is discretized by the conforming finite element method in space and by the Newmark method in time. In these papers this method was coupled with the DG technique for the simulation of compressible flow. It is logical to ask, if it would be suitable to use DG techniques for the solution of flow as well as elasticity problems. Here we shall pay attention to the solution of the dynamic elasticity problem by the DG method applied to the space discretization. The discretization in time is carried out by the backward Euler (BE) difference or general backward difference formula (BDF) or the DG method in time. We are concerned with linear elasticity model as well as nonlinear St. Venant-Kirchhoff model. In this case the nonlinear

discrete problem is solved by the Nawton-Raphson method. Numerical experiments show that as a most accurate technique the space-time DG method appears and gives equally accurate results in the case of the benchmark as in [6]. For details we can refer to works [2] (linear dynamic elasticity) and [5] (nonlinear dynamic elasticity).

The compressible Navier-Stokes system in a time-dependent domain is written in the ALE form and discretized by semi-implicit space-time DG method. This method is very efficient, because on each time level it is necessary to solve only one linear algebraic system. For details see [1].

The coupled FSI problem is solved by the so-called staggered approach, which means that both problems are solved at a given time instant separately. The approximate solutions are required to fulfill certain transient conditions, which are met through several inner iterations. The DG method can also be used for the construction of the ALE mapping.

Summary

In this paper the DG discretization of a linear elasticity and nonlinear elasticity problem with St. Venant-Kirchhoff material was presented. We paid a special attention to the comparison of several different techniques for the time discretization. The space-time discontinuous Galerkin method showed promising results, in particular the ability to use a larger time step without suffering from the numerical dissipation. The results of numerical experiments demonstrate that the DG method can successfully be applied to all problems involved in FSI: fluid flow, large elastic material deformation and the construction of ALE mapping.

Acknowledgments: This research was financially supported by the projects 13-00522S (M. Feistauer) and P101/11/0207 (J. Horáček) of the Czech Science Foundation and by the grant SVV-2015-260226 of the Charles University in Prague (M. Hadrava and A. Kosík).

References

[1] J. Česenek, M. Feistauer, A. Kosík, DGFEM for the analysis of airfoil vibrations induced by compressible flow, Z. Angew. Math. Mech. 93 (2013) 387–402.

[2] M. Feistauer, M. Hadrava, J. Horáček, A. Kosík, Numerical solution of fluid-structure interaction by the space-time discontinuous Galerkin method, in: Finite Volumes for Complex Applications VII - Elliptic, Parabolic and Hyperbolic Problems,FVCA 7, Berlin, June 2014, edited by J. Fuhrmann, M. Ohlberger and C. Rohde, Springer, Cham, 2014, pp. 567–575.

[3] M. Feistauer, J. Hasnedlová-Prokopová, J. Horáček, A. Kosík, V. Kučera, DGFEM for dynamical systems describing interaction of compressible fluid and structures, J. Comput. Appl. Math. 254 (2013) 17–30.

[4] J. Hasnedlová, M. Feistauer, J. Horáček, A. Kosík, V. Kučera, Numerical simulation of fluid-structure interaction of compressible flow and elastic structure, Computing 95 (2013) 343–361.

[5] A. Kosík, M. Feistauer, M. Hadrava, J. Horáček, Numerical simulation of the interaction between a nonlinear elastic structure and compressible flow by the discontinuous Galerkin method, Applied Mathematics and Computation (to appear).

[6] S. Turek, J. Hron, Proposal for numerical benchmarking of fluid-structure interaction between an elastic object and laminar incompressible flow, in: Fluid-Structure Interaction: Modelling, Simulation, Optimization, edited by H.J. Bungartz and M. Schäfer, Springer, Berlin, 2006, pp. 371-385.

21st International Conference **ENGINEERING MECHANICS 2015**
Svratka, Czech Republic, May 11 –14, 2015
Paper **#008, pp. 62–63**

Nonlinear Behaviour of Concrete Foundation Slab

Josef Fiedler[a]*, Tomáš Koudelka[b]

Czech Technical University in Prague, Faculty of Civil Engineering, Thákurova 7, Praha 6

[a]josef.fiedler@fsv.cvut.cz, [b]koudelka@cml.fsv.cvut.cz

Keywords: foundation slab, layered model, double Drucker-Prager, concrete plasticity model, finite element method

Abstract: A layered model is used for nonlinear analysis of a foundation concrete slab. Calculation is performed using interaction with elastic Winkler-Pasternak subsoil model and considering plastic yielding of slab layers. Two Drucker-Prager yield criterions define a nonlinear material model for concrete. Computation is done by SIFEL solver using the Finite Element Method.

Introduction

The contribution is dedicated to nonlinear analysis of concrete foundation slab. Computation is performed by SIFEL [1], a specialized software package used for solving mechanical and transport problems and being developed at Faculty of Civil Engineering, Czech Technical University in Prague. SIFEL has been already used for the solution of foundation slab problem [2] but it has been extended by two new material models, a concrete plasticity model using two Drucker-Prager (DP) yield conditions and a layered model for plate/shell structures. These two material models are briefly described in this paper.

Double Drucker-Prager concrete plasticity model

By the joining of two DP yield conditions [3], a plasticity material model that solves space stress states can be obtained. Using proper parameters one of the conditions is set to describe tensile behaviour of concrete and the other condition is intended to approximate concrete in compression.

General DP yield function is defined as follows

$$f(\boldsymbol{\sigma}) = \alpha_\phi I_1(\boldsymbol{\sigma}) + \sqrt{J_2(\boldsymbol{\sigma})} - \tau_0 \tag{1}$$

where α_ϕ and τ_0 are the parameters of the model. τ_0 represents the shear strength and α_ϕ is connected with friction angle**.** I_1 is the first invariant of stress tensor and J_2 is the second invariant of deviatoric stress tensor. This yield condition creates a cone if it is displayed in the principle stress space.

Each yield condition is set by using parameters α_ϕ and τ_0 according to which stress area it is supposed to describe [4]. These parameters are related to strength in tension and compression of concrete. The problem of stress return areas and first derivative singularities, which are located in the intersection of DP conditions and at the top of the cone, is solved on the level of the stress invariants. Softening procedure is added to the model for the tensile stress area and, in the case of plane stress problem, a special treatment for the transverse stress component is applied.

Layered model for plate/shell structures

To simplify calculation, a general plate/shell structure may be represented by its middle plane. By usage of a layered model [5], material properties across the thickness of a structure are took into account without making of full 3D topology. The layered model divides structures into small layers where each layer is considered to be in the plane stress state and is given its own values of

deformation ($\varepsilon_x, \varepsilon_y, \gamma_{xy}$) and stress ($\sigma_x, \sigma_y, \tau_{xy},$). Deformation and stress components of the j-th layer are driven by the following equations

$$\boldsymbol{\varepsilon}_j = \boldsymbol{\varepsilon}_0 + z_j \boldsymbol{\kappa}, \qquad \boldsymbol{\sigma}_j = \boldsymbol{D}_j \boldsymbol{\varepsilon}_j, \tag{2}$$

where $\boldsymbol{\varepsilon}_0$ represents the deformation of the middle plane, $\boldsymbol{\kappa}$ stands for the bending curvatures, z_j determines the distance of the j-th layer from the middle plane and $\boldsymbol{D}_j$ is considered to be a stiffness matrix for the plane stress state. All contributions to stress resultant forces from individual layers are added and constitutive relation between stress resultant forces and deformations can be written

$$\begin{Bmatrix} \boldsymbol{n} \\ \boldsymbol{m} \end{Bmatrix} = \sum_{j=1}^{n} \begin{bmatrix} t_j \boldsymbol{D}_j & z_j t_j \boldsymbol{D}_j \\ z_j t_j \boldsymbol{D}_j & z_j^2 t_j \boldsymbol{D}_j \end{bmatrix} \begin{Bmatrix} \boldsymbol{\varepsilon}_0 \\ \boldsymbol{\kappa} \end{Bmatrix}, \tag{3}$$

where t_j denotes the thickness of the j-th layer, $\boldsymbol{n}$ and $\boldsymbol{m}$ are the stress resultant forces.

The model is implemented into SIFEL solver in such way that there is a possibility to assign different material models to each layer and to perform a nonlinear calculation with them. For instance, it is possible to compute plasticity analysis of structure considering various yield conditions for layers.

Application of the models

The above described models can be used in simulation of reinforced concrete slabs, walls or shells where concrete layers may be defined by the double DP model and reinforcement layers may be directed by J2 plasticity. The implementation of the presented material models was motivated by a real engineering problem of a foundation slab in a storage hall exposed to a concentrated load. This problem has been analysed with help of the implemented models and the results from the simulation together with all further findings will be presented at the conference contribution.

Acknowledgement: This paper was supported by project SGS15/031/OHK1/1T/11 - "Pokročilé numerické modelování v mechanice konstrukcí a materiálů"

References

[1] J. Kruis, T. Koudelka, T. Krejčí, Simple Finite Element (SIFEL), 2001-2015. Available from: http://ksm.fsv.cvut.cz/~sifel/.

[2] T. Koudelka, T. Krejčí, J. Šejnoha, Modelling of Sequential Casting Procedure of Foundation Slabs, Proc. of the Eleventh Int. Conf. on Civil, Structural and Environmental Engineering Computing, Civil-Comp Press Ltd (2007), No. 115.

[3] E.A. de Souza Neto, D. Perić, D.R.J. Owen, Computational Methods for Plasticity – Theory and Applications. 1st ed. Wiley, Chichester, 2008.

[4] M. Jirásek, Z. P. Bažant, Inelastic Analysis of Structures. 1st ed. Wiley, Chichester, 2002.

[5] H.-T. Hu, W. C. Schnobrich, Nonlinear finite element analysis of reinforced concrete plates and shells under monotonic loading. Computers & structures, 38 (1991) 637-651.

21st International Conference **ENGINEERING MECHANICS 2015**
Svratka, Czech Republic, May 11 –14, 2015
Paper **#150, pp. 64–65**

Punching Resistance of Flat Slabs

Ľudovít Fillo[a], Tomáš Augustín[b], Ján Hanzel[c], Veronika Dvoranová[d]

Faculty of Civil Engineering at SUT in Bratislava, Radlinskeho 11, 81368 Bratislava, Slovakia

[a]ludovit.fillo@stuba.sk, [b]tomas.augustin@stuba.sk,
[c]jan.hanzel@stuba.sk, [d]veronika.dvoranová@stuba.sk

Keywords: flat slab, punching, shear resistance

Abstract: Results of latest experiments have revealed that the maximum punching resistance defined from crushing of concrete struts at the perimeter of a column is an insufficient criterion for limitation of maximum shear forces at the vicinity of the columns. Therefore further limitation has been accepted.

Limits of punching resistance

There are two possible ways of structural failure due to the punching. The first one is strut diagonal failure (crushing of concrete) at control perimeter u_0 of the column. The second one is the shear-tension failure of concrete or transverse reinforcement in area surrounded by the basic control perimeter u_1.

The maximum shear force was limited by compressive capacity of the struts at the column perimeter. The new limit is based on the punching resistance of a member without shear reinforcement $v_{Rd,c}$, Eq. 1.

$$v_{Rd,cs} = 0.75 v_{Rd,c} + \left(\frac{1.5.d}{s_r}\right)\frac{A_{sw}.f_{ywd,ef}}{u_1.d} \le k_{max}.v_{Rd,c}. \quad (1)$$

Punching failure depends also on a position of column in plan of a building [4]. There are several types of column - slab contacts illustrated on typical flat slab plan - Fig. 1. By taking into account the loading area of the column, there is a possibility to substitute the influence of imbalanced bending moments and taking the coefficient β=1. For this decisive loading area, column C, graphs of relation between the design uniform distributed load and the heights of flat slab were created.

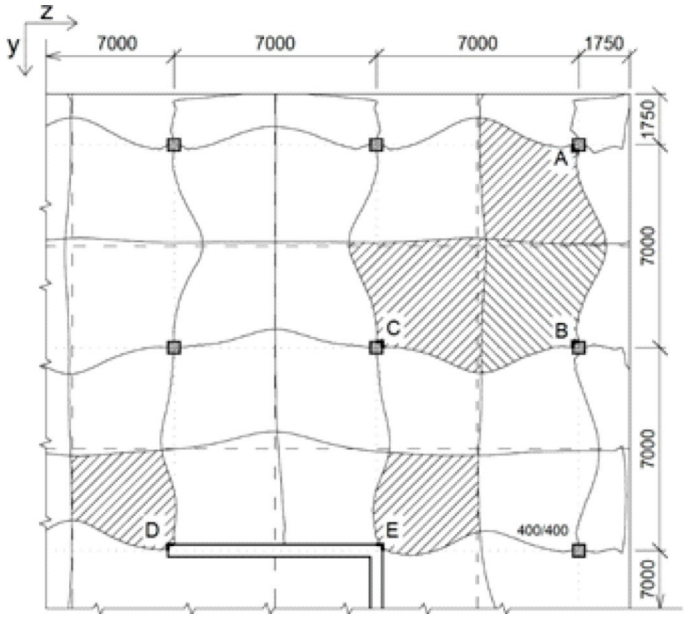

Fig. 1: Analyzed plan of flat slabs

Analysis of minimum flat slab height

The graph in Fig. 2 was created for typical floor of the building (Fig. 1) with flat slabs and column distance of 7 m. By design of flat slab height 175 mm the shear-tension failure arises by load 11.5 kN/m^2 - ρ = 0.005 and 14.5 kN/m^2 - ρ = 0.01. The shear-tension failure precedes the failure of diagonal struts, which should arise by 22.9 kN/m^2. Diameter of main slab bars was ϕ18 and concrete cover 28 mm. The maximum allowable deflection (l_y/250), was reached also by this thickness of slab 175 mm. The nonlinear deflection with cracks and creep of concrete was simulated according to the scheme of Fig. 1 using program Scia Engineer.

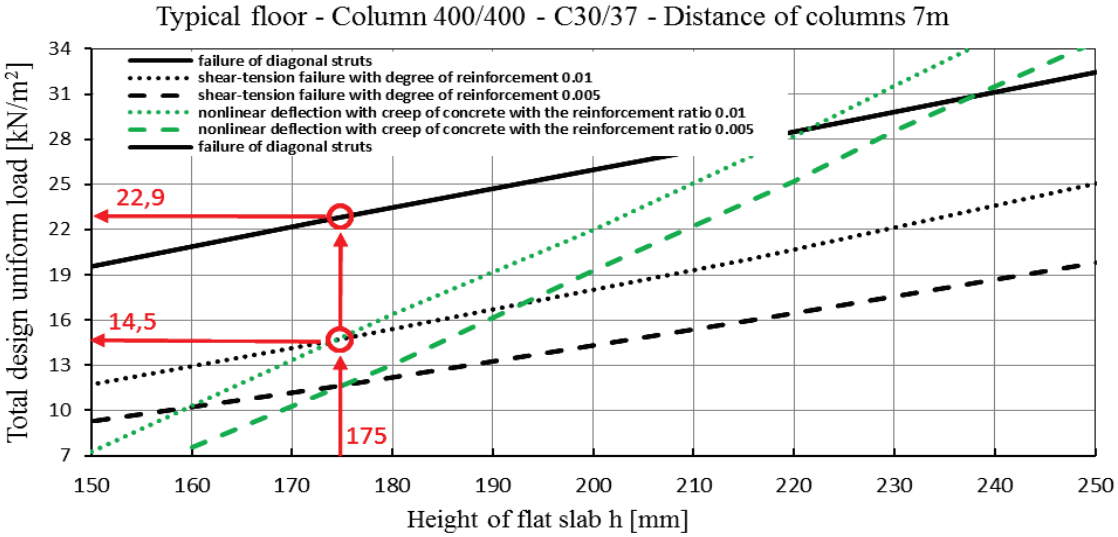

Fig. 2: Minimal flat slab heights for distance of columns 7 m, typical floor (column C-Fig. 1), C30/37, main horizontal reinforcement ϕ18, ρ = 0.01 a 0.005; k_{max} = 1.9.

Conclusions

The problem of flat slab punching was presented in the paper. Coming from limits of shear resistance by CEN TC250 SC2 there was an option to create graphs for control of minimal necessary height of flat slabs. The surrounding of central column C (Fig.1) was analysed for two grades of slab reinforcement ratio 0.01 and 0.005. The presented analyses were carried out with k_{max}=1.9 where shear reinforcement consists of double headed studs. By all analysed cases the shear-tension failure precedes the failure of diagonal struts and so decides about the height of flat slabs.

Acknowledgement: Authors gratefully acknowledge Scientific Grant Agency of the Ministry of Education of Slovak Republic, the Slovak Academy of Sciences VEGA č. 1/0696/14 and the Slovak Research and Development Agency under the contract No APVV–0442-12.

References

[1] L. Fillo, J. Halvonik, The Maximum Punching Shear Resistance of Flat Slabs. In: Concrete and Concrete Structures, Conference Vrátna SK (2013) 376-381.

[2] S.L. Burtscher, G. Rinnhofer, V. Benko, J. Kollegger, Destructive large-scale tests on highly reinforced spun concrete columns (Zerstörende Großversuche an hochbewehrten Schleuderbetonstützen). Bauingenieur, Band 78 (2003) 187-193.

[3] J. Hanzel, L. Majtánová, J. Halvoník, Punching Resistance of Flat Slabs without Shear Reinforcement. In 21. Concrete Days 2014. Proceedings of Conference. Praha: ČCS, 2014. 6p.

21st International Conference **ENGINEERING MECHANICS 2015**
Svratka, Czech Republic, May 11 –14, 2015
Paper **#134, pp. 66–67**

Numerical Simulation of Flows through Labyrinth Seals

Jiří Fürst

Department of Technical Mathematics, Czech Technical University in Prague, Faculty of Mechanical Engineering, Prague, Czech Republic

Jiri.Furst@fs.cvut.cz

Keywords: labyrinth seals, rotordynamics, finite volumes

Abstract. A numerical code for calculation of leakage flow and rotordynamic coefficients of labyrinth seals has been developed. The code is based on the solution of Reynolds-averaged Navier--Stokes equations combined with a two-equation turbulence model. The numerical solution is achieved with finite volume method and the rotordynamic coefficients are evaluated from several simulations with different rotor precessions. The solution is compared to single control volume based bulk flow method [2].

Introduction

Labyrinth seals are commonly used in turbines and compressors to dissipate energy and reduce the amount of leakage flow. Unfortunately the rotor vibrations cause a non-uniformity in the circumferential pressure distribution which in turn produces forces acting on the rotor and can cause the rotor to become unstable. The prediction of rotordynamic coefficients and leakage flow for a straight-through teeth on stator labyrinth seal is the main subject of this work.

Flow field and rotordynamic coefficients calculation

The code is based on the implicit 3D finite volume scheme with AUSM type flux splitting for convective terms and central approximation for viscous terms. The system of Navier-Stokes equations is combined with standard two-equations SST $k-\omega$ model. The steady state solution is sought for precessing rotor in the rotating frame of reference whose angular speed corresponds to the precession. The forces acting on the rotor are evaluated for each precession speed and finally the rotordynamic coefficients (i.e. stiffness coefficients K, k, and damping coefficients D, d) are calculated using least-squares method from (see [1])

$$F_r/\epsilon = -(K + d\Omega), \tag{1}$$

$$F_t/\epsilon = k - D\Omega. \tag{2}$$

Here F_r and F_t are the radial and tangential components of the force, ϵ is the rotor displacement, and Ω is the precession angular speed.

Results

The simulation has been run for straight-through type of seal with parameters given in the table 1. The predicted leakage flow rate 0.222 kg/s corresponds well to the reference solution obtained with OpenFOAM package (0.223 kg/s) as well as with simple bulk-flow (0.208 kg/s) and with experimental data [1] (0.205 kg/s). The table 2 shows calculated force components for different precession speeds relative to rotor angular speed.

Table 1: Geometrical and operationg parameters of the labyrinth seal with 8 teeth on stator.

Shaft radius	75.578	mm	Tooth clearance	0.229	mm
Tooth width	0.152	mm	Tooth height	3.175	mm
Tooth pitch	3.175	mm			
Inlet total pressure	18.3	bar	Inlet temperature	300	K
Inlet swirl	12	m/s	Outlet pressure	10.248	bar

Table 2: Force components for various precession speeds

	PFR=0	PFR=1/4	PFR=1/2	PFR=3/4	PFR=1
F_{rad} [N]	-0.57	0.09	0.75	1.40	2.06
F_{tan} [N]	2.50	2.59	2.74	2.95	3.22

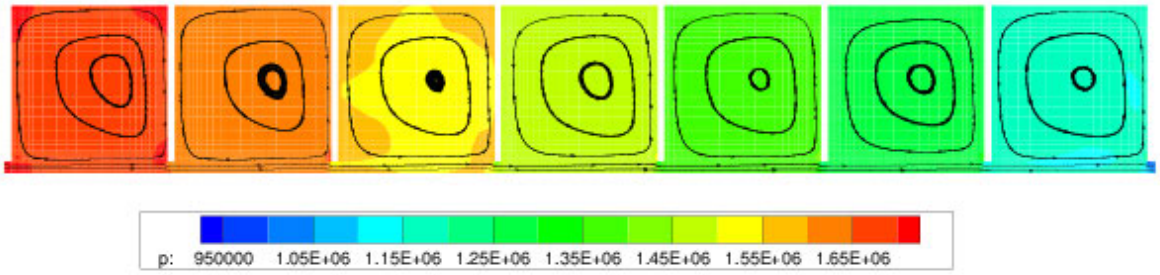

Fig. 1: Pressure distribution and streamlines in 2D cut through labyrinth seal.

Summary

The code for calculating leakage flow and rotordynamic coefficients has been developed. The predicted leakage flow rate corresponds very well experimental data as well as with correlation based bulk-flow and with fine mesh solution using OpenFOAM package. The calculated force components agree for PFR=0 with OpenFOAM solution.

Acknowledgements: The work was supported by the Grant Agency of the Czech Technical University in Prague, grant No. SGS 13/174/OHK2/3T/12.

References

[1] J. Schettel, R. Nordmann. Rotordynamics of turbine labyrinth seals: a comparison of CFD models to experiments. Eighth Internation Conference on Vibrations in Rotating Machinery, (7), 2004.

[2] B. P. Williams, R. D. Flack, Calculation of Rotor Dynamic Coefficients for Labyrinth Seals. International Journal of Rotating Machinery, 4 (1998) 257–269.

21st International Conference **ENGINEERING MECHANICS 2015**
Svratka, Czech Republic, May 11 –14, 2015
Paper **#220, pp. 68–69**

Fracture Toughness Testing for Improving the Safety of Gas Pipelines

Ľubomír Gajdoš[a]*, Martin Šperl[b]

Institute of Theoretical and Applied Mechanics of the AS CR,
Prosecká 76, 190 00 Prague, Czech Republic

[a]gajdos@itam.cas.cz, [b]sperl@itam.cas.cz

Keywords: fracture toughness, pipe bands, CT specimens

Abstract: For standard fracture mechanical tests flat specimens (principally CT or SENB) are required. This brings problems for investigating fracture mechanical properties of thin-walled pipes because it is necessary to straighten the pipe bands [1]. However, this operation causes internal stresses to be induced not only in the semi-product subjected to straightening but also in finished specimens. A question therefore arises to what extent are then the magnitudes of the fracture toughness determined representative for the actual cylindrical wall. To solve this problem fracture mechanics tests were carried out on flat (straightened) CT specimens as well as on curved CT specimens with the natural curvature. The R – curves as well as the resulting parameters of the fracture toughness, obtained for both types of CT specimens, were compared and it was concluded that the fracture toughness of the pipe material determined on straightened CT specimens was practically the same as that obtained on curved CT specimens.

Experimental

Curved CT specimens simulate, to some extent, stress conditions in the pipeline wall loaded by internal pressure. In order to ensure the application of the load in the hoop direction, it was necessary to design and manufacture a fixture that would enable to convert the straight force, generated by the loading machine, to the tangential one, i.e. a force which would act along a circle of the identical diameter to that of the pipe. Such a fixture was designed and manufactured on the basis of the work of Evans, Kotsikos and Robey [2].

In collaboration with RCP Prague we have developed a force converter for tangential loading of curved CT specimens. Its 3D schematic picture is shown on Fig. 1. The straight force, applied at the jaws of the testing machine, is transferred by a pin to the upper and bottom arm of the force converter. Motion of the arms of the force converter around the connecting hinge provides a tangential action of the force at the holes of a curved CT specimen relative to the circumscribed circle around the connecting hinge that goes by central cylindrical area of the specimen.

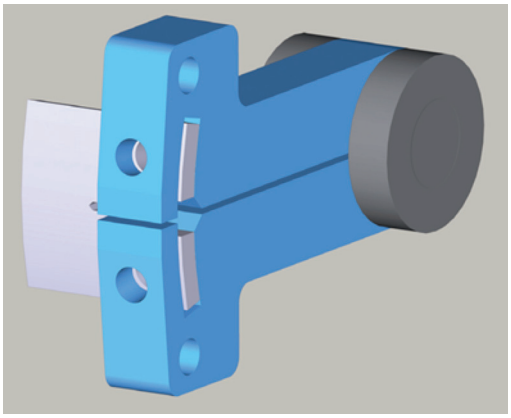

Fig. 1. A force converter

It is apparent that the force converter is bound only to certain specific cross section dimensions of the pipe. For experimental research of the effect of pipe band straightening on fracture toughness values a gas linepipe DN 250 (Ø 266/8) made from low-C steel ČSN 411353 was chosen. The reason for this was a high curvature of the cylindrical surface of the pipe so that the eventual effect of straightening of the pipe band could be very apparent. Fracture toughness characteristics were determined on the basis of R-curves following the standard [3].

Results

It was found that the R curve obtained on curved CT specimens exhibited a lower gradient than that determined on flat (straightened) specimens. This is very likely to be associated with strain hardening of the semiproduct during straightening. However, the lower position of the R curve determined on curved specimens does not mean any significantly lower values of fracture toughness characteristics. For example, the J_m value is lower by 1.1 %, the $J_{0.2}$ value is lower by less than 3 %, and the J_{in} value is even higher than that obtained on flat (straightened) CT specimens. In terms of absolute values these differences are 2.9 N/mm for J_m, 4.6 N/mm for $J_{0.2}$, and 29.7 N/mm for J_{in} in favour of curved CT specimens. Considering a scatter of the results in the form of $(J - \Delta a)$ points given by both the natural process of the subcritical crack growth and inaccuracies in determination of the J integral, especially crack extension during monotonic loading of specimens, it can be stated with a high reliability that the fracture toughness of the pipe material determined on straightened CT specimens is practically the same as that obtained on curved CT specimens.

Acknowledgment: This work was supported by Technology Agency of the Czech Republic Centre of Competence No. TE02000162.

References

[1] Ľ. Gajdoš et al.: Structural Integrity of Pressure Pipelines. Transgas, a.s., Prague, 2004

[2] J. T. Evans, G. Kotsikos, R. F. Robey: A Method for Fracture Toughness Testing Cylinder Material. Engineering Fracture Mechanics, Vol. 50, No. 2, 1995, pp. 295-300

[3] Metallic Materials - Unified Method of Test for the Determination of Quasistatic Fracture Toughness. International Standard ISO 12135, 2002

21st International Conference **ENGINEERING MECHANICS 2015**
Svratka, Czech Republic, May 11 –14, 2015
Paper **#043, pp. 70–71**

Numerical and Experimental Study of Control Algorithm for Unloading System in Mechatronic Device for Gait Reeducation

Grzegorz Gembalczyk

Silesian University of Technology, Department of Theoretical and Applied Mechanics,
Konarskiego 18A, 44-100 Gliwice, Poland

Grzegorz.Gembalczyk@gmail.com

Keywords: control system simulation, gantry control system, parameter optimization

Abstract: This paper presents the results of simulations and experimental research on unloading system used in mechatronic device for gait reeducation. This device works like a special purpose crane, which is equipped with a system for control over keeping up the movement of a crane. Thus, winch can follow the patient and relieve him with a constant value of the force in the vertical direction [3].

First part of the publication regards the simulation study and includes for example: identification of the kinematics, development of the physical model of the winch system and the assembly of the computational model in the MATLAB / Simulink software. The numerical model of device was developed using the multibody systems methodology.

One of the important parts of the numerical model of the crane is description of a BLDC motor model and identification of its parameters. In this case, motor behavior was modeled using a transfer function based on Strejc model [7].

$$K_{eng}(s) = \frac{k}{(1+sT_1)^n} \tag{1}$$

The values of the model parameters were determined in the estimation process, using a genetic algorithm [1,5].

The next part of the paper deals with the concept of the control algorithm for relief system.

This algorithm requires continuous measurement of the relieving force. A new strain gauge load cell has been designed [4] to facilitate this measurement. The concept of the control system concept is shown in a diagram in Fig. 1.

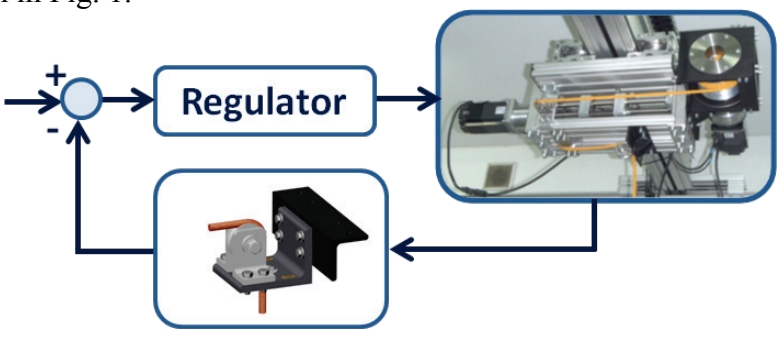

Fig. 1: Scheme of control system

The initially estimated parameters of the proportional-integral-derivative controller are continuously adjusted by a feedback loop. The transmittance of the whole controller was expressed by the equation [3]:

$$K_{reg}(s) = k_p\left(1 + \frac{1}{sT_c} + \frac{sT_D}{1+sT}\right) \tag{2}$$

The complete drive system of the winch is equipped with two engines. One of them provides a quick response to changes in relief force. The other one controls height of the handle.

In this paper we resent results of the tests with the first engine only. This motor is connected via a planetary gear with a drum winding.

Values of the controller settings were estimated using the numerical simulation. In optimization process, the error signal was minimized. Forcing signal was replicated in the center of gravity of person- with gait impairment [2,6]. Obtained results have been verified during the bench tests.

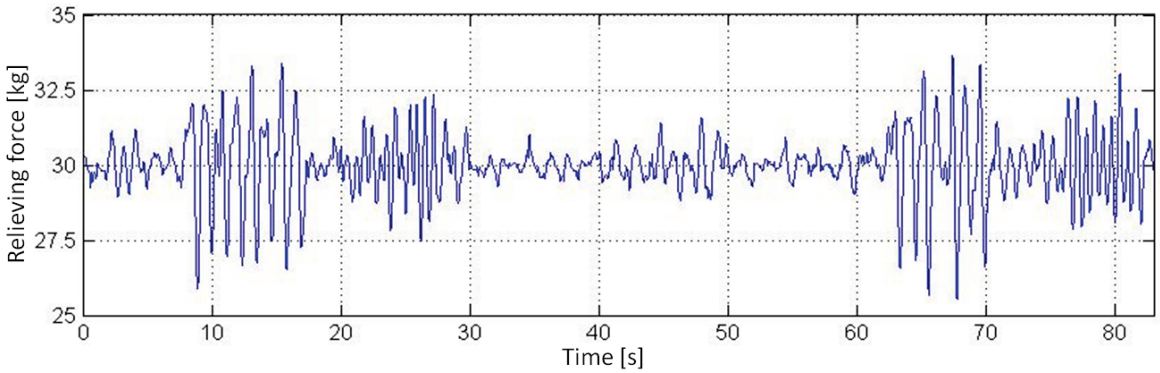

Fig. 2: Values of the relieving force as a function of time

References

[1] M. B. Anandaraju, P. S. Puttaswamy, J. S. Rajpurohit, Genetic Algorithm: An approach to Velocity Control of an Electric DC Motor. International Journal of Computer Applications, 26 (2011) 37-43.

[2] K. Bellad, S.S. Hiremath, M. Singaperumal, S. Karunanidhi, Optimization of PID Parameters in Electro-Hydraulic Actuator System Using Genetic Algorithm. Applied Mechanics and Materials, 592-594 (2014) 2229-2233.

[3] S. Duda, K. Kawlewski, G. Gembalczyk, Concept of the System for Control over Keeping Up the Movement of a Crane. Mechatronic systems and materials VI: Trans Tech Publications, 220/221 (2015) 339-344.

[4] G. Gembalczyk, S. Duda, Projekt i walidacja urządzeń pomiarowych – siły w linie i kąta wychylenia liny zawiesia suwnicy, Modelowanie Inżynierskie, 47 (2013) 75-81.

[5] A. Kapun, M. Curkovic, A. Hace, K. Jezernik, Identifying dynamic model parameters of a BLDC motor, Simulation Modelling Practice and Theory, 16 (2008) 1254–1265.

[6] J. Wei, A Novel PID Controller Parameter Optimization Method, Applied Mechanics and Materials, 738-739 (2015) 1077-1081.

[7] A. Żuchowski, Nietypowe metody eksperymentalnego wyznaczania parametrów zastępczego modelu Strejca, Pomiary Automatyka Kontrola, 59 (2013) 55-58.

21st International Conference **ENGINEERING MECHANICS 2015**
Svratka, Czech Republic, May 11 –14, 2015
Paper **#121, pp. 72–73**

Resistance of Composite Steel-Concrete Columns with Solid Steel Profile

Štefan Gramblička[a]*, Juraj Frólo[b]

Slovak University of Technology in Bratislava, Faculty of Civil Engineering,
Department of concrete structures and bridges, Radlinského 11, 810 05 Bratislava, Slovakia

[a]stefan.gramblicka@stuba.sk, [b]juraj.frolo@stuba.sk

Keywords: composite column, solid steel profile, residual stresses

Abstract: Composite steel-concrete columns with solid steel profiles are characterized as high-resistance columns. Design of these columns is limited in practice due to absence of simplified design method according to EN 1994-1-1 [1]. Reasons are residual stresses in steel profile caused by fabrication process and limitation strains in concrete. Recommendations have been determined for simplified design method according to EN 1994-1-1 for composite columns with cross-section type of high strength concrete filled steel tube with solid steel profile. These recommendations have not been verified yet in application of columns with cross-section type of solid steel profile covered by reinforced concrete.

Introduction

Composite steel-concrete columns with solid steel profile are often used to increase the resistance of columns in combination with small dimensions of cross-section. Higher bending resistance is possible to reach by combination with steel tube. Solid steel profile allows to reach more slender columns. These columns include two types of cross-section. Concrete filled steel tubes with solid steel profiles and solid steel profiles covered by reinforced concrete (Fig. 1). Standard [1] does not contain the design-rules according to simplified design method because of residual stresses in solid steel profile and strain limitations in concrete with centrally situated solid steel profile.

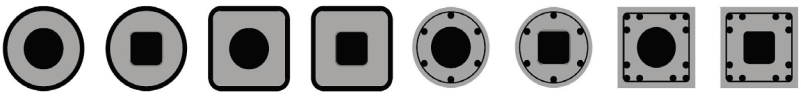

Fig. 1: Types of cross-sections of composite steel-concrete columns with solid steel profile

Design of composite steel-concrete columns according to EN 1994-1-1

Simplified design method is based on cross-section interaction curve assuming full plastic behavior of materials and neglecting the strain gradient in cross-section. Influences of real strain gradient and strain limitations in concrete are covered by reduction factor of plastic bending capacity α_M. This reduction factor α_M depends on grade steel ($\alpha_M=0,9$ for steel grade up to S355 or $\alpha_M=0,8$ up to S460). Strain limitations in concrete cause wide elastic areas in steel parts of cross-section. This effect is especially obvious in cross-section with central solid steel profile (Fig. 2). It leads to significant deviation against material full plastic assumption. Residual stresses arising during fabrication process due to uneven temperature distribution in cross-section by cooling process. Residual stresses in solid steel profile cause reduction of flexural stiffness. These effects had been investigated on columns with section of concrete filled steel tube with solid steel profile [4]. Results and conclusions show that:

- Dimension of solid steel profile has influence on ratio of steel and concrete. Different concrete-steel ratio influences differences between full-plastic resistance and reduced resistance by α_M. It follows that reduction factor α_M must be variable value depending on dimension and steel grade.
- Equivalent imperfection is close to value L/400. This equivalent imperfection must be corrected by factors of steel grade, dimension of solid steel profile and related slenderness of column.

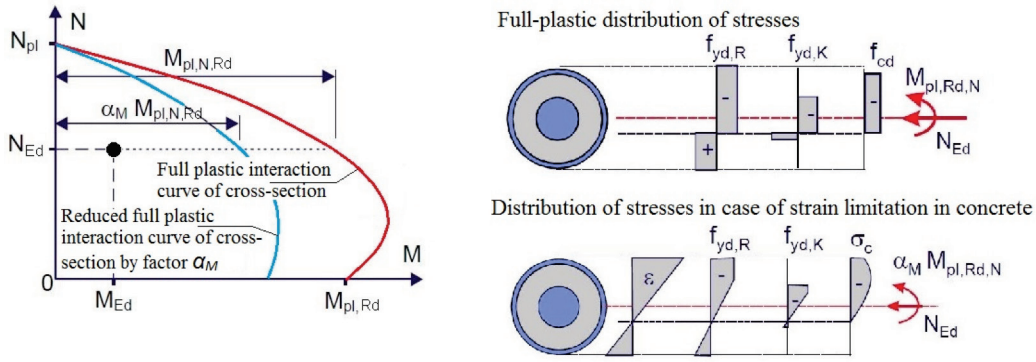

Fig. 2: Full-plastic distribution of stresses and influence of strain limitation in concrete [3]

Experimental research of composite steel-concrete columns with solid steel profile covered by reinforced concrete

It has not been verified yet if mentioned recommendations are applicable for design of composite steel-concrete columns with solid steel profile covered by reinforced concrete. Actual experimental research (Fig. 3) should lead to determine reduction factor α_M, equivalent imperfection and buckling curve for composite columns with investigated cross-sections. For short-term laboratory tests a fully encased in reinforced concrete cross-section with a circular steel profile was chosen. A total of 6 columns in two series were tested.

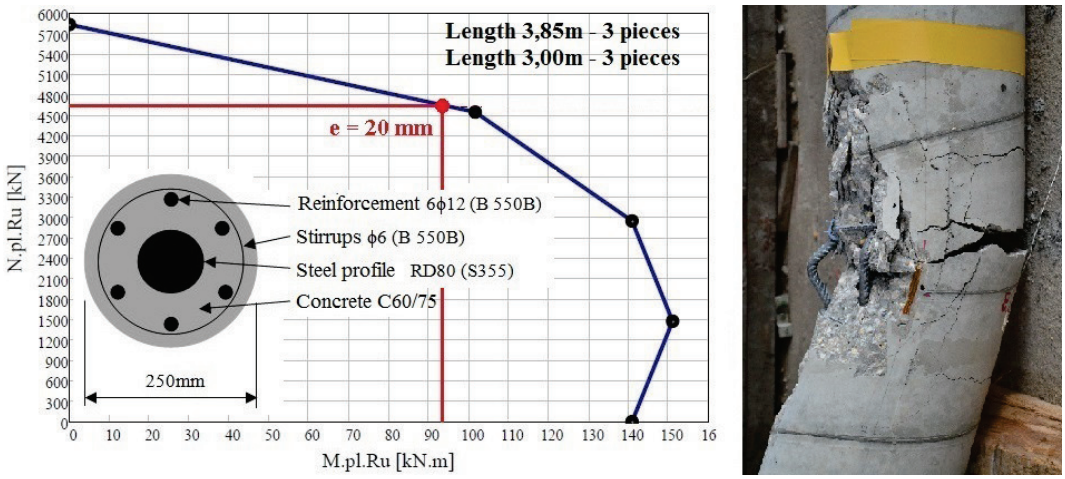

Fig. 3: Interaction diagram and failure of tested composite column

Acknowledgement: This contribution was prepared with the financial support of Slovak Grant Agency VEGA 1/0696/14.

References

[1] EN 1994-1-1 Design of composite steel and concrete structures, Part 1-1 General rules and rules for buildings, 2004

[2] R. Bergman, G. Hanswille, New design method for composite columns including high strength steel. In: International Proceedings on the 5th international conference composite construction in steel and concrete V., South Africa, 2004.

[3] G. Hanswille, M. Lippes, Design of composite columns made of concrete filled tubes with inner massive core profiles and high strength materials, International conference on composite construction in steel and concrete 2008, Colorado, Devil´s Thumb Ranch in Tebernasch, Colorado, July, 2008

[4] M. Lippes, Zur Bemessung von Hohlprofil–Verbundstutzen aus hochfesten Stahlen und Betonen. Institut für Konstruktiven Ingenieurbau Bergische Universitat Wuppertal, November 2008.

21st International Conference **ENGINEERING MECHANICS 2015**
Svratka, Czech Republic, May 11 –14, 2015
Paper **#207, pp. 74–75**

Response of a Non-Linearly Damped Duffing Oscillator Including Non-Linear Restoring Force by Using a Variational Approach

Ardeshir Guran

Institute of Structronics, Montreal, Canada

ardeshir.guran@gmail.com

Keywords: variational approach, parameterized perturbation method, nonlinear oscillators, undamped Duffing oscillator

Abstract: In this paper, we proposed to use approximation methods for solving undamped nonlinear Duffing's equation including nonlinear restoring forces. The purpose is the application of variational approach and parameterized perturbation method to gain the natural frequency and response of the system in a class of Duffing's oscillators. It is shown the variational approach is an explicit method with high validity for the solution of strongly nonlinear oscillatory systems.

Introduction

Nonlinear oscillatory systems are important in engineering because many practical engineering components are modeled using this systems such as elastic beams supported by two springs, mass-on-moving-belt, nonlinear oscillations of a pendulum and vibration of a milling machine. Various kinds of analytical and numerical methods were used to handle the problem and other nonlinear problems such as Non–perturbation methods, variational iteration method, homotopy perturbation method, perturbation techniques, energy balance method, Lindstedt–Poincaré method, parameter–expansion method, variational approach, and Parameterized perturbation method. In this paper, we apply the variational approach and Parameterized perturbation method to the undamped nonlinear Duffing's oscillator.

Description of the Duffing's Oscillator with nonlinear restoring forces

The differential equation:

$$\ddot{x}(t) + x(t) + \varepsilon\,\alpha\, x(t)^3 = 0, \qquad \varepsilon > 0 \tag{1}$$

Is called the Duffing's oscillator which x and t are generalized dimensionless displacement and time variables, respectively, and α and ε are constant parameters in nonlinear Duffing's oscillator. It can be the model of a structural system which includes nonlinear restoring forces (for example springs).

The exact frequency for a dynamic system governed by Eq. 1 can be derived as in Eq. 2:

$$\omega_e(A) = 2\pi \left(4 \int_0^{\pi/2} \frac{dt}{\sqrt{1 - \frac{\alpha\varepsilon}{2} A^2 (1 + \cos^2 t)}} \right)^{-1} \tag{2}$$

Solution using Parameterized perturbation method

The procedure to find the solution of Eq. 1 by means of parameterized perturbation technique is given elsewhere. The closed form solution is:

$$x(t) = A\cos\omega t + \left(\frac{A^3 \alpha\, \varepsilon}{32\omega^2}\right)\left(\cos(3\omega t) - \cos(\omega t)\right) \tag{3}$$

where:

$$\omega = \frac{1}{2}\sqrt{4 + 3\alpha\,\varepsilon A^2} \tag{4}$$

Solution procedures for Duffing equation using variational approach

This Solution given in reference [8]

$$x(t) = A\,\cos(\frac{1}{2}\sqrt{4+3\alpha\,\varepsilon\,A^2}t) \tag{5}$$

Table 1: Comparison of angular frequencies in Eq. 1 from various approximations of the Variational approach and the Parameterized perturbation method with the exact solution

Constants			Results			
A	α	ε	Exact solution ω_e	Variational approach ω	Parameterized perturbation ω	percentage error
1	-1/6	0.5	0.94119	0.96825	0.96825	2.80 %
1	-1/6	1	0.88889	0.93542	0.93542	4.98 %
1	-1/6	3	0.72727	0.79058	0.79058	8.00 %
1	-1/6	5	0.66667	0.70710	0.70710	5.72%

Summary

Nonlinear Duffing's oscillator is sometimes used as an approximation for the pendulum. Approximate analytical approaches have been developed for solving the undamped nonlinear Duffing's oscillator including nonlinear restoring forces. These approaches can be easily extended and applied to other nonlinear oscillation problems in engineering and science.

References

[1] R. H. Abraham, J. E. Marsden, Foundations of mechanics, AMS Chelsea Publishing, Rhode Island, 2000.

[2] G. Duffing, Erzwungene Schwingungen bei veränderlicher Eingenfrequenz und ihre technische Bedeutung, Druck und Verlag von Fridr. Vieweg & Sohn, Braunschwige, 1918.

[3] A. Guran, F. J. P. Rimrott and Georg Duffing (1861 - 1944): seventy years of Duffing equation, UTME, Toronto, 1988.

[4] F. J. P. Rimrott, Georg Duffing (1861 - 1944), Technische Mechanik, 14 (1994) 77–82.

[5] I. Kovacic, J. B. Brennan, Background: on Georg Duffing and Duffing equation, In: The Duffing Equation, Wiley, (2011), pp.1-23.

[6] L. Cvecicanin, Ninety years of Duffing's equation, Theoretical and Applied Mechanics, 40 (S1) (2012) 49-63.

[7] O.E. Rössler, Excerpt translation of Erzwungene Schwingungen bei veränderlicher Eingenfrequenz undihre technische Bedeutung (Forced vibration with variable natural frequency) by Georg Duffing (Reference 2 above), private communication, 2013.

[8] A. Guran, Georg Duffing (1861-1944), and the origin of Duffing equation: response of a non-linearly damped Duffing oscillator including nonlinear restoring force by using a variational approach, Computational Mechanics, 29th Conference, Spicak, Czech Republic, Nov. 4-6, 2013

21st International Conference **ENGINEERING MECHANICS 2015**
Svratka, Czech Republic, May 11 –14, 2015
Paper **#056, pp. 76–77**

Simulation of Damage in Hybrid Composite Cell Structure

Jiří Had[a] *, Milan Růžička[b]

ČVUT v Praze, Fakulta strojní, Ústav mechaniky, biomechaniky a mechatroniky,
Technická 4, 166 07 Praha 6, Česká republika

[a]jiri.had@gmail.com, [b]Milan.Ruzicka@fs.cvut.cz

Keywords: composite, damage, non-uniform transformation field analysis, homogenization

Abstract: A novel type of hybrid cell composite structure has been developed and used for many practical applications. Main goal of this paper is the simulation of damage of this new composite structure. Experimental results of damage of cell structure are presented at first. Modified Non-uniform Transformation Field Analysis was proposed for simulation of damage progress. Basis of this modification are briefly described.

Introduction

At this time, a novel type of hybrid cell composite structure is a common way to produce thick-walled beam applications. Typical macroscopic sub-cells in the cross section structure are formed by the stamping process of partially cured and axially-oriented high modulus carbon fibre bundles. Each bundle is wrapped around by a thin layer of high strength fibres. Example of the cell composite structure used in hybrid spindle beam is in Fig. 1. This new material structure has its own specific stiffness properties and specific damage behavior and failure modes, respectively. Complex failure can be documented on example of fracture area of beam loaded in bending in Fig. 2. In this example, damage is developed in each sub-cell. Most of the cross-section is failed due to compressive loading and only narrow area by tensile failure. Complex modeling of damage progression even in a few cells would demands of tremendous computational performance.

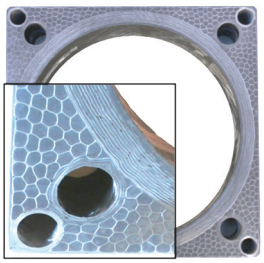

Fig. 1: Example of hybrid spindle beam with cell structure filling the corners

Fig. 2: Fracture area of beam loaded in four-point bending

Simulation of damage progression of the hybrid cell composite structure

The first goal is to focus effort on observation of real properties of cell structure. Static strength of cell structure and its building parts were measured in longitudinal and transverse direction and in shear loading. Static bending behavior was measured in four-point bending configuration and damage progression was monitored during the loading. On this experimental basis, failure and damage behavior of whole cell structure and first of all behavior of building constituents are determined. Generally, cell composite structure is built from parts with mostly brittle micro-behavior (UD composite) and from materials with plasticity. It means the gradual damage of the parts of cell structure and therefore it changes its mechanical response.

Modified Non-uniform Transformation Field Analysis (NTFA) was developed to simulate damage progression. Original method (see [1]) was developed for materials exhibiting elasto-plastic behavior. This method is based on assumption that field of plastic strain in each phase can be decomposed on finite set of fields, called plastic modes. Modification of the method is based on

introducing damage modes instead of plastic modes and specific behavior of proposed damage modes. Procedure of NTFA method is based on two steps. Identification of damage modes and calculation of auxiliary operators are calculated at first and these operations are performed only once. In the second step iterative calculation of macroscopic state is performed.

Several nonlinear FEM simulations of failure of building parts have to be performed for identification of damage modes. The FEM model is based on the periodic system of the cell structure and consisting from the cells and their overwinding. FEM model of PUC of cell structure is loaded in normal and shear loading direction. Moreover analyses with loading in normal direction are duplicated for tension and compression. Common failure criteria are used for all parts of PUC. Damage modes have found in specific material directions of each constituents of cell structure.

Macroscopic state can be decomposed into sum of certain contribution of building parts with their damage modes. Evolution of damage in every damage modes is based on experimental observation. In generally, numerical models of damage modes consist of elasticity and ultimate failure and combination of plastic behavior with subsequent degradation mechanism. They have different behavior in tensile and compressive loading. Each material damage mode can fail ultimately but even failed mode can contribute to macroscopic state in certain directions. Moreover failed damage mode in compressive loading has still certain residual stiffness. General material model of damage mode is in Fig. 3. Modified NTFA method was incorporated into FEM code and verified in several four-point bending tests. Example of verification results is in Fig. 4.

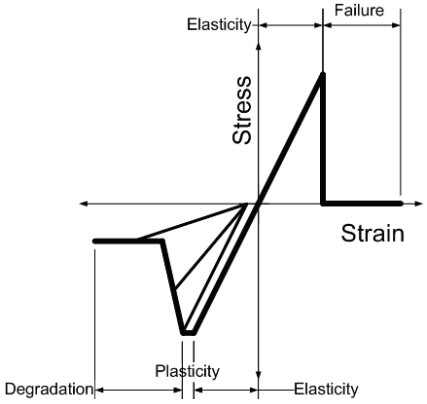

Fig. 3: Schematic material model of damage mode

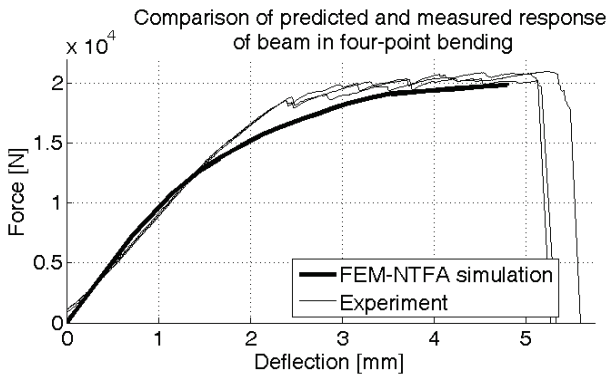

Fig. 4: Verification of the simulation

Summary

Research of newly formed material structure was done. Damage progression was simulated using modified hierarchy homogenization method. New formulation of damage modes and specific material behavior of constituent is used in presented modified NTFA method. Verification of proposed concept is based on comparison predicted bending behavior with experiment.

Acknowledgements: The authors would like to thank the Ministry Technology Agency of the Czech Republic for supporting this research in the framework of project no. TA02010543. Support from the CompoTech Plus Company is also gratefully acknowledged.

References

[1] J.C. Michel, P. Suquet, Computational analysis of nonlinear composite structures using the nonuniform transformation field analysis. Computer methods in applied mechanics and engineering, 193 (2004) 5477-5502.

[2] V. Lasová, J. Vacik, R. Kottner, Investigation of Dynamic Properties of Hybrid Laminate Structure, in: Trebuna, F: (Ed), 5th International Conference on Modelling of Mechanical and Mechatronics Systems. Procedia Engineering, 48 (2012) 358-366.

21st International Conference **ENGINEERING MECHANICS 2015**
Svratka, Czech Republic, May 11 –14, 2015
Paper **#086, pp. 78–79**

Finite Element Modelling of the Effect of Stiffness and Damping of Vocal Folds Layers on their Vibrations and Produced Sound

Petr Hájek[1,a]*, Pavel Švancara[1,2,b], Jaromír Horáček[2,c], Jan G. Švec[3,d]

[1]Institute of Solid Mechanics, Mechatronics and Biomechanics, Brno University of Technology, Technická 2896/2, 616 69, Brno, Czech Republic

[2]Institute of Thermomechanics, Academy of Sciences of the Czech Republic, Dolejškova 1402/5; 182 00, Prague; Czech Republic

[3]Department of Biophysics, Palacky University Olomouc, 17. listopadu 12, 771 46, Olomouc; Czech Republic

[a]y126528@stud.fme.vutbr.cz, [b]svancara@fme.vutbr.cz, [c]jaromirh@it.cas.cz, [d]svecjang@gmail.com

Keywords: Biomechanics of voice, Simulation of phonation, Fluid-structure-acoustic interaction, Finite element method.

Abstract: The study presents a two-dimensional (2D) finite element (FE) model of the fluid-structure-acoustic interaction during self-sustained oscillation of the human vocal folds (VF). The FE model combines the FE models of the VF, the trachea and the simplified human vocal tract shaped for phonation of Czech vowel [a:]. The developed FE model comprises large deformations of the VF tissue, VF contact, fluid-structure interaction, morphing the fluid mesh according to the VF motion (Arbitrary Lagrangian-Eulerian approach), solution of unsteady viscous compressible airflow described by the Navier-Stokes equations and airflow separation during the glottis closure. The effect of stiffness and damping of lamina propria on VF vibrations and produced sound are analyzed. Such variation of the lamina propria properties can be caused by certain VF pathologies such as sulcus vergeture.

Introduction

Production of human voice is an acoustic problem including fluid-structure interaction (FSI). There are many computational models published in literature. Zhao et al. [1] developed 2D axisymmetric FE model with prescribed movement of VF. In recent works of the authors [2] FE model of flow-induced oscillations of the VF was developed. In this paper is presented newly developed 2D FE model of phonation with in literature widely used M5 geometry of the VF [3].

Method

The 2D FE model was developed using the program system ANSYS 15.0. Vocal folds tissue was considered as four-layered (see Fig. 1) with homogenous isotropic material properties of each layer including several variants for values of Young's modulus (E_{SLP}) and damping ratio of the lamina propria.

Results and discussion

Examples of the resulting maximum and minimum values of the acoustic pressure in particular locations of the vocal tract are shown in Table 1. From the results we can for example observe that increasing Young's modulus (E_{SLP}) of lamina propria leads to increase of maximum pressure under the VF.

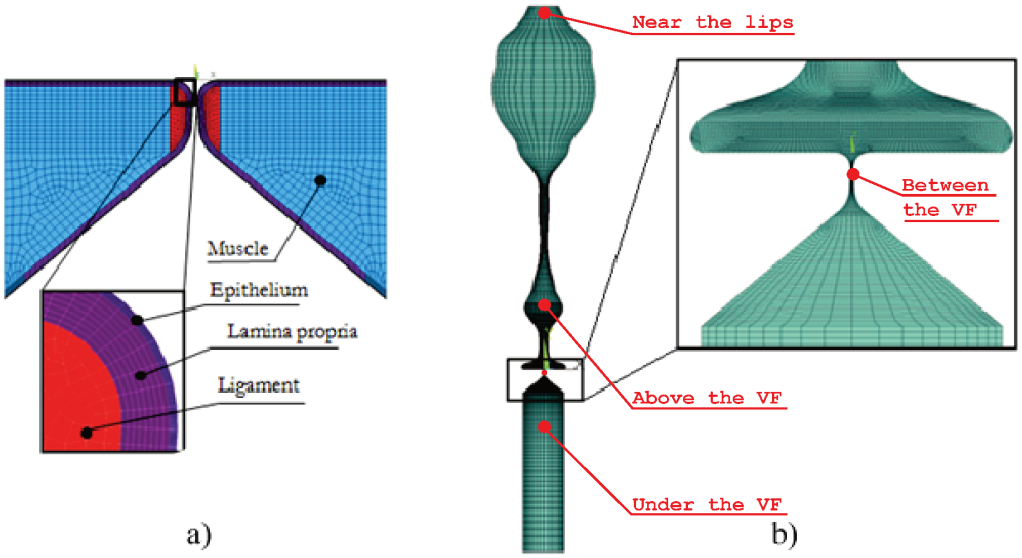

Fig. 1: a) FE model of the four layered tissue of the VF b) FE model of the acoustic spaces of the trachea and the vocal tract for Czech vowel [a:], measuring points are emphasised.

Tab. 1: Computed values of the acoustic pressures in particular locations of the vocal tract.

E_{SLP}	Acoustic pressure [Pa]							
	under the VF		between the VF		above the VF		near the lips	
	max	*min*	*max*	*min*	*max*	*min*	*max*	*min*
1500	307,19	-42,26	381,18	-366,72	214,54	-329,76	23,75	-21,37
2000	334,37	-43,89	373,21	-397,37	213,38	-343,25	23,27	-21,00
2500	329,83	-3,31	411,76	-348,94	188,33	-340,80	21,04	-18,14
3000	339,52	0,03	389,37	-377,89	170,09	-328,68	18,93	-17,39
4000	354,17	0,03	358,33	-432,26	184,45	-355,92	19,29	-16,96
5000	372,15	0,03	445,51	-368,07	192,06	-352,48	19,48	-19,21

Summary

The developed FE model can be used to study the effects of pathological changes in VF tissue on their vibrations and the produced sound.

Acknowledgement This work was supported by specific research project of Brno University of Technology No. FSI-S-14-2344 and by the Grant Agency of the Czech Republic by the project No P101/12/1306.

References

[1] W. Zhao, C. Zhang, S. H. Frankel, L. Mongeau, Computational aeroacoustics of phonation, Part I: Computational methods and sound generation mechanisms, Journal of the Acoustical Society of America, 112/5 (2002) 2134–2146.

[2] P. Švancara, J. Horáček, V. Hrůza, FE modelling of the fluid-structure-acoustic interaction for the vocal folds self-oscillation, in: Vibration Problems ICOVP 2011, Springer, Berlin, (2011), p. 801-807.

[3] R. C. Scherer, D. Shinwari, K. J. De Witt, C. Zhang, B. R. Kucinschi, A. A. Afjeh, Intraglottal pressure profiles for a symmetric and oblique glottis with a divergence angle of 10 degrees, Journal of the Acoustical Society of America, 109/4 (2001) 1616-1630.

21st International Conference **ENGINEERING MECHANICS 2015**
Svratka, Czech Republic, May 11 –14, 2015
Paper **#143, pp. 80–81**

Numerical Solution of Humid Air Flow with Non-Equilibrium Condensation

Jan Halama[a], Miroslav Vrátný[b]

Department of Technical Mathematics, Faculty of Mechanical Engineering, Czech Technical University Prague, Karlovo nám. 13, 12135 Praha 2, Czech Republic

[a]Jan.Halama@fs.cvut.cz, [b]Miroslav.Vratny@fs.cvut.cz

Keywords: humid air, transonic flow, Laval nozzle, condensation

Abstract: Fast expansion of humid air (e.g. flow around an aircraft or a flow in the test section of a wind tunnel) may initiate the condensation of water vapor into tiny droplets. The latent heat released has non-negligible effect on the structure of a considered flow field. This contribution presents the model for humid air flow at high velocities, which is based on the former model [3] originally developed for the simulation of wet steam flow.

Model of humid air flow

Development of numerical algorithms for flow simulations is not possible without relevant experimental data. Some cases, e.g. transonic flow in a turbine cascade, are very sensitive even on minute changes of geometry of flow conditions [2]. The working fluid in experiments is often the air with some remaining humidity. The latent heat released due to condensation may affect the measured data. Numerical simulation of such condensation could help to estimate the measurement uncertainty.

We consider a simplified model of humid air composed of dry air, water vapor and tiny liquid droplets. We consider the same velocity for all components, therefore the flow of the whole mixture can be modeled by set of transport equations

$$\frac{\partial}{\partial t}\big(A(x)W_k\big) + \frac{\partial}{\partial x}\big(A(x)F_k\big) = P_k + A(x)Q_k, \tag{1}$$

where $A(x)$ is the cross-sectional area of the nozzle and the first three components of W_k, F_k, P_k and Q_k are

$$\begin{bmatrix} \rho \\ \rho u \\ e \end{bmatrix}, \quad \begin{bmatrix} \rho u \\ \rho u^2 + p \\ (e+p)u \end{bmatrix}, \quad \begin{bmatrix} 0 \\ pA'(x) \\ 0 \end{bmatrix}, \quad \begin{bmatrix} 0 \\ 0 \\ 0 \end{bmatrix}, \tag{2}$$

with ρ, u, p and e denoting the mixture density, velocity, pressure and total energy per unit volume respectively. We consider the non-equilibrium model for the condensation of water vapor in the form of transport equations for the moments of droplet spectra $Q_n = \int_0^\infty r^n N(r)dr$ with distribution function $N(r)$. The remaining components of W_k, F_k, P_k and Q_k are

$$\begin{bmatrix} \rho\chi \\ \rho Q_2 \\ \rho Q_1 \\ \rho Q_0 \end{bmatrix}, \quad \begin{bmatrix} \rho\chi u \\ \rho Q_2 u \\ \rho Q_1 u \\ \rho Q_0 u \end{bmatrix}, \quad \begin{bmatrix} 0 \\ 0 \\ 0 \\ 0 \end{bmatrix}, \quad \begin{bmatrix} \frac{4}{3}\pi r_c^3 J\rho_l + 4\pi\rho G_2\rho_l \\ r_c^2 J + 2\rho G_1 \\ r_c J + \rho G_0 \\ J \end{bmatrix}, \tag{3}$$

with χ, J and r_c denoting the mass fraction of liquid phase, nucleation rate and critical radius of droplet. The term $G_n = \int_0^\infty r^n N(r) g(r) dr$ models the growth of existing droplets with droplet growth velocity $g(r)$, for more details see [1, 3]. The considered system of equations (1) has the same form as the model for wet steam flow. The main differences are hidden in closing relations [1]. The composition of humid air is specified by the maximum mass fraction χ_{max} of water in both gaseous and liquid phases.

Results of numerical simulations

The first tests have been performed by the in-house finite difference Lax-Friedrichs method. The latent heat release was implemented by the 'switch' model, i.e. we solve only first three transport equations and the vapor jumps from metastable state into the equilibrium state in the point x_N, where specified vapor sub-cooling is reached

$$\chi = \begin{cases} 0, & x < x_N, \\ \chi_{eq}, & x \geq x_N, \end{cases} \tag{4}$$

Such simple model is able to approximate the pressure of pure steam ($\chi_{max} = 1.0$) along nozzle axis, see the Fig. 1. The experimental data are from [4]. The second graph with Mach number distribution along the nozzle axis show the effect of condensation in humid air flow with $\chi_{max} = 0.18$.

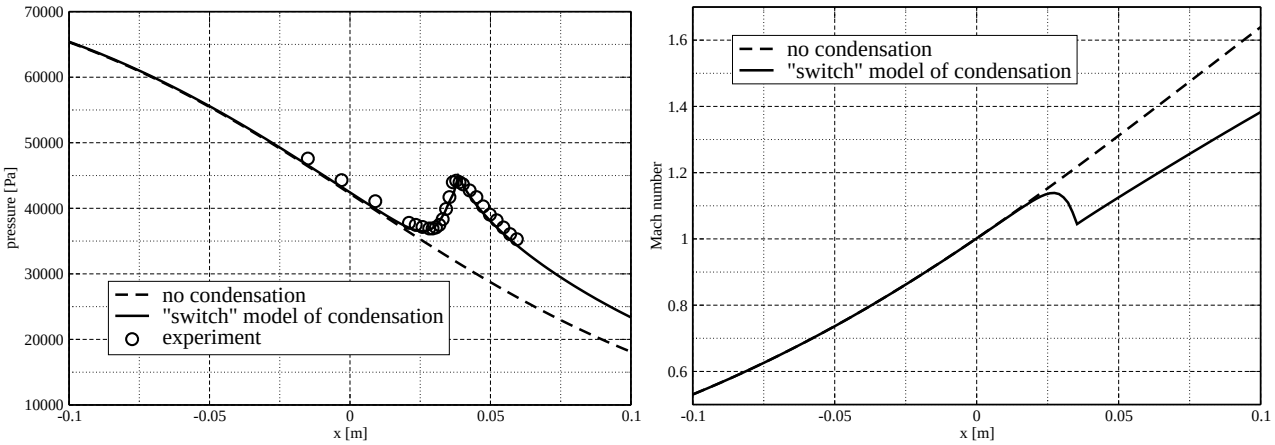

Fig. 1: Pressure in pure steam flow (left) and Mach number in humid air flow (right) along the axis of Barschdorff nozzle [4].

Acknowledgements: The support of the grant No. SGS13/174/OHK2/3T/12 of the Grant Agency of the Czech Technical University in Prague is gratefully acknowledged.

References

[1] P. Kelleners, Simulation of inviscid compressible multi–phase flow with condensation, Annual Research Briefs 2003, Center for Turbulence Research, University of Twente (2003).

[2] M. Luxa, R. Dvořák, D. Šimurda, J. Vimmr, Pneumatic Measurements Downstream of a Radial Turbine Nozzle Cascade, Journal of Thermal Science 19 (2010) 42ï 46.

[3] J. Halama, F. Benkhaldoun, J. Fořt, Flux Schemes Based Finite Volume Method for Internal Transonic Flow with Condensation, International Journal for Numerical Methods in Fluids 65 (2011) 953ï 968.

[4] D. Barschdorff, Verlauf der ZustandgröÇen und Gasdynamische Zuammenhänge der Spontanen Kondensation Reinen Wasserdampfes in Lavaldüsen, Forsch. Ing.-Wes. 37 (1971) 146ï 157.

21st International Conference **ENGINEERING MECHANICS 2015**
Svratka, Czech Republic, May 11 –14, 2015
Paper **#025, pp. 82–83**

Statistical Safety Evaluation of EC2 and MC 2010 – Model for Assessment of Punching Resistance of Footings

Ján Hanzel[a*], Lucia Majtanova[b], Jaroslav Halvonik[c]

Slovak University of Technology in Bratislava, Radlinskeho 11, 81368 Bratislava, Slovakia

[a]jan.hanzel@stuba.sk, [b]lucia.majtanova@stuba.sk, [c]jaroslav.halvonik@stuba.sk

Keywords: reinforced concrete, foundation footings, punching, shear resistance.

Abstract: Assessment of punching resistance according to EC2 is based on the empirical model which was introduced in the Model Code 1990. In the current Model Code 2010 is presented a new physical model which is based on the *"Critical Shear Crack Theory"* by Muttoni and Schwartz [1]. Calculation of punching resistance of foundation slabs and footings was derived in both models using the principles which are valid for flat slabs. In addressing this issue it opens a space for discussion and analysis of possibilities to update, these models in a case of foundation members.

Introduction

The assessment of punching resistance of foundation members without shear reinforcement in EC2 is based on iterative process where the critical control perimeter u_{crit} has to be found. Distance of this perimeter measured from the face of a column is a_{crit}. For each size and type of the foundation footing is the distance a_{crit} different. In Tab.1 are introduced distances a_{crit} which were derived for footings with different shear slenderness and effective depth. For intermediate values the linear interpolation can be used.

Tab. 1: Dependence $a_{i.crit}/d_i$ on the shear-span-depth-ration a_i/d_i for effective depth d_i

$d_{i.footing}$	a_i/d_i	0,8	0,9	1,0	1,2	1,3	1,4	1,5	1,6	1,7	1,8	2,0	2,1	2,2	2,4	2,5
200	$a_{i.crit}/d_i$	0,40	0,45	0,49	0,57	0,62	0,66	0,70	0,74	0,79	0,83	0,91	0,96	1,00	1,08	1,13
400	$a_{i.crit}/d_i$	0,38	0,41	0,45	0,52	0,56	0,60	0,63	0,67	0,71	0,74	0,82	0,85	0,89	0,96	1,00
750	$a_{i.crit}/d_i$	0,36	0,39	0,42	0,48	0,52	0,55	0,58	0,61	0,64	0,68	0,74	0,77	0,80	0,87	0,90
1100	$a_{i.crit}/d_i$	0,34	0,37	0,39	0,45	0,48	0,51	0,54	0,56	0,59	0,62	0,68	0,71	0,73	0,79	0,82
1450	$a_{i.crit}/d_i$	0,33	0,36	0,38	0,43	0,46	0,49	0,51	0,54	0,57	0,59	0,64	0,67	0,70	0,75	0,78

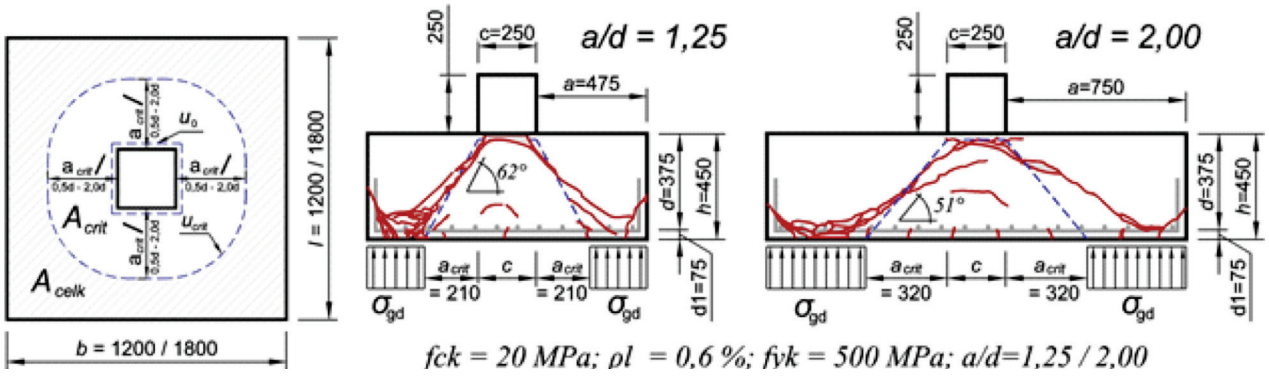

Fig. 1: Influence of shear slenderness a/d on the position of a_{crit}

Punching resistance V_{Rdc} [MN] can be determined according to the (1) as the product of shear strength v_{Rdc} [MPa] and the area surrounded by the critical control perimeter over the effective depth d [m]. The punching resistance then can be expressed as:

$$V_{Rd,c} = v_{Rd,c} * u_{crit} * d \text{ [MN]} \quad (1)$$

$$v_{Rd,c} = C_{Rd,c} * k_h * (100 * \rho_l * f_{ck})^{1/3} * (2d / a_{crit}) \geq v_{min} * (2d / a_{crit}) \text{ [MPa]} \quad (2)$$

The ratio $2d/a_{crit}$ [-] represents the favorable effect of concrete struts to shear resistance.

MC2010 model determines punching resistance without shear reinforcement V_{Rdc} depending on the development of the critical shear crack. The critical shear crack development depends mainly on the slab rotation ψ at the support. The shear resistance of structure without shear reinforcement can be determined as:

$$V_{Rd,c} = k_\psi * (f_{ck})^{1/2} / \gamma_C * b_0 * d_v \geq V_{Ed,red} \text{ [MN]} \quad (3)$$

Rotation of the structure ψ is expressed by factor k_ψ, which takes into account size effect, shear slenderness, aggregate size, and strains in the main reinforcement, e.g. bigger diameter of the aggregates increases the wedge effect of grain in a shear crack and increases resistance V_{Rdc} [MN]. It has to be noted that the model was primarily derived from the tests of the flat slabs [2], [3], [4] and then extrapolated to massive structures such as footings, foundations strips and slabs.

Both models were exposed to statistical evaluation of the safety using results of 48 experimental tests performed on the foundation footings with different shear slenderness and effective depth. The statistical analysis has shown that the EC2 model is pretty safe because $P_{k,0.05}$ is significantly higher than 1. Opposite current MC2010 model seems to be better calibrated with $P_{k,0.05}$ approaching to 1. Update of MC2010 improved precision of the model but due to the high value of COV the safety of the model descended deep below 1.

Tab. 2: Statistical evaluation of safety models EC2 a MC2010

Model	$C_{Rk,c}$ [MPa]	Factor k_ψ	Number of experiments [n]	The average value of [m_x]	Coefficient of variation [V_x]	The characteristic value [$P_{k,0.05}$]
EC2	0,180	-	48	2,408	0,2448	1,388
EC2[1)]	0,240	-	48	1,806	0,2448	1,041
MC2010	-	MC2010	48	1,566	0,2226	0,955
-	-	CCST EC2	48	1,284	0,2181	0,800

[1)] Update of the EC2 model by different value of $C_{Rk,c}$

References

[1] A. Muttoni, J. Schwartz, Behaviour of Beams and Punching in Slabs without Shear Reinforcement, In: IABSE Colloquium, Vol. 62, Zurich, Switzerland, 1991, pp. 703-708.

[2] A. Muttoni, M. Fernández Ruiz, Shear strength of members without transverse reinforcement as function of critical shear crack width, ACI Structural Journal, 105 (2008) 163-172.

[3] A. Muttoni, M. Fernández Ruiz, The levels of approximation approach in MC 2010: applications to punching shear provisions, Structural Concrete, Ernst&Sohn, Germany, 13 (2012) 32-41.

[4] C. Siburg, M. Ricker, J. Hegger, Punching shear design of footings: critical review of different code provisions, Structural Concrete, Ernst&Sohn, Germany, 3 (2014) 1-27.

21st International Conference **ENGINEERING MECHANICS 2015**
Svratka, Czech Republic, May 11 –14, 2015
Paper **#251, pp. 84–85**

Uncertainty Analysis of Earth Dam

Jan Havelka[a], Jan Sýkora[b], Anna Kučerová[c]

Department of Mechanics, Faculty of Civil Engineering, Czech Technical University in Prague,
Thákurova 7/2077, 166 29 Prague, Czech Republic

[a]jan.havelka.1@fsv.cvut.cz, [b]jan.sykora.1@fsv.cvut.cz, [c]anicka@cml.fsv.cz

Keywords: uncertainty analysis, groundwater flow, stochastic finite element method

Abstract: In this contribution we focus on the practical application of the uncertainty propagation in groundwater flow environment [1] using stochastic finite element method [2,3,4], where the uncertain part is taking place in the spatial distribution of the transport properties. From the engineering point of view, it is crucial to choose an optimum between the safety and costs. These criteria are affected by the combination of technology, knowledge and experience of engineers. The essential parts in the prediction of system behavior is the structure geometry and soil properties, represented here by the earth dam with its subsoil and diffusion coefficient, respectively. Such coefficient is usually determined either by the expert guess or very few test drills, whereas the majority of the subsoil properties remains uncertain. The aim of this contribution is to obtain more information and reduce the risks in the system by introducing a stochastic expansion of the underlying deterministic problem.

Introduction

Uncertainty propagation have become popular approach to investigate and predict behaviour of various systems [4,5]. The progress of computer technology then enables to solve more complex models and consequently to get more information about system itself. Such a complex problem is here represented by the extension of deterministic material model with uncertain inputs, which may take origin in the lack or inaccuracy of measurements.

Groundwater flow model

The system is governed by diffusion equation in following form

$$\begin{aligned} -\nabla_{\mathbf{x}} \cdot (\kappa_m(\mathbf{x},\mathbf{y})\nabla_{\mathbf{x}} u(\mathbf{x},\mathbf{y})) &= \widetilde{f}(\mathbf{x}), \qquad \mathbf{x} \in D,\, \mathbf{y} \in \mathbb{R}^m, \\ \mathbf{n}(\mathbf{x}) \cdot (\kappa_m(\mathbf{x},\mathbf{y})\nabla_{\mathbf{x}} u(\mathbf{x},\mathbf{y})) &= \widetilde{f}_N(\mathbf{x}), \qquad \mathbf{x} \in \partial D_N,\, \mathbf{y} \in \mathbb{R}^m, \\ u(\mathbf{x},\mathbf{y}) &= \widetilde{f}_D(\mathbf{x}), \qquad \mathbf{x} \in \partial D_D,\, \mathbf{y} \in \mathbb{R}^m, \end{aligned} \tag{1}$$

where the uncertain term is introduced by material parameter $\kappa_m(\mathbf{x},\mathbf{y})$ [m/s], which in our case consists of log-normally distributed random variables. Spatial discretization is conducted using finite elements and Karhunen-Loève expansion [2] with exponential covariance core is used for stochastic discretization.

The relevant tasks in terms of reliability of such structures are basically the probability of occurrence and position of seepage point and probability of exceeding a critical value of velocity for certain type of soil. With a little additional effort, one can reconstruct the probability density function of the solution in each node of finite element mesh which represents a transformation of random inputs by given equation Eq. 1. Aforementioned relevant quantities can be therefore derived from the probability density function of the solution.

One can also derive basic statistical moments of the solution, i.e. the variance and mean of hydraulic heads, see Fig. 1 and Fig. 2 respectively.

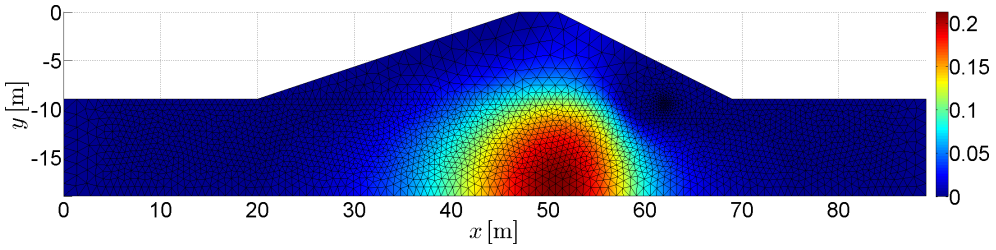

Fig. 1: Variance of hydraulic heads u [m^2]

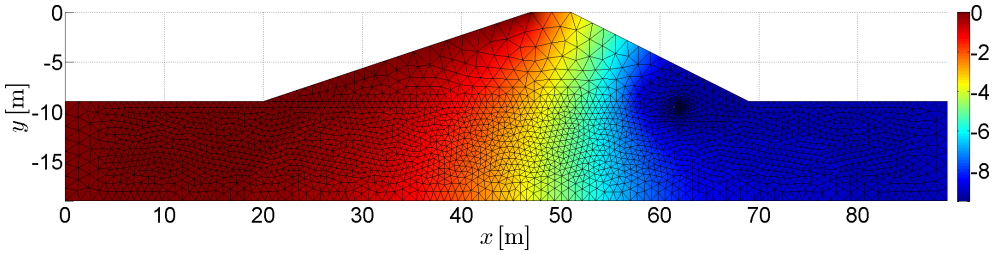

Fig. 2: Mean of hydraulic heads u [m]

Acknowledgements: The support by the Czech Science Foundation through project No. 15-07299S is gratefully acknowledged. We would also like to thank the Grant Agency of the Czech Technical University in Prague, grant No. SGS15/030/OHK1/1T/11.

References

[1] Y. Zhang, Groundwater flow and solute transport modeling, Dept. of Geology and Geophysics, University of Wyoming, 2011.

[2] D. Xiu, Numerical methods for stochastic computations: a spectral method approach, Princeton University Press, 2010.

[3] R.G. Ghanem, P.D. Spanos, Stochastic Finite Elements: A Spectral Approach, Springer New York, 1991.

[4] A. Keese, Numerical solution of systems with stochastic uncertainties. A general purpose framework for stochastic finite elements, PhD thesis, Department of Mathematics and Computer Science, TU Braunschweig, Germany, 2003.

[5] B. Rosić, Variational Formulations and Functional Approximation Algorithms in Stochastic Plasticity of Materials, PhD thesis, Department of Mathematics and Computer Science, TU Braunschweig, Germany, 2013.

Evaluation of Fracture Tests of Concrete Specimens via Advanced Tool for Experimental Data Processing

Ivana Havlikova[1,a] *, Petr Frantik[1,b], Jan Masek[1,c], Jakub Sobek[1,d], Hana Simonova[1,e], Vaclav Vesely[1,f], Zbynek Kersner[1,g], Stanislav Seitl[2,h], Ildiko Merta[3,i], Andreas Schneemayer[3,j]

[1]Brno University of Technology, Faculty of Civil Engineering, Institute of Structural Mechanics, Veveri 331/95, 602 00 Brno, Czech Republic

[2]Academy of Sciences of the Czech Republic, v. v. i., Institute of Physics of Materials, Zizkova 22, 616 62 Brno, Czech Republic

[3]Vienna University of Technology, Faculty of Civil Engineering, Institute for Building Construction and Technology, Karlsplatz 13/206-4, A-1040 Vienna, Austria

[a]havlikova.i@fce.vutbr.cz, [b]kitnarf@centrum.cz, [c]MasekJ3@study.fce.vutbr.cz, [d]sobek.j@fce.vutbr.cz, [e]simonova.h@fce.vutbr.cz, [f]vesely.v1@fce.vutbr.cz, [g]kersner.z@fce.vutbr.cz, [h]seitl@ipm.cz, [i]ildiko.merta@tuwien.ac.at, [j]andreas.schneemayer@tuwien.ac.at

Keywords: Concrete, wedge splitting test, processing of data, Double-*K* fracture model.

Abstract: Cement-based composites are traditionally used building materials. Concrete is the basic representative of this type of materials which exhibit the so called quasi-brittle response. Quantification of mechanical fracture parameters is performed using fracture tests on specimens with a stress concentrator. Load versus crack mouth opening displacement (*P–CMOD*) diagrams are recorded during these tests. In order correctly to evaluate these diagrams an advanced own developed software tool was used for the data filtering and appropriate modifications. In this paper, the programmed Java utility is generally introduced and its utilization demonstrated on the set of recorded *P–CMOD* diagrams, which are further evaluated using Double-*K* fracture model.

Introduction

Concrete is the most commonly used material in civil engineering structures. Its resistance to stable crack propagation expressed via values of mechanical fracture parameters such as fracture toughness, fracture energy, tensile strength, modulus of elasticity etc., is quantified through evaluation of fracture tests on specimens with a stress concentrator – typically the three-point bending test or wedge splitting test (WST). Records from these experiments in the form of diagrams showing load versus deflection or load versus crack mouth opening displacement (*P–CMOD* diagrams) are evaluated using one of relevant fracture models; the *P–CMOD* data are typically processed/purified for further analysis.

Double-*K* fracture model presents one of such approaches; it combines concepts of the cohesive crack model and the equivalent elastic crack model. Its advantage is that it describes different levels of crack propagation: an initiation part which corresponds to the beginning of stable crack growth (at the level where the stress intensity factor, K_{Ic}^{ini}, is reached), and a part featuring unstable crack propagation (after the unstable fracture toughness, K_{Ic}^{un}, has been reached).

In the presented research, the GTDiPS software for filtering and other modifications the recorded diagrams is introduced in general features. Subsequently, this software is applied on the set of *P–CMOD* diagrams from wedge splitting tests on concrete specimens. Further, in this way the modified diagrams are evaluated using Double-*K* fracture model.

Fracture tests and methods of evaluation of the recorded data

Cube-shaped specimens were prepared and subjected to wedge splitting test (see Fig. 1) at the Research Center of Building Construction and Maintenance, Vienna University of Technology (TU Wien). For details of the concrete mixture, specimen curing and preparation for the fracture test see the full-length paper.

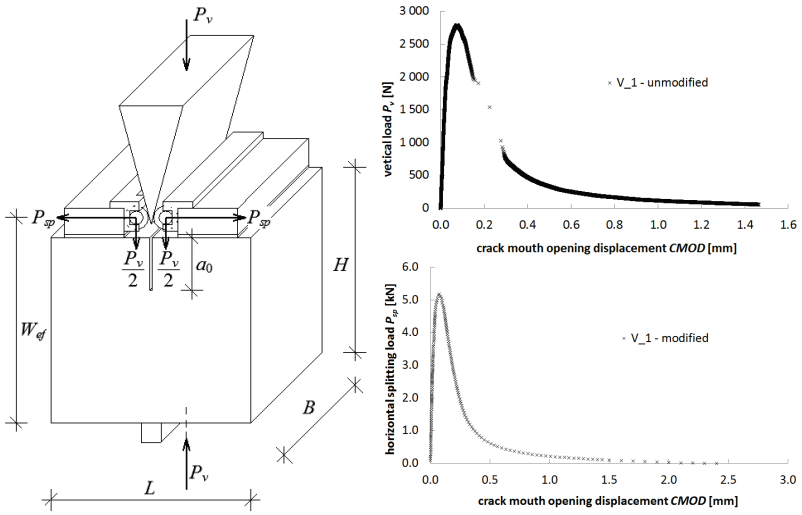

Fig. 1: Wedge splitting fracture test geometry (a), recorded P_v–*CMOD* curve (b), processed P_{sp}–*CMOD* curve (c)

The GTDiPS application serves for processing extensive point sequences by using advanced transformation methods. Each point sequence may contain an arbitrary number of dimensions. The GTDiPS application offers an intuitive GUI for efficient work with transformation methods as well as for browsing and saving the results. The recorded P_v–*CMOD* point sequences (see Fig. 1b) are purified and transformed by a number of implemented techniques into P_{sp}–*CMOD* sequences for their further processing via fracture models.

From the processed diagrams the input data for the Double-*K* fracture model were deducted, i.e. the maximum load $P_{sp,max}$ and its corresponding critical crack mouth opening displacement $CMOD_c$, and the load $P_{sp,i}$, which is deducted from the linear part of the diagram, and its corresponding $CMOD_i$ value. Subsequently, the unstable fracture toughness K_{Ic}^{un} and the cohesive fracture toughness K_{Ic}^{c} were calculated. For details on the numerical procedure with the implemented Double-*K* fracture model see the full length paper. Note that special shape function (*K*-calibration curve) for calculation of the values of fracture toughness and compliance function for calculation of the value of critical effective crack length were created for the utilized test geometry based on ANSYS FEM calculations.

Results

Mean values (and coefficients of variation) of selected results – after eliminating far-off measurements – are summarized in Table 1: elasticity modulus *E*, fracture toughness K_{Ic}^{un}, and the K_{Ic}^{ini}/K_{Ic}^{un} ratio, i.e. the ratio expressing the resistance to stable crack propagation, respectively.

Table 1: Mean values of selected parameters (coefficients of variation in %)

	E [GPa]	K_{Ic}^{un} [MPa·m$^{1/2}$]	K_{Ic}^{ini}/K_{Ic}^{un} [–]
V set	28.4 (9.1)	0.941 (9.5)	0.204 (30.3)

Acknowledgement: This paper has been worked out under the project No. LO1408 "AdMaS UP – Advanced Materials, Structures and Technologies", supported by Ministry of Education, Youth and Sports under the „National Sustainability Programme I" and under the project GAČR 13-03662S (FRAPA) supported by Grant Agency of the Czech Republic.

21st International Conference **ENGINEERING MECHANICS 2015**
Svratka, Czech Republic, May 11 –14, 2015
Paper **#180, pp. 88–89**

CFD Analysis of the Coolant Flow in Fuel Assembly of the VVER1000 Type Reactor

Václav Heidler[a], Jan Vimmr[b], Ondřej Bublík[c]

[1]Department of Mechanics, Faculty of Applied Sciences, University of West Bohemia, Univerzitni 8, 306 14 Pilsen, Czech Republic

[a]v.heidler@kme.zcu.cz, [b]jvimmr@kme.zcu.cz, [c]obublik@kme.zcu.cz

Keywords: lattice Boltzmann method, incompressible Newtonian fluid, fuel assembly, grid-to-rod fretting

Abstract: The paper deals with the simulation of 3D coolant flow in a fuel assembly of the reactor VVER 1000 of the Temelín Nuclear Power Plant. Because of a very complex geometry and a large computational domain, it is a very computationally-demanding task. With this in mind, some measure of simplification is inevitable. The mathematical model of 3D coolant flow is solved using in-house software based on the lattice Boltzmann method.

Introduction

Due to the transverse coolant flow in the core of a pressurized water reactor (PWR), fuel rods are excited to oscillate. Provided that there are some inaccuracies in manufacturing of fuel rods and grids, it is quite likely that the mechanical vibrations cause excessive wear of their cladding in the areas of contact with the grids. This grid-to-rod fretting phenomena (GRTF) can, during the operation, results in breaking the first safety barrier with subsequent leakage of fissile products into the primary coolant. Predictive simulations of GRTF involve turbulence flow, structural dynamics, contacts and wear.

The aim of the present study is to compute the turbulent flow in the fuel rod assembly using the lattice Boltzmann method (LBM) to find out if it is an appropriate numerical method for this type of computationally-demanding calculations.

Methods

The lattice Boltzmann equation is directly derived from the Boltzmann equation, which describe the time evolution of the particle distribution function $f = f(\boldsymbol{x}, \boldsymbol{u}; t)$, by discretization in both time and phase space.

$$f_\alpha(t + \Delta t, \boldsymbol{x} + \boldsymbol{e}_\alpha \Delta t) = f_\alpha(t, \boldsymbol{x}) + \Omega_\alpha, \tag{1}$$

where f_α, α = 1,2,…19 are the distribution functions corresponding to each microscopic velocity. We discuss the D3Q19 model, which is shown in Fig.1. The collision operator on the right-hand side of Eq. (1) is for the multi-relaxation time model [4]

$$\boldsymbol{\Omega} = \boldsymbol{M}^{-1}\boldsymbol{S}[(\boldsymbol{M}\boldsymbol{f}) - \boldsymbol{m}^{\boldsymbol{eq}}]. \tag{2}$$

Matrix $\boldsymbol{M}$ is the transformation matrix composed of the 19 orthogonal basis vectors. The moments of distribution functions $\boldsymbol{m} = \boldsymbol{M}\boldsymbol{f}$ are labeled as

$$\boldsymbol{m} = \left(\rho, e, \epsilon, j_x, q_x, j_y, q_y, j_z, q_z, 3p_{xx}, 3\pi_{xx}, p_{ww}, \pi_{ww}, p_{xy}, p_{yz}, p_{xz}, m_x, m_y, m_z\right). \tag{3}$$

$\boldsymbol{m}^{eq}$ is the vector composed of the equilibrium moments given in Eq. (4) and $\boldsymbol{S}$ is the diagonal collision matrix containing collision parameters (the eigenvalues of the collision matrix $\boldsymbol{M}^{-1}\boldsymbol{S}\boldsymbol{M}$). The some recommended values can be found in [4].

$$
\begin{aligned}
m_0^{eq} &= \rho, \\
m_3^{eq} &= \rho_0 u_x, \\
m_5^{eq} &= \rho_0 u_y, \\
m_7^{eq} &= \rho_0 u_z, \\
m_1^{eq} &= e^{eq} = \rho_0\left(u_x^2 + u_y^2 + u_z^2\right), \\
m_9^{eq} &= 3p_{xx}^{eq} = \rho_0\left(2u_x^2 - u_y^2 - u_z^2\right), \\
m_{11}^{eq} &= p_{zz}^{eq} = \rho_0\left(u_y^2 - u_z^2\right), \\
m_{13}^{eq} &= p_{xy}^{eq} = \rho_0 u_x u_y, \\
m_{14}^{eq} &= p_{yz}^{eq} = \rho_0 u_y u_z, \\
m_{15}^{eq} &= p_{xz}^{eq} = \rho_0 u_x u_y,
\end{aligned} \qquad (4)
$$

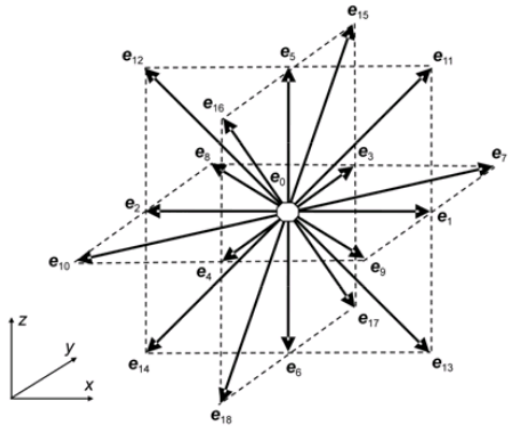

Fig. 1: D3Q19 lattice model

where ρ_0 is a constant density and ρ a density variation. The macroscopic quantities density and momentum are given by

$$\rho = \sum_\alpha f_\alpha, \qquad \rho_0 \boldsymbol{u} = \rho_0 \sum_\alpha \boldsymbol{e}_\alpha f_\alpha. \qquad (5)$$

Summary

We have implemented the lattice Boltzmann method for solving large-eddy simulation of the coolant flow in the fuel assembly using multiple-relaxation-time model, recursively refined meshes using hierarchical block structured grids and parallelization using Coarray Fortran. Next task is to add energy equation into our in-house software and consequently the buoyancy force.

The obtained numerical results will be presented and discussed in detail at the conference.

Acknowledgement: This study was supported by the internal student grant project SGS-2013-036 of the University of West Bohemia.

References

[1] L. Sandoval, D.Walter, Revisiting grid refinement algorithms for thelattice Boltzmann method, Thèse de doctorat, Univ. Genève, 2012, no. Sc. 4520.

[2] P.A. Skordos, Initial and boundary conditions for the lattice Boltzmann method, Phys.Rev. E 48 (1993) 4823-4842.

[3] J. Tölke, M. Krafczyk, M. Schulz, E. Rank, Lattice Boltzmann simulations of binary fluid flow through porous media. Philos Trans Roy. Soc. Lond. A 360 (2002) 535–545.

[4] D. d'Humie`res, I. Ginzburg, M. Krafczyk, P. Lallemand, L-S. Luo, Multiple-relaxation-time lattice Boltzmann models in three dimensions, Philos. Trans. Roy. Soc. Lond. A 360 (2002) 437–451.

[5] L-S. Luo, Unified theory of the lattice Boltzmann models for nonideal Gases, Phys. Rev. Lett. 81 (1998) 1618–1621.

[6] O. Filippova, D. Hänel, Boundary-fitting and local grid refinement for LBGK models. Int. J. Mod. Phys. C 8 (1998)1271–1279.

21st International Conference **ENGINEERING MECHANICS 2015**
Svratka, Czech Republic, May 11 –14, 2015
Paper **#227, pp. 90–91**

Engineering Properties of Alkali Activated Fly Ash Foams

Petr Hlaváček[a]*, Vít Šmilauer[b], Jan Vorel[c]

Faculty of Civil Engineering, Czech Technical University in Prague, Thákurova 7, 166 29, Prague 6, Czech Republic

[a]petr.hlavacek@fsv.cvut.cz, [b]vit.smilauer@fsv.cvut.cz, [c]jan.vorel@fsv.cvut.cz

Keywords: alkali activation, foam, Young's modulus, compressive strength, thermal conductivity

Abstract: Inorganic foams were prepared from alkali activated fly ash and aluminum powder blowing agent. Curing process was accelerated by thermal treatment at 80 °C for 12 hours. Bulk densities ranged between 420 and 800 kg/m^3, depending on batch proportions. Compressive strength was found in the range 3.7-9.0 MPa, Young's modulus 0.6-1.1 GPa, thermal conductivity 0.14-0.16 W/m/K. Young's modulus was reproduced using 2D numerical simulations and analytical homogenizations.

Introduction

The cement-based autoclaved aerated concrete (AAC) is a lightweight inorganic construction material, in Europe well known since 1920's. A Swedish architect Johann Erikksson patented the AAC in 1923. Fly ash-based foam was first mentioned in Costopoulos' patent in 1987 [1, 2, 3].

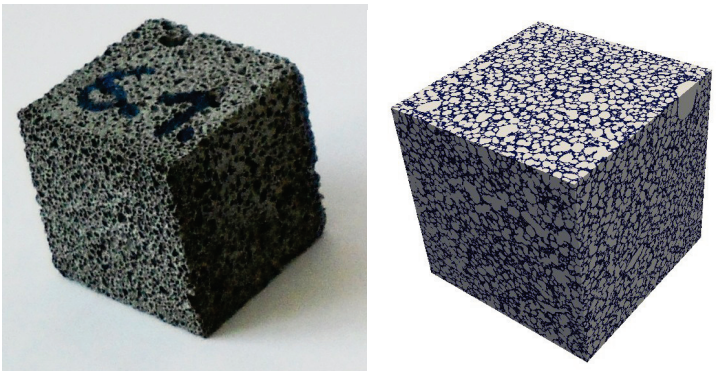

Fig. 1: Left, typical specimen of alkali activated fly ash foam, bulk density 600 kg/m^3, porosity 75%. Right, visualization of CT-scanned foam microstructure.

This work aims at reproduction of measured Young's modulus of alkali-activated fly ash foam (FAF). The FAF is Portland cement-free inorganic foam synthesized at temperatures below 80°C from alkali-activated fly ash and aluminum powder as a blowing agent [4]. Hydrogen liberation during the activation process leads to a closed-pore network. Figure 1 shows a typical FAF specimen.

Results

Finite element simulations on 2D representations and analytical homogenizations aimed at reproducing the FAF elasticity. The intrinsic Young's modulus of alkali-activated paste is of 35.35 GPa and the Poisson's ratio is set at 0.2 [4]. The numerical simulations were done on 2D regular mesh with 500x500 elements with an element size 40 μm. The horizontal edges are loaded by prescribed displacement, while the vertical edges are kept free; averaged vertical stress and strain provide the effective Young's modulus. Mori-Tanaka method and self-consistent scheme [5] were used in the analytical homogenizations.

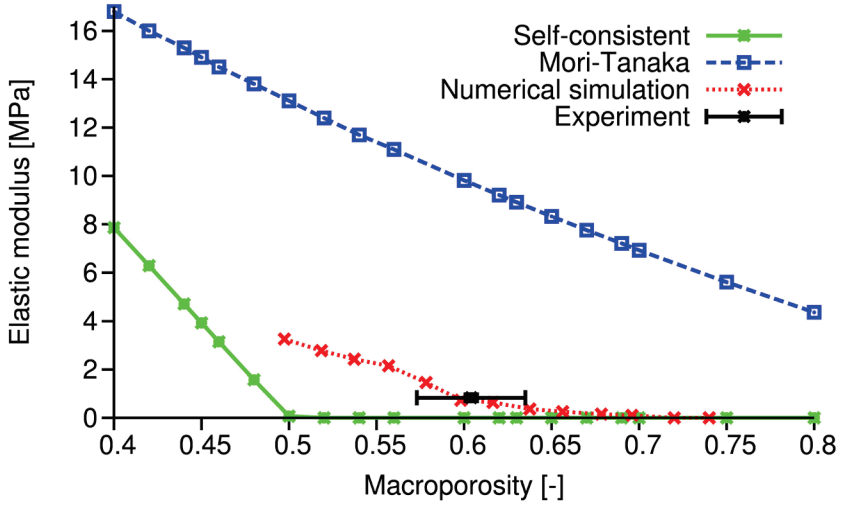

Fig. 2: Comparison of analytical homogenizations of effective Young's modulus of fly ash foam with numerical prediction and measured data.

Additionally, thermal conductivity was reproduced using FFT-based Galerkin method by Jaroslav Vondřejc, CTU in Prague [6].

Acknowledgement: This publication was supported by the European social fund within the framework of realizing the project "Support of inter-sectoral mobility and quality enhancement of research teams at Czech Technical University in Prague", CZ.1.07/2.3.00/30.0034. Period of the project´s realization 1.12.2012 – 30.6.2015.

References

[1] N.G. Costopoulos, H.K. Newhouse, Building material manufacturing from fly ash, U.S. Patent 4,659,385. (1987)

[2] R.C. Pytlik, J. Saxena, Autoclaved Cellular Concrete: The Building Material for the 21st Century. In: F.H. Wittmann (Ed.), Advances in autoclaved aerated concrete, Rotterdam/Brookfield: A.A. Balkema, 1992 pp. 1-18.

[3] N. Narayanan, K. Ramamurthy, Structure and properties of aerated concrete: a review, Cement and Concrete Composites 22 (2000) 321–329.

[4] P. Hlaváček, V. Šmilauer, F. Škvára, L. Kopecký, R. Šulc, Inorganic foams made from alkali-activated fly ash: Mechanical, chemical and physical properties, Journal of the European Ceramic Society 35 (2015) 703–709.

[5] A. Zaoui, Continuum Micromechanics: Survey, Journal of Engineering Mechanics 128 (8) (2002) 808–816.

[6] J. Vondřejc, J. Zeman, I. Marek, Guaranteed upper-lower bounds on homogenized matrix by FFT-based Galerkin method, (2014), submitted for publication (2015), arXiv:1404.3614.

21st International Conference **ENGINEERING MECHANICS 2015**
Svratka, Czech Republic, May 11 –14, 2015
Paper **#140, pp. 92–93**

Unsteady Flow Past a Circular Cylinder Using Advanced Turbulence Models

Jiří Holman

CTU in Prague, Faculty of Mechanical Engineering, Karlovo náměstí 13, Praha 2, Czech Republic
Jiri.Holman@fs.cvut.cz

Keywords: hybrid RANS-LES, URANS, X-LES, EARSM, TNT, finite volume method, turbulent flow

Abstract: This work deals with the numerical simulation of unsteady compressible turbulent flow past a circular cylinder. Turbulent flow is modeled by two different methods. The first is based on the system of URANS equations closed by the two equation TNT model or modified EARSM model. Second method is based on the X-LES model which is a hybrid RANS-LES method. Numerical solution is obtained by the finite volume method. Presented results are for the subcritical turbulent flow characterized by Re=3900.

Introduction

Compressible turbulent flows are described by the system of Navier-Stokes equations [1]. Numerical solution leads to the direct numerical simulation which resolves all turbulent scales. Unfortunately, this approach is usually unusable even for the cases with low Reynolds numbers because very accurate numerical method and very fine mesh are required. Another option is modeling of turbulent effects. The first modeling aproach in this work is based on the unsteady Reynolds averaged Navier-Stokes equations (URANS, [2]) where all turbulent scales are modeled by the model of turbulence. Second approach is a hybrid method which uses URANS equations together with model of turbulence when computational mesh is coarse and large eddy simulation (LES, [2]) when computational mesh is fine enough for direct resolution of turbulent scales.

Models of turbulence and numerical method

We are using two different models of turbulence in the case of full URANS approach. The first model is Kok's two equation TNT k-ω model [3]. Second one is explicit algebraic model of Reynolds stresses (EARSM, [4]) which is based on the TNT model equations with recalibrated model constants which are more suitable in conjunction with the EARSM model [5]. Hybrid RANS-LES method is the XLES model [6] which consists from the k-equation subgrid-scale model used in the LES regions and TNT model [3] used in the URANS regions.

Numerical solution is obtained by the second order finite volume method. Inviscid fluxes are approximated by the HLLC scheme [7] with MUSCL reconstruction [8]. Viscous fluxes are approximated by central differencing on the dual mesh [7]. For advancing in time the explicit two stage TVD Runge-Kutta method is used [7].

Results and conclusion

Solved case is a flow of the air past a circular cylinder with diameter $D = 6.18 \cdot 10^{-4}$ m and inlet Mach number $M_\infty = 0.3$. This regime corresponds to Reynolds number $Re = 3900$. For the numerical

Table 1: Evaluation of Strouhal number for the flow past a circular cylinder with $Re = 3900$.

Model	URANS TNT	URANS EARSM	X-LES	Experiment
St	0.197	0.215	0.212	0.215± 0.005

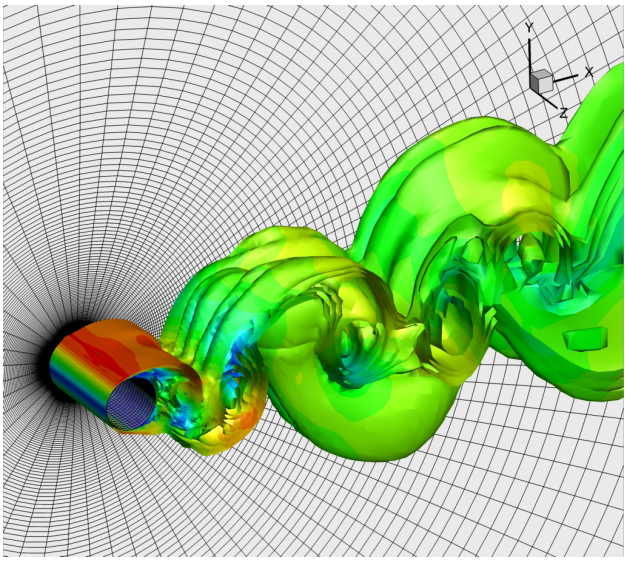

(a) Instantaneous vorticity magnitude isosurfaces in time $t = 10^{-3}s$, X-LES model.

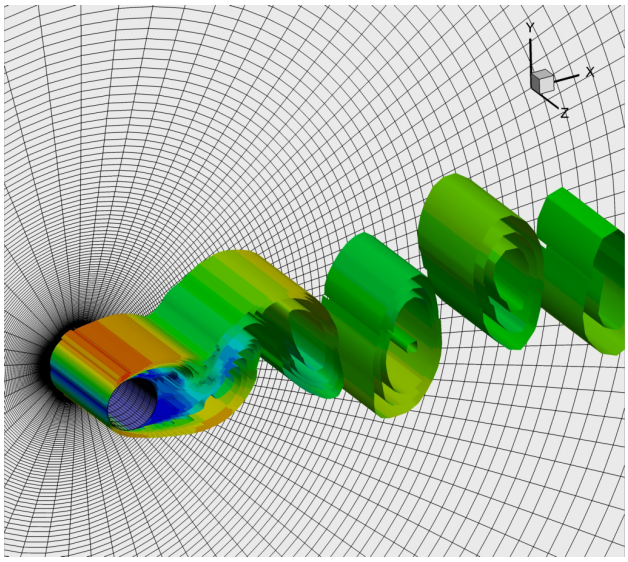

(b) Instantaneous vorticity magnitude isosurfaces in time $t = 10^{-3}s$, EARSM model.

Fig. 1: Numerical solution of turbulent flow past a circular cylinder, $Re = 3900$.

solution is used structured O-type grid with 290304 cells. Fig. 1 shows comparison of instantaneous vorticity magnitude colored by velocity magnitude. Strouhal number is evaluated in Table 1. Results show that both X-LES and EARSM models are able to predict correct Strouhal number but X-LES model provides more detailed full three-dimensional flow field.

Acknowledgment: The work was supported by the Grant no. GAP101/12/1271 and Grant no. P101/10/1329 of the Grant Agency of Czech Republic.

References

[1] J. H. Ferziger, M. Peric, Computational Methods for Fluid Dynamics. Springer, 1999.

[2] D. C. Wilcox, Turbulence Modeling for CFD, DCW Industries, Inc. La Canada, California, 1994.

[3] J. C. Kok, Resolving the Dependence on Freestream Values for $k = \omega$ Turbulence Model. AIAA Journal, 38 (2000) 1292–1295.

[4] S. Wallin, Engineering turbulence modeling for CFD with focus on explicit algebraic Reynoldes stress models, disertation thesis, Royal Institutte of Technology, 2000.

[5] J. Holman, J. Fürst, Numerical Simulation of Compressible Turbulent Flows Using Modified EARSM model, Numerical Mathematics and Advanced Applications - ENUMATH 2013, Springer, 2014.

[6] S. H. Peng, W. Haase, Advances in Hybrid RANS-LES Modeling. Springer, 2007.

[7] J. Holman, Numerical solution of compressible turbulent flows in external and internal aerodynamics. Diploma thesis CTU in Prague, 2007 (in Czech).

[8] H. Deconinck, E. Dick, Computational Fluid Dynamics 2006, Springer, 2006.

21st International Conference **ENGINEERING MECHANICS 2015**
Svratka, Czech Republic, May 11 –14, 2015
Paper **#144, pp. 94–95**

Analysis of Machine Tool Spindles under Load

Michal Holub[1,a]*, Jan Vetiska[1,b], Josef Knobloch[1,c], Petr Minar[2,d]

[1]Institute of Production Machines, Systems and Robotics, Brno University of Technology, Technicka 2896/2; 619 69, Brno; CZ

[2]Intemac Solutions s.r.o., Blanenska 1288/27, 664 34, Kurim, CZ

[a]holub@fme.vutbr.cz, [b]vetiska@fme.vutbr.cz, [c]knobloch@fme.vutbr.cz, [d]minar@intemac.cz

Keywords: spindle error, machine tool, multi-body model, measurement

Abstract: This paper deals with a new experimental approach to analyze radial, axial and tilt error motions of machine tool spindles under load. This work focuses on the identification error of the spindle movements under different machine operation conditions between 500 - 5000 rev / min and loads in range 50 - 500 N. Errors of the spindle movements are measured on cylindrical workpiece using capacitance sensors for different loads. The analysis of measurements of radial, axial and tilt error motions of machine tool spindle indicates dependence between loads and measured errors. The integration of the error measurements to novel multi-body dynamic models of machine tool spindles is very important for prediction of machine behavior during a cutting process.

Introduction

Spindles belong to the most important structural nodes of machine tools (MT). Running accuracy of the spindle of turning and milling machines has a major impact on resulting geometric and dimensional accuracy of a future workpiece. To these structural nodes of MT significant challenges are posed concerning parameters of performance, accuracy and service life [1]. In terms of the optimal spindle design for a cutting process, activities are performed in the area of static stiffness, dynamic behavior improvement, temperature stability and geometric accuracy of spindles. For simulation models of spindles and their verification various methods of measurement and identification of necessary parameters are introduced, such as the necessity to identify the external conditions entering the simulation models. Publications [2] deal with the proposal for temperature and static models of machine tool spindles. The models then provide information on rotation and displacement of axes, which are experimentally verified by laser and capacitance proximity sensors.

Another area of research is design of appropriate measurement methods and the use of various technologies to collect information about sought variables. Publication [3] describes the use of a magnetic load of a measurement artefact for causing a loading force on the spindle with a maximum load of 1.000 N. The observed deviation is only a radial one and describes spindle stiffness. Measurement of the radial deviation is described for high speed spindles in publication [4]. The paper presents test of running accuracy of spindles in the unloaded condition. The contemporary measuring procedures do not allow to assess the impact of the load on the running accuracy of the spindle.

Task formulation

Concerning precise MT, a great deal of emphasis is placed on running accuracy of machine tool spindles. One of the tasks is to control the accuracy of spindles by defined load conditions during the production stage. Another task is to increase the performance, reliability and accuracy of new machine tool spindles. This objective can be achieved at the spindle

design stage by means of various computing devices. One of the tools that can be used for creating models and simulations is Multi-body system (MBS). On the basis of simulation runs optimal construction of machine tools spindles can be designed. This publication introduces the measurement of running accuracy of spindles at a defined speed and with radial static load. It also mentions the outputs of a model created in MBS. The load size of a spindle caused by operation conditions is chosen according to publication [5]. Concerning small milling machines, the cutting force ranges from 300 - 800 N depending on depreciation of the tool, passive force of 50 - 150 N, normal force of 250 - 500 N, with a cutting speed of 35 m/min and work piece material with a diameter of 1. 8159.

Multi-body dynamic model

MBS modelling is one of the possible approaches to creating complex models of parts and also whole MT. It enables to include compliant behavior in the models as well [6]. Creating a quality model requires its verification. For testing of behavior of new MT in development it is necessary to gain testing data by measurement. The model of a spindle is assembled according to V-model VDI 2206 and static and dynamic behaviour are both monitored there. The CAD data of MCV 754 QUICK machine were used as input and the complete model was designed for SW ADAMS. See Fig. 1 for the verification of static stiffness of the spindle without the change of rotation.

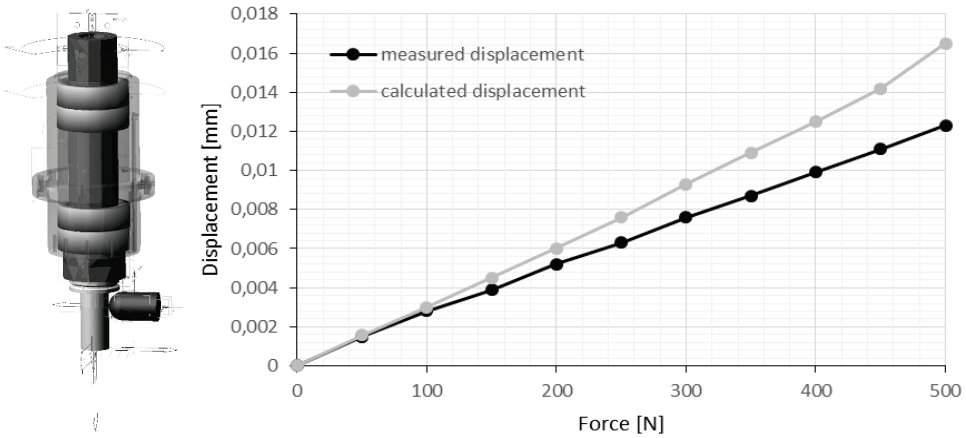

Fig. 1: Dependence of displacement of a spindle on radial load at rest

References

[1] E. Abele, Y. Altintas, C. Brecher, Machine tool spindle units. CIRP Ann - Manuf Technol 59 (2010) 781–802.

[2] E. Uhlmann, J. Hu, Thermal Modelling of a High Speed Motor Spindle. Procedia CIRP 1 (2012) 313–318.

[3] A. Matsubara, T. Yamazaki, S. Ikenaga, Non-contact measurement of spindle stiffness by using magnetic loading device. Int J Mach Tools Manuf 71 (2013) 20–25.

[4] K. Fujimaki, K. Mitsui, Radial error measuring device based on auto-collimation for miniature ultra-high-speed spindles. Int J Mach Tools Manuf 47 (2007) 1677–1685.

[5] Z. Fiala, M. Piska, A. Jaros, On the analysis of the sound spectrum at machining of the glass-polyester composite material. MM Sci J 2014, p. 201403.

[6] T. Brezina, Z. Hadas, J. Vetiska, Simulation behavior of machine tool on the base of structural analysis in multi-body system. in: Proc. 15th Int. Conf. Mechatronics, MECHATRONIKA 2012, 2012.

21st International Conference **ENGINEERING MECHANICS 2015**
Svratka, Czech Republic, May 11 –14, 2015
Paper **#198, pp. 96–97**

Aero-Acoustic and Vibration Characteristics of Self-Oscillating Artificial Vocal Folds

Jaromír Horáček[1,a*], Vítězslav Bula[1,b], Vojtěch Radolf[1,c], Tomáš Vampola[2,d], Miroslava Dušková[3,e]

[1]Institute of Thermomechanics, ASCR, Dolejškova 5, 18200 Prague, Czech Republic

[2]Department of Mechanics, Biomechanics and Mechatronics, Faculty of Mechanical Engineering, Czech Technical University, Technická 4, 16607, Prague; Czech Republic

[3]Institute of Macromolecular Chemistry, Academy of Sciences of the Czech Republic, Heyrovského nám. 1888/2, 16206 Prague, Czech Republic

[a]jaromirh@it.cas.cz, [b]bula@it.cas.cz, [c]radolf@it.cas.cz, [d]Tomas.Vampola@fs.cvut.cz, [e]m.duskova@imc.cas.cz

Keywords: fluid-structure interaction; flutter; biomechanics of voice; modeling of phonation.

Abstract: The study presents in vitro measurements of phonation characteristics performed on developed 1:1 scaled replica of human vocal folds. The measured aerodynamic, vibration and acoustic characteristics are in good agreement with the values found in humans.

Introduction

Voice production is a complex physical process, which involves airflow coming from the lungs, self-oscillating vocal folds and acoustics of the resonance cavities of the human vocal tract. The vocal folds, excited by the airflow, generate a primary sound which propagates in the airways of the vocal tract modifying its spectrum and producing the final acoustic signal radiated from the mouth. Understanding basic principles of voice production is important for detection of laryngeal pathologies and treatment of laryngeal disorders. The physical models of voice production are important tools for experimental verification of developed theoretical models of phonation and in the development of the vocal folds prosthesis [1].

Method

The vocal folds made of silicon rubber were excited by airflow with synchronous measurement of the flow-induced vocal fold vibrations using laser vibrometer, two high speed cameras, the subglottic dynamic and mean air pressures and the radiated sound. A general scheme of the measurement set up and the used experimental techniques were described in detail in [2]. The airflow coming from the model of trachea was increased step by step from the phonation onset up to the airflow rate and subglottic pressure, which are in the range of physiologically relevant values for a normal human voice production.

Results and summary

The vocal folds model created by a silicon cover filled by a liquid phonated in the interval of the airflow rate $Q \cong 0.08 - 0.6$ l/s and subglottic pressure $P_{sub2} \cong 0.28 - 1.7$ kPa having realistic maximum vibration amplitudes, so-called glottis opening $MaxGO \cong 0 - 2.6$ mm. Corresponding to a bass voice, the fundamental frequency increased with the flow rate from 80 Hz at the phonation onset up to $F_0 \cong 103$ Hz while the peak sound level of the generated acoustic signal at the distance 20 cm from the vocal folds increased from 62 dB up to $L_p \cong 90$ dB.

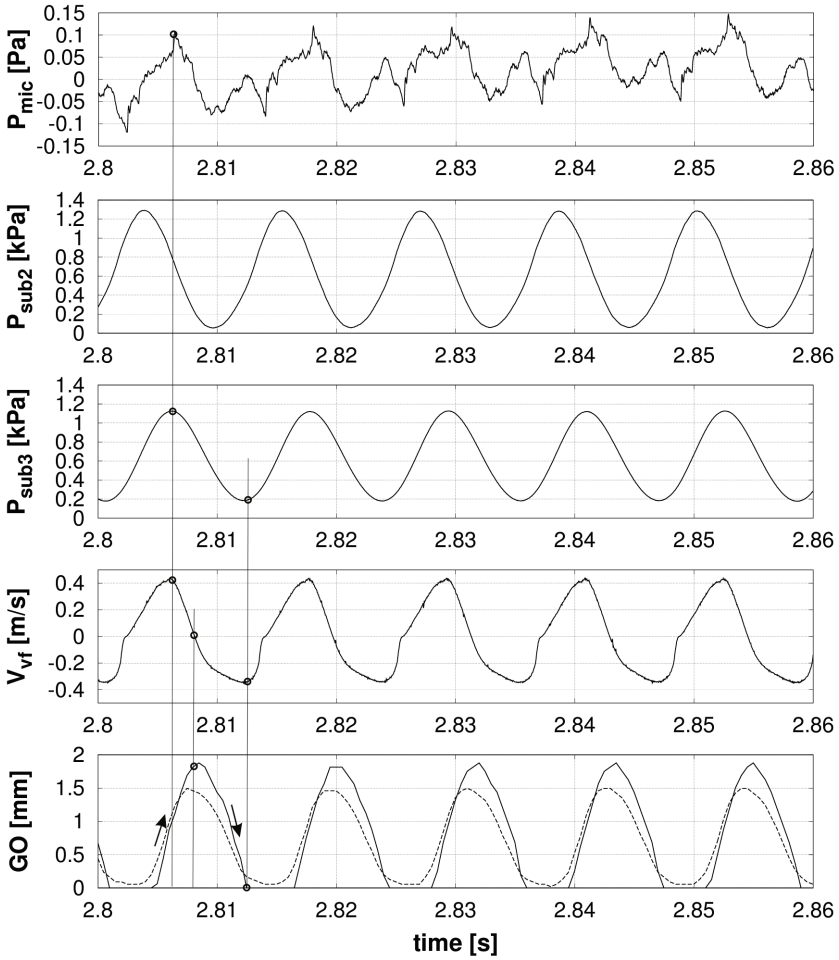

Fig. 1: Measured and evaluated signals for the vibrating vocal folds model for the flow rate Q=0.15 l/s, mean tracheal subglottic pressure P_{sub2}=0.67 kPa and F_0=86 Hz.

Fig. 1 shows the example of the measured signals during phonation. The peaks of the microphone signal (P_{mic}) correlates with the peaks of the vocal folds surface velocity in the vertical direction (V_{vf}) as well as with the subglottic pressure measured just before the glottis entrance (P_{sub3}), which is delayed after the subglottic pressure measured in the trachea (P_{sub2}). The signals of the glottis opening (GO) show that the closed time of the glottis, i. e. when GO=0 for the glottis motion in the horizontal direction (full line), is nearly 0.4 of the vibration period, and that the maximum displacement of the glottis in the vertical direction (dashed line) is slightly phase shifted and corresponds to zero of the vocal folds velocity (V_{vf}=0). The negative maximum of the velocity ($V_{vf}\cong$ -0.35 m/s) is just before the glottis closer where the minimum of the subglottic pressure P_{sub3} exists.

In summary, the results show that the maximum energy from the airflow is transferred to the acoustic energy during the opening phase of the glottis where are the maxima of the subglottic pressure P_{sub3}, the vertical vocal folds velocity V_{vf} and the peak sound level L_p of the sound (P_{mic}).

Acknowledgement: The work has been supported by the grant project GACR No P101/12/1306.

References

[1] G.J. Verkerke, S.L. Thomson, Sound-producing voice prostheses: 150 years of research. Annu. Rev. Biomed. Eng. 16 (2014) 215–45.

[2] J. Horáček, V. Bula, V. Radolf, P. Šidlof, Impact stress in a self-oscillating model of human vocal folds. Advances in Vibration Engineering, 13 pp., accepted 16.10. 2014.

21st International Conference **ENGINEERING MECHANICS 2015**
Svratka, Czech Republic, May 11 –14, 2015
Paper **#199, pp. 98–99**

Performance of Fibre Reinforced Concrete Specimens Subjected to Impact Loading

Alena Horska[a] *, Pavel Jiricek[b], Marek Foglar[c]

CTU in Prague, Faculty of Civil Engineering, Department of Concrete and Masonry Structures,
Thákurova 7, 166 29, Prague, Czech Republic, Tel: +420 224 354 630

[a]alena.horska@fsv.cvut.cz, [b]pavel.jiricek@fsv.cvut.cz, [c]marek.foglar@fsv.cvut.cz

Keywords: fibre-reinforced concrete, impact loading, drop-weight experiment

Abstract: Impact resistance of concrete structures gains high importance nowadays, as the man-made disasters (such as terrorism, car crashes, etc.) occur increasingly. Development and testing of blast and impact resistant materials is highly required. This paper shows outcomes of the experiments focused on FRC performance under impact loading.

Introduction

Besides tensile strength of plain concrete itself, both reinforcement and speed of loading influence tensile resistance of concrete specimen. The dependence of concrete strength on strain rate is expressed by DIF (Dynamic increase factor). To study the effect of high strain rates on FRC specimens, drop-weight experiments were undertaken.

Experimental Set Up

For the experiment tile-shaped concrete samples were prepared. The samples with unified size of 300 x 300 mm differed in thicknesses, varying the values of 30, 60 and 120 mm. The concrete mixture was reinforced with polypropylene or steel fibres. Several samples were reinforced with basalt fabric placed in one or two layers. Also samples with no reinforcement were prepared.

Impact loading of specimens was induced using drop-weigh mechanism. The steel drop-weight consisted of central shaft and several disc attached to it. Variable amount of steel discs enabled to regulate impacting weight (reaching 20.6, 46.4 and 75.2 kg). At the bottom disc the hemispherical tip was attached, so that the impact load was concentrated. The drop-weight was lifted by the hoist to its maximal height of approx. 2.8 m above the tested concrete sample. From its top position the drop-weight was released reaching impact velocity of approx. 7.2 m/s. The specimens were supported on two of their edges by steel beams and were hit in the centre.

Fig. 1: Steel frame with hoist.

Fig. 2: Specimen supported by beams.

Fig. 3: Burden discs of different weights

Evaluation

The progress of deflection of the specimen was captured by high-speed camera. The video record was decomposed into separate frames. The frames were graphically processed to obtain instantaneous velocity of the steel burden. Velocity-time dependence of the burden was plotted. Also the time dependence of deflection of the specimen was obtained.

The deceleration of the burden after collision with the specimen represents impact resistance of the specimen. Specimens causing grater deceleration of the burden prove themselves more impact resistant. The behaviour comparison of samples of different reinforcement but equal thickness and weight of burden was the centre of interest. Knowing the deceleration of the burden, the impact force could be calculated.

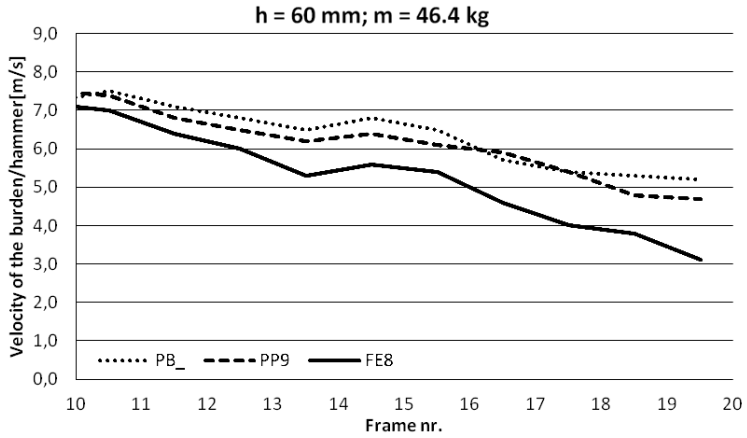

Fig. 4: Behaviour comparison of differently reinforcement specimens.

Fig. 5: Crack pattern of specimen.

One third of all samples of each thickness and reinforcement was subjected to three-point bending test. The mechanical resistance of concrete specimen depends on strain rate; in general, dynamic increase factor (DIF) increases with increasing strain rate.

Numerical simulations

According to the experimental conditions, numerical simulations were prepared. Material models were adopted from previous impact loading experiments. The aim was to validate the used material models in conditions of current experiment and in case of discrepancy between experimental data and simulation to calibrate the material model.

Summary

The aim of this paper is to compare behaviour of differently reinforced FRC samples subjected to impact loading from both experimental and numerical point of view. According to the experimental results, the main factors influencing FRC impact resistance are type, material and volume of the used dispersed reinforcement.

Acknowledgements: The financial support of the Czech Science Foundation grant project 13-30441S is gratefully acknowledged.

21st International Conference **ENGINEERING MECHANICS 2015**
Svratka, Czech Republic, May 11 –14, 2015
Paper **#032, pp. 100–101**

To the Analytical Analysis of the Internal Dynamics of Nonlinear Time Heteronymous Planetary Differential Systems

Milan Hortel[a*], Alena Škuderová[b]

Institute of Thermomechanics, AS CR, v. v. i., Dolejškova 5, 182 00 Prague 8, Czech Republic

[a]hortel@it.cas.cz, [b]skuder@it.cas.cz

Keywords: nonlinear dynamics, time heteronymous systems, damping in gear meshes

Abstract: The light high-speed transmission systems with minimum dimensions and weights may show a wide spectrum of properties extending from the regular - periodic solutions to irregular ones of chaotic character. The method of transformation of differential boundary value problems to equivalent nonlinear integro-differential equations with solving kernels of Green's type and the method of successive approximations are applied for analytical analysis of dynamic phenomena.

Introduction

For example, at a mass discretisation and with lightening holes in the cogwheel discs, the mathematical physical model of weakly and strongly nonlinear parametric, due to damping in gear time heteronymous, planetary transmission systems with spur gears is given by expression, [1]

$$\begin{aligned}&\mathbf{M}\mathbf{v}'' + \left[{}_1\mathbf{K}(\beta,\delta_i,H) + {}_1\mathbf{k}_d(t)\right]\mathbf{v}' + \sum_{K_1>1}\left[{}_{K_1}\mathbf{K}(D,D_i,H) + {}_{K_1}\mathbf{k}_d(t)\right]\left|\mathbf{w}'(\mathbf{v}')\right|^{K_1}\operatorname{sgn}(\mathbf{w}'(\mathbf{v}'))\\ &+ {}_1\mathbf{C}(\varepsilon,\kappa,Y_n,U_n,V_n,H,t)\,\mathbf{v} + \sum_{K>1}{}_K\mathbf{C}(\varepsilon,\kappa,I_n,H,t)\,\mathbf{w}^K(\mathbf{v}) = \mathbf{F}(a_n,b_n,\overline{\varphi},H,t),\quad K_1 = 2;3\end{aligned} \tag{1}$$

where $\mathbf{v}$ means generally the n-dimensional vector of displacement of system, $\mathbf{w}^K(\mathbf{v})$ is the K-th power of vector $\mathbf{v}$ defined by expression $\mathbf{w}^K(\mathbf{v}) = \mathbf{D}(\mathbf{w}(\mathbf{v})\mathbf{w}^{K-1}(\mathbf{v}))$. $\mathbf{D}(\mathbf{w}(\mathbf{v}))$ denotes the diagonal matrix, whose elements at the main diagonal are comprised by elements of vector $\mathbf{w}(\mathbf{v}) \equiv \mathbf{v}$. $\mathbf{M}$ is the matrix of mass and inertia forces, ${}_1\mathbf{K}, {}_1\mathbf{k}_d(t)$ and ${}_{K_1}\mathbf{K}, {}_{K_1}\mathbf{k}_d(t)$ are matrices of linear and nonlinear constant and time variable damping forces, respectively, ${}_1\mathbf{C}$ and ${}_K\mathbf{C}$ are the matrices of quasilinear and nonlinear reversible forces, respectively, $\mathbf{F}(t)$ is the vector of nonpotential external excitation with components a_n, b_n and the phase angle $\overline{\varphi}$. H is the Heaviside's function, which allows to describe the motions (contact bounces) due to strong nonanalytical nonlinearities, for example due to technological tooth backlash $s(t)$. The corresponding *constant* linear or nonlinear coefficients of damping are denoted by β, δ_i or D, D_i, respectively. The linear parametric stiffness functions are denoted by the symbols Y_n, U_n, V_n and nonlinear parametric functions, so-called parametric nonlinearities, by the symbol I_n. ε and κ are the coefficients of the mesh duration, and the amplitude modulation of the *resulting* linear tooth stiffness function $C(t)$, t is the time.

Method of analysis

Based on the quantitative evaluation of each member of vector equation system (Eq.1) of the given planetary system with kinematic constraints, this can transform into form [1], [2]

$$\mathbf{F}(\mathbf{v}) \equiv \mathbf{M}\mathbf{v}'' + {}_1\mathbf{C}(H)_k\,\mathbf{v} = \mu\,\mathbf{V}(\mathbf{v}'',\mathbf{v}',\mathbf{v},\ldots,H,\alpha,t), \tag{2}$$

where μ is a small parameter, $\mathbf{V}$ functional operator containing all nonlinearities, parametric functions, damping and nonpotential excitation sources of vibration, α factor of frequency

variation and ${}_1\mathbf{C}(H)_k$ regular matrix of linear reversible forces (both symmetrical and asymmetrical). For periodic solutions with period 2π, the boundary conditions are then

$$N_{n1} \equiv \mathbf{v}(t+0) = \mathbf{v}(t+2\pi), \qquad N_{n2} \equiv \mathbf{v}'(t+0) = \mathbf{v}'(t+2\pi). \tag{3}$$

Due to limited extent of the contribution, the *successive* approximation method to the differential boundary problem (Eq.2, Eq.3) of equivalent integrodifferential equation system will be indicated for the analytical solution of this deterministic multi-frequency excited system briefly only for the case of a *symmetric* matrix of reversible forces, by means of E.Schmidt's method of split cores.

Introducing normal coordinates $\hat{\mathbf{v}}$, further simultaneous transfer of diagonal matrix $\mathbf{M}$ on unit one $\mathbf{E}$, symmetric matrix ${}_1\mathbf{C}(H)_k$ on the diagonal one ${}_1\hat{\mathbf{C}}(H)_k$ and the introducing Green's influence function (Müller's-Breslau's method) with variables t, ξ complying with the given boundary conditions of solved differential boundary problems, then we get to the differential boundary problem Eq.2, Eq.3 equivalent integrodifferential system of equations after longer calculations and integration both for regular – nonresonant $\lambda_n(H) \neq M_k^2$, and singular - resonant $\lambda_n(H) = M_k^2$ cases, where $\lambda_n(H)$ are the eigen values of boundary problem.

$$\begin{aligned}\hat{v}_n(t) = &\int_0^{2\pi} \left[\frac{\overline{v}_{n0}^2}{\lambda_n(H)} + \sum_{m=1}^{\infty} \frac{\overline{v}_{nm}(t)\,\overline{v}_{nm}(\xi) + \overline{w}_{nm}(t)\,\overline{w}_{nm}(\xi)}{\vartheta_{\lambda_n(H)}^{\lambda_{nm}(H)} \lambda_{nm}(H) - M_m^2} \right] \times \hat{V}_n(\hat{v}'', \hat{v}', \hat{v}, H, \alpha, \xi)\, d\xi \\ &+ \sum_{i=1}^{p} \delta_{\lambda_i(H)}^{M_k^2} \left(r_{2i-1}\overline{v}_{nM}(t) + r_{2i}\overline{w}_{nM}(t) \right),\end{aligned} \tag{4}$$

where the expression in square brackets represents solving the core - *Green's empty resolvent* in an extended sense of word. $\lambda, \overline{v}, \overline{w}$ are eigen values independent on linkage of main part of the system (Eq.2), r_{2i-1}, r_{2i} are then branching parameters resulting from branching equations[2]

$$\begin{pmatrix} r_{2i-1} \\ r_{2i} \end{pmatrix} = \int_0^{2\pi} \hat{v}_n(\xi) \begin{pmatrix} \overline{v}_{nM}(\xi) \\ \overline{w}_{nM}(\xi) \end{pmatrix} d\xi\,. \tag{5}$$

Conclusion

When matrices of reversible forces ${}_1\mathbf{C}(H)_k$ in main part of Eq.2 are asymmetrical, the solution may lead to difficulties, compared with case of a symmetric matrix with the normal coordinates. There is necessary then make the transformation of differential boundary problem and solution integrodifferential equations for linkage dependent main part of Eq.2 in the original coordinates $\mathbf{v}$. For a limited range of paper, will deal with this issue in next expanded publications.

References

[1] M. Hortel, A. Škuderová, Lineární, nelineární – kvadratické a kombinované časově heteronomní tlumení v záběrech ozubení ve vnitřní dynamice nelineárních parametrických soustav, Colloqium Dynamics of Machines 2014, IT AS CR, v.v.i., Prague, Ed. L. Pešek, 53-64.

[2] M. Hortel, Integrodifferentialgleichungen in der Analyse von Phänomenen in nichtlinearen parametererregten Systemen. In: Recent Advances in Mechanics of Solids and Fluids Bd. 1-3, Technische Universität Wien, 28. November 1997.

Acknowledgement: Study has been elaborated with institutional support RVO 61388998 in the Institute of Thermomechanics AS CR, v.v.i. and with TACR support, project Nr. TA04011656.

21st International Conference **ENGINEERING MECHANICS 2015**
Svratka, Czech Republic, May 11 –14, 2015
Paper **#115, pp. 102–103**

Approximate Calculation of Eigen-Values of Linear Viscously Damped System with Passive Damping Element

Stanislav Hračov

Institute of Theoretical and Applied Mechanics AS CR, v.v.i.,
Prosecká 76, 19000, Prague, Czech Republic

hracov@itam.cas.cz

Keywords: complex eigen-solution, non-classical damping, passive damping device

Abstract: The paper presents an approximative method for eigen-solution of non-classically damped linear system representing classically damped structure equipped with passive damping element (viscous damper). The proposed procedure avoids using a numerically demanding state-space approach. It operates in the original dimension of the problem and utilizes the real eigen-modes for its further size reduction. The method is based on the dividing of the damping matrix to classical and non-classical part and the application of the perturbation strategy. The accuracy of the procedure is demonstrated by considering numerical examples.

Theoretical background

The proposed method is based on the division of the damping matrix of the linear viscously damped system, which represents the structure with the damper, in the form:

$$\mathbf{C} = \mathbf{C_p} + \mathbf{d} \cdot \mathbf{d^T}. \tag{1}$$

Matrix $\mathbf{C_p}$ is the proportional part of the damping matrix, while the product consisting of vector $\mathbf{d}$ stands for the non-proportional part arising from the presence of the damper. The eigen-values λ of the complete system are given, see [1], by solving the equation:

$$\frac{1}{\lambda} + \sum_{i=1}^{n} \frac{\tilde{d}_i^{\,2}}{\lambda^2 + \lambda \widetilde{C}_{p_{i,i}} + {\omega_i}^2} = 0, \tag{2}$$

where n is a number of the eigen-modes of the complete system, $\tilde{d}_i$ is given by product of transposed i-th eigen-mode and vector $\mathbf{d}$. Element $\widetilde{C}_{p_{i,i}}$ is i-th diagonal element of modal damping matrix $\widetilde{\mathbf{C}}_p$ calculated from matrix $\mathbf{C}_p$ and ω_i is i-th undamped angular eigen-frequency of the system. The solution of the j-th eigen-value λ_j can be sought in a form:

$$\lambda_j = \lambda_{0,j} + \Delta\lambda_j. \tag{3}$$

Symbol $\lambda_{0,j}$ stands for the known or easily obtained eigen-solution of the same system with e.g. different damping ratio of the damper, while $\Delta\lambda_j$ represents its deviation from the exact solution λ_j. Inserting solution (3) into Eq. (2) and performing few mathematical operations lead to:

$$\begin{aligned} &\prod_{i=1}^{n} \left(\alpha_{i,j} + \beta_{i,j}\Delta\lambda_j + \Delta\lambda_j^2\right) + (\lambda_{0,j} + \Delta\lambda_j) \sum_{l=1}^{n} \tilde{d}_l^{\,2} \prod_{\substack{i=1 \\ i\neq l}}^{n} (\alpha_{i,j} + \beta_{i,j}\Delta\lambda_j + \Delta\lambda_j^2) = 0. \\ &\alpha_{i,j} = \lambda_{0,j}^2 + \lambda_{0,j}\widetilde{C}_{p_{i,i}} + {\omega_i}^2, \qquad \beta_{i,j} = 2\lambda_{0,j} + \widetilde{C}_{p_{i,i}}. \end{aligned} \tag{4}$$

After expansion of Eq. 4 the numerically favorable simplification consisting in keeping only the first or the first two powers of $\Delta\lambda_j$ can be made. Then $\Delta\lambda_j$ is easily calculated and subsequently the eigen-value λ_j can be determined.

Numerical experiments

The accuracy of the suggested approach was analysed for the numerical model of the existing tower with the vibration absorber. The exactness of its calculated eigen-solution was investigated parametrically for a set of various damping ratios of the absorber ($\zeta_d = 0 \div 0{,}9$), while the proportional damping matrix of the tower remained constant (structural damping ratio $\zeta = 0{,}005$). Two approximate eigen-solutions which differed in the selection of the reference values λ_0 in Eq. (3) were calculated. The first selection λ_0 was represented by the eigen-values λ_p corresponding to the classically damped system. In the second case the eigen-values λ_n of the realistically damped system, which were calculated under the assumption of the neglecting of the off-diagonal elements of the modal damping matrix, were chosen. The eigen-values λ_n are often used as the approximate eigen-solution of non-classically damped systems and thus served together with the exact eigen-solution for the comparison and the assessment of the suitability of the proposed method. The accuracy was assessed in terms of the relative errors that were calculated separately for the imaginary and the real part of the eigen-values. The most significant errors for the solutions using the first two powers of $\Delta\lambda$ are depicted in Fig. 1.

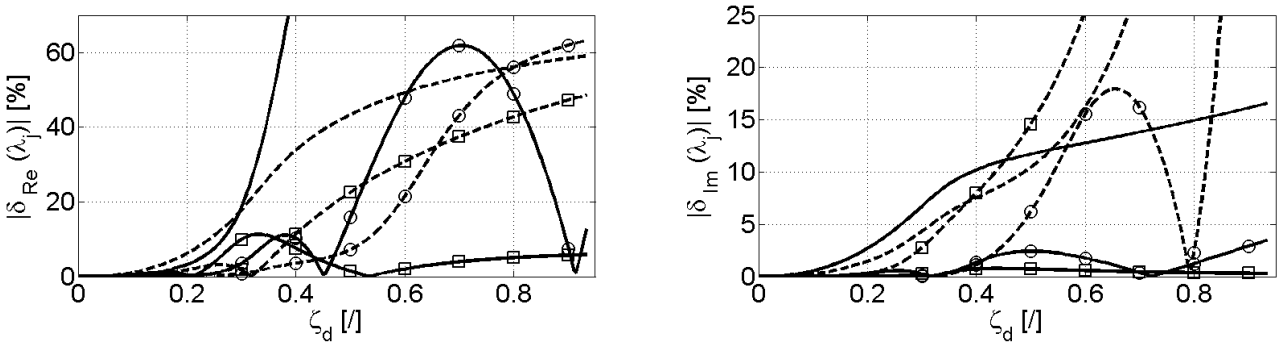

Fig. 1: The percentage relative error of the real (left) and imaginary (right) part of calculated eigen-values λ_j as a function of damping ratio ζ_d (solid line - 2^{nd} eigen-value; dashed line - 3^{rd} eigen-value) (no markers - traditional approximate solution λ_n; ○ - proposed solution based on λ_n; □ - proposed solution based on λ_p)

The comparison of the proposed and the exact eigen-solutions showed higher errors in the real (damping) than in the imaginary (frequency) part of the eigen-values. The method provided acceptable and higher accuracy than the traditional approximate approach in the whole investigated interval of ζ_d for the eigen-values, that were not directly connected with the frequency tuning of the absorber. The significant errors came up for eigen-values which were close to eigen-value of the absorber, i.e. for the second and the third eigen-value. In these cases the method provided sufficient accuracy (below 10%) only in the limited interval in the vicinity of the classical damping ratio. Nevertheless in comparison with the classical approximate solution λ_n the range of the applicability is wider. The best result was reached for the solution using two powers of $\Delta\lambda$ and based on initial values λ_n. In this case the limiting value of the damping ratio of the absorber for which the errors were reasonable was 35%, while for traditional approximative approach it was only 25%. Beyond this value the errors were significant and more sophisticated approach should be employed.

Acknowledgements: The kind support of the Czech Science Foundation project No. 13-41574P and of the RVO 68378297 institutional support are gratefully acknowledged.

References

[1] M. Gürgöze, Proportionally damped systems subjected to damping modifications by several viscous dampers, Journal of Sound and Vibration 255 (2002) 407–412.

21st International Conference **ENGINEERING MECHANICS 2015**
Svratka, Czech Republic, May 11 –14, 2015
Paper **#012, pp. 104–105**

Numerical Solution of Wet Steam Flow through Blade Stage

Vladimír Hric[1,a], Jan Halama[2,b]

[1]Dpt. of Technical Mathematics, FME CTU, Karl. nám. 13, CZ-12135 Prague 2, Czech Republic

[2]Institute of Thermomechanics, AS CR, Dolejškova 5, CZ-18200, Prague 8, Czech Republic

[a]vladimir.hric@fs.cvut.cz, [b]jan.halama@fs.cvut.cz

Keywords: wet steam, nucleation, two-phase, blade

Abstract: We present in a rather simple way an engineering approach to numerical modeling of transonic flow of wet steam through the blade-to-blade channel. Due to the non-equilibrium vapor-to-liquid phase transfer process additional transport equations must be append to the traditional system of equations which describes fluid flow. We limit our flow model to the laminar case (compressible Navier-Stokes equations). Further, we assume zero difference in velocities of vapor and liquid phase (no-slip condition), low mass fraction of liquid phase (less than 8 per-cent) and homogeneous dispersion of droplets in vapor steam. Obtained results are in satisfactory accordance with experimental measurements.

Introduction

When the expansion of a condensable fluid (e.g. dry steam) is rapid and the expansion curve cross the equilibrium saturation, initially superheated steam remains dry until certain supersaturation (or supercooling) is attained. Therefore, naive equilibrium modeling of flow field parameters cannot be used. In the wet region as the expansion and supercooling proceed, critical clusters of molecules of liquid water are continuously created, but these clusters can further grow to the water droplets only if critical work of formation of the second phase is exceeded (otherwise clusters decay). This occurs at the region of maximum supercooling (so-called Wilson region). In the steam turbines condensation occurs in the last stages. Presence of water droplets results in the additional losses and are the cause of blade erosion. Hence, reliable and accurate CFD simulations can be interesting for turbines' manufacturers.

Flow model

Following hyperbolic system of partial differential equations is numerically solved

$$\frac{\partial W}{\partial t}+\frac{\partial F}{\partial x}+\frac{\partial G}{\partial y}=\frac{\partial P}{\partial x}+\frac{\partial R}{\partial y}+S_n+S_g \tag{1}$$

Vectors W, F, G, P, R, S have eight componenents (in 2D) and take the form

$$\begin{aligned}
W &= \{\rho,\rho u,\rho v,\rho E,\rho Q_0,\rho Q_1,\rho Q_2,\rho y\}^T\\
F &= \{\rho u,\rho vu,\rho u^2+p,\rho Eu+pu,\rho Q_0u,\rho Q_1u,\rho Q_2u,\rho yu\}^T\\
G &= \{\rho v,\rho uv,\rho v^2+p,\rho Ev+pv,\rho Q_0v,\rho Q_1v,\rho Q_2v,\rho yv\}^T\\
P &= \left\{0,\tau_{xx},\tau_{xy},u\tau_{xx}+v\tau_{xy}+\lambda\tfrac{\partial T}{\partial x},0,0,0,0\right\}^T\\
R &= \left\{0,\tau_{xy},\tau_{yy},u\tau_{xy}+v\tau_{yy}+\lambda\tfrac{\partial T}{\partial y},0,0,0,0\right\}^T\\
S_n &= \{0,0,0,0,J,r_cJ,r_c^2J,4\pi\rho_\ell r_c^3J/3\}\\
S_g &= \{0,0,0,0,0,\ \ldots\\
&\quad \ldots\ \rho\left(aQ_{-1}+bQ_0+cQ_1\right),2\rho\left(aQ_0+bQ_1+cQ_2\right),4\pi\rho_\ell\rho\left(aQ_1+bQ_2\right)+3c\rho y\}
\end{aligned} \tag{2}$$

where W is vector of conserved variables, F and G are vectors of inviscid fluxes, P and R are vectors of viscous fluxes, S_n is liquid mass source due to nucleation, S_g is liquid mass source due to growth of

droplets, ρ is density of the whole mixture, u and v are components of velocity vector, E is total energy of mixture and consists of internal energy of vapor phase, internal energy of liquid phase, energy stored in the phase interface and kinetic energy of mixture, p is static pressure, Q_i is i-th moment of droplet number distribution function, y is wetness, τ_{ij} are components of shear stress tensor, λ is coefficient of thermal conductivity of vapor phase and T is absolute temperature. This system of equation is solved by the cell-centered finite volume discretisation process with inviscid flux scheme of AUSM type. Symmetrical splitting of Strang is employed in order to resolve stiff character of the system. Closure of the system comprises of equation of state for vapor phase suitable for CFD purposes [6], simple relations for saturated liquid parameters, relation for nucleation rate J [3] and droplet growth model in the form $g(r) = a/r + b + cr$ [5, 4].

Basic results and conclusion

We validate the above mentioned flow model on the flow through Bakhtar cascade [1, 2]. Presented flow model gives slightly shifted zone of nucleation onset comparing to the experimental results. Distribution of wetness and droplet size are in good accordance with other researchers.

Acknowledgments: The support of the grant GA ČR 101/11/1593 and the grant No. SGS13/174/OHK2/3T/12 of CTU in Prague is gratefully acknowledged.

References

[1] F. Bakhtar, M. Ebrahimi, R.A. Webb: On the Performance of a Cascade of Turbine Rotor Tip Section Blading in Nucleating Steam, part 1, Surface Pressure Distributions, IMechE Proc Instn Mech Engrs 209 (1995) 115–124.

[2] F. Bakhtar, M. Ebrahimi, B.O. Bamkole: On the Performance of a Cascade of Turbine Rotor Tip Section Blading in Nucleating Steam, part 2, Wake Traverses, IMechE Proc Instn Mech Engrs 209 (1995) 169–177.

[3] F. Bakhtar, J.B. Young, A.J. White, D.A. Simpson: Classical Nucleation Theory and Its Application to Condensing Steam Flow Calculations, Proc IMechE 219(C) (2005) 1315–1333.

[4] A.J. White: A Comparison of Modelling Methods for Polydispersed Wet-Steam Flow, Int J Numer Meth Engng 57 (2003) 819–834. 1

[5] M.J. Moore, C.H. Sieverding: Two-Phase Steam Flow in Turbines and Separators, Hemisphere Publishing Corp. (1976).

[6] J. Hrubý, J. Pátek, M. Duška, An Analytical Formulation of Thermodynamic Properties of Dry and Metastable Steam Suitable for Computational Fluid Dynamics Modelling of Steam Turbine Flows, J Power and Energy 228 (2014) 120–128.

21st International Conference **ENGINEERING MECHANICS 2015**
Svratka, Czech Republic, May 11 –14, 2015
Paper **#197, pp. 106–107**

Study of Surface Quality and Mechanical Properties of Composite Material Based on Natural Reinforcement

Zuzana Hutyrová[1, 2a*], Dušan Mital'[2,b], Marta Harničárová[1,3,c], Jozef Zajac[2,d], Ján Valíček[3,4,5 e]

[1]Nanotechnology Centre, VŠB – TU Ostrava, Czech Republic

[2]Faculty of Manufacturing Technologies of TUKE with seat in Prešov, Slovakia

[3]Institute of Physics, Faculty of Mining and Geology, VŠB – TU Ostrava, Czech Republic

[4]Institute of Clean Technologies for Mining and Utilization of Raw Materials for Energy Use, VŠB – TU Ostrava, Czech Republic

[5]RMTVC, Faculty of Metallurgy and Materials Engineering, VŠB – TU Ostrava, Czech Republic

[a]zuzana.hutyrova@vsb.cz, [b]dusan.mital@tuke.sk, [c]marta.harnicarova@vsb.cz, [d]jozef.zajac@vsb.cz, [e]jan.valicek@vsb.cz,

Keywords: metrotomography, composite material with natural fiber, mechanical properties

Abstract: The term WPC refers to any composite material containing 2 basic components → natural fibers (used as reinforcements because of their: relatively high strength, rigidity, low cost) and plastics (the key indicator in their manufacture is to establish a sufficiently effective link of components). From the point of view of machinability, WPCs are classified as easy to work materials – as shown in the studies [1-4], etc. However, in machining, the heterogeneity of material plays an important role. Any surface defects arising as a result of "incorrect" machining lead to additional costs for repair. During machining, not only set parameters of the technology of machining process are relevant, but also mechanical properties and compatibility of the material. As an experimental material, wood filled plastic was used with a volume ratio: 30/70 % – HDPE/wooden filling. The profile was subjected to non-destructive testing method by X-rays (inspection by overexposure – to control volume defects) and testing to mechanical properties (tensile and bending test according to ISO 6892, or ISO 178).

Quality of the resulting machined surface is closely linked to the characteristics of the material (whether mechanical or physical). The values of studied mechanical properties change along the extruded profile – as demonstrated by the carried out tests (tensile test and triaxial bending test). The values of ultimate strength of individual samples differ by less than 10 MPa, despite the fact that they have been taken from the central part of the profile parallel to the axis of extrusion (differences are recorded in Tab. 1). The set deformation work is very low as for both uniaxial compressive load, and the tensile load – which may be under selected conditions in practice

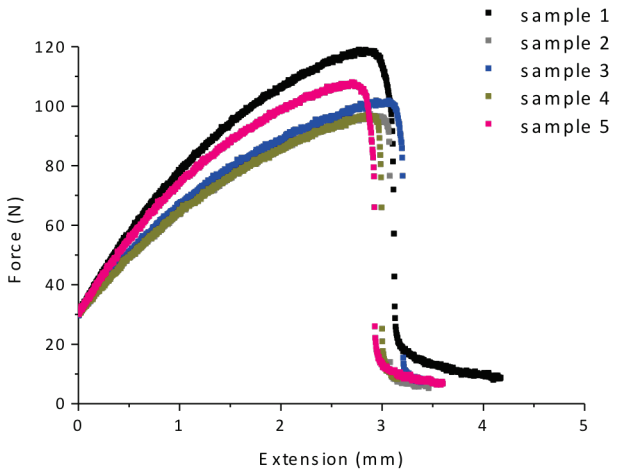

Fig. 1: Load diagram – triax bending test of samples: 1 – 5

Table 1: Values of mechanical properties after tensile testing

No. of sample	Yield point [MPa]	Elogation [%]	Reduction [%]	Deformation work [mJ]
1	24	2.8	2.0	20.4
2	15	2.9	0.4	12.4
3	24	3.4	0.8	24.1
4	15	5.1	0.4	13.5
5	* defect			

*Probably because of the occurrence of a defect, the test sample 5 was already broken at 200 N, so the result is not mentioned.

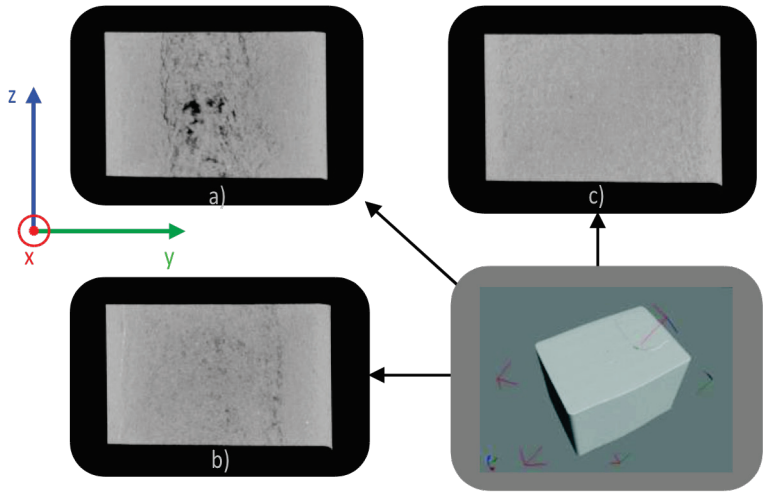

Fig. 2: Cuts in the direction of plane movement in the z-axis at a distance of:
a) 40.5 mm, b) 30.5 mm, c) 20.5 mm (after X-ray inspection)

problematic. The non-destructive examination method using X-rays helps to visualize internal defects in a material – Fig. 2 (porosity, course and shape of cavities). The presented images show changing compatibility of the material (in different cuts). The material compatibility increases from the axis of extrusion (material core) to the edges of the profile. The improper positioning of the turned profile into the area with a high density of "air" bubbles caused their transfer to the surface in a form of cracks, which adversely affected the surface quality and appearance.

Acknowledgement: This research has been elaborated in the framework of the project Institute of Clean Technologies for Mining and Utilization of Raw Materials for Energy Use, Reg. No. CZ.1.05/2.1.00/03.0082, the IT4Innovations Centre of Excellence project, reg. no. CZ.1.05/1.1.00/02.0070 supported by Operational Programme 'Research and Development for Innovations' funded by Structural Funds of the European Union and state budget of the Czech Republic, the project RMTVC No. LO1203 and the project New creative teams in priorities of scientific research, reg. No. CZ.1.07/2.3.00/30.0055.

References

[1] N. F. Zhu, W.J. He, P. Liu, Study on Cutting Temperature for Wood Plastic Composite. Proceedings of the 19th International Wood Machining Seminar, Nanjing, China, 21-23. October 2009, p. 39-49, ISBN: 978-7-5023-6224-9.

[2] X.L. Guo, Effect of Spindle Speed on Surface Qualities in WPC Sawing. Advances in Functional Manufacturing Technologies, 33 (2010) 487-491.

[3] D. Saloni, U. Buehlmann, R.T. Lemaster, Tool Wear Cutting Wood Fiber-Plastic Composite Materials. Forest Product Journal, 61 (2011) 149-154.

[4] Z. Šomšáková, Z. Zajac, P. Michalik, M. Kasina, Machining of Wood Plastic Composite (Pilot Experiment). Materiale Plastice, 49 (2012) 55-57.

21st International Conference **ENGINEERING MECHANICS 2015**
Svratka, Czech Republic, May 11 –14, 2015
Paper **#050, pp. 108–109**

Void Fraction Based Two Phase Flow Model of Natural Draft Wet-Cooling Tower

Tomáš Hyhlík

Department of Fluid Dynamics and Thermodynamics, Faculty of Mechanical Engineering, Czech Technical University in Prague, Technická 4, 166 07 Prague 6, Czech Republic

tomas.hyhlik@fs.cvut.cz

Keywords: two phase flow modelling , wet-cooling tower, moist air, void fraction, supersaturation

Abstract: The article deals with an improvement of recently developed model of natural draft wet-cooling tower flow, heat and mass transfer [1]. The aim of present work is to make model more correct from the point of view of thermodynamics of two-phase flow. Void fraction of gas phase is included in governing equations. Homogeneous equilibrium model, where the two phases are well mixed and have the same velocity, is used. The main advantage of present approach is correct modelling of supersaturated moist air flow especially in the case where supersaturation occurs due to temperature decrease.

Mathematical Model

Void fraction of gas phase is a fraction of gas volume in two phase mixture over the total volume of the mixture. Overall density of two phase mixture can be expressed by using void fraction of gas phase as [2]

$$\rho = \alpha\rho_g + (1-\alpha)\rho_l, \tag{1}$$

where ρ_l is the density of water liquid and density of gas phase is a sum of the dry air density ρ_a and the density of water vapour ρ_v

$$\rho_g = \rho_a + \rho_v. \tag{2}$$

If density is introduced in this way it is possible to calculate dry air mass fraction w_a, water vapour mass fraction w_v as and water liquid mass fraction w_l as

$$w_a = \frac{\alpha\rho_a}{\rho},\ w_v = \frac{\alpha\rho_v}{\rho},\ w_l = \frac{(1-\alpha)\rho_l}{\rho}. \tag{3}$$

It is possible to show that

$$w_a + w_v + w_l = 1. \tag{4}$$

The ratio of gas mass fraction to liquid mass fraction is

$$\frac{\alpha\rho_g}{(1-\alpha)\rho_l} = \frac{\alpha(\rho_a+\rho_v)}{(1-\alpha)\rho_l} = \frac{w_a+w_v}{1-w_a-w_v}, \tag{5}$$

It is very interesting that it is possible to formulate the system of governing equations where there are only overall continuity equation, overall momentum balance, dry air continuity equation and overall equation of energy. The system of governing equations has to be closed by using the definition of internal energy and by using the equation of state. The system of governing equations can be written for the case of quasi one-dimensional flow as

$$\frac{\partial(\mathbf{W}A)}{\partial t} + \frac{\partial(\mathbf{F}A)}{\partial z} = \mathbf{Q}, \tag{6}$$

where vector of conservative variables **W**, vector of fluxes **F** and vector of sources **Q** are

$$\mathbf{W} = \begin{bmatrix} \rho \\ \rho v \\ \rho w_a \\ \rho e \end{bmatrix}, \mathbf{F} = \begin{bmatrix} \rho v \\ \rho v^2 + p \\ \rho w_a v \\ (\rho e + p)v \end{bmatrix}, \mathbf{Q} = \begin{bmatrix} A(z)\sigma_v(z) \\ p\frac{\mathrm{d}A}{\mathrm{d}z} - A(z)(\rho g + \zeta\rho\frac{v^2}{2}) \\ 0 \\ A(z)(\sigma_q(z) + \rho g v) \end{bmatrix}. \tag{7}$$

The density of overall energy e is

$$e = u + \frac{v^2}{2}, \tag{8}$$

where internal energy u is defined as

$$u = c_{v_s}(p,T)t + w_v(p,T)\left(l_{TR} - \frac{p_{TR}}{\rho_{TR}}\right), \tag{9}$$

where l_{TR} is heat of vaporisation in the triple point, p_{TR} is the triple point pressure and ρ_{TR} is the density in triple point. Temperature in degrees of Celsius is t and temperature in Kelvins in T. Mixture specific heat capacity is

$$c_{v_s}(p,T) = w_a c_{v_a} + w_v(p,T)c_{v_v}t + [1 - w_a - w_v(p,T)]c_{v_w}, \tag{10}$$

where c_{v_a}, c_{v_v} and c_{v_w} are constant volume specific heat capacities of dry air, water vapour and water liquid respectively. Equation of state can be written as

$$p = r_s(p,T)\rho_g(p,T)T(p,T), \tag{11}$$

where r_s is gas constant of the mixture of dry air and water vapour and temperature in Kelvins can be expressed as

$$T(p,T) = \frac{u - w_v(p,T)\left(l_{TR} - \frac{p_{TR}}{\rho_{TR}}\right)}{c_{v_s}(p,T)} + 273.15. \tag{12}$$

The key part of this model of two phase flow is solving of temperature and pressure based on the Eq. 9 and Eq. 11. The two equations for pressure and temperature are non-linear mainly because water vapour mass fraction is the function of saturation pressure at given temperature

$$w_v(p,T) = 0.622 w_a \frac{p_v(T)}{p - p_v(T)}. \tag{13}$$

The saturation pressure at given temperature can be calculated e.g. by using IAPWS formulation.

Acknowledgement: This work has been supported by The Technology Agency of the Czech Republic under the project Advanced Technologies for Heat and Electricity Production - TE01020036.

References

[1] T. Hyhlík, Concept of CFD model of natural draft wet-cooling tower flow, in: EJP Web of Conferences, Volume 67, 2014, 02044, DOI: 10.1051/epjconf/20146702044

[2] S. M. Ghiaasiaan, Two-Phase Flow, Boiling and Condensation in Conventional and Miniature Systems, Cambridge University Press, (2008)

21st International Conference **ENGINEERING MECHANICS 2015**
Svratka, Czech Republic, May 11 –14, 2015
Paper **#201, pp. 110–111**

Load Carrying Capacity of Steel Arch Reinforcement Taking into Account the Geometrical and Physical Nonlinearity

Petr Janas[a], Lenka Koubová[b], Martin Krejsa[c,*]

VSB–Technical University of Ostrava, Faculty of Civil Engineering, Department of Structural Mechanics, Ludvika Podeste 1875/17, 708 33 Ostrava–Poruba, Czech Republic

[a]petr.janas@vsb.cz, [b]lenka.koubova@vsb.cz, [c]martin.krejsa@vsb.cz

Keywords: steel arch reinforcements, large displacement, geometrical nonlinearity, physical nonlinearity, effective bending stiffness, rotating capacity, cross-section classes

Abstract: The paper deals with the calculation of the load carrying capacity of the steel arch reinforcements of underground and mine workings respect for the resulting large displacement and physical nonlinearities. Solution is based on the application of the so-called effective bending stiffness, which is defined as a function of the normal forces and bending moment. The results of the numerical analysis are compared with the values of the load carrying capacity, which have been experimentally obtained using strain-stress test of mining reinforcement. The computational procedure was also applied to software that allows you to very effectively calculate the load carrying capacity of steel arch reinforcements.

Introduction

Steel arch reinforcements are mounted usually from special rolled profiles. They are designed to have a sufficient plastic reserve and withstand large displacements. These profiles are significantly more complex from a geometric point of view than the profiles applied in steel constructions of buildings and civil engineering structures. This fact does not count in the EC3 [4] - profiles of steel arch reinforcements cannot be correctly classified in the relevant cross-section class according to this standard.

Therefore, attention was also the inclusion of the TH-29 profile to the corresponding cross-section class during the development of steel H500M in the framework of the project TA CR TA01010838 for the arch reinforcement specified particularly for the mining and underground construction [3]. The basis for this classification were mathematical modelling and bending tests.

Modelling of bending tests of this profile as well as whole sets of steel arch reinforcement is based on the knowledge of effective bending stiffness of this profile. The effective bending stiffness is a function of the bending moment and normal force. For clarity of its expression it should be expressed as a function of the relative rotation dφ considering the variable value of axial forces [1]. The effective bending stiffness was derived from the results of the modelling using the finite element method.

The rotating capacity of cross-section is evaluated for its classification. This rotating capacity shall be determined according to the relation:

$$R = (\varphi - \varphi_{pl})/\varphi_{pl} \,. \tag{1}$$

The angle φ_{pl} is the rotation of the pin supported beam under three-point bending test on the increasing part of the function $\varphi = F(M)$ for the value of the bending moment $M = M_{pl}$. The rotation φ for the same value of the bending moment is the value on the decreasing part of the chart (refer with: Fig. 1).

The value of rotating capacity R for the cross-section classification in class 1 is not fixed in EC 3 [4]. The comment to the American AISC LRFD [5] gives the value $R = 3$ for cross-section class 1, while Japanese AIJ LSD [6] gives $R = 4$.

The values of R for the TH-29 profile of the steel H500M were intended for modelling of bending tests and experimentally as well. Rotating capacity of the profile according analysis is

sufficient for inclusion in cross-section class 1 and is substantially greater in the load profile at its root - profile is more stable. This fact is reflected in the curves of the effective bending stiffness. Their validity was confirmed by the good agreement between results of mathematical modelling of the mining reinforcements under the load [2] and the experimental load tests.

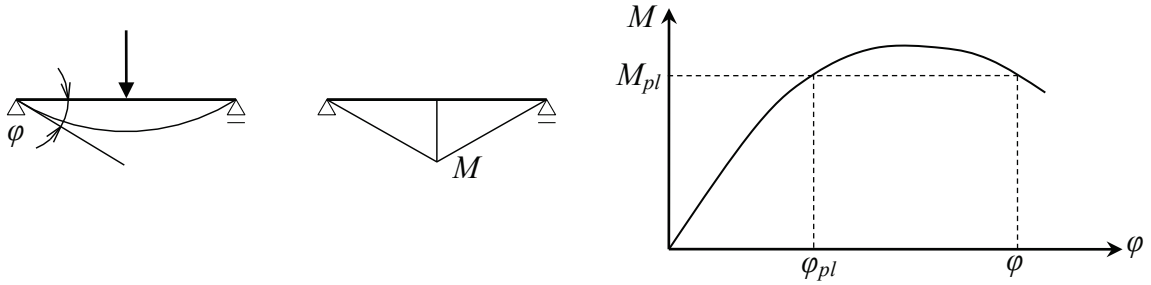

Fig. 1: Scheme of bending tests and the curve of bending moment and rotation

The software titled *Calculation of Load Carrying Capacity of Steel Arch Reinforcements of Corridors from the TH-29 Profile and TH-34 Profile of Steel H500M (31Mn4) – VÚOOVCH TH29/H500M and TH34 TH29/H500M* was developed as utility for the operative calculations of yielding and unyielding steel arch reinforcement with the focus to the resulting load carrying capacity in accordance with EC3 [4]. Alternatively it can be determined also for the higher value of limit bending moment when the load is applied on the root of the profile (for details see [8]).

Acknowledgement: This project has been completed with the financial support provided to VSB–Technical University of Ostrava by the Czech Ministry of Education, Youth and Sports from the budget for conceptual development of science, research and innovations for the year 2015.

References

[1] A. Markopoulos, P. Janas and J. Podesva, Effective bending stiffness of TH-29 profile, in: New Trends in Statics and Dynamics of Building 2010, Slovak University of Technology in Bratislava (2010) p 101-102, ISBN: 978-80-227-3373-1.

[2] L. Koubova, Displacement method in nonlinear mechanics, thesis, VSB-Technical University of Ostrava (2012).

[3] Z. Vasek, P. Janas, Steel products for use in ground and mining engineering, in: Modeling in Mechanics 2012, VSB-Technical University of Ostrava (2012) ISBN: 978-80-248-2694-3.

[4] CSN EN 1993-1-1 ed. 2 (731401), Eurocode 3: Design of steel structures - Part 1-1: General rules and rules for buildings, Czech Standards Institute (2011).

[5] AISC LRFD, Load and Resistance Factor Design Specification for structural steel buildings, American Institute of Steel Construction (AISC) (1994).

[6] AIJ LSD, Standard for Limit State Design of Steel Structures, Architectural Institute of Japan (AIJ) (1990).

[7] P. Janas, I. Kolos, R. Fojtik, Classification of steel mine support sections as per EC3 classification, Advanced Materials Research, 969 (2014) 63-66, DOI: 10.4028/www.scientific.net/AMR.969.63.

[8] P. Janas, User manual for the Calculation of Load Carrying Capacity of Steel Arch Reinforcements of Corridors from the TH-29 and TH-34 Profile of Steel H500M (31Mn4) VUOOVCH, in: fast.vsb.cz [online], Ostrava, CR, 2013 [cit. 2015-03-05], available online https://www.fast.vsb.cz/export/sites/fast/228/cs/software/vuoovch-uzivatelska-prirucka.pdf

21st International Conference **ENGINEERING MECHANICS 2015**
Svratka, Czech Republic, May 11 –14, 2015
Paper **#216, pp. 112–113**

Experimental Measurement of Elastic-Plastic Fracture Parameters Using Digital Image Correlation Method

Ivan Jandejsek[a]*, Ľubomír Gajdoš[b], Martin Šperl[c], Daniel Vavřík[d]

[1]Institute of Theoretical and Applied Mechanics AS CR, v.v.i,
Prosecká 76, Prague 9, 19000, Czech Republic

[a]jandejs@itam.cas.cz, [b]gajdos@itam.cas.cz, [c]sperl@itam.cas.cz, [d]vavrik@itam.cas.cz

Keywords: *J*-integral, CTOD, DIC

Abstract: This paper presents possibilities of an experimental measurement of elastic-plastic fracture parameters such as *J*-integral, CTOD and *J*-resistance curve of ductile materials with single specimen test employing the Digital Image Correlation method. Main advantage of this approach is that it allows evaluation of the parameters directly from its definitions in contrast to current standardized measurements defined mostly by ASTM where parameters are evaluated indirectly. Successful experimental results of the fracture parameters evaluation and determination of its critical values in the case of Aluminum alloy and low strength steel are presented.

Introduction

The Elastic-plastic fracture mechanics (EPFM) or nonlinear fracture mechanics deals with the situation when the vicinity of a crack tip undergoes large-scale yielding before the crack growth. In other words, the assumption of small-scale yielding used in the linear elastic fracture mechanics theory (LEFM) is not valid. It is well-known fact that this situation occurs in the case of high ductile materials (such as aluminum alloys or low/medium strength steels), plane stress loading conditions and thin-sheet specimens. Two fundamental concepts in the EPFM theory for materials under monotonic loading are the *J*-integral [1] and the crack tip opening displacement (CTOD) [2]. Both parameters describe a stress tip condition in an elastic-plastic body and can serve as a fracture toughness criterion. In EPFM the fracture toughness can be expressed as a single critical value of the *J*-integral or CTOD, or as a resistance curve, where the parameter values are plotted against a crack extension. Current standards defined mostly by the American Society for Testing and Materials (ASTM) include testing procedure for J_C, *J*-resistance curve and $CTOD_C$ [3]. The common feature of all standard procedures is that the toughness parameters are evaluated indirectly using simplified relations and load-displacement curve of the loading test. In terms of engineering practice, it is understandable and sufficient in many cases because such measurements are not demanding and time-consuming. However, this can be risky in the special cases such as high ductile materials or thin-sheet nonconventional specimens.

In this work precise experimental measurement of strain and stress fields in the vicinity of a crack allows an evaluation of the *J*-integral directly from its definition. The optical nature of the method allows simultaneous measurement of CTOD and crack length during loading which made possible to build the *J*-resistance curve. The method was employed in the case of fracture toughness determination of aluminum alloy and low strength steel.

Experimental

The first fracture experiment was carried out with a flat thin-sheet specimen made of aluminum alloy (ČSN 424415.21) with a symmetric central notch so-called middle tension (MT) specimen. Acquired optical data of the crack vicinity served for full-field strain and stress evaluation in this region. On the basis of these fields the *J*-integral was evaluated in each recorded loading step. The crack length extension during stable growth was obtained directly from the acquired images. The assembled resulting *J*-resistance curve is shown in Fig. 1. Fracture toughness of the material in the

terms of critical value of the *J*-integral was extracted from the curve. The second experiment was carried out with low strength steel (ČSN 411373) used in pipeline industry. In this case, a comparison measurement of the CTOD evaluated by the DIC method and the δ_5 measured using standard displacement gauge was carried out.

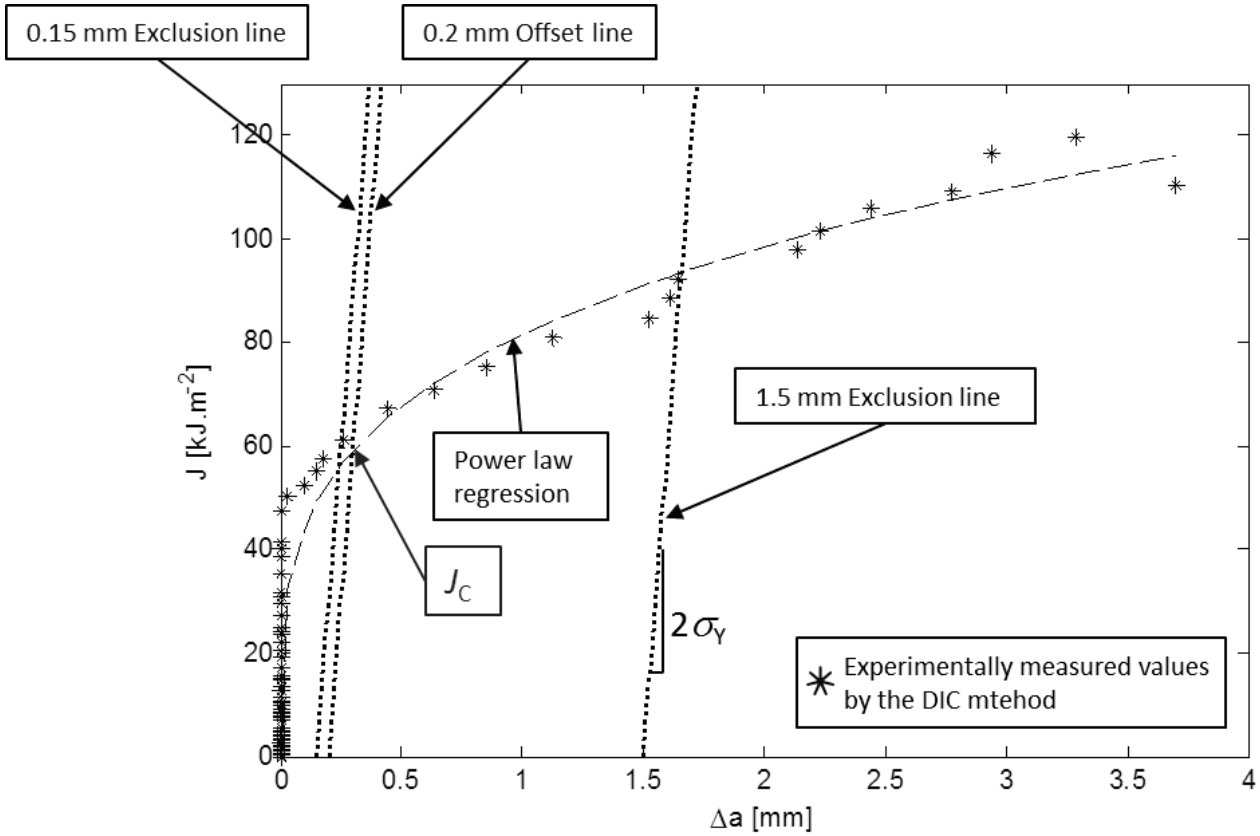

Fig. 1: Experimentally measured J-resistance curve of aluminum alloy using the DIC method.

References

[1] A.A. Wells, Application of fracture mechanics at and beyond general yielding, Br Weld J, 10 (1963) 563–70.

[2] J.R. Rice, A path independent integral and the approximate analysis of strain concentration by notches and cracks, J Appl Mech 35 (1968) 379–86.

[3] T.L. Anderson, Fracture Mechanics: Fundamentals and Applications, CRC Press, 1995.

[4] D. Vavřík, I. Jandejsek, Experimental evaluation of contour J integral and energy dissipated in the fracture process zone, Eng Fract Mech 129 (2014) 14–25.

21st International Conference **ENGINEERING MECHANICS 2015**
Svratka, Czech Republic, May 11 –14, 2015
Paper **#112, pp. 114–115**

Risk-Based Inspection of Some Components of Power Plant Prunéřov-II

Jan Janošťák[a]*, Jakub Stoniš[b], Zdeněk Ramík[c]

VÍTKOVICE ÚAM a.s., Purkyňova 648/125, 612 00 Brno, Czech Republic

[a]jan.janostak@vitkovice.cz, [b]jakub.stonis@vitkovice.cz, [c]zdenek.ramik@vitkovice.cz

Keywords: risk-based inspection; RIMaSys system; power plant Prunéřov-II

Abstract: The paper deals with rendering of Risk-Based Inspection method (RBI) for use in maintenance system on "retrofit" power plant Prunéřov-II (EPR-II). Data collected during inspections are stored in database of RIMaSys system. Assessment of inspection data may be used for planning next inspections and to keep the risk of failure of power plant inspected components under control. RIMaSys computer code developed in VÍTKOVICE ÚAM a.s. company was used.

1. Introduction

Risk level analysis is very important not only in business and financial transactions, but in industry too. In heavy industry, chemical industry, aircraft industry and others is risk level analysis used for fitness for service management and inspection planning.

Use of RBI method [1] for assessment of risk of several components of power plant Prunéřov-II (EPR-II) is presented in this paper. For inspection data collection and assessment system RIMaSys developed in VÍTKOVICE ÚAM a.s. company is used.

2. Risk-Based Inspection method (RBI)

Risk-Based Inspection is modern and powerful process based on planning of inspections, visual examinations and nondestructive inspection techniques of equipment. Risk is defined by combination of probability and consequence of equipment failure. Probability and risk can be estimated in one of three ways.

Qualitative RBI is based on experience and expertise of visual testing and nondestructive inspection techniques. Most of components are assessed by qualitative approach, the aim is to obtain wide overview of state of technical preservation of equipment.

Quantitative RBI considers structural degradation and damage in probabilistic manner, so measurement data (wall thickness, size of defect and so on) are necessary for assessment. Only the most important components are assessed by quantitative approach.

Semi-quantitative RBI is between above approaches.

In progress from qualitative to quantitative RBI the results are more accurate, but the cost and the time to achieve them grow up.

3. Software system RIMaSys

The RIMaSys system [2] developed in VÍTKOVICE ÚAM a.s. company is based on RBI method. System consists of two program parts, RIMaSys for PC runs on Windows based computer and RIMaSys for mobile devices, such as smartphones and tablets, runs on operating system Android – almost all types of mobile devices with different screen size are suitable.

During inspection of the power plant components tablet with RIMaSys is used for data collection. RIMaSys running on PC is used for power plant equipment inspection planning, export inspection data sheet to tablet and import collected inspection data from tablet.

Assessment of inspection data, which are stored in MSSQL database type file on hard disk with RIMaSys on PC, may be used for planning next inspection and other analyses. Screen-shots of RIMaSys system for tablet are shown in figures Fig. 1 and Fig. 2.

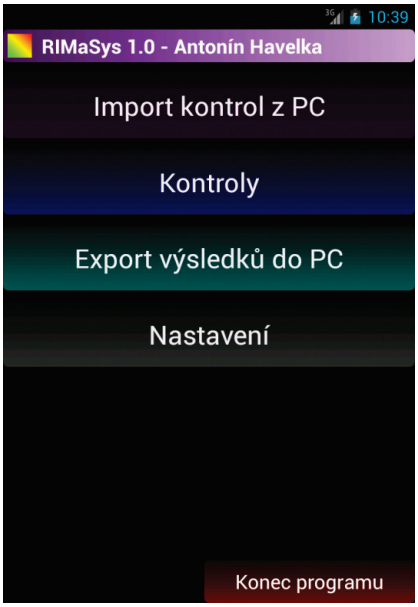

Fig. 1: RIMaSys window for tablet

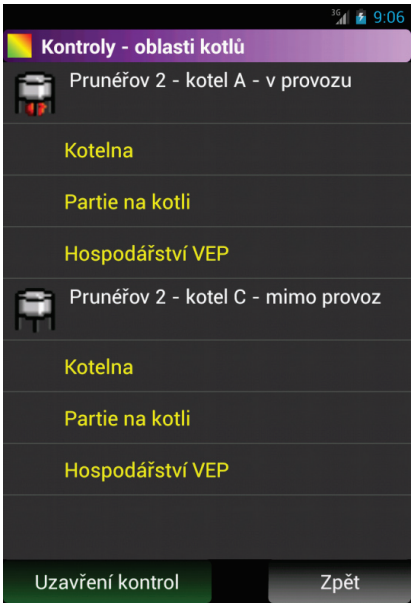

Fig. 2: List of inspection areas

4. Conclusion

Assessment of risk of failure of selected inspected components of power plant Prunéřov-II (EPR-II) is based on RBI method.

The RIMaSys system developed in VÍTKOVICE ÚAM a.s. company is used for inspection, planning, collection data in MSSQL database type file and assessment.

Summary

The paper describes aims stated in paper introduction. Use of RBI method for assessment of selected power plant Prunéřov-II components is presented. RIMaSys computer code developed in VÍTKOVICE ÚAM a.s. company is introduced.

Acknowledgement: This work has been supported by research project VG20132015109 granted by Ministry of the Interior of the Czech Republic.

References

[1] J. Gottvald, J. Stoniš, P. Ryšavý, S. Vejvoda, Z. Kala, Projekt č. VG20132015109, report VÍTKOVICE ÚAM a.s., arch. č. V3053/13, Brno, 2013.

[2] J. Janošťák, J. Stoniš, Z. Ramík, Projekt č. VG20132015109, report VÍTKOVICE ÚAM a.s., arch. č. V3105/14, Brno, 2014.

21st International Conference **ENGINEERING MECHANICS 2015**
Svratka, Czech Republic, May 11 –14, 2015
Paper **#254, pp. 116–117**

Properties of Commercially Available, Ready-to-Use Mortars for the Restoration of Historic Renders and Masonry

Dana Janotová[1,a*], Krzysztof Niedoba[1,b], Petr Gláser[1,c], Petr Šašek[2,d], Roman Fabeš[2,e]

[1]Institute of Theoretical and Applied Mechanics, AS CR,
Prosecká 76, 190 00 Praha 9, Czech Republic

[2]ITAM-Centre of Excellence Telč,
Batelovská 486, 588 56 Telč, Czech Republic

[a]krivankova@itam.cas.cz, [b]niedoba@itam.cas.cz, [c]glaser@itam.cas.cz,[d]sasek@itam.cas.cz,
[e]fabes@itam.cas.cz,

Keywords: renovation plasters, renders, compatibility, mechanical properties, water/vapour transport properties, thermal properties

Abstract: There is a wide range of premixed, dry mortars, on the market, designed with the reconstruction of historic renders and masonry in mind. The use of such materials has some advantages, including good workability and standard quality, however, due to unknown composition, being a secret of a manufacturer, it is frequently impossible to predict their influence on the substrate and on the ageing. If the ready-to-use mortar is to be applied during the renovation of the historic masonry, it is necessary to know: how close the mortars' properties match the properties of the original material; will the repair be durable enough and will it degrade faster than the original material. Technical information, provided by the manufacturer, does not contain such data. The only parameters given, are the strength, porosity of hardened mortar and water vapour diffusion coefficient, however, it is not specified in which conditions these values were measured.

Within the project "Conditions and requirements of compatible care of the historical inorganic porous materials" the authors work on the development of a list of most important, so called critical properties of the mortars, that significantly affect the durability of the repair and as such must be followed in terms of the material compatibility. These properties can be divided into three different groups: a) properties related to the pore system, influencing the water and water vapour transport throughout the porous material, b) mechanical resistance and adhesion to the original substrate, c) response to the temperature variations.

In this study, we compare the key properties of six commercially available mortars, the compositions of which, according to what manufacturers claim, meet the demands of cultural heritage protection; some of them even comply with the WTA requirements. The following mortars were tested:

- WE – porous, air lime-based mortar, without cement, designed to render humid masonry, composed of stone or brick
- CE – mortar with the binder based on lime and pozzolana, without cement. Mortar is to be applied manually in the interior or exterior.
- EX – mortar belonging to CS II group (according to DIN EN 998 – 1), containing special admixtures, creating specific pore geometry
- BA – hydrophobic, porous, lime-trass render, with high water vapour permeability, for manual application
- RE – contains lime and trass, to be used as joint mortar. In a hardened state it has improved resistance against sulphates, low susceptibility to cracks formation and frost-mediated damage
- MA – mortar based on lime, eco-pozzolana and synthetic fibers, designed for structures made of natural stone, bricks or tuff

The size of samples was chosen to match the real thickness of the renders. Thus, the mechanical properties (flexural and compressive strength, Young modulus) and humidity transport-related properties (water accessible porosity and capillary absorption coefficient) were measured using 20x20x100mm samples. Water vapour permeability was measured using 12x70 round samples and the thermal expansion was measured on cylinders, 12x20mm. Samples of each mortar were prepared according to the guidelines provided by the manufacturer. The results obtained are shown in Table 1.

First of all, one can observe significant differences in mechanical properties of particular mortars. Together with mixing water content, that can vary slightly, within the range given by the manufacturer, this allows for adjustment of the render according to the strength of the substrate. Interestingly, it was found, that hydrophobic mortar, though slowly, still absorbs water. EX mortar, having relatively high porosity and low strength, is characterised by surprisingly low permeability. Such a combination of properties is rather disadvantageous. In contrast to this, BA mortar has similar strength, even higher porosity and very good permeability of water vapour. As regards higher strength renders, one would obviously choose MA, as it has low water absorption coefficient, relatively high water vapour permeability and favourable relation between strength and Young modulus. In conclusion, based on our experience and on the literature, we suggest to follow several simple rules:

- In the environment where frost can damage the object, stronger mortar is better than the weaker one, however it cannot be of higher strength than the substrate.
- The thermal expansion of the render should be similar to thermal expansion of the substrate, especially on the south and west façades.
- As water is always undesired in the masonry and even the hydrophobic render does absorb some water, porous renders with high pore size should be used where possible.

Table 1: The key properties of six commercially available mortars.

Mortar	Flexural strength (ČSN EN 12372) [MPa]	Compressive strength (ČSN EN 1926) [MPa]	Young's modulus (ČSN EN 14580) [GPa]	Porosity accesible to water (RILEM Test No.I.2. 1989) [vol. %]	Capillary absorption coeficient (ČSN 1925) [$kg.m^{-2}.hod^{-0,5}$]	Dry cup diffusion factor coefficient (ČSN EN ISO 12572) 0/33 μ [-]	Thermal expansion coefficient in tempereture range -20 +80°C [$\times 10^{-6}$ K^{-1}]
WE	4,5 ±0,4	9,0 ±0,7	2,3 ±0,6	29,0 ±0,3	4,0 ±0,1	22,2 ±2,0	between 5 and 6
MA	6,1 ±1,0	13,6 ±1,0	1,7 ±0,2	28,4 ±0,3	1,8 ±0,1	25,3 ±1,7	between 1 and 9
RE	6,1 ±0,7	10,8 ±0,7	2,2 ±0,4	29,9 ±1,0	3,8 ±0,2	26,4 ±1,2	between 7 and 19
BA	1,2 ±0,4	1,5 ±0,2	1,3 ±0,2	56,6 ±0,2	2,4 ±0,2	13,6 ±0,4	between -6 and 19
EX	1,2 ±0,1	2,0 ±0,2	2,9 ±1,0	46,9 ±0,6	4,2 ±0,3	12,7 ±1,0	between 0 and 19
CE	1,0 ± 0,2	1,6 ±0,2	1,6 ±0,4	31,6 ±0,6	5,3 ±0,6	16,0 ±0,5	between 5 and 23

Acknowledgement: The authors gratefully acknowledge support from the Czech Ministry of Culture NAKI Project DF12P01OVV018 entitled "Conditions and requirements of compatible care of the historical inorganic porous materials".

21st International Conference **ENGINEERING MECHANICS 2015**
Svratka, Czech Republic, May 11 –14, 2015
Paper **#081, pp. 118–119**

Parameter Identification of Heterogeneous Materials from a Set of Destructive Experiments

Eliška Janouchová[a], Anna Kučerová[b], Jan Sýkora[c]

Faculty of Civil Engineering, CTU in Prague; Thákurova 7/2077; 166 29, Prague; CZ

[a]eliska.janouchova@fsv.cvut.cz, [b]anicka@cml.fsv.cvut.cz, [c]jan.sykora.1@fsv.cvut.cz

Keywords: uncertainty quantification, heterogeneous materials, uncertain parameter identification, stochastic inversion problem, principal component analysis, Markov chain, Monte Carlo sampling

Abstract: Structural parameters such as material properties involve uncertainties which need to be considered in an appropriate reliability analysis. The contribution focuses on stochastic parameter estimation of heterogeneous materials based on observations from a set of destructive experiments.

Introduction

Heterogeneous character of building materials causes spatial variations of mechanical parameters affecting the structural system behaviour under the loading. This phenomenon can be observed during laboratory testing on a set of specimens made of the same material. In order to investigate the structural reliability properly, these inherent uncertainties in material parameters have to be captured by a corresponding stochastic model. Calibration of such a model can be formulated as a search for probabilistic description of its parameters providing the distribution of the model response corresponding to the distribution of the observed data, i.e. a stochastic inversion problem.

Uncertainties can be divided into two main categories according to whether a source of nondeterminism is irreducible or reducible [1]. Our goal is to quantify aleatory (irreducible, inherent, stochastic) uncertainty which corresponds to real variability of properties in the heterogeneous material, while epistemic (reducible, subjective, cognitive) uncertainty arising from our lack of knowledge is supposed to be reduced by any new measurement according to the coherence of learning [2].

Inverse problems are often ill-posed, because the function mapping the parameters to the responses is not injective so it is also non-invertible. The most common method of parameter estimation is based on minimisation of the difference between the experimental data and the model response. In the last decades probabilistic methods to modelling of uncertainties have became applicable thanks to a growing computational capacity. The probabilistic approach restates the inverse problem as well-posed in an expanded stochastic space by modelling the parameters as well as the observations as random variables with their probability distributions [3]. Several methods for uncertainty quantification in probabilistic settings have been proposed in the literature. They are mainly based on choosing a particular type of probability density function (pdf) of variables and the corresponding parameters of this distribution are provided by e.g. maximum likelihood method [4] or Bayesian inference [5]. Authors in [6] represent random variables by a polynomial chaos expansion and identify its coefficients from the data. An extensive overview on stochastic modelling of uncertainties can be found in [7].

This contribution concentrates on stochastic parameter identification of heterogeneous materials. The proposed method quantifying the aleatory uncertainties concentrates on using a probabilistic method to represent the source of uncertainty and then Markov chain Monte Carlo (MCMC) sampling [8] to compute the moments of the parameters' distribution through a deterministic model.

Stochastic identification method

The developed method is initially inspired by the Bayesian inference where all the available information are combined in resulting updated distribution of the parameters. The underlying problem of its practical application to real experimental data is an appropriate formulation of the a priori pdf of

parameters and function representing the distribution of experimental measurements. As it is focused on the quantification of irreducible uncertainty in the data, the influence of the prior information is suppressed and an non-informative uniform a priori pdf is employed.

We consider a situation where available observations are obtained within a set of destructive experiments, each performed on a different set of specimens. Simple multiplication of pdfs constructed for data from each experiment may lead to underestimating the parameter variance due to underlying assumption of independence among observations from different experiments. Despite the independence of specimens, the observations may be correlated due to their physical meaning described by the material model and hence their dependence on the same material parameters.

The proposed methodology is based on transformation of the data by principal component analysis (PCA) into a set of independent quantities [9]. The PCA requires information about mutual correlations among data from particular experiments, which needs to be estimated using the prior knowledge about the underlying model. Considering only a reasonable number of the principal components in stochastic model updating allows eliminating the influence of experimental errors to a certain extent.

Summary

The contribution is focused on developing a method for identification of parameters along with their variations in heterogeneous materials from a set of experiments. The procedure is based on MCMC sampling of a combination of the non-informative prior pdf and PCA-based pdf of experimental data where correlations between particular observed variables and measurement errors are eliminated.

Acknowledgement: This outcome was financially supported by the Czech Science Foundation, project No. 15-07299S, and the Grant Agency of the Czech Technical University in Prague, grant No. SGS15/030/OHK1/1T/11.

References

[1] W. L. Oberkampf et al., Error and uncertainty in modeling and simulation. Reliability Engineering and System Safety 75 (2002) 333–357.

[2] P. Mantovan, E. Todini, Hydrological forecasting uncertainty assessment: Incoherence of the GLUE methodology. Journal of Hydrology 330 (2006) 368–381.

[3] J. Kaipio and E. Somersalo, Statistical and Computational Inverse Problems. New York: Springer-Verlag, 2005. 339 p. Applied mathematical sciences. ISBN 03-872-2073-9.

[4] J. R. Fonseca et al., Uncertainty identification by the maximum likelihood method. Journal of Sound and Vibration 288 (2005) 587–599.

[5] A. Gelman et al., Bayesian data analysis. 2nd ed. Boca Raton, Fla.: Chapman, 2004. 668 p.

[6] M. Arnst, R. Ghanem, C. Soize, Identification of Bayesian posteriors for coefficients of chaos expansions. Journal of Computational Physics 229 (2010) 3134–3154.

[7] C. Soize, Stochastic modeling of uncertainties in computational structural dynamics — Recent theoretical advances Journal of Sound and Vibration 332 (2013) 2379–2395.

[8] C. J. Geyer, Handbook of Markov Chain Monte Carlo. In: Introduction to Markov Chain Monte Carlo. Boca Raton, Fla.: CRC Press, 2011, pp. 3-48. ISBN 978-1-4200-7942-5.

[9] I. Jolliffe, Principal component analysis. 2nd ed. New York: Springer, 2002. 487 p.

21st International Conference **ENGINEERING MECHANICS 2015**
Svratka, Czech Republic, May 11 –14, 2015
Paper **#176, pp. 120–121**

Measuring of a Nose Landing Gear Load during Take-Off and Landing

Ivo Jebáček[a] *, Marek Horák[b]

[1]Brno University of Technology, Institute of Aerospace Engineering,
Technická 2896/2 616 69 Brno, Czech Republic

[a]jebacek@fme.vutbr.cz, [b]horak@fme.vutbr.cz

Keywords: Airplane, landing gear, in-flight, load, measurement, strain gauge, calibration

Abstract: This article provides information about in-flight measurement of a small sport aircraft. The strain gauges were used as sensors for load monitoring on the nose landing gear structure. To obtain overall forces the calibration procedure was necessary to do. After the calculation of strain gauge coefficients the equations for calculating of total force, total force direction and individual force components were determined. During test flights the data acquisition system was installed into the aircraft. The data from strain gauges were collected together with other flight parameters like speed, altitude and data from inertial measurement unit which determine the exact movements of the aircraft before landing. The data recorded during fifty-six flights were analysed to obtain loads acting in the aircraft structure. These results were compared with calculated values.

Introduction

Generally, in-flight testing is a very important part of aircraft development. Its results are necessary for aircraft certification and helpful for further aircraft development. Landing gear is one of the most important components of the aircraft. It is used for aircraft take-off, landing, taxiing, parking and steering on the ground. Measuring of the landing gear loads during flight tests is necessary in order to verify the structural design loads, which were used for landing gear design. The same data provide useful information for landing gear fatigue analysis.

Specimen

The landing gear load was measured on a small two-seated sport aircraft with maximum take-off weight of six hundred kilograms. For purpose of measurement, the aircraft nose landing gear leg and aircraft itself were equipped with twenty strain gauges, two pressure transducers, GPS receiver, inertial measurement unit and two independent data acquisition systems. Data from this equipment were needed for description of the take-off and landing conditions as speed, height, positional angles, angular velocities and accelerations in three perpendicular directions.

Four full Watson's bridges were used to measure of nose leg ground load. Each of these bridges is composed of four active strain gauges. In order to determine the load based on the responses of strain gauge bridges, it was necessary to perform the calibration.

Calibration

Calibration means finding the relation between the measured responses of strain gauge bridges and external load. Calibration was done in test laboratory at the Brno University of Technology before the test flights program started. The result of the calibration is matrix of calibration coefficients. Only on the basis of knowledge of these calibration coefficients can be determine the force resultant magnitude and direction, which acts on the landing gear during take-off and landing.

These parameters were measured directly during test flight to determine the landing gear load:

- axial force in one section of nose landing gear leg arm structure
- two perpendicular bending moments in one section of nose landing gear leg arm structure
- torque moment in one section of nose landing gear leg arm structure
- nose wheel steering angle

After the test flights, based on measured values, matrix of calibration coefficients and the lending gear geometry, the magnitude and direction of force resultant was calculated.

Flight tests and results

Fifty-six test flights with various take-off and landing conditions were done. Some flights were performed on concrete runway and some flights on grass runaway. Landings first on the main landing gear as well as landing on three points simultaneously were performed. To achieve the maximum nose landing gear ground reaction, the mass configuration of the airplane was a maximum take of weight and forward centre of gravity position in all cases.

The results of measurement are the load spectrum for different flight techniques and conditions and especially the values of maximal magnitude of force resultant and its direction which acts on the landing gear during take-offs and landings. A typical landing spectrum of nose gear ground load is shown in Fig. 1.

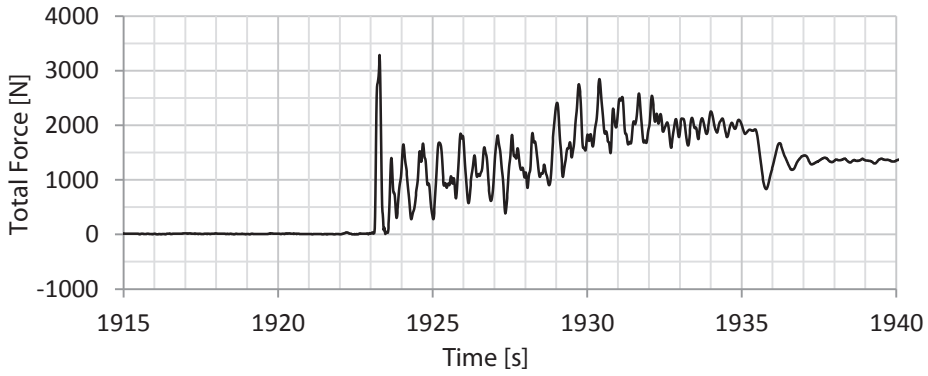

Fig. 1: Typical landing spectrum of nose gear ground load

Conclusion

As a part of in-flight measurement, characteristic spectra of light sport aircraft nose landing gear ground load were obtained. The measured data can be used to validate the methods of load calculation as well as for fatigue analysis of this type of aircraft structural components.

References

[1] I. Jebacek, M. Horak, Possibilities and methods of in-flight loading measurement, Aviation 16 (2012) 47-50.

[2] K. Xiangjun, L. Ningning, L. Chunsheng, X. Xianbo, L. Bo, X. Bing, Landing gear ground load measurement and verification test for a large passenger jet, Procedia Engineering 99 (2015) 1423-1433.

[3] T.H. Skopinski, S.A. William, Calibration of strain-gage installation in aircraft structures for the measurement of flight loads, NACA Report 1178, 1953.

[4] A.-N. Tang, Z.-T. Zhou, J.-T. Cao, A technique of landing gear loads calibration with strain gauges, in: ICAS 2010, paper ICAS2010-P3.1.

21st International Conference **ENGINEERING MECHANICS 2015**
Svratka, Czech Republic, May 11 –14, 2015
Paper **#137, pp. 122–123**

Aerodynamic Characteristics of Steam Turbine Prismatic Blade Section

Tomáš Jelínek[a]*, Petr Straka[b], Milan Kladrubský[c]

Výzkumný a zkušební letecký ústav, a.s., Beranových 130, 199 05, Prague, Czech Republic

[a]jelinek@vzlu.cz, [b]straka@vzlu.cz, [c]kladrubsky@vzlu.cz

Keywords: prismatic blade cascade, high pressure nozzle, high-speed flow, Reynolds number effect, flow separation, RANS

Abstract: For the needs of high-performance steam turbines producer the data of a blade section measurement have been analyzed in detail by experimental and numerical approach. The blade section is used on prismatic blades in high and medium pressure steam turbine parts. The linear blade cascade was tested at four pitch/chord ratios at two different stagger angles. The blade cascade was tested under two levels of Reynolds number in the range of output izentropic Mach numbers from 0.4 to 0.9.

The inlet of the test section was measured pitch-wise by five-hole probe to determine the inlet flow angle. The free stream turbulence of inlet flow was determined of 2.5% what is very close to the operating conditions on first high pressure stages. Two-dimensional flow field at the center of the blades was traversed pitch-wise downstream the cascade by means of a five-hole needle pressure probe to find out the overall integral characteristics. The blade loading was measured throughout surface pressure taps at the blade center. An in-house code based on a system of Favre-averaged Navier-Stokes equation closed by non-linear two-equation EARSM k-ω turbulence model was adopted for the predictions. The code utilizes an algebraic model of bypass transition valid both for attached and for separated flows taking into account the effect of free-stream turbulence and pressure gradient. Results are presented by integral characteristic in means of kinetic energy loss coefficient and velocity or pressure distribution in the blade wakes or on the blade surface. In this article, the effect of investigated criteria and comparison of experimental and numerical approach are presented and discussed.

Introduction

The common procedure for the designers of turbine stages is to test experimentally the optimized blade sections during or after the optimization process to obtain the aerodynamic characteristics. It is also necessary for filling the databases which are used during subsequent design procedures. Therefore, the detailed testing in aerodynamic wind tunnel was performed on a blade section used for prismatic nozzle blades of a new reaction stage and several criteria on this blade section were investigated.

Although the blades in steam turbines of 40-300MW power operates mainly on Reynolds number (Re) in range of $1.10^6 – 1.10^7$ where the turbulent boundary layer occurs, it is important to study the flow in such levels of Re where the boundary layer transition emerge somewhere on the blade, because at this moment the aerodynamic efficiency starts decreasing [1]. For the investigated blade section model and the conditions in the non-pressurized wind tunnel the $Re = 5.10^5$ in overall Mach number range is maximum value. Therefore the two levels of Re ($2{,}5.10^5$ and 5.10^5) were chosen for investigation.

The purpose of testing the blade section on several pitch/chord ratios (t/c) and at two different stagger angles (γ) is based on the whole turbine stage design procedure: In the last steps of the stage design the stage nozzle is turned around the radial axes and the optimal turbine stage mass flow is set. Therefore the two utmost positions of γ were tested. The t/c ratio is also a sensitive criterion how to balance the losses of the stage [2].

For the numerical study of blade section characteristics the model by system of Reynolds-averaged Navier-Stokes equations enclosed by non-linear two-equation EARSM k-ω turbulence

model was used. The turbulence model is supplemented by an algebraic bypass-transition model proposed by Straka and Příhoda [3].

Results and discussions

In Fig. 1 the overall results of kinetic energy loss versus Mach number obtained by experimental tests and CFD data are displayed for selected investigated criteria. In the article the data in selected regimes are supplemented by pressure distribution in wakes and blade loading.

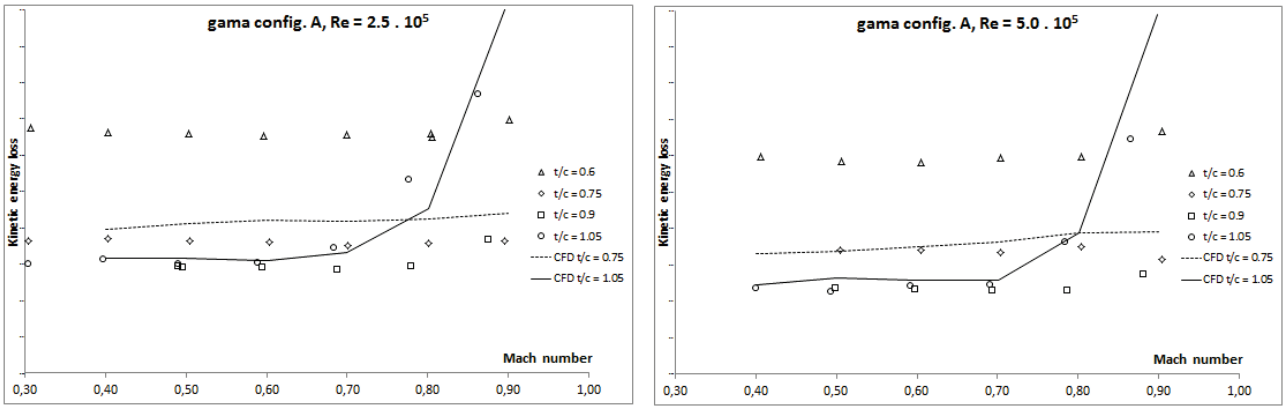

Fig. 1: Overall characteristics for selected criteria

1. Effects of investigated criteria (Re, t/c, γ). Common Re effect on the kinetic energy loss coefficient is that with decreasing the Re the loss coefficient increase. It is affected by boundary layer´s character in subsonic regimes. The laminar boundary layer (forming on lower Re) is wider and such the losses are higher. By transition to turbulent boundary layer the velocity in boundary layer increases and losses such decrease. Fig. 1 presents the comparison of overall level of kinetic energy loss coefficient for two Re levels and the definite influence of Re on the point where the losses begin to increase (due to boundary layer separation).

The results confirm that the optimum of t/c ratio is about 0.75. When the ratio further increase the kinetic energy loss coefficient still decrease but for higher Mach numbers (0.8-0.9) the boundary layer begins to separate and the loss coefficient increases.

2. Comparison of experimental and CFD data. The comparison of CFD and experimental data shows the same trends of the investigated criteria and very good comparison of integral characteristics. The CFD results predict little higher losses (approx. 5% higher as compared with exp.). The character of boundary layer is captured very well for t/c = 1.05. For lower values of t/c CFD results predict probably boundary layer translation later than it is happened physically during experiment. The trends character of kinetic energy loss coefficient matches the laminar boundary layer on the blade so therefore the losses are predicted litter higher. The more detailed analysis is given in the article.

Acknowledgement: The work was performed with help of long term institutional support kindly provided by Ministry of Industry and Trade of the Czech Republic.

References

[1] H. Moustapha, et al, Axial and Radial Turbines, Concept NREC, Vermont, 2003.

[2] S.L. Dixon, Fluid Mechanics, Thermodynamics of Turbomachinery, Pergamon Press, Ltd., Oxford, 2005.

[3] P. Straka, J. Příhoda, Application of the algebraic bypass-transition model for internal and external flows, in: Proc. Conf. Experimental Fluid Mechanics, TU Liberec, pp. 636-641 (2010).

21st International Conference **ENGINEERING MECHANICS 2015**
Svratka, Czech Republic, May 11 –14, 2015
Paper **#231, pp. 124–125**

Mechanical Properties of 3D Auxetic Structures Produced by Additive Manufacturing

Ondřej Jiroušek[1,a*], Petr Koudelka[2,b], Tomáš Fíla[2,c]

[1]Faculty of Transportation Sciences, Konviktská 20, 110 00 Praha 1, Czech Republic

[2]Institute of Theoretical and Applied Mechanics, Academy of Sciences of the Czech republic, Prosecká 76, Praha 9, Czech republic
[a]jirousek@fd.cvut.cz, [b]koudelkap@itam.cas.cz, [c]fila@itam.cas.cz

Keywords: auxetic structure, direct 3D printing, finite element method, digital image correlation

Abstract: Three distinct auxetic structures were produced by direct 3D printing based on parametric CAD models. Mechanical properties of the structures were established by static compression tests where strain fields on the surface of the specimens was measured by non-contact optical method. Parametric finite element (FE) model of each structure was then subjected to a virtual compression test and mechanical properties obtained from the FE simulations were compared to the experimentally assessed values. After verification, the parametric FE models were used to establish relationships between various design parameters (porosity, rod thickness, internal angles, etc.) and overall mechanical properties (particularly stiffness).

Introduction

Auxetic materials are materials with negative Poisson's ratio, i.e. unlike other materials, auxetics become thicker in the direction perpendicular to the applied strain when stretched. This phenomena is caused by their specific microstructure either at the molecular or macroscopic level. Auxetics thus posses interesting properties such as high energy absorption and fracture resistance [1]. This predetermines them for applications such as body armor, padding and robust shock absorbing material.

Methods

Three different types of auxetic structures were designed and printed (see Fig. 1): i) two-dimensional cut missing-rib, ii) two-dimensional inverted (re-entrant) honeycomb and iii) three-dimensional inverted honeycomb. These structures were then printed using VisiJet EX200 (3D Systems, USA) UV curable acrylic material suitable for high resolution 3D printing with accuracy approx. $328 \times 328 \times 606$ DPI ($25 - 50\,\mu$m resolution). The samples were tested in uni-axial compression experiments to obtain stress-strain response of each microstructure.

Parametric FE model of each auxetic structure has been developed. The geometries have been discretized either with linear 3D hexahedral solid elements or with beam elements, each having 6 degrees of freedom at every nodal point. Beam elements were based on Timoshenko beam theory which includes shear-deformation effects. To inversely calculate the stress-strain relationship of the structures the model must include both geometric and material nonlinearities. In this study material model was considered elasto-plastic with von Mises yield criteria coupled with bilinear isotropic work hardening. Loading has been prescribed in 100 loading steps, i.e. in each step $0.1\,\%$ deformation was applied. Furthermore to take post-buckling behaviour of the thin beams subjected to the large compression into account used strain measures have to also account for higher order terms. Thus in our analyses material stress-strain properties were input in terms of true stress versus logarithmic strain. In every loading step reaction forces originating at the supports have been calculated and the true stresses and strains have been derived.

The FE models were used for description of deformation behaviour of auxetic structures which allows for easy and fast prediction and optimization of the effective mechanical characteristics that

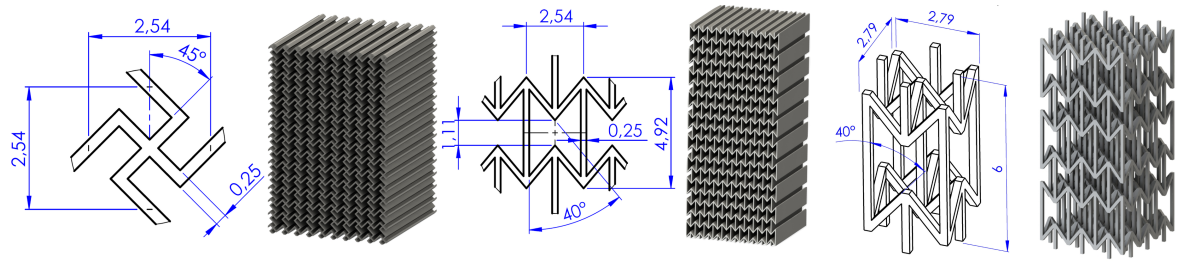

Fig. 1: Auxetic structures used in the study: a) cut missing-rib structure, b) 2D re-entrant structure, c) 3D re-entrant structure

facilitates material's design for specific application. Although there are many analytical models available in the literature, here we used numerical approach only. One reason is that the analytical models assume small deflections neglecting axial deformation of the struts [2]. The other reason is that for investigation of very large deformations one must include for the self-contact between the individual struts. The analytical models are effective only when simplifying assumptions such as small deflection theory and linear elastic material properties are used. In contrary FE approach can be used to prove not only the concept of negative Poisson's ratio and/or to optimize parameters of the structure (e.g. the re-entrant angle, relative density, struts' thickness) but also to maximize the effective parameters of resulting constructs (i.e. deformation energy per unit volume, yield strength of the structure, compressive strength) according to specific requirements.

Stress-strain curves were assessed from the FE simulations inversely, i.e. from reaction forces calculated at the restrained side of the sample. Using such inverse FE simulations it is relatively easy to obtain not only the stress-strain curves for each considered sample, but it is also possible to establish the stresses and strains arising at individual struts from the deformation of the structure. Hence strains can be easily compared to the experimentally obtained values from the digital image correlation at the same positions (i.e. individual markers).

Results

Mechanical behaviour of three different porous microarchitectures exhibiting in-plane and volumetric negative Poisson's ratio was studied both experimentally and numerically. True stress - true strain diagrams in compression were derived and compared for each structure. FE models of all considered microarchitectures were developed and their ability to predict mechanical response of the studied constructs was assessed by comparing numerically and experimentally obtained stress-strain diagrams. Deformation response of the cut missing-rib structure was well captured by the FE model up to 20 % strain. Simulations of re-entrant honeycomb structures showed good correlation of yield point and strain softening characteristics up to 10 % strain. The FE models can be readily used for optimization of the auxetic structures for a specific application.

Acknowledgment: The research was supported by the Czech Science Foundation (research project No. 15-15480S) and by RVO: 68378297.

References

[1] R. Lakes, Foam Structures with a Negative Poisson's Ratio, Science, 235 (1987) 1038–1040.

[2] W. Voigt, Lehrbuch der Kristallphysik, Teubner, Leipzig, 1928.

21st International Conference **ENGINEERING MECHANICS 2015**
Svratka, Czech Republic, May 11 –14, 2015
Paper **#067, pp. 126–127**

VVER-440 Steam Generator's Two-Phase Flow Analysis

Lukáš Joch[1,a]*, Roman Krautschneider[2,b]

[1]Brno University of Technology, Faculty of Mechanical Engineering, Energy Institute, Technická 2896/2, 616 69 Brno, Czech Republic

[2]Institute of Applied Mechanics Brno, Ltd., Resslova 972/3, 602 00 Brno, Czech Republic

[a]jochl@uam.cz, [b]krautschneiderr@uam.cz

Keywords: horizontal steam generator, thermal-hydraulic analysis, two-phase flow, user defined functions

Abstract: The subject of this report is creation of three-dimensional thermal-hydraulic model of horizontal steam generator for Dukovany nuclear power plant. A procedure is presented for simulation and analysis of secondary side of PGV-440 steam generator for nominal and increased reactor power load. A two-fluid approach is applied for modeling physical processes inside the steam generator. Physical models were implemented in ANSYS Fluent CFD environment using User Defined Functions (UDFs). Results from this thermal-hydraulic numerical model can be used for various other subsequent nuclear power plant operations and safety analysis.

Introduction

Steam generator (SG) is one of the most important components of nuclear power plant (NPP) with pressurized water reactors (PWR). The main purpose of this component is heat transfer from the radioactive primary side to the secondary side of SG where steam is generated. Therefore the service life of NPP is closely connected with service life of SG.

Corrosive impurities (iron oxides) concentrated in the secondary side are main problem of SG which decreases designed service life. As a result of thermal-hydraulic processes, the impurities are accumulated in so-called critical zones which are cause increased degradation of heat-transfer tubes (HTT) [1].

Removing these impurities is carried out by periodical and continual operated blowdown system. In order to achieve high blowdown efficiency, the location of critical zone must be known for designing blowdown circuit arrangements [2].

Due to complications related to the measurements of SG and lack of large experimental facilities it is very difficult to describe multi-phase flow on the secondary side. A detailed insight into two-phase flow on the secondary side can be obtained by a three-dimensional thermal-hydraulic numerical simulation.

Methodology

There have been published several works dealing with thermal-hydraulic analysis of horizontal SG in the world. Every NPP with VVER-440 or VVER-1000 reactors has unique design of SG components, therefore it is necessary to create a specific numerical model for SG of Dukovany NPP.

This NPP is equipped by 6 PGV-440, with identical design for each of its four units. A two-fluid approach is applied to model two-phase flow on the secondary side of SG [3]. Certain simplifications, whose the most significant is the modeling of HTT as a porous media, are made.

Special multiphase flow model was developed and implemented in ANSYS Fluent CFD environment using UDFs for the accurate presentation of steam generation processes [4].

The governing equations are solved using six-equation model. This model is based on conservation equations of mass, momentum and energy at two-phase interfaces, as well as between two fluid phases and tube bundles. The two-phase flow interface transfer processes are completed

by closure laws. By using UDFs for mass, momentum and energy source terms, better convergence of numerical analysis was achieved [5].

Results

Obtained data from thermal-hydraulic numerical model provide complete insight of velocity distributions and steam volume fraction (Fig. 1 and Fig. 2). These results can be used for detailed analysis of impurities concentration and obtained data are essential for improvement of blowdown efficiency.

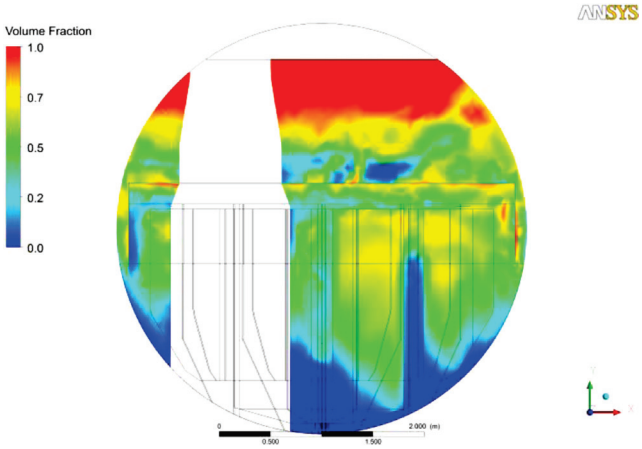

Fig. 1: SG cross section view with steam volume fraction

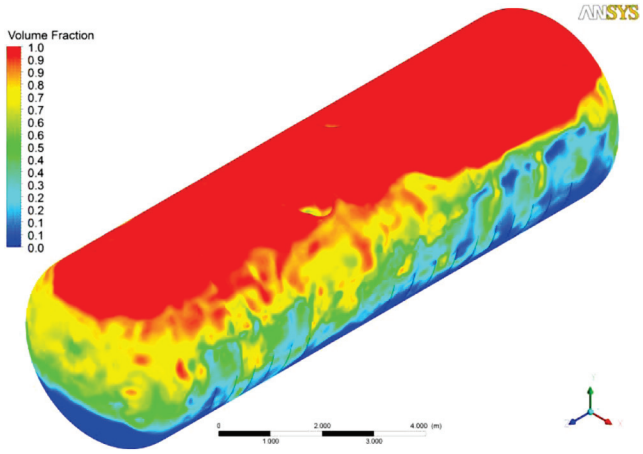

Fig. 2: SG isometric view with steam volume fraction

Conclusions

This report deals with thermal-hydraulic analysis of horizontal steam generator of Dukovany nuclear power plant VVER-440. Due to accumulation of corrosive impurities it is important to know processes which occur on the secondary side of steam generator.

A two-fluid approach is applied for modeling of physical processes inside the steam generator. Physical models were implemented in ANSYS Fluent CFD environment using UDFs.

Results from numerical simulation of two-phase flow can be used in steam generator design, reconstruction, in nuclear power plant operation and safety analyses or for improvement of blowdown circuit and feed water arrangements.

References

[1] N.B. Trunov, S.B. Ryzhov, S.E. Davidenko, Horizontal steam generators: problems and prospects, Thermal Engineering, 58, (2011) 179–183.

[2] I.O. Budko, Yu.F. Kutdjusov, S.I. Gorburov, New technology for purging the steam generators of nuclear power plants, Power Technology and Engineering, 45 (2011) 120–124.

[3] V.D. Stevanovic, Z.V. Stosic, M. Kiera, U. Stoll, Horizontal steam generator thermal-hydraulics at various steady-state power levels, 10th International Conference on Nuclear Engineering, 2002, pp. 767–779.

[4] K. Gerbely, S. Gabor, R. Tamas, Modeling of boiling water flow in the horizontal steam generator of the Paks nuclear power plant, 26th CADFEM users´ meeting, 2008, pp. 1–7.

[5] V. Hovi, M. Ilvonen, CFD-simulation of the VVER-440 steam generator with porous media model, 8th International Seminar on Horizontal Steam Generators, Podol'sk, 2010, pp.1–15.

21st International Conference **ENGINEERING MECHANICS 2015**
Svratka, Czech Republic, May 11 –14, 2015
Paper **#256, pp. 128–129**

Exprimental Modal Analysis of a Rectangular Plate with Embedded Piezoelectric Actuators and Sensors

Miroslav M. Jovanović[1,a,*], Ardeshir Guran[2,b], Aleksandar M. Simonović[3,c], Nemanja D. Zorić[3,d], Nebojša S. Lukić[1,e], Slobodan S. Ilić[1,f]

[1]Serbian Armed Forces, Technical Test Center, Vojvode Stepe 445, 11000 Belgrade, Serbia

[2]Institute of Structronics, Montreal, Quebec, Canada

[3]University of Belgrade, Faculty of Mechanical Engineering,
Kraljice Marije 16, 11120 Belgrade, Serbia

[a]mjovano@sbb.rs, [b]ardeshir.guran@gmail.com, [c]asimonovic@mas.bg.ac.rs,
[d]nzoric@mas.bg.ac.rs, [e]nesaluca@ptt.rs, [f]slobodan.ilic@vs.rs

Keywords: modal analysis, natural frequency, piezoelectric actuator, PVDF sensors, vibration

Abstract: This paper present experimental modal analysis of rectangular thin plates with embedded Piezoelectric Actuators and Sensors. This study gives the difference in natural frequencies of the rectangular plate without and with integrated PZT actuator and PVDF sensors with the aim to define the structural changes before the development of active control vibration system.

Introduction

Integration of actuators and sensors on structure area have changed its modal parameters. The optimization of sizing and location of actuators and sensors for active vibration control of flexible structures has been shown as the one of the most important issues in the design of active structures since these parameters have a major influence on the performance of the control system.

Modes (or resonances) are inherent properties of a structure. Resonances are determined by the material properties (mass, stiffness, and damping properties), and boundary conditions of the structure. Each mode is defined by a natural (modal or resonant) frequency, modal damping, and a mode shape. If either the material properties or the boundary conditions of a structure change, its modes will change. For instance, if piezoelectrical actuator is embedded on structure, the modes of structures will be changed.

Experimental set-up and modal analysis of rectangular plate

Aluminum rectangular plate was used for experimental determination of first three natural frequencies. The experimental set-up was in CFFF configuration and excited at opposite side of clamped side. The response acceleration are measured with two piezo film sensors. PVDF sensors are integrated on clamped side of the plate as shown in Figure 1.

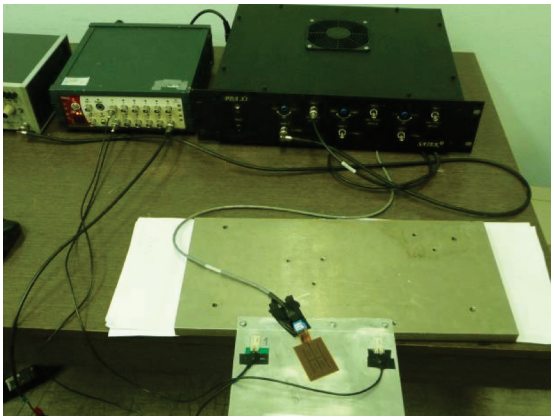

Fig. 1: Plate with integrated PZT actuator and PVDF sensors

The response measurements were acquired, using the multi-channel signal analyzer NetdB 12, and its matched software dBFA Suite, with sampling rate of 12800 Hz.

Table 1 shows Experimental results of the first three natural frequencies for plate without the PZT actuator.

Table 1: Experimental results for plate without the PZT actuator

Modes	Modes	
	Frequency [Hz]	Phase [φ]
1	10.8367	4.64
2	39.9698	179.40
3	70.2782	3.31

The experimental results of the first three natural frequencies for rectangular plate after mounting the piezoelectric actuator are given in Table 2.

Table 2: Experimental results of plate with the PZT actuator

Modes	Modes	
	Frequency [Hz]	Phase [φ]
1	10.5769	1.37
2	39.7837	174.77
3	67.6411	1.13

Natural frequencies of the thin rectangular plate before and after embedded piezoelectric actuators, which are evaluated from experimental methods given in this study are not in compliance.

Local increase of the plate stiffness, with mounted actuator, is given the increase in natural frequencies of whole plate. The mass of the actuator has a lower effect on natural frequencies than its stiffness.

In experiment, the local increase of stiffness from mounted actuator and sensors has a lower effect on natural frequencies in relation of added mass. The added mass is overall mass of glue (epoxy, etc.) and connection cables (sensors and actuator). The experimental result shows that the increase in total mass of the system decreases the frequencies of the first three modes.

Conclusion

In this paper, the first three natural frequencies of a thin rectangular plate before and after integration of the piezoelectric actuator are determined by experiment.

Based on experimental result it is concluded that the consequences in changes of natural frequencies in the process of integration of the sensors and actuators on real structure can approach the system to the working frequencies of external forces, and to reinforce the vibration of the structure.

References

[1] M.M. Jovanović, A. Guran, A.M. Simonović, N.D. Zorić, N.S. Lukić, S.S. Ilić, Estimation the Changes in Modal Parameters of a Rectangular Plate with Embedded Piezoelectric Actuators and Sensors, Proceeding of 12th International Symposium on Stability, Vibration, and Control of Systems (SVCS 2015), Prague, Czech Republic, 2015.

[2] R.C. Fuller, J.S. Elliott, A.P. Nelson, Active Control of Vibration, Academic Press, New York, 1996.

21st International Conference **ENGINEERING MECHANICS 2015**
Svratka, Czech Republic, May 11 –14, 2015
Paper **#051, pp. 130–131**

Preliminary Investigations of Machine Frame Vibration Damping Using Eddy Current Principle

George Juraj Stein[a]*, Peter Tobolka[b], Rudolf Chmúrny[c]

Institute of Materials and Machine Mechanics, Slovak Academy of Sciences,
Racianska 75, SK - 83102 Bratislava, Slovak Republic

[a]ummsste@savba.sk, [b]ummstob@savba.sk, [c]ummschmu@savba.sk

Keywords: eddy current damping, magnetic stiffness, machine frame, multi physics modeling

Abstract. A novel approach to vibration attenuation, based on the eddy current principle, is described. The combined effects of all magnetic forces acting in the oscillatory system attenuate frame vibrations. A mathematical model of the forces balance in the oscillatory system was derived before. Some experimental results from a mock-up machine frame mechanically loaded by a rotating machine and excited at resonance are presented.

Introduction

Vibrations of rotating machinery, mounted on a flexible frame (raft), may interfere with frame eigenfrequencies and resonances can occur. Because of low structural damping the resonance vibrations may exceed the limits of safe operation. Various passive damping methods are used. Apart of visco-elastic and friction dampers occasionally dampers employing electro-magnetic damping principles are used. A very thorough research on their contemporary use is presented in the paper [1]. Author has shown a remarkable attenuation of the excited eigenmodes of cantilever beam transversal vibrations. The first author has analysed an oscillatory system analogous to that one described here; however, with additional coil wound around the permanent magnet [2, 3].

The difficulty of the study of the electro-magnetic dampers in general is their inherent non-linearity, as the physical phenomena are dependent on inverse of the square of the acting distance. It is a non-linear multi-physics problem, which calls for inevitable simplification and linearization.

Experimental device description

The lay-out of the analyzed electro-mechanical system is depicted in Fig. 1. The rotating machine (pos. 1) is situated on a flexible frame, to which a ferromagnetic yoke (pos. 2) is fixed. Below the yoke a rotationally symmetric pot-type core (3) is situated at a static distance d_0. In the axis of the pot core an axially polarized permanent magnet is situated. The mechanical system may be treated as an SDOF oscillatory system with additional magnetic forces. Theoretical analysis of the first order effects was made elsewhere. Here some preliminary experimental results are presented.

Preliminary measurements

The experimental set-up consisted of a frame, fixed to two supporting rigid structures, onto which a commercial small compressor was rigidly fixed. The compressor was loaded by additional dead weight, to excite the frame near its first resonance frequency by machine rotation. Frame vibrations were measured by a MEMS type accelerometer CXL04LP3 (Crossbow, USA) – pos. 4 in Fig. 1; firstly without the damping device and then with the damping device for two different static distances d_0. Acceleration autospectrum, obtained by frequency analysis, is depicted in Fig. 2.

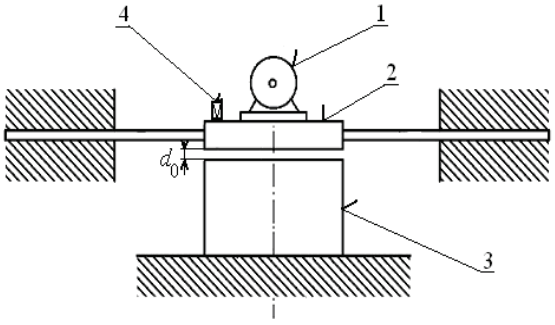

Fig. 1: Schematic lay-out of the treated electro-mechanical oscillatory system.

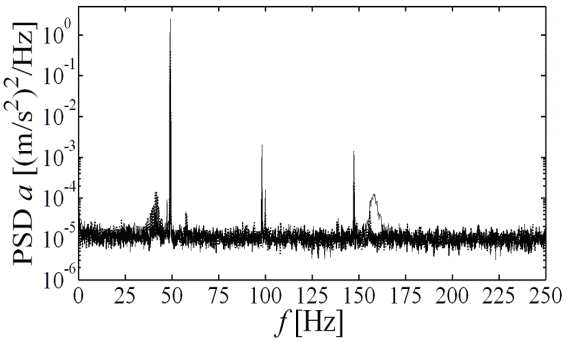

Fig. 2: Autospectrum of acceleration of frame vibrations.

In the autospectrum three marked peaks are seen at the asynchronous rotation frequency and its second and third multiple, as well as the second harmonic of the mains frequency. Enlarged details of each peak are depicted in Fig. 3, where the influence of the damping device is clearly seen.

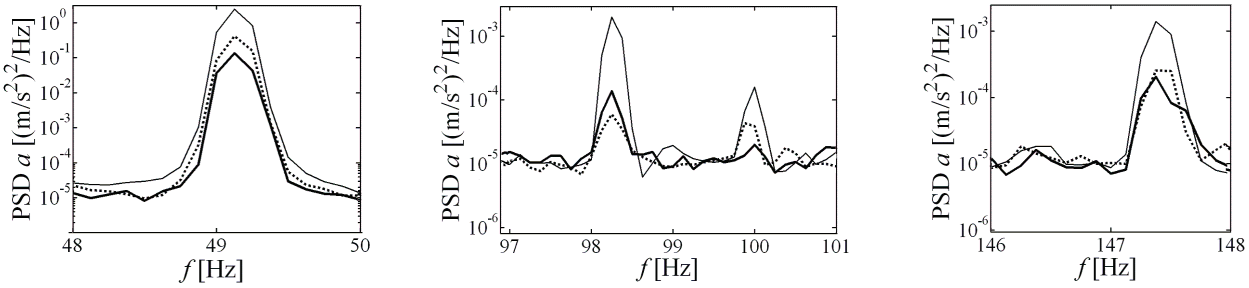

Fig. 3: Details of the peaks in the autospectrum: (a) at the rotational speed, (b) second harmonic and mains second harmonic, (c) third harmonic (── frame, ── d_0 = 0.45 mm, ···· d_0 = 0.53 mm).

Conclusion

From the presented preliminary results the good vibration attenuation in resonance due to the eddy current damper is visible. Up to 12 dB attenuation is attainable at resonance (Fig. 3a). However, because the damping is proportional to vibratory velocity, outside of the resonance frequency band the vibration attenuation is much lower or not present at all.

Acknowledgement: The reported research was conducted within the project No. 2/0058/13 of the Slovak VEGA Grant Agency. The subject of the paper was lodged as a patent application with the Patent Office.

References

[1] H.A. Sodano, J-S. Bae, Eddy current damping in structures. The Shock and Vibration Digest 36 (2004) 468–479.

[2] G.J. Stein, R. Darula, S. Sorokin, Control of forced vibrations of mechanical structures by an electromagnetic controller with a permanent magnet. in: Proceedings of Intl. Conference on Noise and Vibration Engineering (ISMA 2012), Katholieke Universiteit Leuven, (2012) p. 385-393.

[3] G.J. Stein, R. Chmúrny, Damping of beam transversal vibrations by a permanent magnet with coil. Conference: Engineering Mechanics 2013. Institute of Thermomechanics Academy of Sciences, Prague (2013), p. 541-552.

21st International Conference **ENGINEERING MECHANICS 2015**
Svratka, Czech Republic, May 11 –14, 2015
Paper **#170, pp. 132–133**

The Influence of Autocorrelation Length of Random Strength in Stochastic Discrete Simulations

Jana Kaděrová[a], Jan Eliáš[b], Miroslav Vořechovský[c]

Institute of Structural Mechanics, Faculty of Civil Engineering, Brno University of Technology,
Veveří 331/95, 602 00 Brno, Czech Republic

[a]kaderova.j@fce.vutbr.cz, [b]elias.j@fce.vutbr.cz, [c]vorechovsky.m@fce.vutbr.cz

Keywords: concrete, lattice–particle model, random field, bending, autocorrelation length

Abstract: The contribution studies an influence of the autocorrelation length of a random field of local tensile strength and fracture energy on the fracture process zone in concrete beams. Experimentally obtained data on bending of concrete specimens of four different sizes with and without notch were simulated by discrete lattice-particle model enhanced by stochastic extension. The simulations reveal an interesting and clear dependence of the peak load on the autocorrelation length in terms of the mean value and also variability. For example, when the autocorrelation length in unnotched specimens equals roughly the fracture process zone size, the average specimen strength is significantly reduced.

Introduction

Concrete and other similar cementitious composites belong among the most commonly used materials in civil engineering. Concrete is a highly heterogeneous material with quasi-brittle behavior. For the proper understanding of this behavior, a development of advanced complex numerical models is necessary. The models should allow a description and prediction of the material's strength as well as its post-critical response.

Besides models describing the material as a continuum, the meso-scale discrete models can be also employed. Classical lattice models represent the material as a system of elasto-brittle elements forming a lattice with geometry independent of the inner material structure. Nevertheless, due to their fine resolution, these models demand long computational time and therefore such a modeling strategy is not suitable for larger structural elements. A model with a less dense lattice, where the nodes correspond to individual aggregates, seems to be a suitable compromise. These models are termed as the *lattice–particle* models. The contacts between adjacent elements (large particles) generally have a nonlinear constitutive law (for example linear elastic branch followed by a nonlinear softening branch).

Discrete lattice-particle model

One advantage of meso-scale models lies in the incorporation of spatial material variability by modeling its inner meso-structure. Although here being referred to as the *deterministic model*, the response of this model varies due to the heterogeneity of the inner structure, which is constructed by generated spheres of random diameters and random positions, representing the individual mineral aggregates in concrete. Furthermore, an additional stochastic description, capturing the variability in some model parameters of material, can be considered and modeled by a random field. In the present contribution, parameters of the lattice–particle model developed by Cusatis [1] are modeled by stationary random field. Such a model was used to simulate bending experiments on concrete beams [2, 3] and is referred here to as the *stochastic model*.

Selected parameters of the contacts were considered as randomly spatially varying. They were described by a single random field with Gauss-Weibull probability distribution [4] and squared exponential autocorrelation function (with autocorrelation length l_c as an additional parameter). Parameters of the deterministic and stochastic models were identified using the response of concrete beams of four different sizes and three different notch lengths loaded in bending [3].

Deterministic and stochastic simulations

The variability of response caused by the random location and diameter of particles was evaluated with the results of deterministic model and compared with the results of stochastic simulations. In stochastic simulations, four parameters (tensile and shear strength and fracture energy in tension and in shear) were selected to be modeled as random and linearly dependent on each other. Therefore, the variability of all four parameters was represented by a single random field. The mean value of each random parameter was equal to the parameter values used in the deterministic model and the coefficient of variation was fitted on some experimental data (see [3] for more details).

Comparing both types of simulations, there is a significant increase in response variance (of strength as well as of fracture energy) of notched beams after the consideration of variability of input variables. The mean value of both quantities kept unchanged. For the unnotched beams, the decrease in the mean strength could be observed, which can be explained by a higher probability of the occurrence of weaker spots at the bottom face of the beam, where the crack can initiate. The random field helps the strain to localize into narrower zones and the numerical calculation to converge compared to deterministic simulations.

The main conclusion from the stochastic simulations of notched and unnotched bent beams with various autocorrelation lengths are as follows: In *unnotched* beams with $l_c \to \infty$ the random parameters take constant random values over the volume of the specimens and therefore the variability of nominal strength is composed of the variability measured in deterministic models plus the variability due to random local strength. The mean value is not influenced. When $l_c \to 0$, the nominal strength is virtually similar to the strength of deterministic models because the whole FPZ (fracture process zone) of relatively large size has a homogenized strength of randomly varying local strengths. When, however, l_c is approximately equal to the size of FPZ, the average nominal strength of the whole beam attains its minimum that is lower than the strength of the deterministic model.

In *notched* specimens, the ability to sample from many possible weak zones to form a decisive FPZ is limited by the stress concentration. Therefore, the effect of autocorrelation length on the mean strength vanishes. However, the autocorrelation length influences the variability in nominal strength. When l_c reaches the ca $3 \cdot d_{max}$, the variability suddenly increases.

Acknowledgement: This outcome has been achieved with the financial support from Specific University Research (No. FAST-J-15-2664) and by the Czech Science Foundation (Nos. 15-19865Y and GC13-1941J). The support is gratefully acknowledged.

References

[1] G. Cusatis, L. Cedolin, Two-scale study of concrete fracturing behavior, Eng Fract Mech 74 (2007) 3–17.

[2] J. Eliáš, M. Vořechovský, J. Skoček, Z.P. Bažant, Stochastic discrete meso-scale simulations of concrete fracture: Comparison to experimental data. Eng Fract Mech 135 (2015) 1–16.

[3] J. Kaděrová, J. Eliáš, Simulations of Bending Experiments of Concrete Beams by Stochastic Discrete Model, In: Key Eng Mat 627 (2014) 457–460.

[4] Z.P. Bažant, S.-D. Pang, Activation energy based extreme value statistics and size effect in brittle and quasibrittle fracture. J Mech Phys Solids 55 (2007) 91–131.

21st International Conference **ENGINEERING MECHANICS 2015**
Svratka, Czech Republic, May 11 –14, 2015
Paper **#082, pp. 134–135**

Calibration of Hypoplastic Models for Soils

Tomáš Kadlíček[a]*, Tomáš Janda[b], Michal Šejnoha[c]

Thákurova 7/2077, 166 29 Praha 6 Dejvice, Czech Republic

[a]tomas.kadlicek@fsv.cvut.cz, [b]tomas.janda@fsv.cvut.cz, [c]sejnom@fsv.cvut.cz

Keywords: hypoplasticity, fine grained soils, coarse grained soils, calibration, parameters.

Abstract: The paper is concerned with hypoplastic models for both coarse and fine grained soils. It concentrates on the description of models parameters and presents procedures for their evaluation based on laboratory tests.

Introduction

The theory of hypoplasticity offers a sound approach to the modeling of soil behavior which considerably differs from classical plasticity theories represented for example by the Mohr-Coulomb or Cam-Clay material models. Unlike these models it allows for the description of nonlinear response of soils from the onset of loading as well as upon unloading. It captures most of the principal features of the soil behavior including the dependence of the soil stiffness on void ratio and stress level. Although the essential material parameters can be calibrated on the bases of standard laboratory tests, the hyploplastic models are still far from being generally accepted. The objective of this paper is thus to provide a suitable tool for the estimation of model parameters exploiting laboratory measurements and numerical simulations to bridge the gap between the theoretical formulation of hyploplastic models and their application in engineering practice.

Hypoplastic model for coarse grained soils

This model was put forward already in 1996 [1] and at the present time is generally accepted as a hypoplastic model for sand. It introduces eight parameters φ_c, h_s, n, e_{d0}, e_{c0}, e_{i0}, α and β, which can be divided into groups according to the laboratory tests and methods necessary for their determination.

We begin with the critical angle of friction φ_c. This angle is possible to evaluate as an angle of repose φ_{rep} for a soil with the grain size larger than 0.1mm. For soils containing grains smaller than 0.1mm the friction angle φ_c can be determined from standard triaxial shear test. Two other parameters h_s and n control the slope and curvature of the limiting void ratio curve represented by Eq. (1), which describes the evolution of void ratio e_i under isotropic compression as

$$e_i = e_{i0} \exp[(-3p/hs)\exp(n)]. \tag{1}$$

Notice that parameter h_s can be directly extracted from the Eq. 1 upon time differentiation. Parameters controlling the position of limiting void ratio curves in the e x ln(p) plane are e_{d0}, e_{c0}, e_{i0} (see Fig. 1). The limiting void ratio e_{c0} might be evaluated by the means of undrained triaxial shear test or oedometric test. In case of triaxial test, the parameters h_s and n have to be evaluated in advance. When adopting eodometric test, the parameter e_{c0} can be associated with the initial void ratio providing the soil sample is in its loosest state. The limiting void ratio e_{i0} is the theoretical value of the loosest possible state having analogy with a distribution of spheres in a gravity-free space. For that reason the value of $e_{i0} = 1.2e_{c0}$ was proposed as a representative one. The void ratio of maximal density e_{d0} can be acquired by cyclic shearing with a small amplitude at constant pressure and additionally evaluated from oedometric test using parameters h_s and n and Eq. 1. The last two parameters α and β control the evolution of stiffness and pyknotropy factors [1,2]. These parameters can be found numerically by simulating the triaxial shear test.

Hypoplastic model for fine grained soils

The hypoplastic model for clay [2] consists of five parameters φ_c, ν, λ^*, κ^* and N, which are much similar to those defining the Cam-Clay model. First two parameters can be evaluated from the results of triaxial test while other three follow from oedometric or isotropic compression test.

The the critical state friction angle φ_c can be estimated from the results of triaxial shear test displayed in the form mean stress-deviatoric stress diagram. The parameter ν controls the ratio of bulk modulus K to the shear stiffness G. A suitable way of how to determine the parameter ν is to perform a parametric study of the triaxial shear test. In order to minimize errors resulting from sample defects, it is advisable to determinate parameters φ_c and ν from the set of at least three triaxial tests.

Establishing parameters λ^*, κ^* and N requires performing the isotropic compression test or alternatively the oedometric test (see Fig. 2). Parameters λ^* and κ^* represent slopes of the *NCL* (Normal Consolidation Line) and isotropic unloading line, respectively, and are read out from the $\ln(e + 1)$ x $\ln(p)$ plane. Conveniently, the test might be executed on the reconstituted soil samples and *NCL* is then reached under a lower loading pressure. Parameter N, similarly to parameters e_{d0}, e_{c0} and e_{i0} in the coarse grained soil moded, specifies the position of *NCL* in $\ln(e + 1)$ x $\ln(p)$ plane and represents the value of void ratio corresponding to the mean stress $p = 1$. When deriving the parameter N from the oedometric test, its value has to be adjusted in consideration of the correct position of *NCL*. [2]

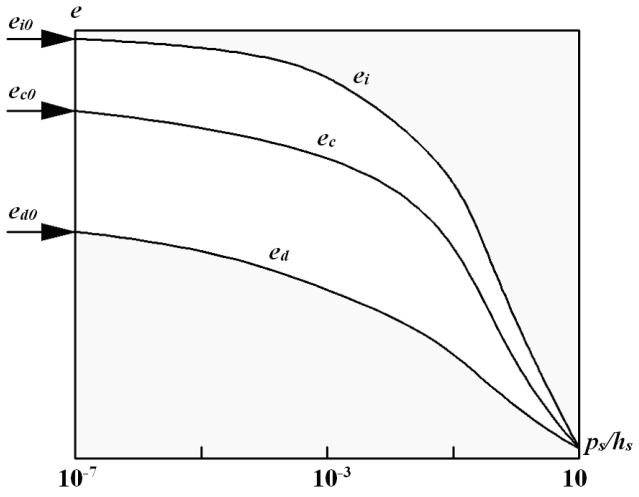

Fig. 1: Evolution of limiting void ratios

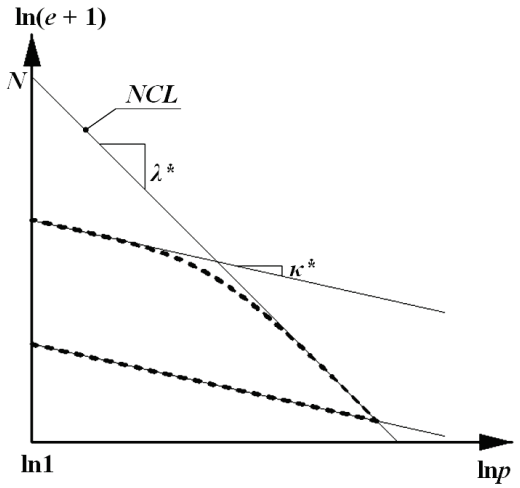

Fig. 2: Progression of an isotropic compression test

Summary

A brief overview of material parameters of two hypoplastic material models was given together with their possible evaluation from a suitable combination of basic laboratory tests and simulations. It is our current effort to developed an automotive numerical tool to make the calibration process as simple as possible and thus to brink these models to the point of practical applications.

Acknowledgement: The financial support provides by the projects TA04031603 and SGS15/031/OHK1/1T/11 is gratefully acknowledged.

References

[1] G. Gudehus, A comprehensive constitutive equation for granular materials, Soil and foundations, 36 (1996) 1-12.

[2] D. Mašín, A hypoplastic constitutive model for clays, International Journal for Numerical and Analytical Methods in Geomechanics 29 (2005) 311–336.

21st International Conference **ENGINEERING MECHANICS 2015**
Svratka, Czech Republic, May 11 –14, 2015
Paper **#149, pp. 136–137**

Detail Topometrical FEM Optimization of Wing Structural Panel

Tomáš Katrňák[a]*, Jaroslav Juračka[b]

Brno University of Technology, Faculty of Mechanical Engineering,
Institute of Aerospace Engineering, Technická 2896/2, Brno 61669, Czech Republic

[a]katrnak@fme.vutbr.cz, [b]juracka@fme.vutbr.cz

Keywords: FEM, topometrical optimization, wing structure, stress analysis

Abstract: The detail topometrical optimization of the critical wing part of the aircraft is presented in this article. The integral lower wing structural panel of the aircraft in the CS-23 Commuter category is selected for the optimization. The first case demonstrates significant weight savings using the modern FE optimization methods for determined structural constraints. The practical aircraft operation and additional regulation requirements affect optimization constraints in the second case. The detail optimization also consists of the FE model validation, stress analyses and complex load capacity analyses, which are necessary for designed structural modifications with an optimal stress distribution.

Introduction

The modern finite element optimization methods allow to design an optimal stress distribution on complex structural parts. The structural optimization is a process of such design which fulfills all the requirements and minimizes weight or other efficiency decreasing factors. The weight of the structure is the objective function of an optimization. The structural shape and dimensions constitute a design space.

Accuracy and usability of the optimization process could be divided to certain stages. First, the preliminary study of the optimization possibilities and estimated weight savings could be done. The general constrains according to mainly the structural or material requirements are applied. This case could demonstrate significant weight savings and other advantages.

The second stage involves more practical requirements into account. The real aircraft operation, certain specific load cases and certification requirements must be used in the aircraft design. The next stage reflects also the production costs, manufacturing technique and technological demands.

The initial and also the second detail optimization stages of the wing structure are presented in this paper. The utilization of modern optimization methods, real operation conditions and certification requirements are described in detail.

Optimized aircraft structure

The presented optimization and analyses were made on a demand of the aircraft producer and the main purpose was to obtain the optimal structural design and to select locations for weight savings at the wing structure of the L 410 NG aircraft, which is designed in CS-23 Commuter category. An inspected aircraft part is the complex metal semi-shell wing structure with attached engine mounts, integral fuel tanks and rudders.

The main focus was put on the integral lower wing panel, presented in Fig. 1. There each skin or stringer segment could be produced with different thickness on this milled wing panel. All strength, stiffness and certification requirements specified by the producer must be fulfilled. Also the Damage tolerance philosophy is utilized in this design to increase the aircraft fatigue durability.

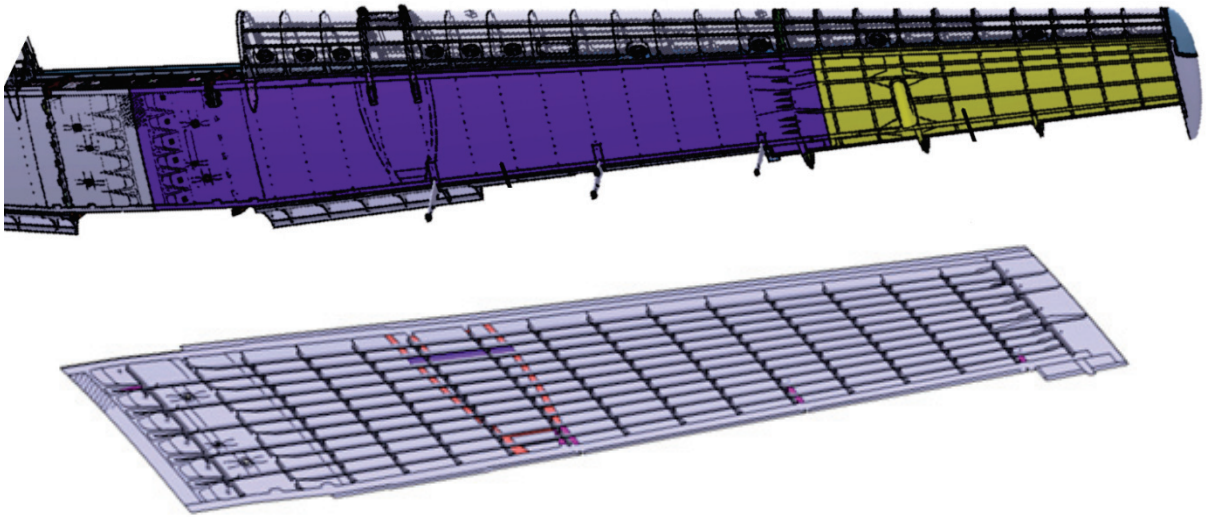

Fig. 1: Detail of wing structure and optimized lower wing panel

Optimization process

For our purposes, the deterministic gradient methods implemented in the MSC.NASTRAN software were used. The specific types of the structural optimization are topological and topometrical optimizations.

The topometrical optimization is the proper shape optimization solution for this case, where distances and number of stiffeners must be kept in the design. Its example is presented in Fig. 2, where only the element thicknesses of panel skins and stringers are modified to the maximal material utilization.

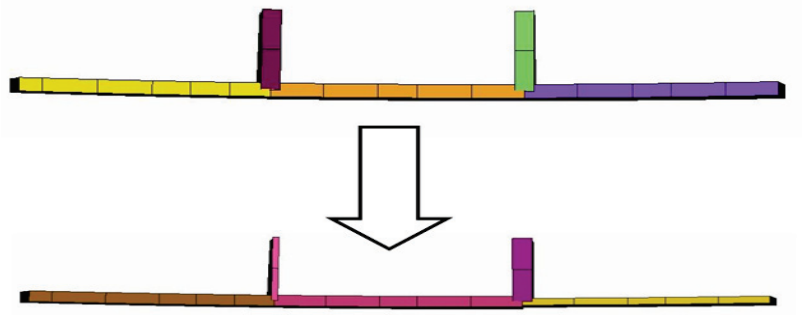

Fig. 2: Example of thickness optimization of panel skins and stringers

Acknowledgement: These outputs were supported by the project TE02000032 - Advanced Aerostructures Research Centre. This project was realized with financial support from national budget of the Technology Agency of the Czech Republic.

21st International Conference **ENGINEERING MECHANICS 2015**
Svratka, Czech Republic, May 11 –14, 2015
Paper **#127, pp. 138–139**

Multibody Based Tool for Simulation of the Turbocharger Rotor Dynamics

Jiří Knotek[a]*, Pavel Novotný[b], Ondřej Maršálek[c]

Brno University of Technology, Faculty of Mechanical Engineering,
Technická 2896/2, 616 69 Brno, Czech Republic

[a] knotek@iae.fme.vutbr.cz, [b] novotny.pa@fme.vutbr.cz, [c] marsalek@fme.vutbr.cz

Keywords: turbocharger, floating ring bearing, finite element method, Reynolds equation

Abstract: The turbocharger is a unique example of the rotating machinery. Not only for its very high speed, but also because of its compact design and difficult operating conditions (i.e. high temperature, harsh vibrations, etc.). Moreover, measuring of most parameters characterizing the rotor dynamics is a very difficult task. Thus, it is advantageous to replace the real turbocharger with a computational model and determine the turbocharger rotor dynamics using such a simulation tool.

The first part of the paper describes the theoretical background of the simulation tool. The second part presents the example of the simulation results and the last part discusses the possibility of experimental verification of the simulation tool.

The theoretical background can be divided in to two parts – theory of the hydrodynamic model of the floating ring journal bearing; and the theory of the rotor modeling and modal reduction. The whole model is designed as the uncoupled hydrodynamic model, and the structural solution is used (i.e. the hydrodynamic solution is solved separately and its results are imported to the solution of the rotordynamics itself).

The hydrodynamic model of the floating ring bearing is treated as two separate oil films (i.e. inner and outer oil film). The inner oil film separates the shaft from the floating ring and the outer oil film separates the floating ring from the housing bore. Moreover, the knowledge and experience of our research team were used at the first stage of the development of the turbocharger simulation tool.

The hydrodynamic pressure distribution in the oil film is solved separately for the inner and outer oil film. The solution is based on the nonlinear Reynolds differential equation, which is based on the modified Navier-Stokes equation and continuity equation transformed for cylindrical shape of the bearing oil gap. The basic form of the Reynolds equation is well-known, but more important is the form of the equation after simplifications (Eq. 1) which enables to use the uncoupled solution.

$$\frac{\partial}{\partial x}\left(\frac{h^3}{\eta}\frac{\partial p}{\partial x}\right)+\frac{\partial}{\partial z}\left(\frac{h^3}{\eta}\frac{\partial p}{\partial z}\right)=6U\frac{dh}{dx}+12\frac{dh}{dt} \tag{1}$$

The equation is solved by iterative numerical solution, using Gauss-Seidel method. The solution also considers cavitation and pin tilting effect. On the other hand, for the purpose of the hydrodynamic solution, the deformation of the shell and pin is neglected. The pressure distribution depends mainly on the dimensionless oil film thickness, which is described in Eq. 2.

$$H=1+\left(\varepsilon-Z\cdot\gamma\cdot(1-\varepsilon)\right)\cdot\cos\varphi+\delta\cdot Z\cdot\sin\varphi\cdot\sqrt{1-(\varepsilon+(1-\varepsilon)\cdot|\gamma|^2)} \tag{2}$$

The second main part of the theoretical background deals with the modeling of the turbocharger rotor. The rotor is created in three stages; firstly the shaft is discretized by the FE method, then the

modal reduction of the FE model is performed, and in the last step the rotor is assembled in the MBS environment.

Several types of results are determined using the simulation model – e.g. bearing eccentricity, floating ring speed, power loss, wheel nose displacement, etc. For example, the Fig. 1 shows the Waterfall diagram of the displacement on the compressor wheel nose. Speeds of the floating rings, rotor and its combination, and their multiples are plotted in the diagram. This type of plot helps to track down the vibration modes and to determine their cause.

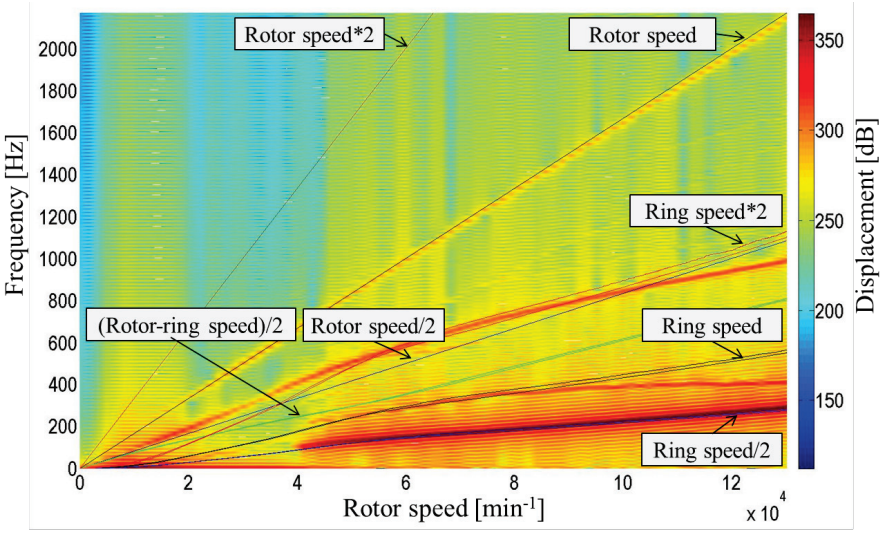

Fig. 1: The Waterfall diagram of the displacement on the compressor wheel nose

Summary

This short paper presents the basics of the turbocharger model developed by our research team. This model aims to help designers to develop new turbochargers quicker, cheaper and more effective combining both simulation and experimental measuring. The current turbocharger model can be considered a foundation for further development and improvement of each part of the model.

Acknowledgement: This work is an output of NETME CENTRE PLUS research activities (project no. LO1202) and is funded by the Ministry of Education, Youth and Sports under the *National Programme for Sustainability I.*

21st International Conference **ENGINEERING MECHANICS 2015**
Svratka, Czech Republic, May 11 –14, 2015
Paper **#108, pp. 140–141**

Fresh Concrete Flow through Reinforcing Bars using Homogenization Approach

Filip Kolařík[a], Bořek Patzák[b], Jan Zeman[c]

Department of Mechanics, Faculty of Civil Engineering, CTU in Prague,
Thákurova 7, 166 27, Prague, CZ

[a]filip.kolarik@fsv.cvut.cz, [b]borek.patzak@fsv.cvut.cz, [c]zemanj@cml.fsv.cvut.cz

Keywords: flow, fresh concrete, homogenization, Variational Multiscale Method

Abstract: Mechanical performance, surface quality, and durability of concrete structures is to a significant extent influenced by the casting process. Thus, predicting the flow behavior of concrete in the formwork, and identification of critical zones, has become an important part of the design procedure of concrete mixes. The aim of the present contribution is to model the effect of reinforcing bars in the single-fluid approach by means of computational homogenization. Flow in parts of the domain without any reinforcement is governed by Stokes equations. In areas with the reinforcement, governing equation is Darcy law, which is obtained by averaging the velocity on the microscale.

Introduction

The modeling of fresh concrete casting is an important issue for construction industry but also very interesting problem from the computational point of view. One of the main issues represents the effect of reinforcement on the flow of fresh concrete. In the case of traditional reinforcement, the reinforcing bars represent obstacles to the flow of fresh concrete, see [1] for wider discussion. Direct modeling of each reinforcing bar individually is theoretically possible, but usually not affordable, as the mesh would have to be locally very fine and simulations too time-consuming. Natural way how to avoid this difficulty is to consider the reinforced area as a porous medium and employ multiscale approach. In this work, we follow procedure introduced in paper [2], where so-called variational multiscale method is combined with usual separation of scales.

Description of the problem

Fresh concrete is in our approach considered as a single homogeneous fluid with Bingham model as a constitutive relation. For the time being, we restrict ourselves to steady state flow. This can be justified by the fact that flow of the concrete is slow enough so the inertia effects are negligible. Following methods introduced in [2], we employed variational multiscale method. After formulation of the Stokes problem in the weak sense, the trial and test functions corresponding to pressure are decomposed into subscale and macroscale parts. According to that decomposition, standard weakly formulated Stokes problem splits into subscale and macroscale problem as well. The macroscale problem represents continuity equation, while the subscale remains the Stokes problem. Next step consists in introducing intrinsic averages and in decomposing the whole domain into union of non-overlapping subdomains (referred to as RVE's). Averaging applied to the macroscale problem leads to (non-linear) Darcy law, which relates macroscale effective seepage velocity field with pressure gradient in the pores. The seepage velocity is obtained by averaging velocity over the RVE, where the flow is driven by macroscopic pressure gradient. The whole problem is solved using FEM, linear approximations for both velocities and pressures have been used. Numerical scheme for both the Stokes and the Darcy problem was stabilized by Variational Multiscale Method proposed in [3] due to Babuška-Brezzi condition.

Numerical examples

The solution obtained by homogenization technique is compared with direct simulation, where the reinforcement is modeled explicitly. The results are shown in Fig. 1.

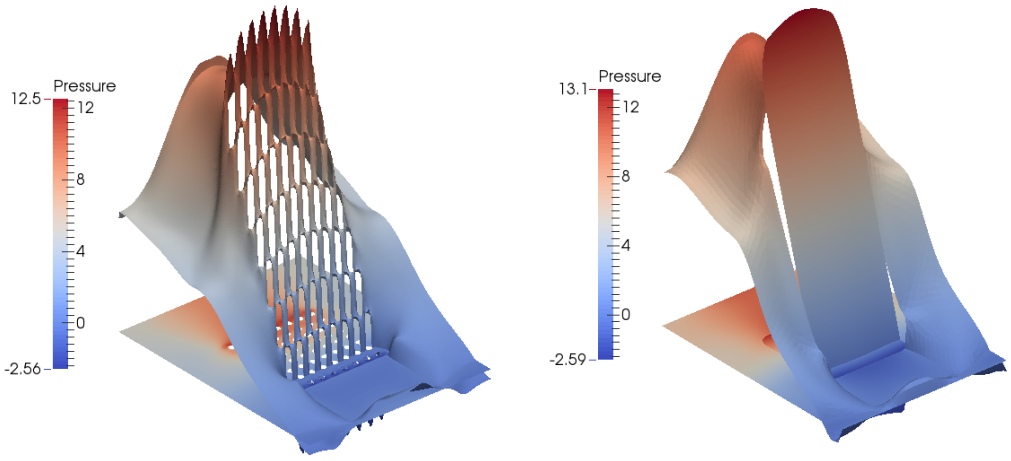

Fig. 1: Flow through the reinforced area - Comparison of fully resolved solution (on the left) and homogenized solution (on the right).

Summary

In this paper, we showed homogenization approach to modeling of the influence of reinforcement to the flow of fresh concrete. The model was validated against direct numerical simulation and results are in a very good agreement.

Acknowledgement: The research was carried out within the the project SGS15/031/OHK1/1T/11 — Advanced numerical modeling in mechanics of structures and materials and the authors gratefully acknowledge the financial contribution of the MŠMT ČR.

References

[1] N. Roussel et al., Computational modeling of concrete flow: general overview Cement and Concrete Research 37 (2007) 1298–1307.

[2] C. Sandström, Fredrik Larsson, Variationally consistent homogenization of Stokes flow in porous media Journal for Multiscale Computational Engineering 11 (2013) 117–183.

[3] T. J. R. Hughes et al., The variational multiscale method - a paradigm for computational mechanics Computer Methods in Applied Mechanics and Engineering 166 (1998) 3–24.

21st International Conference **ENGINEERING MECHANICS 2015**
Svratka, Czech Republic, May 11 –14, 2015
Paper **#013, pp. 142–143**

Partitioned Equations of Motion for Wave Propagation Problems in Solids

Radek Kolman[1,a], Sang Soon Cho[2,b], K.C. Park[3,c]

[1]Institute of Thermomechanics, v.v.i., Academy of Sciences of the Czech Republic, Dolejškova 5, Prague 8, Czech Republic

[2]Korea Atomic Energy Research Institute, 999-111 Daedeok-Daero, Yuseong-gu, Daejeon, Republic of Korea

[3]Center for Aerospace Structures, University of Colorado at Boulder, Boulder, CO 80309 - 0429, Colorado, USA

[a]kolman@it.cas.cz, [b]sscho96@kaeri.re.kr, [c]kcpark@colorado.edu

Keywords: decomposition of equations of motion in solids, longitudinal and shear waves in solids

Abstract: We present a decomposition of equations of motion in solids into a $curl$-zero (longitudinal) component and a $divergence$-zero (shear) component. Partitioned equations of motion are needed for accurate finite element numerical modelling of wave propagation problems. In that case, each equation of motion is integrated separately with corresponding critical time step size in explicit time integration. By this approach, dispersion behaviour of the finite element method and mainly spurious oscillations in numerical results can be suppressed.

Introduction

A novel explicit time integration method in finite element computations of wave propagation problems in solids has been presented in [1, 2, 3]. This technology is based on separate integration of longitudinal and shear waves with each critical time step size respecting different wave speeds. The mentioned time integration scheme is the three-time step scheme in the predictor-corrector form and it produces excellent results without spurious oscillations near theoretical wavefronts. In this paper, we give a theoretical framework for a wave orientated decomposition of the equations of motion in solids.

Decomposition of displacement fields and equations of motion

From the vector analysis [4], we know that a vector field $\mathbf{p}(\mathbf{x})$ with described boundary conditions, which is defined on a bounded Lipschitz domain $\Omega \subset \mathbb{R}^3$, $\mathbf{x} \in \Omega$, and is twice continuously differentiable, can be decomposed into two parts: an $irrotational$ (curl-free) component which can be expressed by the gradient of a scalar function and a $rotational$ (divergence-free) component which can be expressed by the curl of a vector function. This decomposition of a vector field is called the $Helmholtz$ decomposition [4, 5].

In the Helmholtz decomposition, the vector field $\mathbf{p}$ is given by the sum of the gradient of a scalar potential ϕ and the curl of a vector potential $\boldsymbol{\psi}$ as

$$\mathbf{p} = \operatorname{grad}\phi + \operatorname{curl}\boldsymbol{\psi} \quad \text{with the condition} \quad \operatorname{div}\boldsymbol{\psi} = \mathbf{0} \tag{1}$$

The proof of the Helmholtz decomposition of a vector field on arbitrary domains and with prescribed non-homogeneous boundary conditions can be found in [6]. Here, formulæ for the scalar potential ϕ and the vector potential $\boldsymbol{\psi}$ have been also derived.

For the following text, we denote expressions $\mathbf{p}_1 = \operatorname{grad}\phi$ and $\mathbf{p}_2 = \operatorname{curl}\boldsymbol{\psi}$. The main properties of the Helmholtz decomposition of the vector field $\mathbf{p}$ decomposed by Eq. 1 are following

$$\operatorname{div}\mathbf{p} = \operatorname{div}\mathbf{p}_1, \quad \operatorname{curl}\mathbf{p} = \operatorname{curl}\mathbf{p}_2, \quad \operatorname{curl}\mathbf{p}_1 = \mathbf{0}, \quad \operatorname{div}\mathbf{p}_2 = 0 \tag{2}$$

These expressions serve for derivation of a decomposition of equations of motion in solids.

The equations of motion in solids (the law of balance of linear momentum) [5] defined on a domain $\Omega \subset \mathbb{R}^3$ take the vector form as

$$\operatorname{div} \boldsymbol{\sigma} + \mathbf{b} = \rho \ddot{\mathbf{u}} \tag{3}$$

where we assume that Dirichlet and Neumann boundary conditions of the problem are defined. Here, $\boldsymbol{\sigma}$ is the Cauchy stress tensor, $\mathbf{b}$ is the volume intensity vector, $\ddot{\mathbf{u}}(\mathbf{x}, t)$ is the acceleration vector field, $\mathbf{x} \in \Omega$ is the position vector, t is the time and ρ is the mass density. Each vector field, taking place at the equations of motion Eq. 3 (i.e. $\operatorname{div} \boldsymbol{\sigma}$, $\mathbf{b}$ and $\ddot{\mathbf{u}}$), can be decomposed by the Helmholtz decomposition into two parts: irrotational (marked with the subscript L) and rotational (marked with the subscript S). We suppose that boundary conditions for $\ddot{\mathbf{u}}$ and $\operatorname{div} \boldsymbol{\sigma}$ should be also respected. Then, we have got

$$(\operatorname{div} \boldsymbol{\sigma})_L + (\operatorname{div} \boldsymbol{\sigma})_S + \mathbf{b}_L + \mathbf{b}_S = \rho \ddot{\mathbf{u}}_L + \rho \ddot{\mathbf{u}}_S \tag{4}$$

If the operators div and the operator curl are applied on Eq. 4 and with respect to Eq. 2, it yields

$$\operatorname{div}\big[(\operatorname{div}\boldsymbol{\sigma})_L + \mathbf{b}_L - \rho \ddot{\mathbf{u}}_L\big] = 0, \qquad \operatorname{curl}\big[(\operatorname{div}\boldsymbol{\sigma})_S + \mathbf{b}_S - \rho \ddot{\mathbf{u}}_S\big] = \mathbf{0} \tag{5}$$

The two last equations are vanished only if it is valid

$$(\operatorname{div} \boldsymbol{\sigma})_L + \mathbf{b}_L = \rho \ddot{\mathbf{u}}_L, \qquad (\operatorname{div} \boldsymbol{\sigma})_S + \mathbf{b}_S = \rho \ddot{\mathbf{u}}_S \tag{6}$$

These two last equations are the sought decomposed system of the equations of motion in solids.

In the case of linear elastodynamic theory of an isotropic homogeneous body and neglecting of body forces, the equation Eq. 6left describes propagation of longitudinal waves and the equation Eq. 6right controls propagation of shear waves [5].

Summary

We presented a technique for decomposition of equations of motion in solids into longitudinal and shear components. These partitioned equations of motion serve for accurate numerical modelling of wave propagation problems. In [2, 3], a specific explicit time integration method using the partitioned equations of motion in finite element computation has been published. Further, the discrete longitudinal and shear operators as counterparts of the operators div and curl, which are able to guarantee the decomposition of an arbitrary discretized vector field by the linear finite element method as the sum of the $curl$-zero (longitudinal) and $divergence$-zero (shear) components, have been found in [2, 3].

Acknowledgements: The work of R. Kolman has been supported by the grant projects GACR, No. GAP101/12/2315, and the grant project TACR, No. TH01010772. All grant projects supported by the Czech Science Foundation (GACR) and the Technology Agency of the Czech Republic (TACR) were realized within institutional support RVO:61388998.

References

[1] K.C. Park, S.J. Lim, H. Huh, Int. J. Numer. Meth. Eng. 91 (2012) 622-643.

[2] S.S. Cho, K.C. Park, H. Huh, Int. J. Numer. Meth. Eng. 95 (2013) 212-237.

[3] R. Kolman, S.S. Cho, K.C. Park, submitted to Int. J. Numer. Meth. Eng. (2015).

[4] J.W. Gibbs, Vector Analysis (Yale University Press: New Haven 1901).

[5] J.D. Achenbach, Wave Propagation in Elastic Solids (North-Holland, Amsterdam 1973).

[6] H. Sohr, The Navier-Stokes Equations. An Elementary Functional Analytic Approach (Birkhäuser Verlag, Basel 2001).

21st International Conference **ENGINEERING MECHANICS 2015**
Svratka, Czech Republic, May 11 –14, 2015
Paper **#217, pp. 144–145**

Deformation Mechanisms of Auxetic Microstructures for Energy Absorption Applications

Petr Koudelka[a*], Michaela Neuhäuserová[b], Tomáš Fíla[c], Daniel Kytýř[d]

Czech Technical University in Prague, Faculty of Transportation Sciences,
Konviktská 20, 110 00 Prague 1, Czech Republic

[a]xpkoudelka@fd.cvut.cz, [b]neuhamic@fd.cvut.cz, [c]filatoma@fd.cvut.cz, [d]kytyr@fd.cvut.cz

Keywords: auxetic structure, compression, quasi-static testing, digital image correlation

Abstract: In this work parametric modelling was utilized to design and produce two types of porous microarchitectures with auxetic compressive properties suitable for deformation energy mitigation applications such as blast and bullet protection. The samples were directly produced from acrylic material using a high resolution 3D printer and their compressive mechanical characteristics were tested. Two different structures exhibiting in-plane negative strain dependent Poisson's ratio were selected for the analysis: i) two-dimensional inverted (re-entrant) honeycomb and ii) two-dimensional cut missing-rib. Stress-strain relationships were established from a set of quasi-static compression experiments where the strain fields were evaluated using digital image correlation applied to measure the full-field displacements on the samples' surface. From the displacement fields true strain – true stress curves were derived for each sample and relative elastic moduli were evaluated.

Introduction and methods

Recently much effort has been concentrated on development of advanced materials providing high impact energy absorption capabilities for applications where weight is a crucial factor. One of possible solutions are porous solids (i.e. open or closed cell foams) which are advantageous by their low specific weight and thus high specific stiffness. However usage of most foam types including metallic foams is impossible for certain applications (including blast protection) as it may be necessary to use materials with relatively high compressive strength [1]. One of possible approaches how to deal with absorption of enormous amounts of deformation energy during blast and impact loading of structures is to produce a highly optimized porous structure taking advantage of negative Poisson's ratio of its skeleton [2].

In this paper two microstructures utilizing in-plane negative Poisson's ratio were produced by direct 3D printer Pro Jet HD3000 (3D Systems, USA) utilizing multi-jet modelling technology. Samples were produced from VisiJet EX200 (3D Systems, USA) UV curable acrylic material suitable for high resolution 3D printing with resolution $328 \times 328 \times 606$ DPI (x, y, z) and layer thickness 0.036 mm. In this mode accuracy of printing was approx. $0.025 - 0.05$ mm and the production process took 11 hours. Two different structures exhibiting in-plane negative strain dependent Poisson's ratio were selected for the analysis: i) two-dimensional inverted (re-entrant) honeycomb (porosity 73.2 %, Fig. 1 left, upper) and ii) two-dimensional cut missing-rib (porosity 72.8 %, Fig. 1 left, lower).

Quasi-static uni-axial compressive experiments were performed using in-house developed loading setup based on a novel modular compression/tension loading device suitable for both optical and X-ray observation of deformation processes equipped with U9b force transducer (HBM, Germany) with nominal force capacity 2 kN. Deformation of the samples was optically observed using a CCD camera and digital image correlation (DIC) method was used for strain-field evaluation [4] and calculation of true strain - true stress relationships.

Results and conclusion

True stress – true strain diagrams from experimental quasi-static compression tests were plotted for both microstructures as shown in Fig. 1 right. It can be seen that cut missing-rib microstructure exhibits

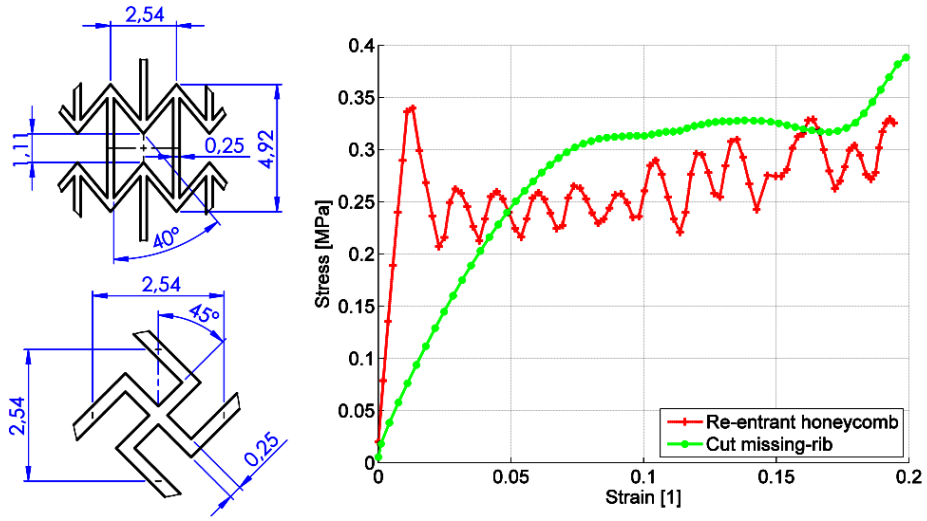

Fig. 1: Schematics of investigated microstructures (left) and true stress - true strain relationships determined using DIC (right).

initial compressive behaviour very similar to a closed-cell porous solid [3]. The initial linear elastic part is followed by apparent yield point and compaction region with constant stress plateau. These parts are then at approx. 17.5 % strain followed by region of localized densification due to negative Poisson's ratio of the unit cell and repeated decreases of stress that can be attributed for ruptures of beams due to excessive bending. Response of the re-entrant honeycomb microstructure to compressive loading is significantly different. After the initial linear elastic region 30 % drop of stress is followed by cyclic increases and decreases of stress levels in the specimens with apparent progressive trend. Following visual inspection of individual projections during deformation the occurrence of cycles can be attributed to collapse of individual layers of unit cells in the microstructure. From the elastic parts relative elastic moduli were evaluated resulting in $E_{\mathrm{r,cut}} = 4.46 \cdot 10^{-3}$ for the cut missing-rib structure and $E_{\mathrm{r,inv}} = 2.37 \cdot 10^{-2}$ for the inverted honeycomb structure. It has been shown that DIC method is suitable for characterization of deformation and mechanical characteristics of auxetic constructs produced by direct 3D printing.

Acknowledgment: The research has been suported by the Czech Science Foundation (project no. 15-15480S).

References

[1] Y. Sugimura, J. Meyer, M. Y. He, H. Bart-Smith, J. Grenestedt, A.G. Evans, On the mechanical performance of closed cell Al alloy foams, Acta Materialia, 45 (1997) 5245–5259.

[2] M. Grujicic, J. Galgalikar, J. S. Snipes, R. Yavari, S. Ramaswami, Multi-physics modeling of the fabrication and dynamic performance of all-metal auxetic-hexagonal sandwich-structures, Materials & Design, 51 (2013) 113–130.

[3] O. Jiroušek, T. Doktor, D. Kytýř, P. Zlámal, T. Fíla, P. Koudelka, D. Vavřík, Journal of Instrumentation, X-ray and finite element analysis of deformation response of closed-cell metal foam subjected to compressive loading, 8 (2013) C02012.

[4] I. Jandejsek, J. Valach, D. Vavřík, Optimization and Calibration of Digital Image Correlation Method, in: P. Šmíd (Ed.), Proceedings of Experimental Stress Analysis 2010, Univerzita Palackého v Olomouci, Olomouc, pp. 121–126.

21st International Conference **ENGINEERING MECHANICS 2015**
Svratka, Czech Republic, May 11 –14, 2015
Paper **#053, pp. 146–147**

Experiment E7/0,3 – Time Behaviour of Active Pressure of Non-Cohesive Sand after Wall Translative Motion

Petr Koudelka

Institute of Theoretical and Applied Mechanics CAS, v.v.i.,
Prosecká 76, 190 00 Praha 9, Czech Republic

koudelka@itam.cas.cz

Keywords: lateral earth pressure, non-cohesive material, sandy mass behaviour, wall movement modus, pressure at rest, pressure time instability

Abstract: A new experiment denominated as E7/0,3 with *active* pressure of non-cohesive quartz sand on a rigid moved wall was performed at the Institute of Theoretical and Applied Mechanics in the last year. The wall was translative moved towards active direction (out of the mass) at a position of supposed acting of active pressure value, then the wall motion was stopped and time pressure stability was monitored. After more than three months the wall was moved at the last position of 100 mm from original position before the experiment. The experiment ran four and a half months.
The paper will present the first results of monitored active pressures of sensors during a consolidative phase after active wall movement of 1.357 mm. The experiment will be repeated to be proved the results (Experiment E8/0,3).

Introduction

Long-term experiment E7/0,3 with *active* lateral pressure of sandy mass is a part of a long-term research of lateral earth pressure of non-cohesive granular masses at the Institute of Theoretical and Applied Mechanics running from 1998. A complete set of experiments with *passive* pressure ran in period 2010 -2014 [1] when all three basic modes of wall movement (rotations about the top and toe, translative motion) were tested two times (experiment sets E5 and E6), altogether six long-term experiments with the same sand to be proved mass behaviour during each wall movement modus. The presented experiment E7/0,3 ran in the second half of 2014 year. A repeated same experiment E8/0,3 is running contemporaneously (March, 2015).

Experiment E7/0,3

Experimental equipment. It was availed the same developed advanced equipment such as for the previous experiments [1] with passive pressure however, with shorter sandy sample space. Sizes of sandy sample were as follows: wide of 0.98 m, height of 1.20 m, length of 1.375 m (previous experiments – length of 3.0 m). Side walls are transparent (glass). Numbers of bi-component pressure sensors in a front moved wall (5) and a stable back wall (6) were the same but there were used more sensitive sensors for lower pressures.

Frequency of pressure registration was of 50 ÷ 1 Hz. Movement of the wall was measured by four instrument kinds: potential-electric sensors, optic-electric sensors, turns of engine and directly by electronic digital calliper.

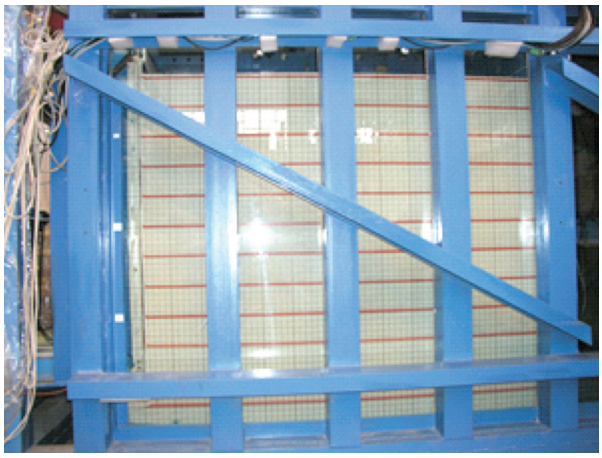

Fig. 1: View at the right side of the sample after translative motion of the front wall (seen left) of *1.36 mm* to left. Deformations are not yet visible.

Sample. There is used the same sharp quartz material of size of 0.3 mm repeatedly and as well as for the experiment E7/0,3. Compaction of the mass was homogeneous and not too high similarly to previous masses using also a special exact compacting instrument (n=*47.0 %*, I_D = *0.55*, unit weight γ = *1494 kg/m*^{3}).

Visual monitoring. A surface of the sample was scanned by one camera during movement of the front wall continuously. Slow processes into the sample were sensed using little black glass globules placed closely to the left equipment side by a camera continuously. Decreases and slip surfaces into the sample were registered by means of red sand strips placed closely beside the right glass side wall using a camera.

Experiment flow. The **e**xperiment was in progress in three motional phases applying front wall translative motion and three reconsolidation phases (without a motion). The first motional phase tested an influence of *active* micro movement of the front wall from an original position of u = *0 mm* at position of u = *-0.28 mm*, i.e. behaviour in a range of pressure at rest. The second motional phase followed after 5 days at wall position of u = *-1.36 mm*, i.e. supposed full mobilization position of *active pressure* according to EN 1997-1 (Annex C). Then time behaviour of the mass consolidated along of 97 days was monitored (see Fig. 2). The last motional phase at position of u = *100.42 mm* made it be possible to monitor behaviour of the mass in a range of full shear strength mobilization and further during destruction of the mass. Consolidation pressures of the failed mass were monitored 23 days after. A movement velocity of the front wall during all motional phases was of *0.0049 mm/min*.

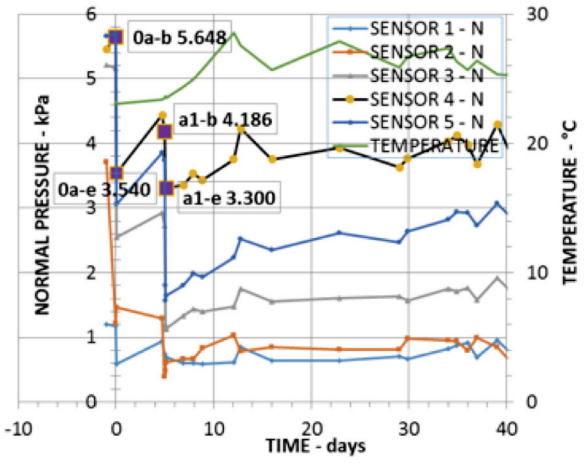

Fig. 2: Histories of normal components of pressure according to all five sensors placed in the moved wall and a history of structure temperature.

Time behaviour of the mass

Histories of normal components of pressure (left vertical axis) acting on the moved wall during initial forty days are shown in Fig.2 together with relevant temperature of the equipment structure (right vertical axis). Seemingly vertical sensors pressure histories (very short time duration – 1 hour, resp. 4 hours) represent the two initial motional phases with pressure at rest (0a) and with active pressure (a1 – nearly minimal value). The sensors are numbered from above. Pressure time behaviour according all five sensors is almost the same and is marked out for the sensor 4 (*depth 0.665 m*) in detail. The motional phases show very considerable rapid decreases while the consolidation phase pressures increase more slowly but very considerable too. Conclusions will be made after a finish of repeated E8/0,3.

References

[1] P. Koudelka, Double Case of Passive Pressure Acting on Wall Rotated about the Top. In: Proc. 7th IC on Case Histories in Geotechnical Engineering (#3.15b), Wheeling (Chicago, Ill.), Apr.29-May 4, 2013. S. Prakash, Missouri University of Science and Technology, Rolla, MO, USA. ISBN 1-887009-18-3 (Abs.v.), ISBN 1-887009-17-5 (2013) ps.10.

21st International Conference **ENGINEERING MECHANICS 2015**
Svratka, Czech Republic, May 11 –14, 2015
Paper **#092, pp. 148–149**

Modelling of Moisture Transport Influenced by Damage in Concrete Structures

Tomáš Koudelka[a], Jaroslav Kruis[b]

Faculty of Civil Engineering of Czech Technical University in Prague,
Thákurova 7, Praha 6, 16629, Czech Republic

[a]koudelka@cml.fsv.cvut.cz, [b]jk@cml.fsv.cvut.cz

Keywords: damage, moisture transport, coupled problems, concrete

Abstract: The paper describes model of the moisture transport in concrete material where the permeability is influenced by the crack opening which is determined by the scalar isotropic damage model. These models are used for the simluation fourpoint shear test coupled with moisture transport and simulation of storage tank.

Extended abstract

The paper deals with the fully coupled heat and moisture transport in heterogeneous quasi-brittle materials such as concrete. Generally, the mechanical behaviour of concrete material is nonlinear and it is different in tension and compression. Due to applied load, void nucleation and crack growing appear in the original solid skeleton which lead to changes in porosity and reduction of Young's modulus. There are two main approaches for the description of the crack growing - damage or fracture mechanics. In this contribution, the damage mechanics [1] is used for the description of mechanical behaviour because we assume materials and structures in serviceability states rather than the limit state. Therefore, the concept of smeared cracks is more suitable and it can be relatively easily connected with transport processes. The scalar isotropic damage model was used in this paper due to its simplicity and because the initial transport properties are assumed to be also isotropic.

The heat and moisture transfer is modelled by the Kunzel's model [2]. Two unknowns are introduced in the model, relative humidity and temperature. The model divides overhygroscopic region into two subranges - capillary water region and supersaturated region, where different conditions for water and water vapor transport are considered. For the description of simultaneous water and water vapor transport, the relative humidity is chosen as the only moisture potential for both hygroscopic and overhygroscopic range. This model uses certain simplifications but nevertheless, the model describes all substantial phenomena and the predicted results comply well with experimentally obtained data, which is the main advantage of the model. Also determination of the material properties can be obtained quickly from the common laboratory tests. Contrary to that advantages, the model suffers by numerical difficulties in the case the relative humidity approaches the fully saturated state. The sorption isotherm is nearly vertical and its derivatives are extremely high.

It is usually assumed that the mechanical behaviour is influenced by the heat and moisture transport (temperature and water content are used for determinantion of strains) while the description of transport processes is usually not affected by the mechanical models. In the case of damage evolution, the damage growth increases the porosity which results in faster moisture transport and therefore this phenomena should be taken into account. If the damage parameter is relatively small (smaller than 0.1), the transport process is affected moderately and it can be described by explicit formula for the permeability. If the damage parameter is close to one, material is severely damaged and transport resembles convection described by the Hagen-Poiseuille law [3]. For the intermediate cases of the damage state, the permeability can be obtained by interpolation. This numerical approach is tested on examples of four-point shear test and numerical simulation of a storage tank that were computed by SIFEL [4] with help of the above implemented models.

The following figures Fig. 1 and Fig. 2 depict the distribution of damage parameter ω and volumetric moisture content w in the case of four-point shear test of concrete specimen saturated from the bottom surface by water.

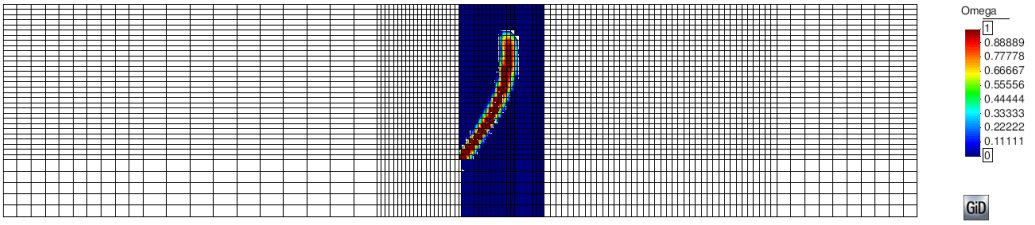

Fig. 1: Four-point-shear problem: distribution of the damage parameter ω.

As the evolved damage parameter (as seen in Fig 1) influences the permeability, distribution of the volumetric moisture content differs from an undamaged state and a strip with higher moisture content can be seen in Fig. 2.

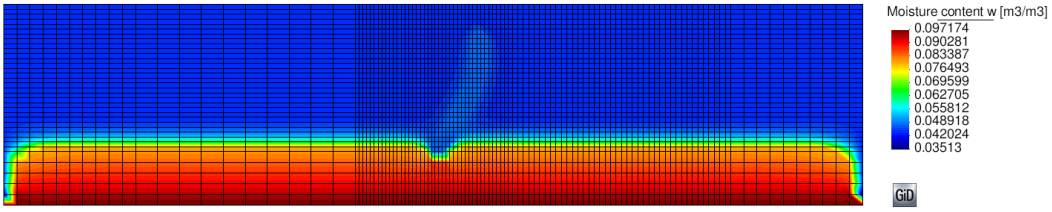

Fig. 2: Four-point-shear problem: distribution of the volumetric moisture content w.

Acknowledgement: This paper was supported by project No. 13-18652S of Grant Agency of Czech Republic which is highly appreciated.

References

[1] J. Lemaitre, J.L. Chaboche, Mechanics of solid materials(Cambridge University Press, Cambridge, UK 1994).

[2] H.M. Kunzel, Simultaneous Heat and Moisture Transport in Building Components (Fraunhofer Institute of Building Physics, Fraunhofer IRB Verlag Stuttgart 1995).

[3] G. Pijaudier-Cabot, F. Dufour, M. Choinska, Multiscale Modeling of Heterogenous Materials: From Microstructure to Macro-scale Properties, Wiley, (2010) p. 277-292

[4] Open source software package SIFEL http://mech.fsv.cvut.cz/šifel/

21st International Conference **ENGINEERING MECHANICS 2015**
Svratka, Czech Republic, May 11 –14, 2015
Paper **#155, pp. 150–151**

Wing Geometry Design Using Glauert's Method

Tomáš Koutník

Institute of Aerospace Engineering, Faculty of Mechanical Engineering,
Brno University of Technology, Technická 2, 619 69 Brno

koutnik@fme.vutbr.cz

Keywords: Glauert's method, wing planform, lift distribution

Abstract: Glauert's solution of Prandtl's lifting line theory is a quick method widely used for analysis of the spanwise lift distribution on planar wings. In this article, its use on an inverse problem is demonstrated. The concept is tested by morphing the initial rectangular wing planform to reach demanded lift distribution. Results are compared with theoretical assumptions, solution obtained from CFD simulation and tunnel measurement results.

At the beginning of each aircraft design its concept and configuration has to be set. Planform of the wing in this early stage of the project results mostly from designer's experience. Then is the geometry modified iteratively until desired spanwise lift coefficient distribution and stall characteristics of the wing are reached. Glauert's solution of Prandtl's lifting line theory is suitable for this type of preliminary analysis on wings with higher aspect ratio. This paper demonstrates feasibility of this method also for preliminary design of the wing planform from known lift coefficient distribution.

For testing purposes, the initial rectangular wing planform was modified to reach the target shape with lift coefficient known from literature or CFD computations. Since the lift coefficient in each section is proportional to its chord, based on equation

$$c(\theta) = \frac{4 \cdot b \cdot \sum_n A_n \cdot \sin(n \cdot \theta)}{c_l(\theta)} \tag{1}$$

from the lifting line theory it is possible to manipulate dimension directly. Then the normalization of the wing area is necessary, so the aspect ratio of the wing remains constant. Number of iterations needed depends on required accuracy and complexity of the target function, but entire process is very fast on today's computers.

Early test cases were very simple and compared only against the also lifting line based software Glauert III, which is used at the Institute of Aerospace Engineering for preliminary analyses of the lift coefficient distribution. Then more realistic arrangements were examined, where the best fitting variant was that including complete lift curves of used airfoils at the input. This approach requires higher effort in pre-processing stage and longer computational times, but considering the overall speed of computations with the lifting line theory is this cost still tolerable.

Fig. 1 shows the wing cord distribution along the wingspan designed according to the reserve in lift coefficient prescribed for each section. Because of better accuracy nonlinear inputs for each of 75 sections were used. Approximately 30 iterations were needed to complete the solution with total wall clock time less than 30 seconds. It was found, that the best performance of this design method corresponds to prescribed reserve with the form of the smooth curve.

As is presented, the method can be used especially for design of composite wings, where the planform shape can be manipulated freely. Accuracy of results is sufficient for the preliminary design unaffected by the fuselage, which can change aerodynamic characteristics of the aircraft significantly. The main advantage of this method is absence of the manually driven iterative design process, but the result represents only the aerodynamicist's point of view and in some cases can be rejected by structural engineers as unacceptable. In conclusion, additional constrains for the wing planform and also the manipulation of the spanwise twist distribution should be involved.

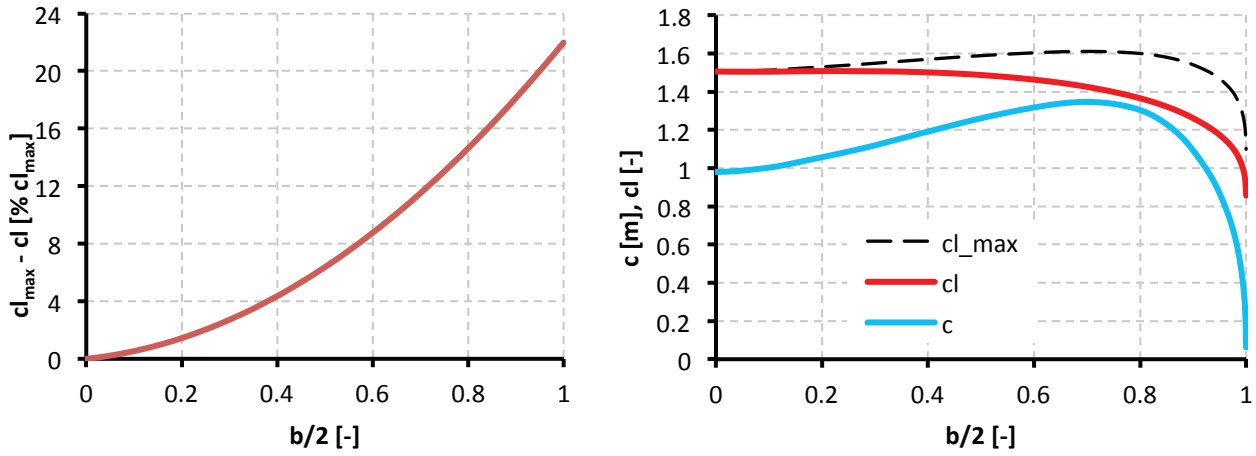

Fig. 1: Prescribed reserve in sectional lift coefficient (left) and corresponding wing chord and lift coefficient distribution obtained from nonlinear lifting-line theory (right)

References

[1] P. Schoř, Non-Linear Lifting Line Theory Application to Glider Aerodynamic Design, diploma thesis, Faculty of Mechanical Engineering, Brno University of Technology, Brno, 2011.

[2] E.O. Pearson, A.J. Evans, F.E. West, Effects of Compressibility on the Maximum Lift Characteristics and Spanwise Load Distribution of a 12-Foot-Span Fighter-Type Wing of NACA 230-Series Airfoil Sections. NACA-ACR-L5G10. NACA, Langley Memorial Aeronautical Laboratory, 1945.

[3] J.C. Sivells, R.H. Neely, Method for calculating wing characteristics by lifting-line theory using nonlinear section lift data, NACA-TN-1269. NACA, Langley Memorial Aeronautical Laboratory, 1947.

[4] J.D. Anderson, Fundamentals of aerodynamics. McGrav-Hill, Inc., 1984.

[5] F. Vaněk, Glauert III (uživatelská příručka), Institute of Aerospace Engineering, Faculty of Mechanical Engineering, Brno University of Technology. Brno.

21st International Conference **ENGINEERING MECHANICS 2015**
Svratka, Czech Republic, May 11 –14, 2015
Paper **#094, pp. 152–153**

The Influence of Internal Structure Change on Sandstone Strength

Kateřina Kovářová

Department of Geotechnics, Faculty of Civil Engineering, Czech Technical University,
Thákurova 7, 166 29 Prague 6, Czech Republic

katerina.kovarova@fsv.cvut.cz

Keywords: sandstone, internal structure, mercury porosimetry, x-ray microtomography, strength

Abstract: During their "life" sandstones are influenced by actions of weathering processes which usually lead to changes in their internal structure. Porosity and the character of pore space is one of the main factors affecting the resistance to weathering processes and, consequently, to the changes of mechanical-physical properties of these stones. Rock material is generally negatively influenced especially during the winter period. The effect of salt crystals and ice formation depends on the character of pore space, including the pore size distribution. Our research was focused on three commonly used Czech Cretaceous sandstones – Hořice, Božanov and Kocbeře. These stones were exposed to the accelerated durability test and then the change of uniaxial compressive strength was determined. We used the mercury porosimetry and X-Ray microtomography methods to evaluate the changes of pore space properties. Use of these methods enabled more detailed understanding of the processes inside the stone structure and their influence on strength characteristics of sandstones.

Introduction

The weathering processes influence the technical properties of sandstones especially during the winter season thanks to the frost and deicing salt action. These two weathering agents significantly influence the stone internal structure, i.e. pore space, which consequently leads to the deterioration of technical parameters. The uniaxial compressive strength is the most commonly used mechanical parameter enabling the evaluation of deterioration and also durability of a stone.

Experimental material and procedure

Three Czech Cretaceous sandstones (Hořice, Božanov and Kocbeře) were exposed to the accelerated durability test, according to the procedure described by Kovářová et al. [1]. Two sets of cubic stone samples were treated by a cyclic thermal exposition in a climatic chamber with the temperature ranging from – 14°C to 14°C. The samples were soaked for 24 hours in distilled water and in 2.5% solution of NaCl before and during the treatment. The treatment regime consisted of 56 freeze/thaw cycles in total.

To evaluate the rate of deterioration, the uniaxial compressive strength (hereafter UCS) was determined as an arithmetic mean of measured values on ten samples of each sandstone type before and after undergoing both climatic treatments. Hg porosimentry and X-Ray microtomography methods were used to determine the internal structure changes. The total cumulative volume of pores, volumes of meso-, macro- and coarse pores, and the total porosity were determined using coupled Pascal 140 + 240 porosimeters by Thermo Electron – Protec. Small cylinder samples with the diameter 1 cm and the height 1.5 cm were measured by microCT phoenix|x-ray nanoton180 at 90 kV, 100 μA with timing 2 s and 2880 projections. Voxel size was 5 μm and experimental arrangement enabled the evaluation of pores with diameter > 5 μm [1].

Results

Uniaxial compressive strength. The UCS is by many authors considered one of the most important durability indicators. Generally, it is stated that the UCS decreases with an increasing number of freeze/thaw cycles [e.g. 2], however, these statements do not correspond with some of the results we gained, as is obvious from the following table (Table 1). The UCS increased after the climatic treatment with distilled water in Hořice sandstone and also after the climatic treatment with sodium chlorite in Kocbeře sandstone.

Table 1: Average values of UCS [MPa], including percentages changes (in parentheses).

	Hořice sandstone	Božanov sandstone	Kocbeře sandstone
Untreated samples	51	75.2	87.6
F/T cycles + H_2O	54.9 (+ 7.65)	73 (- 2.93)	76.9 (- 12.21)
F/T cycles + NaCl	44.6 (-12.55)	68.7 (- 8.64)	92.4 (+ 5.48)

Mercury porosimetry and X-Ray microtomography. According to statements of many authors [e.g. 2], the decrease of UCS is accompanied by the increase of porosity. The porosity measurement using only Hg porosimetry did not provide convincing results, which would confirm the previous statements. Using the results of mercury porosimetry and X-Ray microtomography, the *residual porosity* of pores with the diameter > 5 μm was calculated [1]. The *residual porosity* consists of closed pores, which are not possible to detect using only mercury porosimetry and other standard penetration methods of porosity determination. Average values of the residual porosity are summarized in the following table (Table 2).

Table 2: Residual porosity of pores with diameter > 5 μm [%].

	Hořice sandstone	Božanov sandstone	Kocbeře sandstone
Untreated samples	7.11	3.31	1.84
F/T cycles + H_2O	5.69	3.11	7.16
F/T cycles + NaCl	9.24	5.56	5.12

Conclusion

The residual porosity development in Hořice and Božanov sandstones explains the reason of increasing UCS after the climatic treatment. For example, the residual porosity in Hořice sandstone increased and the UCS decreased after the climatic treatment with NaCl, whereas the increase of UCS was accompanied with the residual porosity decrease after the climatic treatment with distilled water. Only the Kocbeře sandstone showed a different development and coherency of the studied parameters after the climatic treatment with NaCl. The UCS increased with the residual porosity increase. This can be explain thanks to the X-Ray microtomography detection limit. We can assume, that the internal structure changes occure even below 5 μm and, therefore, it cannot be ruled out, that the residual porosity of pores < 5 μm significantly decreased and this caused the UCS increase.

Acknowledgement: This paper has been supported by the project LAPIDARIUS (Project No. DF12P01OVV020, supported by the Ministry of Culture of the Czech Republic).

References

[1] K. Kovarova, R. Sevcik, Z. Weishauptova, Comparison of mercury porosimetry and X-ray microtomography for porosity study of sandstones, Acta Geodynamica and Geomaterialia. 9 (2012) 541-549.

[2] L. Gonzáles de Vallejo, M. Ferrer, Geological engineering, Taylor & Francis Group, London, 2011.

21st International Conference **ENGINEERING MECHANICS 2015**
Svratka, Czech Republic, May 11 –14, 2015
Paper **#128, pp. 154–155**

Implementation of k-kL-ω Turbulence Model for Compressible Flow into OPENFOAM

Martin Kožíšek[1,a] *, Jiří Fürst[2,b], Jaromír Příhoda[1,c], Piotr Doerffer[4,d]

[1]Department of Institute of Thermomechanics AS CR, v. v. i., Academy of Sciences of the Czech Republic, Prague, Czech Republic

[2]Department of Technical Mathematics, Czech Technical University in Prague, Faculty of Mechanical Engineering, Prague, Czech Republic

[3]The Szewalski Institute of Fluid-Flow Machinery, Polish Academy of Sciences, Gdańsk, Poland

[a]kozisek.martin@seznam.cz, [b]jiri.furst@fs.cvut.cz, [c]prihoda@it.cas.cz, [d]doerffer@imp.gda.pl

Keywords: turbulence, CFD, transition, RANS, OpenFOAM

Abstract: The article deals with the results of implementation of k-k_L-ω turbulence model for compressible transitional flow into OpenFOAM. This model was firstly proposed by Walters and Leylek (2005) and utilizes the approach of laminar kinetic energy in order to predict transition between laminar and turbulent flows. The performance of implemented model has been tested for the case of flow over the flat plate and flow through VKI turbine cascade. The properties of the implementation of k-k_L-ω model for compressible flow simulations into OpenFOAM are discussed.

Introduction

OpenFOAM is the open-source CFD software package which utilizes the finite volume method. Although OpenFOAM (version 2.3.0) includes k-k_L-ω model for incompressible flow calculations, this ready-made code gives us wrong results even for basic test cases. Note that the clarification of errors in this code are available in [1]. We implemented k-k_L-ω turbulence model for compressible flow in order to build reliable turbulence model for investigation of compressible flow through turbine cascades.

Mathematical model

The viscid flow of perfect compressible gas was described by the set of Favre-averaged Navier-Stokes equations. The transitional turbulence model k-k_L-ω [2] uses the Boussinesq hypothesis to determine the Reynolds stress tensor. Three transport equations are solved for the turbulent kinetic energy k_T, the laminar kinetic energy k_L and the specific dissipation rate ω.

Results

The implementation of k-k_L-ω into OpenFOAM was applied for solving 2D compressible flow through VKI turbine cascade [4, 5]. The mesh consists of 62049 quadrilateral and triangular cells. The structured hyperbolic mesh is situated near the blade with $y^+ \leq 1$. $M_{2is} = 0.0884$, $Re_{2c} = 590000$, inlet turbulent intensity Tu = 1.5%, dynamic viscosity $\mu = 1.2984\text{e-}5$ and inlet angle $\alpha = 0°$ are considered. Boundary conditions are shown in Table 1. Fig. 1 shows distribution of skin friction coefficient $C_f = 2\tau_w / (\rho_e U_e^2)$ on the suction side related to free-stream velocity U_e at $y = 0.05$ m and $\rho_e = 1.1885$ kg/m^3.

Conclusions

The comparison with experiment data [4, 5] shows that our implementation of k-k_L-ω model as well as standard k-k_L-ω model supplied in commercial CFD package FLUENT underestimate friction

coefficient. The figure suggests that calculated boundary layer is near to separation, but the position of transition onset is captured well. The transition is driven by threshold constants without any dependence on pressure gradient of external flow. It can be reason of difference between CFD results and experiment data. The future development will aim to investigation of the pressure gradient dependency as well as improvement of the turbulent heat transfer model.

Table 1: Boundary conditions. The homogenous Neumann condition is marked ZG. Other boundary conditions are periodic.

	U (m/s)	p (kPa)	T (K)	k_T (m^2/s^2)	k_L (m^2/s^2)	ω (s^{-1})
Inlet	$\alpha = 0°$	$p_{tot} = 100.548$	$T_{tot} = 293.7$	0.037922	0	16
Outlet	ZG	$p_{stat} = 100$	ZG	ZG	ZG	ZG
Blade	0	ZG	ZG	0	0	ZG

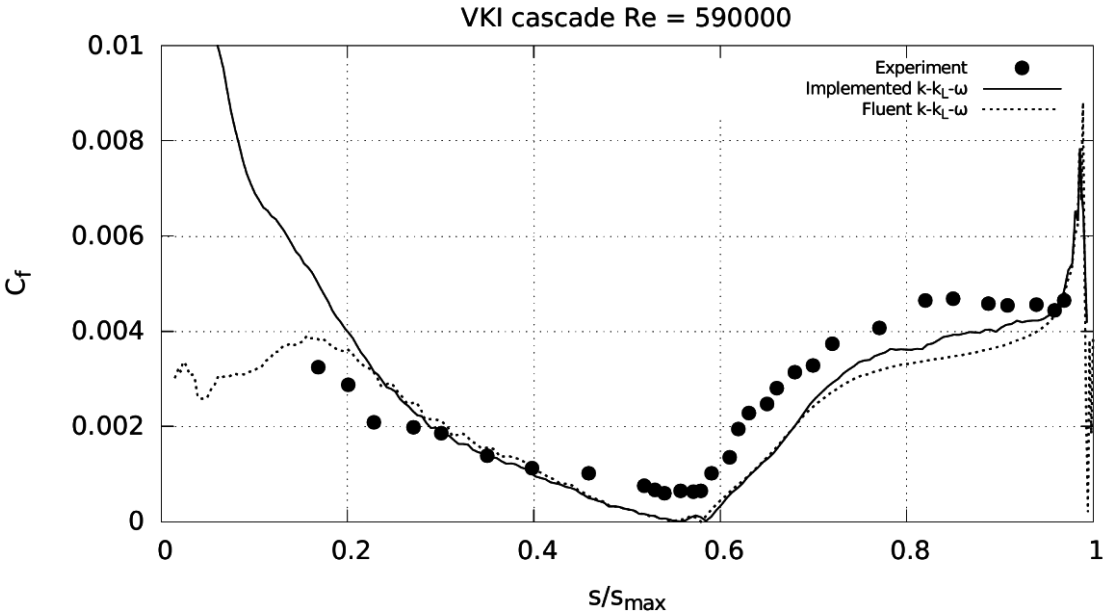

Fig. 1: Distribution of the skin friction coefficient along the suction side of the VKI blade.

References

[1] Fürst, J., Numerical simulation of transitional flows with laminar kinetic energy, in: Engineering Mechanics 18th International Conference, Svratka, Czech Republic, 2012, pp. 309-315.

[2] Walters D. K., Leylek J. H., A new model for boundary layer transition using a single-point RANS approach, in: Journal of Turbomachinery, 126, 2005, pp. 193-202.

[3] Coupland, J., Flat plate transitional boundary layers, in: ERCOFTAC classic database, 2009, information on http://cfd.mace.manchester.ac.uk/ercoftac/

[4] Canepa E., Cattanei A., Pittaluga F., Ubaldi M., Zunino P., Transitional boundary layer on the on suction side of a turbine blade at different Reynolds numbers, in: 5th European conference on turbomachinery, Prague, Czech Republic, 2003, pp 911–923.

[5] Ubaldi M., Zunino P., Campora U., Ghiglione A., Detailed velocity and turbulence measurements of profile boundary layer in a large scale turbine cascade, in: ASME Paper, 1996, 96-GT-42.

Acknowledgements: The work was supported by the Grant Agency of the Czech Technical University in Prague, grant No. SGS 13/174/OHK2/3T/12. The authors would like to express their thanks to the Technology Agency of the Czech Republic, which supported this research under grant No. TA03020277, to the Czech Science Foundation for the grant No. P101/12/1271 and for institutional support RVO 61388998.

21st International Conference **ENGINEERING MECHANICS 2015**
Svratka, Czech Republic, May 11 –14, 2015
Paper **#186, pp. 156–157**

Numerical Investigation of Wind Effects on the Perforated Structures

Radomil Král[a], Stanislav Pospíšil[b]

Institute of Theoretical and Applied Mechanics, v.v.i.,
Prosecká 76, CZ-190 00 Prague 9, Czech Republic

[a]kral@itam.cas.cz, [b]pospisil@itam.cas.cz,

Keywords: CFD, perforated surface, resistance barrier, wind effect, screen boundary condition.

Abstract:. The paper deals with a numerical analysis of wind effects on structures with perforated surfaces. The solution based on FEM model is governed by the stabilized Navier-Stokes equations for incompressible fluid. Special attention is given to perforated screens. Such a partly resistance barrier always introduces considerable numerical difficulties resulting from the complexity of a flow distortion when the fluid is passing through. For simplification, the barrier is assumed as a thin screen with specific resistance parameters where the fluid flow mechanism needs not be resolved. The general influence of a screen on the flow field is a loss in the normal momentum component and the change in flow direction. On the other hand, to simulate the fluid mechanics authentically it requires to specify the relevant input parameters that can be determined by an experiment or by using a corresponding handbook.

Introduction

A great part of scientific and expert reports concerning the wind effects on structures are based on numerical modeling. Generally, in isolated cases when the problem is too complex and/or is of high social importance, the theoretical models are replaced with experimental testings in the wind tunnels. In a case that a structure with perforated surfaces is considered, the tunnel study is recommended provided the model scale is reasonable low. If a large scale is needed for any reason, the perforated surfaces become very complicated from both the similarity requirements and the measurement point of view. Then the numerical analysis prevails, however, relevant boundary conditions and parameters simulating the resistance barrier have to be imposed correspondingly.

In this paper, the overall wind loads with respect to the effect of perforation and wind direction are studied on a civil/architecture engineering structure in the shape of an airship. The wooden structure of more than $42\,\mathrm{m}$ length and $9\,\mathrm{m}$ in diameter is supported by two slender columns and several guy cables fix the structure horizontally. The external surface is covered by wooden perforated cladding with a regular grid. The upper part of the structure is protected by a pre-tensioned impermeable foil, see Fig. 1 left.

Numerical analysis and resistance barrier specification

The effects of the wind are examined for several loading cases in association with the wind direction. To compare the influence of the perforation, both the porous and the solid surface of the airship cladding are assumed. The acting wind is characterized by a logarithmic velocity profile for an urban terrain type with no turbulence component in the inlet. The mean speed corresponds to category I with a low intensity.

The perforated surface is investigated using a thin barrier to flow at which by solving the relevant boundary conditions the pressures drop and loss in normal momentum velocity component arises. This approach utilizes the method of the step function where two approximation solutions are calculated at each nodal point depending on the screen side orientation to the flow. The unknown velocity **u** and

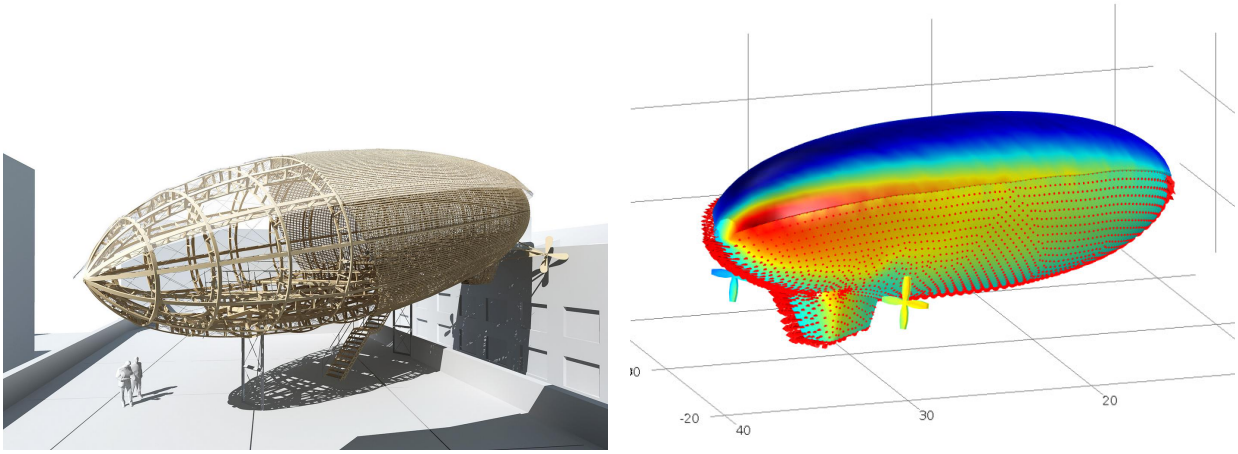

Fig. 1: Architectural visualization by Martin Rajniš© (left) and pressure distribution over the outer surface with velocity vectors (right). The top part is protected by insulating foil.

the pressure p are solved across the screen by imposing the set of conditions:

$$2\Big[\rho\big(\mathbf{u}\cdot\mathbf{n}\big)^2+p-\mathbf{n}^T\Big\{\mu\Big(\nabla\mathbf{u}+\big(\nabla\mathbf{u}\big)^T\Big\}\mathbf{n}\Big]_-^+ = -K\rho(\mathbf{u}_-\cdot\mathbf{n})^2, \tag{1a}$$

$$\mathbf{n}\times\mathbf{u}_+ = \eta(\mathbf{n}\times\mathbf{u}_-), \tag{1b}$$

$$\big[\rho\mathbf{u}\cdot\mathbf{n}\big]_-^+ = 0, \tag{1c}$$

where ρ is the fluid density, μ is the dynamic viscosity and $\mathbf{n}$ is unit normal exterior vector. The signs $+$ and $-$ refer to the upstream and downstream side of the barrier, respectively, and the operator $[-]_-^+$ indicates the product of the difference between the sides. Eq. (1a) represents quadratic dependency of the pressure loss on the normal velocity component. The Bernoulli's principle is applied taking the dynamic and static pressure and viscous effects into account. The rate of the pressure loss is given by the resistance coefficient K whose value depends on the geometrical properties of the screen and the Reynolds number Re. The coefficient K can be determined by means of an experimental testing, or estimated from relevant handbook, see e.g. [1]. Parameter η stands for the flow refraction expressed in Eq. (1b) in terms of K as $\eta=\sqrt{K^2/16+1}-K/4$. This relation covers a wide range of industrial applications.

In Fig.1, the axonometric views on the perforated structure are shown. The left figure presents the architectural ideas in the final form, while the FEM solution is displayed on the right. This representative image shows the pressure relations over the external surface with velocity vectors when both sides of the perforated screen are considered. The red color indicates the positive pressure, dark blue represents the suction. Integrating the total stress over double-sided surface, component force effects generated by the wind were evaluated and used as the basis for the static design of the guy anchorage and the supports.

Acknowledgment: The kind support of the Czech Science Foundation project No. GP14-34467P and of the RVO 68378297 institutional support are gratefully acknowledged.

References

[1] E. Fried, I.E. Idelchik, Flow Resistance: A Design Guide for Engineers. Taylor & Francis, London, (1998).

21st International Conference **ENGINEERING MECHANICS 2015**
Svratka, Czech Republic, May 11 –14, 2015
Paper **#179, pp. 158–159**

Nonlinear Analysis of Fire Resistance of Composite Steel-Concrete Tube Column

Juraj Kralik[a]*, Alzbeta Grmanova[b], Maros Klabnik[c]

Slovak University of Technology in Bratislava, Faculty of Civil Engineering,
Department of Structural Mechanics, Radlinskeho 11, SK-810 05 Bratislava, Slovakia

[a]juraj.kralik@stuba.sk, [b]alzbeta.grmanova@stuba.sk, [c]xklabnik@stuba.sk

Keywords: fire safety, composite steel concrete columns, transient thermal conduction

Abstract: Generally, three different approaches can be applied for analysis of a fire safety: A time factor, bearing capacity factor, and the temperature factor. Three types of columns (a steel tube filled with concrete; an encased steel cross-shaped profile; reinforced-concrete column of a circular cross-section) were investigated using the transient temperature analysis. Heat transfer in composite columns as well as the effects of boundary conditions represented by normalized temperature curve, were monitored during a period of two and a half hour [1, 2].

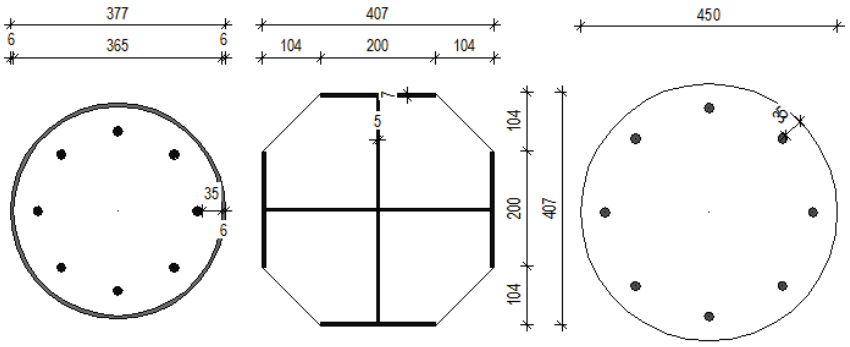

Fig. 1: Analyzed columns: C1- steel tube filled with concrete, C2- encased steel cross-shaped profile, C3 - reinforced-concrete column

Introduction

The fire process can be divided into four basic phases: Ignition, Growth, Fully developed and Decay. Overall ignition occurs, when the temperature between 400 to 600°C is exceeded, while the heat from floor releases by the highest rate, i.e. 20kW/m^{2}s. There remains only a small chance to survive for persons who failed to escape the fire site. The temperature before the overall ignition is rather low and the fire is localized in its epicenter. The action of a fire-fighting crew as well the evacuation of humans is possible. Casualties indicated in international statistical indexes, range from 0,0004 to 0,04%. Economic losses range from 1,6 to 5,9% from the Gross National Product. 85 % of fire casualties occur during fires of residential buildings [3]. Considering the above mentioned factors, one can see that fire safety is an important part that has to be involved in the building structures design.

Temperature analysis

For a proper investigation of the fire resistance of a structure, it is necessary to determine the time-temperature curve. The temperature changes dynamically and it is given by a normalized temperature curve [4].

Basic equation of the non-stationary heat conduction can be written in following form $\mathbf{C\dot{T}+KT=Q}$, where **K** - matrix of thermal conductivity, **T** - vector temperatures in nodes, **Q** - vector of heat flow, **C** - matrix of thermal accumulations, $\dot{\mathbf{T}}$- time derivation of vector **T** .

Boundary conditions and calculation

Numerical simulation of heat transfer in the structure was analyzed using the ANSYS software with use of elements for the thermodynamic analysis. Two-zone model was used for the calculation. Two different normalized temperature curves were defined. Models were divided in their middles into two parts lengthwise. Each model was loaded by lower temperature in its bottom part and by higher temperature in its upper part. Two model situations were investigated: Model Situation 1 – Fire load acts on the whole diameter of a column; Model Situation 2 – Fire load acts on the half of diameter. Boundary conditions valid for the model were specified using applicable elements. Altogether six situations were modeled, two for each column. The results obtained for each Model Situation were strongly affected by quality of mesh.

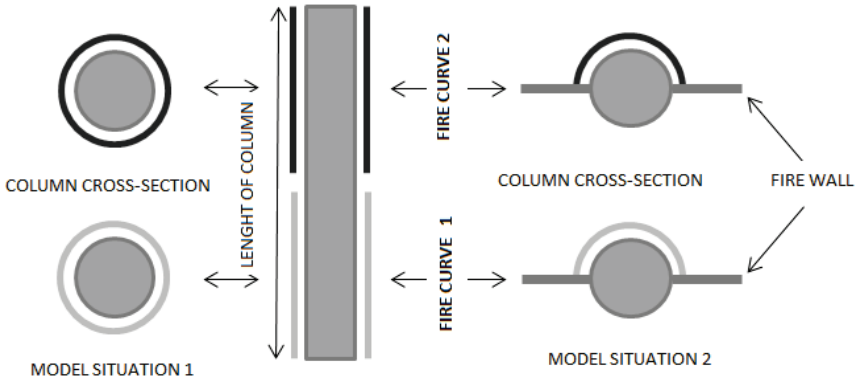

Fig. 2: Fire scenario for the transient analysis

Summary

The investigations have proved a considerable drawback of an encased steel cross-shaped column: the steel which is unprotected on the surface, continually progresses into the core what enforces the degradation of the concrete strength considerably. In this type of column in time 2 hours, the area of concrete which is not damaged by heat effects, is by approx. 30% smaller compared to a steel tube filled with concrete. The maximum temperature difference in this type of column under the uniform load occurs in time approx. 1 hour, namely in the concrete part of profile. Here, in the undisturbed core the temperature is only 28 ºC, while the temperature of damaged concrete on column's edge is 786ºC. In Model Situation 2 the maximal temperature difference is in time approx. 80 minutes in the value of 950ºC.

Acknowledgements: This paper was written with support of Slovak Grant Agency VEGA, project number 1/1039/12.

References

[1] M. Chladna, Fire Safety of Composite Structures, STU, Bratislava, 2005 (in Slovak).

[2] M. Holicky, J. Markova, Principles of Design Building Structures, CKIAT, Prague, 2007 (in Czech).

[3] A. Buchanan, Structural Design for Fire Safety, John Wiley and Sons Ltd, West Sussex, 2001.

[4] J. Kralik, Safety and Reliability of Nuclear Power Buildings in Slovakia. Earthquake-Impact-Explosion, STU, Bratislava, 2009.

21st International Conference **ENGINEERING MECHANICS 2015**
Svratka, Czech Republic, May 11 –14, 2015
Paper **#178, pp. 160–161**

Probabilistic Nonlinear Analysis of Bubble Tower Structure due to Extreme Pressure and Temperature

Juraj Králik[1,a*], Juraj Králik, jr.[2,b]

[1] Faculty of Civil Engineering STU Bratislava, Radlinského 11, Slovakia

[2] Faculty of Architecture STU Bratislava, Námestie slobody 19, Slovakia

[a]juraj.kralik@stuba.sk, [b]kralik@fa.stuba.sk

Keywords: probability, nonlinearity, extreme, pressure, temperature, nuclear power plant

Abstract: This paper presents an application of the probabilistic analysis of structural resistance of the bubble tower structure of a VVER 440/213. The evaluation is based on an extension of the smeared crack model developed on basis of Kupfer's bidimensional failure criterion, rotated crack, CEB-FIP model of failure energy and implemented into the ANSYS system. The non-linear analysis was considered for the median values of the input data and the probabilistic analysis models the uncertainties of loads, material resistance and other modeling issues.

Introduction

The definition of the fragility curve for containment of a nuclear power plant (NPP) generally represents a crucial step for the level 2 probabilistic safety assessment (PSA L2), where the probability of containment failure can be evaluated as the convolution of the fragility curve with the load curve (SSG-4). The assessment of the structural strength of the containment of a nuclear power plant has acquired even a greater importance in the framework of post-Fukushima stress tests where the assessment of the safety margin and off-design conditions.

In the case of the loss-of-coolant accident (LOCA) the steam pressure expand from the reactor hall to the bubble condenser. Hence, the reactor hall and the bubble condenser are the critical structures of the NPP hermetic zone.

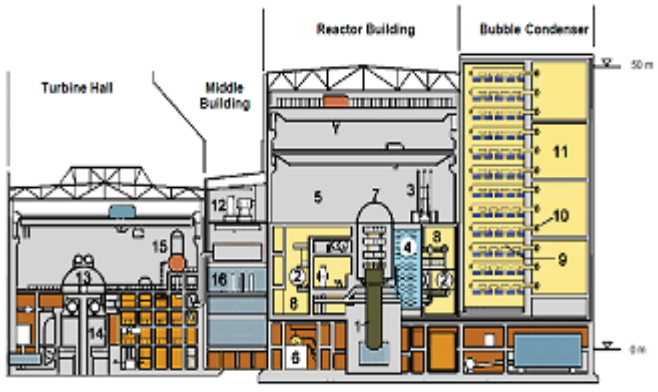

Fig. 1: Section plane of NPP VVER 440/213

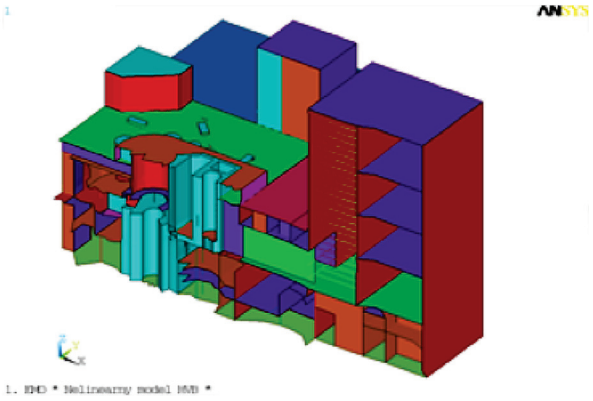

Fig. 2: Calculation FE model

The present work analyses the impact of combination of pressure load with thermal load that can arise in extreme situation related to severe accident progression. For the purpose, a detailed finite-element analysis of the concrete structure was carried out with ANSYS software and the program CRACK [1, 2] were provided to solve this task.

The theory of large strain and rate independent plasticity were proposed during the high overpressure loading using the SHELL181 layered shell element from the ANSYS library [1]. The layered approximation and the smeared crack model of the shell element are proposed. The processes of the concrete cracking and crushing are developed during the increasing of the load.

The limit of the finite element damage is controlled by the failure energy [3]. The program CRACK based on the presented nonlinear theory of the layered reinforced concrete shell was adopted in the software ANSYS [1, 2].

Evaluation of the fragility curve

The previous design analyses of the containment failure determine the critical area of this structure. The semi probabilistic methods were applied for the probabilistic analysis of the containment failure in this paper. The probabilities of the containment failure were considered in the critical structure areas on the basis of the nonlinear deterministic analysis of them for various levels of the overpressure. The probability of containment failure is calculated from the probability of the reliability function in the form

$$p_f = P\left(\frac{1}{t}\sum_{l=1}^{N_{lay}} F_u^l\left(I_{\varepsilon 1}; I_{\varepsilon 2}; \varepsilon_u\right) t_l > 0\right) \qquad (1)$$

where $F_u^l(.)$ is the Kupfer's failure function.

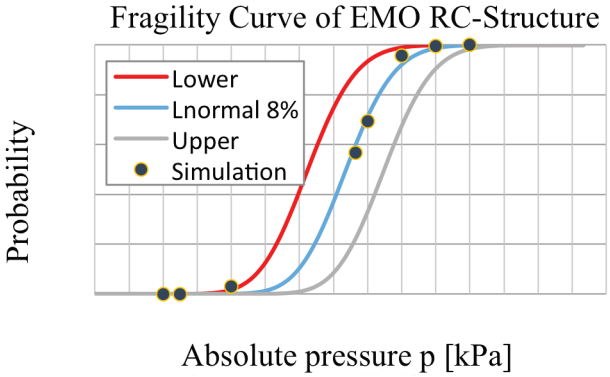

Fig. 3. Idealized fragility curves with boundary ±5%

Summary

The probability analysis of the loss of the concrete containment integrity was made for the overpressure loads from 250kPa to 500kPa using the nonlinear solution of the static equilibrium considering the geometric and material nonlinearities of the reinforced concrete shell layered elements. The uncertainties of the loads level (temperature, dead and live loads), the material model of the composite structure (concrete cracking and crushing, reinforcement), and liner and other influences following from the inaccuracy of the calculated model and the numerical methods were taken into account in the Monte Carlo simulations (Králik, 2009). The probability of the loss of the concrete containment integrity is less than 10^{-6} for the original structural model. The containment failure is equal to 0,050422906 for the overpressure 275,5 kPa.

Acknowledgements: The project was performed with the financial support of the Grant Agency of the Slovak Republic (VEGA 1/1039/12).

References

[1] J. Králik, Safety and Reliability of Nuclear Power Buildings in Slovakia. Earthquake-Impact-Explosion. Published by STU Bratislava, 307p. (2009).

[2] J. Králik, Nonlinear Probabilistic Analysis of the Reinforced Concrete Structure Failure of a Nuclear Power Plant Considering Degradation Effects. In: Applied Mechanics and Materials Vols. 249-250 (2013) pp 1087-1098, © Trans Tech Publications, Switzerland (2013).

[3] Z. P. Bažant, S. D. Pang, M. Vořechovský, D. Novák, Energetic-statistical size effect simulated by SFEM with stratified sampling and crack band model. International Journal for Numerical Methods in Engineering (Wiley), 71 (2007) 1297–1320.

Probabilistic Assessment of Historic Reinforced Concrete Bridge

Jan Krejsa[1,a*], Miroslav Sýkora[1,b], Michal Drahorád[2,c]

[1] CTU in Prague, Klokner Institute, Solinova 7, Prague 6, 166 08, Czech Republic

[2] CTU in Prague, Faculty of Civil Engineering, Thakurova 7, Prague 6, 166 29, Czech Republic

[a] jan.krejsa@klok.cvut.cz, [b] miroslav.sykora@klok.cvut.cz, [c] michal.drahorad@fsv.cvut.cz

Keywords: bridge, reinforced concrete and probabilistic assessment

Abstract: More than 50 % of investments in construction are related to existing structures. This ratio is even greater for bridges due to continuous degradation, ever increasing traffic intensities and general lack of authorities for rehabilitations. That is why effective assessment of the load bearing capacity of existing bridges is becoming a crucial issue. Respecting this situation the paper is aimed to the probabilistic assessment of historic reinforced concrete bridge and the comparison of obtained results with the partial factor method.

Methods for assessment of existing bridges

In the Czech Republic the assessment of an existing road bridge is based on determination of load bearing capacity V_i in accordance with ČSN 73 6222:2013 which assumes three different types of traffic conditions:

- V_1 is determined for the crossing of a defined two-axle vehicle with a uniform loading representing common traffic,
- V_2 is determined for the crossing of defined single three-axle or single six-axle vehicle with restricted access of other vehicles (a more unfavourable vehicle is taken into account) and
- V_3 is determined for the crossing of a special nine-axle vehicle with defined track on a bridge and prescribed speed.

The most adverse transversal position of the vehicles for V_1 and V_2 and of the uniform load for V_1 is taken into account.

Partial factor method. Nowadays existing bridges are mostly assessed by the partial factor method. This method is calibrated for new structures and it can hardly reflect real bridge-specific conditions in reliability analysis. Conservative values of these factors have been intentionally proposed to cover most situations in design when information about real material properties and/or structural geometry are unavailable. Therefore, this method may be inappropriate for the assessment of an existing bridge.

Probabilistic method. Probabilistic assessment is based on target reliability index β derived from probability of failure P_f according to ČSN EN 1990:2010 and ČSN ISO 13 822:2015. Partial, reduction and combination factors, and characteristic values are not considered in the probabilistic analysis. Basic variables for assessment of load bearing capacities V_i are described by a probabilistic distribution with specified characteristics.

Assessment of load bearing capacity

The case study is focused on a single span bridge built in 1908. The bridge consists of four main longitudinal reinforced concrete girders stiffened by several transversal bracings, reinforced concrete slab and stone masonry abutment. The load bearing capacities V_i are assessed for the main load bearing structure (reinforced beams and slab). Statistical parameters of basic variables are based on previous experience and measurements.

Assessment by partial factor method. Assessment of the load bearing capacities V_i by the partial factor method is conducted for all the girders at each cross section in the grid of 0.5 m. The partial

factors for bridge design according to ČSN EN 1990:2010 are taken into account. The critical load bearing capacities for a critical cross section are shown in Table 1.

Table 1: Load bearing capacities V_i for the applied methods

	Load bearing capacity of the bridge [t]				
	Partial factor method	Probabilistic method			
		$\beta = 2.3$	$\beta = 3.1$	$\beta = 3.8$	$\beta = 4.3$
V_1	40	66	58	52	48
V_2	56	100	88	78	72
V_3	106	188	165	148	138

Assessment by probabilistic method. The probabilistic assessment is performed only in critical cross sections identified by the partial factor method due to computational demands. Table 1 provides the load bearing capacities V_i for different target reliability indices β. It appears that V_i decreases with increasing β.

Comparison of applied methods. It appears that the probabilistic method leads to 40 % higher results of the load bearing capacities V_i for a commonly accepted β = 3.8 (middle failure consequences) than the partial factor method. However, this may be different in case of severe conditions of a bridge. It is foreseen that the probabilistic method provides more accurate estimates of load bearing capacities than the partial factor method for new structures when statistical parameters of basic variables are available. Comparison of load bearing capacities V_1 for different target reliabilities β is shown in Fig. 1.

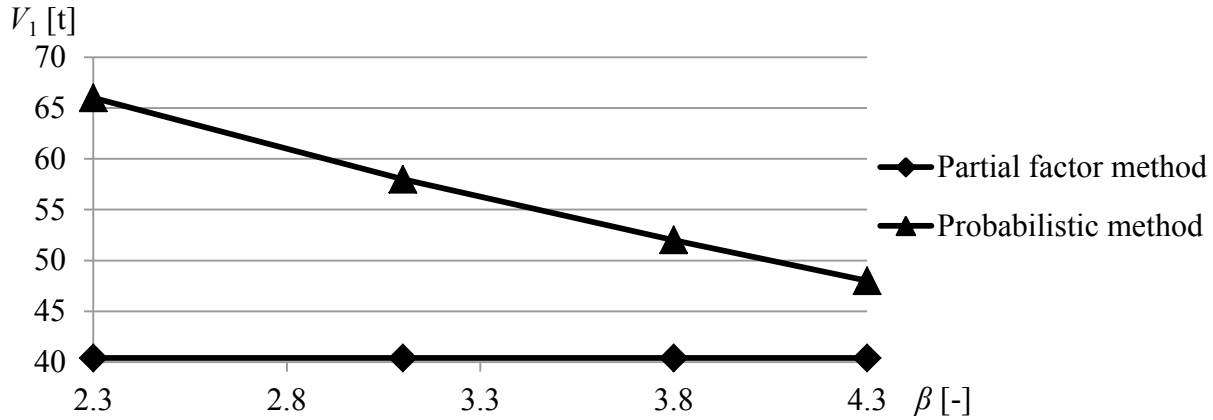

Fig. 1: Load bearing capacities V_1 for different reliability indices β

Conclusions

The assessment of the load bearing capacities of the historic bridge indicates that:

- Partial factor method for structural design is easier to compute than the probabilistic method, but in most cases it is overly conservative,
- Probabilistic method facilitates straightforward consideration of different target reliability indices,
- Load bearing capacities assessed by probabilistic method are about 40 % higher for the commonly accepted target reliability index 3.8.

Acknowledgement: The study is a part of the research project NAKI DF12P01OVV040 supported by the Ministry of Culture of the Czech Republic.

21st International Conference **ENGINEERING MECHANICS 2015**
Svratka, Czech Republic, May 11 –14, 2015
Paper **#190, pp. 164–165**

Problems of Lamella Flanges in Steel Bridge Construction

Vladimír Křístek[2,a], Miroslav Škaloud[1,b], Jaromír Kunrt[3,c], Shota Urushadze[1,d]*

[1]ITAM ASCR, v.v.i., Prosecká 76, 190 00 Praha 9, Czech Republic

[2]Czech Technical University, Thákurova 7, 166 29 Praha 6, Czech Republic

[3]Engineering Academy of the Czech Republic, Národní třída 3, 111 21, Prague, Czech Republic

[a]vladimirkristek@seznam.cz,[b]skaloud@itam.cas.cz, [c] kunrt.jaromir@seznam.cz,
[d]urushadze@itam.cas.cz

Keywords: bridges, lamella flanges, repeated loading, breathing, limit states

Abstract: As the plate elements of ordinary lamella flanges always exhibit unavoidable initial geometrical imperfections, a gap always occurs between them, into which the loaded lamella is pressed under load. Given the fact that the loading is many times repeated, the above phenomenon is also many times repeated, a pronounced cumulative damage process being thereby generated. This leads, as it became manifest during the authors´ tests, to the initiation and propagation of fatigue cracks in the longitudinal fillet welds connecting the individual lamellas, which can, of course, imperil the safety and useful lifetime of the bridge structure concerned.

Introduction

Lamella flanges have lately grown popular with the designers of steel bridges, because – in their belief – they provide us with the possibility of avoiding very thick flange plates in steel bridge structures. This belief is based on the assumption that the lamellas are perfectly plane and, therefore, in perfect contact everywhere, so that the loading from one lamella is transmitted into the other via pure compression, and that the perfect interaction of both lamellas is materialized by means of boundary fillet welds connecting both of the two lamellas. This simple assumption is, however, far from reality: it is not in the means of steel fabricators, not even in the means of those which are very progressively equipped, to produce perfectly plane flange lamellas. Then both lamellas exhibit unavoidable initial curvatures, which in combination form a gap between the lamellas, and consequently the directly loaded lamella are pressed into this gap. As the loading acting on every bridge is many times repeated, the aforesaid phenomenon is also many times repeated, (we can say that the lamellas „breathe“), and then an unavoidable cumulative damage process in the lamellas comes to being.

Experimental investigation

The aim of this investigation was to examine whether, due to the breathing of the lamellas, significant cumulative damage was generated such as to endanger the whole structural system.

The corresponding test specimens were materialised as a transverse cut-out from the lamella flange of a bridge in the neighbourhood of Prague, the width of the specimen being 250 mm, and the specimen acting compositely with a concrete slab (this again being compatible with the situation in the bridge concerned). The whole model was tested in the upside-down position, so that the plate elements of the lamella flange were above the concrete slab. The top plate element was repeatedly loaded by a force modelling the reactions of the inclined webs in the system of the whole box girder. The related test set-up is shown in Fig. 1.

In the course of the investigation, two models were tested, and therefore two tests carried out. The first of them started by a static, one-cycle loading experiment (which also provided the authors with useful information), and then was continued by a typical cyclic loading test, during which the model was subjected to many times repeated cycles of loading. The objective of this repeated

loading test, which played the role of a pilot test for the whole examination, was to prove that the phenomenon of lamella breathing could significantly affect the performance of a lamella flange system. Therefore the gap between the two lamella plates in this first test was chosen large, namely as 12mm.

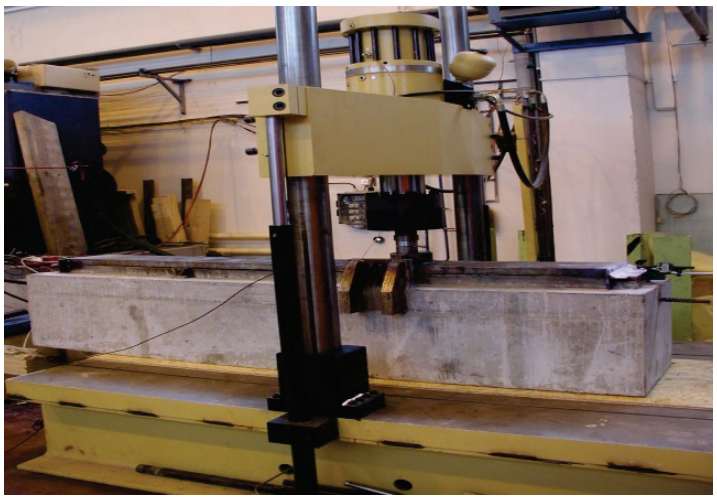

Fig. 1: The test set-up used

The other experiment already had quantitative objectives and was tailored to the real situation in an ordinary lamella-flange system. That is why the gap between the lamella plates was chosen much smaller (as 5.5 mm), with the view to reflect a possible combination of manufacture tolerances of the lamella plates in question.

The results of the static test were also used to determine the maximum amplitude to be safely applied during the cyclic loading experiment. A sinusoidal frequency of 2 Hz was used, and the cyclic loading was continued until the fatigue crack, generated by the cumulative damage process induced by the repeated loading, reached the whole length of the fillet weld connecting both of the two lamellas.

The welds of the first model cracked completely after 129 353 loading cycles, i.e. already after a few hours of testing. The importance of a real danger of lamella flange breathing, and of its impact on the limit state of the whole bridge structure, was therefore already demonstrated by this pilot test.

Of course, the results of, and the conclusions drawn from, the second test , where the gap between the flange lamellas realistically depicted the situation occurring in ordinary lamella flanges currently used in steel bridge construction, are of a much greater practical importance. There the fatigue crack initiated at 578 558 loading cycles, then propagated under further repeated loading, and covered the whole length of the weld (and thereby heralded a complete failure of the weld) after 1 256 293 loading cycles.

The experiments clearly demonstrated that the performance of the lamella flanges at the limit state is significantly influenced by a phenomenon which is still not taken into account. The authors´ experimental investigation proved the possibility of threats to the reliability and safety of the bridge due to the failure of the longitudinal boundary fillet welds connecting the plates of the lamella flanges, and consequently due to the disruption of their primary function necessary to ensure the desired action of the plates of the lamella flanges as a composite system.

The fatigue phenomenon studied, whose probability increases with the increasing number of heavy vehicles crossing the bridge, can result in very severe problems that may occur after many years of service of the bridge.

Acknowledgments: The kind support of the Czech Science Foundation Project No. GC13-34405J and of the RVO 68378297 institutional support are gratefully acknowledged.

Acoustic Metamaterial Behaviour of 3D Periodic Structures Assembled by Robocasting

Alena Kruisová[1,a], Hanuš Seiner[1,b], Petr Sedlák[1,c], Michal Landa[1,d], Benito Román-Manso[2,e], Pilar Miranzo[2,f], Manuel Belmonte[2,g]

[1]Institute of Thermomechanics, Czech Academy of Sciences, Dolejškova 5, 182 00 Prague 8, Czech Republic

[2]Institute of Ceramics and Glass (ICV-CSIC), Campus de Cantoblanco, Kelsen 5, 28049 Madrid, Spain

[a]alena@it.cas.cz, [b]hseiner@it.cas.cz, [c]psedlak@it.cas.cz, [d]ml@it.cas.cz, [e]mbelmonte@icv.csic.es, [f]pmiranzo@icv.csic.es, [g]mbelmonte@icv.csic.es

Keywords: elasticity, anisotropy, metamaterials, acoustic waves, band structure

Abstract: Ultrasonic measurements combined with numerical modelling are used to analyze the elastic and acoustic properties of morphologically complex ceramic bodies assembled by the Robocasting technique. It is shown that the micromechanics of the robocast periodic scaffolds leads to several metamaterial-like wave propagation phenomena. Besides the expectable prominent elastic anisotropy and the frequency band structure resulting from the periodicity of the scaffold, a wave-mode mixing is observed that disables the conventional distinguishing between quasi-longitudinal, quasi-shear, and pure shear modes for propagation in the symmetry planes of the structure. This paper proves the capability of Robocasting, as a versatile three-dimensional (3D) printing method, to produce tailored acoustic metamaterials with very low damping and outstandingly strong acoustic anomalies.

Robocasting is a free-form additive-manufacturing method for fabrication of cellular ceramic materials with regular complex architectures [1]. Besides the already well-explored suitability of the robocast scaffolds for applications in advanced filtering [2] or bone tissue engineering [3], these cellular materials posses also unique acoustic properties [4], similar to those of the so-called acoustic metamaterials. Among these properties, the frequency band-gap structure and the extremely strong anisotropy leading to refraction anomalies are the most noteworthy.

In this contribution, we present an analysis of vibrational properties and related macroscopic (effective) elasticity of robocast silicon carbide scaffolds densified by spark plasma sintering (SPS). The experimental method used for such an analysis is the resonant ultrasound spectroscopy (RUS,[5, 6]), that is, in combination with finite elements modeling (FEM), able to determine all independent anisotropic elastic moduli of the scaffold. The main part of the analysis is carried out on tetragonal architectures shown in Fig.1; however, due to the high versatility of the Robocasting method, several different architectures can be designed and prepared. As illustrative examples of this versatility, properties of scaffolds with monoclinic and hexagonal arrangements of the rods are presented, and compared to the tetragonal case.

It is shown that the analyzed scaffolds exhibit outstandingly strong acoustic anomalies, in particular in the acoustic energy focusing and acoustic wave mode mixing, and simultaneously also very low internal friction parameters, comparable to those of bulk silicon carbide ceramics. This makes the robocast materials promising candidates for applications in acoustic energy engineering, such as in lensing or cloaking devices.

Acknowledgement: This work was supported by the AdMat Project of Czech Science Foundation (14-36566G).

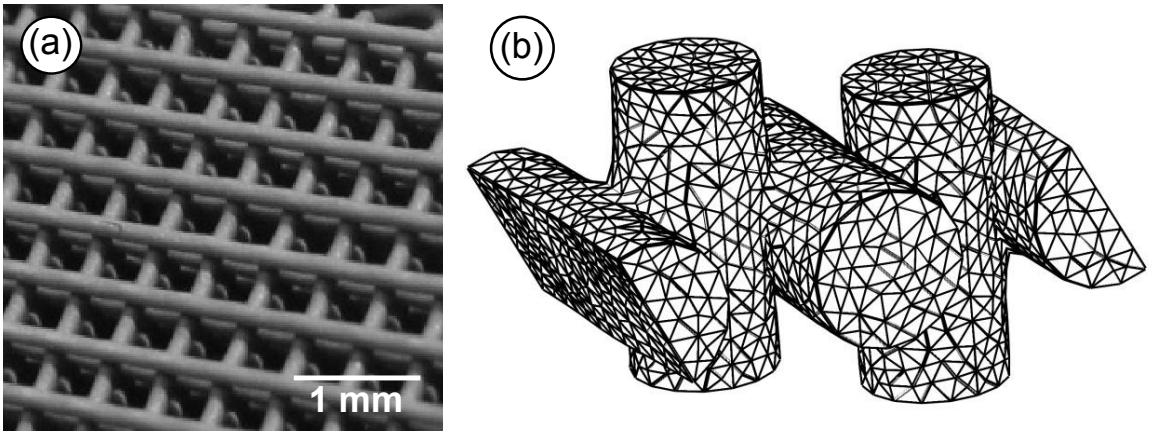

Fig. 1: (a) the regular structure of the robocast scaffold after the SPS; (b) a finite elements model of a scaffold under prescribed shear loading.

References

[1] K. Cai, B. Román-Manso, J. E. Smay, J. Zhou, M. I. Osendi, M. Belmonte, P. Miranzo, Geometrically Complex Silicon Carbide Structures Fabricated by Robocasting. J. Am. Ceram. Soc. 95 (2012) 2660–2666.

[2] B. Román-Manso, S. M. Vega-Díaz, A. Morelos-Goméz, M. Terrones, P. Miranzo, M. Belmonte, Aligned carbon nanotube/silicon carbide hybrid materials with high electrical conductivity, superhydrophobicity and superoleophilicity. Carbon 80 (2014) 120–126.

[3] P. Miranda, E. Saiz, K. Gryn, A. P. Tomsia, Sintering and robocasting of $\beta-$tricalcium phosphate scaffolds for orthopaedic applications, Acta Biomater. 2 (2006) 457–466.

[4] A. Kruisová, H. Seiner, P. Sedlák, M. Landa, B. Román-Manso, P. Miranzo, M. Belmonte, Acoustic metamaterial behavior of three-dimensional periodic architectures assembled by robocasting. Appl. Phys. Letters 105 (2014) 211904.

[5] R. G. Leisure and F. A. Willis, Resonant Ultrasound Spectroscopy. J. Phys.: Condens. Matter 9 (1997) 6001–6029.

[6] P. Sedlák, H. Seiner, J. Zídek, M. Janovská, M. Landa, Determination of All 21 Independent Elastic Coefficients of Generally Anisotropic Solids by Resonant Ultrasound Spectroscopy: Benchmark Examples. Exp. Mech. 54 (2014) 1073–1085.

21st International Conference **ENGINEERING MECHANICS 2015**
Svratka, Czech Republic, May 11 –14, 2015
Paper **#189, pp. 168–169**

Effect of Pulsating Water Jet Peening on 316L Stainless Steel

Tomáš Kruml[1,a]*, Petr Hlaváček[2,b], Josef Foldyna[2,c],
Jiří Tobiáš[1,d], Jiří Man[1,e]

[1] Institute of Physics of Materials, AS CR, Žižkova 22, 616 62 Brno, Czech Republic

[2] Institute of Geonics AS CR, Studentská 1768, 708 00 Ostrava, Czech Republic

[a]kruml@ipm.cz, [b]petr.hlavacek@ugn.cas.cz, [c]josef.foldyna@ugn.cas.cz, [d]tobias@ipm.cz,
[e]man@ipm.cz

Keywords: pulsating water jet, surface cold working, 316L steel, fatigue

Abstract: High-speed pulsating water jet was applied on polished surface of 316L stainless steel. Surface slip bands appeared after this treatment. In the most severe conditions, microcracks were formed. Hardness measurement showed that the affected layer is thinner than 60 μm. Application of the pulsating water jet has beneficial effect on the fatigue life of the material.

Introduction

Hardening of surface of ductile alloys by cold-working processes is often used in order to increase surface hardness, prolongate fatigue life by creating near-surface compressive stresses, remove nonhomogeneous residual stresses from the machining or even reduce corrosion. The most used surface cold-working process is the shot peening; other reported methods are e.g. deep rolling, laser shock peening or surface mechanical rolling [1-2]. This paper refers about recently developed method of surface treatment using high-speed pulsating water jet (PWJ). Theory of generating the pulsating water jet is described in [3] and the effect of its application on Al surface in [4].

Experiment

Material. Austenitic stainless steel 316L was supplied in a form of rods with 22 mm in diameter. The rods were cold worked which results in relatively high yield stress for this steel of 417 MPa.
Pulsating water jet. Specimens with carefully polished surface were subjected to PWJ generated at various water pressures from 20 to 30 MPa and moving on the specimen surface with various velocities. In these conditions, every place on the specimen is hit by 10^4-10^5 water droplets.
Characterization. Surface of specimens after the application of PWJ was observed by SEM-FEG Tescan Lyra. Microhardness was measured using head ZHU0.2. Fatigue experiments were performed using MTS servohydraulic testing machine and specimens with cylindrical gauge length.

Results & Discussion

The surface of flat polished specimens after the PWJ treatment was observed by the SEM. Slip bands were formed during the process. The surface density of bands and their height varied according the conditions of the PWJ process. In the most severe treatment (20 MPa), the bands are very pronounced and even microcracks appeared within such bands (Fig. 1a). The bands are different from those formed in standard fatigue test; they consist of sharp steps (Fig. 1b).

Microhardness was measured on specimen´s cross-section. No effect of the PWJ is observed (Fig. 2a), however, the indents were made 60 μm from the surface or farther. The surface layer affected by the PWJ is thus thinner than 60 μm. Effect of the PWJ (20 MPa) on fatigue life is shown in Fig. 2b. It is visible that for high stress amplitudes σ_a there is no difference in lifetime but for low σ_a the beneficial effect of the PWJ appears.

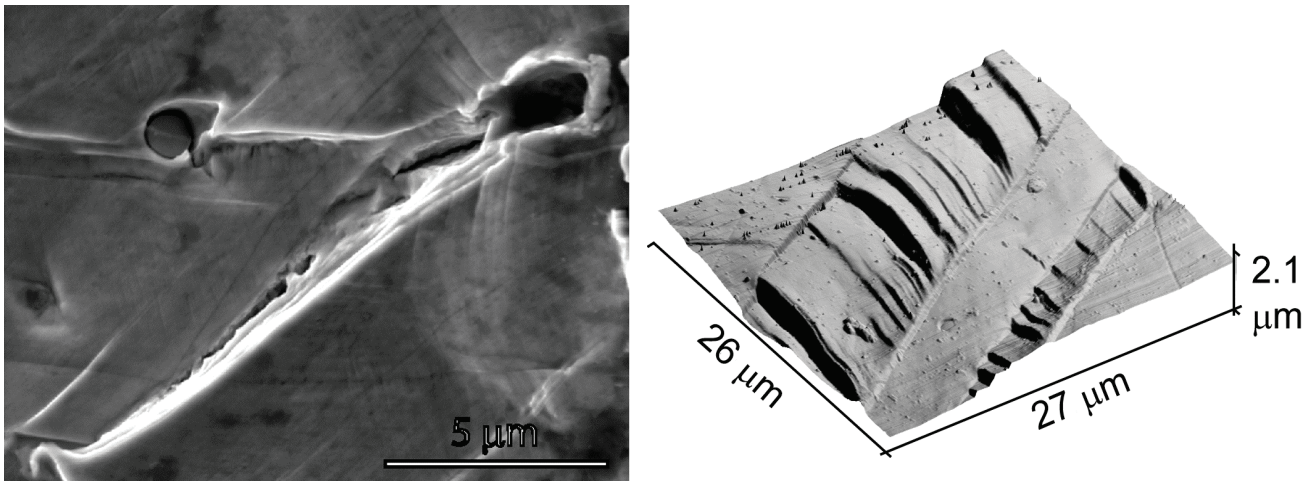

Fig. 1: a) Detail of surface bands and small cracks, b) AFM 3D imaging of the surface bands.

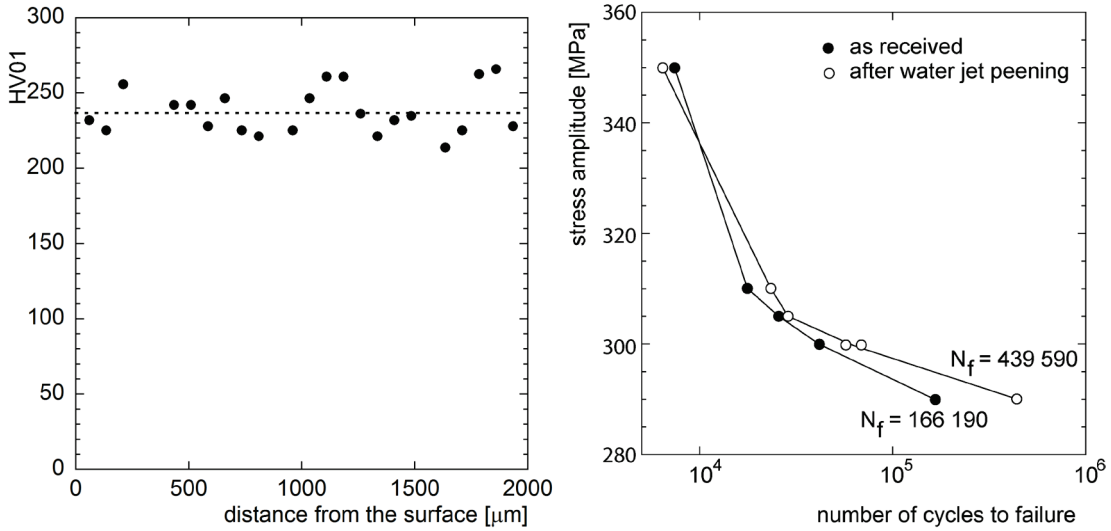

Fig. 2: a) Microhardness as a function of the distance from the surface. b) S-N curves of the as-received material and specimens with the surface treated by the pulsating water jet.

Summary

The PWJ process is a new possibility for surface cold-working treatment. The hardened surface layer is thinner than in the case of shot peening, but the beneficial effect on fatigue life is comparable.

References

[1] H.W. Huang, Z.B. Wang, J. Lu, K. Lu, Fatigue behaviors of AISI 316L stainless steel with gradient nanostructured surface layer, Acta Mat. 87 (2015) 150–160.

[2] I. Altenberger, B. Scholtes, U. Martin, H.W. Oettel, Cyclic deformation and near surface microstructures of shot peened or deep rolled austenitic stainless steel AISI 304, Mat. Sci. Eng. A 264 (1999) 1–16.

[3] J. Foldyna, Use of Acoustic Waves for Pulsating Water Jet Generation, in: M.G. Beghi (Ed.) Acoustic Waves - From Microdevices to Helioseismology, Intech 2011, 323–342.

[4] J. Foldyna, L. Sitek, J. Ščučka, P. Martinec, J. Valíček, K. Páleníková, Effects of pulsating water jet impact on aluminium surface. Journal of mat. proces. technology 209 (2009) 6174–6180.

21st International Conference **ENGINEERING MECHANICS 2015**
Svratka, Czech Republic, May 11 –14, 2015
Paper **#165, pp. 170–171**

Decreasing of Sliding Friction in Hydraulic Piston Damper

Michal Kubík[a] *, Ivan Mazůrek[b], Jakub Roupec[c]

Brno University of Technology, Brno, Czech Republic

[a]y115760@stud.fme.vutbr.cz, [b] mazurek@fme.vutbr.cz, [c] roupec.j@fme.vutbr.cz

Keywords: hydraulic piston damper, hydraulic damper, piston rod seal

Abstract: The published paper deals with the decreasing of sliding friction in hydraulic cylinder with double-ended piston rod. The hydraulic cylinder extrudes oil through the throttling gap placed in the external bypass, and so the throttling gap works as a hydraulic damper. Commercial hydraulic cylinder is the simplest way to ensure the fluid flow through the bypass. The hydraulic piston is manufactured with minimal leaking around the piston rod and maximal sealing of the piston. It results in high friction losses particularly caused by piston and piston rod sealing. This causes the undesired increase of force in whole range of velocities. The main goal of this paper is a proposal of suitable design and material selection which decreases friction losses. The measurement of all components, which contribute to the increase of shear friction, is described (piston rod sealing, piston sealing, dust cover, sliding tapes). The piston rod sealing has a significant effect on the total frictional force. New seals were designed and measured. The material NBR with suitable design modification of seal preload is the best solution for low shear friction operation of hydraulic cylinder.

Introduction

The majority of the available hydraulic damping systems have a seal of moving parts which creates the friction losses. This friction losses have a negative influence on the effectiveness of the damping system. For the progressive semi-active damping system is this problem significant. The friction losses in the system cause decreasing of a dynamic range (ratio of maximal to minimal damping force) which has negative influence to effectiveness of the damping system [1].

An important group of damping systems forms the systems where hydraulic fluid is extruded through the throttling gap placed in the external bypass by hydraulic cylinder. The most affordable option is commercially manufactured hydraulic cylinder which creates flow through external bypass. This hydraulic cylinder is manufactured with minimal leakage around the piston rod and maximal sealing of the piston. This causes large friction losses.

The main goal of this paper is a proposal of suitable design and material selection which decreases friction losses in commercial available hydraulic cylinder.

Materials and methods

In the paper, two experiments are presented. The first experiment should detect which component of hydraulic cylinder creates significant friction losses. Between piston rod and hydraulic press, the load cell and positon sensor were placed. Data acquisition system Dewetron and software Dewesoft were used. Commercially available hydraulic cylinder with double-ended piston rod (piston rod ø18, piston ø32, stroke 50 mm) was measured. This variant contains a few sliding tapes (piston rod and piston) from PTFE/Bronze, two piston rod seal T20 (Novathan), two dust covers PU5 and piston seal Omegat OMK. The friction for 4 different configurations was measured – 1) original state, 2) removed dust cover, 3) removed dust cover + piston rod seal and 4) removed dust cover + piston rod seal + piston seal.

The second experiment was composed of hydraulic cylinder, hydraulic pulsator Inova, load cell and position sensor. The tested hydraulic cylinder was assembled from measured piston rod seal, sliding tapes and piston seal. The piston rod seal T20 from Novathan, modified (change preload)

T20 from NBR and compact seal PTFE/NBR were measured. The whole hydraulic system was filled with damping oil. Inlet and outlet from hydraulic cylinder were connected by hydraulic hose. Hydraulic pulsator generated a movement of hydraulic piston (sin 1 Hz, stroke 20 mm).

Results

The results indicate that dust cover, piston seal, sliding tapes of piston and piston rod have minimal influence of the total friction losses. The piston rod seal has a significant effect to total friction losses. For this reason, different piston rod seals were measured (Fig. 1). The smallest friction losses exhibits the modified piston rod seal T20 from NBR. The friction force for this variant was in the range of 20 to 25 N.

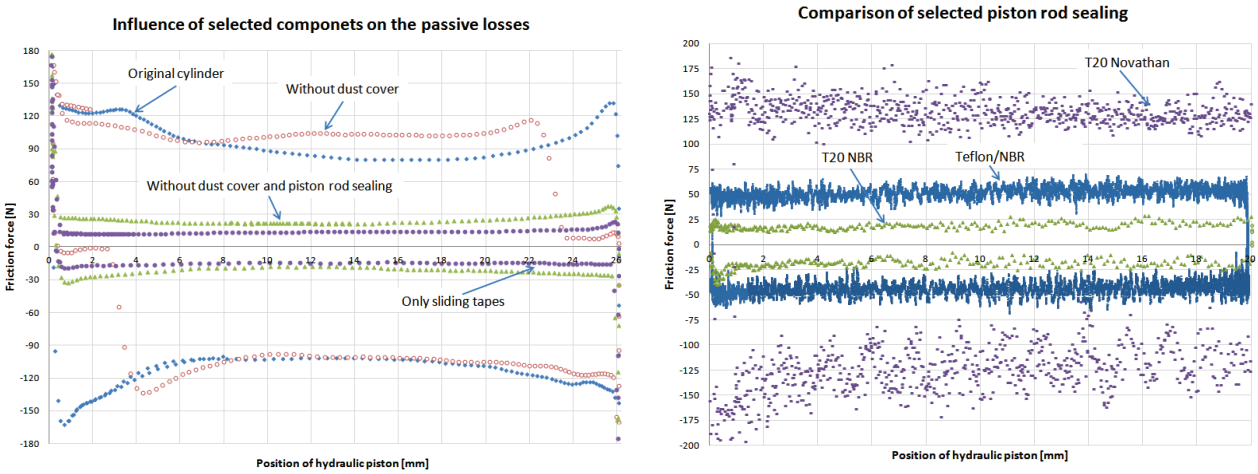

Fig. 1: Influence of components on the passive losses (left), comparison of piston rod sealing (right)

Conclusion

Modified piston rod seal from NBR had the smallest friction losses. However, this type of seal exhibits significant dependence of friction losses on the pressure in hydraulic system. Therefore, the piston rod seal from NBR is suitable for low pressure in hydraulic systems. For higher pressure in damping system, PTFE/NBR piston rod seal is more suitable, according to preliminary measurement. This type of seal exhibits a small dependence of pressure on friction losses.

Acknowledgement: This work was developed with the support of the grant FSI-S-14-2329 and CZ.1.07/2.3.00/30.0039. Project LO1202, obtained with financial support from the Ministry of Education, Youth and Sports under the program NPU I.

References

[1] G. Yang, B.F. Spencer, J.D. Carlson, M.K. Sain, Large-scale MR fluid dampers: modeling and dynamic performance considerations, Engineering Structures, 2002, vol. 24 (2002) 309-323. DOI: 10.1016/s0141-0296(01)00097-9.

21st International Conference **ENGINEERING MECHANICS 2015**
Svratka, Czech Republic, May 11 –14, 2015
Paper **#030, pp. 172–173**

Computational Model of ATV Vehicle for Real-Time Simulation

Pavel Kučera[a] *, Václav Píštěk[b]

Brno University of Technology, Faculty of Mechanical Engineering, Institute of Automotive Engineering, Technická 2896/2, 616 69 Brno, The Czech Republic

[a] kucera@iae.fme.vutbr.cz, [b] pistek.v@fme.vutbr.cz

Keywords: ATV, Simulink, NI VeriStand, computational model, motor, tire

Abstract: The paper deals with description of a computational model of ATV vehicle in Simulink software. This computational model is created using the basic elements of own library and represents the main driveline parts for the simulation of longitudinal and lateral vehicle dynamics. The article describes the design and function of the computational model and demonstrates the usage of ATV model in the NI VeriStand software. It can be simulated on the hardware for real-time testing. In conclusion; a simulation of drive is done to verify the functionality of the assembled model.

Introduction

Virtual software are already common instruments for the development of prototype vehicles. It helps to accelerate the testing of vehicle behaviour and cost reduction. The available software libraries are already prepared for various applications in the automotive industry and user only changes the input parameters of the vehicle. If the libraries are not sufficient for users; they can create their own which is also the case here. This paper deals with the creation of computational model of ATV vehicles and the possibility to simulate it in real time by using National Instruments hardware and software.

Computational model of ATV vehicle

The computational model of ATV vehicle is based on vehicle design described in [1]. There is a detailed description of the construction ATV vehicle and its parameters. These parameters are used as input values for the simulation model of ATV. The computational model is created using own library in the Simulink software. This library contains blocks describing the main parts of the powertrain and blocks of the longitudinal and lateral vehicle dynamics that are created and described in [2; 3]. The library contains blocks of computational model of the engine; transmission; brakes; tires and directional dynamics of the vehicle. Each of these blocks contains an interface for entering input parameters. These parameters can be changed by the user. The user can enter the engine torque curve; moments of inertia; gear ratio; shaft torsional stiffness and damping; parameters of disc brakes etc. The block of tire is used for the calculation of longitudinal and lateral force; aligning moment and transient behaviour of the tire. The main block describes the directional dynamics of ATV vehicle and vertical load of tires. The library also contains other blocks for assembling different vehicles and configuration. Here only blocks used to build ATV vehicles are mentioned.

Simulation of ATV vehicle and compiling of the computational model

A simple demonstration of the function of the vehicle computational model is shown in Fig. 1. The vehicle design; computational model; trajectory of the vehicle and graphical interface in the NI VeriStand software are displayed here. The simulation was performed in Simulink software. The vehicle started moving and accelerating. Then the vehicle turned to the left about 360 degrees; and then to the right. After 16 s the vehicle began to brake and then stopped. After 22 s; the vehicle

began to move again. To assess the correct behaviour of the vehicle; a standard driving test and comparison with the real measurement must be done. As it is a prototype; the simulation can be verified only in accordance with theoretical assumptions.
The computational model developed in Simulink software can be used for real-time applications in NI VeriStand software. Combining these two software packages and setting parameters of fixed step; the model can be compiled into dynamically linked libraru (.dll file). This file can be loaded in the NI VeriStand software and run in real time on the appropriate hardware. The user can create an interface for displaying the output data from the simulation. Inputs data are driven by external user intervention. Another option is to add a graphical interface programmed using VRML and NI Labview. The user can simulate the drive of a prototype vehicle in the real-time by these tools and analyse its behaviour influenced by a real driver.

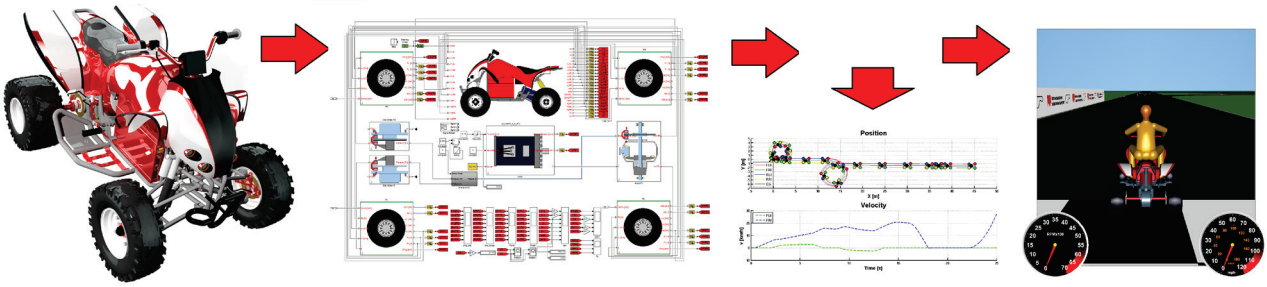

Fig 1: Scheme of development of ATV vehicle

Summary

The paper describes a computational model of ATV vehicle which can be used to simulate different driving modes of vehicles; i.e. acceleration; steering; braking etc. An important factor of this model is the possibility of its use on the device for real-time testing. Developers can test the behaviour of the vehicle before starting its production; which saves time; and the model can be further expanded and used for the development of mechatronic systems.

Acknowledgement: This work is an output of cooperation between internal BUT research project Reg. No. FSI-S-14-2334 and NETME Centre; regional R&D centre built with the financial support from the Operational Programme Research and Development for Innovations within the project NETME Centre (New Technologies for Mechanical Engineering); Reg. No. CZ.1.05/2.1.00/01.0002 and; in the follow-up sustainability stage; supported through NETME CENTRE PLUS (LO1202) by financial means from the Ministry of Education; Youth and Sports under the „National Sustainability Programme I".

References

[1] P. Kučera, Design of All-Terrain Vehicle with Electric Drive. Brno: Brno University of Technology; Faculty of Machanical Engineering; 2011. 114 p. Supervisor Ing. Petr Porteš; Dr.

[2] P. Kučera, V. Píštěk, Simulink block library for assembling a vehicle. *Perner's Contacts* [online]. 2014; vol. IX; no. 2; p. 38-47 [cit. 2015-02-23]. Available from: http://pernerscontacts.upce.cz/35_2014/Kucera.pdf

[3] T.D. Gillespie, Fundamentals of Vehicle Dynamics; Society of Automotive Engineers; Warrendale; PA; 1992. ISBN 1-56091-199-9.

Prediction of Optimal Load and Performance of Thermal Batteries

Milena Kušnerová[a]*, Jan Valíček[b], Marta Harničárová[c]

VŠB-Technical University of Ostrava, Czech republic

[a]milena.kusnerova@vsb.cz, [b]jan.valicek@vsb.cz, [c]marta.harnicarova@vsb.cz

Keywords: Thermal battery, internal resistance, optimal load, optimal performance.

Abstract: Direct conversion of heat into electrical energy is one of appropriate alternatives to generating electric current in conventional ways. Although thermal batteries are now usually used beyond the reach of energy distribution networks, however, prospectively, their wider use could be considered. In particular, more than 50 % of the energy used in homes, in car engines it is up to 70 %, is being lost as waste heat (for example – heated car exhausts, waste heat from refrigerators, computers, or solar panels can be used to power electrical circuits in those appliances).

Historically, in manufacturing the first thermal batteries, only metals (tellurium, antimony, germanium, silver) were used, later then different alloys and semiconductors. Lead telluride is considered to be the most effective thermoelectric material, but it is not allowed because of its toxicity. Material researchers from the University of Osaka achieved promising results with the use of nickel and iron, but with the addition of thallium, i.e. also a toxic element. Researchers from General Motors very intensively examine skutterudites allowing heat absorption and passage of electric current, and conveniently with regard to relatively high temperature differences [1]. Further development of thermoelectrically efficient materials in the future should be oriented in particular to an environmental thrift and a relatively high efficiency, i.e. to material and structural resistance to high temperature differences (in the hundreds of degrees Celsius), which would allow to utilize significant waste heat from high-temperature processes (e.g. in steel production, etc.).

To demonstrate a sample measurement of proposed performance characteristics, classical thermal batteries of ternary alloys have been chosen. Ternary alloys are characterised (compared to metals or semiconductors) by relatively convenient values of material coefficients. Using them, for example, for the temperature difference from 400 to 1 000 K, theoretically up to 30 % of material efficiency can be achieved. Practically, however, the temperature differences tend to be lower in the use of waste heat (as a result of heat dissipation into the surrounding environment and to the equipment itself). Even high temperature differences, however, do not guarantee a high level of efficiency of thermal batteries of ternary alloys, because under relatively high temperature differences, the thermal batteries are considerably amortisable.

Measuring internal resistance of thermal battery

Impairment of efficiency in thermal battery amortisation is primarily caused by growing internal resistance R_i. The temperature developments of the internal resistance of thermal batteries of ternary alloys was measured; the measurement results were then compared with the indirect measurements of internal resistance (computationally), namely repeatedly under comparable operating conditions and the corresponding temperature differences ΔT (U_S Seebeck thermoelectric and electromotoric voltage, I thermal current, R resistance of load).

$$R_i(\Delta T) = \frac{U_S(\Delta T) - I \cdot R}{I} \tag{1}$$

The thermal battery of ternary alloys can be evaluated as a source of hard voltage; the terminal voltage under load is detected as the smaller, the greater thermal current is taken. So, if the thermal battery has very small internal resistance compared to external load resistance, the terminal voltage under load varies very little. The problem arises when the thermal battery is thermally amortised.

Amortised thermal batteries behave in an electrical circuit as non-linear elements, i.e. they exhibit non-linear current-voltage characteristics.

Performance measurement and optimum load determination

Thermal batteries of ternary alloys heated by an external heat source were a source of Seebeck electro-motoric voltage. Performances of 3 classic thermal batteries were measured, namely under various loads at different equi-temperature levels. For this purpose, measurements of the 1 temperature of walls, 2 current, 3 terminal voltages under various loads (resistance standards) were made. Under comparable conditions, the measurements showed a qualitatively comparable character of the dependence of performance on load resistance and a comparable character of the dependence of performance on the temperature difference between the thermal battery walls. The optimum load R_{opt} was found by the method of least squares as maximum performance squares were sought using a local extreme of functions as follows

$$P_{max} = U_{max} \cdot I_{max}. \tag{2}$$

These maximum performance squares were inscribed in the appropriate performance triangles for the given temperature difference ΔT between the thermal battery walls. The straight line of the optimum load was a connecting line of all maximum performance levels P_{max} of all equi-temperature levels of the carried out measurements (Fig.1).

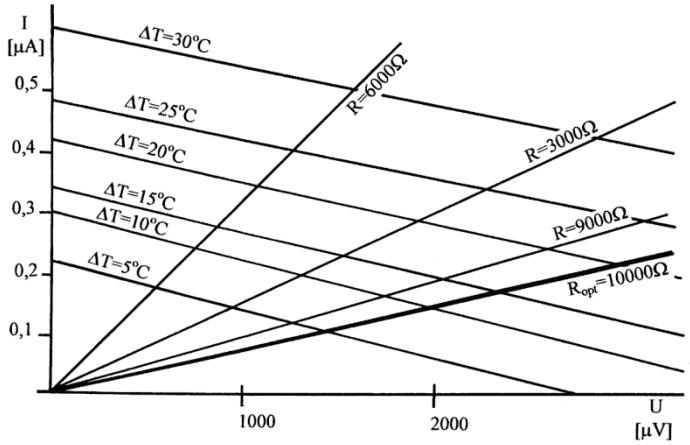

Fig. 1: Character of the dependence of performance of the thermal battery of ternary alloys (thermal current and thermal voltage under load R) for a temperature difference between the thermal battery walls ΔT and prediction of the optimum load R_{opt} for maximum performance.

Conclusions

In conclusion, it can be said that for each thermal battery with regard to its specific material, geometric and structural properties, a maximum permissible operating internal resistance to be specified and the internal thermal battery resistance to be continuously monitored. In addition, such optimum operating load of each thermal battery was determined in order to submit the maximum possible performance linearly dependent on the temperature difference between its walls.

References

[1] Skutterudites: The heat scavengers. New Scientist, 2990 (2014) 40-41.

21st International Conference **ENGINEERING MECHANICS 2015**
Svratka, Czech Republic, May 11 –14, 2015
Paper **#045, pp. 176–177**

Analysis of the Boundary Problem with the Preference of Mass Flow

Martin Kyncl[a], Jaroslav Pelant[b]

Výzkumný a zkušební letecký ústav, a.s., Beranových 130,199 05 Prague, Czech Republic

[a]kyncl@vzlu.cz, [b]pelant@vzlu.cz

Keywords: turbulent flow, the Navier-Stokes equations, finite volume method, boundary conditions, 3D, Riemann problem

Abstract: We work with the numerical solution of the turbulent compressible gas flow, and we focus on the numerical solution of these equations, and on the boundary conditions. In this work we focus on the outlet boundary condition with the preference of given mass flow. Usually, the boundary problem is being linearized, or roughly approximated. The inaccuracies implied by these simplifications may be small, but they have a huge impact on the solution in the whole studied area, especially for the non-stationary flow. The boundary condition with the preference of mass flow is sometimes being implemented with the use of some iterative process, guessing the correct values (for the pressure, density, velocity) in order to match the given mass flow through the boundary. In our approach we try to be as exact as possible, using our own original procedures. We follow the exact solution of the initial-value problem for the system of hyperbolic partial differential equations. This complicated problem is modified at the close vicinity of boundary, where the conservation laws are supplied with the additional boundary conditions. We complement the boundary problem suitably, and we show the analysis of the resulting uniquely-solvable modified Riemann problem. The resulting algorithm was coded and used within our own developed code for the solution of the compressible gas flow (the Euler, NS, and RANS equations). The examples show good behaviour of the analyzed boundary condition.

The problem

The main problem of this boundary condition is to solve the following system (conservation laws in 1D), equipped with one-side initial condition and the complementary condition (preference of mass flow at the boundary).

$$\begin{aligned}
&\frac{\partial \varrho}{\partial t} + \frac{\partial u\varrho}{\partial x} = 0 && \varrho(x,t) = \varrho_L, \quad x < 0 \\
&\frac{\partial \varrho u}{\partial t} + \frac{\partial (p + \varrho u^2)}{\partial x} = 0 && u(x,t) = u_L, \quad x < 0 \qquad \varrho(0,t)u(0,t) = G_\star \\
&\frac{\partial \varrho(\varepsilon + \frac{1}{2}u^2)}{\partial t} + \frac{\partial (\varrho u(\varepsilon + \frac{1}{2}u^2) + pu)}{\partial x} = 0 && p(x,t) = p_L, \quad x < 0
\end{aligned} \tag{1}$$

Here ϱ is the density, p pressure, u velocity, $\varepsilon = p/\varrho(\kappa - 1)$ is the specific internal energy, κ is the adiabatic constant, $G_\star$ is prescribed mass flow (per unit area). This problem has a unique (entropy weak) solution for the reasonable input data $\varrho_L, u_L, p_L, \kappa, G_\star$. The complete analysis of this problem is based on the solution of the Riemann Problem for the Euler equations.

Example

The developed software with presented boundary condition was used for the simulation of the compressible turbulent flow in the 3D axis-symmetrical channel. Axis x is the axis of symmetry. At the geometry crosscut shown at Fig. 1., the inlet is located at the upper part of the boundary, the outlet is located right. The computational mesh in 2D crosscut consisted of 73x97 quadrilaterals. The initial condition was formed by the state $\theta^o = 273.15,\ v_1^o = 0,\ v_2^o = 0,\ v_3^o = 0,\ p^o = 101325$. The

boundary condition conserving the total pressure, total temperature, and zero tangential velocity, with $\theta_o = 273.15, p_o = 101325$ was used at the inlet. At the outlet, the boundary condition with preference of mass flow was used, with $G_\star = 4.0$ in average. At each face, the value $G_\star$ was computed (in each iteration) in order to match the average (across the whole boundary). Other boundaries were considered as wall: The boundary condition preffering the zero normal velocity was used in the case of the inviscid flow. For the viscous flow, this condition was modified by the zero velocity at the wall, and wall temperature $\theta_{WALL} = 273.15$ was set. Further $k_{WALL} = 0$ and $\omega_{WALL} = c_\omega \frac{6\mu}{\beta \varrho y_s^2}$, $c_\omega \frac{6}{\beta} = 120$. Here by y_s we mean the distance between the face and the center of the neighbouring element.

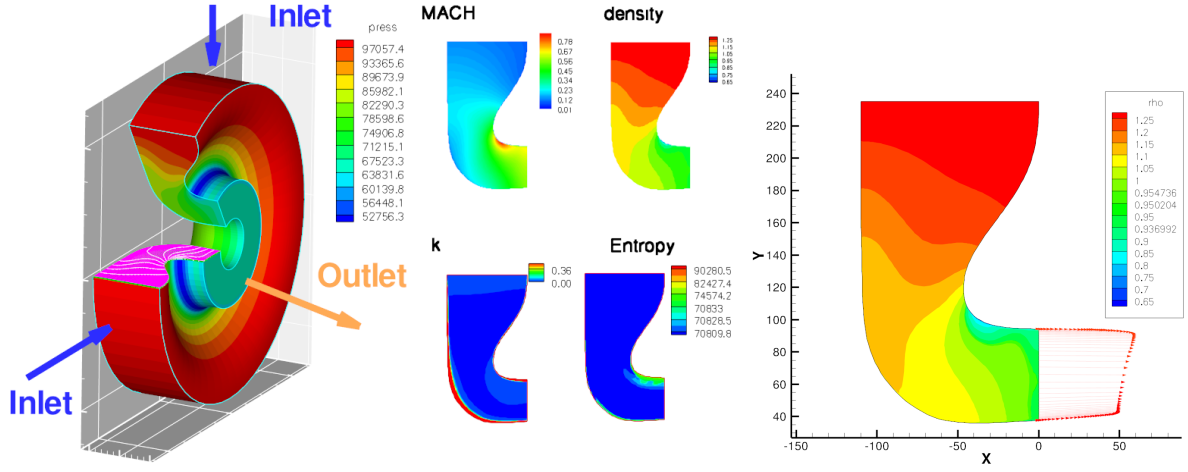

Fig. 1: 3D axis-symmetrical turbulent flow, 3D geometry shape, results at chosen 2D crosscuts.

Summary

This paper shows the analysis of the outlet boundary condition by preference of mass flow, based on the modification of the Riemann problem for the Euler equation.

Acknowledgment: This result originated with the support of Ministry of Industry and Trade of Czech Republic for the long-term strategic development of the research organisation. The authors acknowledge this support.

References

[1] C. J. Kok, Resolving the Dependence on Freestream Values for the k- Turbulence Model, AIAA Journal, 38 (2000) 1292–1295.

[2] M. Kyncl, J. Pelant, Applications of the Navier-Stokes equations for 3D viscous laminar flow for symmetric inlet and outlet parts of turbine engines with the use of various boundary conditions. Technical report R3998, VZLÚ, Beranových 130, Prague, (2006).

[3] M. Kyncl, Numerical solution of the three-dimensional compressible flow. Master's thesis, Prague, (2011). Doctoral Thesis.

[4] M. Kyncl, J. Pelant, Outlet Boundary Condition by the Preference of Mass Flow. Technical report R6155, VZLÚ, Beranových 130, Prague, (2014).

[5] M. Kyncl, J. Pelant, Implicit method for the 3d RANS equations with the k-w (Kok) Turbulent Model. Technical report R5453, VZLÚ, Beranových 130, Prague, 2012.

21st International Conference **ENGINEERING MECHANICS 2015**
Svratka, Czech Republic, May 11 –14, 2015
Paper **#225, pp. 178–179**

Deformation Behaviour of Gellan Gum Based Scaffold Subjected to Compression Loading

Daniel Kytyr[1,2,a], Tomas Doktor[1,2,b], Marcel Adorna[2,c], Michaela Neuhauserova[2,d], Jan Sleichrt[1,2,e], Nela Fenclova[1,2,f], Ana Gantar[3,4,g] , Sasa Novak[3,4,h]

[1]Institute of Theoretical and Applied Mechanics, CAS, v. v. i, Prosecká 76, 190 00 Prague, Czech Republic

[2]Czech Technical University in Prague, Faculty of Transportation Sciences, Department of Mechanics and Materials, Konviktska 20, 120 00 Prague 1, Czech Republic

[3]Department for Nanostructured Materials, Jožef Stefan Institute, Jamova cesta 39, 1000 Ljubljana, Slovenia

[4]Jožef Stefan International Postgraduate School, Jamova cesta 39, 1000 Ljubljana, Slovenia

[a]kytyr@itam.cas.cz, [b]doktor@itam.cas.cz, [c]adornmar@fd.cvut.cz, [d]neuhamic@fd.cvut.cz, [e]sleicjan@fd.cvut.cz, [f]fenclova@itam.cas.cz, [g]ana.gantar@ijs.si, [h]sasa.novak@ijs.si

Keywords: scaffold, gellan gum, compressive loading, digital image correlation

Abstract: This work presents deformation behaviour of gellan gum and gellan gum - bioactive glass composites as novel hydrophilic materials for production of scaffolds in the field of bone-tissue engineering. According to recent studies such materials are attractive for personalized design of implants thanks to their biocompatibility and wide range of available fabrication methods. Batch of samples was subjected to uni-axial compression loading in a custom designed loading device to obtain their elastic and plastic characteristics. Deformation response was derived from full-field optical strain measurements based on digital image correlation method. The acquired results show a reinforcement effect bioactive glass and its significant influence to the elastic modulus.

Introduction

Gellan Gum (GG) has been recently very popular for tissue engineering applications because of its tunable physical and mechanical properties [1]. To expand its use in bone tissue regeneration bioactive glass (BG) particles (highly bioactive and osteogenic material) were added to the polymer matrix [2]. For the clinical application description of deformation response to the external loading is an essential property for every newly synthesized material. However, proper estimation of overall mechanical properties of such a material with complex microstructure requires employment of optical strain measurement together with precise position control and force readout.

Gellan gum scaffold samples

Pure GG and GG-BG composite samples in shape of cylinder with diameter $4.0-4.5$ mm and height $6.0-8.0$ mm were synthesized based on procedure in detail described in [2]. Faces of the samples with porosity $80-90$ % (weight of $80-130$ mg) were carefully polished to obtain suitable plan-parallelism for compression testing.

Experimental procedure

Compression test was performed using custom uni-axial loading device designed with respect to high-precison testing of small biological samples and artificial tissues. Planetary gear unit P42-25

(Transtecno, Italy) with minimal backlash attached to micrometer screw 7T173-20 (Standa, Lithuania) enabled $2\,\mu\mathrm{m}\cdot\mathrm{s}^{-1}$ loading rate. The device was equipped with high accuracy load-cell HBM U9C (Hottinger Baldwin Messtechnik, Germany) with $50\,\mathrm{N}$ load capacity connected to OM 502T (Orbit Merret, Czech Republic) programmable indicator for force readout. Strains were derived from optically measured deformations evaluated using digital image correlation (DIC). For this purpose images of the loaded specimens were acquired by high-resolution CCD camera (Manta G-504B, AVT, Germany) attached to bi-telecentric zoom lens TCZR 072 (Opto Engineering, Italy). Homogeneous illumination of loading scene was povided using laboratory LED light source KL 2500 (Shott, Germany). Strain was evaluated from the acquired image sequence using custom DIC software [3] based on Lucas-Kanade tracking algorithm [4].

Results and conclusions

Compressive material properties of GG cylindrical scaffolds were measured. Stress-strain curves were derived from optically measured deformations. From the slope of elastic linear parts in the stress-strain diagrams Young's moduli were estimated. However full field strain evaluation was limited by depth of field corresponding to $25\,\%$ of samples diameter nevertheless preliminary results showed suitability of the method for testing of highly porous soft synthetic materials. Reinforcement effect of the BG was observed. Elastic modulus of GG-BG composite was significantly higher compared to pure GG samples.

Acknowledgements: The research was supported by Grant Agency of the Czech Technical University in Prague (grant no. SGS15/225/OHK2/3T/16) and by institutional support RVO: 68378297. The Slovenian Research Agency is acknowledged for its financial support of the PhD study of the co-author, Ms. Ana Gantar.

References

[1] E.R. Morris, K. Nishinari, M. Rinaudo, Gelation of gellan – A review, Food Hydrocolloids 28 (2012) 373–411.

[2] A. Gantar, L.P. da Silva, J.M. Oliveira, A.P. Marques, V.M. Correlo, S. Novak, R.L. Reis, Nanoparticulate bioactive-glass-reinforced gellan-gum hydrogels for bone-tissue engineering, Materials Science and Engineering C, 43 (2014) 27–36.

[3] I. Jandejsek, J. Valach, D. Vavřík, Optimization and Calibration of Digital Image Correlation Method, in P. Šmíd, et al. (Eds), 48^{th} International Scientific Conference on Experimental Stress Analysis, (2010), p. 121–126.

[4] B.D. Lucas, T. Kanade, An iterative image registration technique with an application to stereo vision, in: Proceedings of Imaging Understanding Workshop, 1981, pp. 121–130.

21st International Conference **ENGINEERING MECHANICS 2015**
Svratka, Czech Republic, May 11 –14, 2015
Paper **#109, pp. 180–181**

Reliability of Approach Slabs and Modelling of Transition Zones of Bridges

Kamil Laco[a], Viktor Borzovič[b]

Stavebná fakulta, STU v Bratislave, Radlinského 11, 810 05 Bratislava, Slovak Republic

[a]kamil.laco@stuba.sk, [b]viktor.borzovic@stuba.sk

Keywords: approach slab, elastic support, modelling of interaction

Abstract: The approach slab is the structural member of transition zones, which compensates a different settlement of bridge abutment and a road embankment. The main reason of different settlement is the consolidation of soil under the slab and the abutment. The geometry of approach slab, its length and the thickness is defined on the basis of differential settlement of embankment and the abutment. The static behaviour of slab is defined as a slab on elastic soil. The reinforced concrete slab is supported with the line rigid support on the one edge, and the rest of slab area interacts with the soil. The civil engineers design the reinforcement in those slabs based on the simplified structural scheme, without considering the elastic area support. This scheme is the simple supported slab on the both ends**.**

The paper is dealing with the comparing of different structural models of the reinforced concrete approach slabs. The complex models of transition zones with the brick elements of the soil and the interaction with the reinforced concrete slab with the soil embankment are compared with the simplified models used by civil engineers. The analysis was performed on the transition zone of highway bridge from Slovakia based on its geometry and the subsoil consistence. The approach slab has length of 6.0 m and is 10.15 m wide. The thickness of slab is 350 mm. The height of embankment behind the abutment is 9.5 m. As an alternative 250 and 350 mm thickness of the slab was analysed.

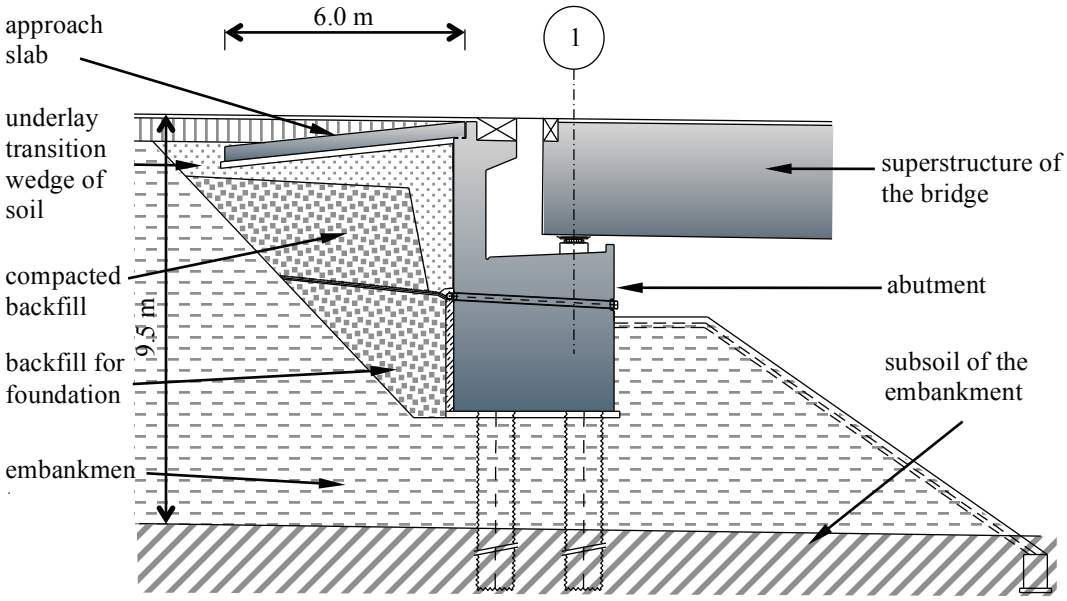

Fig. 1: Analysed approach slab of the bridge on the highway road

What is the reliability and the safety of using simplified models shows the parametric studies, where the results of different soil stiffness and the thickness of slab for various structural models are

compared. The structural models were divided into 2 groups. With the constant stiffness of subsoil under the approach slab and linearly changing stiffness along the slab length. The linearly decreasing stiffness from the maximum value on the free end to the minimum on the edge that is supported by the abutment. This should simulate the void that may develop below the slab caused by the erosion of embankment or by water percolation and the infiltration. The reference model to compare with, was the simple supported slab on the both ends.

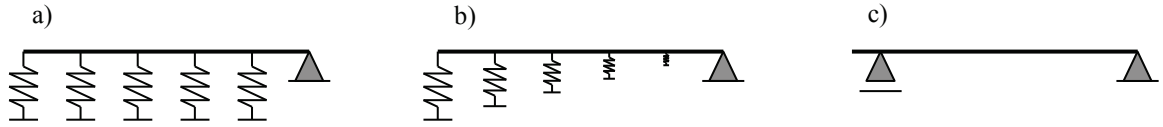

Fig. 2: The alternatives of models of approach slab (right edge – connection with abutment, left edge – free end of approach slab)

The selected models of soil for analysis were: single parameter Winkler model, two-parameters Winkler-Pasternak model, iterative procedure for obtaining soil resistance coefficient via Soil-In from SCIA Engineer and 3D finite soil elements model with Sofistik software.
The backfill for transition zone is in the most cases sand or sand-gravel compacted soil. For the analysis was chosen 8 representative values of stiffness parameters from gravel G1-GW to G5-GC and sand from S1-SW to S3-SF.

The loads of construction was based on STN EN 1991-2/NA. Selected load model was LM1 with a coefficient γ_{Qi} and γ_{q1} equals 0.9. The most loaded lane was placed on the edge of approach slab. The areas of tandem of wheels was enlarged according to the 30° angle of force redistribution to 1.2 x 1.2 m. The analysis of models is based on the maximum bending moment of the approach slab. Therefore the vehicle was placed in the middle of the slab.

The reason for the analysis of design reliability of approach slab was the conservative structural scheme of approach slab as simply supported slab on the both ends. Also the effect of consideration of void creation in transition zone, which could cause a significant loss of soil material under the slab. The paper tries also assess ability of real usage of these complex calculations in practise in the terms of time difficulty, effectivity and the reliability of design of approach slabs.

Acknowledgement: This work was supported by the Slovak Research and Development Agency under the contract No APVV–0442-12.

References

[1] V. Borzovič, J. Halvonik, Navrhovanie prechodových dosiek mostov pozemných komunikácií, in Betonárske dni 2010: Zborník prednášok. Bratislava, STU v Bratislave, 2010. ISBN 978-80-8076-089-2. s. 115-120.

[2] N. Jendželovský, Modelovanie základových konštrukcií v MKP, Bratislava, Nakladateľstvo STU, 2013. ISBN 978-80-227-3860-6. s. 94.

[3] J. Frankovská, M. Súľovská, P. Turček, Zakladanie stavieb: Podklady k navrhovaniu, plošné a hĺbkové základy, Bratislava, Nakladateľstvo STU, 2013. 160 s. ISBN 978-80-227-4018-0.

[4] OTN 73 6244 : Prechody na cestných a diaľničných mostoch. Praha, 1981.

21st International Conference **ENGINEERING MECHANICS 2015**
Svratka, Czech Republic, May 11 –14, 2015
Paper **#103, pp. 182–183**

Utilization of Artificial Neural Network Based Response Surface Method for Reliability Analysis of Structures

David Lehký[a], Martina Šomodíková[b]

Institute of Structural Mechanics, Faculty of Civil Engineering, Brno University of Technology,
Veveří 331/95, 602 00 Brno, Czech Republic
[a]lehky.d@fce.vutbr.cz, [b]somodikova.m@fce.vutbr.cz

Keywords: artificial neural network, Latin hypercube sampling, load bearing capacity, probability of failure, reliability index

Abstract: The key step of the reliability and lifetime assessment of structures is the determination of reliability level, described by failure probability or reliability index. Some of the simulation or approximation techniques can be used for this purpose. In case of large structures analyzed using the nonlinear finite element method, it is necessary to develop more efficient procedures, reducing the number of evaluations of original limit state function to a minimum. Here, artificial neural network based response surface method in combination with small-sample simulation technique Latin Hypercube Sampling is utilized for the approximation of a limit state function. Thanks to ability of artificial neural network to generalize it is efficient to fit limit state function with a sufficiently small number of simulations.

Introduction

A utilization of the response surface method (RSM) can be a suitable solution if time-consuming nonlinear finite element method (FEM) analysis of structures is applied and the crude Monte Carlo (MC) simulation method can not be used because of millions of simulations needed. In polynomial RSM, the limit state function (LSF) is approximated using a suitable polynomial function in most cases of first or second order. Parameters of surrogate function are adjusted with regard to several discrete points obtained from evaluations of original LSF and failure probability is then calculated by utilization of classical simulation methods or first-order reliability method (FORM). In case of large structures, artificial neural network based response surface method (ANN-RSM) in combination with small-sample simulation technique Latin Hypercube Sampling (LHS) can be utilized as a powerful parallel computational system, reducing the number of evaluations of original LSF to a minimum.

In proposed ANN-RSM a feed-forward multi-layer network type is used [1]. Artificial neurons are organized into several layers and the signal moves from the input nodes through the nodes in hidden layers (if any) to the output node. Feed-forward network is trained using "supervised" learning, where a set of example pairs (p, y), $p \in \mathbf{P}$, $y \in \mathbf{Y}$ is introduced to the network and the aim is to find a function in the allowed class of functions that matches the examples best. The stratified simulation LHS method is used for selection of artificial neural network training set elements to emphasize the efficiency.

Application

The ANN-RSM was applied for reliability calculation of a single-span post-tensioned composite bridge in the Czech Republic (see Fig. 1 left). Normal load bearing capacity of the bridge was assessed using computational tools of advanced nonlinear mechanics based on FEM and fully probabilistic approach. Numerical model was created in ATENA 2D software [2]. Stochastic parameters of random input variables were defined using FReET software [3] according to appropriate recommendations.

At first, sensitivity analysis was performed to capture the most important variables. The repetitious deterministic FEM analyses with random realizations generated by LHS were performed and the sets

of structural responses and corresponding vectors of input random variables serve as a training set for ANN training using appropriate optimization technique. Trained ANN was used as a surrogate LSF for consequent reliability analysis where failure probability or reliability index were calculated by utilization of classical simulation methods or FORM method. In case of simulation methods millions of simulations can be used thanks to very fast evaluation of surrogate LSF compared to original one.

By reason of time-consuming nonlinear analyses, only serviceability limit states (SLS, the limit state of decompression and limit state of cracking) were investigated. The value of normal load bearing capacity was assessed considering the common bridge type. It was assumed $\beta = 0$ $(p_f = 0.5)$ for both SLS. Results are summarized in Fig. 1 right as a comparison of proposed ANN-RSM method with classical simulation method LHS in combination with Cornell reliability index, approximation method FORM, and first order response surface method (RSM-linear).

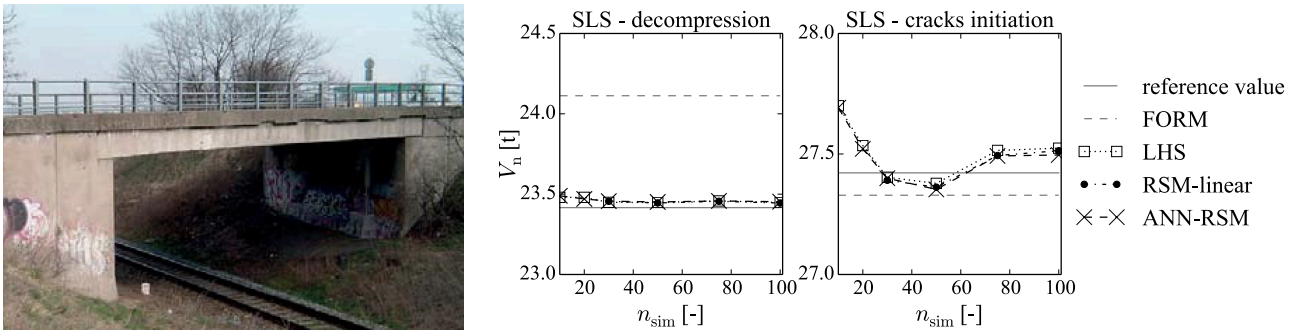

Fig. 1: Side view of the analyzed bridge (left); Comparison of normal load bearing capacity V_n obtained by various methods and using different number of simulations n_{sim} (right)

Summary

Artificial neural network based response surface method in combination with small-sample simulation technique Latin Hypercube Sampling has been proposed. The method was applied to a single-span post-tensioned composite bridge in the Czech Republic to assess the normal load bearing capacity and reliability of the structure within the framework of fully probabilistic nonlinear analysis. Results of ANN-RSM were compared with those obtained by other reliability methods.

Acknowledgement: The authors give thanks for the support of the project no. 15-07730S (FIRBO) of the Grant Agency of the Czech Republic (GACR) and of the project of the specific university research at Brno University of Technology no. FAST-J-15-2712.

References

[1] A. Cichocki, R. Unbehauen, Neural networks for optimization and signal processing. John Wiley & Sons Ltd. & B.G. Teubner, Stuttgart 1993.

[2] V. Červenka, L. Jendele, J. Červenka, ATENA Program Documentation – Part 1: Theory, Cervenka Consulting, Prague 2012.

[3] D. Novák, M. Vořechovský, B. Teplý, FReET: Software for the statistical and reliability analysis of engineering problems and FReET-D: Degradation module. Advances in Engineering Software, 72 (2014) 179–192. http://dx.doi.org/10.1016/j.advengsoft.2013.06.011.

21st International Conference **ENGINEERING MECHANICS 2015**
Svratka, Czech Republic, May 11 –14, 2015
Paper **#234, pp. 184–185**

Consolidation Testing of Porous Limestone Using Lime Nanomaterials: Optimization, Assessment of Stone Mechanical and Structural Characteristics

Dana Macounová[1,a]*, Karol Bayer[2,b], Elisabeth Ghaffari[3,c], Michaela Navrátilová[1,d], Zuzana Slížková[1,e], Johannes Weber[3, f]

[1]ITAM – Centre of Excellence Telč, Batelovská 486, 588 56 Telč, Czech Republic

[2]University of Pardubice, Faculty of restoration, Jiráskova 3, 570 01 Litomyšl, Czech Republic

[3]University of applied arts in Vienna, Institute of arts and technologies, Salzgries 14/1, 1010, Vienna, Austria

[a]macounova@itam.cas.cz, [b]karol.bayer@upce.cz, [c]ghaffari@chello.at, [d]navratilova_m@seznam.cz, [e]slizkova@itam.cas.cz, [f]johannes.weber@uni-ak.ac.at

Keywords: limestone, nanomaterials, consolidation, testing, mechanical characteristics.

Abstract: In consequence of an array of degradation mechanisms there is a change of stone characteristics used in historic objects. One of the negative changes is deterioration of mechanical properties, which may often lead to losses of original substance and gradual disintegration of works of art or handcraft made of stone. To prolong the lifespan of such damaged cultural-heritage objects a process called consolidation is often carried out within the framework of conservation treatment. During the process of conservation treatment the damaged stone is impregnated with a consolidating material, which is to provide the stone with a new binder capable of renewing its cohesion to a certain extent. Currently, a wide range of organic and inorganic consolidating agents of various characteristics is available, from synthetic polymers to silicic acid esters. Long-term experience shows that not only is the consolidating effect of the actual agent important, but also its lifespan and impact on the subsequent aging of the treated stone. Thus, in the past few years more emphasis has been laid on the compatibility or – to express it more precisely – the material similarity of the agents used in the process of conservation and restoration of works of art or handcraft.

As a result of this requirement there is an effort to use such materials to consolidate stone, which after hardening will have a similar composition to that of the original rock/stone matrix before the consolidation. Within the area of consolidation of calcareous rocks such as limestone there has been quite an intense research in the possibilities of the use of nanomaterials on the basis of calcium hydroxide. Such relatively modern consolidating agents have a high potential to provide – in terms of material – a more suitable equivalent to the consolidants on the basis of silicates.

Even if there is a difference in material, these are used abundantly for consolidation of calcareous materials (which applies not only to the instance of stone). New, in terms of material, suitable nanolime products are made as stable nanosols of calcium hydroxide dispersed in alcohol media. The size of calcium hydroxide particles ranges between 100 and 200 nm with ethanol, isopropyl alcohol or n-propanol serving as dispersion media most often.

At present, the application of consolidating agents on actual objects is preceded by quite detailed studies and testing on reference materials corresponding with their characteristics and composition to the stone used on the historic objects. Testing and subsequent assessment of the mechanical characteristics changes (not only on the surface but also in depth) may not be executed directly on actual works of art or at times, these may be carried out to a limited extent. Of course, the main purpose is to preserve the original work of art and to prevent it from possible damage. Among other reasons, there are restricted options to test on actual objects and a problematic comparison of the test results on substrates of variable characteristics. When working on objects in-situ a critical moment might occur because of their unknown conservation history (e.g. hydrophobization of

surface) or other changes in the surface caused by their exposition in the exterior associated with degradation (sulfation and others, water soluble salts etc.). Therefore, tests are carried out on specimens prepared from undamaged types of stone matching the rocks for which the tested consolidant is designated. Yet, in this case the testing material used does not correspond with the degraded stone and does not simulate its characteristics on actual objects where there is usually an increase in porosity and a substantial decline in strength due to weathering processes.

Within the project of Nanolith there have been tests to use nanolime products as an option to consolidate selected types of Leitha limestone, which are mostly porous, biodetritic limestone used for historic sculptural and architectonic purposes in the regions of Eastern Austria and South of Bohemia and Moravia. Particularly, the selection of a suitable testing substrate or – as a matter of fact – suitable test specimens was crucial part of testing and optimization of nanolime products application. Based on experience of previous, similarly focused tests a method for the preparation of the specimens was chosen which would facilitate simulation of a degraded material and at the same time provide homogeneity and reproducibility of their preparation. The aim was to prepare a material of very similar characteristics to those of heavily degraded limestone, i.e. with high porosity and very low strength. The test specimens were prepared by pressing down limestone sand of the same grain and mineralogical composition as selected types of Leitha limestone. Microscopic analysis proved that a substrate could be prepared to match the degraded stone. A rather simple technique was developed to guarantee not only the preparation of the specimens of desired characteristics, but also sufficient homogeneity of the samples essential regarding the reproducibility of the consolidation testing results. To a certain extent the characteristics can be influenced by granulometric composition of the sand used.

A series of tests with a few types of nanolime products was carried out on test specimens prepared in this way, while various options of application and application conditions were tested and compared. Consolidation effectivity was assessed and compared mutually on the basis of mechanical characteristics measurements. Compressive strengths were compared directly, whereas the method of ultrasound transmission was used as an indirect indicator of changes in strength. Ultrasound transmission was also used to discover potential strength gradients originating in possible differences in distribution caused by application of the consolidating agent only on one side of the test specimen (a phenomenon possibly occurring in actual objects too). Consolidation effect could be proved in all the cases of the specimens. After consolidation and hardening of the consolidating agent as a result of formation of calcium carbonate from calcium hydroxide there is an increase in compressive strength as well as increased ultrasound velocity (p-waves). Changes in structure of the consolidated material and depth distribution of the consolidant were studied by microscope using optical and scanning electron microscopy.

Results of the testing were then used while applying nanolime products on several actual objects. Effective consolidation of degraded parts of stone could be proved again using ultrasound transmission.

Acknowledgement: The authors gratefully acknowledge support from European Regional Development Fond, the programme European Territorial Co-operation Austria-Czech Republic 2007-2013 entitled “Nanolith” M00264 („Použití nanomateriálů pro udržitelnou konzervaci historických sochařských a architektonických děl z litavských vápenců”).

21st International Conference **ENGINEERING MECHANICS 2015**
Svratka, Czech Republic, May 11 –14, 2015
Paper **#191, pp. 186–187**

Mechanics of Laser Cut Stent Grafts

Štěpán Major[1,a], Vladimír Kocour[1,b], Štěpán Hubálovský[2,c]

[1]Institute of Theoretical and Applied Mechanics/Academy of Sciences,
Prosecká 809/76, 190 00 Prague 9, Czech Republic

[2]Department of Informatics, Faculty of Science, University Hradec Králové,
Rokitanského 62,500 03 Hradec Králové, Czech Republic

[a]major@itam.cas.cz, [b]kocour@itam.cas.cz, [c]stepan.hubalovsky@uhk.cz

Keywords: stent-grafts, nitinol, finite element analysis, fatigue, fracture

Abstract: This article is dedicated to a finite element analysis of tubular, laser cut stent grafts with peak-to peak bridge geometry under representative cyclic loading conditions for abdominal aortic aneurysm repair. Cardiovascular diseases are the principal cause of death in the developed world. For computational analysis, ANSYS software was employed to study the mechanical behavior of stents. Contrary to conventional engineering materials, nitinol stent fracture is not stress based but strain based. The effects of crimpling and cyclic pressure loading on stent–graft fatigue life were simulated and analyzed.

Introduction

Stent-grafts are tubes made out of wire or by cutting laser meshes that are inserted into arteries to help keep them open so blood can flow properly. The stent is mounted on a balloon catheter and delivered to the site of blockage. Endovascular aneurysm repair has clear benefits when compared with conventional open surgery in terms of less trauma, earlier return to daily activities, reduced mortality, and lower morbidity. However, stent–graft failure, i.e., implant migration, device fatigue, and endoleaks resulting potentially in abdominal aortic aneurysms rupture, remains a major concern [1,2,3].

Stent graft geometry and material

Peak-to peak bridge geometry of stents. Virtually all previously published analyzes, however, dedicated stents with a diamond shape geometry [1,3]. This study is dedicated to stents with peak-to peak bridge geometry, see Fig. 1.

Material. Nitinol alloys exhibit two closely related and unique properties: and shape memory. Shape memory is the ability of nitinol to undergo deformation at one temperature, then recover its original, undeformed shape upon heating above its "transformation temperature". Superelasticity occurs at a narrow temperature range just above its transformation temperature; in this case, no heating is necessary to cause the undeformed shape to recover, and the material exhibits enormous elasticity, some 10-30 times that of ordinary metal. A self-expandable nitinol stent-grafts repair utilizes these characteristics rather well. Cooled to less than 5 C, it fully transforms into martensite and hence becomes very deformable and easily compressed into a small catheter. Contrary to conventional engineering materials, nitinol fracture is not stress based but strain based.

Modeling

Geometry modeling. Nitinol stent model with a total of 16 bridges or cells and 5 rings built into the tubular stent. Because stent and graft are sutured together, a tight, rigid contact is assumed to simulate the interaction between stent and graft interaction between stent and graft. Fully expanded stents has a length L of 20 mm, an outer diameter D of 5 mm, a thickness s of 0.1 mm.

Material modeling. The two materials of the artery wall, arterial tissue and stenotic plaque, were modelled using a 5-parameter third-order Mooney–Rivlin hyperelastic constitutive equation. This has been found to adequately describe the non-linear stress-strain relationship of elastic arterial tissue. The general polynomial form of the strain energy density function in terms of the strain invariants, given by [1,3] for an isotropic hyperelastic material is

$$W(I_1, I_2, I_3) = \sum_{i,j,k=0}^{\infty} a_{ijk} \, (I_1 - 3)^m (I_2 - 3)^n (I_3 - 3)^o \tag{1}$$

$$a_{000} = 0$$

where W is the strain-energy density function of the hyperelastic material, I_1, I_2 and I_3 are the strain invariants and a_{ijk} are the hyperelastic constants.

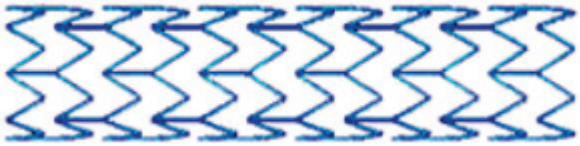

Fig. 1: Peak-to-peak bridge geometry of stent-graft.

Simulation

The ANSYS Finite Element Analysis package, in combination with user-defined material subroutines for the nitinol material properties, was employed to calculate the stress and strain fields. The governing equation for the structure(s) was the condition for static equilibrium, where zero body loads were applied:

Stent is loaded by: 1) Crimping is used to compress an expanded stent graft into a delivery system; 2) In the sealing section, the arterial wall prevents the stent graft from completely expanding, which implies the stent is under compression and the graft material may not encounter significant tensile stress. 3) When the stent graft is deployed in the artery main body of stent-graft is under cyclic loading as a result of pulsatile blood flow.

Results

It was found that the maximum strain is located at the strut's internal side, bridge connection. The maximum crimping strain for NITI is 7.8%, which is lower than in the case of diamond shape stents. Thus, in terms of crimping performance, the peak-to-peak bridge geometry of stents is preferable to diamond shape geometry. Under representative cyclic pressure loading, sealing stents are located in the safe zone of the fatigue life zone.

References

[1] C. Kleinstreuer, Z. Li, C.A. Bascian, S. Seelecke, M.A. Farber, Journal of Bimechanics, 41 (2008) 2370–2378.

[2] C. Lally, F. Dolan, P.J. Prendergast, Journal of Bimechanics, 38 (2005) 1574–158.1

[3] W. Maurel, Y. Wu, Y., N. Magnenat Thalmann, D. Thalmann, Biomechanical Models for Soft-Tissue Simulation. Springer, Berlin 1998.

21st International Conference **ENGINEERING MECHANICS 2015**
Svratka, Czech Republic, May 11 –14, 2015
Paper **#252, pp. 188–189**

The Influence of Deformation of the Frame of Testing Device on the Accuracy of Brazilian Test and Indirect Assessment of Young Modulus

Štěpán Major[a], Daniel Vavřík[b], Vladimír Kocour[c], Jan Bryscejn[d]

[1]Institute of Theoretical and Applied Mechanics/Academy of Science,
Prosecká 809/76, 190 00 Prague 9, Czech Republic

[a]major@itam.cas.cz, [b]vavrik@itam.cas.cz, [c]kocour@itam.cas.cz, [d]bryscejn@itam.cas.cz

Keywords: split test, Brazilian disc, tensile strength, portable testing device, finite element analysis

Abstract: This article deals with determination of mechanical properties based on indirect measurements of brittle building materials like stones using portable device. Due to the fact, that the material samples may change their properties during transportation, it is preferred to test samples on site. For these reasons, portable testing device was developed. The testing machine operates on the split test principle. The device also shall to serve for estimation of other mechanical characteristics of the tested material, such as Young's modulus, compressive strength or flexural strength, etc. This paper concentrates on the effect of deformation of frame on the accuracy of indirect determination of mechanical properties.

Introduction

Direct assessment of elastic modulus E, tensile strength σUT or fracture toughness KIC of brittle materials represent a difficult problem for experimental instrumentation. Therefore alternative solutions have been proposed [1,2]. One of these alternative solutions, called the Brazilian test, has been popular for determining tensile strength for brittle building materials mainly due its simplicity. The Brazilian test is performed by compression with diametrically opposite concentrated loads on a disc specimen. When the specimen dimensions and maximum force at the moment of the fracture of sample is known, it is possible to calculate the tensile strength of material. If we know the relationship between load and displacement/deformation, it is possible to estimate other parameters of the material.

Experimental device

The testing device is primarily intended for split tests of core samples. Weight of the device is approximately 25 kg. The loading is performed by moving the lower grips upward. The lower grip is lifted by wedge mechanism. Linear movement of the wedge is implemented by screw rotation. Maximal loading force is limited by 100 kN. Loading force is registered by logger from measuring bolt. Force data are imaged by data-logger display and can be recorded by a computer in digital form. Loading displacement data are obtained directly by measuring instruments based on optoelectronics sensors and by non-directly by counting of the loading screw revolutions, both types of data can be recorded by a computer in digital form. Interchangeable jaws with different ratios $R_{jaw}/R_{specimen}$ are installed in the testing machine. The custom written software is used to control the test equipment. This software allows calculation of tensile strength R_T, compressive strength R_C and flexural strength R_F using data obtained from the test device, without further operator intervention.

Theory

Brazilian test and calculation of tensile strength. Theoretical basis for the split test is analytical solution developed by Hondros for determination of elastic modulus and Poisson's ratio [1]. That failure is expected to initiate at the center of disc. The tensile strength R_T is expressed as

$$R_T = \frac{2F_{\max}}{\pi LD}, \tag{1}$$

where P is line load [N/m], L is thickness of the disc, and D is diameter of the specimen. When using jaws with the radius, a more accurate solution proposed by Koukoulis can be used.

Estimation of Young modulus. In the case of the known relationship between displacement and load, other mechanical properties such as Young modulus can be determined. Estimation of Young modulus can be based on following relationships

$$A(\Delta x) = \Delta x \cdot F(\Delta x), \tag{2}$$

$$\sum_{i=1}^{i_{max}} \left(F_{measured}(x_i) - F_{simulated}(x_i)\right)^2 = \psi\left(E_{simulation}, \sigma_{simulation}\right), \tag{3}$$

where A is deformation work, Δx, resp x_i are the displacement, F is loading force, and E is Young modulus. Subscription indicates values measured directly by sensors. Subscription simulation indicates simulated values.

Experiments and effect of frame deformation

Specimens were prepared from sandstone by core drilling. The specimens were obtained in dry condition. Diameter of the specimens was 47-50 mm and length was about 70 mm. Specimens were loaded to final rupture by the developed portable loading device. Result of split test shows that the tensile strength σ_{UT} differs only a little from that obtained by other methods. In the case of other variables such as E, however, there are significant differences (order of 10 or more), which do not allow practical use of measurements of E. This behavior can be explained by the growing influence of deformation of the devices frame on indirect measurements. If the model based on the relationships Eqs. 2 and 3 is corrected by deformation of the frame, the results are better. For further practical use it is necessary to implement a set of additional measurements to create a table of corrections. These corrections must be implemented to the control software. The problem, however, is gaining generally valid correction because results differ for tests carried out for only one type of material (error between 20-150% depending on the sample). Deformation of the frame, jaws and the samples can be simulated by Finite Element Method. In order to refine results further, it is necessary to implement additional measurements.

Results

Corrections based on the relationships Eqs. 2 and 3 improve results of measurement. Implementation of the corrections to the control software improves accuracy of the measurement.

Acknowledgement: This work has been supported by Project NAKI DF11PØ1OVVØØ.1

References

[1] Š. Major, I. Jandejsek, J. Valach, D. Vavřík. Portable Device for Indirect Assessment of Strength in Tension of Building Materials and Problem of Boundary Condition, Applied Mechanics and Materials, 486 (2014) 307–312.

[2] S.K. Koourkolis, Ch.F. Markides, P.E. Chatzistergos, The Brazilian Disc under parabolically varying load: Theoretical and experimental study of the displacement field, International Journal of Solids and Structures, 49 (2012) 959–972.

21st International Conference **ENGINEERING MECHANICS 2015**
Svratka, Czech Republic, May 11 –14, 2015
Paper **#024, pp. 190–191**

Failure of Window Glass Plate under Blast Load

Daniel Makovička[1,a] *, Daniel Makovička, Jr.[2,b]

[1]CTU in Prague, Klokner Institute, CZ166 08 Prague 6, Šolínova 7, Czech Republic

[2]Static and Dynamic Consulting, CZ284 01 Kutná Hora, Šultysova 170/8, Czech Republic

[a]daniel.makovicka@klok.cvut.cz, [b]d.makovicka @makovicka.cz

Keywords: window glass, blast load, dynamic response, assumption, failure

Abstract: The paper deals with the response analysis of interaction of a gaseous shock wave and a glass plate structure with particular reference to the character of excitation wave and material characteristics of structure. The goal of this analysis is the determination of hypothesis of failure of window glass plate on the basis of the actual plate rotation during extreme plate displacement. Pressures greater than the ultimate stress or plate rotation bring to the collapse of the glass plate structure.

Introduction

The explosion of an explosive medium generates a pressure wave in the centre of the explosion. Its intensity and history are determined by the chemical properties of the explosive and its reaction with ambient environment. The pressure wave begins propagating from the explosion centre in approximately spherical wave fronts which reflect from and are modified by their impact on the surface of window or other structure parts. The effect of pressure in the propagating wave, together with the reflected wave form the magnitude of the load applied to the structure and its history. Particularly in closed spaces of rooms, industrial halls, etc., in which multiple reflections take place, it is the very size of such closed spaces that is dominant for the load intensity [2].

The explosion, consequently, generates a pressure wave (Fig. 1) the dominant effect of which on a standard window structure is manifested, as a rule, by the flexure of the glass window plate.

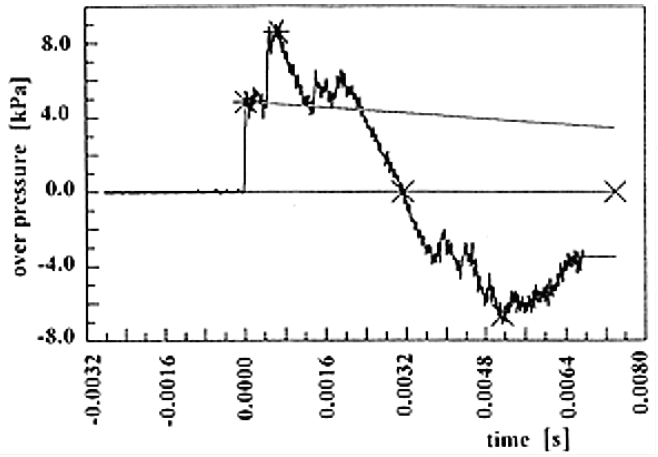

Fig. 1: Example of measured time history

Window structure response and its assumption

For determination of static load bearing capacity of glass plate the bending four-point tests was carried out. By static load test the resulting load bearing capacity is lower then it should be found by dynamic test. Consequently the static load test indicates safety enough values of load bearing capacity of glass plate structure and its resistance. In case of more complex dynamics accidents, it is possible to use approximately the following characteristics determined by comparison of static and dynamic test of window glass plates (3 mm thickness and span of about 1 m): flexural dynamic strength in tension (for time duration of blast load about 1 ms) is 56 MPa in relation to the mean

long-term (static) strength 13 MPa. The uncertainty of the so determined ultimate bearing capacity is usually approximately 30 % with the exception of glass types of distinctly different strength and strain characteristics. The dynamic strength for window and approximately for common window glass is 56/13=4.3 times higher. The stress/strain ratio can be considered linear in the whole load interval up to the ultimate strength (the deviation from linearity does not exceed 3%).

Experimental verification [1] has revealed that the moment of glass plate failure is influenced decisively by the rotation of the glass plate middle plane. Under the overpressure in the shock wave the glass plate first deflects in the load direction. These extreme glass deflections take place only under the effect of the underpressure phase, i.e. in the load direction towards the explosion centre. These extreme deflections correspond with the actual limit rotation 6°of the glass plate. The way of damage (failure) is based on the location of the place where the ultimate rotation is exceeded in the dominant vibration mode [3]. Physically this is manifested by the fact that for the analysed load the first cracks open in the 1/3 - 1/4 of the span of the analysed glass structure. The diagram of limit bearing capacity of square glass plates (for new and 10-year old glass) for overpressure p_m of incident wave and time of its duration τ is given on the Fig. 2.

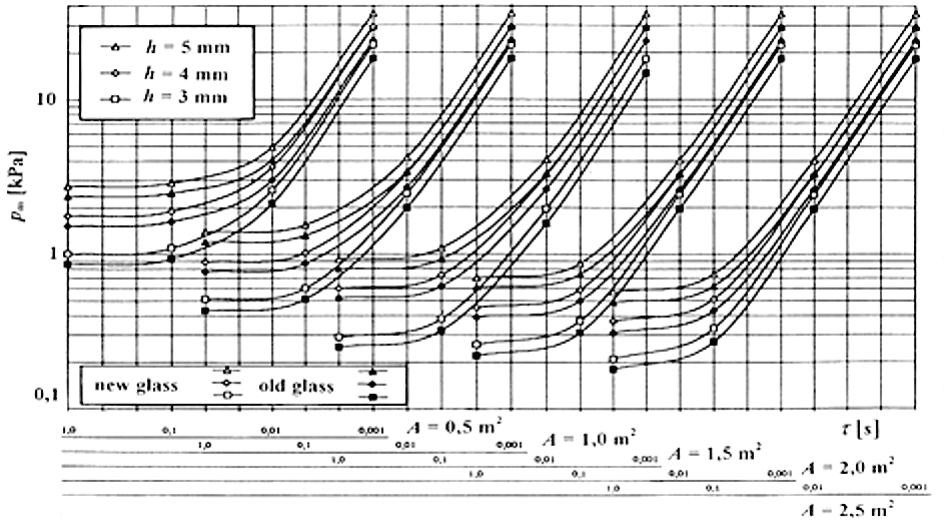

Fig. 2: Limit bearing capacity of glass plate under blast wave load

Conclusion

Analyses of dynamic bending of window glass plate, depending on the parameters of the structure and the impact wave have been computed and compared with experimental results. The limit angle of window glass plate and its limit bearing capacity are derived and discussed. The excess of these parameters result in the collapse of the structure.

Acknowledgment: The paper is based on outcomes of the research project VG20122015089 supported by the Ministry of the Interior of the Czech Republic, for which the authors would like to thank the Ministry.

References

[1] D. Makovička, Load bearing capacity of window structures under explosion pressure effects (in Czech), Stavební obzor, 4 (2002) 100-103.

[2] D. Makovička, B. Janovský, Handbook of explosion protection for buildings (in Czech), CTU Publishing House, Prague, 2008.

[3] D. Makovička, D. Makovička, Jr., Blast load of building structure, Mechanical Engineering, No 1, 21 (2014) 11-18.

21st International Conference **ENGINEERING MECHANICS 2015**
Svratka, Czech Republic, May 11 –14, 2015
Paper **#126, pp. 192–193**

Numerical Solution of Micro-Lubrication in Internal Combustion Engine Journal Bearing

Ondřej Maršálek[a]*, Pavel Novotný[b], Jiří Knotek[c]

Brno University of Technology, Faculty of Mechanical Engineering,
Technická 2896/2, 616 69 Brno, Czech Republic

[a]marsalek@fme.vutbr.cz, [b]novotny.pa@fme.vutbr.cz, [c]knotek@iae.fme.vutbr.cz

Keywords: asperity radius, contact pressure, flow factor, rough surface

Abstract: All technological processes leading to the final surface visage of mechanical components create on its surface characteristic pattern. These surface patterns subsequently play a significant role in terms of their function and lubrication, particularly in the case of surface contact pairs. However, inclusion of the actual surface patterns of machine parts as one of the input parameters of the computational simulation of friction losses is still not common. This article describes a complex computational model for solving the frictional losses for directionally oriented and non-oriented sliding surfaces.

The first part of this article provides information regarding the description of surface roughness. Attention is paid to the two basic possibilities of obtaining the surface characteristics – namely those obtained by measurement (3D scanning surface) or those obtained using a specialized software generator. The software generator of surface characteristics is based on the relation:

$$z(x,y) = \frac{\sigma}{\sqrt{nm}} \sum_{k=1}^{n} \sum_{l=0}^{m} \eta_{x+k,y+l} \,. \tag{1}$$

The second part of this contribution describes the behaviour of thin lubricating layers depending on the lubricated surfaces topologies. The generally accepted simplification of similar tasks accepts the assumption of zero velocity near the lubricated surface. On the other hand, the computational approach described in this paper takes into account flow of the lubricant between each asperity, which is governed by the Reynolds equation. The described procedure provides a sort of loss coefficients of the oil flow (flow factors) that are specific for the technology of the resulting surface, the material, coating, or surface finishing method that gives its final form. The directional dependence of the analysed surface is determined by its autocorrelation function, which is given in Eq. 2.

$$R(\tau_i,\tau_j) = \frac{1}{(M-i)(N-j)} \sum_{l=1}^{N-j} \sum_{k=1}^{M-i} \eta(x_k,y_l)\eta(x_{k+i},y_{l+j}) \tag{2}$$

The resulting flow factors – form one of the inputs for the general solution of Reynolds equation (Eq. 3), which is the basic core of the hydrodynamics solver. Its numerical solution is generally known and is often used to describe the hydrodynamic lubrication regime.

$$\frac{\partial}{\partial x}\left(\phi_x \frac{\rho h^3}{12\eta}\frac{\partial p}{\partial x}\right) + \frac{\partial}{\partial y}\left(\phi_y \frac{\rho h^3}{12\eta}\frac{\partial p}{\partial y}\right) = \frac{U_1+U_2}{2}\frac{\partial(\rho h_T)}{\partial x} + \frac{U_1-U_2}{2}\sigma\frac{\partial(\rho\phi_s)}{\partial x} + \frac{\partial(\rho h_T)}{\partial t} \tag{3}$$

One of the outcomes of the computational sub-models mentioned above is number of pairs of surface protrusions in the contact (unique for the type of surface and ratio of height of the

lubricating layer) and combined roughness of both surfaces. The full-length article gives examples of generated and scanned surfaces, examples of the surface roughness pattern impact on flow factors, and also examples of friction losses analysis. Regarding the automotive industry, the computational model can be applied, for example, to the piston ring pack, journal bearings, camshaft and others.

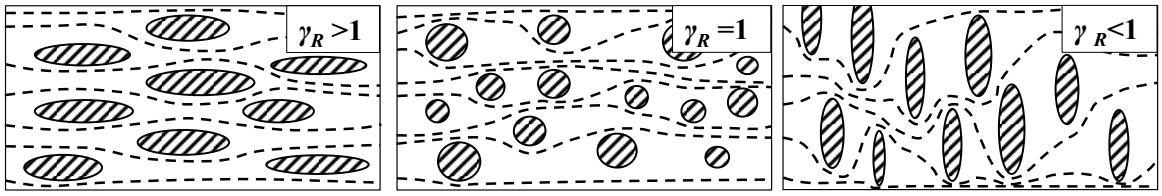

Fig. 1: Illustrative shapes of contact areas of longitudinally oriented (γ_R >1), isotropic (γ_R =1) and transversely oriented surfaces (γ_R <1)

The following tables list results of two sample analyses of crankshaft main bearing. The first table lists results for the case of naturally aspirated three cylinder internal combustion engine. In the second case the load was applied on the bearing from over-pressured internal combustion engine. Three different configurations of surface pattern of bearing shell (according to Fig. 1) were tested in both cases together with the case when the impact of flow factors was not considered.

Table 1: Results of analysis of naturally aspirated internal combustion engine slide bearing

γ_R	-	1	1/3	3	[-]
min h/σ	1.05	1.30	1.20	1.22	[-]
average h/σ	6.03	6.26	6.10	6.23	[-]
h/σ **< 4**	27.00	25.70	26.49	27.80	[%]
P_{ztr}	152.23	154.78	157.95	154.09	[W]

Table 2: Results of analysis of over-pressured internal combustion engine slide bearing

γ_R	-	1	1/3	3	[-]
min h/σ	0.77	1.01	0.94	0.91	[-]
average h/σ	5.22	5.47	5.31	5.43	[-]
h/σ **< 4**	30.00	28.70	29.90	29.31	[%]
P_{ztr}	169.70	174.26	178.94	173.24	[W]

When the results from both tables are compared, it is evident that the greatest differences are in case of transversally oriented surface pattern (γ_R <1) and when the flow factors were not considered. This difference reaches ones of percent. Wrong design of partial mechanical components can cause big mechanical losses of the final machine.

Acknowledgment: Outputs of this project, named NETME CENTRE PLUS (LO1202), were created with financial support from the Ministry of education, youth and sports of the Czech Republic under the program supporting research, experimental development and innovation: "National Programme for Sustainability I." This support is gratefully acknowledged.

21st International Conference **ENGINEERING MECHANICS 2015**
Svratka, Czech Republic, May 11 –14, 2015
Paper **#218, pp. 194–195**

Numerical Calculation of Coefficient of Force for Cylindrical Shape Smokestack Covered with Corrugated Iron

Vladimira Michalcova[a] *, Lenka Lausova[b]

Faculty of civil engineering, VSB-Technical University of Ostrava,
Ludvika Podeste 1875/17, Ostrava-Poruba, 708 33, Czech Republic

[a]vladimira.michalcova@vsb.cz, [b]lenka.lausova@vsb.cz

Keywords: circular cylinder, drag coefficient, aerodynamic roughness, CFD, DES model

Abstract: This paper deals with the influence of the shape of covering at smokestack to the resultant of load from wind effects. Calculation according to current standard takes into account only size of the wave-height of shaped sheets regardless of the shape of the waves, which leads in some cases to a substantial increase of the coefficient of force. The aim of this paper is to determine the equivalent coefficient of force for a cylindrical shape smokestack, which is covered with corrugated iron. The flow around smokestack is designed in software Ansys Fluent using the DES model. The calculated coefficient of force for the real roughness of a smokestack is compared with the values specified in the standard.

Introduction

Determination of load from wind effects at smokestacks depends on Reynolds number *Re* describing the flow, geometry of structure and surface roughness. Valid standard distinguishes the type and shape of roughness up to 3 mm. In the case of higher values, the equivalent roughness is determined from empirical relationship, which only takes into account the height of inequality, not its shape. This sometimes leads to a high increase of the coefficient of force. There can be assumed a fully developed turbulence in the boundary layer around the smokestack walls covered with corrugated sheets. This process is very complicated physical experiment because of the high *Re* [1,2,3]. There are given high demands on the number of cells in numerical modeling of the real covering, currently it is not realistic for a desktop PC [4,5,6]. The article deals with the possibilities of compensatory equivalent aerodynamic roughness of corrugated iron and defining the aerodynamic drag coefficient of flow around covered cylinders. The problem is solved by finite volume CFD code in software Ansys Fluent.

There is simulated a wind flow around a real smokestack of circular section of diameter 3.36 m. Cladding is made from corrugated sheet SP 18/76 with the wave height 18 mm. The basic wind speed is estimated to 22 m/s. Airflow with $Re = 5.5 \cdot 10^6$ is far in the supercritical region.

The solution is divided into two phases. In the first phase, the task is modeled as a turbulent flow in rough pipe, which has got one meter in diameter and 20 meters in length. The geometry of the walls is identical to the geometry of the sheet (Fig. 1). This is a 2D axially symmetric problem, which is solved in a steady state way using the SST k-ω model. This simulation is chosen because it allows a feedback control with published measured values of pressure losses. Seeking equivalent aerodynamic roughness, which software Ansys Fluent offers, is determined on the bases of the assessed loss of pressure and velocity.

In the second phase, the air flow around the smokestack is modeled in 3D (Fig. 2) in order to define the demanded aerodynamic drag coefficient required to calculate the effects of wind loads on structures. The model of smokestack is covered by non-profiled sheet. Corrugated sheet geometry is replaced by equivalent aerodynamic roughness which is set by us. The first cells at the smokestack walls are formed by the boundary layer so that the height of the aerodynamic roughness reaches the maximum to mid-height of the first cell wall. The solution of tasks uses unsteady fluid flow analysis using the DES model.

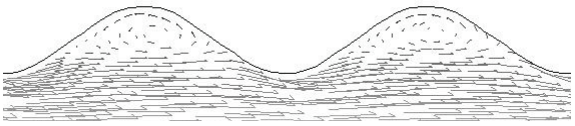

Fig. 1: Velocity vectors in the surroundings of corrugated iron

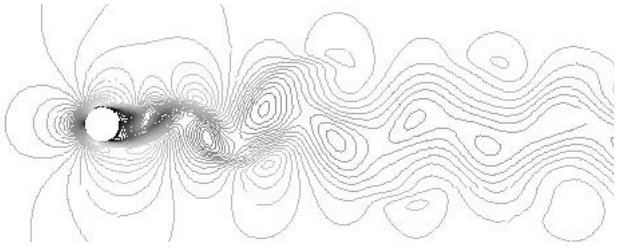

Fig. 2: The formation of vortices behind flow around smokestack

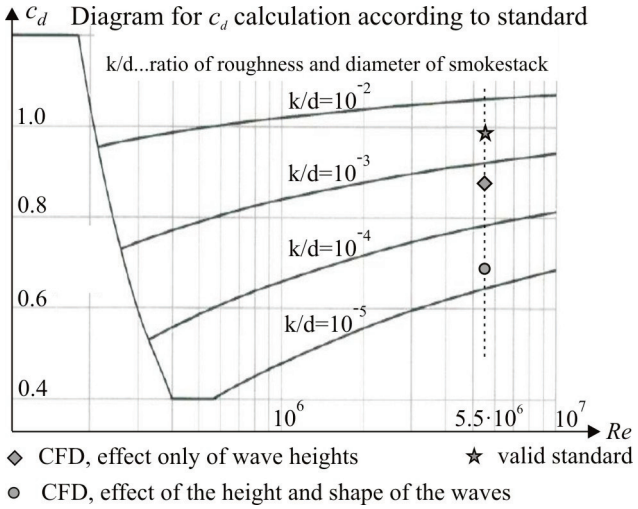

Fig. 3: The value of drag coefficient

Summary

The results show that the standard calculation of the effects of wind on the corrugated iron smokestack is overestimated (Fig. 3). The value of the resistance coefficient computed using CFD code should be considered as approximate only until it is verified by using either a physical experiment or a detailed numerical calculation, which allows the direct simulation of the actual geometry of a covered smokestack. Such task, however, would require a powerful supercomputer, for example that available in the National supercomputing center in Ostrava (http://www.it4i.cz/).

Acknowledgements: This contribution is the result of the research supported by the conceptual development of science, research and innovation for 2015 allocated to the VSB-Technical University of Ostrava by the Ministry of Education, Youth and Sports of the Czech Republic and also by specific grant Support for science and research in the Moravian-Silesian Region in 2014 given by Moravian-Silesian Region.

References

[1] R. Merrick, G. Bitsuamlak, Control of flow around a circular cylinder by the use of surface roughness: A computational and experimental approach. In: Proceeding of the 4th International Conference Advances on Wind and Structures (AWAS08), Jeju, Korea, 2008.

[2] J. Dobes, M. Kozubkova, The influence of numerical models on determining the drag coefficient. In: Proceeding of the International Conference on Experimental Fluid Mechanics, Kutna Hora, Czech Republic, 2013.

[3] A. Roshko, Experiments on the flow past a circular cylinder at very high Reynolds number. Journal of Fluid Mechanics, 10 (2006) 345–356.

[4] P. Catalano, M. Wang, G. Iaccarino, Numerical simulation of the flow around a circular cylinder at high Reynolds numbers. Journal of Heat and Fluid Flow, 24 (2003) 463–469.

[5] M. Breuer, A challenging test case for large eddy simulation: high Reynolds number circular cylinder flow. Journal of Heat and Fluid Flow, 21 (2000) 648–654.

[6] D. Lakehal, Computation of turbulent shear flows over rough-walled circular cylinders. Journal of Wind Engineering and Industrial Aerodynamics, 80 (1999) 47–68.

21st International Conference **ENGINEERING MECHANICS 2015**
Svratka, Czech Republic, May 11 –14, 2015
Paper **#029, pp. 196–197**

Experimental Study of Gas Dispersion over Complex Terrain

Petr Michálek[a] *, David Zacho[b]

Výzkumný a zkušební letecký ústav, a.s., Beranových 130, 19905 Praha 9, Czech Republic

[a]michalek@vzlu.cz, [b]zacho@vzlu.cz

Keywords: gas dispersion experiment, boundary layer wind tunnel, complex terrain model

Abstract: Experimental study of gas dispersion over complex terrain model was performed in VZLU Prague. The terrain model was mounted into a boundary layer wind tunnel and equipped with ground-level gas emission source. Concentration field of the emitted gas was measured using comb suction probe and flame ionization detectors. The results will serve for verification and validation of a new computational dispersion model.

Introduction

The existence of relatively high number of chemical plants in Czech Republic causes an indispensable risk to people living in its neighborhood. Human health and lives can be endangered with many chemical substances stored in the plant areas, e.g. chlorine, ammonia, etc. It is important to know the possible size of an area with lethal concentration of gases in the case of an accident or attack.

The new computational dispersion model, which is being developed in VZLU, is based on numerical simulation of compressible gas flow in the gravitational field and finite volume method of Reynolds-averaged Navier-Stokes equations. The software will use pre-calculated results of flow and dispersion in chosen areas near chemical plants in Czech Republic together with actual meteorological data to estimate the most dangerous area. The estimate will be used by rescue services and firemen to make the rescue action more effective.

The experimental setup and results

The boundary layer wind tunnel (BLWT) in VZLU is an open-circuit wind tunnel with cross section 1.8 m wide and 1.5 m high in test area. The test section for boundary layer development is 13.6 m long and the tunnel is powered with 55 kW fan. Maximal velocity above the boundary layer is 25 m/s, the flow velocity can be measured with hot-wire probes on a traversing mechanism and with a reference Pitot-static tube. The boundary layer simulation has three variants, i.e. agricultural, suburban or urban boundary layer can be simulated in the BLWT according to Eurocode 1 [1].

The terrain model was manufactured from lightweight boards on the basis of a digital terrain model of Liberec city. There is a heating plant with gas tanks near the city center, which presents the possible source of gas leakage. The model was manufactured in scale 1:1500 and presents an area of 9.0 km x 2.4 km in full scale. The modeled area is in northwest-southeast direction along the valley of Lužická Nisa River and contains the heating plant and its densely urbanized neighborhood.

To adjust the incoming boundary layer, lightweight boards covered with 4 mm gravel were mounted ahead of the model in the test section. The boards were glued together in steps, so that a continuous transition from flat plane into the terrain model area was ensured. The terrain model was covered with the same 4 mm gravel in order to increase the aerodynamic roughness. Models of significantly high buildings and housing estates were manufactured too. Other buildings were substituted with the gravel. Part of the terrain model is shown in Fig. 1.

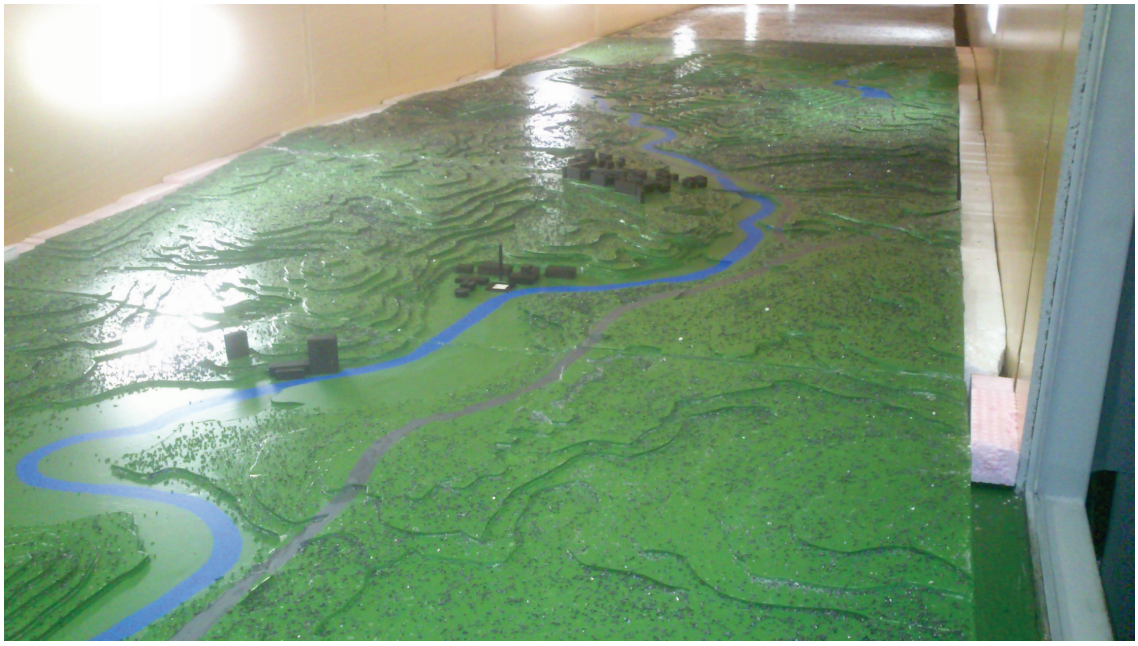

Fig. 1: Front part of the terrain model with emission source (white spot)

Concentration field was measured using suction comb probe, peristaltic pump and four flame ionization detectors (FID). Source emission was air plus ethane as tracer gas dosaged with flow controllers. FID calibration was made with calibration gas mixture with precise concentration 100 ppm of ethane in air. Example of measured longitudinal horizontal concentration profiles for different heights is presented in Fig. 2.

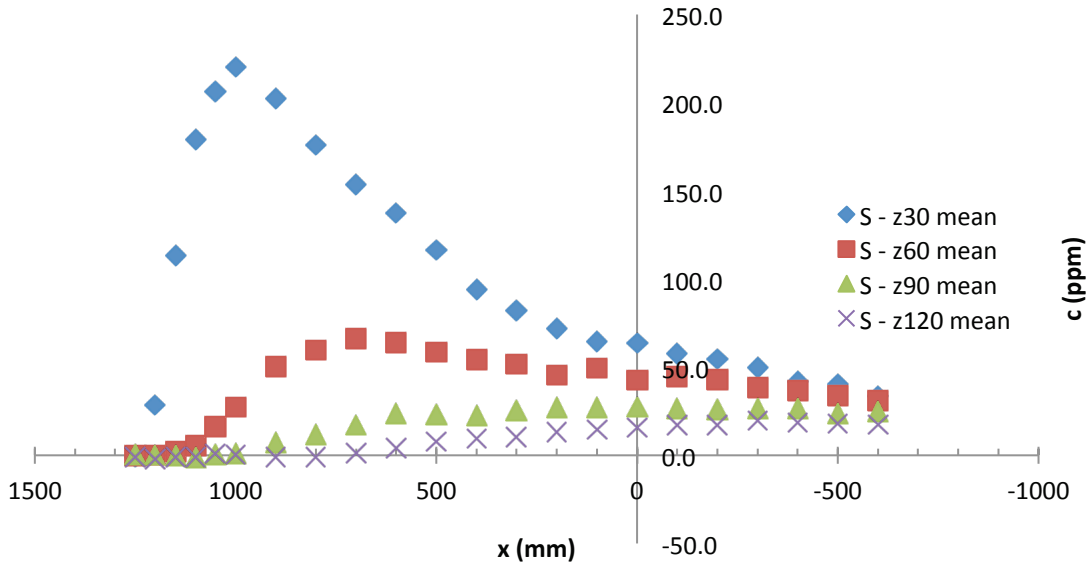

Fig. 2: Horizontal concentration profiles

Acknowledgement: This work was supported by Ministry of the Interior of Czech Republic under project No. VG20122015098 “Scent”.

References

[1] Eurocode 1: Actions on structures – Part 1-4: General actions – Wind loads (EN 1991-1-4), European Committee for Standardisation, Brussels (2005)

21st International Conference **ENGINEERING MECHANICS 2015**
Svratka, Czech Republic, May 11 –14, 2015
Paper **#039, pp. 198–199**

Experimental Verification of the Unloaded Control Valve

Martin Miczán[1,a], Lukáš Bednář[1,b]*, Michal Hoznedl[1,c], Ladislav Tajč[2,d]

[1]DOOSAN ŠKODA POWER s. r. o., Tylova 1/57, 301 28 Plzeň, Czech Republic

[2]The University of West Bohemia in Pilsen, KKE, Czech Republic

[a]martin.miczan@doosan.com, [b]lukas.bednar@doosan.com, [c]michal.hoznedl@doosan.com, [d]ladislav.tajc@doosan.com

Keywords: valve, steam turbine

Abstract: Findings are presented from the tests of unloaded control valve mounted on the steam piping with experimental turbine. The forces applied on the spindle are recorded and compared to design calculation. The forces are evaluated from the pressures on a servo drive piston or they are measured directly using force transducers. The real operational characteristics are compared with characteristics developed for constant inlet pressure.

Introduction

One of the unloaded valve tests was carried out on the model built into the inlet piping of experimental steam turbine. In the model version operation is controlled by the turbine which requires certain relation between the pressure ratio on the valve and the lift of the cone, i.e. the flow area and thus evens the required mass flow. In the real life conditions the valve operation is driven by consumption body, which is in this case the turbine. The turbine operation corresponds with operational characteristics of the valve. When drafting the designs for turbine and corresponding regulation bodies, constant inlet pressure and steam temperature is expected. But it is impossible to rule out variation in parameters. In the real valve implementation additional forces occur that are connected with the sealed system. The aim of the experiment on the steam version of the control valve is to compare the real result with the prediction of forces applied on the cone and the spindle obtained from experiments with a model version of the valve measured in the air tunnel.

Measuring on the valve model in steam piping

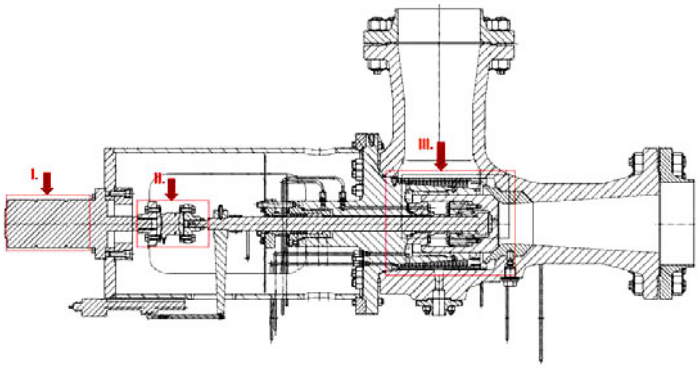

Fig. 1: Control valve for steam operation

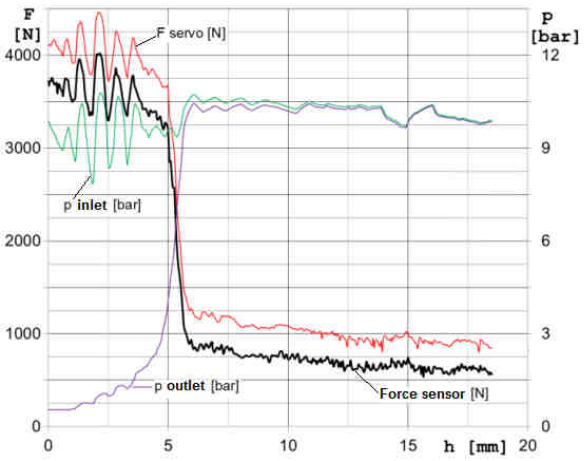

Fig. 2: Forces applied on the valve spindle

Valve arrangement for operation with experimental steam turbine is shown in Fig. 1. The force on the spindle can be determined from the pressures applied on both sides of the servo drive piston and also using the built-in force transducer, see Fig. 2. Operational characteristics are considered for two turbines of different output, where the valve of the same size would be used. Both courses are

marked in the diagram of the mass flow valve characteristics in Fig. 3. In the unloaded valve it is advisable for the stabilizing force which keeps the big cone on the spindle to be sufficiently large in all regimes and to operate always in one direction. Force characteristics for the stabilizing force of the cone and two turbine operational characteristics are for the model version processed in Fig. 4. In the diagram the area of the cone lower loading for a limited area of shear cone lift h / D_h. D_h is the throat diameter of the diffuser under the cone. The smaller the pressure ratio $\varepsilon = p_d / p_0$ defined by outlet pressure p_d and inlet pressure p_0, the bigger the stabilizing force F_{ST}. S_S represents the seal area of the cone. In engineering practices it is necessary for various construction implementations of valves to estimate the forces operating on the valve parts and decide on a required dimensioning of the servo drive.

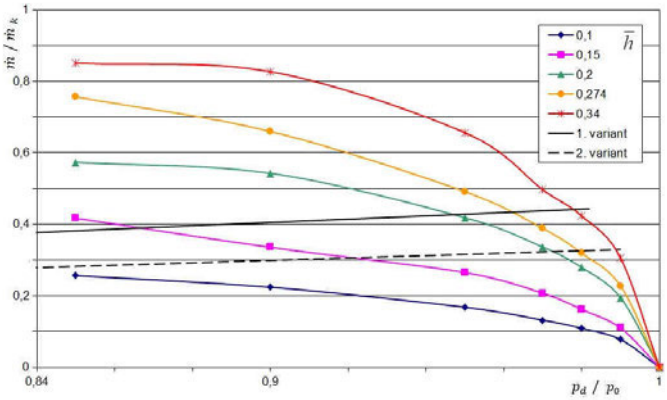

Fig. 3: Mass flow characteristic of the valve

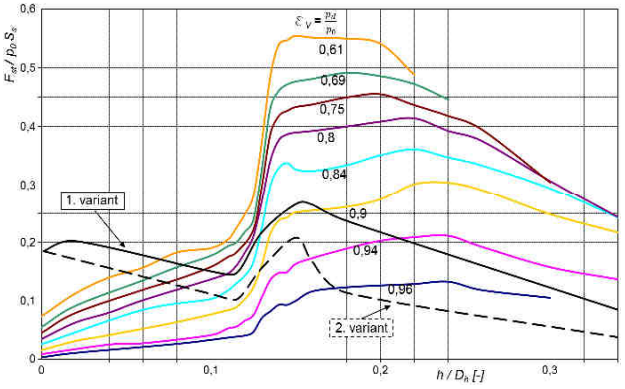

Fig. 4: Force characteristic of the valve

Summary

Experiments on the steam version of unloaded valve confirmed lowering of force needed to tear the big cone from the valve seat up to 1/3 of the original force.

Regarding various limitations occurring while building the valve into the existing steam piping with experimental turbine, it was not possible to test the valve in expected operational states of the turbine. It was necessary to recalculate all the forces from the measured data for designed parameters.

The experiments showed that the friction forces in the servo drive are about 300 N. A similar value is calculated for the valve friction forces. For the unloaded valve operation the predicted and measured forces are in agreement. In the loaded valve operation the measured value is smaller than the predicted one. It can be even negative. The stabilizing force applied on the big cone can be in the whole range positive and it is bigger than the predicted value.

References

[1] M. Miczán, L. Bednář, D. Kovandová, L. Tajč, Experimentální ověření sil působících na kuželku a vřeteno odlehčeného regulačního ventilu ŠKODA bez ochranného síta, Výzkumná zpráva ŠKODA POWER s.r.o., VZTP 1065, 2012

[2] R. Matas, CFD simulace nového typu odlehčeného regulačního ventilu parní turbíny pro vysoké parametry páry, Zpráva NTL při ZČU Plzeň, NTL 02-04/086, 2008

[3] F. Straka, Numerická simulace proudění v odlehčeném ventilu ŠKODA a určení namáhání vřetena od aerodynamických sil, Diplomová práce FS ZČU Plzeň, 2012

21st International Conference **ENGINEERING MECHANICS 2015**
Svratka, Czech Republic, May 11 –14, 2015
Paper **#041, pp. 200–201**

Quasicontinuum Approach Applied to Inelastic Materials

Karel Mikeš

Czech Technical University in Prague, Faculty of Civil Engineering,
Thákurova 7, 166 29 Praha 6, Czech Republic
karel.mikes.1@fsv.cvut.cz

Keywords: quasicontinuum method, discrete particle model, microplane model.

Abstract: The quasicontinuum (QC) method was proposed by Tadmor, Ortiz and Phillips [3] in 1996. The original application of this computational technique was a simulation of large atomistic systems with regular lattices described by long-range conservative interaction potentials. Extension to non-conservative interaction was done by Beex et al. [1]. In the present work, the QC technique is applied to an irregular set of particles connected by discrete plastic links representing e.g. a fibrous material. QC models for plastic materials are constructed within the framework of the microplane theory. Accuracy, efficiency and specific properties of QC microplane models are evaluated by comparison of results with the pure particle approach.

Methodology

The key idea of QC is to reduce the computational cost by reducing degrees of freedom (DOF) of the fully atomistic approach. Instead of dealing with all atoms, a small relevant subset of atoms is selected to represent the whole system. These atoms, the so-called repatoms, are used to approximate the DOF of other atoms. atoms. In applications of the QC idea to particle models, the selected representative particles are referred to as the repnodes.

The description of the 2D material with plastic properties is based on the idea of microplanes. The relation between the stress and strain vectors is used on planes with various orientations, so-called microplanes. The macroscopic stress and strain tensors are obtained by a summation of all these vectors under the assumption of kinematic constraint. The orientation of each microplane is defined by its unit normal $\boldsymbol{n}$. The strain vector ε^n on the microplane is the projection of the strain tensor, $\varepsilon_i^n = \varepsilon_{ij} n_j$. Then the normal strain on the microplane is

$$\varepsilon_N = n_i \varepsilon_i^n = n_i \varepsilon_{ij} n_j. \tag{1}$$

The constitutive elasto-plastic law is defined on microplane level and the macroscopic stress tensor is obtained by integral formula

$$\sigma_{ij} = \frac{2}{\pi} \int_\Omega \sigma_N n_i n_j. \tag{2}$$

Numerical simulations have been performed using the open-source finite element code OOFEM [2]. In OOFEM implementation, nodes with interpolated DOF are realized with a special type of node called hanging node. Linear interpolation of hanging nodes is used. Links connecting particles are modeled as perfectly elasto-plastic.

Results

The proposed model has been tested in uniform tension. The geometry of the tested example is depicted in Fig. 1 (left). A significant narrow region is realized in the middle and final plastic mechanism is expected there. If this region is realized with repnodes, the QC model provides very accurate description. But if this region is realized only with microplane elements, the final plastic mechanism is not captured exactly; see Fig. 2. The QC model with repnodes is compared with the fully resolved particle model. The strain error in the last time step is depicted in Fig. 1 (right). Time saving is more than 20%.

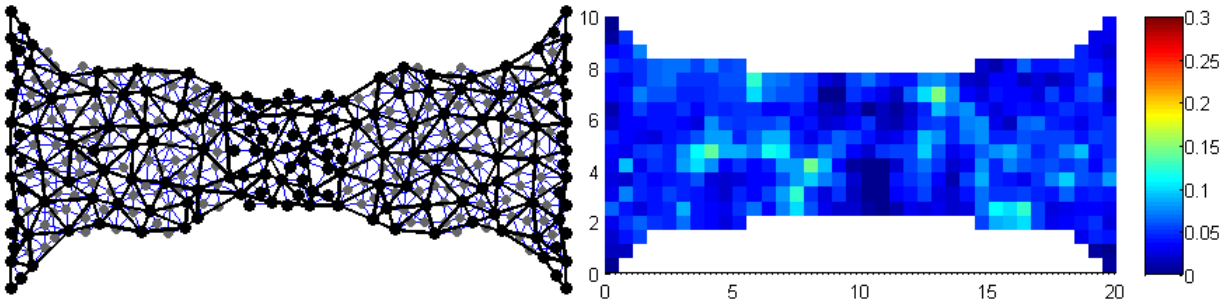

Fig. 1: Interpolation mesh with repnodes and absolute strain error divided by submitted strain.

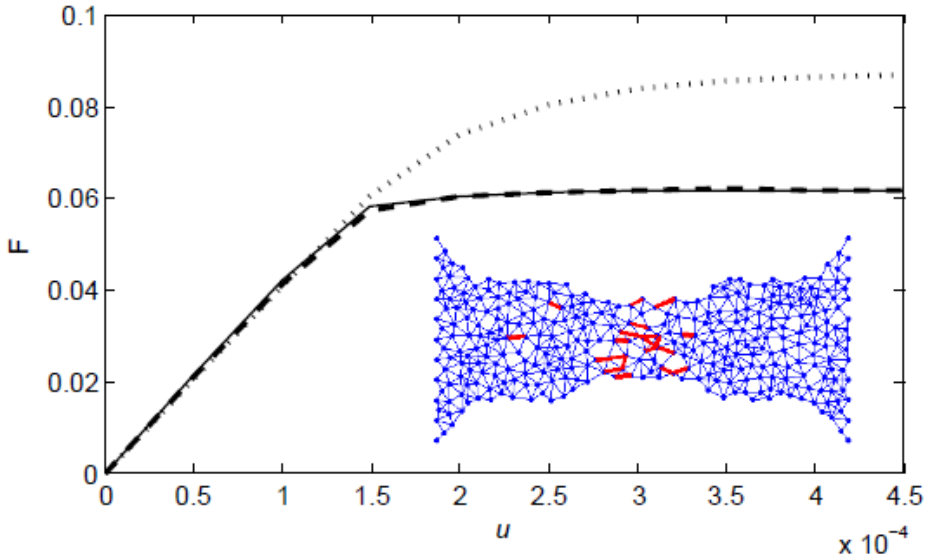

Fig. 2: Force-displacement diagram for fully resolved particle model (solid), microplane model with repnodes in the narrow region (dashed) and without extra repnodes (dotted). Deformed particles with links in plastic state (red).

Conclusions

The QC-based method leads to a substantial reduction of unknown DOF and computational demand. The error caused by this reduction can be effectively reduced by suitably setting the region of high interest. Finally, a significant simplification of the problem can be reached at the price of an acceptable error. The presented example shows that the QC microplane model provides a very good description of the particle model with plastic links if the final plastic mechanism is captured by repnodes.

Acknowledgement: The financial support of this research by the Grant Agency of the Czech Technical University in Prague (SGS project No. 15/031/OHK1/1T/11) and by the Czech Science Foundation (GAČR project No. 14-00420S) is gratefully acknowledged.

References

[1] L. Beex, R. Peerlings, M. Geers, A multiscale quasicontinuum method for dissipative lattice models and discrete networks. Journal of the Mechanics and Physics of Solids, 64 (2014) 154–169.

[2] B. Patzák, OOFEM – an object-oriented simulation tool for advanced modeling of materials and structures. Acta Polytechnica, 52 (2012) 59–66.

[3] E.B. Tadmor, M. Ortiz, R. Phillips, Quasicontinuum analysis of defects in solids. Philosophical Magazine A, 73 (1996) 1529–1563.

21st International Conference **ENGINEERING MECHANICS 2015**
Svratka, Czech Republic, May 11 –14, 2015
Paper **#195, pp. 202–203**

Microindentation Assessment of Climatic Loading Impacts on Polymer Sealants

Jiří Minster[a]*, Petr Šašek[b]

[1]Institute of Theoretical and Applied Mechanics AS CR , v. v. i.,
Prosecká 76, Prague 9, 109 00 Czech Republic

[a]minster@itam.cas.cz, [b]sasek@itam.cas.cz

Keywords: microindentation, climatic loading, polymer sealants

Abstract: Sun light, especially the short-wave ultra-violet part of the sun spectrum, together with influence of moisture, are the most enlarged and the most effective sources of climatic damage of polymers. The effects of the both influences became stronger with enhanced temperature. Sun light on the one hand supports the forming of transverse chemical bonds between macromolecules and on the other hand results in their breakdown. This causes a strengthening or softening of polymers. The amount of changes and the dominant process depends on the radiation dose and on the influencing wave length. Every kind of chemical bond has its own critical wave length, which, with sufficient amount of energy, brings a reaction. Ageing, as a result of climatic loading, is therefore very closely connected with a structure of a real material.

Microindentation is one of possible methods for assessing influences of a climatic loading on mechanical properties of polymers. Indentation test is checked by the history either of a power or an indent depth. The information about the hardness, Young modulus and viscoelastic properties of the investigated material can be received afterwards from measured data. The investigated materials were tested in their native standard form and also after four model types of physical-chemical ageing. Time-dependent properties of the sealants were assessed by the method of indentation creep. One hundred indentation creep tests were conducted for each sealant and type of ageing. A motivation for this work was a requirement to assess an influence of a climatic loading on the basic mechanical properties of sealants, used for a creation and a repair of mosaics.

Investigated materials

A group of six polymer sealants was selected for measurements. Their commercial names, production plants, compositions and their short marks for distinguishing are given in Table 1.

Tab. 1: Investigated materials

Commercial name of the sealant	Production plant	Composition	Mark of the sealant
Akryl Exterier	Den Braven	One-component sealant on the basis of acrylate dispersion	A
Mapeflex AC4	Mapei	One-component acrylate sealant in water dispersion	B
Mapeflex MS45	Mapei	One-component quickly hardening elastic thixotropic sealant on the basis of hybrid silan polymer	C
Multisil	Remmers	Silicone- caoutchouc sealant	D
MS 150	Remmers	Elastic sealant on the basis of hybrid polymers	E
MultiSil NUW	Remmers	Silicone- caoutchouc sealant	F

The investigated materials were tested in their native standard form (STAND) and also after several model types of physical-chemical ageing:

a) after one month placement in the conditions of enhanced temperature, moisture influence and ultra violet radiation (UV)
b) after three month placement in the temperature 60 °C (60)
c) after three month placement in the temperature 60 °C with the relative humidity 80 % (60M80)
d) after one month cycle of 2 hours soaking in water with subsequent freezing (VM).

Methods of measurements and results

The system Hysitron TI 750D TriboIndeter™, equipped by the Berkovich indenter, was used for testing. The basic mechanical characteristics were measured using quasi-static mode Basic QS Trapezoid. Its output represent reduced Young modulus and hardness. Indentation creep is defined by the history of loading $P(t')=P_o*H(t')$, where $H(t')$ represents the Heaviside function. The equation for viscoelastic compliance $D(t)$ has a form dependent on the history of the indent depth $h(t)$.

$$D(t) = 2\, h^2(t) / [\pi(1-\nu^2)\, P_c \tan \alpha] \quad (1)$$

ν is the Poisson´s coefficient, α is the effective angle of the Berkovich indenter. The average viscoelastic compliance values of the sealant with the smallest influence of the climatic loading on the investigated mechanical characteristics are presented in Fig. 1.

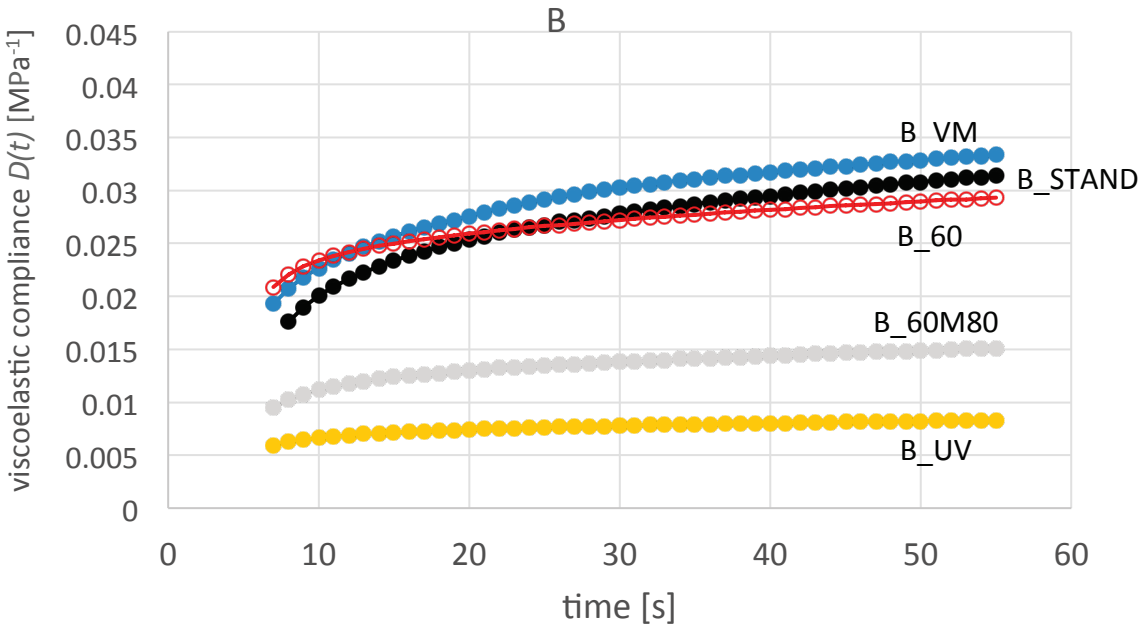

Fig 1: Viscoelastic compliances of the B sealant

Conclusion

Present results have confirmed microndentation technique to be a suitable methodology to assess changes of basic mechanical properties of sealants caused by photo-degradation processes and climatic influences.

Acknowledgement: This work was supported by the Ministry of Culture Grant DF12P01OVV017.

21st International Conference **ENGINEERING MECHANICS 2015**
Svratka, Czech Republic, May 11 –14, 2015
Paper **#110, pp. 204–205**

Influence of the Primary Breakup Conditions on the Droplet Size of the Spray Generated by Twin Fluid Atomizers

Marek Mlkvik[1,a] *, Matous Zaremba[1,b], Philipp Stähle[2,c], Heike P. Schuchmann[2,d], Volker Gaukel[2,e], Jan Jedelsky[1,f]

[1]Brno University of Technology, Technická 2896/2, 616 69 Brno, Czech Republic

[2]Karlsruhe Institute of Technology, Institute of Process Engineering in Life Sciences, Section I: Food Process Engineering, Kaiserstraße 12, 76131 Karlsruhe, Germany

[a]mlkvik@fme.vutbr.cz, [b]y116215@stud.fme.vutbr.cz, [c]philipp.staehle@kit.edu, [d]heike.schuchmann@kit.edu, [e]volker.gaukel@kit.edu, [f]jedelsky@fme.vutbr.cz

Keywords: twin-fluid atomizers, Y-jet atomizer, effervescent atomizer, CFT atomizer, primary breakup, spray

Abstract: Main goal of this study is to relate the measured droplet sizes, characterized by the Sauter mean diameter (ID32), to the conditions of the primary breakup defined mainly by the Weber number (We). To compare different atomizing techniques, we investigated four twin-fluid atomizers with different mechanisms of internal mixing: Y-jet atomizer, outside in gas (OIG) and outside in liquid (OIL) effervescent atomizers and in-house invented CFT atomizer. Our results shows, that for the OIL, OIG and CFT atomizer a common relation between the working parameters (pressure drop- Δp, gas to liquid ratio- GLR) and measured droplets sizes, normalized regarding to the critical Weber Number (We_{crit}) in the primary breakup area, is found Increasing trend of the normalized droplet diameter with increasing GLR and Δp indicates the decreasing efficiency of atomization process, which is in accordance with current knowledge of energy conversion in twin fluid atomizers. The Y- jet atomizer shows a different trend which is related to the considerably lower We at primary breakup site.

Introduction

Atomization by twin fluid nozzles with internal mixing is a complex process which starts by injection of liquid and gas into a mixing chamber and finishes by ejection of the mixture and the formation of stable spherical droplets. This work describes the influence of primary breakup conditions on droplet size, which is a first approach in our effort to find a general link between the working parameters of selected atomizers and the quality of the spray (related to droplet size).

Experiment

Experiments were conducted on a cold test bench equipped with four twin fluid atomizers: Y-jet, OIL, OIG and CFT atomizer [Fig. 1]. The working parameters of the atomizers were defined by input pressure (Δp = 1.4 *MPa*) and gas to liquid ratio (GLR = 2.5, 5, 10 and 20 %). To investigate the effect of viscosity on the droplet size, two solutions of maltodextrin and de-ionized water (μ = 60 and 143 *mPa·s*) were used as the working liquids.

The primary breakup was investigated by the high-speed imagining. Captured images were processed to describe the breakup by dimensionless numbers [1]. Droplet size was measured by a laser diffraction system (Malvern Spraytec) at the distance 100 *mm* downstream to the discharge orifice. To find general relation for the droplet size, the measured Sauter mean diameter of the spray (ID32) was normalized by the value $d_{max} = We_{crit} \cdot \sigma / \rho \cdot \omega^2$, where σ denotes liquids surface tension, ρ denotes density of gas. Symbol ω is for liquid to gas velocity difference at the primary breakup site and the W_{ecrit} = 1.18 [2] denotes the critical Weber number of spherical droplets.

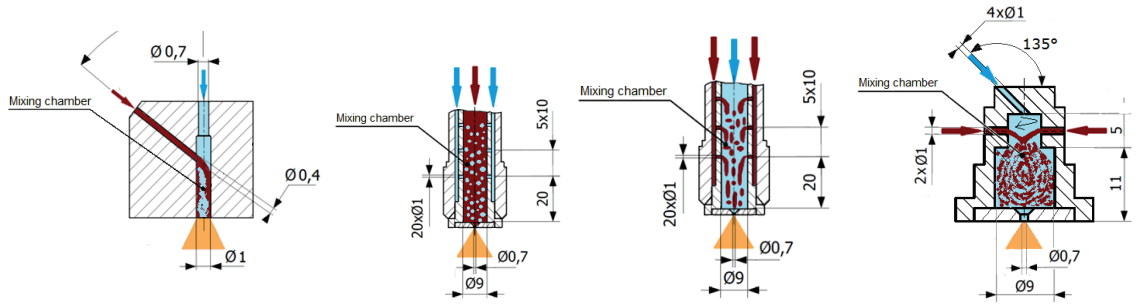

Fig. 1: Used atomizers, a) Y-jet atomizer, b) OIG atomizer, c) OIL atomizer, d) CFT atomizer

Results and discussion

Fig. 2 shows that for the OIG, OIL and the CFT atomizer a common relation between the working parameters of the atomizer (GLR, Δp) and the normalized spray drop size can be found for OIL, OIG and CFT atomizer. The Y-jet atomizer differs from the previous ones by design of the mixing chamber and internal flow, which leads to a different breakup mechanism from the other ones [1] and finally to a different relation of the normalized spray drop size on GLR.

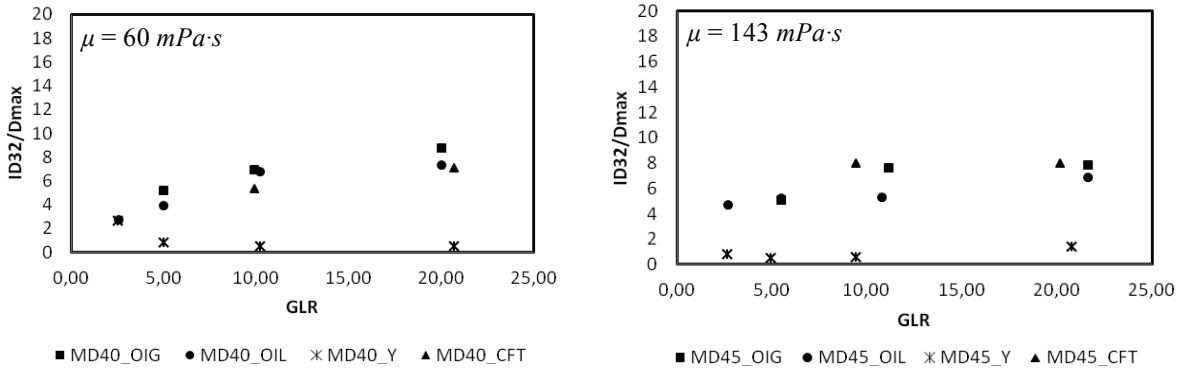

Fig. 2: Normalized droplet size for input pressure 0.14 *MPa*, ID32/D_{max} [-], GLR [*%*]

Acknowledgement: Authors acknowledge financial support from project № 101/11/1264 funded by the Czech Grant Agency, from project NETME CENTRE PLUS (LO1202) co-funded by the Ministry of Education, Youth and Sports within the support programme „National Sustainability Programme I“ and project № CZ.1.07/2.3.00/30.0005 of Operational Program Education for Competitiveness of Ministry of Education, Youth and Sport of the Czech Republic.

References

[1] M. Mlkvik, P. Stähle, H. P. Schuchmann, V. Gaukel, J. Jedelský, Investigation of near nozzle flow of high viscous liquid in twin- fluid atomizers, in: Proceedings of the 25th international symposium on transport phenomena, Krabi, Thailand: KMITL, 2014. pp. 1-8.

[2] A. Lefebvre, Atomization and sprays, Hemisphere publishing corporation, 1989, ISBN 0-89116-603-3

21st International Conference **ENGINEERING MECHANICS 2015**
Svratka, Czech Republic, May 11 –14, 2015
Paper **#157, pp. 206–207**

Adaptive Updating of Meta-Models in Hyperspherical Domains

Eva Myšáková[a], Matěj Lepš[b]

Faculty of Civil Engineering, CTU in Prague, Thákurova 7, 166 29, Prague, CZ

[a]eva.mysakova@fsv.cvut.cz, [b]leps@cml.fsv.cvut.cz

Keywords: design of experiments, meta-modeling, design domain, hypercube, hypersphere

Abstract: The meta-modeling is frequently used method for analysis of the complex systems. Its basic part constitutes the design of experiments (DoE) - it is crucial to select the training points with consideration. Therefore the appropriate design domain where the points are to be spread has to be selected. The meta-models are usually constructed within the domain in shape of hypercube. In this contribution we propose the alternative - the hyperspherical design domain.

Introduction

A Design of Experiments (DoE) is a set of the design points whose coordinates correspond to combinations of values of system's input variables [1]. It plays an essential role in meta-modeling which is often used method for analysis of the complex systems' behavior [2]. The purpose of meta-models is approximation of the system response in cases where the evaluation of the original model is costly or highly time-consuming. The meta-model is constructed based on (i) training data - the design points - spread over the domain of real input parameters and (ii) responses of the original model corresponding to those design points. For good meta-model predictions the positions of design points have to be selected carefully. Furthermore the meta-model usually needs to be updated by addition of more training points into appropriate areas of the design domain.

The training points are traditionally generated within the domain in a shape of hypercube. This contribution deals with alternative procedure: the points are placed within the hyperspherical domain - which seems to be effective e.g. for solving reliability-based problems [3]. The additive points are then found using two-objective strategy - the new points are added (i) into the areas that are not still covered well and (ii) into the areas interesting for the response of the meta-model.

Meta-model construction in hypercube

The adaptive updating briefly described in Introduction and discussed for example in [4] originally operates in hypercubical domain. More precisely the domain for the meta-model construction has the shape of a unit hypercube. The domain in a real parameter space is generally a hyperprism because individual parameters differs in their values and distributions. We set the bounds for meta-model construction as 0.15% and 99.85% quantiles ($\mu \pm 3\sigma$ in case of normal distribution; μ is mean and σ is the standard deviation). Outside these bounds the meta-model has to extrapolate the response value. Then uniform space-filling DoE is created in the hypercube, the responses corresponding to the points in real parameter domain are computed by the original model, and the meta-model is constructed. Usually the quality of the meta-model prediction is not precise enough and therefore the meta-model has to be updated by addition of new design points into the DoE.

Motivation

As dimension grows we face problem that the majority of added points are placed on the border of the domain, see Figure 1. It can be caused by the character of the model response - the interesting areas lie outside the selected bounds and therefore the new points are placed as far as possible. The second explanation relates to the shape of the domain. The hypercube simply has too many borders and from

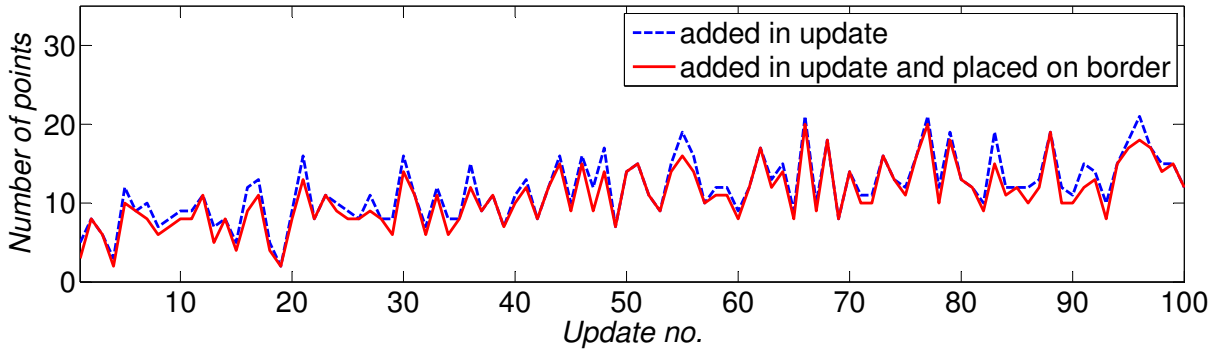

Fig. 1: Points added in individual updates of meta-model constructed within hypercubical domain.

the previous experience it is known that even a good space-filling design of experiments often has the biggest hole on the border object of the design domain (vertex, edge and so forth). Therefore the alternative is proposed - to build the meta-model within the hyperspherical domain.

Hyperspherical design domain

The main idea is to construct the meta-model within the domain in a shape of a hypersphere, which is inscribed in a unit hypercube, because the meta-model usually operates in $[0, 1]^n$ space; n is dimension. In real parameter space the corresponding domain has hyperellipsoidal shape. For simple comparison of the results we set the ellipsoidal semiaxes such that the volume of the hyperellipsoid is same as the volume of the hyperprism in the previous case of hypercubical design domain. So the volume of the real parameter space area covered by the meta-model remains the same in both cases. At first the initial design of experiments in the hypersphere is created [5]. This design is generated in a unit hypersphere (unit radius, centered at the origin), therefore it has to be transformed (i) into the real parameter space (hyperellipsoid) to get the responses of the original model and (ii) into the hypersphere (inscribed in a unit hypercube) for meta-model construction. The procedure is tested on examples with different dimension and various parameter distributions.

Acknowledgement: The authors gratefully acknowledge the financial support from the Czech Science Foundation, project No. 15-07299S, and the Grant Agency of the Czech Technical University in Prague, the grant SGS15/030/OHK1/1T/11.

References

[1] D. C. Montgomery, Design and Analysis of Experiments, Wiley, 8 edition, (2012).

[2] A. Forrester, A. Sóbester, A. Keane, Engineering Design via Surrogate Modelling: A Practical Guide, John Wiley & Sons Ltd, (2008).

[3] V. Dubourg, Adaptive surrogate models for reliability analysis and reliability-based design optimization, Ph.D. thesis, Université Blaise Pascal, Clermont-Ferrand, France, (2011).

[4] E. Myšáková, A. Pospíšilová, M. Lepš, Optimized Design of Computer Experiments: A Review, In: Computational Methods for Engineering Technology, (2014).

[5] E. Myšáková, M. Lepš, Uniform Space-filling Design of Experiments in Hypersphere, In: Proceedings of the 5th Conference Nano and Macro Mechanics NMM 2014, (2014).

21st International Conference **ENGINEERING MECHANICS 2015**
Svratka, Czech Republic, May 11 –14, 2015
Paper **#021, pp. 208–209**

Non-Linear Normal Modes in Dynamics – Discrete Systems

Jiří Náprstek[a*], Cyril Fischer[b]

ITAM AS CR, Prosecká 76, 190 00 Prague 9
[a]naprstek@itam.cas.cz, [b]fischerc@itam.cas.cz

Keywords: nonlinear dynamic systems, non-linear normal modes, discretization, multi-scale method

Abstract: The aim of the paper is to inform about main features of Non-linear Normal Modes (NNM) as a powerful tool for investigation of multi-degree of freedom (MDOF) dynamic systems. In particular, it is shown how this concept can be used to investigate forced resonances of non-linear symmetric systems including non-linear localization of vibrational energy. NNMs can provide a valuable tool for understanding essentially non-linear dynamic phenomena having no counterparts in linear theory and which do not enable analysis using linearized procedures. Discrete MDOF systems are considered in this study. A couple of possible approaches are outlined together with some demonstrations of numerical results.

Introduction

The most popular concept of dynamic systems investigation consists in decomposition into linear normal modes (LNM) which serve as independent separable orthogonal space. These modes are energy invariant and therefore motion consisting of a single mode at any instant will correspond only to this mode for all time. The widespread view being very reliable in the linear domain motivated an idea of expansion into the non-linear domain.

The first self-contained theoretical background of extension into the non-linear domain is ascribed to R.M. Rosenberg [1] and later to R. Rand [2]. Massive development of NNM including theoretical background, numerical implementation, applications and propagation in the community of dynamics has been started by Vakakis e.g. [3] or monograph [4], etc. and simultaneously by A.H. Nayfeh, e.g. [5]. The concept of NNM seems to be more and more popular as a powerful tool for investigation of complicated non-linear dynamic systems, see many papers which appeared recently e.g. [6]. Besides analytical studies dealing with qualitative investigation, many computer implementation have been developed and widely used in daily practice of engineering system design. Well known packages are available, e.g. AUTO, MATCONT, CL-MATCONT, etc.

Definition outline for systems with concentrated masses

The NNM of an undamped discrete or continuous system can be regarded as a synchronous periodic oscillation where all material points of the system reach their extreme values or pass through zero simultaneously. When a discrete system vibrates in an NNM the corresponding oscillation is represented by a line in its configuration space which is termed modal line. Linear systems possess straight modal lines since their coordinates are related linearly during a normal mode oscillation. In non-linear systems the modal lines can be either straight or curved. The later cases are typical in non-linear discrete systems since straight non-linear modal lines reflect rare special symmetries of the system.

For discrete systems Rosenberg defined similar NNM that correspond to straight modal lines in configuration space and non-similar NNM that correspond to curved modal curves. While LNM are all similar, non-linear discrete (or discretized continuous) systems possess basically non-similar modes and similar are rather exceptional. Let us demonstrate the concept of similar and non-similar NNM at the autonomous TDOF system:

$$\begin{aligned} \ddot{x}_1 + x_1 + x_1^3 + K(x_1 - x_2)^3 &= 0, \\ \ddot{x}_2 + x_2 + x_2^3 + K(x_2 - x_1)^3 &= 0. \end{aligned} \tag{1}$$

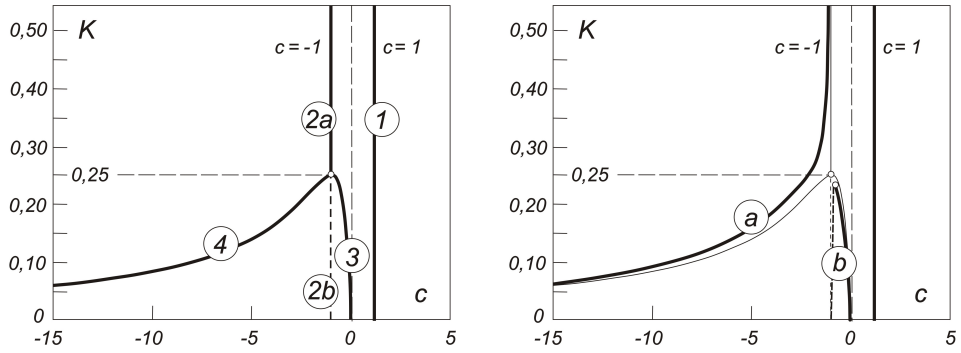

Fig. 1: Proportionality coefficient c as a function of the stiffness K

where K is a symbolic non-linearity rate of the connecting spring. Linear part of this spring is omitted. If the system (1) includes similar NNM a constant parameter c should exist:

$$x_2(t) \;=\; c \cdot x_1(t) \tag{2}$$

Constant c indicates a proportionality of both coordinates x_1, x_2 during every period of eigen vibration and approves an existence of a similar NNM. Fig. 1 - left picture - corresponds with Eqs (1) and shows two similar NNMs - branches 1 and $2a$ (branch $2b$ is unstable) and two non-similar NNMs - branches 3 and 4. Fig. 1 - right picture - presents the case of modified system Eqs (1) which admits slightly different parametr K in both equations and other "non-symmetries". The relevant plots in the right picture demonstrate that purely similar NNMs don't exist any more. The NNMs should be investigated in other way distinguishing global NNMs (close to similar NNMs) and local NNMs (close to non-similar NNMs). In general we can see, that the nonlinear system can include more NNMs than is the number of its degree of freedom.

Conclusion

Let us stress that similar NNM are not generic. Their appearance require quite severe symmetry conditions to be fulfilled and so the similar NNM are rather exceptional in an exact meaning of the term. On the other hand NNM quite often remember shape of a linear counterpart, but anyway their shape changes with level of energy, nodes are moving, etc. These facts makes investigation of NNM more difficult to evaluate, but this concept is still one of the most effective procedure of MDOF nonlinear systems investigation.

Acknowledgement: The kind support of the Czech Science Foundation project No. 15-01035S and of the RVO 68378297 institutional support are gratefully acknowledged.

References

[1] R.M. Rosenberg, On non-linear vibrations of systems with many degrees of freedom. Adv. Appl. Mech., 9 (1966) 155–242.

[2] R. Rand, Non-linear normal modes in two-degree-of-freedom system. J. Appl. Mech., 6 (1971) 545–547.

[3] A.F. Vakakis, Non-linear normal modes (NNMs) and their applications in vibration theory: an overwiev. Mech. Syst. Signal. Pr., 11 (1997) 3–22.

[4] A.F. Vakakis, L.I. Manevitch, Y.V. Mikhlin, V.N. Pilipchuk , A.A. Zevin, Normal modes and localization in non-linear systems. Wiley, New York, 1996.

[5] A.H. Nayfeh, S.A. Nayfeh, On nonlinear modes of continuous systems. J. Vib. Acoust., 116 (1994) 129–136.

[6] G. Kerschen, M. Peeters, J.C. Golinval, A.F. Vakakis, Non-linear normal modes, Part I: A useful framework for the structural dynamicist. Mech. Syst. Signal. Pr., 23 (2009) 170–194.

21st International Conference **ENGINEERING MECHANICS 2015**
Svratka, Czech Republic, May 11 –14, 2015
Paper **#250, pp. 210–211**

Modification of Protective Lime Coating Systems for the Porous Limestone Using Lime Nanomaterials: Assessment of Mechanical Properties and Ageing Resistance

Michaela Navrátilová[1,a]*, Karol Bayer[2,b], Elisabeth Ghaffari[3,c], Dana Macounová[1,d], Zuzana Slížková[1,e], Johannes Weber[3, f]

[1]ITAM – Centre of Excellence Telč, Batelovská 486, 588 56 Telč, Czech Republic

[2]University of Pardubice, Faculty of restoration, Jiráskova 3, 570 01 Litomyšl, Czech Republic

[3]University of applied arts in Vienna, Institute of arts and technologies, Salzgries 14/1, 1010, Vienna, Austria

[a]navratilova_m@seznam.cz, [b]karol.bayer@upce.cz, [c]ghaffari@chello.at, [d]macounova@itam.cas.cz, [e]slizkova@itam.cas.cz, [f]johannes.weber@uni-ak.ac.at

Keywords: lime coatings, nanolime products, Leitha limestone, adhesion, cohesion, aging tests

Abstract: Within the area of care for sculptural and architectonic monuments of limestone in Austria there has been a historic continuity of use of protective lime coatings. In the regions of Upper and Lower Austria, Vienna and Burgenland mainly Leitha limestone (named after the Leitha Mountains) are dealt with. In Czech lands such approach was disrupted from 19th century by application of the "purist" idea of bare surface of stone. Nevertheless, this treatment of stone surface has been coming back into use for many various reasons in the past few decades. Requirements for preservation of pieces of art and handcraft made of limestone using lime coatings are most often applied in the regions of Vysočina, South Moravia and South Bohemia, which directly border on the Northern States of Austria. Owing to the resource locations of Leitha limestone in these regions, there is a higher representation of cultural heritage monuments made of this type of stone in the Czech Republic.

Based on existing findings and practical experience, besides other favourable characteristics lime coatings and even nanolime products fulfil also the theoretical requirement for so called material compatibility with limestone – stones consisting of mainly calcium carbonate. Having followed the instructions for their application conditions they should not cause any undesirable physical or chemical changes in the treated material. Nowadays their use corresponds to the current requirements of cultural heritage preservation for retreatibility and reconservation. Their characteristics and relatively easy removability does not prevent prospective conservation and restoration treatments in the future and at the same time they provide long-term and repeatable preventive care. Their limited adhesion to the types of limestone with compact surfaces of low porosity and soakability might be considered as a certain drawback of the use of lime coatings for surface preservation. In addition, their decreased resistance to the impacts of environment and corrosion could be viewed as a problem; currently these would include above all air pollution by acid atmospheric pollutants and the effects of water soluble salts.

Within the Nanolith project (cross-boundary Austrian-Czech collaboration), there has been a series of tests carried out focused on possible modifications of protective lime coating systems by means of alcohol nanosuspensions of calcium hydroxide. The purpose of the modification was to increase the lifespan of lime coating systems in exterior conditions with the use of various types of nanolime products. Within the described experiment, nanolime products were tested in various combinations as primers as well as final fixatives of lime coating systems. The purpose of the testing was to find out if the proposed combination of lime coatings with nanolime products positively influenced adhesion of the coatings to the stone surface, their cohesion and resistance to aging in exterior conditions. Part of the testing was to determine suitable application conditions and the way of application of nanolime products.

Choosing suitable methods to assess the characteristics and resistance of individual modified coating systems proved to be quite difficult. The inconveniences were caused by the absence of available published papers dealing with the given issues as well as norms and standards designated for lime of inorganic coatings testing generally. Because of such limitations, partially modified methods based on existing norms in the field of organic coatings testing and the methodology proposed by the ITAM AS CZ / CET Telč in collaboration with FR UPCE were used.

Choosing and finding a suitable substrate – a support for the application of the tested lime coating systems was not easy either. For the given type of sedimentary stone a notable variation might have been expected in the physical characteristics of the prepared test specimens, which makes the testing result assessment more difficult. Adhesion of coating treatment is closely related to the differences of these characteristics, mainly to soakability, porosity or compactness of stone, thus also their lifespan to a great extent. For that reason, individual test specimens, which differed in the above mentioned characteristics, were set with these parameters and subsequently taken into account when the resistance of the applied system of lime coatings was assessed.

As support for the testing of modified lime coating systems test specimens of Leitha limestone from the quarry near the municipality of Loretto (Burgenland) in Austria were used. For the preparation of the lime coating slaked lime from Dullinger Kalk in Austria was employed. Nanolime products were chosen from the product line of the firm IBZ Freiberg from Germany. For the primary adhesive layer – primer – nanoproducts CaLoSiL® E50 (concentration of 50 g Ca(OH)2 / a litre of the product) and CaLoXiL® Lime Glaze (concentration of 120 g Ca(OH)2 /a litre of the product) were chosen. For the final fixative layer – fixative – nanosuspension CaLoSiL® E25 (concentration of 25 g Ca(OH)2 / a litre of the product) was used.

For the testing itself and the assessment of characteristics of the lime coating systems the following testing and assessment methods were used: cross cut adhesion test for the assessment of adhesion of the coating system to the surface of stone; climatic accelerated aging testing – cyclic changes of temperature and relative humidity, exposure to mixed air pollution by the gases of SO_2 a NO_x and resistance to salt crystallization using sodium chloride; water resistance test; water drop test of paint wettability; resistance test by dropping with hydrochloric acid – assessment of coating system resistance to acidic pollutants; peeling test – assessment of adhesion and cohesion of the coatings; drying test; test of application of a fixative to pigmented lime coatings – assessment of optical changes of tinted lime coatings after the final fixative application; tests of suitable application method of a fixative – assessment of the distribution of the fixative during application; visual assessment in dispersed day light and sharp raking light; study of the microstructure of surface layers – microphotography by means of a special camera; optical and scanning electron microscopy; setting the basic physical characteristics of the support with the coating system – bulk density; open porosity accessible by water; water absorption and pore size distribution.

The results of laboratory testing have suggested that in the tests of modified lime coating systems similar trends can be observed. Treatment of the support (limestone) under the lime coating itself by means of a primer based on lime nanosuspension increased adhesion, resistance and durability of the lime coating on all the types of lime test specimens. A positive effect has been noted both in the case of limestone of high porosity, soakability and structured on the surface as well as in the problematic ones with compact surfaces, lower porosity and soakability. The best results have been achieved with the use of CaLoXiL® Lime Glaze – a highly concentrated nanosuspension. Application of a fixative – less concentrated lime nanosuspension CaLoSiL® E25 – a final fixing layer of lime coating seems to have been positive only if the by homogenous distribution using low concentration of lime nanosuspension.

Acknowledgement: The authors gratefully acknowledge support from European Regional Development Found, the programme European Territorial Co-operation Austria-Czech Republic 2007-2013 entitled "Nanolith" M00264 („Použití nanomateriálů pro udržitelnou konzervaci historických sochařských a architektonických děl z litavských vápenců").

21st International Conference **ENGINEERING MECHANICS 2015**
Svratka, Czech Republic, May 11 –14, 2015
Paper **#125, pp. 212–213**

Dynamic Analysis of Cables on Pulleys Using the New Algorithm

Ivan Němec [a], Hynek Štekbauer [b]*

Institute of Structural Mechanics, Faculty of Civil Engineering, Brno University of Technology,
Veveří 331/95, 602 00 Brno, Czech

[a]nemec.i@fce.vutbr.cz, [b]stekbauer.h@fce.vutbr.cz

Keywords: pulleys, RFEM, dynamics, finite element method

Abstract: This paper demonstrates application of a new algorithm for calculation of cables on pulleys. This brand new algorithm enables taking into account the magnitude of radius of each pulley. It has been implemented in the RFEM program because of its significantly higher accuracy and high efficiency compared to the previous algorithm. The paper contains the comparison of the commonly used algorithm, which ignores pulley radius, and the new algorithm. The solutions obtained by explicit finite element method are presented.

Introduction

Pulleys are used for their mechanical advantage (Fig.1). That is why pulleys are a part of many building and machine structures, they can be seen e.g. at crane structures, cableways and even in a car engine. The set of pulleys is often a complex system too complicated for hand calculation and therefore there is an effort to enable calculation of such structures with the aid of computer programs. For pulleys which are part of load bearing structures and dynamic effects are taken into account, manual calculation is completely impossible.

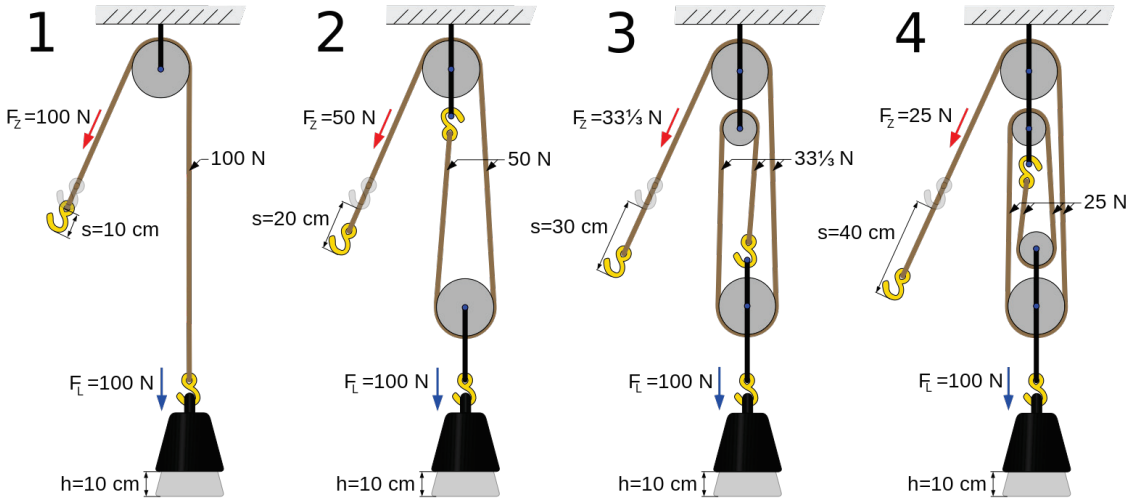

Fig. 1: Efficiency of pulley system [1]

Algorithms for the calculation of cables on pulleys

Besides simulators like MapleSim, which do not allow detailed static and dynamic calculation of pulleys and structures connected to them, there are two possible approaches for solving cables on pulleys.

The first approach is a connection of pulleys by 1D elements only in the centre of each pulley (Fig.2a) or at the intersection of real cable sections (Fig.2b) and defining behaviour of such system to find equivalent solution [2, 3]. Such a solution lacks any consideration of the radii of pulleys, which inevitably leads to inaccurate results. In the first case (Fig.2a) spatial geometry of cables in the model is changed and in the second case (Fig.2b) reaction occurs in the node located out of the structure. This approach is used in programs such as LS-DYNA or RFEM.

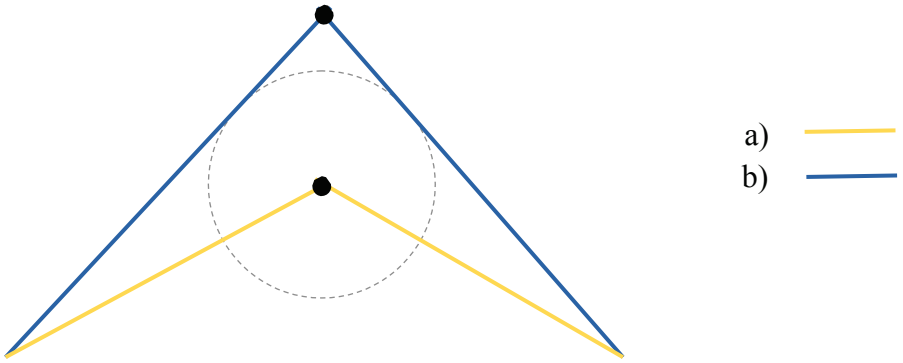

Fig. 2: Connection possibilities of two cables in node for the first approach

The second approach is modelling of each pulley and cable using 3D elements and between these elements adding other contact elements for correct behaviour of multibody system. This solution is indeed accurate for the correct model, but it is extremely laborious to create a mathematical model and calculation is also extremely time-consuming. Because of the difficulty mentioned above, use of this approach is impossible for large structures. Such approach can be used with programs like ANSYS, Nastran and Abaqus.

The current algorithm, used in the RFEM program, utilizes the first approach and for some input parameters too many iterations are required, which leads to long computing times. That is why the new algorithm was developed. The new algorithm, implemented in the RFEM program, combines advantages of previous two approaches mentioned above. These advantages are simplicity and speed of pre-processing and processing in the first approach and more accurate geometry in the second approach. This enables fast and accurate solution of pulleys using 1D elements.

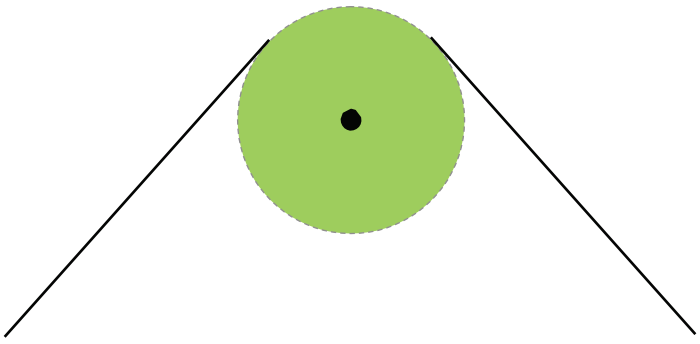

Fig. 3: New algorithm geometry

References

[1] cs.wikipedia.org, (2015). Pulley. (online) Available at: http://cs.wikipedia.org/wiki/Kladka#mediaviewer/File:Four_pulleys.svg (Accessed 6 Feb 2015).

[2] F. Ju and Y. Choo, Dynamic Analysis of Tower Cranes, Journal of Engineering Mechanics, 131 (2005) 88-96.

[3] F. Ju and Y. Choo, Super element approach to cable passing through multiple pulleys, International Journal of Solids and Structures, 42 (2005) 3533-3547.

Issue of Rigidity of the Ball Screw Nut Exposed to Bending Stress during Bending Stress of the Ball Screw

Lubomír W. Novotný[1,2,a,*], Jiří Marek[1,3,b], Tomáš Marek[1,c]

[1]VUT in Brno, UVSSaR Faculty of Mechanical Engineering, Technická 2896/2, 616 69 Brno

[2]TOSHULIN, a.s., Wolkerova 845, 768 24 Hulín, Czech Republic

[3]KSK-Kuřim, a.s., Blanenská 1277/37, 664 34 Kuřim, Czech Republic

[a]lubomir.novotny@toshulin.cz, [b]jiri.marek@ks-kurim.cz, [c]y116370@stud.fme.vutbr.cz

Keywords: geometric precision, ball screw, laser, FEM calculations, machine tools, machine tool axis, bending loading, nut

Abstract: Ball screws and nuts represent the inseparable part of machine-tool building. The thread lead accuracy ranges in hundredths of millimetres per 1 m. In addition to the undesirable phenomena caused by heat (dilatability) and, e. g., torsional and transverse oscillations, the bending stress of the ball screw is considerably undesirable too. This stress and at the same time behaviour are transferred to the bending stress of the ball screw nut. This has a very harmful influence on setting of the ball screws, when the machine tool is assembled. Using the analysis by means of the FEM method, the paper conducts a survey of deformation issue of the arrangement "machine – ball screw – ball screw nut" during the assembly stage as well as a survey of compensation possibilities and other technical measures determined to limit the undesirable deformations and stress of the ball screw originating already in the manufacturing stage of the machine tool.

Introduction

The ball screws and nuts are utilized at designing of machine tools [3] for transformation of the rotary motion to the translation motion. The machine tools represent precise manufacturing machineries which must comply with the dimensional and geometric requirements of the products and manufacturing technology.

According to the literature researches, the current knowledge level about internal kinematics and dynamics of the ball screws is not too large. It is limited predominantly on the description of the ball behaviour in the carrying part of the nut thread under the ideal geometric and loading conditions. At the current time the engineering designers and research workers dealing with the ball screws are interested in the contact tasks in the carrying part and their influence on the mechanism rigidity. For example, these issues have not been elaborated yet – the dynamic behaviour of the balls in the stage of their entering the thread and leaving the carrying part as well as the kinematic and dynamic behaviour of the balls in the transducer. Moreover, the coherence is not known with the processes taking place inside the nut and their external manifestations. The main aim of this analysis is to find the influence of the screw position towards the nut at the assembly of this design group. When the assembly is performed, the ball screw nut is bending-stressed, which is undesirable, and it is not known whether and how this stress is transferred and reflected in the assembled machine tool. The description and analysis of the issue contained in the text are the application issues which all manufacturers of machine tools are confronted with. Nevertheless, the authors do not know whether the issue has been already explored in the similar way.

Fig. 1 shows the design type execution of the drive for the linear motion axis [1]. The ball screw does not move and the nut is driven by the servomotor. The internal force effects – the force interaction among the screw, the nut and the balls can be expressed as the functional dependence. The contact relations and also the forces (force F_k) in the ball screw thread can be examined analytically or by means of the numerical methods (Fig. 2) [1]. Fig. 3 shows the dependence of the contact force (F_k) on the ball size (D_w) and the prestressing intensity (δ, i. e. at deformation loading) [1].

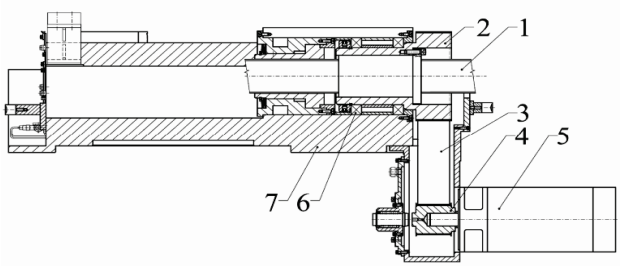

Fig. 1: Schema of the drive for the linear motion.

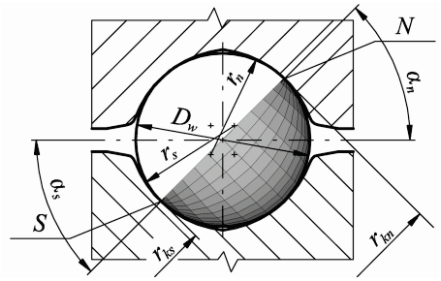

Fig. 2: Contact relations in the ball screw.

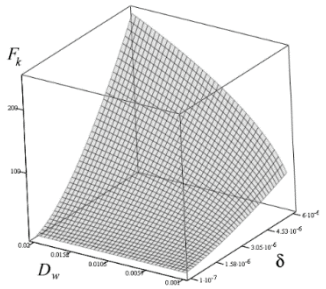

Fig. 3: Dependence of the contact force on the ball size and prestressing intensity.

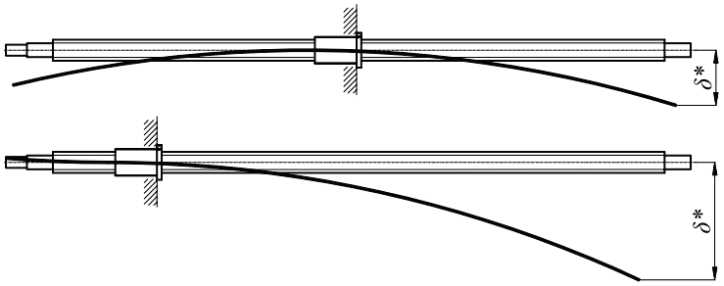

Fig. 4: Dependence of the screw deformations on the position of the nut.

Fig. 4 shows the situation which happens commonly at the machine-tool assembly. The ball screw nut is fixed with the frame through the flange. The ball screw (nut, this depends on the fact whether the screw or the nut can be rotated at the assembly) gets towards the screw from the middle position when the deformation (δ*) is the smallest (Fig. 4). If the nut is at the ball screw end, it is obvious that the screw deformations (δ*) are considerably bigger. When the assembly is performed incorrectly, these deformations are brought into the machine geometric inaccuracy and the brought bending stress of the ball screw nut reduces its service life. The nut service life can be calculated analytically [2]. However, as it is shown and the long-term observance of this issue, the theoretical values are not in accordance with the practical ones. The paper shows how the nut pliability can influence the paradoxical service life increase of the design group "ball screw and nut".

Summary

The paper shows that the way of calculation and external manifestations of the ball screw properties used in the text can be applied to the mechanism development as well as to the check of its operational condition at the machinery where it is used, i. e. at the machine tool. The numerical calculations show the behaviour of this motion mechanism (e. g. the nut pliability) which the analytical calculations are not able to catch (they are not able to work with it).

References

[1] L. Novotný, Analýza dějů v kuličkových šroubech a maticích. Brno: Vysoké učení technické v Brně, Fakulta strojního inženýrství, 2006.

[2] J. Marek, Modifikovaný výpočet životnosti kuličkového šroubu akceptující nepřesnosti vzniklé při jeho montáži. KSK Kuřim 2015, p. 8, číslo zprávy 25-2015/TOS.

[3] J. Marek, a kol., Designing of CNC Machine Tools III. 1st ed. Praha: MM publishing, 2014, 684 p. MM special edition. ISBN 978-80-260-6780-1.

21st International Conference **ENGINEERING MECHANICS 2015**
Svratka, Czech Republic, May 11 –14, 2015
Paper **#203, pp. 216–217**

Methodology of Geometry Testing and Measuring of Oversized Machine Tool Components and Their Verification Using the FEM Method

Lubomír W. Novotný[1,3,a]*, Oldřich Učeň[2,3,b]

[1]VUT in Brno, UVSSaR Faculty of Mechanical Engineering, Technická 2896/2, 616 69 Brno

[2]VŠB – TU Ostrava, Fakulta strojní, 17. listopadu 15, 708 33 Ostrava – Poruba

[3]TOSHULIN, a.s., Wolkerova 845, 768 24 Hulín, Czech Republic

[a]lubomir.novotny@toshulin.cz, [b]oldrich.ucen@toshulin.cz

Keywords: geometric precision, guideways, laser, FEM calculations, machine tools, machine tool frame, rotating screw

Abstract: The paper deals with the issue of geometric precision measuring at large parts (especially at castings having big dimensions) in their manufacturing stage. The large parts of machine-tool frames are required to have their geometric tolerances in thousandths of millimetres. The production or cooperation abilities of the particular company must be adapted to these demands and it is also necessary to adapt the company metrological equipment and measuring procedures to them. The standard measuring equipment cannot be used in most cases, because the particular parts are too large. For this reason, it is necessary to search such methods and procedures which enable to perform measuring with the relevant result. It could be considered to use e. g. 3D scanners. Unfortunately, their measuring precision has not reached the required tolerances up to now. For example, the HandyPROBE 3D scanner measures with the precision of 0,022 mm [1].

Introduction

The size of geometric tolerances can be presented on the example of the vertical machining centre column, see Fig. 1. The straightness tolerance is 0,005 mm and the flatness tolerance is 0,01 mm, when the guideways are approx. 2000 mm long.

To provide measuring of the column, the measuring methodology was elaborated by means of the available means and devices to enable the check of the ground guideways. The measuring jig was designed for measuring, this measuring jig has the basic carrying part which the holders are attached to. These holders are specified to fix the dial gauges. The carrying part has five tilting supports which are located in two rows and their spacing is 300 mm. When measuring is performed, the jig moves along the column and measuring is performed in steps by 300 mm.

Fig. 1: CAD model of column

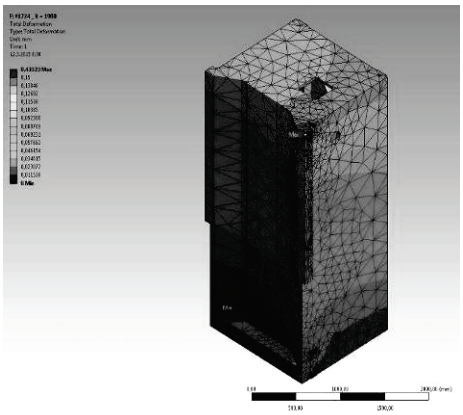

Fig. 2: Deformation of column

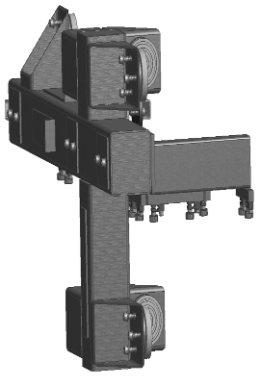

Fig. 3: Gauges holders

The jig slight turning in relation to the initial value is measured in the particular measuring positions by means of the laser and two water levels. The water levels and laser are located on the carrying part of the measuring jig. Using the values obtained in this way, it is possible to determine the shape of the column guideways which the tilting supports move along.

There are altogether 8 dial gauges located in the holders. These dial gauges are set to zero at the measuring beginning and they measure successively the profile of the column guideways, while the jig moves. The dial gauge zero setting is performed on the precise measuring plate so that perpendicularity and parallelity can be guaranteed in relation to the check plate. The values measured by means of the water levels and laser are added to the values measured by means of the dial gauges. The measured column can be also loaded statically and measuring can be performed at loading in the horizontal position as well as in the vertical position. The problems at these load tests consist in the fact that it is very difficult to deform the parts (to load them by force), when these parts are freely located on the floor, etc. (thus, if they are not assembled on the machine). On the contrary, when the parts are assembled in the machine frame, it is not possible to measure the deformations of the parts to the whole extent (one frame part always covers another frame part).

Summary

Measuring of the external impacts (machining accuracy, geometric precision, etc.) of the internal force effects at the machine-tool motion axes (moving of big masses) was implemented in dependence on the design made by the paper authors within the prototype tests, research and development activities of TOSHULIN, a. s company. Measuring was performed at those machines, where the authors participated by the FEM calculations (see Fig. 2) [2] and design work (design of the jig, etc.). E. g. at the machine with the rotating screw, the author created the just measured horizontal motion axis (X-axis), the whole machine frame and other functional units. Moreover, this machine also enables to influence the dynamic properties of the machine frame by utilization of the materials damping vibrations and noise, which is also based on the knowledge obtained at the research activity performed by TOSHULIN, a. s. company and on the experiments designed by the authors of this paper. The numerical simulation of this experiment is performed in [3].
The measured data (by measuring device, see Fig. 3) serve not only to provide the column check according to the manufacturing drawing but also to compare the calculated values by means of the FEM calculations. These calculations serve for the analysis of the machine behaviour as the whole unit as well as for the analysis of the particular parts of the future machine, which shall enable the precise and stable machining. The measured data serve to assess correlation with calculations. The modifications at grinding are also performed in accordance with the measuring data so that the better results can be reached at the geometric tolerances.

References

[1] Dotykové skenery CMM: Portable Coordinate Measuring Machine (CMM). [online]. [cit. 2015-03-13]. Available on: http://www.3d-skenovani.cz/dotykove-skenery-cmm.

[2] Deformace stojanů obráběcích center: Interní výzkumná zpráva H1415009. TOSHULIN, a.s. Hulín, 2014.

[3] J. Marek, et al., Konstrukce CNC obráběcích strojů III. 1. vydání. Praha: MM publishing, 2014, 684 s. MM speciál. ISBN 978-80-260-6780-1.

21st International Conference **ENGINEERING MECHANICS 2015**
Svratka, Czech Republic, May 11 –14, 2015
Paper **#060, pp. 218–219**

Reduction of Pneumatic Tyred Roller Fuel Consumption

Tomáš Panáček[1,a] *, Milan Klapka[2,b]

[1]Inst. of Machine and Industrial Design, BUT, Technická 2896/2, 616 69, Brno, Czech Republic

[2]Inst. of Automation and Computer Science, BUT, Technická 2896/2,
616 69, Brno, Czech Republic

[a]panacek@fme.vutbr.cz, [b]klapka.m@fme.vutbr.cz

Keywords: kinetic energy regeneration, numerical simulation, optimization, evolutionary algorithms

Abstract: This article deals with optimization of operational parameters of an energy regeneration module for a heavy vehicle. Recently there was developed energy regeneration module for a pneumatic tyred roller with hydrostatic drive. It was necessary to optimize its operational parameters to achieve good results in experimental tests on the actual vehicle. Optimization process was based on a numerical model of the vehicle using a parallelized modification of the differential evolution algorithm as an optimizer. Suggested parameter values were subsequently verified experimentally on the vehicle by analysis of the fuel consumption.

Introduction

In order to fully utilize the potential of the energy regeneration module [1] and considering the low operational speed of the vehicle, various operational parameters of the module – such as timing of control processes or the pressures in accumulators – needed to be optimized. A lumped parameter numerical model tyred roller created in Matlab was used for simulation of vehicle operation [2]. Concurrently, the differential evolution algorithm was applied for optimization of the operational parameters of the energy regeneration module.

Fig. 1: Energy regeneration module prototype mounted to the vehicle

Optimization

One iteration of optimization consists of two stages. The first stage ensures proper setting of initial conditions for assessment of total fuel consumption through the second stage of simulation.

The input parameters were

$$\boldsymbol{x} = (p_{acH0};\ p_{acHAccelStop}; T_{HM}; R_{HM}). \tag{1}$$

The objective function is defined as follows:

$$f(\boldsymbol{x}) = \frac{q}{s}\ , \tag{2}$$

where q [g] is the total mass of fuel consumed through second stage of simulation and s [m] is the distance driven by the vehicle by defined conditions.

The asynchronous parallel optimizer [3] (based on the differential evolution algorithm [4]) was applied to minimize the objective function (2). The optimizer is implemented outside Matlab/Simulink platform using the simulation model in Matlab/Simulink to evaluate the objective function.

Optimization process and results

Several operational modes of the vehicle drive were optimized. The default operational mode (*Free Run*) is without active regeneration. The other two modes utilize the energy regeneration module: deceleration with energy regeneration enabled (*Decel*) and acceleration of the vehicle with the use of the energy stored (*Accel*).

Utilizing the optimizer the fuel consumption of the vehicle was reduced from 2.76 g/m of fuel to 2.54 g/m (by 7.97 %) while maintaining the performance of the vehicle (see Fig. 2) during simulation.

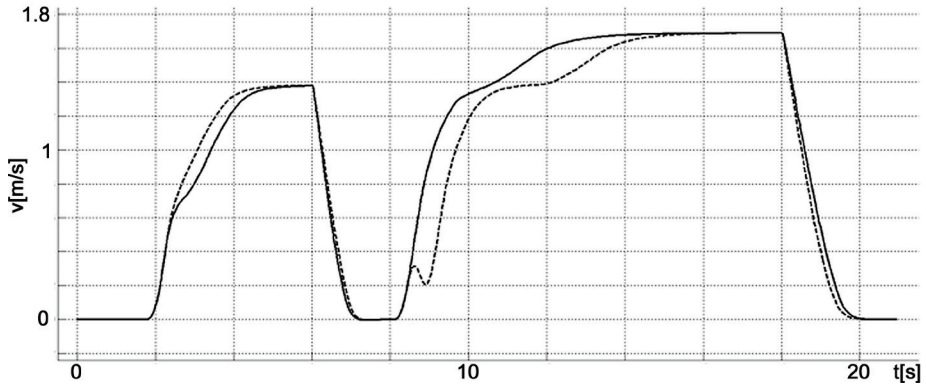

Fig. 2: Time response of the vehicle speed with default setting of the regeneration module (dashed) and optimized setting (full line)

Conclusions

The optimizer was used with the simulation model of the vehicle. The results of the optimization process suggested the settings of the operational parameters of the energy regeneration module on the vehicle. These settings need to be experimentally verified by driving the vehicle. Although there are expected some limitations of suggested settings beyond the capability of the control system of the vehicle, there is good potential for further lowering the fuel consumption and increasing the efficiency of the regeneration process as verified by a preliminary driving test.

Acknowledgement: The results of this project NETME CENTRE PLUS (LO1202) were obtained with the financial support of the Ministry of Education, Youth and Sports under the „National Sustainability Programme I" and with support of the of the BUT grant nr. FSI-S-14-2329.

References

[1] Z. Němec, J. Nevrlý, Influence of Short-circuit Valve on Hydraulic Recovery of Vehicle Kinetic Energy. In 55th Int. Conf. of Machine Design Departements. Praha, ČVUT, 239 – 244, 2014.

[2] J. Nevrlý, Z. Němec, P. Noskievič, Use of Matlab/Simulink and Amesim for simulation of hydraulic recovery of kinetic energy. In Proceedings of The 4th International conference ANTiM, University „UNION – Nikola Tesla", Belgrade, Serbia, 2014.

[3] T. Panáček, M. Klapka, Z. Němec, Optimization of valve manifold timing sequence using differential evolution algorithm. In Engineering mechanics 2014, Book of full texts. Prague: Institute of Termomechanics, Academy of Sciences of the CR, 2014, 468-471, 2014.

[4] R. Storn, Differential Evolution for Continuous Function Optimization [online] (cit. 2.8.2013). Available on http://www.icsi.berkeley.edu/~storn/code.html.

21st International Conference **ENGINEERING MECHANICS 2015**
Svratka, Czech Republic, May 11 –14, 2015
Paper **#133, pp. 220–221**

Parallel Solver for Large Thermo-Elasto-Plastic Finite Element Problems

Petr Pařík

Institute of Thermomechanics, AS CR, Dolejškova 1402/5, 182 00 Prague 8, Czech Republic

parik@it.cas.cz

Keywords: sparse direct solver, finite element method

Abstract: The article deals with the implementation and verification of a numerical solver for large heat transfer problems in the context of the finite element analysis. Large problems are defined as problems whose solution on contemporary computers is computationally difficult. The solver builds on the numerical methods for an efficient direct solution of large linear elastostatic problems, developed in earlier works. The solver is integrated within our in-house finite element code PMD. Verification is carried out on several large thermo-elasto-plastic problems from real-world engineering practice.

Introduction

Direct solution methods [1] are particularly important in the Finite Element Method (FEM) [2] since they enable the factorization (the most time demanding part of the solution) to be performed only once for a given problem and subsequently to solve it for any number of right-hand sides (load cases), which is especially useful in complex problems (thermo-elasto-plastic, dynamic, etc.).

The presented approach to an efficient implementation of a sparse direct solver focuses on minimizing the required amount of both the storage space and the computational time required for the direct solution of a large problem. This is achieved particularly by using a modified minimum ordering algorithm to reduce the fill-in, therefore, reducing the number of numerical operations needed to compute the solution [3]. Both the factorization and the substitution algorithms are parallelized to fully exploit today's multi-core and multi-processor computers. The global coefficient matrix is assembled and stored in-core throughout the computation, using an efficient sparse matrix storage format. Although that leads to considerably high memory requirements, in practice, it does not present a significant problem for today's computers. The finite element Fortran code PMD [4] is used as the framework for the presented implementation of a sparse direct solver.

Problem formulation

The solution of a linear equation system can be written in the matrix form simply as

$$\mathbf{A}\mathbf{x} = \mathbf{b}, \tag{1}$$

where **A** is the coefficient matrix, **x** is the unknown solution vector and **b** is the righ-hand side vector. In solid continuum mechanics, **A** may refer to the stiffness or conductivity matrix, **x** to the displacement or temperature vector, and **b** to the external loading forces or thermal loading.

Moreover, especially in the context of FEM, a single problem almost always needs to be solved for many right-hand sides (load cases), thus, vectors **x** and **b** in Eq. 1 actually become matrices. Furthermore, the global coefficient matrix **A** obtained from the finite element discretization is singular, therefore, equation system Eq. 1 cannot be solved unless boundary conditions, which are a part of the finite element problem formulation, are taken into account.

For a complete solution of a combined thermo-elasto-plastic problem, iterative non-linear numerical solution methods are needed [2]. From the computational point of view, they involve matrix-vector and vector-vector operations that are however not as computationally intensive as the underlying solution of linear equation system, which plays major part in each iteration.

Results

In Table 1, selected largest computed problems are listed along with their order n (number of unknowns), block-order N (number of diagonal blocks), frontwidth n_{fw}, number of nonzero matrix blocks N_{nz} and number of nonzero matrix elements n_{nz}.

Computational times are presented in Table 2, where the sparse direct solver clearly demonstrates its efficiency over the existing frontal solver.

Table 1: Test problems‘ parameters.

Problem no.	n	N	n_{fw}	N_{nz}	n_{nz}
1	1,129,747	257,861	7,582	13,548,221	216,454,160
2	1,739,211	579,737	4,719	124,138,819	1,115,504,693
3	1,909,577	439,287	5,214	29,584,204	484,886,739
4	1,973,550	657,85	12,873	218,994,791	1,968,939,519
5	2,858,631	952,877	18,828	667,395,241	6,003,699,588
6	3,022,848	695,05	11,342	65,174,392	1,063,250,512

Table 2: Solution time for test problems.

Problem no.	Frontal solver [hrs]	Sparse direct solver [min]
1	4.49	17
2	3.56	49
3	4.12	47
4	22.38	115
5	> 99.99	253
6	17.17	120

Conclusion

A distinct approach to the direct solution of large thermo-elasto-plastic problems was presented. Efficient sparse matrix storage and necessary algorithms were implemented into a sparse direct solver, which was thoroughly tested on real-world engineering problems from solid continuum mechanics. The results obtained from the numerical tests confirmed the solver's efficiency and scalability. High memory requirements of the solver were anticipated and will present gradually less a problem with the ever-increasing capacity of computers.

The potential of the implemented sparse direct solver is fully utilized within the solution procedures for nonlinear heat transfer and inelastic finite element problems.

Acknowledgement: The work was supported by TA CR project No. TH01010772 within the institutional support RVO 61388998.

References

[1] A. George, J.W.H. Liu, Computer solution of large sparse positive definite systems, Prentice-Hall, Englewood Cliffs, NJ, 1981.

[2] K.J. Bathe, Finite Element Procedures, Prentice-Hall, Upper Saddle River, NJ, 1996.

[3] P. Pařík, An out-of core sparse direct solver for large finite element problems, CTU reports Vol. 1 No. 15, Czech Technical University Press, Prague, 2011.

[4] PMD version 11.0, information on http://www.pmd-fem.com/

21st International Conference **ENGINEERING MECHANICS 2015**
Svratka, Czech Republic, May 11 –14, 2015
Paper **#007, pp. 222–223**

Development of Technology of Controlled Wave Effects on Low-Carbon Array

Michail V. Pavlenko

University of Science and Technology «MISIS», Department of «TB and GD».
Leninsky Ave 6, 119991 Moscow

mihail_mggy@mail.ru

Keywords: methane, vibration effect, frequency, the array effect, well array, technology

Abstract: The coal production in low-permeability gas-bearing coal seams brings the problems with advance methane recovery from coal array to reduce gas emission in a goaf.

Technology of advance methane recovery from low-permeability coal array aimed at improving safety in coal mines. This stimulates the development of new technology methods improving the properties and state of the environment.

Given the great heterogeneity of the coal properties of the array and the complexity of the exposure active, effective effort is possible only through a series of sequential engineering impacts.

Technology of underground coal array involves solution of the problem of effective management of gassing using vibration and reservoir wells. In this regard, the proposed technological scheme of methane recovery is designed with consideration of the conditions of occurrence of the layer and the desired level of reduction of natural recoil of methane,

To solve this problem, the proposed technology managed wave action, which provides an intensive extraction of methane gas from the low-permeability coal array at the stage of preparation of the reservoir to the hollow.

Introduction

In the activities aiming at improving safety and working conditions in coal mines, there is a need to develop new ways to manage the properties and state of the environment.

The development of research on vibration exposure stimulated interest in doing experiments in the laboratory and field experiments on the mine field.

Results studies and generalizations

Given the great heterogeneity of the data requirements and complexity properties of coal-bearing strata, effective control is possible only through a series of sequential engineering impacts, and until, as happened unloading coal strata, and was found to be the sources of free gas [1].

Technology of underground coal array involves the solution of the problem of effective management of gassing the use of wave action, and wells drilled both from the surface and from underground workings.

In this regard, the technological scheme (Fig.1.) and methods for determining the parameters of methane designed with mining and geological conditions of occurrence of the layer and the desired level of reduction of natural gas ampleness.

However, there is a common origin in engineering means to control gas in coal mines. This General principle is the need to ensure access to remote areas of coal-bearing strata and increase gas recoil from coal seams that it is important to perform the specified engineering solutions.

Because such training is conducted in advance to conduct mining operations or, at least, to conduct experimental work, engineering construction, which enables the preparation may also be a well drilled from the surface [2].

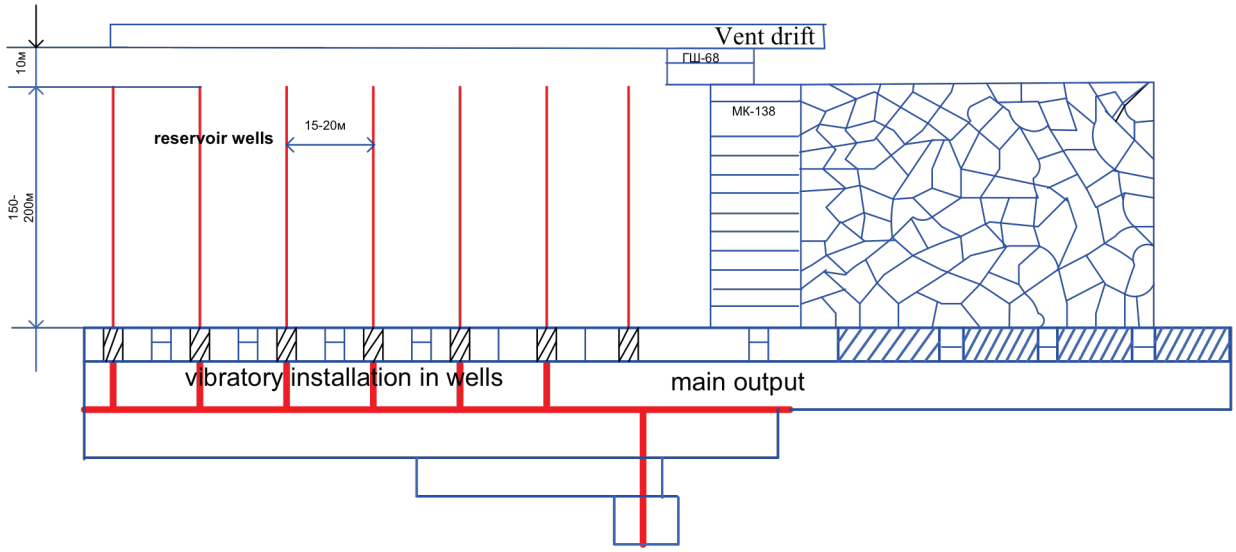

Fig. 1: Technological scheme vibration through underground wells

Development of variants of technological schemes of preparation of a mine field is reduced to drawing up sequence, the combination of influences: drilling method and location of wells, the number of pumped liquid, the exposure time, the required level of reduction of gas-bearing reservoir. So many variants of technological chains, qualitatively different at any stage of the impact, is the set of estimated technological options.

When choosing the method and scheme of complex processing of coal seam occurs the necessity of several competing variants of diversity training array. When choosing the method and circuit of the integrated effect probable cases when you will be limited to one option. The specific option scheme of complex processing of a mine field for safe and efficient testing is based not only on the General principle of selection of the determining factors, but also largely determines the type of work undertaken equipment and significant factors.

To solve this problem is developed and tested on a number of mines the new method is a method of vibration on gas-saturated coal array in order to intensify gas emissions from coal-fired array and its subsequent removal by means of degassing to reduce the concentration of methane in the atmosphere workings [3].

Conclusion

The decrease in methane content coal array is achieved in the process of vibration amplifying diffusion processes, which provide a reduction in the natural the methane content part of the coal seam, increase the filtering process gas from remote areas of the array.

The developed technology of vibration exposure allows you to reduce methane in the mine workings in the impact zone.

References

[1] M.V. Pavlenko, A.L. Kolosov, A. L. Sambursky, The vibration exciter of vibrations as an effective impact on coal array GORN.-M.: Moscow state mining University. 2001.-№ 6, 2001..

[2] M.V. Pavlenko, N.A. Desyaterik, C.D. Rozhon, Vibration impacts on low-permeability coal seam with the aim of changing its state GORN.-M.: Moscow state mining University №. 7, 2001.

[3] A.I. Panisko, C.D. Rozhon, M.V. Pavlenko, Study of the process of methane output from coal mass at vibrohvostami GORN. -M.: Moscow state mining University. - No. 8.1999.

21st International Conference **ENGINEERING MECHANICS 2015**
Svratka, Czech Republic, May 11 –14, 2015
Paper **#006, pp. 224–225**

Acoustic Standing Waves in Primary Circuit of NPPs with WWER 1000 MW

Ladislav Pečínka[a]*, Miroslav Švrček[b]

ÚJV Řež, a. s., Hlavní 130, 250 68 Husinec - Řež, Czech Republic

[a]ladislav.pecinka@ujv.cz, [b]miroslav.svrcek@ujv.cz,

Keywords: acoustic, standing waves, primary circuit, WWER 1000 MW, Whittaker method

Abstract: Acoustic standing waves in primary circuit of the NPPs with WWER 1000 MW reactor is possible classify as in whole primary circuit or only in reactor pressure vessel with partial penetration in the hot leg. Typical feature of these waves is the dependence on the coolant temperature which increase or decrease during increasing or decreasing of the reactor power. Exact solution of the eigenvalue problem represents the six order determinant. The first (lowest) frequency is influenced by the water volume in the pressurizer. To obtain the analytical solution the Whittaker method is applied to the original six order determinant. As the result we obtain the two order one and finally the very simply but exact equation is obtained.

Introduction

Acoustic standing waves represent special type of exciting forces acting on the reactor internals. As a important part of the reactor diagnostic this ones are detected using installed pressure sensors on the cold and hot legs. To explain some specific features of this phenomenon basic theory is derived and numerical results presented.

Basic theory

Simplified schema of the loop with pressurizer is illustrated in the Fig.1. In the upper part of the reactor pressure vessel is supposed small volume of steam. In normal operation conditions in pressurizer is certain volume of coolant and above is the steam. The height of the coolant volume depend on the coolant temperature and as the result the value of first acoustic frequency changed. The same is valid for steam volume in reactor pressure vessel.

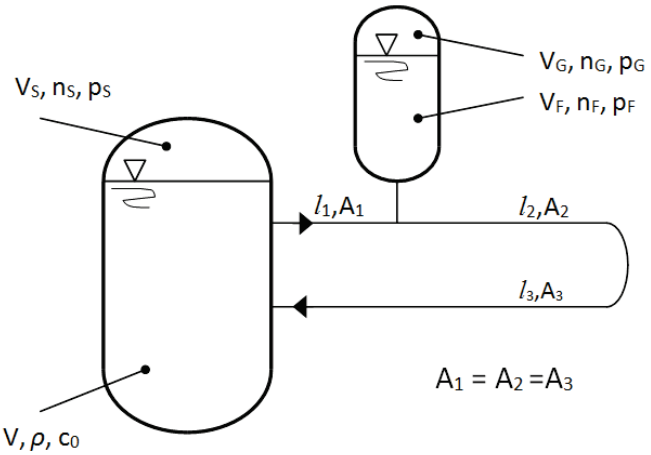

Fig.1: Scheme of the loop with pressurizer

The basic theory is published in paper [1], resulting determinant of the system of equations takes the form:

$$0 = \begin{vmatrix} \cos\frac{\Omega_n l_1}{c_0} & \sin\frac{\Omega_n l_n}{c_0} & -\frac{A_2}{A} & 0 & -1 & 0 \\ -\sin\frac{\Omega_n l_1}{c_0} & \cos\frac{\Omega_n l_1}{c_0} & 0 & -1 & 0 & 0 \\ 0 & 0 & \cos\frac{\Omega_n l_2}{c_0} & \sin\frac{\Omega_n l_2}{c_0} & 0 & -1 \\ 0 & 0 & -\sin\frac{\Omega_n l_2}{c_0} & \cos\frac{\Omega_n l_2}{c_0} & 0 & -\frac{A_2}{c_0\rho(\frac{V_G}{n_G P_G}+\frac{V_f}{c_0\rho})\Omega_n} \\ -1 & \frac{1}{A}(\frac{V}{c_0}+\frac{\rho c_0 V_s}{n_s p_s})\Omega_n & 0 & \sin\frac{\Omega_n l_3}{c_0} & \cos\frac{\Omega_n l_3}{c_0} & 0 \\ 0 & -1 & 0 & \cos\frac{\Omega_n l_3}{c_0} & -\sin\frac{\Omega_n l_3}{c_0} & 0 \end{vmatrix} \quad (1)$$

For assessment of first (lowest) frequency it is realistic to suppose $l_1 \doteq 0$. After application of the Whittaker method t we obtainas the resul the two order determinant and the resulting equation

$$f_1 = \frac{1}{2\pi}\sqrt{\frac{1}{\frac{\rho l_2}{A_2}+\frac{\rho l_1}{A_1}}\left(\frac{1}{\left(\frac{V_g}{n_G p_G}+\frac{V_f}{\rho c_0^2}\right)}+\frac{1}{\left(\frac{V_S}{n_S p_S}+\frac{V+A_3 l_3}{\rho c_0^2}\right)}\right)} \quad (2)$$

First term in the bracket represents influence of the pressurizer and second one the influence of steam in reactor pressure vessel.

Numerical results

The input data in normal operation conditions are as followes

$V = 148.3 m^3$; $V_f = 55 m^3$; $V_g = 24 m^3$

$l_1 = 6.86$ m; $l_2 = 25.1$ m; $l_3 = 53.39$ m;

$A_1 = 0.567 m^2$; $A_2 = 0.094 m^2$;

Results of numerical calculations are illustrated in tables 1 and 2

Table 1: Influence of increasing water volume in pressurizes

$V_s[m^3]$	55	60	65	70	75	79
f [Hz]	0.76	0.768	0.792	0.836	0.937	1.23

Table 2: Influence of steam in % of V in reactor pressure vessel

V_s[%]	0.1	0.5	2	4	6	8	10
f_1 [Hz]	0.751	0.724	0.647	0.585	0.543	0.514	0.49

Summary

Theoretical analysis of the acoustic pressure pulsations has been performed. Eigenvalues of the six order determinant represent frequency spectrum of this problem. Special attention has been paid to obtain the lowest eigenfrequency. Simple formula has been derived. Using numerical sensitivity analysis we can conclude that this one represent diagnostic symptom describing upset operation states of the primary circuit.

References

[1] L. Pečínka, Exact Solution of the coolant Resonant States in the Primary Circuit of the Reactor, Dynamic of Machines, National Colloquium with International. Participation, February 7-8,2006, Prague, in Czech Language only

21st International Conference **ENGINEERING MECHANICS 2015**
Svratka, Czech Republic, May 11 –14, 2015
Paper **#122, pp. 226–227**

Mars Probe Soft Landing Test in the Earth Conditions

Jan Pejchar[a], Miloš Daniel[b], Robert Popela[c]

Institute of Aerospace Engineering, Brno University of Technology, Czech Republic

[a]pejchar@fme.vutbr.cz, [b]daniel@fme.vutbr.cz, [c]popela@fme.vutbr.cz

Keywords: the Mars, interplanetary probe, soft landing, ballistic recovery system, probe subscale model

Abstract: Presented paper informs about the FP7 project SPARTAN (SPAce exploration Research for Throttleable Advanced eNgine) that is mainly dedicated to design and develop high efficient and green propellant propulsion technology based on using hybrid fuel rocket engines. This technology is needed for further space exploration and precise landing on any planet surface in the solar system. This article pays particular attention to the SPARTAN Lander, which demonstrates developed technology capability in the Earth conditions. The article contains aerodynamic shape study, subscale model free fall testing and ballistic recovery system design and testing.

Introduction

Soft landing ability, with the payload that cannot withstand heavy impact load and should be smoothly delivered onto precisely selected place on the extraterrestrial bodies without or with low atmosphere density, is the key technology for future manned and unmanned missions.

European Space Agency established the project "View on The Long-Term International Scenario for Space Exploration" [1]. There is disclosed an intention for manned and future early robotic preparatory exploring missions towards the Moon and the Mars. In response to ESA exploration plans, the FP7 project SPARTAN (SPACE exploration Research for Throttleable Advanced eNgine, SPACE SPA.2010.2.1-04 GA n. 262837) was established. The main aim of the project is to design fully throttleable engines for soft planetary landing by using the hybrid fuel rocket engines technology. It allows smoother and wider throttle range in comparison to solid rocket engines, which are intrinsically simpler, safer and able to use green propellants in comparison to liquid powered rocket engines.

Since 2010, when project started, Lander demonstrator structure has been designed and manufactured as well as its internal structure and driving systems. During autumn 2014 the project reached the final phase and recently is facing the last challenge, i.e. the full scale test. The full scale soft landing test serves as verification of the development process of the entire series of preparatory tests. The whole system has to work as one unit which contains the newly designed engines commanded by On Board Computer (OBC) algorithms according to data from the Guidance and Navigation Center (GNC) in order to smoothly touch down on the ground by Landing gear.

The full scale test conditions are derived from the planet Mars requirements and adjusted by the Earth and the Mars mass ratio. The test is dedicated to the last phase of landing, when Lander has already passed Mars upper atmosphere layers, pilot parachute has deployed and Lander is steadily descending towards the ground. Lander releases the main parachute and decelerates to 30 m/s (for atmosphere average density on the ground $\sim$0.020 kg/m3 [2] and Lander weight 1000 kg). In precise altitude, above the ground, the thrusters are fired and decelerate the Lander up to zero velocity at 0.5 m above the ground where they are turned off.

Full scale test starts with Helicopter hovering when demonstrator hangs in altitude 220 m above the ground and is subsequently released. Lander descents 50 m by free fall and reaches velocity 30 m/s. At this moment the thrusters are fired and throttled due to the GNC and OBC commands. Lander decelerates up to 0.2 m above the ground and engines are turned off. Impact energy is damped by landing gear.

Lander demonstrator

Lander demonstrator was designed with respect to planned mission. Its shape and overall design is based on mechanical and aerodynamic study and corresponds with ordinary designs of extraterrestrial probes and satellites. Lander body has a shape of octagon truncated pyramid where each vertex contains landing gear hinge.

Designed shape was carefully analyzed by CFD. The main purpose was to check an aerodynamic derivation what shows lander free fall phase stability or possibility of spin and fail. This critical topic was further investigated and subscale model was tested in free fall phase.

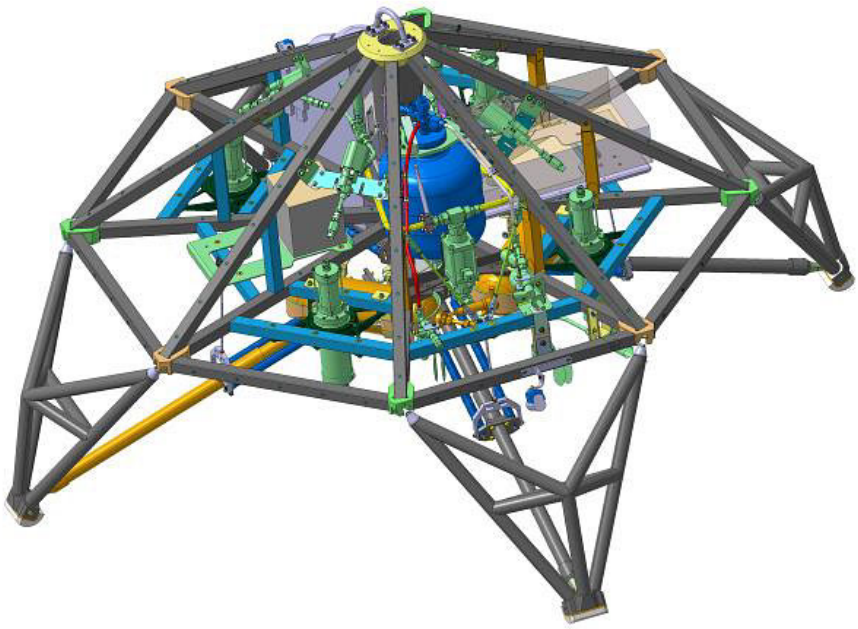

Fig. 1: Lander demonstrator design

References

[1] The NASA-ESA Comparative Architecture Assessment, [online], [ref. 2014-09-18], available from: http://www.nasa.gov/pdf/259237main_NASA_ESA_CAA-Report.pdf .

[2] Mars/Earth Comparison, [online], [ref. 2014-09-19], available from: http://nssdc.gsfc.nasa.gov/planetary/factsheet/marsfact.html

[3] GRS 3/ 450 datasheet, [online], [ref. 2014-09-20], available from: http://www.galaxysky.cz/grs-450-472-5-p17-cz .

[4] M. George, E. Kisiellowski, D.S. Douglas, Investigation of the downwash environment generated by V/STOL aircraft operating in the ground effect. USAAVLABS technical report 68–52 1968.

[5] Pyro actuators datasheet [online], [ref. 2014-09-20], available from: http://www.iss-cz.com/default/view?language=en&pageId=34 .

[6] Ch. Wolowicz, J. Bowman, W. Gilbert, Similitude requirements and scaling relationship as applied to model testing, NASA technical paper 1435, 1979.

21st International Conference **ENGINEERING MECHANICS 2015**
Svratka, Czech Republic, May 11 –14, 2015
Paper **#214, pp. 228–229**

Micromechanical Homogenization of Ultra-High Performance Concrete

Veronika Petráňová[a]*, Sajdlová Tereza[b], Němeček Jiří[c]

[1]Czech Technical University in Prague, Department of Mechanics, Faculty of Civil Engineering, Thákurova 7, 166 29 Prague 6, Czech Republic

[a]veronika.petranova@fsv.cvut.cz, [b]tereza.sajdlova@fsv.cvut.cz, [c]jiri.nemecek@fsv.cvut.cz

Keywords: UHPC, effective elastic properties, SEM, nanoindentation, Mori -Tanaka

Abstract: Mechanical properties and durability of Ultra-High Performance Concretes (UHPC) are closely associated with composition and microstructure of tested samples. In this work, determination of effective elastic properties of UHPC composite was performed for a representative volume element using combination of microstructural investigations (scanning electron microscope imaging, image analysis of back scattered electron micrographs and nanoindentation) and analytical methods of micromechanics. Based on the volumetric content and micromechanical behavior of individual components an effective elastic modulus of the whole composite was predicted and compared with macroscopically measured value with good agreement.

Introduction

Ultra-High Performance Concrete (UHPC) widely used in building industry represents promising material with excellent durability and mechanical properties. Depending on final application UHPC can be designed by mixing of common raw materials (cement, water and aggregates, plasticizer), reactive powder (e.g. microsilica) and/or small fiber reinforcement improving material parameters in addition. Properties of concrete are commonly assessed from macroscopic point of view, nevertheless, its mechanical behavior is related to its composition and microstructure. Overall mechanical behavior of a heterogeneous material including concrete can be best calculated from measured data on individual phases, their volume fractions and possible interphase interactions. For this task, description of individual UHPC components and their micromechanical characterization can be performed using, e.g., scanning electron microscopy (SEM) equipped with energy dispersive X-ray detector (EDX) and nanoindentation. To determine the effective properties of the concrete sample in a statistical sense homogenization of phase properties from a representative volume element (RVE) involving all the material phases in a sufficient content can be performed with the aid of micromechanics [1,2]. In this paper, we evaluated the effective elastic properties of UHPC containing microsilica and steel fibers using homogenization based on Mori-Tanaka method.

Materials and methods

Phase detection and volume content of the phases was performed on a polished cross section (2.2 cm^2) of UHPC with SEM Mira II LMU (Tescan corp., Brno) equipped with energy dispersive X-ray detector (Bruker corp., Berlin). The content of individual phases in concrete was calculated using Image processing toolbox in MATLAB. Elastic material constants were determined with nanoindenter Nanohardness tester (CSM Instruments) in micrometer scale. Overall elastic stiffness of the composite was estimated assuming spherical inclusion geometry and perfect bond of the phases at the microscale with the Mori-Tanaka homogenization scheme. The resulting effective Young´s modulus was compared with experimental values measured on macroscopic laboratory specimens (100x100x400 mm) with impulse excitation method.

Results

Based on image analysis of BSE micrographs the major phases in concrete were basalt aggregates with grain size ranging from 5 mm to 300 μm, aluminosilicate binder (mainly calcium-silica hydrates and unhydrated clinker), steel fibers and pores. Classification of individual phases and their ratios were determined by means of BSE intensity level image analysis. The aggregate was found to have mineralogically heterogeneous microstructure (composed of apatite, magnetite, olivine and feldspar) and was homogenized separately from the rest of the phases.

Cementitious composite are often characterized with the weak interfacial zones (ITZ) between matrix and aggregate. This is not the case of the UHPC sample where virtually no ITZ was detected by SEM and nanoindentation as a possible result of low water/binder ratio and presence of microsilica in the composition. The results of the image analysis and a two-step homogenization (step 1 = homogenization of aggregate, step 2 = homogenization of other composite phases) are summarized in Tab. 1.

Table 1: UHPC composition based on image analysis, elastic moduli of individual phases from nanoindentation and effective values of composite elastic modulus.

Phase	Phase content [%]	Elastic modulus [GPa]	Poisson's ratio	Effective elastic modulus [GPa]
Aggregate (composed of apatite, magnetite, olivine, feldspar and pores in aggregate)	37.5	131.3*	0.2	46.6
Binder (incl. clinker and microsilica)	57.9	29.4†	0.2	
Pores (in cement matrix)	2.8	0	0	
Fibers	2	200	0.3	

*value from nanoindentation on individual phases and homogenized (step 1), †from nanoindentation

Summary

Combination of image analysis and analytical homogenization was used to estimate effective elastic modulus of a heterogeneous UHPC sample. The homogenized sample Young's modulus was assessed as 46.6 GPa. The value is generally in accordance with the value measured on laboratory specimens with the impulse excitation method which gives dynamic elastic modulus (51 GPa). The small discrepancy between the values can be caused by dissimilar testing methods. Dynamic methods are known to give higher elastic moduli compared to static tests (which is the case of nanoindentation). The other possible reason lies in not exact representativeness of the area scanned in image analysis causing underestimation of the real volumetric content of some phases (especially large aggregate volume). The image analysis could be refined by an extension of the analyzed area.

Acknowledgement: Financial support of the Czech Science Foundation (project 14-19561S and P105/12/G059) and the Grant Agency of the Czech Technical University in Prague (SGS14/121/OHK1/2T/11) is gratefully acknowledged.

References

[1] J. Němeček, V. Králík, J. Vondřejc, Micromechanical analysis of heterogeneous structural materials, Cem. Con. Res. 36 (2013) 85–92.

[2] L. Sorelli, G. Constantinides, F.J. Ulm, F. Toutlemonde, The nano-mechanical signature of Ultra High Performance Concrete by statistical nanoindentation techniques. Cem. Con. Res. 38 (2008) 1447–1456.

21st International Conference **ENGINEERING MECHANICS 2015**
Svratka, Czech Republic, May 11 –14, 2015
Paper **#048, pp. 230–231**

Stability of Stainless Steel Prestressed Stayed Columns

Radek Pichal[a] *, Josef Machacek[b]

Czech Technical University in Prague, Faculty of Civil Engineering
Thakurova 7, 166 29 Prague, Czech Republic

[a]radek.pichal@fsv.cvut.cz, [b]machacek@fsv.cvut.cz

Keywords: cable supported structure, cross-arm, linear analysis, nonlinear analysis, stability, stainless steel, stayed column, 3d analysis

Abstract: The paper deals with extremely slender stainless steel columns reinforced for stability by prestressed cable stays running over one central crossarm. Such columns, with the un-stayed slenderness L/r round about 300, are more and more used as the attractive exterior supports of important structures. The structural arrangement can vary according to number of stays, number of cross arms, material of structural elements etc. While some linear bifurcation 2D stability analysis (LBA) and geometrically nonlinear elastic analysis with imperfections (GNIA) were published in the years past, 3D analysis for specific boundary conditions and stainless steel were not published. The brief summary of tests with stainless steel stayed elements performed recently at the laboratory of CTU in Prague is presented. The main part of the paper describes 3D stability analysis of unstayed and prestressed stayed columns as the first part of envisaged research concerning 3D materially and geometrically nonlinear analysis with imperfections (GMNIA) to analyze the test results. FE 3D models of LBA using prestressed stays preventing any compression force are used and optimal prestressing analyzed to receive the maximal critical buckling loading. In the conclusion the comparison with tests is provided.

Tests and numerical results

Tests. The three stayed columns of 1.4301 grade stainless steel acc. to Fig. 1 were tested under various prestressing. The column and crossarms were circular tubes Ø 50.0x2.0 – 5000 and Ø 25.0x1.5-(2x250) [mm], respectively. Macalloy cables of Ø 4 mm (sliding on the cross bars) were prestressed to give the required prestress. Initial and progress deflections were measured using potentiometers and 3D scanning [1]. The collapse loads in Fig. 1 were assessed from enormous deflections, while the buckling load $N_{cr.max}$ = 27.4 kN corresponds to 3D linear buckling analysis.

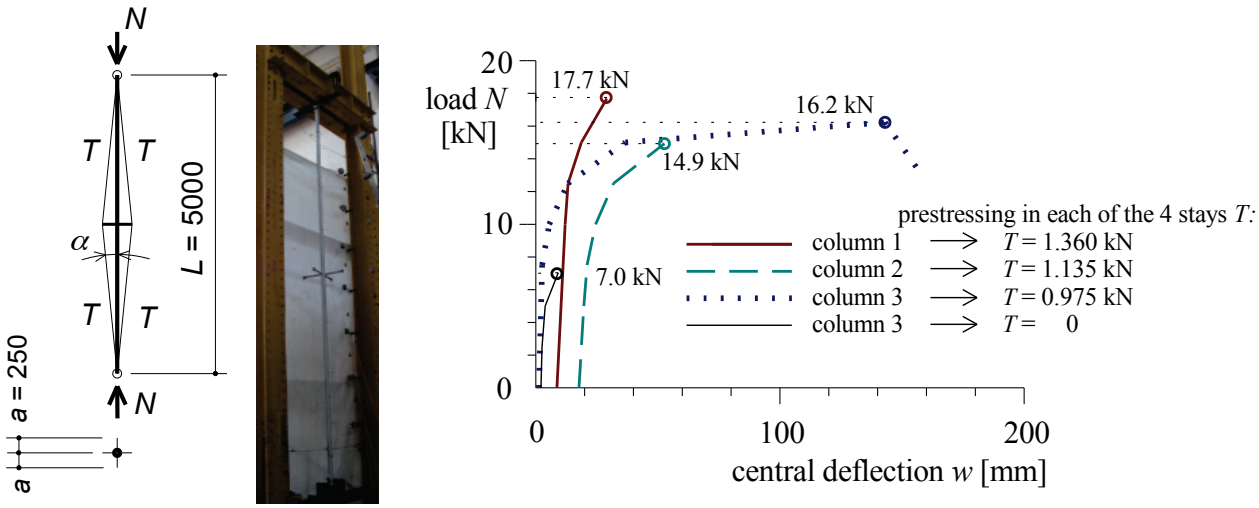

Fig. 1: Test layout and load-deflection relationship

The amplitudes of initial deflections (with shapes approaching to half sine wave) of the columns 1, 2 and 3 were 8.5 mm (i.e. $L/588$), 18.4 mm (i.e $L/272$) and 1.6 mm (i.e. $L/3125$) respectively. At collapse the deflection modes were symmetrical.

3D stability analysis. Euler's critical load of the tested column without prestressing (linearized E = 200 GPa, I = 87010 mm^4, L = 5000 mm) is $F_E = F_{cr,1}$ = 6.87 kN, the second critical load $F_{cr,2}$ = 27.48 kN. Analytical formulas based on elastic behavior, hinged joints of stays to crossarms and buckling in the plane of the crossarm member [2] give T_{min} (total pretension of stays small enough for buckling load equal to Euler load) and T_{opt} (total pretension of stays giving maximal buckling load $N_{cr,max}$). Based on axial (K_c, K_{ca}, K_s) and bending (B_c, B_{ca}, 0) stiffnesses of the column, crossarm and stay, the values are:

$$T_{min} = C_1 N_E = \frac{\cos\alpha}{2K_c\left(\frac{1}{K_s}+\frac{2\sin^2\alpha}{K_{ca}}+\frac{2\cos^2\alpha}{K_c}\right)} N_E = 0.0354 \cdot 6.87 \cdot 10^3 = 0.24 \cdot 10^3 \text{ N} \quad (1)$$

$$N_{cr,max} = \frac{(kl)^2 E_c I_c}{(L/2)^2} = \frac{(3.635)^2 \cdot 2 \cdot 10^5 \cdot 87009.6}{2500^2} = 36.79 \cdot 10^3 \text{ N} \quad (2)$$

$$T_{opt} = C_1 N_{cr,max} = 0.0354 \cdot 36{,}79 \cdot 10^3 = 1.30 \cdot 10^3 \text{ N} \quad (3)$$

in which symmetrical mode of buckling acc. [2] gives (kl) = 3.78 and predominant asymmetrical one - on the contrary to tests, (kl) = 3.635. The buckling load according to 3D nonlinear buckling analysis (NLBA using SCIA Engineer soft.) *with the optimal prestressing* of the 4 stays was performed with two boundary conditions: i) the stays joined with the crossarms as ideal hinges, ii) the stays sliding on the crossarms (which is convenient arrangement for the structure assembly). The first case gives $N_{cr.max}$ = 36.6 kN, the second one $N_{cr.max}$ = 27.4 kN.

Maximum load-carrying capacity. The experimental results were compared with analytical formulas according to [3], based on nonlinear analysis (ABAQUS soft.). Asymmetric buckling modes were considered according to the analysis. The values for columns 1, 2 and 3 were received taking into account amplitudes of the initial deflections conservatively as $L/400$, $L/200$ and $L/1000$ and result into N_{max} = 15.5, 15.6 and 20.0 [kN] respectively. Therefore, in comparison with tests (Fig. 1), the recommended procedure with safety factor γ_M = 1 is for *stainless steels* rather unsafe.

Summary

The brief insight into test behavior, analysis and design of steel prestressed stayed column is provided. Experimental results give global path of the behavior and indicate predominant influence of initial imperfections which decrease the load-carrying capacity in respect to critical loading received from 3D LBA. Optimum prestressing and the design capacity using 3D GMNIA for a spectrum of stainless steel stayed columns is under investigation.

Acknowledgment: The support of the Czech Grant Agency GACR grant No. 103/13/25781S is gratefully acknowledged.

References

[1] K. Servítová, J. Macháček, Prestressed stainless steel stayed columns, in: L. Dunai et al. (Eds.), EUROSTEEL, Publ. ECCS, Budapest, 2011, pp. 1767-1772.

[2] R.J. Smith, G.T. McCaffrey, J.S. Ellis, Buckling of a single-crossarm stayed column, J. Struct Div ASCE, 101(ST1) (1975) 249-268.

[3] M.A. Wadee, L. Gardner, A.I. Osofero, Design of prestressed stayed columns, J. Constr Steel Res, 80 (2013) 287-298.

21st International Conference **ENGINEERING MECHANICS 2015**
Svratka, Czech Republic, May 11 –14, 2015
Paper **#147, pp. 232–233**

Helical Reinforcements Can Be Replaced with Glass Reinforcements

Luboš Podolka

Institute Department of Civil Engineering, University of Technology and Economics in Czech Budejovice, Street Circular No. 517/30; 370 01, Czech Budejovice; CZ,

podolka@mail.vstecb.cz

Keywords: helical reinforcement, glass reinforcement

Abstract: The article focuses on the practical use of composites able to replace helical stainless steel reinforcements, i.e. composites glued into a groove or into a borehole. The paper describes experiments performed with elements reinforced by glass and helical stainless steel reinforcements in the laboratories of the Klokner Institute of the Czech Technical University in Prague (KI CTU). The experiments were subsequently evaluated and compared with a mathematical model created using the ATENA software and technical information provided by the company HELIFIX CZ s.r.o.

Introduction

Strengthening and reconstructing of constructions is a subject of extensive research focused on possible applications of new technologies or innovations of the existing ones. New materials are being studied that should be used in order to improve building durability while effectively using reconstruction costs in comparison to the costs of new constructions, including maintenance costs. That is why experimental or in situ load tests are performed on constructions in order to specify applicability of new materials. The tests are subsequently evaluated and different methods of construction strengthening are compared in terms of the appropriateness of a method, effectiveness of a reconstruction plan, rehabilitation or a comprehensive renovation of a building. The article focuses on the practical use of composites able to replace helical stainless steel reinforcements, i.e. composites glued into a groove or into a borehole. The paper describes experiments performed with elements reinforced by glass and helical stainless steel reinforcements in the laboratories of the Klokner Institute of the Czech Technical University in Prague (KI CTU). The experiments were evaluated and compared with a mathematical model created using the ATENA software and technical information provided by the company HELIFIX CZ s.r.o.

Description of the experiments performed in the KI CTU laboratories

The elements were three little beams made of C 30/37 XC1 concrete the dimensions of which were 150 x 150 x 200 mm. An 8x10 mm groove was made on one side of the beams and a Φ5 mm glass reinforcement was put in the groove.

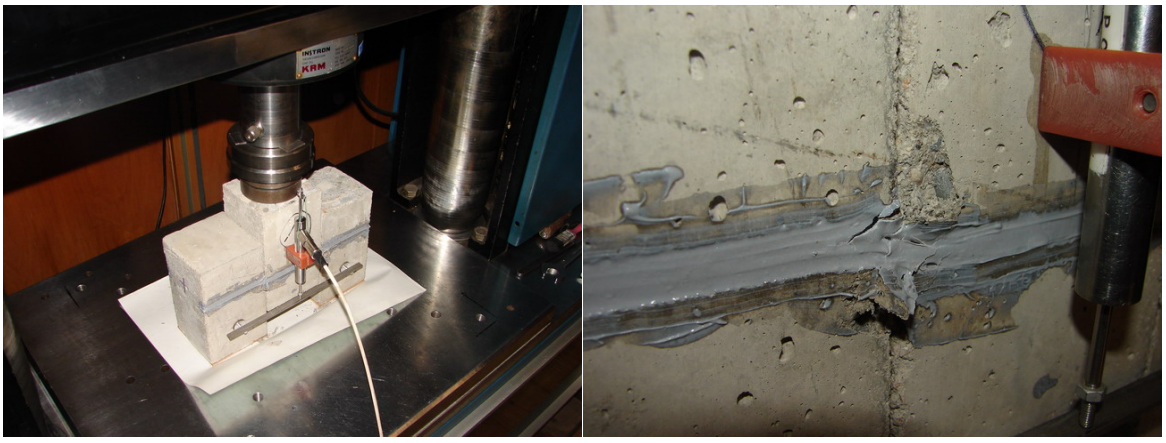

Fig. 1: View of the sample placed in a press and detail of the joint damaged by a shear force.

Verification of the experimental data on a model created using the Atena software

The above described experimental elements were modelled using the ATENA software so that we could observe the behaviour of the element in the point of the shear-loaded joint, i.e. the transfer of forces from the reinforcement into both concrete elements joined by the glass reinforcement in the groove or the borehole.

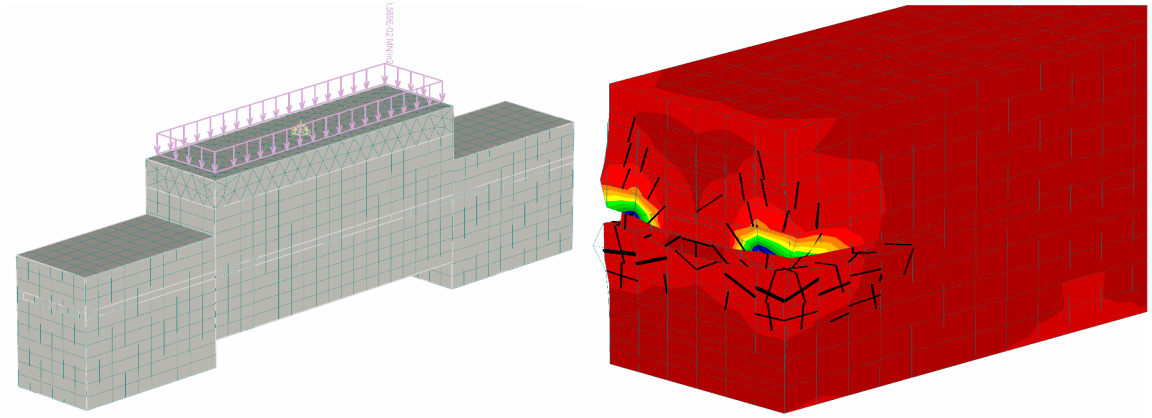

Fig. 2: View of the model created using the ATENA software and detail of the damage on the model in the point where reinforcements were put into the groove.

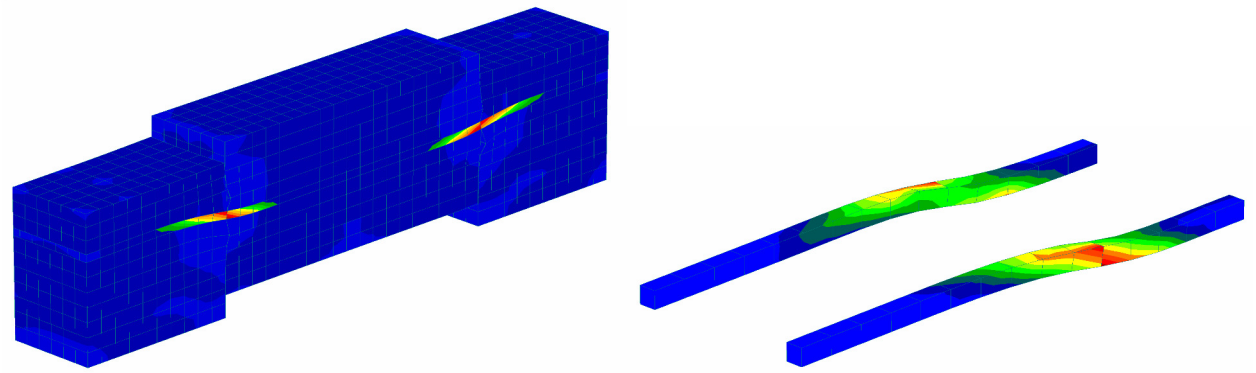

Fig. 3: View of tension isolines in a concrete elements and a glass reinforcement.

Bearing capacity of a pair Φ6 mm Helifix rods in the groove would be : 2 x 7.52 = 15.04 kN (1)
Considering the safety factor s = 1.6 x 1.2 = 1.92 (2)
32 / 1.92 = 16.6 kN (3)

Summary

After having compared the results of the experiments with the bearing capacities declared in the data sheets provided by the company Helifix CZ s.r.o., we can state that glass rods are able to replace helical reinforcements. That can lower the costs needed for rehabilitation of typical panel joint failures.

Acknowledgement: This paper was supported by the company STADO CZ, s.r.o. (www.stado.cz)

References

[1] STADO CZ, s.r.o. data sheets

[2] Helifix CZ, s.r.o. data sheets

21st International Conference **ENGINEERING MECHANICS 2015**
Svratka, Czech Republic, May 11 –14, 2015
Paper **#200, pp. 234–235**

Statistical Evaluation of Three and Four-Point Bending Tests of FRC

Adam Podstawka[a]*, Marek Foglar[b], Vladimir Kristek[c]

CTU in Prague, Faculty of civil engineering, Department of concrete and masonry structures,
Thákurova 7, 166 29, Prague, Czech Republic, Tel: +420 224 354 630

[a]adam.podstawka@fsv.cvut.cz, [b]marek.foglar@fsv.cvut.cz, [c]kristek@fsv.cvut.cz

Keywords: fiber reinforced concrete, testing of materials properties, force-deflection diagram, numerical modeling, statistical evaluation

Abstract: Paper compares and discusses three-point bending and four-point bending tests of fiber reinforced beams. A numerical modeling, stochastic and statistical analysis are used to determine which layouts of testing are more suitable for identification of mechanical and fracture properties of fiber reinforced concrete.

Introduction

Mechanical properties of fiber reinforced concrete (FRC) are commonly tested on the beam-shaped specimens loaded by bending moment and by the corresponding shear force.

The mechanical approach according to the RILEM and Eurocode [5] recommendations, use the three-point bending test of notched specimens. Presence of the notch clearly predefines the position of the initial crack which generally is not able to respect the actual fiber distribution.

When the engineering approach according to Czech and German standards [2, 3] is used, the fracture characteristics of FRC are tested using the four-point bending tests. At the specimens without the notch, the macro-crack propagates at the weakest cross-section.

For decision which method is more suitable for identification of material characteristic of FRC, three methods were used: method of tensile chord, method of direct evidence and method of dispute.

Method of tensile chord [7] is quite simple, but very effective. The expected damage zone is divided into elements (10 in case of four-point, 1 above the notch in the case of three-point). The value of tensile strength was randomly generated and then statistically evaluated. On this example, it was shown that due to lower statistical sensitivity, the four-point bending test without notch is more suitable for testing of material characteristics of FRC specimens.

More sophisticated method of direct evidence follows up the method of tensile chord and confirms the greater statistical sensitivity of three-point bending test arrangement. The numerical simulations and probabilistic approach were used in this method. The primary assumption of the numerical approach was to perform the numerical analysis of FRC based on previously published approaches [1, 4, 8, 9]. The material model 3DNLC2U was used for the non-linear analysis. Only this material model 3DNLC2U can appropriately describe real behavior of FRC including its characteristic peak and following hardening or softening (see Fig. 1).

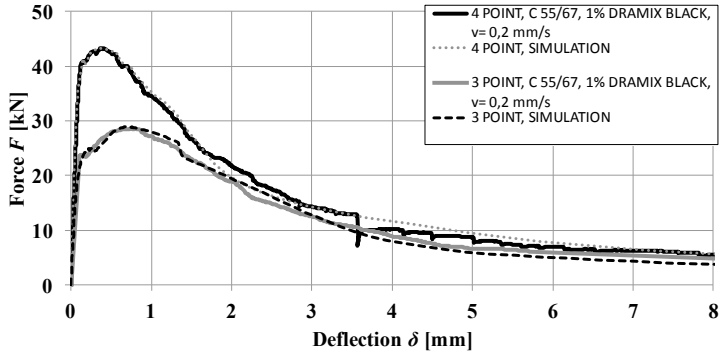

Fig. 1: Comparison of numerical simulations and experiments

It was determined that the selected material parameters are not mechanical properties of real material, but only parameters of material model. There is no generation of random simulations.

Therefore, the method of dispute must be used. The numerical simulations and probabilistic approach were again used in this method. Main idea was that the mechanical properties of the weakest cross-section determine mechanical properties of whole specimen and it´s absolutely necessary determine it. For both types of bending tests, the typical weakened cross-sections in the damage zone were chosen. These weakened cross-sections must be located around the notch in case of three-point bending test, because bending moment is reduced with the increasing distance. The sections considered are located 5, 15, 30 and 45 mm from the notch. The arbitrary position is in the middle third of span in the case of four-point bending test. The selected parameters of the material model of these weakened sections were assigned to probabilistic models according [6]. The results confirmed that three-point bending test cannot locate the weakest cross-section (cross-section with the lowest tensile strength and/or with the smallest amount of fibers). On the contrary, the four-point bending test always locates the weakest cross-section (in the middle third of span).

Summary

The main purpose of this paper was to determine which bending test is more suitable for testing of mechanical and fracture properties of FRC. It was determined that three-point bending test arrangement with the notch is not able to locate the weakest cross-section, which is absolutely essential for non-homogeneous material, such as FRC. The four-point bending test can precisely localize the weakest (representative) cross-section, which is the basic assumption to obtain representative results. Moreover, four-point bending test investigates about 40-200 times larger area of possible crack appearance. Based on the above statements it is possible to argue that four-point bending test is only suitable for identification of the material parameters of FRC.

Acknowledgements: Support from the Grant Agency of the Czech Republic, Grant Project No. 13-30441S, is gratefully acknowledged.

References

[1] M. Kovář, M. Foglar, Analytické vyjádření mechanických a lomových vlastností vláknobetonu, in: 20. Betonářské dny 2013, Česká betonářská společnost ČSSI, Praha, 2013, pp. 258-263.

[2] TP FC 1-1, Technické podmínky 1: Vláknobeton - Část 1: Zkoušení vláknobetonu, Českomoravský beton, a.s., Praha, 2007, p. 34.

[3] DAfStb-Richtlinie Stahlfaserbeton, Deutscher Ausschuss Für Stahlbeton, Berlin, 2010, p. 52.

[4] Kovar M, Foglar M., An analytical description of the force–deflection diagram of FRC. Composites: Part B (2014), http://dx.doi.org/10.1016/j.compositesb.2014.10.021

[5] RILEM TC 162-TDF, Test and design method for steel fibre reinforced concrete, Bending test, Final recommendation, Materials and Structures, 35 (2002) 579–582.

[6] JCSS probabilistic model code part 3: Resistance models, 3.01Concrete properties, 2002, http://www.jcss.byg.dtu.dk/Publications/Probabilistic_Model_Code

[7] M. Kovar, V. Kristek, M. Foglar, A. Podstawka, Three or four-point bending tests for identification of material characteristics of fiber reinforced concrete, in: Proceedings of 10th CCC Congres Liberec 2014, Czech Concrete Society, Praha, 2014.

[8] M. Kovář, M. Foglar, P. Veselý, Vliv rychlosti zatěžování vláknobetonu na jeho pevnostní a lomové charakteristiky, Konstrukce, (2013) 36-39.

[9] M. Foglar, M. Kovar, Conclusion from experimental testing of blast resistance of FRC and RC bridge decks, International Journal of Impact Engineering, 59 (2013) 18-28.

21st International Conference **ENGINEERING MECHANICS 2015**
Svratka, Czech Republic, May 11 –14, 2015
Paper **#016, pp. 236–237**

Two Approaches to the Simulations of City Bus Driving Tests

Pavel Polach[1,a], Jaroslav Václavík[2,b]

[1]Výzkumný a zkušební ústav Plzeň s.r.o. (Research and Testing Institute Plzeň), Section of Materials and Mechanical Engineering Research, Tylova 1581/46, 301 00 Plzeň, Czech Republic

[2]Výzkumný a zkušební ústav Plzeň s.r.o. (Research and Testing Institute Plzeň), Section of Testing and Calibration Laboratories, Tylova 1581/46, 301 00 Plzeň, Czech Republic

[a]polach@vzuplzen.cz, [b]vaclavik@vzuplzen.cz

Keywords: vehicle dynamics, bus, handling behaviour, multibody model, simulation, experimental measurement

Abstract: The Triple Hybrid Hydrogen Bus project comprises research and development, implementation and a test operation of a city bus with hybrid electric propulsion using hydrogen fuel cells. The mass distribution and the total bus mass are rather different from common buses. This is, among others, the reason for investigating the bus driving stability. In order to obtain a tool for dynamic analysis, multibody models of the bus were created. Verification of multibody models was performed based on the comparison of simulation results and experimental measurements focused on handling behaviour of the bus. To perform the simulations two approaches were used: the initial position of the bus multibody model at the beginning of the simulation of the manoeuvre depends on the bus motion trajectory and the initial position of the bus multibody model at the beginning of the simulation of the manoeuvre is set an equilibrium position.

Introduction

The TriHyBus (abbreviation of the Triple Hybrid Hydrogen Bus) project comprises research and development, implementation and a test operation of a 12-meter city bus (see Fig. 1) with a hybrid electric propulsion using hydrogen fuel cells.

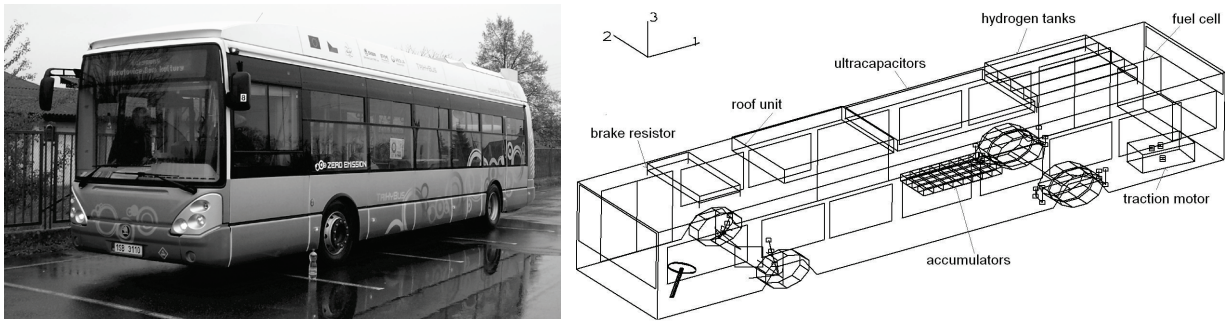

Fig. 1: TriHyBus at experimental tests and visualization of the TriHyBus multibody model in the *alaska 2.3* simulation tool

The mass distribution and the total bus mass differ from those at common buses. This is, among others, the reason for investigating the bus driving stability [1]. In order to obtain a tool for dynamic analysis multibody models of the bus were created using the *alaska* simulation tool. The aim of the simulations with the verified TriHyBus multibody models is the calculation of courses of kinematic and dynamic quantities giving information about the investigated properties of the vehicle at selected operational situations.

Testing manoeuvre and simulation results

Testing manoeuvres focused on the driving stability of the TriHyBus were performed with an empty real bus in the Řípská parking place in Mělník (Czech Republic) in November 2012 [1].

In this paper results from experimental measurements and computer simulations of the severe double lane change manoeuvre according to ISO 3888-1, Test Drive No. 6, are given.

The simulation of the test drive starts when the real TriHyBus reaches the speed of 15 km/h and ends when the real bus speed is lower than 15 km/h (simulating the vehicle starting with zero speed should cause certain problems when comparing the results [1]). In [1] there was presented the approach to the simulations, at which the initial position of the bus multibody model at the beginning of the simulation of the manoeuvre depended on the bus motion trajectory. Comparing the results from the experimental measurements and the simulations presented in [1], it is evident that a certain coincidence of results exists, but it is not perfect (especially time histories of relative deflections of the air springs – see Fig. 2). In order to improve coincidence of results from the experimental measurements and the simulations further approach to the simulations was tested: the initial position of the bus multibody model at the beginning of the simulation of the manoeuvre was set an equilibrium position (the bus body roll angle and the bus body yaw angle, which were measured during the test drive in the moment of the real TriHyBus achieving the speed of 15 km/h, were introduced as initial conditions).

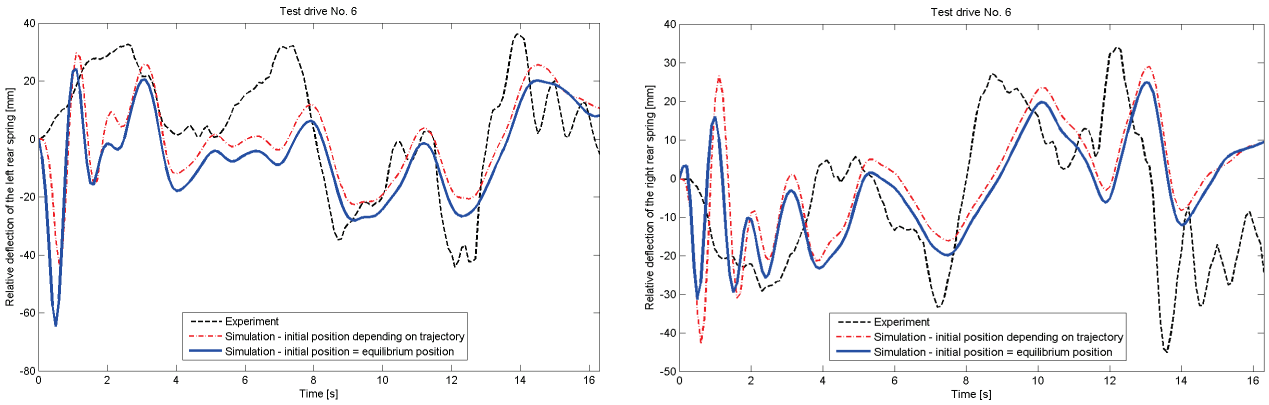

Fig. 2: Time histories of relative displacement of the left and right air springs before the rear axle

Conclusions

From the results given in Fig. 2 it is evident, that neither the configuration, in which the initial position of the bus multibody model at the beginning of the simulation of the manoeuvre was set an equilibrium position, had proved useful.

As it has been stated in [1], the ignorance of the actual air pressure in air springs of the TriHyBus suspension has the most significant impact on correlating experimental measurements and simulation results (it is the source of "unsuccessful" using the configuration, in which the initial position of the bus multibody model was the equilibrium one, among others).

Further testing manoeuvres with the real TriHyBus were performed in the year 2014. Time histories of air pressure in the air springs were measured, in addition to the monitored quantities measured at testing manoeuvres in November 2012. After processing the measured data it will be possible to improve the existing bus multibody models. The characteristics of air springs in the bus multibody models will not be only functional dependent of the forces acting on the springs and the spring deflections, but in addition they will be considered to be functionally dependent on the pressure of the air springs.

References

[1] P. Polach, J. Václavík, Investigation of Lateral Dynamics of Triple Hybrid Hydrogen Bus, in: Z. Dimitrovová, J. R. de Almeida, R. Gonçalves (Eds.), Proceedings of 11th International Conference on Vibration Problems, Associação Portuguesa de Mecânica Teórica, Aplicada e Computacional, Lisbon, 2013, USB flash drive.

21st International Conference **ENGINEERING MECHANICS 2015**
Svratka, Czech Republic, May 11 –14, 2015
Paper **#233, pp. 238–239**

Variation of Strouhal Number on Iced Cable in Sub-Transitional Range

Stanislav Pospíšil[1,a,*], Piotr Górski[2,b], Sergej Kuznetsov[1,a],
Marcin Tatara[2,c], Ante Marušić[3,d]

[1]Institute of Theoretical and Applied Mechanics, ASCR, v.v.i., Czech Republic,

[2]Department of Road and Bridges, Opole University of Technology, Poland

[3]Institute of Fluid Mechanics, University of Zagreb, Croatia.

[a]pospisil@itam.cas.cz, [b]p.gorski@po.opole.pl, [c]m.tatara@po.opole.pl, [d]marusic@itam.cas.cz

Keywords: bridge cable, ice accretion, Strouhal number, angle of attack, vortex shedding frequency

Abstract: The influence of ice accretion, angle of attack and Reynolds number on the flow field around iced cables of the cable-supported bridges is not clearly understood. The paper presents results of a wind tunnel investigations of Strouhal number of stationary iced cable model of cable-supported bridges. The investigations were carried out in a Climatic Wind Tunnel Laboratory of ITAM. The methodology leading to the experimental icing of the inclined cable model in the climatic section of the laboratory was prepared. For the aerodynamic investigations the iced cable model in a smaller scale was reproduced with combination of photography and 3-D printing procedure. The Strouhal number (St) was determined within the range of the Reynolds number (Re) between 2.4×10^4 and 16.4×10^4, based on the dominant vortex shedding frequency measured in the flow behind the model. The model was orientated at three principal angles of wind attack for each of the Re. Good agreement with the generally reported value in the sub-critical Re range for a circular cylinder was obtained.

Introduction

The change of the cross-section of the cable due to the ice accretion has a significant influence on the flow field around the cables and its aerodynamic [1]. In this case, an asymmetric airflow around the cable appears, thus, an asymmetric distribution of the wind pressure on its surface exists. For this reason, three aerodynamic coefficients, i.e. drag, lift and moment coefficients depending on the angle of the wind attack should be taken into account. Moreover, in such conditions, an aeroelastic instability of an iced cable known as galloping instability may occur if the specific criteria are met. It is well documented that the amplitude of galloping of ice accreted cables or transmission lines could be very large, [2]. The analysis of the vortex excitation response of the iced cables requires, among others, knowledge of the Strouhal number, which characterizes the vortex shedding frequency and is necessary for determination of critical wind velocity at which the largest amplitudes due to the vortex excitation are observed. This manuscript presents the method and the results of a wind tunnel investigations of St of stationary iced cable model with respect to different angles of wind attack. The methodology leading to the experimental icing of the inclined cable model in the climatic section of the laboratory was prepared. The shape of the ice on the cable was registered by a photographic method with combination of numerical image analysis. St number was determined within the range of the Re between 2.4×10^4 and 16.4×10^4, based on dominant vortex shedding frequency measured in the flow behind the model. The model was oriented at three principal angles of wind attack for selected values of the Re.

Ice accretion on cable

Different types of ice can be rise in different climatic conditions, i.e. in different combinations of temperature, wind velocity, angle of wind attack and droplets of the rain. For the purpose of this research, the most common natural conditions, expected at Central European geographical condition, were selected, causing smooth evenly distributed ice accretion together with frozen rivulets on the cable within a mild rain, relatively low wind velocity (2.8 m/s) and the temperature slightly below 0^oC.

After several preliminary tests, 40 min cooling exposure time was selected as sufficient from the point of view of ice creation. During the experiment, the model was inclined in a horizontal plane to the airflow direction at the angle of 60^o. The angle was found from several preliminary tests as one, at which the ice ribs on the bottom side of the model are distinctive. The final ice shape on the cable model was compared to the reference pictures from real situations. The characteristic ice ribs (frozen rivulets on the bottom side of the model) were created and used for further examination. On the upper part of the model the ice shape was similar to the circular shape. The cross-section of the cable with an ice became strongly non-symmetrical with the dimensions 0.192 m in high and 0.181 m in width. The cooling and icing procedure was carried out on a scale of 1:1, thus, no scaling factors were considered. Surface (roughness, material) effect on the flow around the cable during icing procedure is negligible because of low wind velocity, also relatively big drops were simulated and effect of the flow deflection near the surface of the cable on drop trajectory is negligible. Three configuration were selected with respect to the wind angle attack on the cable, see Fig. 1.

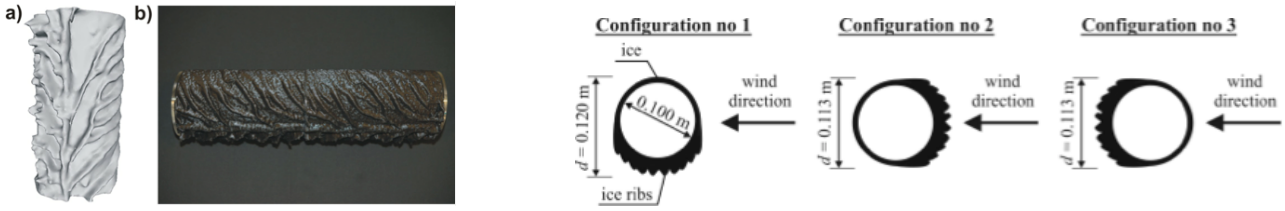

Fig. 1: Left: Ice on the cable segment - a) digital model, - b) printed section; Right: Ice configurations.

Conclusion, results

The experimental creation of the ice on an inclined cable model of cable-supported bridges was carried out in the climatic chamber of the wind tunnel of CET ITAM. The St was investigated for the stationary iced cable model with respect to three principal angles of wind attack. The ice accretion process produced the asymmetrical and irregular iced cross-section of the cable model with rounded edges of the ice ribs accreted on the bottom side of the model (with maximal surface roughness of 18%) and with the quasi-circular shape on its upper part (with minimal surface roughness of 0.73%).

At first configuration initially, in the range of $Re = 2.5 \times 10^4 \div 6.1 \times 10^4$, the St values linearly decrease from $St = 0.199$ to 0.189. In the range of $Re = 6.1 \times 10^4 \div 9.9 \times 10^4$, St suddenly increases to $St = 0.206$ and for $Re > 9.9 \times 10^4$, St again decreases to $St = 0.198$. As for the second configuration the St number is changing in the range of $St = 0.201 \div 0.205$ and seems to be independent of Re. All obtained St values are 12% to 14% higher than $St = 0.18$ used as reference. The variability of the St for this configurations can be incidental and may be caused by the randomness of the vortex excitation. The St number determined for the third configuration strictly depends on Re. Its values were initially in the range of $St = 0.186 \div 0.187$ for $Re = 2.4 \times 10^4 \div 4.6 \times 10^4$, while in the range of $Re = 4.6 \times 10^4 \div 9.5 \times 10^4$, St number suddenly increased to maximum value $St = 0.215$. In the range of $Re = 9.5 \times 10^4 \div 15.8 \times 10^4$, St number remain in the range of $St = 0.205 \div 0.215$. Effect of the change of wind direction on the iced cylinder can thus be attributed to the experimental data by [3] obtained at different surface roughness of the cylinder.

References

[1] C. Demartino, H.H. Koss, C.T. Georgakis, F. Ricciardelli, Effects of ice accretion on the aerodynamics of bridge cables. J. Wind Eng. Ind. Aerod. 138 (2015) 98--119.

[2] Y. Zhitao, L. Zheng-Liang, S. Eric, E.J. William, Galloping of a single iced conductor based on curved-beam theory. J. Wind Eng. Ind. Aerod. 123 (2013) 77--87.

[3] M.M. Zdravkovich, Flow around circular cylinders, Volume 1: Fundamentals. Oxford University Press, USA, 1997.

21st International Conference **ENGINEERING MECHANICS 2015**
Svratka, Czech Republic, May 11 –14, 2015
Paper **#078, pp. 240–241**

Reconstruction of Random Media via Multi-Objective Optimization

Adéla Pospíšilová[a], Matěj Lepš[b]

Department of Mechanics, Faculty of Civil Engineering, Czech Technical University in Prague, Thákurova 7, Praha 6, Czech Republic

[a]adela.pospisilova@fsv.cvut.cz, [b]leps@cml.fsv.cvut.cz

Keywords: image reconstruction, multi-objective optimization, non-dominated sorting genetic algorithm II, two-point probability function, lineal path function

Abstract: To simplify numerical analyzes of complicated real microstructures, a material representation in terms of Representative Volume Element (RVE) has been introduced. It is based on a binary (black and white) image, which statistically resembles the corresponding real microstructure. To characterize microstructure and assess the proximity of the compressed representation to the reference microstructure, several statistical descriptors are usually employed. In one of the approaches to construction of RVE, a unit cell is derived from the optimization procedure formulated in terms of selected statistical descriptors. The aim of our work is to resolve this issue by multi-objective optimization techniques. The goal is to approximate as closely as possible the true Pareto front as a trade-off of competing objectives.

Introduction

Most of the current multi-scale methods (e.g. FE^2) require a substitution of the complicated microstructure (simple examples in Fig. 1) with a relatively small representation, called a statistically equivalent periodic unit cell (SEPUC) [1] that has the same or very similar properties to the original microstructure. A similarity between the original microstructure and its surrogate is appraised e.g. by statistical descriptors. One of the possible procedures how to construct a SEPUC is to utilize an optimization methodology with a statistical descriptor as a part of the optimized objective function. The choice of only one statistical descriptor to capture majority of the microstructure features is not a trivial task and is usually governed by the related computational cost. Formulation of a multi-objective optimization task in which several statistical descriptors are optimized at the same time allows to avoid this difficult selection. Moreover, involving more descriptors strengthen credibility of the representation.

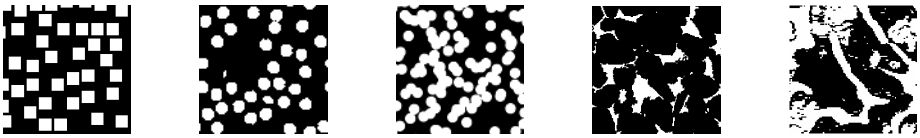

Fig. 1: Examples of optimized microstructures.

Yeong and Torquato [2], for example, optimize chosen statistical descriptors by a simulated annealing, which is single objective optimization algorithm. They use two-point probability and lineal path functions to capture long- and short-range features of the media. The objective function is taken as a weighted sum of the mean square errors between the target descriptors and those corresponding to the reconstructed medium. Here, difficulty lies in the proper adjustments of weights, which influences both the morphology of reconstructed media and complexity of the optimization problem.

Methodology

In this contribution, the goal is to approximate as closely as possible true Pareto front as a trade-off between competing objectives by a real multi-objective optimization algorithm. The Non-Dominated

Sorting Genetic Algorithm II (NSGA-II) [3] seems to be a suitable methodology for this problem. The NSGA-II is a multi-objective ($\mu + \lambda$) evolutionary algorithm, where the offsprings are selected firstly in accordance with their position on the approximated Pareto front and secondly, with their interpoint (crowding) distance. A new population is created by a special mutation operator based on swapping of two pixels from different phases in a grid. This operator ensures that the volume fraction of all phases remains the same during the whole procedure. In paper [4] is shown, that the swapping based mutation operator is sufficient for this type of optimization algorithms. Therefore, no crossover operator has been used.

For statistical description of the media, we incorporate the same two descriptors as in [2]. Namely, we use the two-point probability function (S2) [5] giving the probability of the ends of a vector with the given length and orientation falling in the same phase. This characteristics is suitable for capturing long-range order correlations. It can be efficiently enumerated with discrete Fast Fourier Transformation making it thus suitable for optimization algorithms. The second objective function, the lineal path function (L2) [5] captures a short-range order characteristic as it states the probability of finding the whole vector being embedded in the same phase. It thus statistically describes the convex part of phase connectivity (in the case of a matrix phase) and the averaged shape of an inclusion (in the case of inclusion phase).

Conclusions

This contribution serves for a verification of the multi-objective reconstruction of heterogeneous materials described in a pixel form. Since the objective function leading the reconstruction process is multi-modal, a genetic algorithm has been used. The possible multi-modality of the selected statistical descriptors is bypassed by the multi-objective approach, i.e. taking into account more than one statistical descriptor at once.

Acknowledgement: This work was supported by Czech Science Foundation, grant No. 15-07299S and by the Grant Agency of the Czech Technical University in Prague No. SGS15/030/OHK1/1T/11. Also, we would like to thank Jan Havelka for providing us a procedure for the lineal path function.

References

[1] J. Zeman, M. Šejnoha, From random microstructures to representative volume elements. Modelling and Simulation in Materials Science and Engineering, 15 (2007) 325–335.

[2] C.L.Y. Yeong, S. Torquato, Reconstructing random media, Physical Review E, 57 (1998) 495–506.

[3] K. Deb, S. Agrawal, A. Pratab, T. Meyarivan, A Fast Elitist Non-Dominated Sorting Genetic Algorithm for Multi-Objective Optimization: NSGA-II, in M.S. et al. (Editor), Proceedings of the Parallel Problem Solving from Nature VI Conference, pages 849–858. Springer. Lecture Notes in Computer Science No. 1917, Paris, France, 2000.

[4] A. Kučerová, M. Lepš, Z. Vitingerová, Contributions to numerical and experimental investigation of building materials and structures, Volume 1, Chapter Comparison of optimization algorithms suitable for microstructure reconstruction, pages 95–100, CTU in Prague, 2008.

[5] S. Torquato, Random heterogeneous materials: Microstructure and macroscopic properties, Springer-Verlag, 2001.

21st International Conference **ENGINEERING MECHANICS 2015**
Svratka, Czech Republic, May 11 –14, 2015
Paper **#096, pp. 242–243**

Mechanical Properties of Fiber Reinforced Lime-Based Mortar Evaluated from Four-Point Bending Test

Michal Přinosil[a] *, Petr Kabele[b]

Czech Technical University in Prague, Faculty of Civil Engineering,
Thákurova 7, 166 29, Praha 6, Czech Republic

[a]michal.prinosil@fsv.cvut.cz, [b]petr.kabele@fsv.cvut.cz

Keywords: lime-based mortar, fiber composite, tensile strength, strain hardening

Abstract: In this paper, tensile properties of a high-performance fiber reinforced lime-based mortar is experimentally investigated using four-point bending test. In the study, we consider several sets of the mortar with two types of the matrix (pure lime, lime-metakaolin) and two types of polyvinyl alcohol fibers in four volume fractions (0.5÷2.0%). As the reference, we consider two sets of specimens made of plain mortar without reinforcement. The main investigated parameters are cracking strength (initiation of the first crack), ultimate tensile strength and Young's modulus of elasticity. Moreover, we deal with the character of stress-displacement diagram, whether after initiation of cracking occurs softening or the response has hardening character and the specimen breaks in multiple cracking.

Introduction

Lime-based mortars were used in history for construction of buildings and monuments. At the present time, when maintenance and restoration are performed, it is desirable to use material with the same composition in order to ensure compatibility (in terms of mechanics, transport processes, aesthetic look, etc.) [1]. These materials could be characterized by low strength and low deformation capacity, which result in a poor durability of repairs.

In order to avoid these drawbacks, our team develops a new high-performance lime-based mortar reinforced with short synthetics fibers. Our intention is to systematically design the composition, so that under tensile loading the composite exhibits tensile hardening, multiple cracking and material retains its macroscopic integrity [2]. The main objective of this work is to clarify influence of matrix composition and fiber reinforcement on tensile characteristics evaluated using four-point bending test. This paper follows a previous study focused on fracture properties [3].

Materials

The composite consists of the matrix and the fiber reinforcement. The filler is represented by fine grained quartz sand with maximum particle size 0.3 mm (manufactured by Sklopísek Střeleč, a.s.) and the binder is represented by hydrated air lime powder CL90 (made by Čertovy schody a.s.) and metakaolin Mephisto L05 (made by ČLUZ s.r.o., Nové Strašecí). As the fiber reinforcement, we selected two types of polyvinyl alcohol fibers REC 15×12 and RSC 15×8 (made by Kuraray Company, Ltd.).

In our previous work, we optimized composition of pure matrix with regard to tensile strength and Young's modulus of elasticity [4]. Based on the results, we proposed grading curve, ratio of the filler and the binder (3:1 in mass), ratio of the lime and the metakaolin (3:1 in mass) and water ratio (0.3, calculated as ratio of weight of water and all dry ingredients). In this work, we consider two types of the matrix (pure lime - L, lime-metakaolin - LM), both types of fibers (REC, RSC) in four volume fractions (0.5%, 1.0%, 1.5%, 2.0%).

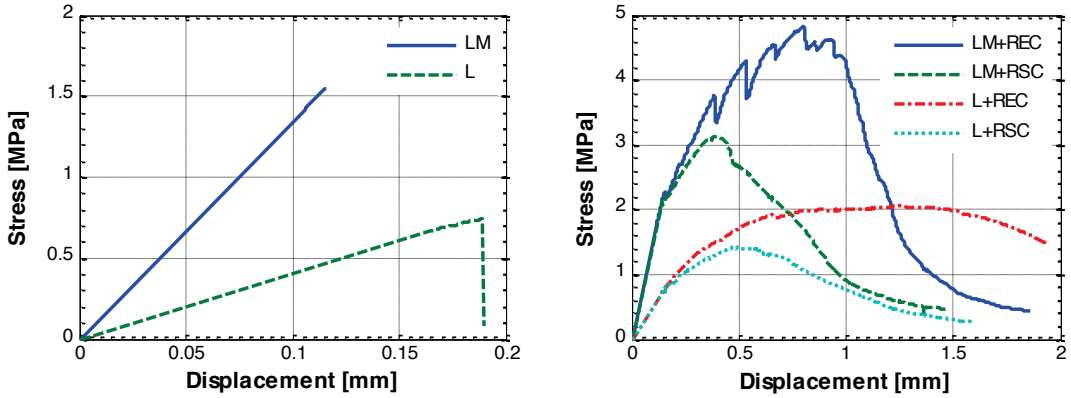

Fig. 1: Typical stress-displacement diagrams of specimens: without reinforcement (left), with fiber reinforcement in volume fraction 0.5% (right)

Methodology and testing set-up

From each proposed mixture, a set of 6 standard beams 40×40×160 mm was prepared and stored in laboratory conditions approximately for one year. Four-point bending test was performed using the MTS Alliance RT/30 machine with controlled crosshead displacement. The span of outer supports was 120 mm and the span of inner supports was 60 mm. During the test, all important data (applied force, crosshead displacement) were continuously recorded. Moreover, high resolution images of front side of each specimen were taken for digital image analysis of crack development. Bending stress was calculated from applied force and the geometry.

Results and conclusions

Figure 1 shows typical stress-displacement diagrams for specimens without reinforcement (left) and with reinforcement in volume fraction V_f = 0.5% (right). The results reveal that the mortar with lime-metakaolin matrix has higher values of tensile strength (cracking and ultimate) and Young's modulus of elasticity. Response of pure mortar is brittle, but even a small volume fraction of fibers improves it to softening character and for several configurations (the most obvious for lime-metakaolin matrix reinforced with REC 15×12) the response has hardening character and the mortar exhibits multiple cracking. The amount of cracks was determined using image analysis.

Acknowledgement: The presented research has been carried out with the financial support of the Czech Technical University in Prague, as part of the project no. SGS15/031/OHK1/1T/11.

References

[1] J. Lanas, J.I. Alvarez, Masony repair lime-based mortars: Factors affecting the mechanical behavior. Cement and Concrete Research. 33 (2003) 1867-1876.

[2] V.C. Li, C.K.Y. Leung, Steady-state and multiple cracking of short random fiber composites, ASCE Journal of Engineering Mechanics. 118 (1992) 2246-2264.

[3] M. Přinosil, P. Kabele, Fracture Properties of Fiber Reinforced Lime-Based Mortar, in: T. Plachý, et al. (Eds), Proceedings of the 5th Conference Nano & Macro Mechanics. CTU in Prague, Prague, 2014, pp. 143-152.

[4] M. Přinosil, P. Kabele, Influence of composition on tensile and fracture properties of lime-based mortar, in: T. Plachý, et al. (Eds), Proceedings of the Conference Nano & Macro Mechanics 2013. CTU in Prague, Prague, 2013, pp. 163-170.

21st International Conference **ENGINEERING MECHANICS 2015**
Svratka, Czech Republic, May 11 –14, 2015
Paper **#113, pp. 244–245**

Definition of Effective Material Properties of Recycled Plastic: Image Analysis and Homogenization

Zdenka Procházková[1,a*], Vlastimil Králík[1,b],
Karel Doubrava[2,c], Michal Šejnoha[1,d]

[1]Department of Mechanics, Faculty of Civil Engineering, Czech Technical University in Prague, Thákurova 7, Prague 6, 16629, The Czech Republic

[2]Department of Mechanics, Biomechanics and Mechatronics, Faculty of Mechanical Engineering, Czech Technical University in Prague, Technická 4, Prague 6, 16607, The Czech Republic

[a]zdenka.prochazkova@fsv.cvut.cz, [b]vlastimil.kralik@fsv.cvut.cz, [c]Karel.Doubrava@fs.cvut.cz, [d]sejnom@fsv.cvut.cz

Keywords: recycled plastic, viscoelastic material, plastic bridges, Mori-Tanaka

Abstract: The influence of foaming agent on the properties of steel-reinforced beams made of recycled plastic material is studied in the paper. The foaming agent creates a porous core in the recycled plastic elements, which must be reflected when deriving the effective properties to be used in macroscopic simulations. To that end, standard image analysis combined with nanoindentation and the Mori-Tanaka micromechanical model will be adopted to identify elastic material properties of the plastic material both inside and outside of the core. These are expected to enter an independent macroscopic analysis of the steel-bar reinforced beams.

Introduction

An ever-increasing amount of plastic waste is a global problem with negative impact on our natural ecosystem [1]. A mechanical recycling process means that the plastic is melted only by heat and pressure and no intermolecular connections are created. The resulting recycled material is then a mixture of plastics with lower material properties than the original material and therefore a novel combination with steel reinforcement was developed. The use of recycled plastic in new structures promises the possibility of turning large amounts of plastic waste into sustainable construction. Hence, it is imperative to understand the structural properties of steel reinforced recycled plastic beams so that their capacity can be exploited while extending their application.

Production

The recycled plastic products are typically produced by injection process. Cut pieces of assorted plastic waste are heated to 200˚C. Under this temperature the plastic becomes liquid and then is pressed into a steel mold of a required shape. In the case of steel reinforced beams, the steel bars are placed in the mold ahead of injection of the plastic melt. The liquid plastic is then injected into the mold from one end and the beam is filled along its entire length. For production of the thick-wall plastic products it is necessary to use foaming agents during the plastic melt process. The foaming agent helps to create enough pressure within the plastic product to maintain the required shape and therefore each recycled plastic beam has three distinctive regions – a porous core in the center, a plastic shell and isolated locations with steel bars.

Testing

Although the material is clearly rate and time depended, as can be seen from rate dependent tensile tests shown in Fig. 1a, we concentrate here on the derivation of effective elastic properties only. To that end, we combine standard nanoindentation measurements with the Mori-Tanaka micromechanical model. To distinguish between the two regions the nanoindentation tests were

performed both outside and inside the core at different temperatures. The influence of location and the effect of temperature on the measured elastic moduli are evident from Fig. 1b. These measurements clearly show and effect of foaming agent during the curing process on the resulting material stiffness.

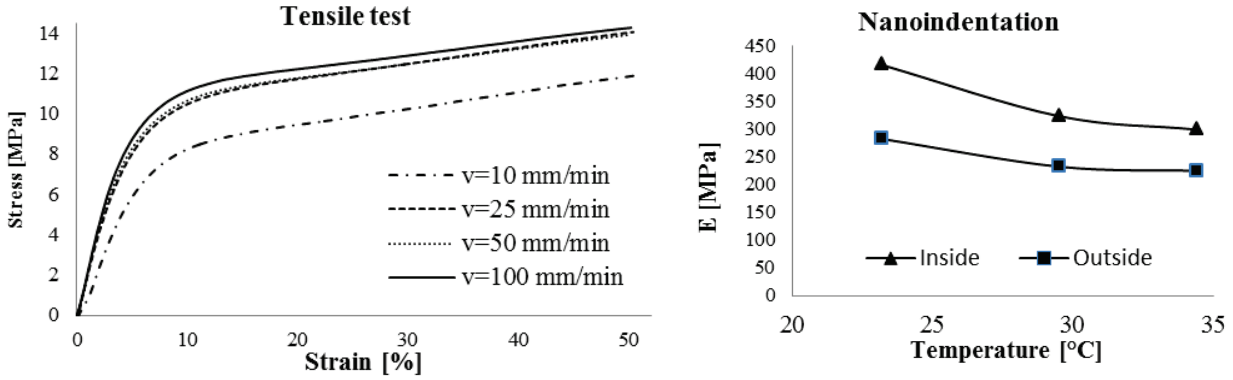

(a) (b)

Fig. 1: a) Tensile test stress-strain curve of recycled plastic under different strain rates, b) Evolution of Young's modulus measured by nanoindentation as a function of temperature

Image analysis and Mori-Tanaka Method

It has also been recognized that the production process results in variation of porous core along the beam axis as shown in Fig. 2. Clearly, the further from injection point the smaller the core gets but with increasing size of the pores. However, from the homogenization point of view, which draws up on the assumption of statistically uniform distribution of spherical pores, this plays no role. Here, the Mori-Tanaka micromechanical model [2] will be adopted assuming the volume fraction of pores is derived from 2D images of real material, Fig. 2(a,b). This is possible if accepting Delesse's law. This computational step is currently under investigation.

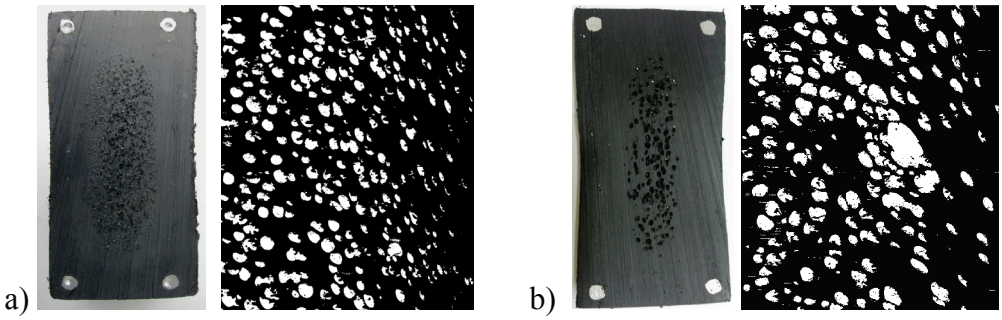

Fig. 2: Porosity of the foamed core from different distances from the side of the injection of the beam a) 200 mm and b) 2800 mm.

Acknowledgment: This research was made with the continuous support of Lankhorst Engineered Products and the research project No. SGS15/031/OHK1/1T/11.

References

[1] R.C. Thompson, C.J. Moore, F.S. vom Saal, S.H. Swan, Plastics, the environment and human health: current consensus and future trends, Phil. Trans. Roy. Soc. B: Biological Science, (2009) 2153-2166.

[2] M. Sejnoha, J. Zeman, Micromechanics in Practice, WIT Press, 2013.

21st International Conference **ENGINEERING MECHANICS 2015**
Svratka, Czech Republic, May 11 –14, 2015
Paper **#037, pp. 246–247**

Dynamics of Simple Planet Gearing Model

Ladislav Půst[a] *, Luděk Pešek[b]

[1]Institute of Thermomechanics AS CR, Dolejškova 5, Prague 8, Czech Republic

[a]pust@it.cas.cz, [b]pesek@it.cas.cz

Keywords: planet gearing box, flexible pin, free and forced vibration, response curves

Abstract: Planetary gears have several advantages over parallel axis gears. Flexible pins of planets enable better power flow distribution in planet subsystems and increase the input torque density. Analysis of proposed simple mathematical model explains basic dynamical properties of planetary gearing with flexible pins, influence of pins' stiffness on frequencies and modes of free vibrations as well as on the response curves on external harmonic excitation.

Introduction

Planetary gearboxes have in comparison to the single parallel-axes mechanical gear transmission systems advantage in minimizing of weight of produce at given power due to distribution of internal force flow into several planet branch circuits [1, 2]. However the modal and spectral dynamic properties of such gearings are more complicated and therefore they need detailed dynamic analysis. The increased compliance of planetary gears axes can have essential influence on internal dynamic properties and very strongly can change also the reliability and service live of the whole product.

Presented paper is oriented on the first stage of mathematical model design, in which a detailed analysis of influence of compliance pivots of planetary gears on dynamic properties is mainly studied. The simplest plane type of gearings with three planetary subsystems has been selected from the many possibilities of basic types of planetary gearings. It is supposed that the central sun wheel, planet wheels as well as outer annulus ring wheel have cylindrical double helical (herring-bone) gearings. As this kind of gearings has an essential smaller variation of contact stiffness against the direct spur gearings, this stiffness variability is not taken into account and in addition also teeth contact compliance can be neglected with respect to the elastic deformation of planetary gears pins.

The steady contact in gearings without any interruption is asserted by means of preloading on the sun and outer rig gears. External dynamic excitation load is realized by means of harmonic moment acting on outer annulus gear.

The development of dynamic mathematical model of planetary gearing set starts on the simplest structure and will continue with the successive improvement. This procedure will be coordinated with the development of laboratory experimental investigation of gearing set prototype. The first stage of dynamic mathematical model of planetary gearing set is based on these assumptions:

a) Plane motion of all gearing wheels.
b) Rigid wheels, with inertia parameters Θ_1, Θ_2, Θ_3, m.
c) Rigid, exact gearings.
d) Compliant planet wheels pivots, stiffness k.
e) Entire system is without damping, linear.
f) Axes of the central sun and outer annulus rig wheels are fixed, wheels can only rotate.
g) All planetary gear wheels move identically.
h) Radial components of teeth contact forces acting on the planet gears are in balance, so that forces in teeth contacts can be replaced by the tangential components.

Equations of motion

Planetary wheels work as idle gear wheels in this transversal-torsion dynamic model, the motion of which can be described by means of three angles of rotation $\varphi_1, \varphi_2, \varphi_3$ of ring, planet and sun wheels and of tangential translation of planet wheel described by $r_4\varphi_4$. Graphical representation of kinematical situation is plotted in Fig. 1 and expressed by equations containing also two contact forces F_1, F_2.

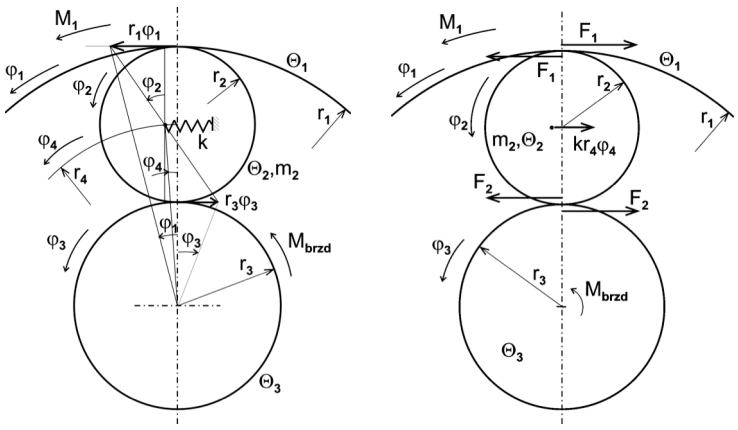

Fig. 1: Kinematical situation

$$
\begin{aligned}
r_1\varphi_1 &= \quad r_2\varphi_2 + r_4\varphi_4 \\
r_3\varphi_3 &= -r_2\varphi_2 + r_4\varphi_4 \\
\Theta_1\ddot{\varphi}_1 &= -F_1 r_1 + M_{inp}(t) \\
\Theta_2\ddot{\varphi}_2 &= \quad F_1 r_2 - F_2 r_2 \\
m r_4\ddot{\varphi}_4 + k r_4\varphi_4 &= F_2 + F_1 \\
\Theta_3\ddot{\varphi}_3 &= -F_2 r_3 + M_{outp}
\end{aligned}
\tag{1}
$$

Solution

After eliminating contact forces F_1, F_2 and angles φ_1, φ_3 we get couple of equations with two unknown variables φ_2, φ_4. Theirs rearrangement gets expressions for modes and frequencies of free vibrations as well as for forced vibrations and corresponding response curves.

Summary

In the study of flexible pins stiffness effects on the dynamic behaviour of planetary gears, the following conclusions have been obtained:

Eigenfrequencies and eigenmodes of gearing set with fixed planetary carrier were ascertained for several values of flexible pin's stiffness, for several magnitudes of inertia moment of ring gear and of central sun gear.

Properties of forced vibrations were analysed by means of response curves. Comparison of responses obtained by application of sinusoidal excitation with constant amplitude of force moment with responses obtained at sinusoidal excitation with constant amplitude of displacement showed differences both in positions of resonance zones and in amplitudes of vibrations.

Acknowledgements: This work has been elaborated in a frame of the grant project TA04011656.

References

[1] Z. Doležal, Řešení planetových vysokootáčkových převodů metodou komplexních dynamických poddajností. In: Proc. Dynamics of machines, Prague, Liblice, (1977), 85-90.

[2] M. Hortel, A. Škuderová,: Dynamika nelineárních parametrických planetových soustav s kinematickými vazbami. Report ÚT AVČR Z-1512/14, (2014)

21st International Conference **ENGINEERING MECHANICS 2015**
Svratka, Czech Republic, May 11 –14, 2015
Paper **#064, pp. 248–249**

Mathematical Modelling of the Sensitivity of Acoustic Resonance Properties to a Change in Volume of Lateral Cavities of the Human Vocal Tract

Vojtěch Radolf

Institute of Thermomechanics AS CR, v.v.i., Dolejškova 1402/5, 182 00 Praha 8, CZ

radolf@it.cas.cz

Keywords: piriform sinus, vocal tract model, biomechanics of voice, formant frequency

Abstract: An analysis of acoustic resonant properties of the human vocal tract including piriform sinuses was done using 1D mathematical model. Resulted changes caused by the lateral cavities correspond to recent findings of 3D computational models.

Introduction

Lateral cavities of the human vocal tract (VT) play specific role in the speech spectra. It was shown by several authors that piriform sinuses (PS), side branches in the bottom part of the pharynx, decrease formant frequencies in the lower frequency region. Besides, these cavities cause spectral minima in a region of 4 to 5 kHz as was proved by Dang and Honda in [1]. Detailed computational analysis of 3D acoustical mode shapes done by Vampola et al. [2] revealed that PS additionally contribute extra resonances. In this paper a simplified mathematical model is used to describe this issue.

Mathematical Model

The acoustical system was described by the wave equation of an acoustical duct with variable cross-section A and viscosity losses (specific acoustic resistance r_N)

$$\frac{\partial^2\phi}{\partial x^2}+\frac{1}{A}\cdot\frac{\partial A}{\partial x}\cdot\frac{\partial\phi}{\partial x}-\frac{1}{c_0^2}\cdot\left(\frac{\partial^2\phi}{\partial t^2}+c_0\cdot r_N\cdot\frac{\partial\phi}{\partial t}\right)=0\,. \tag{1}$$

The system was modelled in frequency domain using conical acoustical ducts, considering the radiation impedance at lips. Geometry of the model has been derived from CT images of the human vocal cavities for vowel /a:/, see [3]. The following values of fluid density, dynamic air viscosity, and speed of sound were used, respectively: $c_0 = 353\,ms^{-1}$; $\rho = 1.2\,kgm^{-3}$, $\mu = 1.8\cdot10^{-5}\,kgm^{-1}s^{-1}$.

Results

Geometry of the computational model including PS of nominal volume size is depicted in the upper panel of Fig. 1. Corresponding transfer functions from the glottis to the position of lips and to the closed ends of PS are shown below. Moreover the transfer function of the VT model without PS is plotted with black dashed line. The volume of PS was changed from zero to the nominal value for which the normalized volume was $V_N = 1$, the length of both PS kept constant at 20 mm. New pair of resonances around 5 kHz followed by an antiresonance frequency were detected in the results. The formant frequencies lying below the first new resonance of PS lowered with increasing PS volume, whereas the others increased, see Fig. 2.

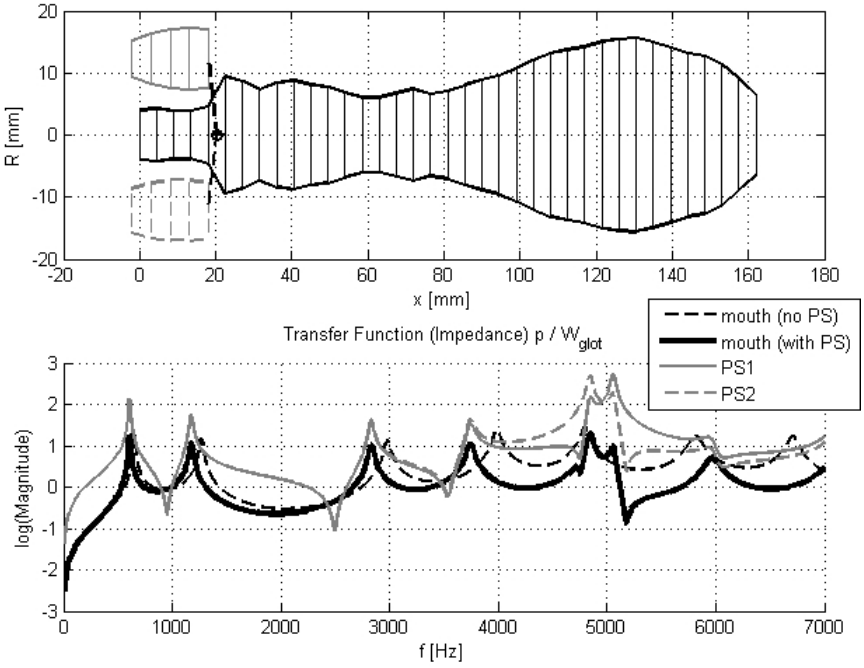

Fig. 1: Top: Geometry of the VT model with PS of normalized volume $V_N = 1$. Bottom: Transfer function from glottis
a) to lips without PS (black dashed),
b) to lips including PS (black solid),
c) to PS1 cavity (grey solid),
d) to PS2 cavity (grey dashed).

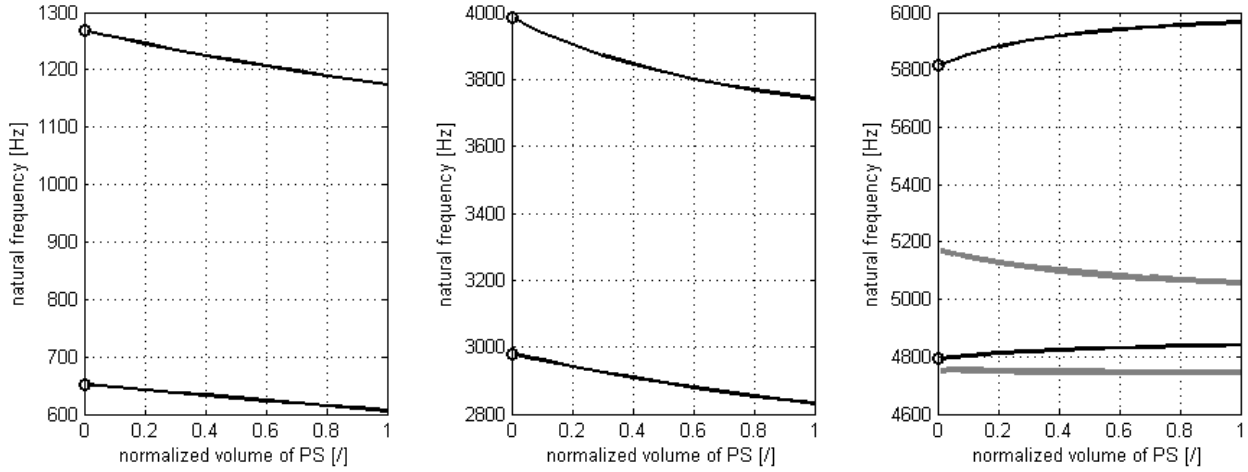

Fig. 2: Natural frequencies of the VT model in dependence on normalized volume of PS. Grey lines depict resonances that disappear when $V_N = 0$.

Summary

Although the simplified 1D model cannot capture higher-frequency transversal mode shapes, the resulted changes caused by PS correspond to recent findings of 3D computational models [3].

Ackonwledgement: The study was supported under the grant of the Czech Science Foundation No P101/12/P579.

References

[1] J. Dang, K. Honda, Acoustic characteristics of the piriform fossa in models and humans, J. Acoust. Soc. Am. 101 (1997) 456-465.

[2] T. Vampola, J. Horáček, A.M. Laukkanen, J.G. Švec, Human vocal tract resonances and the corresponding mode shapes investigated by three-dimensional finite-element modelling based on CT measurement, Logoped. Phoniatr. Vocol. (2013) 1-10, DOI: 10.3109/14015439.2013.775333.

[3] T. Vampola, A.M. Laukkanen, J. Horáček, J.G. Švec, Vocal tract changes caused by phonation into a tube: A case study using computer tomography and finite-element modeling, J. Acoust. Soc. Am. 129 (2011) 310-315.

21st International Conference **ENGINEERING MECHANICS 2015**
Svratka, Czech Republic, May 11 –14, 2015
Paper **#202, pp. 250–251**

Measuring of Driving and Impact Dynamics of Cyclists

Zuzana Radová[a]*, Luboš Nouzovský[b]

Faculty of Transportation Sciences, Horská 3, Prague 2, 128 03, the Czech Republic

[a]radova@fd.cvut.cz, [b]nouzolub@fd.cvut.cz

Keywords: cyclist riding dynamic, trajectory measurement, passive safety, biomechanical load, bicycle helmet

Abstract: The contribution is aimed at detection of cyclists' dynamics in standard and non-standard situations. From forensic experts point of view there are significant both, ie. riding dynamics of cyclist and also post-crash motion in case of collision with passenger car.

To determine the riding trajectory, it is necessary to devise a measuring apparatus and devise methods for measuring and processing of the collected data. Measuring involves combination of several procedures such as accelerometric measuring, photogrammetry and GPS use.

In the term of post-crash motion the paper deals with the biomechanical analysis of load exerted on the child cyclist in configuration typical for cyclists (sudden enter the road or the case of non-giving way; the car front vs. the left side of the cyclists).

Introduction

In case of riding dynamics, trajectory of a bicycle-rider system has, even when moving straight forward, a sine pattern – a sinusoidal waveform. The amplitude of this "macrowave", as well as the amplitude of a "microwave" generated by the swaying of a bicycle along the macrowave, is influenced by many factors. The magnitude of the macrowave can be directly affected by riders themselves – by their own volition and concentration on riding. This does not apply to the microwave.

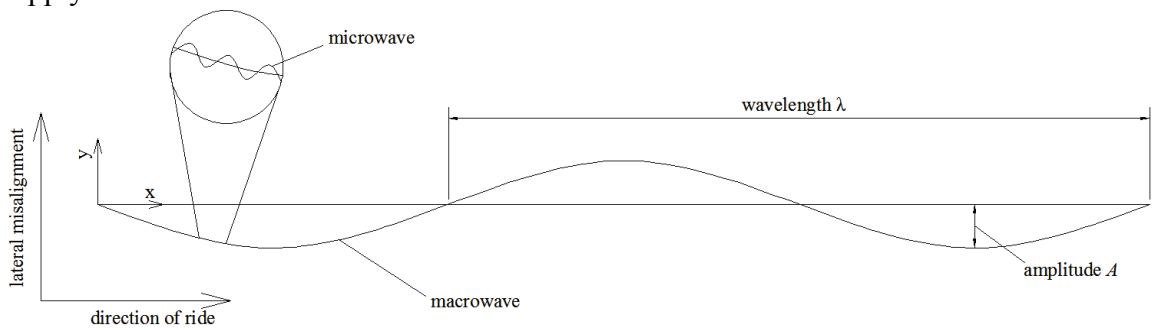

Fig. 1: Illustration of linear motion

During collision with a passenger car, the cyclist moves along a trajectory which depends on the collision speed, the shape of the front vehicle structure and its rigidity and pedestrian´s or cyclist´s initial position towards the vehicle. Because of number of factors affecting the course of impact, it is a process with a high degree of variability.

Material and method

For the riding dynamics trajectory detection the test bike was fitted with multifunctional accelerometric device, GNSS receiver, field computer. This measuring apparatus enabled to collect data essential for the description of the cyclist's motion such as acceleration, angular velocity and position-time data.

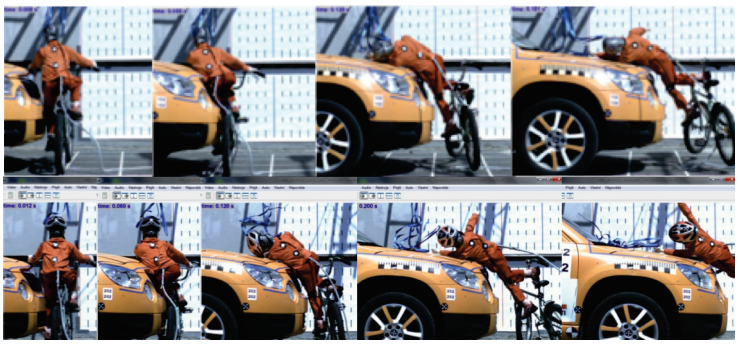

Fig. 2: Image sequence of two tests: the same configuration - with/without bicycle helmet

Performed passive safety tests were focused on vehicle front part, which is usually tested by impactors with respect to certified methodology 78/2009 ECE. In terms of boundary conditions the limit case of conflict of the child cyclist (height 117 cm, weight 22 kg) with a passenger car was tested. Two tests were performed in the same configuration and nominal collision speed, the first one with a bicycle helmet and the second one without the helmet.

Additional third test was performed in following configuration vehicle front part – back of cyclist (insufficient breaking, uncontrolled avoidance manoeuvre…) Using the accelerometers in the head, chest, pelvis and knee of the dummy acceleration fields were detected, which is the cyclist exposed during the primary (contact with the vehicle) and secondary collision (contact with the vehicle road surface).

Results

From the results of the test of riding dynamics measurements (man, 25 years, intermediate experienced rider, sunny weather and no wind, road without grade) can be preliminarily said that the width of the riding corridor is a significantly wider, when the start of the motion is captured. When start is included, the corridor width is about 70 cm. Conversely, the continuous driving corridor size (as a sum of the greatest opposite amplitudes) is approximately 20 cm. It is important to note that captured curve represents only the trajectory of a point through space – the measuring apparatus. It is therefore necessary to add the width of bicycle-rider system.

For the evaluation of performed dynamic tests were chosen biomechanical criteria that are frequently used for classification of biomechanical load in passive safety tests, for example for the head load evaluation the Head Performance Criterion was used, where the input value are accelerations measured at the head centre of gravity. The resulting HPC value should not be greater than 1000.

Tab. 1: HPC values for performed tests in the first configuration

Test No.	Contact with the vehicle		Contact with the road surface	
	HPC_{15}		HPC_{15}	
	[-]	limit	[-]	limit
102 – without helmet	**47.9**	1000	**1325.0**	1000
202 – with helmet	**30.7**	1000	**104.7**	1000

Conclusion

Aim of the presented method of measuring and processing of cyclist's riding data is classification and quantification of particular factors, which affects the movement. This information should be used not only for forensic experts, but also for the general public.

Results of passive safety tests were interpreted by values of biomechanical load and severity of potential injuries, as well as a documentation of final positions. In addition, the positive impact of bicycle helmets has been demonstrated to the general public within an awareness campaign.

21st International Conference **ENGINEERING MECHANICS 2015**
Svratka, Czech Republic, May 11 –14, 2015
Paper **#129, pp. 252–253**

Computer Simulation of the Behavior of the Piston Ring Pack of Internal Combustion Engines

Peter Raffai[a]*, Pavel Novotný[b], Jozef Dlugoš[c]

Faculty of Mechanical Engineering, Brno University of Technology, Brno, Czech Republic

[a]raffai@iae.fme.vutbr.cz, [b] novotny@fme.vutbr.cz, [c] dlugos@iae.fme.vutbr.cz

Keywords: piston ring, simulation model, mechanical losses, lubrication, asperity contact

Abstract: Due to stricter pollutant emission regulations for internal combustion engines the increase of the effectiveness of power units got even more into the center of attention in the last few decades. Therefore, the need for the optimization of even smaller engine parts – like piston rings – became more discussed, and their research and development became more important. The main objective of this project was to develop a computational model for the simulation of the behavior of the piston ring pack, capable of supporting the design process of new piston rings with lower friction losses.

Applied theory

For the determination of the instantaneous pressures above, behind and below the rings in the calculation a labyrinth model is used, which divides the volumes created by the rings-piston assembly into chambers. The pressures are determined from the volumetric flow of the gases between the chambers. This model presumes the gas flow through the piston ring gap to be an isentropic orifice flow between two volumes [1].

In case of gas flow through a small clearance between the ring and the piston groove a one-dimensional Reynolds equation is used to calculate the mass flow, assuming flow to be laminar [2].

The determination of the mass flows in and out of each volume is carried out in each time step, while the pressures in the crevices are calculated using the mass conservation equation in combination with the equation of state for ideal gas.

Concerning the lubrication regime – in case enough oil is present between the ring and the liner, hydrodynamic lubrication is considered. The given problem is described by the Reynolds equation which defines the relationship between the lubricant pressure and the lubricant film shape. Since the ring-liner contact pair due to its characteristics can be considered as an infinitely long flat sliding bearing, the 2-dimensional Reynolds equation can be further simplified [3]:

$$\frac{d}{dx}\left(\phi_x \frac{h^3}{12\eta}\frac{dp_A}{dx}\right) = \frac{U}{2}\frac{dh_{TA}}{dx} + \frac{U}{2}\sigma_C \frac{d\phi_s}{dx} + \frac{dh_{TA}}{dt} \tag{1}$$

In cases where the oil supply is insufficient, and the asperities of surface roughness come to contact, mixed, or boundary lubrication regime is calculated. Pure boundary lubrication is solved according to Greenwood and Tripp, where the nominal pressure due to the elastic deformation of the surface roughness peaks can be calculated as [4]:

$$p_c = \frac{8\pi}{5}(\eta\beta\sigma)KF_{5/2}\left(\frac{h}{\sigma}\right) \tag{2}$$

Further input variables entering the computation, like the temperature distribution of the piston and its deformations due to operation were calculated using FEM approach on the basis of Ortjohann's proposition [5].

The utilized numerical approach incorporates an iterative solution for the force equilibrium calculation for each crank angle by the use of a modified Newton-Raphson method for better approximations to the roots. The blow-by calculation is speeded up by utilizing the 4th order Runge-Kutta method for the iterative solution. To achieve another significant acceleration in the

solution time, variable time step is utilized, although the time step is reduced only in a few places where convergence is more problematic.

Experimental validation

The experimental validation of each numerical method is undoubtedly desired. For the purpose of this project an experimental setup for determining the amount of blow-by gases has been built. The setup involves a commercial three-cylinder spark ignition engine with the blow-by measuring device from AVL. The obtained results show good correlation to the calculated values, as it can be seen in the graph in Fig. 1.

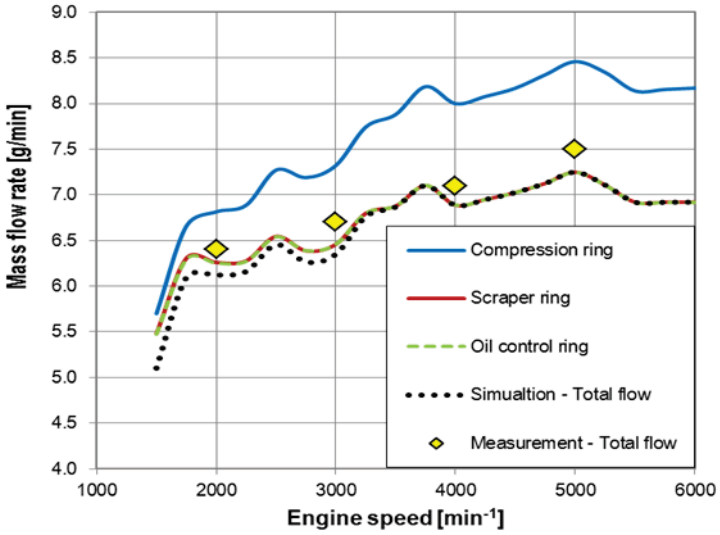

Fig. 1: Gas blow-by through piston ring pack.

Conclusions

By incorporating the above presented theory, besides others, into the numerical scheme, the force balance on each ring is solved at every time step of the calculation. Lastly, the developed computational model is applied to a standard inline three-cylinder passenger car petrol engine to obtain computational results of the identical engine as utilized in the experiment.

Acknowledgement: This work is an output of NETME CENTRE PLUS research activities (project no. LO1202) and is funded by the Ministry of Education, Youth and Sports under the *National Programme for Sustainability I.*

References

[1] S. Furuhama, T. Tada, On the flow of gas through the piston-rings: 1st report, The discharge coefficient and temperature of leakage gas, Bulletin of JSME. 4 (1961) 684-690.

[2] K. Wannatong et.al., Simulation algorithm for piston ring dynamics, Simulation modelling practice and theory. 16 (2008) 127-146.

[3] N. Patir, H. Cheng, An average flow model for determining effects of three-dimensional roughness on partial hydrodynamic lubrication, J. of Lubrication Technology. 100 (1978) 12-17.

[4] J. Greenwood, J. Tripp, The contact of two nominally flat rough surfaces, in: Proceedings of the Institution of Mechanical Engineers. 185 (1970) 625-634.

[5] T. Ortjohann, A. Voncken, S. Pischinger, piston ring dynamics simulation based on FEA software, MTZ worldwide. 69 (2008) 36-41.

21st International Conference **ENGINEERING MECHANICS 2015**
Svratka, Czech Republic, May 11 –14, 2015
Paper **#055, pp. 254–255**

Parallel Computing Procedure for Dynamic Relaxation Method on GPU Using NVIDIA's CUDA

Václav Rek[a], Ivan Němec[b]

Institute of Structural Mechanics, Brno University of Technology, Veveří 95; 602 00, Brno, CZ

[a]rekv@seznam.cz, [b]nemec@fem.cz

Keywords: finite element method, dynamic relaxation, finite difference method, central difference method, parallel computing, GPU, GPGU, NVIDIA CUDA

Abstract: This paper introduces a procedure for parallel computing with the Dynamic Relaxation method (DR) on a Graphic Processing Unit (GPU). This method facilitates the consideration of a variety of nonlinearities in an easy and explicit manner. Because of the presence of inertial forces, a static problem leads to a transient dynamic problem where the Central Difference Method is used as a method for direct integration of equations of motion which arise from the Finite Element model. The natural characteristic of this explicit method is that the scheme can be easily parallelized. The assembly of a global stiffness matrix is not required. Due to slow convergence of this method, the high performance which GPUs provide is strongly suitable for this kind of computation. NVIDIA's CUDA is used for general-purpose computing on graphics processing units (GPGPU) for NVIDIA's GPUs with CUDA capability.

Introduction

Dynamic Relaxation (DR) method is basicaly an explicit integration scheme for solution of equations of motion by Central Difference Method, which is commonly used in Dynamic Analysis. DR was originaly introduced by Day [1] for the finite difference analysis of concrete pressure vessels and in the next years was investigated mainly by P. Underwood [2]. The conditional stability character of explicit methods leads in some cases to necessity to use exceptionaly small integration step. As a consequence, the method was time consuming and remained at the mere periphery of scientific interest. Since year 2006, when CUDA (Compute Unified Device Architecture) was introduced by NVIDIA company, explicit methods have become more attractive. Availability of a huge number of parallel threadsdirectly implemented in hardware enabled their effective usage.

In the past, it was common to use CPU (Central Processing Unit) for parallel run of computional time-consuming tasks. Parallel programming was especially supported by software libraries OpenMP (Open Multi-Processing), MPI (Message Passing Interface) etc. These libraries for parallel run of variety of computations in computational mechanics are very well known to interested researchers especially for domain decomposition method (see [3]). CUDA and related technologies like OpenCL (Open Computing Language) or Microsoft Direct-Compute are currently investigated by many researchers. Their applications occurs in research interested mainly in information technologies, in algorithms for artificial inteligence (diagnosis and synthesis of voice, image recognition, etc.), for programming of shaders for production of special effects in computer visualization or in computational fluid dynamics (see [6]).

Paradigm of usage of CUDA technology in computer science is also available for computional structural mechanics and dynamics, namely for explicit methods.

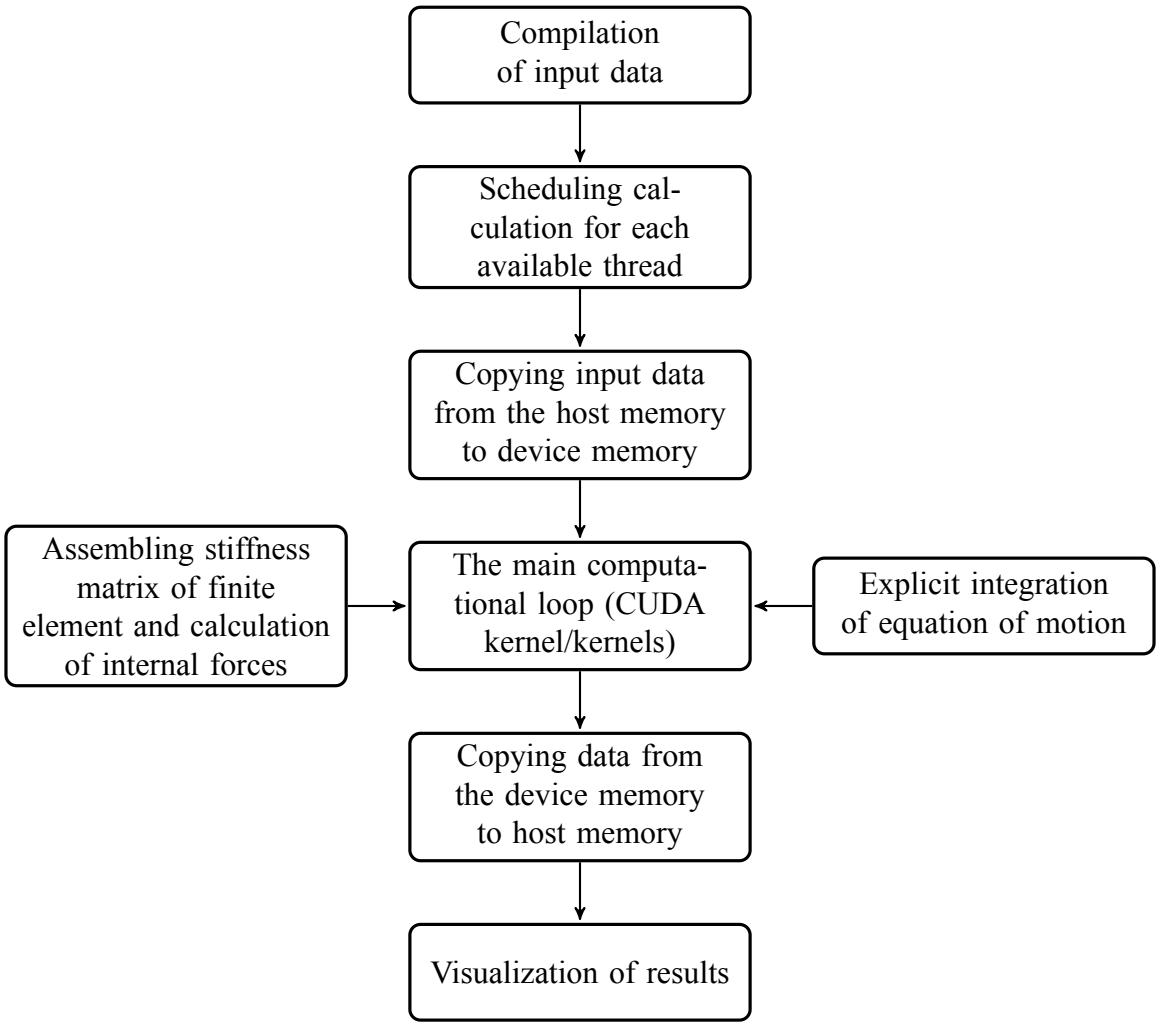

References

[1] A.S. Day, An Introduction to Dynamic Relaxation, The Engineer 219 (1965) 218-221.

[2] P. Underwood, Dynamic Relaxation, Computational Methods for Transient Analysis (1983) 245-265.

[3] J. Kruis, Domain Decomposition Methods for Distributed Computing, Saxe-Coburg Publications, 2006.

[4] E. Oñate, Structural Analysis with the Finite Element Method. Linear Statics: Volume 1: Basis and Solids, Springer, 2009.

[5] E. Oñate: Structural Analysis with the Finite Element Method. Linear Statics: Volume 2: Beams, Plates and Shells, Springer, 2013.

[6] R. Couturier, Designing Scientific Applications on GPUs, CRC Press, 2013.

[7] S. Cook, CUDA Programming: A Developer's Guide to Parallel Computing with GPUs, Morgan Kaufmann, 2012.

[8] S. Prata, C Primer Plus, fifth ed., Sams Publishing, 2004.

Modelling of the Influence of Vegetative Barrier on Concentration of PM10 and PM2,5 from Highway

Hynek Řezníček[a], Luděk Beneš[b]

Department of Technical Mathematics, Faculty of Mechanical Engineering - Czech Technical University in Prague. Karlovo nám. 293/13, 121 35 Praha 2, Czech Republic

[a]hynek.reznicek@fs.cvut.cz, [b]benes@marian.fsik.cvut.cz

Keywords: dust dispersion, vegetation barrier, RANS equations

Abstract: The influence of different types of the vegetative barrier near a highway on dustiness was studied. Transport, dispersion and sedimentation of pollutants PM10 and PM2.5 emitted from the highway was numerically simulated. Mathematical model was based on the Navier-Stokes equations for turbulent fluid flow in Boussinesq approximation. The AUSM-MUSCL scheme in finite volume formulation on structured ortogonal grid was used. The influence of the shape of the barrier and of its obstructing properties on the concentration of pollutants was studied.

Mathematical model

The air flow in atmospheric boundary layer is described by RANS (Reynolds Averaged Navier-Stokes) equations for the viscous, imcompressible, turbulent and stratified flow with variable density (in general). The system of equations is simplified with Boussinesq approximation, in 2D it is written:

$$\begin{aligned} \frac{\partial u_j}{\partial x_j} &= 0, \\ \frac{\partial \rho'}{\partial t} + \frac{\partial u_j \rho'}{\partial x_j} &= u_2 \frac{\partial \rho_0}{\partial x_2} \\ \frac{\partial u_i}{\partial t} + \frac{\partial u_j u_i}{\partial x_j} + \frac{1}{\rho_0}\frac{\partial p'}{\partial x_i} &= \frac{\partial}{\partial x_j}\nu\left(\frac{\partial u_i}{\partial x_j}\right) - \frac{\rho'}{\rho_0} g \delta_{i2} + T_i, \end{aligned} \tag{1}$$

where u_i ($i \in \{1, 2\}$) are velocity components, ρ' resp. p' are perturbations of density resp. pressure, ρ_0 is background density and T_i is the aerodynamic resistance of the barrier. The viscosity was composed from the molecular kinematic viscosity and the turbulent viscosity $\nu = \nu_m + \nu_T$. The turbulent viscosity was computed from Blackadar algebraic turbulent model (see [1], [2]).

The vegetative barrier was modelled by adding volume force T, which simulates the aerodynamic resistance caused by the vegetation:

$$T_i = r_h |U| u_i, \tag{2}$$

here $|U|$ is the velocity magnitude and r_h is an obstructing coefficient of the vegetative barrier (as in [3]). Different profiles and different values of these coefficients have been tested.

The contaminant is a non-hygroscopic, primary emitted dust which can be considered as passive scalar in the flow field. The transport of concentration c_i size fraction is described by:

$$\frac{\partial \rho c_i}{\partial t} + \frac{\partial (\rho u_1 c_i)}{\partial x_1} + \frac{\partial ((\rho u_2 - v_{si}) c_i)}{\partial x_2} = \frac{\partial}{\partial x_j} D \left(\frac{\partial c_i}{\partial x_j}\right) + Z_i, \tag{3}$$

where v_{si} denotes the sedimentation velocity, D is dispersion coefficient (turbulent in general) and Z_i is loss term due to the vegetation.

Numerical approximation and computational set up

The finite volume AUSM scheme was used for the inviscid terms with MUSCL velocity reconstruction and Hemker-Koren limiter. The inviscid terms was approximated by the central way on dual (diamond type) mesh. The resulting system of ODEs was integrated in physical time by a backward differentiation formula. The time discretization of the equations was done via artificial compressibility method in dual time. The suitable Runge-Kutta multi-stage scheme was used.

The computing domain was 300 × 150 m, the highway is situated in position $x_1 \in \langle 20, 45 \rangle$ m. The vegetative barrier of height h = 15 m is located in position $x_1 \in \langle 50, 80 \rangle$ m. Four dust sources were situated in the center of lanes.

Results and conclusions

First results for velocity field was obtained for simple obstructing coefficient profile:

$$r_h(z) = \begin{cases} r\,\frac{x_2/h}{0.75} & \text{for} \quad 0 \le x_2/h \le 0.75 \\ r\,\frac{1-x_2/h}{1-0.75} & \text{for} \quad 0.75 \le x_2/h \le 1.0. \end{cases} \tag{4}$$

Different constants $r \in \langle 0, 0.5 \rangle$ and different heights $h \in \langle 0, 15 \rangle$ m were tested .

Fig. 1 shows the influence of the vegetative barrier on the horizontal velocity field. The results were obtained for neutrally stratified atmosphere ($\frac{\partial \rho_0}{\partial x_2} = 0$) and for $r = 0.1$ resp. 0.3.

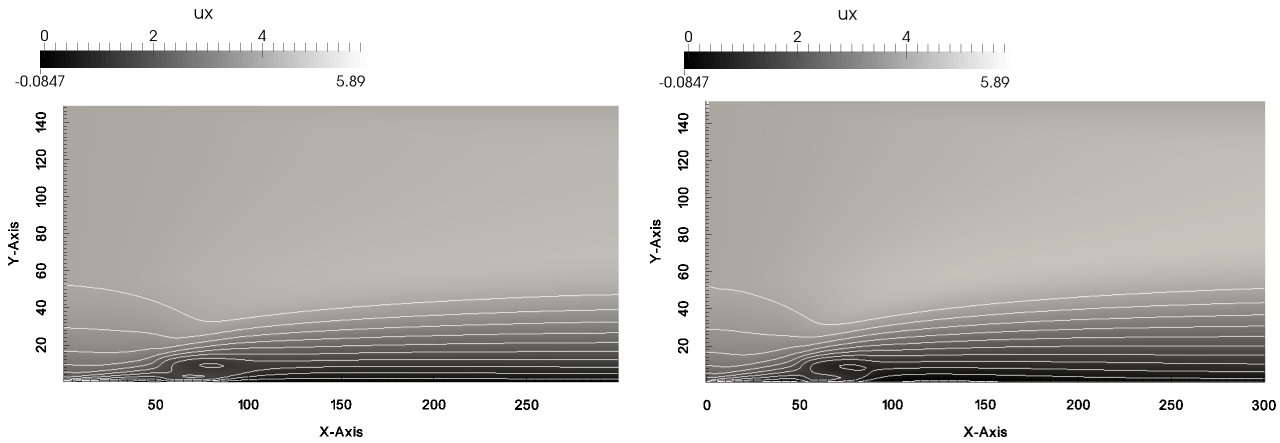

Fig. 1: Isolines of the horizontal velocity fields for $r = 0.1$ (right) and $r = 0.3$ (left)

References

[1] T. Bodnar, et al., Application of compact finite-difference schemes to simulations of stably stratified fluid flows, Appl. Math. Comput., 219 (2012) 3336–3353.

[2] A.K. Blackadar, The vertical distribution of wind and turbulent exchange in a neutral atmosphere, J. Geophys. Res., 67 (1962) 3095–3102.

[3] J.T. Steffens, et al., Exploration of effects of a vegetation barrier on particle size distributions in a near-road environment, Atmospheric Environment, 50 (2012) 120–128.

21st International Conference **ENGINEERING MECHANICS 2015**
Svratka, Czech Republic, May 11 –14, 2015
Paper **#253, pp. 258–259**

ANSYS More than FEM

Radek Řídký[a], László Iván[b]*, Miloslav Popovič[c]
SVSFEM s.r.o., Škrochova 42; 615 00, Brno; CZ
[a]rridky@svsfem.cz, [b]livan@svsfem.cz, [c]mpopovic@svsfem.cz

Keywords: numerical analysis, optimization, ANSYS

Abstract: A standard numerical simulation is only one step in product development. A robust and effective result can be found only in complex of many different but connected analyses. Many years of development in numerical simulations brings extensive multiphysics systems as ANSYS product family. One of the most important step in development process is in optimization of required results.

Introduction

More than 40 years of continual development in FEM simulation methods in ANSYS family shifts technical opportunities in wide range of everyday demands. This long period was started by Dr. John A. Swanson as Swanson Analysis Systems, Inc (SASI) with raw but clever codes for structural physics that could simulate static (stationary), dynamic (moving) and thermal (heat transfer) problems. It enabled to take advantage of currently available computers in combination with many years known mathematical solutions. This longtime process is still in movement now. Not only structural or thermal analyses are able to sufficiently describe nowadays problems that technical engineers should solve. A precision of required simulations goes to particle size less than micrometer but in opposite sometimes a complex fluid simulation solves problems in kilometers of atmosphere. It everything leads to multiphysics solution with general-purpose tools, like ANSYS products are.

Problem description

The simulation system implemented in ANSYS product package grows every year like an evolution process. Structural simulations enable to analyze large models with millions of equations. The interaction of many parts in complicated assemblies is more reliable and quicker. All neither structural nor thermal modules include more independent loads and boundary conditions.

Some steps in FEM analysis systems can be understand as a revolution steps. The process of any numerical simulation was passed from some standalone applications to the complex project environment named ANSYS Workbench. It enabled to implement fluid modules as CFX or Fluent. Besides that more explicit simulation systems were implemented similarly. Many engineers welcomed extensive group of electromagnetics systems.

Actual questions in product development become more and more complex in many physical areas. The multiphysics simulation system can be a solution for this purpose.

Parametrization in FEM

The standard numerical simulation is a complex of many complicated material models, structural models and other physics description. Many inputs are significantly inaccurate or almost unknown. Any competent and efficient tool for this problem can be found in sensitivity study of important inputs of numerical models. The sensitivity study can assess level of influence of any inputs to any outputs. A correlation between any parameters can be observed.

ANSYS product package offer a solution for this process in optimization modules, i.e. optiSLang optimization system. Not only sensitivity can be used with advance but many optimization procedures are available too.

The big advantage of this system is in assessment of the whole product development process. It can be evaluated by a robustness study. It enables to observe quality of any optimized results.

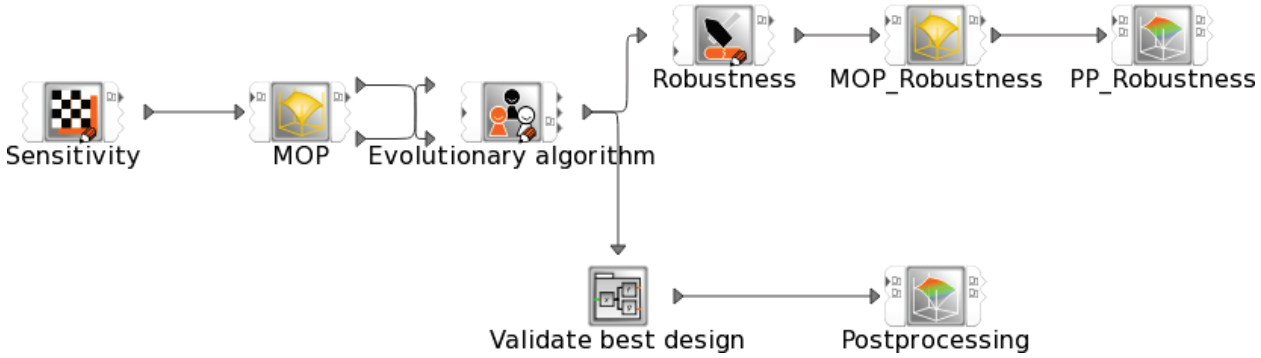

Fig. 1: Optimization process in optiSLang environment.

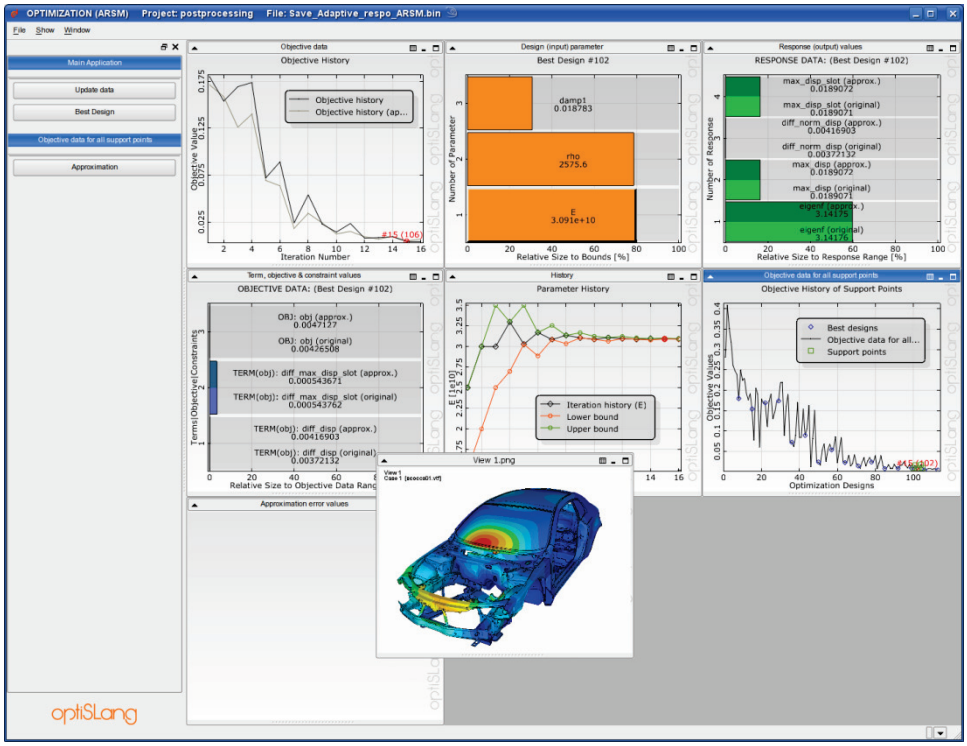

Fig. 2: Example of results of an optimization study.

Conclusion

Not only one numerical simulation brings sufficient results. Actual problems have to be solved in complex multiphysics point of view. Moreover, good stability of results in combination with product costs can be found only in optimized and robust result. Numerical simulation systems are able to solve all those requirements.

21st International Conference **ENGINEERING MECHANICS 2015**
Svratka, Czech Republic, May 11 –14, 2015
Paper **#181, pp. 260–261**

The Dynamic Response of Polymeric Composites

R. Řídký[1,a]*, M. Popovič[1,b], S. Rolc[2,c], M. Drdlová[3,d], J. Krátký[4,e]

[1]SVSFEM s.r.o., Škrochova 42; 615 00, Brno; CZ.
[2]Vojenský výzkumný ústav. s. p., Veslařská 230, 637 00 Brno, CZ.
[3]Výzkumný ústav stavebních hmot, a. s., Hněvkovského 65, 617 00 Brno,CZ.
[4]BOGGES spol. s.r.o., Rudice 1, 679 06 Rudice, CZ.
[a] rridky@svsfem.cz, [b] mpopovic@svsfem.cz, [c] rolc@vvubrno.cz,
[d]drdlova@vustah.cz, [e]josef.kratky@bogges.cz

Keywords: split Hopkinson pressure bar, absorbing materials, polymeric composites, viscoelastic testing bars, explicit LS-Dyna code

Abstract: Knowledge of the properties of soft, viscoelastic materials at high strain rates are important in our understanding of their role during blast or impact events. Although there is a large body of literature containing compressive data, this rarely deals with strain rates above 250 s^{-1} which becomes increasingly important when looking at the design of composite structures where energy absorption during impact events is high on the list of priorities. The high strain-rate characteristics of a specific porous blast energy absorbing material measured by modified Split Hopkinson Pressure Bar apparatus is presented in this study. Testing these low impedance materials using a metallic split Hopkinson pressure bar setup results in poor signal to noise ratios due to impedance mismatching. These difficulties are overcome by using polymeric Hopkinson bars. Conventional Hopkinson bar analysis cannot be used on the polymeric bars due to the viscoelastic nature of the bar material. Implementing polymeric Hopkinson bars requires characterization of the viscoelastic properties of the material used. In this paper, 16 mm diameter Polycarbonate bars are used as Hopkinson pressure bars. This testing technique is applied to materials composed of porous glass/ceramic filler and polymeric binder, with density of 125 - 300 kg/m^3 and particle size in range of 50 μm – 2 mm. Testing of polymeric composites at high strain rates allows the development of better constitutive models that is necessary for next numerical simulations.

Introduction

The aim of this study was to analyze properties of dynamic impact absorbing materials composed of porous glass/ceramic filler and polymeric binder. This complex investigation was based on experimental testing in order to determine an applicable material model for practical material selection and next numerical simulations as well. Two kinds of experiments were performed, dynamic Split Hopkinson Pressure Bar (SHPB) test and surrogate projectile impact on material layer as a verification test. Two types of absorbing with different filler type (trade name Liaver and Liapor) were fully compared.

Problem description

The structure and material properties of analyzed samples did not allow a standard SHPB test because of large impedance difference between analyzed material and testing bars material. Moreover standard steel testing bars can significantly harm an analyzed sample because of high hardness of interaction area and high mass of bars in motion. To ensure accurate measurement, standard steel testing bars were replaced by high sensitivity polymeric bars. An example of recorded input and output strain gauge signals are depicted in Fig. 1.

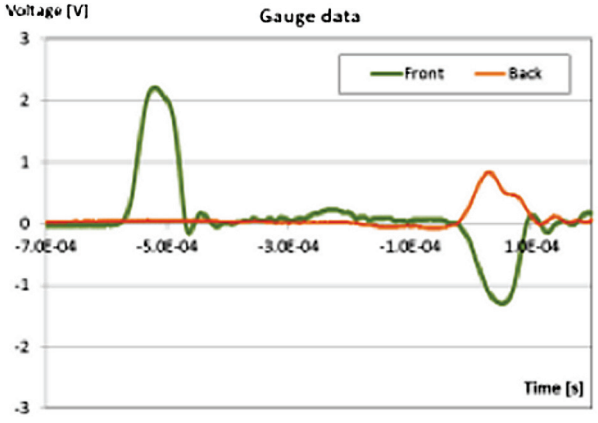

Fig. 1: Experimental data – SHPB test.

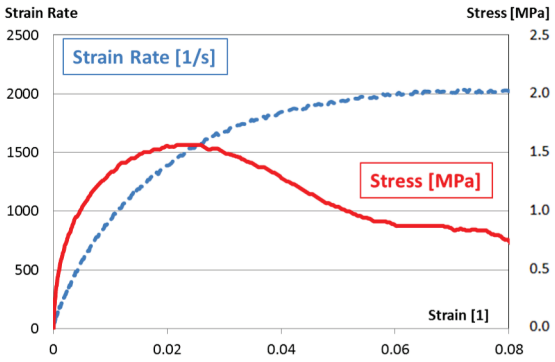

Fig. 2: SHPB result–Stress–Strain–Strain Rate

Measuring the high strain rate response of the above described absorbers, the material of testing bars has to be taken into account due to viscoelastic behavior of the bar during impact wave propagation. Ahonsi [1] implemented this viscoelastic model in wave propagation theory by complex evaluation of testing bars material. It can be defined on the SLS material model that is combination of standard Hook's law and Maxwell material model. The complex behavior of material properties leads to evaluation of measured data in frequency domain. I.e., the attenuation coefficient of bars material referred in [2] is frequency dependent too. Practically measured data should be analyzed by FFT method and afterwards an inverse FFT method can quantify stress, strain and strain rate dependency according to [3].

Numerical material model

The most convenient and universal material model has to be defined based on the results from the first investigation step. More material models were analyzed, the most suitable models were found in LS-Dyna explicit code named Mat_Honeycomb respectively Mat_Crushable_Foam. The major use of the first mentioned model is for honeycomb and foam materials with real anisotropic behavior. A nonlinear elastoplastic material behavior can be defined separately for all normal and shear stresses. The second material model is dedicated to modeling crushable foam with optional damping and tension cutoff. Unloading is fully elastic. Tension is treated as elastic-perfectly-plastic at the tension cut-off value.

Verification of the numerical simulation in real tests

Subsequent experiment was performed due to validation of achieved numerical material models of samples (Liaver and Liapor). This test is based on the surrogate projectile impact on the rectangle sample with dimensions of 100x100x5 mm. This experiment result was compared with an explicit numerical simulation of experiment setup with material model from previous step.

Conclusion

This study analyzed a problem of testing of absorbing materials in high velocity conditions. Whole testing and evaluating procedure was applied to materials composed of porous glass/ceramic filler and polymeric binder, with density of 125 - 300 kg/m^3 and particle size in range of 50 µm – 2 mm. SHPB experimental method adapted for viscoelastic testing bars was used. The obtained material properties were used for adjustment of numerical material model. This numerical model was successfully verified in next experiment including high velocity projectile impact.

Acknowledgement: The authors gratefully acknowledge the financial support from the Grant Agency of the Czech Republic through the project GAČR GA13-22945S.

References

[1] B. Ahonsi, J.J. Harrigan, M. Aleyaasin, On the propagation coefficient of longitudinal stress waves in viscoelastic bars, Int J Impact Eng (2012), doi:10.1016/j.ijimpeng.2012.01.004

[2] H.S.U. Butt, P. Xuea, Determination of the wave propagation coefficient of viscoelastic SHPB: Significance for characterization of cellular materials, Int J Impact Eng, 74 (2014) 83–91.

[3] T.P.M. Johnson, S.S. Sarva, S. Socrate, Comparison of Low Impedance Split-Hopkinson Pressure Bar Techniques in the Characterization of Polyurea, Exp Mech, 50 (2010) 931–940.

21st International Conference **ENGINEERING MECHANICS 2015**
Svratka, Czech Republic, May 11 –14, 2015
Paper **#022, pp. 262–263**

Numerical Simulation of Flow in the Human Vocal Tract

Václav Řidký

Institute of Thermomechanics AS CR, v. v. i.

vaclav.ridky@tul.cz

Keywords: finite volume method, unsteady simulation, dynamic mesh and incompressible flow

Abstract: Numerical simulation of 2D flow in the human vocal tract is important part for the generation of synthetic human voice. Human vocal folds model is changing its position by prescribed harmonic oscillations. The unsteady flow is computed on a dynamic mesh and the solver is a combination of SIMPLE and PISO algorithms. The simulation is performed within the package OpenFOAM and the computational mesh is generated using the generator SnappyHexMesh.

Introduction

Numerical simulation of airflow in vocal folds combines solution of airflow and structure deformation. The numerical simulations are solved in finite volume package OpenFOAM [5]. Motion of the vocal folds is prescribed as a harmonic function. In this case it is prescribed as a mathematical function on the walls which represent the vocal folds. This motion is combination of rotation and translation (motion with two degrees of freedom)

$$x_1 = x_{10} + X_1 * \sin\left(2\pi f * t + x_{1phase}\right) \tag{1}$$

$$x_2 = x_{20} + X_2 * \sin\left(2\pi f * t + x_{2phase}\right), \tag{2}$$

where values with index 1 are components of rotational motion and with index 2 are components of translational motion. The phase shift between the two motions is $\pi/2$. Starting position of vocal folds is at the minimum gap. Frequency of harmonic motion is 100 Hz. The solver Mesquite [1] used for solution of the mesh deformation gives good results even for small glottal gaps, and allows the vocal folds approaching twice closer than the solver based on solution of the Laplacian equations [2] that was used up to now.

Flow is computed as unsteady with time steps dependent on the Courant number. The computational domain is a simple model of human glottis with vibrating vocal folds which are changing the channel geometry in time. The solver is based on a combination SIMPLE and PISO algorithms [4]. The flow is modeled as an incompressible viscous fluid without any turbulence model. It is described by the continuity equation and the Navier-Stokes equations:

$$\frac{\partial \mathbf{u}}{\partial \mathbf{x}} = 0 \tag{3}$$

$$\frac{\partial \mathbf{u}}{\partial t} + \nabla \cdot (\mathbf{u}\mathbf{u}) - \nabla \cdot \nu \nabla \mathbf{u} + \frac{1}{\rho}\nabla p = 0, \tag{4}$$

where $\mathbf{u}$, p and ρ are fluid velocity, pressure, and density and ν is kinematic viscosity.

The boundary conditions for the velocity are set to zero on fixed walls, and equal to the velocity of the moving surface on the vocal folds. Initial distribution of pressure and velocity is a result of stationary solution for minimal gap in order to eliminate transitional processes at the beginning of a dynamic simulation.

Results

The velocity fields from third period of motion of vocal folds are shown in Fig. 1. Simulation is computed on a 2D tetrahedral mesh, the number of elements is 46 k. The air flow separates from the wall and creates large-scale circulation structure. During the maximally open gap (see two results on the right side of Fig. 1) the flow alternately attaches to the upper or lower vocal folds.

Plan for future is computed simulation in 3D with more complex motion of the vocal folds. The next step is to modify the solver to reduce the gap width until the interruption of the flow.

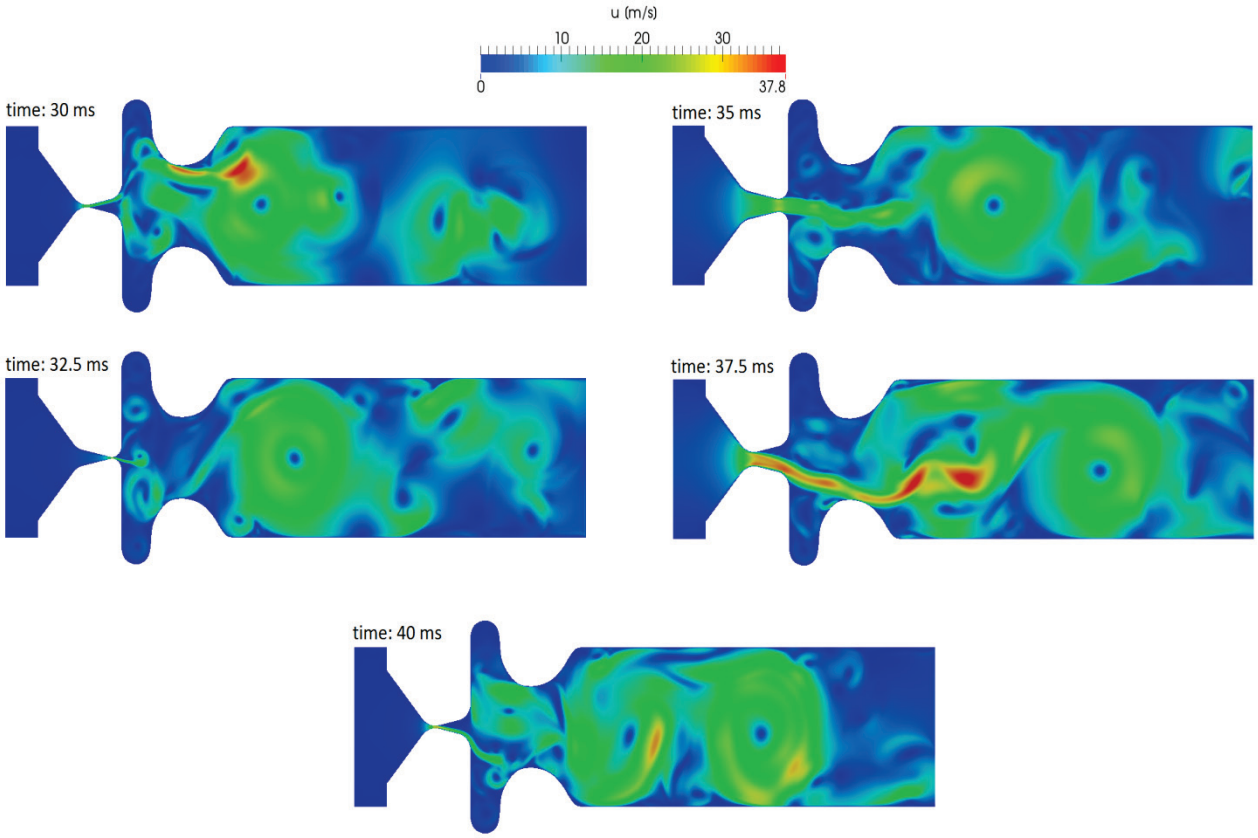

Fig. 1: Velocity fields during the third period of the vocal folds motion

Acknowledgments: The research has been supported by the Czech Science Foundation; project P101/11/0207

References

[1] V. Řidký, P. Šidlof, Numerical simulation of deformation of dynamic mesh in the human vocal tract model, EPJ Web of Conferences 69 (2015) 465-468.

[2] P. Šidlof, S. Zörner, A. Hüppe, Numerical simulation of flow-induced in human voice production, Procedia Engineering 61 (2013) 333-340.

[3] J. H. Ferziger, M. Peric, Computational Methods for Fluid Dynamics, third edition, Springer, Berlin, 2002.

[4] H. Jasak, Error Analysis and Estimation for the Finite Volume Method with Applications to Fluid Flows, PhD thesis, Imperial College, London, 1996.

[5] Information on http:// www.openfoam.org.

21st International Conference **ENGINEERING MECHANICS 2015**
Svratka, Czech Republic, May 11 –14, 2015
Paper **#020, pp. 264–265**

Simple Model of the Cajal-Like Interstitial Cell and Its Analysis

Josef Rosenberg[1,a] *, Milan Štengl[2,b], Miroslav Byrtus[3,c]

[1,3]University of West Bohemia, Dpt. of Mechanics, Univerzitni 8, 30614 Plzen, Czech Republic

[2]Charles University in Prague, Faculty of Medicine in Pilsen, Physiology , Czech Republic

[a]rosen@kme.zcu.cz, [b]milan.stengl@lfp.cuni.cz, [c]mbyrtus@kme.zcu.cz

Keywords: Cajal-like interstitial cells, bladder, nonlinear dynamical system

Abstract: Cajal-like interstitial cells (IC-LC) can be detected e.g. in the bladder wall tissue. The current research proves their important role in both physiological and pathological function of this organ. The authors developed relative simple mathematical model consisting of five nonlinear ODEs. The model accuracy was verified using published experimental results. Presented nonlinear dynamical system was then analyzed using software Matcont. This analysis allowed to simulate the influence of different drugs on the function of the bladder. The drug influence was again compared with the experimental results.

Introduction

To model the pathological events in the lower part of urinary tract (LPUT) like the over-active bladder (OAB) and detrusor over-activity (DO), it seems to be necessary to take into account all cellular types present in the detrusor tissue. Besides the smooth muscle cells (SMC) there are the Cajal-like interstitial cells (ICCLC) and urothelium cells. According to the last investigations (see e.g. the survey [1] and [2]), the ICCLC are involved in the spontaneous contractile activity during bladder filling. For this purpose it's useful to develop relatively simple model based on the current knowledge about these cells ([3], [4], [5]). Such a model allows to study the influence of different drugs using free software packages like MATCONT or XPPAUT. This is the goal of this contribution.

Description of the model

According the above mentioned papers the scheme of ICCLC presented in Fig. 1 was used.

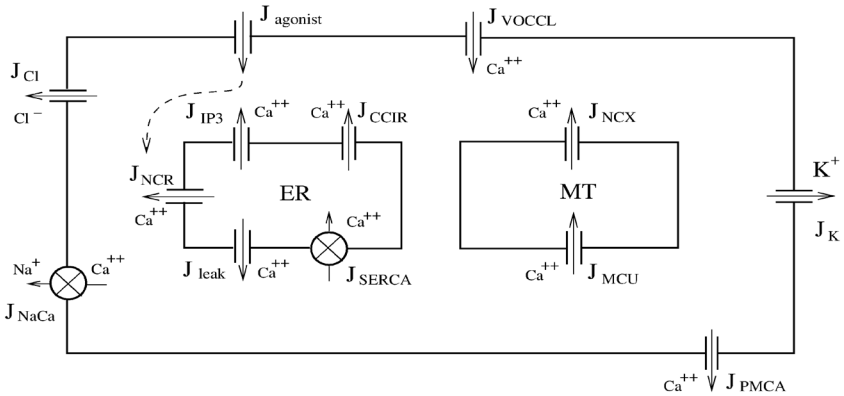

Fig 1: Schema of ICCLC with all fluxes. ER is the endoplasmatic reticulum and MT is the mitochondria.

The basic equations for Ca2++ concentration in cytoplasm (c ev. cc), in ER (c_{ER}), in MT (c_{MT}), for the membrane potential (v) and the variable w are following

$$\frac{dc}{dt} = J_{IP3} - J_{VOCCL} + J_{CICR} + J_{IICR} + J_{Leak} - J_{SERCA} - J_{PMCA} + J_{NaCa} - J_{MCU} + J_{NCX}; \qquad (1)$$

$$\frac{dc_{ER}}{dt} = J_{SERCA} - J_{CICR} - J_{IICR} - J_{Leak}; \tag{2}$$

$$\frac{dv}{dt} = \gamma \cdot [J_{Cl} - J_{VOCCL} - J_{NaCa} - J_K]; \tag{3}$$

$$\frac{dw}{dt} = \lambda \cdot \left[S \cdot \frac{(c+x_w)^2}{(c+x_w)^2 + beta \cdot e^{-\frac{v - z_{Ca3}}{R_K}}} - w \right]; \tag{4}$$

$$\frac{dc_{MT}}{dt} = J_{MCU} - J_{NCX}. \tag{5}$$

On the right hand sides there are the ion fluxes. The corresponding formulas and basic values of parameters was taken from literature, mainly from [5] and [6]. The parameters were then fitted in accordance with published experimental results.

Some results

As an example, in Fig. 2 there is shown the influence of the equilibrium potential of the Na-Ca exchanger zNaCa, which can be advantageously influenced by drug.

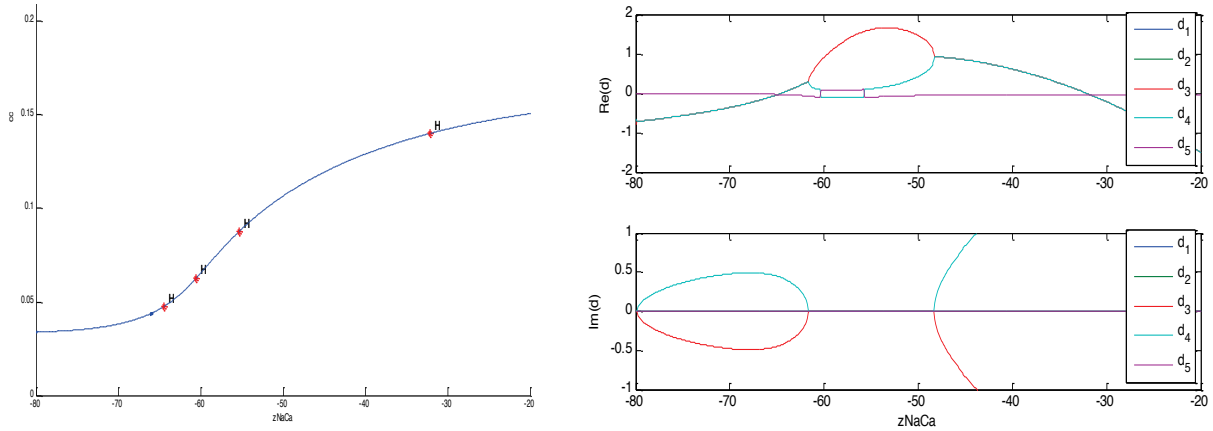

Fig. 2: left: Influence of zNaCa on Ca2++ concentration; right: change of eigenvalues. H are the bifurcation points – comparing with the eigenvalues change, the stability can be determined.

References

[1] K.E. Andersson, A. Arner A., Urinary Bladder Contraction and Relaxation: Physiology and Pathophysiology. Physiol. Rev. 84 (2004) 935-986.

[2] B.T.Drumm et al.,Calcium signalling in Cajal-like interstitial cells of the lower urinary tract. Nat. Rev. Urol. advance online publication 16 (2014) doi:10.1038/nrurol.2014.241.

[3] M.J. Berridge, Smooth muscle cell calcium activation mechanisms. J. Physiol 586.21 (2008) 5047-5061.

[4] J. Deng et al., Identification of T-type Calcium Channels in the Interstitial Cells of Cajal in Rat Bladder, UROLOGY 80 (2012) 1389.e1–1389.e7.

[5] R.A. Faville et al., A biophysically based mathematical model of unitary potential activity in interstitial cells of Cajal. Biophys J. 95 (2008) 88-104.

[6] M. Koenigsberger et al., Calcium dynamics and vasomotion in arteries subject to isometric, isobaric and isotonic conditions. Biophysical Journal. 95 (2008) 2728-2738.

21st International Conference **ENGINEERING MECHANICS 2015**
Svratka, Czech Republic, May 11 –14, 2015
Paper **#083, pp. 266–267**

Long-Term Trends in Annual Ground Snow Maxima for the Carpathian Region

Árpád Rózsás[1,2,a] *, Miroslav Sýkora[1,b], László Gergely Vigh[2,c]

[1]Department of Structural Reliability, Klokner Institute, Czech Technical University in Prague, Solinova 7, 16608 Prague, Czech Republic

[2]Department of Structural Engineering, Budapest University of Technology and Economics, 3-9. Műegyetem rkp., Kmf. 85, Budapest, H-1111, Hungary

[a]rozsas.arpad@epito.bme.hu, [b]miroslav.sykora@klok.cvut.cz, [c]vigh.l.gergely@epito.bme.hu

Keywords: ground snow, non-stationary, maximum likelihood, extreme value theory, structural reliability

Abstract: The current structural design provisions are prevalently based on experience and on the assumption of stationary meteorological conditions. However, the observations of past decades and advanced climate models show that this assumption is debatable. Therefore, this paper examines the long-term trends in ground snow load maxima, and their impact on structural reliability. For this purpose, the Carpathian region is selected, and data from a joint research effort of nine countries of the region are used. According to our knowledge, the long-term trends in extreme snow loads, i.e. annual maxima, for this region has not been sufficiently studied yet.

Methodology and results

Stationary and five non-stationary generalized extreme value (GEV) distributions are fitted to the snow water equivalents (SWE) utilizing the maximum likelihood method. First, a linear line is fitted to the annual snow maxima at every grid point by the least-square method, while the snow-free years are discarded from the analysis. The associated slope parameters are illustrated in Fig. **1**, where the negative values are referring to decreasing trend in time. At 97% of 5895 locations negative trend is detected, whereas a mild increase is observed in the northern part of the region, Slovakia, Czech Republic, and Poland.

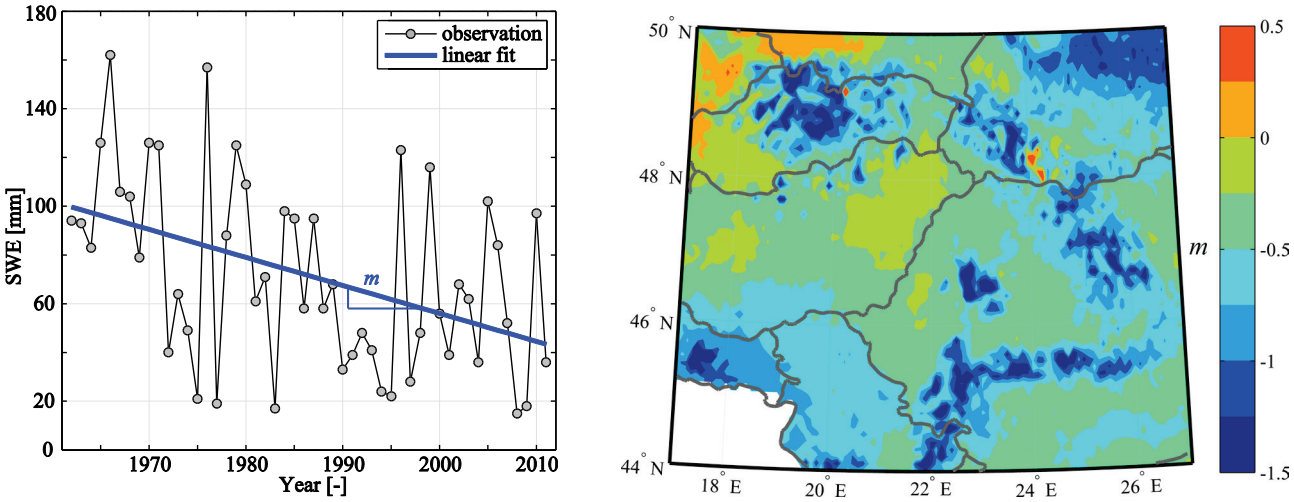

Fig. 1: A representative location with decreasing trend (left), and map of the linear trend line's slope parameter *m* in mm/year (right).

Then statistical and information theory based approaches, likelihood ratio (LR) test and Akaike weights respectively, are used to compare the models and to identify trends. Both approaches reveal that the trend in the annual maxima is better captured by allowing trend in the location parameter

than in the scale parameter of GEV. Hence, the non-stationary model with linear trend in the location parameter (μ1) is used for further study. The characteristic values and confidence intervals are calculated for year 1962 and 2011, for six selected locations. The time trend is deemed practically significant if the stationary estimate is outside of the non-stationary confidence interval. Based on this criterion, only two of the selected locations exhibit practically significant negative trend.

Additionally, reliability analyses are performed for a simple structure to explore the practical significance of the trends. Two locations are examined, one from Hungary with moderate decreasing trend (statistically significant by the LR test), the other one from Ukraine with strong decreasing trend. Reliability is analysed considering a reference period of one year. The location parameter is obtained from the non-stationary model for each of the selected years - 1962, 2011 and 2062. Fig. 2 indicates reliability indices and confidence intervals illustrating effect of parameter estimation uncertainty.

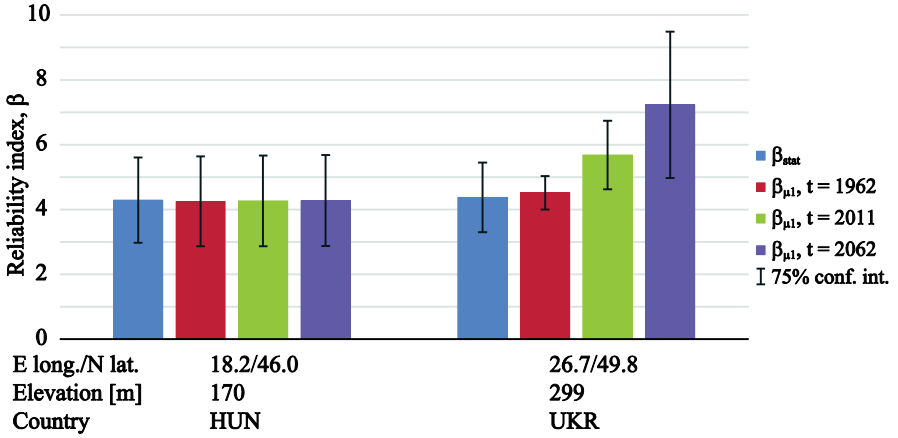

Fig. 2: Reliability indices with 0.75 confidence intervals from ground snow parameter estimation uncertainty.

Conclusions

The main conclusions of the study can be summarized as follows:

- A decreasing trend in annual snow maxima is found for 97% of the studied region.
- The reliability analyses show that the practical significance of time trends not necessary follows the statistical significance. This is largely due to the substantial uncertainty in parameter estimation.
- The simple, limited reliability analyses indicate that for most locations in the region, which are characterized by Fréchet distribution, the negative trend in annual snow maxima has a minor effect on structural reliability, the uncertainty in parameter estimation rules.
- For locations with strong, decreasing trend and Weibull distribution, the impact on structural reliability is practically significant, although the change is favourable from a safety point of view.

Acknowledgement: This work was partly supported by the International Visegrad Fund Intra-Visegrad Scholarship (contract no. 51401089) and by the Ministry of Education, Youth and Sports of the Czech Republic (LG14012 project). The meteorological data were obtained from the CARPATCLIM Database © European Commission - JRC, 2013.

21st International Conference **ENGINEERING MECHANICS 2015**
Svratka, Czech Republic, May 11 –14, 2015
Paper **#123, pp. 268–269**

Parallel Data Mapping between Simplex Finite Element Meshes using Mesh Topology

Daniel Rypl[a], Jan Vesecký[b]

Department of Mechanics, Faculty of Civil Engineering, Czech Technical University in Prague,
Th´akurova 7; 166 29, Prague; Czech Republic

[a]daniel.rypl@fsv.cvut.cz, [b]jan.vesecky@fsv.cvut.cz

Keywords: finite element data transfer, finite element mesh mapping, walking algorithm, mesh traversal, parallelization, threads

Abstract: Presented paper focuses on the transfer of finite element data between simplex finite element meshes representing different discretizations of the same geometrical model. The construction of the localization map, defining for each node of the target mesh, onto which the data are to be transferred, the closest element of the original source mesh, is based on the walking algorithm, performing a traversal between neighbouring elements of the source mesh from an initial element towards the processed node. To make the algorithm efficient and reliable, individual nodes of the target mesh are processed in special order given by the nodal connectivity of the target mesh. The implementation also relies on the classification of the processed meshes to the underlying geometrical model. Once the localization map is available, data from the source mesh are mapped to nodes of the target mesh in parallel (using threads) by the help of shape functions of the elements of the source mesh.

Introduction

A need for transfer of finite element data between finite elements meshes appears commonly in many finite element method based applications. There are several approaches for mapping the field variables. The most common one is based on shape functions of element comprising given point [1, 2], the others use typically the nearest point or set of points [3]. The common denominator of these techniques is the need to localize the node or element of the original mesh nearest to a particular node (or point) of the mesh on which the field variables are to be recovered. Since the recovery is likely to be performed many times during the analysis, in the past the attention was primarily focused on the computational efficiency of the localization process. In this context, the spatial index based approaches using various tree or dynamic cell data structures proved to be especially powerful. However, these approaches use typically only geometrical location/distance to determine the index (position of the node/point within the data structure), which may lead to incorrect results in special cases when dealing, for example, with geometry with curved discrete cracks. In these cases the topological distance should be also considered.

Walking algorithm

In the present approach, the localization process does not rely on any spatial index and the search is performed by a walking algorithm [4, 5] based on the topological information of the mesh and the knowledge from previous searches. The basic idea comes from the fact that elements of the original mesh comprising adjacent nodes of the new mesh are likely to be relatively close to each other. Thus the candidates for localization are always not yet processed neighbours of already localized nodes which are inside or on the boundary of the processed region. The order in which the nodes are processed is controlled by a queue, which must be initialized by (at least) one node, the source element of which is known. This should be either a vertex node, in which case the target element can be quickly identified as one of elements on the original mesh incident to the same (classified to the same vertex or having

identical coordinates) vertex node, or interior node (or a virtual point inside the region (as a last resort)), in which case target element comprising the node (or point) is found by inspecting successively individual elements (classified to the processed region) of the original mesh until the one comprising the node is localized. Once the queue is initialized, it is processed on the first-in first-out basis until it becomes empty. If it is empty but there are still some unprocessed nodes in the target mesh, the queue must be newly initialized by a not yet processed target node(s) and the processing of the queue is invoked again. Once localization of a particular node in the queue is completed, its shape functions within the localized source element are computed and stored for later use during the mapping of the field variables. If the node is outside of its source element then it is marked as provisionally localized. If the node is inside of the source element and it is either interior or boundary classified to an entity of the next lower dimension (with respect to the processed region) then all its not yet processed or provisionally localized neighbour nodes are added to the queue using its source element localized by the walking algorithm as the initial element for their own localization. The advantage of the proposed approach is that it needs no additional searching data structure and relies only on the mesh topology and optionally also on the classification of the mesh with respect to the underlying geometrical model. The disadvantage consists in the fact that all the nodes, not only the selected ones, of the new mesh must be processed to ensure convergence and efficiency of the algorithm. Also the localization of the first node, when performed by intensive search, can be considered a drawback (despite the fact that this search is likely to be computationally less demanding than building the complete searching data structure), especially if performed several times when processing disconnected meshes, for example.

Summary

In this paper, a topology based methodology for the transfer of data between simplex finite element meshes has been introduced. While the standard approaches are based on various spatial decomposition techniques using typically Euclidean distance as the measure of proximity of the objects, the proposed method relies on topological features of the processed meshes and their classification to the underlying geometrical model. The approach proved to be not only reliable but also efficient. Its efficiency is further increased by running the actual mapping of data in several concurrent threads.

Acknowledgments: This work was supported by the Technology Agency of the Czech Republic under project No. TA02011196. Its financial assistance is gratefully acknowledged.

References

[1] S.M. Afazov, A.A. Becker, T.H. Hyde, Development of a Finite Element Data Exchange System for Chain Simulation of Manufacturing Processes, Advances in Engineering Software, 47 (2012) 104–113.

[2] D. Scrimieri, S.M. Afazov, A.A. Becker, S.M. Ratchev, Fast Mapping of Finite Element Field Variables Between Meshes with Different Densities and Element Types, Advances in Engineering Software, 67 (2014) 90–98.

[3] Y. Luo, A Nearest-Nodes Finite Element Method with Local Multivariate Lagrange Interpolation, Finite Elements in Analysis and Design, 44 (2008) 797–803.

[4] O. Devillers, S. Pion, M. Teillaud, Walking in a Triangulation, International Journal of Foundations of Computer Science, 13 (2002) 181–199.

[5] R. Soukal, V. Purchart, I. Kolingerová, Surface Point Location by Walking Algorithm for Haptic Visualization of Triangulated 3D Models, Advances in Engineering Software, 75 (2014) 58–67.

Dynamic Analysis of the Structure Exposed to the Moving Periodic Force and Viscoelastic Models of the Human Body

Vladimír Šána

Czech Technical University in Prague, Faculty of Civil Engineering, Department of Mechanics,Thákurova 7, CZ-166 29 Prague, Czech Republic

vladimir.sana@fsv.cvut.cz

Keywords: human-Induced vibration, human-structure interaction, vibration of footbridges, DLF model, viscoelastic models of human body

Abstract: Submitted paper is focused on dynamic analysis of the footbridge structure, which is represented by the simply supported beam. The continuous beam model was discretized by the FEM to MDOF system and loaded by pedestrians, walking across the structure. Two states of loading are considered in this paper. Firstly, it is the mathematical description of pedestrian's ordinary traffic, where each pedestrian is randomly generated by the Monte Carlo method. Secondly, the movement of single pedestrian, simplified by viscoelastic models, is introduced.

Introduction

The human induced vibration is phenomenon, which designers and structural engineers must take into account during the design of footbridges, grandstands etc. It is essential namely at the structures with some of the natural frequencies inside the range $\langle 1\,\mathrm{Hz}; 3\,\mathrm{Hz}\rangle$, which is typical frequency interval of human walking or running. It means, that the resonance between pedestrians and structure can occurs.

DLF model of pedestrian's ordinary traffic

This is special type of live load induced by humans. Pedestrians walk with random pacing frequencies and with random incoming time during the ordinary traffic. It is significant at structures with very dense traffic, e.g. at footbridges near the underground stations etc. The ordinary traffic of pedestrians has been considered as stochastic process, where each of these pedestrians is simplified by the periodic force defined as

$$P(t) = G + \sum_{j=1}^{N} G\,\alpha_j\,\sin\left(j\,\omega_p\,t - \phi_j\right). \tag{1}$$

where G is static weight of pedestrian, α_j is the dynamic loading factor of j-th harmonic element (DLF), ω_p is circular frequency associated with velocity of motion and ϕ_j is phase shift of j-th harmonic element. *Bachmann's* DLF model was used for the mathematical description of pedestrian. The appropriate multipliers α_j and phase shifts ϕ_j are summarized e.g. in [2].

The Monte Carlo method was used for numerical simulations of ordinary traffic, where number of pedestrians N, velocity of motion v_p (pacing frequency f_p), weight of pedestrians m_p and individual time of incoming τ_p were generated from the uniform distribution of probability. The script, created in MATLAB, can be briefly described by next steps: Set up input param. $\rightarrow$ assembling of struct. matrices $\rightarrow$ generating of random pedestrians (v_p, m_p, N) $\rightarrow$ assembling of right sided vector $\rightarrow$ numerical integration of diff. eq. (Newmark-β) $\rightarrow$ data visualization.

Viscoelastic models of single pedestrian

By using this approach, it was considered, that the human body is replaced by the Kelvin-Voigt element with 1 or 2 degrees of freedom. These models, visualized in Fig. 1, are described by the stiffness and

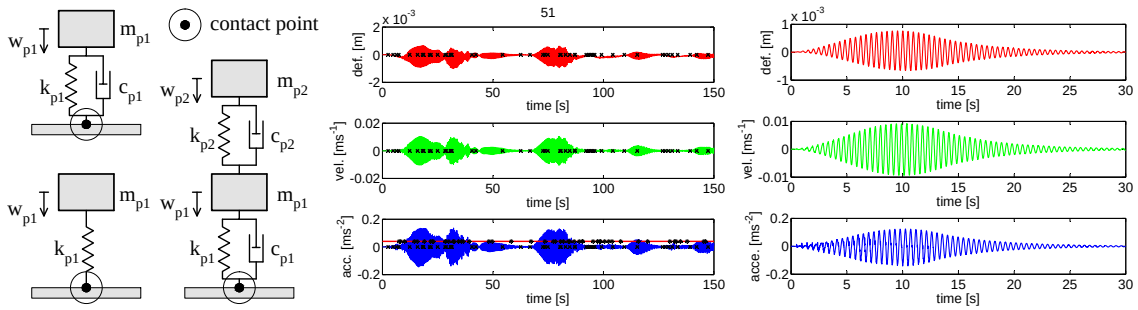

Fig. 1: Viscoelastic models, one realization of ordinary traffic and response of the structural midpoint-viscoelastic model.

viscous parameters, which can be found out hardly. Nevertheless someone is able to find the data in the literature. The viscoelastic parameters of the human body were studied and measured e.g. by *Farah*, *Brownjohn* etc. It was also considered, that model is moving with constant velocity v_p over the structure.

Solution of this problem was carried out separately for the viscoelastic element and for the structure (decoupled problem). Complications with activation of the pedestrian's passive model were solved by using the approximation of trajectory of the centre of gravity (CoG), which was used as input excitation signal for contact point between Kelvin's element and the structure. The algorithm of solution can be written as:

response of K-V model to kinematic exc. $\rightarrow$ calculation of contact force $\rightarrow$ calculation of the response of the structure $\rightarrow$ correction of CoG trajectory by computed deflections $\rightarrow$ back at the beginning of the loop.

Summary

New approaches to modeling of pedestrian's ordinary traffic and movement of single pedestrian have been presented in this paper. The ordinary traffic was simulated by the Monte Carlo method and each of random pedestrians was simplified by DLF *Bachmann's* model. Vibration induced by single pedestrian was described by viscoelastic model with kinematic excitation. The investigated structure was the simply supported beam, which is based on the real structure across Opatovska street in Prague. The numerical results of dynamic analysis are summarized in Fig. 1.

Acknowledgment: This paper has been created thanks to the project SGS No. 14/122/OHK1/2T/11 supported by Czech Technical University, which is gratefully acknowledged.

References

[1] P. Archbold, J. Keogh, C. Caprani, P. Fanning, A Parametric study of Pedestrian Vertical Force Models for Dynamic Analysis of Footbridges Dublin Institute of Technology (2011).

[2] H. Bachmann, W. Ammann, Vibrations in Structures Induced by Man and Machine, Structural engineering documents, International Association for Bridge and Structural Engineering, Zurich, Switzerland. ISBN 3-85748-052-X (1987).

[3] R. Sachse, A. Pavic, P. Reynolds, Human-structure dynamic interaction in civil engineering dynamics: A literature review Shock and Vibration Digest 35 (2003) 3-18.

21st International Conference **ENGINEERING MECHANICS 2015**
Svratka, Czech Republic, May 11 –14, 2015
Paper **#017, pp. 272–273**

Verification of Ductile Fracture Criteria Based on Selected Calibration Tests

František Šebek[a] *, Petr Kubík[b], Jindřich Petruška[c]

Brno University of Technology, Brno, Technická 2896/2, 616 69 Brno, Czech Republic

[a]sebek@fme.vutbr.cz, [b]m3petr@gmail.com, [c]petruska@fme.vutbr.cz

Keywords: ductile fracture, crack initiation and propagation, phenomenological criteria, explicit finite element method, AISI 1045 carbon steel

Abstract: Phenomenological ductile fracture criteria represent, among others, one of powerful tools for prediction of ductile fracture. These criteria are based on evaluating damage throughout the solid body as a response to straining. The damage is influenced by plasticity but not vice versa. Therefore, these criteria are often called uncoupled as they do not mutually couple the damage and plasticity. One of immense advantages of such criteria is a possibility not only to predict the crack initiation but also to follow the propagation based on the damage. Moreover, it is not restricted for one specific locus but the damage is evaluated in the entire solid body and one or more cracks can be tracked simultaneously or sequentially. Ductile fracture criteria are calibrated on the basis of several independent calibration tests under various stress states. One way how to verify calibrated model is to simulate numerically an experimental tests and follow the crack initiation and propagation. In the present study, selected phenomenological criteria were calibrated using various calibration tests. Then, selected calibration tests were simulated together with implemented ductile fracture criteria. In our case, the verification is carried out on tensile cylindrical specimens. Finally, computationally obtained results were compared to the experimentally observed ones and the prediction ability and reliability of selected phenomenological criteria is discussed.

The ductile fracture is comprehensive and complex problematics important in many fields of mechanics [1, 2]. It can be applied to vast different engineering applications [3]. Plasticity of AISI 1045 carbon steel was identified at first and two material constants of Hollomon hardening law [4] were calibrated. Three phenomenological ductile fracture criteria were selected and calibrated on the basis of tensile tests of smooth and notched cylindrical specimens and biaxial tests of notched tube specimens. Material constants of model proposed by Bai and Wierzbicki [5], Extended Mohr–Coulomb criterion [6], and model proposed by Lou et al. [7] were found using the non-linear least square method in the software MATLAB.

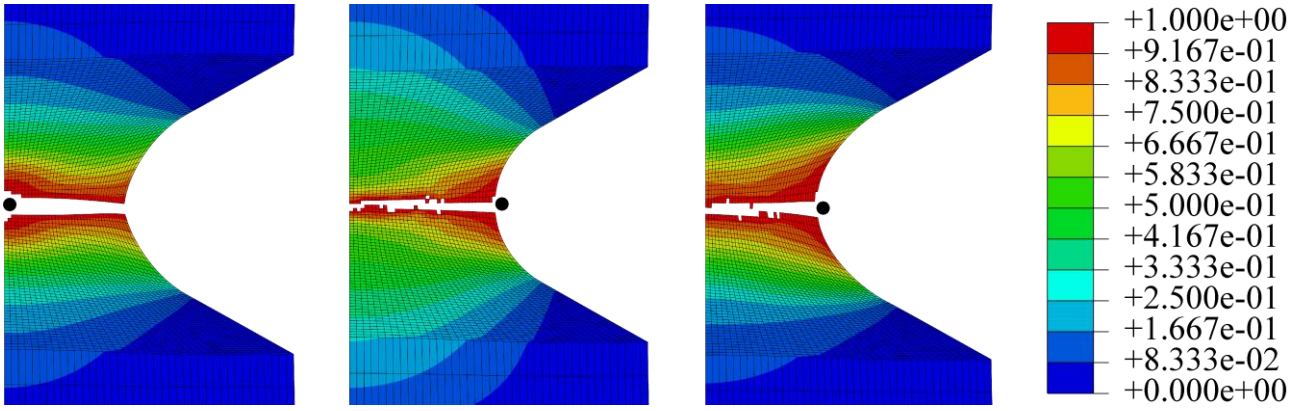

Fig. 1: Field of damage for specimen with notch radius R1.2 from left for model proposed by Bai and Wierzbicki [5], Extended Mohr–Coulomb criterion [6], and model proposed by Lou et al. [7]

Tensile tests of notched cylindrical specimens were simulated to investigate and verify the reliability of selected fracture criteria. The prediction ability was evaluated on the basis of the crack initiation and propagation predicted by each ductile fracture model compared to experimentally observed results. Loci of crack initiation are highlighted by the black circles in Figs. 1 and 2.

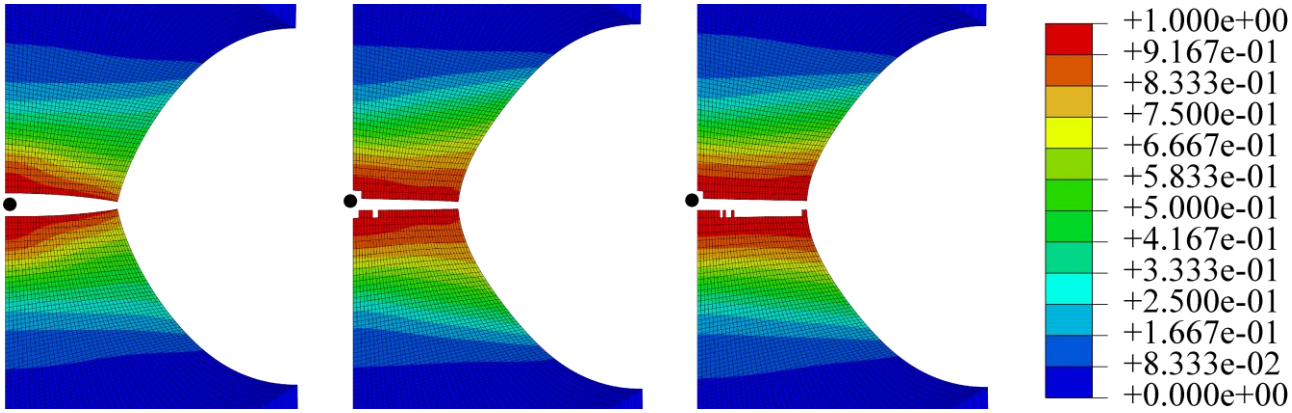

Fig. 2: Field of damage for specimen with notch radius R2.5 from left for model proposed by Bai and Wierzbicki [5], Extended Mohr–Coulomb criterion [6], and model proposed by Lou et al. [7]

The cup and cone fracture was experimentally observed. Fractography revealed [8] that the fracture really initiated in the center of tension cylindrical specimens on the axis of symmetry due to high stress triaxiality. All models predicted the crack initiation well (Figs. 1 and 2) except for the Extended Mohr–Coulomb criterion [6] and model proposed by Lou et al. [7] in case of notched cylindrical specimen with notch radius R1.2 (Fig. 1). Moreover, none of selected models predicted the slant fracture in the final part of the fracture to complete the cup and cone fracture mechanism.

Acknowledgment: This work is an output of cooperation between grant project FSI-S-14-2311 and NETME CENTRE PLUS (LO1202) created with financial support from the Ministry of Education, Youth and Sports under the „National Sustainability Programme I“.

References

[1] J. Petruška, P. Kubík, J. Hůlka, F. Šebek, Ductile Fracture Criteria in Prediction of Chevron Cracks, Adv. Mat. Res. 716 (2013) 653-658.

[2] F. Šebek, J. Hůlka, P. Kubík, J. Petruška. On the Proportionality of Damage Rule in Finite Element Simulations of the Ductile Failure, Adv. Mat. Res. 980 (2014) 189-193.

[3] J. Petruška, T. Návrat, F. Šebek, A new model for fast analysis of leveling process, Adv. Mat. Res. 586 (2012) 389-393.

[4] J. H. Hollomon, Tensile deformation, Trans. AIME 162 (1945) 268-290.

[5] Y. Bai, T. Wierzbicki, A new model of metal plasticity and fracture with pressure and Lode dependence, Int. J. Plast. 24 (2008) 1071-1096.

[6] Y. Bai, T. Wierzbicki, Application of extended Mohr–Coulomb criterion to ductile fracture, Int. J. Frac. 161 (2010) 1-20.

[7] Y. Lou, J.-W. Yoon, H. Huh, Modeling of shear ductile fracture considering a changeable cut-off value for stress triaxiality, Int. J. Plast. 54 (2014) 56-80.

[8] J. Bořkovec, Computer simulation of material separation process, Ph.D. Thesis, Brno University of Technology, 2008 (in Czech).

21st International Conference **ENGINEERING MECHANICS 2015**
Svratka, Czech Republic, May 11 –14, 2015
Paper **#187, pp. 274–275**

Fatigue Crack Front Behavior near the Free Surface

Martin Ševčík[1,a]*, Pavel Hutař[1,b], Andrei Kotousov[2,c], Luboš Náhlík[3,d]

[1]Institute of Physics of Materials, Academy of Sciences of the Czech Republic,
Žižkova 22, 616 62 Brno, Czech Republic

[2]School of Mechanical Engineering, The University of Adelaide, Adelaide, SA 5005, Australia

[3]Institute of Physics of Materials, Academy of Sciences of the Czech Republic,
Žižkova 22, 616 62 Brno, Czech Republic

[a]sevcik@ipm.cz, [b]hutar@ipm.cz, [c]andrei.kotousov@adelaide.edu.au, [c]nahlik@ipm.cz

Keywords: crack front shape; fatigue; free surface, crack closure, numerical model

Abstract: The development of the fatigue crack front shape in the engineering materials is still not fully understood problem. The fatigue crack front shape is influenced by many factors, e.g., crack closure, geometry of the structure, microstructure of the material, free surface effect, etc. The aim of this contribution is to provide experimental and numerical results that could help to quantify the influence of the main effects. The fatigue test results on aluminum is provided with emphasize on the geometry of the crack front. Experimentally obtained fatigue crack front shapes are compared with numerically estimated crack front shapes and discussed in the contribution.

Introduction

Phenomenon of fatigue of materials has already been studied for many years and there still exist many unknowns. One of them concerns the crack front curvature. By inspecting the fatigue fracture surface the initially straight crack front develops into the curved crack front [1].

Experimental observations demonstrated that as soon as the crack front shape is changed into the saturated (final) curved crack front the further crack propagation does not influence the crack front shape [2]. This implies that if the crack front reaches its saturated state the crack growth rate is constant along the crack front.

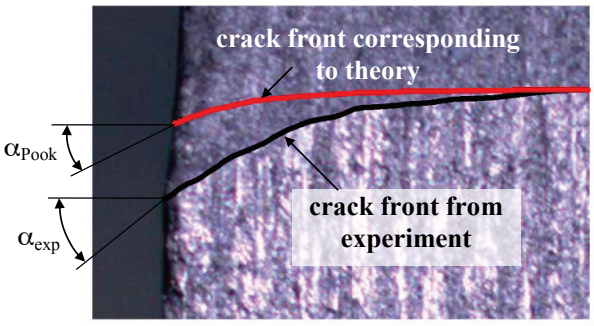

Fig. 1: Development of the fatigue crack front from the initially straight crack front

The intersection of the crack front and free surface is called vertex point. It has been shown that the stress singularity in the vertex point is different than in the centre of the body [4] and this affect the intersection angle between the crack front and the free surface in the vertex point, see Fig. 1. Pook [6] pointed out that the intersection angle depends on the Poisson's ratio, however, this is valid only for the brittle materials. Comparing theoretical crack front shapes and the experimental data obtained on the aluminum it is possible to see discrepancy between crack intersection angles, see Fig. 1. Whereas Pook [6] predicts the intersection angle around 12° the experimental measurement show more than 60°. This discrepancy is not well clarified in the literature. One of the possible explanations could be that the plasticity induced crack closure becomes important and together with the vertex singularity leads to much higher crack front curvature than predicted based on the theory of Pook. Therefore, for the prediction of the crack front shape the assumption of the constant crack closure along the crack front can be used [7].

The aim of this paper is to provide new numerical results obtained by the finite element method, see Fig. 2 where the numerical model is shown. The boundary layer method is used here as it

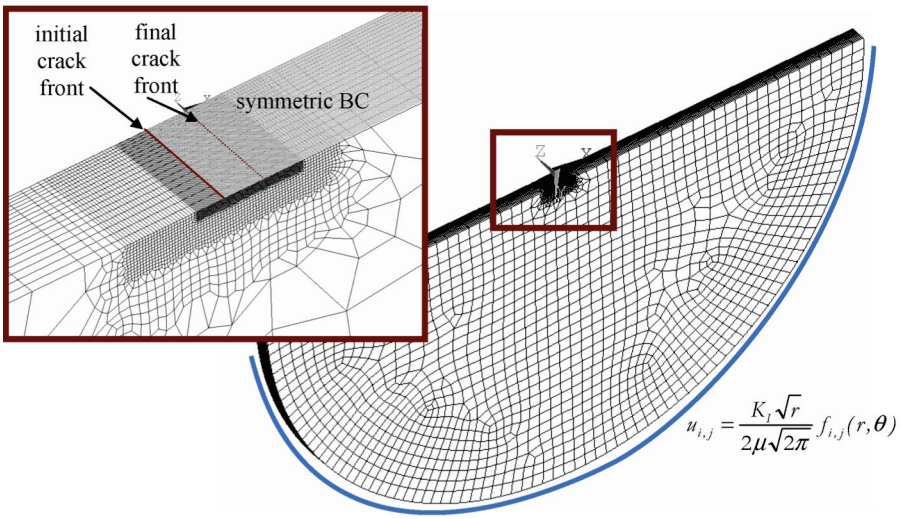

Fig. 2: Preview of the finite element model of the boundary layer method for modeling of the crack closure phenomenon

provides possibility for generalization of the obtained results [8]. The comparison of the straight and curved crack front shape is provided here from the perspective of the plasticity induced crack closure. This contribution contains also an overview of numerical modeling techniques of the plasticity-induced crack closure in the three-dimensional body. The numerically obtained results are compared with the experimentally obtained fatigue crack front shapes found on the aluminum.

Acknowledgement: This work was supported through the grant 15-08826S of the Czech Science Foundation and by the Ministry of Education, Youth and Sports of the Czech Republic throughout the Project No. CZ.1.07/2.3.00/30.0063 - Talented postdocs for scientific excellence in physics of materials.

References

[1] P. Hutař, L. Náhlík, Z. Knésl, The effect of a free surface on fatigue crack behaviour, International Journal of Fatigue. 32 (2010) 1265–1269. doi:10.1016/j.ijfatigue.2010.01.009.

[2] J. Toribio, J.C. Matos, B. González, J. Escuadra, Numerical modelling of crack shape evolution for surface flaws in round bars under tensile loading, Eng Fail Anal 16 (2009) 618–630. doi:10.1016/j.engfailanal.2008.02.014.

[3] A. Kotousov, P. Lazzarin, F. Berto, S. Harding, Effect of the thickness on elastic deformation and quasi-brittle fracture of plate components, Eng Fract Mech 77 (2010) 1665–1681. doi:10.1016/j.engfracmech.2010.04.008.

[4] Z.P. Bažant, L.F. Estenssoro, Surface singularity and crack propagation, International Journal of Solids and Structures. 15 (1979) 405–426. doi:10.1016/0020-7683(79)90062-3.

[5] M. Heyder, K. Kolk, G. Kuhn, Numerical and experimental investigations of the influence of corner singularities on 3D fatigue crack propagation, Eng Fract Mech 72 (2005) 2095–2105. doi:10.1016/j.engfracmech.2005.01.006.

[6] L.P. Pook, Some implications of corner point singularities, Eng Fract Mech 48 (1994) 367–378. doi:10.1016/0013-7944(94)90127-9.

[7] Z. He, A. Kotousov, R. Branco, A simplified method for the evaluation of fatigue crack front shapes under mode I loading, Int J Fract 188 (2014) 203–211. doi:10.1007/s10704-014-9955-3.

[8] S. Roychowdhury, R.H. Dodds Jr., A numerical investigation of 3-D small-scale yielding fatigue crack growth, Eng Fract Mech 70 (2003) 2363–2383. doi:10.1016/S0013- 7944(03)00003-1.

21st International Conference **ENGINEERING MECHANICS 2015**
Svratka, Czech Republic, May 11 –14, 2015
Paper **#117, pp. 276–277**

Tangent Curve Mathematical Model for Illustration of Deformation Curve of Rapeseeds

Riswanti Sigalingging[1,2,a] *, David Herák[1,b], Abraham Kabutey[1,c]

[1]Czech University of Life Sciences Prague, Faculty of Engineering, Department of Mechanical Engineering, Kamycka 129, Praha 6, Czech Republic.

[2]University of Sumatera Utara, Faculty of Agriculture, Department of Agricultural Engineering, Prof. A. Sofyan No. 3 Kampus USU, Medan, Indonesia Republic.

[a]riswanti@usu.ac.id, sigalingging@tf.czu.cz, [b]herak@tf.czu.cz, [c]kabutey@tf.czu.cz

Keywords: oilseeds, theoretical model, mechanical behavior, compression loading

Abstract: Detailed knowledge of mechanical behaviour of oilseeds such as rapeseeds under compression loading is ideal for development of more cost-effective technology for production of oil. The tangent curve mathematical model based on MathCAD software was used to describe the deformation characteristic curves of rapeseeds of moisture content 11.07 (% w. b.) at different pressing force and speed. Compressive force ranged between 100 and 200 kN whiles the speed varied from 10, 30 to 60 mm·min^{-1}. Pressing vessel diameter 100 mm was used to measure the bulk rapeseeds at pressing height 80 mm where the dependency between force and deformation characteristics curves was described in relation to speed and pressing heights between 30 mm and 80 mm at constant compressive force 100 kN. Based on the statistical analysis of the experimental data, the tangent curve model suitably described the force-deformation characteristic curves of bulk rapeseeds. The fitted model was dependent on force and deformation coefficients of mechanical behaviour of the tangent curve mathematical model.

Tangent curve function

Experimentally, the relationship between force and deformation of bulk oilseed such as rapeseeds can be described by function (Eq.1).

$$F(x) = A \cdot \left[\tan(B \cdot x)\right]^n \tag{1}$$

Where A is the force coefficient of the mechanical behaviour (N), B is the deformation coefficient of the mechanical behaviour (mm^{-1}) and n is the exponent of fitted function (-). In terms of the relationship between force and deformation characteristic curves in relation to different vessel diameter and pressing seed height, the tangent curve model (Eq. 1) requires modification based on the experimental boundary conditions that: when the compressive force increases to infinity the deformation reaches the maximum limit, zero compressive force means zero deformation and the integral of Eq. 1 represents the energy [1, 2, 3, 4]. Theoretically, when the force is approaching infinity (Eq. 1) then the limit deformation, δ (mm) (Eq. 2) which is dependent on the pressing seed height H (mm), can be expressed by deformation coefficient of mechanical behaviour [5, 6, 7].

$$\delta = \lim_{F(x)\to\infty} x = \frac{\pi}{2 \cdot B} \tag{2}$$

The relationship between compression coefficient, G (N) and deformation coefficient of mechanical behaviour, B (mm^{-1}) can be expressed as shown in Eq. 3 [2, 6, 7].

$$G = B \cdot H \tag{3}$$

Where H is the bulk seed height (mm) which affects the deformation coefficient of mechanical behaviour, B (mm^{-1}) [3, 4, 6, 7]. From the experimental results the tangent curve equation (Eq.1) can be mathematically modified (Eq. 4) based on the assumption that the porosity of bulk rapeseeds as well as the compressive stress inside the pressing vessel diameter containing the bulk rapeseeds remain constant. Therefore, the tangent curve model as described in (Eq. 4) indicates that the linear experimental data, that is, the dependency between the force and deformation curve can be fitted based on a single vessel diameter and pressing seed height. Equation (Eq. 4) is generated using the Levenberg-Marquardt algorithm [8] which provides numerical solutions to the problem of minimizing deviations in non-linear functions in relation to function parameters.

$$F(x, D, H) = C \cdot D^2 \cdot \left[\text{ta} \left(G \cdot \frac{x}{H} \right) \right]^1 \tag{4}$$

Where C is the stress coefficient of mechanical behaviour ($N \cdot mm^{-2}$), D is the vessel diameter (mm), G is the compression coefficient (-) and H is the bulk seed height (mm). Using Eq. 4, the dependency between force and deformation characteristic curves in relation to vessel diameter and bulk seed height can be described theoretically.

Acknowledgment: The authors would like to acknowledge the support of the Indonesian government under DIKTI Award.

References

[1] D. Herák, G. Gurdil, A. Sedlacek, O. Dajbych, S. Simanjuntak, Energy demands for pressing Jatropha curcas L. Seeds, Biosystems Engineering, 106 (2010) 527–534.

[2] D. Herák, A. Kabutey, A. Sedlacek, G. Gurdil, Tangent curve utilization for description for mechanical behavior of pressed mixture, Research in Agricultural Engineering, 57 (2011) 13–18.

[3] D. Herák, A. Kabutey, A. Sedlacek, Mathematical description of Rape seeds (Brassica napus l.) mixture mechanical behavior under compression loading, Scientia Agriculturae Bohemica, 42 (2011) 31–36.

[4] R. Sigalingging, D. Herák, A. Kabutey, M. Čestmír, M. Divišová, Tangent curve function description of mechanical behavior of bulk oilseeds: a review. Scientia Agriculturae Bohemica, 45 (2014) 259–264.

[5] D. Herák, A. Kabutey, A. Sedlacek, G. Gurdil, Mechanical behaviour of several layers of selected plant seeds under compression loading, Research in Agricultural Engineering, 58 (2012) 24–29.

[6] D. Herák, A. Kabutey, M. Divišová, S. Simanjuntak, Mathematical model of mechanical behaviour of Jatropha curcas L. seeds under compression loading. Biosystems Engineering, 114 (2013) 279–288.

[7] D. Herák., A. Kabutey, M. Divišová, Analysis of tangential curve equation describing mechanical behaviour of Rape seeds (Brassica napus L.) mixture under compression loading, Research in Agricultural Engineering, 59 (2013) 9–15.

[8] D. W. Marquardt, An algorithm for the least-squares estimation of non-linear parameters, SIAM, Journal of Applied Mathematics, 11 (1963) 431–441.

21st International Conference **ENGINEERING MECHANICS 2015**
Svratka, Czech Republic, May 11 –14, 2015
Paper **#177, pp. 278–279**

Road Dust Emission Modelling

Viktor Šíp[a], Luděk Beneš

Faculty of Mechanical Engineering, Czech Technical University in Prague, Czech Republic

viktor.sip@fs.cvut.cz

Keywords: vegetation barrier, particulate matter, RANS modelling, air quality

Abstract: Atmospheric particulate matter (PM) is a well known risk to human health. Vehicular traffic is one of the major sources of particulates in an urban setting.

Here we study a problem of road dust dispersion. Using CFD solver based on RANS equations, we investigate the effect of a vegetation barrier on the concentration of airborne PM induced by road traffic. Simplified 2D model of a porous obstacle adjacent to a road source of PM2.5 and PM10 serves as an idealization of a real-world situation.

Introduction

Near road vegetation barriers have been suggested as a way to mitigate the particulate matter pollution in neighbouring areas. Its effectivity is influenced by a number of parameters: atmospheric conditions, properties of the particulates, vegetation type or its position (see eg. [1], [2] and references therein).

Here we set out to explore the effect of the wind speed on the barrier effectivity using simplified 2D model.

Numerical Model

Flow in the domain is modelled using equations of incompressible turbulent flow,

$$\frac{1}{\beta}\frac{\partial p'}{\partial t} + \nabla \cdot \boldsymbol{u} = 0, \tag{1}$$

$$\frac{\partial \boldsymbol{u}}{\partial t} + (\boldsymbol{u} \cdot \nabla)\boldsymbol{u} + \nabla(p'/\rho_0) = \nu_E \nabla^2 \boldsymbol{u} + \boldsymbol{g} + \boldsymbol{F}, \tag{2}$$

$$\frac{\partial \theta}{\partial t} + \nabla \cdot (\theta \boldsymbol{u}) = k/c_v \left(\nabla \cdot (1/\rho \nabla \theta)\right). \tag{3}$$

Here pressure and density are split into background component in hydrostatic balance and fluctuations, $p = p_0 + p'$ and $\rho = \rho_0 + \rho'$. Vector $\boldsymbol{u}$ stands for velocity, ν_E is the effective viscosity, $\nu_E = \nu + \nu_T$, $\boldsymbol{g}$ is the gravity term, $\boldsymbol{F}$ represent momentum sink due to the vegetation, θ is a potential temperature. Artificial compressibility with parameter β is utilized. Particulate matter C_i is modelled as passive scalar,

$$\frac{\partial \rho C_i}{\partial t} + \nabla \cdot (\rho C_i \boldsymbol{u}) - (\rho C_i u_s)_y = \nabla \cdot (D \nabla C_i) + \rho f_c. \tag{4}$$

Here u_s is settling velocity of the particle and f_c is the source term. Discretization is done by finite volume method, using numerical flux AUSM$^+$-up [3]. Algebraic mixing-length model according to [4] is used to account for the effects of turbulence.

Case settings

Computational domain is 300 m long and 150 m high. Four-lane road is modelled as four line sources of PM10 and PM2.5 particulates, placed at 23.125, 29.375, 35.625 and 41.875 m from the inlet at

height 0.8 m. Intensity of each source is 1 mg/m/s for both PM10 and PM2.5. The vegetation barrier of length 30 m and height 15 m is located at 50 m from the inlet. Size of the computational grid is 300 x 120 cells.

All simulations were performed under assumption of weakly stably stratified atmosphere with inlet velocity according to log wind profile.

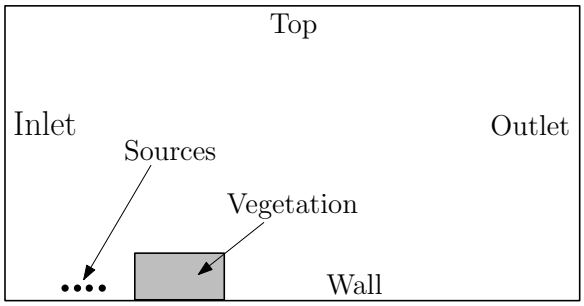

Fig. 1: Sketch of a computational domain.

Results

We investigated the effect of the wind speed on the effectiveness of the filtering by the vegetation block. Four scenarios with wind speeds of 2.5, 5.0, 7.5 and 10 m/s at the top of the domain were considered. For each scenario, two cases were computed - with and without the vegetation block.

In Fig. 2 following quantities of interest are shown: particle mass concentration at 250 m from the inlet at height of 2 m and 10 m for both cases without (C_F) and with vegetation (C_V). Their ratio C_V/C_F, describing the effectivity of the barrier, is shown as well.

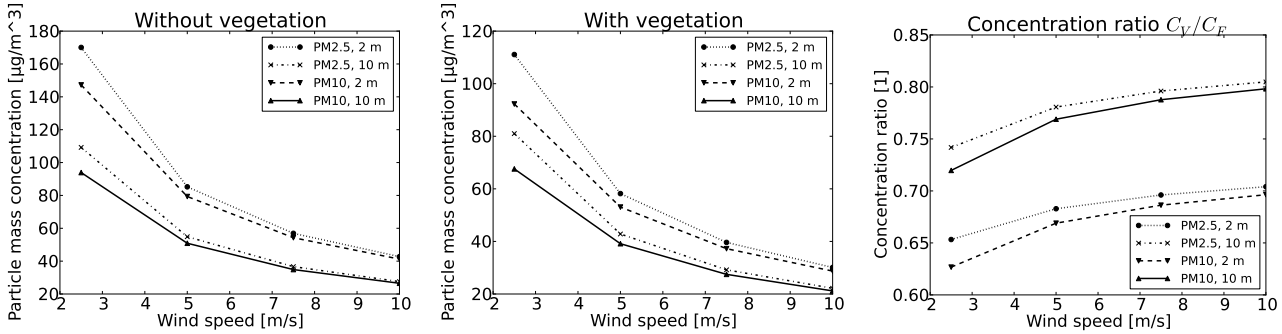

Fig. 2: Particle mass concentration at x = 250 m for case without (left) and with vegetation (middle), and their concentration ratio C_V/C_F (right).

Decreasing efficiency of the barrier with increasing wind speed is indicated by the results. Also, significantly lower effect of the barrier on the pollutant concentration higher above ground is apparent.

References

[1] J.T. Steffents, Y.J. Wang, K.M. Zhang, Exploration of effects of a vegetation barrier on particle size distributions in a near-road environment. Atmos. Environ. 50 (2012) 120–128.

[2] T. Litschke, W. Kuttler, On the reduction of urban particle concentration by vegetation - a review. Meteorol. Z. 17 (2008) 229–240.

[3] M.-S. Liou, A sequel to AUSM, Part II: AUSM+-up for all speeds. J. Comput. Phys. 214 (2006) 137–170.

[4] A.K. Blackadar, The Vertical Distribution of Wind and Turbulent Exchange in a Neutral Atmosphere. J. Geophys. Res. 67 (1962) 3095–3102.

21st International Conference **ENGINEERING MECHANICS 2015**
Svratka, Czech Republic, May 11 –14, 2015
Paper **#184, pp. 280–281**

The "Miracle" of Post-Buckled Behaviour in Thin-Walled Steel Construction and its Breathing-Induced Limitation

Miroslav Škaloud[a], Marie Zörnerová[b], Shota Urushadze[c] *

ITAM ASCR, v.v.i., Prosecká 76, 190 00 Praha 9, Czech Republic

[a]skaloud@itam.cas.cz, [b]zornerova@itam.cas.cz, [c]urushadze@itam.cas.cz

Keywords: thin-walled construction, saving steel, stability, post-buckled behaviour, repeated loading, breathing, limit states

Abstract: Thin-walled construction represents a powerful tool for saving steel and thereby for increasing the competitiveness of steel structures. However, on the other hand, as the limit state of thin-walled structures is substantially affected by stability phenomena, the above concept can be implemented just on the condition of post-buckled behaviour being taken into account in the solution to these stability phenomena. The paper first studies the factors on which the intensity of the very favourable post-buckling reserve of strength depends and then in detail turns attention to the most important among them, viz. the effect of the cumulative-damage process that becomes manifest in the case of bridges and other systems subjected to many times repeated loading.

Introduction

One of the most promising trends in our striving to save steel is to use thin-walled structures, i.e. systems made of slender plate elements. Of course, it can be argued at this juncture that by decreasing the plate thickness we do reduce the consumption of steel, but on the other hand make the system more sensitive to stability phenomena. The situation is however remedied by the stabilizing effect of membrane stresses which come into play when plate deflections are of the order of plate thickness, so that a very significant post-buckled reserve of strength is generated. That is why a great attention has been internationally paid to research on post-buckled behaviour, the authors always striving to play a useful role in these activities.

It goes without saying that the favourable reserve of strength cannot be exploited blindly, and therefore in the full version of the paper the first part is devoted to "mapping" the factors on which the intensity of the beneficial post-buckled behaviour depends. In so doing, the effects of the slenderness of the plate element, its initial imperfections, the kind of loading and its material are analysed.

The main attention is paid to the impact of the cumulative-damage process that comes into being when the structure is subjected to many times repeated loading - as is the case, for example, in steel bridgework.

Experimental investigation into the cumulative-damage process generated by the breathing of the slender web of a thin-walled steel plate girder

As the extent of this paper is limited, we will herebelow concentrate only on the results of the authors´ experiments on the "breathing" of webs subjected to combined shear and bending. It is this kind of loading that governs the design of the webs of bridge girders and similar structures.

One of the test girders in the testing position is shown in Fig.1. It can be seen there that the test girders are fairly large, so that their character is not far from ordinary girders.

The main impact of the cumulative-damage process generated by the "breathing" of the web is the initiation and propagation of fatigue cracks. They initiate in the crack-prone areas at the toes of the fillet welds connecting the breathing web sheet with the girder flanges and stiffeners.

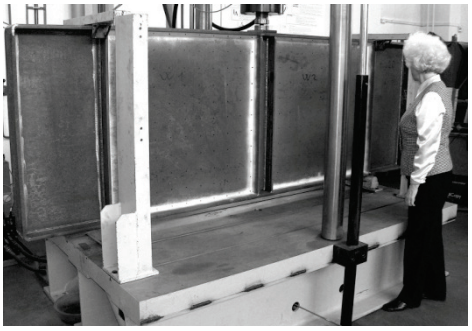

Fig. 1: One of the Prague girders in the testing position

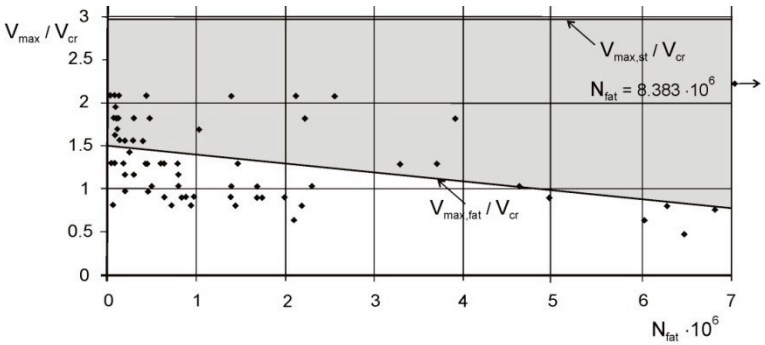

Fig. 2: The cumulative-damage-induced "erosion" of the maximum sustainable load – repeated predominant shear

Partial "erosion" of the post-buckled behaviour in webs subjected to repeated predominantly shear

The results of the writers´ experiments are shown in Fig. 2. The corresponding ratios V_{max}/V_{cr} are plotted on the vertical axis (V_{cr} being the critical shear force), the related numbers N of loading cycles on the horizontal axis.

A very significant impact of the cumulative damage process on the fatigue tests can easily be seen in the figure.

Impact of the breathing phenomenon on design

It follows from the above analysis that the problem of web "breathing" can play a very important role and therefore cannot be disregarded; on the contrary, it can significantly affect the design of steel bridges, crane-supporting girders and other structural systems under the action of many times repeated loads.

In establishing a suitable method for design, the authors follow the general features of the design philosophy according to which two limit states are introduced in the analysis, viz. (i) the fatigue limit state, (ii) that of serviceability.

While the fatigue limit state can be related to the failure of the girder (i.e. to unrepairable damage – which is acceptable in view of the fact that the fatigue limit state can never be attained during the planned life of the girder), the limit state of serviceability should be related to a much more limited, easily repairable degree of damage. In the case of steel girders with "breathing" webs, this means that, in the course of the useful fatigue life of the girder, either no or very small fatigue cracks can develop, such as to be easily kept under control, or easily retrofitted in case of need. That is why this limit state can successfully be used for governing inspections of the structure concerned for the occurrence of breathing-induced fatigue cracks.

The corresponding S-N curves and formulae are given in the full version of the paper.

Summary

It follows from the results of the authors´ research that the cumulative damage process generated in slender webs breathing under many times repeated loads can substantially influence the limit state behaviour and useful life of steel thin-walled structures. Therefore. this phenomenon ought to be taken into account in design.

Acknowledgments: The kind support of the Czech Science Foundation Project No. GC13-34405J and of the RVO 68378297 institutional support are gratefully acknowledged.

21st International Conference **ENGINEERING MECHANICS 2015**
Svratka, Czech Republic, May 11 –14, 2015
Paper **#192, pp. 282–283**

Strengthening of Weak Historic Renders with Traditional and Innovated Consolidation Treatment

Zuzana Slížková[a] *, Dita Frankeová[b]

Institute of Theoretical and Applied Mechanics, Prosecká 76, 190 00 Praha 9, Czech Republic

[a]slizkova@itam.cas.cz, [b]frankeova@itam.cas.cz

Keywords: lime mortar, lime render, consolidating products, lime water, nanolime, consolidation, strengthening

Abstract: The presented study was aimed to proof consolidation effects of different families of consolidants: inorganic agents (lime -based or silica-based solutions or sols), organic agents (silicic acid ester based consolidant) and their combination on the characteristics of weak mortars prepared in laboratory with different types of aggregates. Besides exploring consolidant-substrate interaction also the pozzolanic activity of the aggregate and the binder mortar component after reaction with lime (calcium hydroxide solution) was investigated in order to understand and describe the strengthening mechanism into consolidated mortars. As the study was based on experimental research, the production of mortar test specimens represented an important preliminary work. Different mortar components (various types of sand in terms of phase composition, clay, lime) and the same ratio of the aggregate and the binder were used in various mortar mixtures. Various mineralogical types of aggregate were used with the same grain size distribution (600 pieces of tubes of 40 mm in outer diameter, of the height of 40 mm and depth of 4 mm were prepared for testing the compressive strength, for the tension tests 550 thin plates of dimensions 40 mm x 100 mm x 4 mm were cast and 600 beams 20 x 20 x100mm were made for testing the flexural strength and other characteristics of reference and consolidated mortars). The sand used for mortar specimens was characterized by microscopic examination of thin section and also by X-ray diffraction, X-ray fluorescence spectroscopy and thermal analysis. The pozzolanic activity of the sands (reactivity with calcium hydroxide) was determined by means of the thermal analysis and supplemented by wet silicate analysis. The amount of the effective matter in the consolidant was the same for all agents per the square unit for all mortar types and specimen shape. One set of specimens was prepared as the reference set of mortars without any treatment and the second set was used for the evaluation of various consolidating agent effects.

The following consolidation treatment was studied:

- lime water – saturated solution of calcium hydroxide in distilled water
- dispersion of nanoparticles of calcium hydroxide in alcohols (CaLoSiL IP 15)
- colloidal solution SiO_2 in water
- silicic acid ester solution (TEOS –based)
- colloidal solution SiO_2 and lime water (combination)
- colloidal solution SiO_2 and CaLoSiL IP 15 (combination)
- TEOS and lime water (combination)
- TEOS and CaLoSiL IP 15 (combination)
- barium water - saturated solution of barium hydroxide in distilled water
- ammonium oxalate solution in distilled water

Two months after impregnation procedure, the consolidated specimens were tested and obtained data evaluated. Mechanical tests – compressive, tension and flexural strength, peeling tests, drilling resistance; physical tests focused on porosity a water transport parameters – pore size distribution, water absorption in certain time and a microscopic investigation of new compounds distribution in the depth profile of the treated specimen were performed. Chemical analyses involved thermal analyses, X-ray diffraction, EDXRF and SEM-EDS analyses. Thermogravimetric analysis (TGA) was used for monitoring the pozzolanic reaction extent of different binders and aggregates used in

mortars after reaction with calcium hydroxide. Suspensions consisting of the binder or the aggregate (particle size under 125 microns) and lime (in ratio 1:1) were prepared for this purpose. Resulting reaction compounds were quantified by TGA and their presence was proved by X-ray diffraction. Both analyses confirm, besides the calcium hydroxide and carbonate, the presence of CSH and CAH phases. TGA was also used for investigation of changes in mineralogical composition in lime mortars (ratio lime: aggregate 1: 9) before and after the treatment by consolidating agent. The presence of consolidant unfortunately distorts the area where CSH and CAH phases can be detected, so in this case TGA gave just information about the quantity of calcium carbonate. TGA also confirms that samples were fully carbonated (calcium hydroxide was not present). Hydraulic compounds, detectable by means of XRD, were not found in the samples of mortars. Beside the study of model mortar specimens, also real historic mortar samples were characterized and physical-chemical properties were determined.

The results from experiments focused on lime water efficiency, compared to nano-lime based consolidants, showed that the lime water spraying technology may provide acceptable results on a certain class of ancient lime mortars, from the technical point of view and also from the aesthetic point of view. The treated plasters should ideally be well packed and porous, without compact surface crust layers. However, lime water is not suitable in all situations, and a consolidation effect can be only achieved with a very large number of applications (more than 100), which typically releases and washes away sand grains and the binder of the original surface layers. This changes the appearance of historic surfaces together with apparent white hazing when there are a large number of repeated applications. The risk of mobilizing water-soluble salts in historic plasters is high. If soluble salts are present, the potential damage should be considered carefully.

The lime water treatment was also compared with some other, less labour-intensive technologies. Dispersions of calcium hydroxide in alcohols, which are marketed under the trade name CaLoSiL, were the most promising agents. The major advantage with these agents is that they can be applied much more rapidly than tens to hundreds of lime water cycles and they deliver higher amount of lime in each cycle. While lime water contains only small calcium ions, sized about 0.1 nm, calcium hydroxide particles in CaLoSiL are considerably larger (50-200 nm). This property may limit the use of nanolime dispersions for consolidation of mortars with fine pores or with less pore interconnectivity. Nanolime dispersion CaLoSiL 15 applied to mortar, where the majority of pores were around 100 μm in diameter, was efficient enough to achieve significant strengthening effect after one-day lasting consolidation treatment (7 applications of the consolidant. every 2 hours).

The combined application of lime-based consolidants (lime water, nano-lime dispersions) and silica based consolidants (silica sol, silicic acid ester solution) was studied with finding that both lime water or the calcium hydroxide nano-dispersion are more effective in consolidation of lime mortar when they are applied in combination with silicic acid ester or silica sol consolidant.

The experiments proved on series of model mortars with different aggregate brought the knowledge that the strengthening efficiency due to consolidation is influenced significantly by the aggregate type used in the consolidated mortar.

All the tested consolidation agents showed a positive strengthening effect when they were used for consolidation of poor lime mortar. Entirely different results were achieved when the same consolidants were used for strengthening of soil based mortar. Silicic acid ester solution-based product was efficient for consolidation of this type of mortar.

Study of the pozzolanic activity of various types of sand in mortars showed that the grains of sand may be reactive with calcium hydroxide and can participate in the formation of hydraulic compounds when they are subjected to calcium hydroxide for a long time (several months at room temperature). In treated lime mortar samples, however, the products of this reaction were not detected, probably because of the relatively small amount of these substances in mortar and their X-ray diffraction amorphous character.

Acknowledgement: The authors gratefully acknowledge support from the Czech Ministry of Culture NAKI Project DF11P01OVV012 entitled “New materials and technologies for conservation of monuments´ materials and preventive conservation”.

21st International Conference **ENGINEERING MECHANICS 2015**
Svratka, Czech Republic, May 11 –14, 2015
Paper **#066, pp. 284–285**

Evaluation of Audze-Eglājs Criterion for Orthogonal and Regular Triangular Grids

Magdalena Šmídová[a*], Václav Sadílek[b],
Jan Eliáš[c], Miroslav Vořechovský[d]

Institute of Structural Mechanics, Faculty of Civil Engineering, Brno University of Technology,
Veveří 331/95, 602 00 Brno, Czech Republic

[a]smidova.m@fce.vutbr.cz, [b]sadilek.v@fce.vutbr.cz, [c]elias.j@fce.vutbr.cz,
[d]vorechovsky.m@fce.vutbr.cz

Keywords: Audze-Eglājs criterion, optimization, design of experiments, full factorial design (orthogonal grid), regular triangular design

Abstract: This article describes two deterministic designs that optimally fill a unit hypercube. The motivation is to estimate the lower bound of the Audze-Eglājs (AE) criterion – a criterion for optimization of designs of experiments or for a sample for statistical analyses when uniform filling of sampling space is required.
The construction of the two deterministic designs is described and the analysis of mutual distances of sample points in the designs (the distances are featured in the formula for the AE criterion) is performed. A closed form for evaluation of the AE criterion on these deterministic designs is developed.

Introduction

These days, physical experiments realized in research to get deeper insight into the examined issue are often replaced by computer experiments in order to decrease cost and time necessary for the modelling and realization of the experiment. The principle of the computer experimenting is the evaluation of a certain number of simulations (N_s) of the problem and estimation of an unknown quantity using statistical methods.

As an evaluation of a single simulation may be inadequately time-consuming in case of complex engineering problems, further approximation can be used to decrease the computational time, e.g. the response surface method as described in [1, 2]. Response surface is derived based on limited number of simulations of the real problem. Various requirements may be demanded from such a set of simulations. One of the usual requirements is uniform probability of the simulations evaluated.

To ensure uniform probability, the space of input random variables of the original problem is transformed into a sampling space where all the inputs are mutually independent and are represented by their probabilities. The sampling space is, therefore, a unit hypercube $[0, 1]^{N_v}$, where N_v is the number of input random variables of the original problem. This hypercube should then be filled uniformly with the points that represent individual simulations.

The problem of optimal filling of a space with respect to a predefined criteria is often solved by Monte Carlo type stochastic methods (crude Monte Carlo, Latin Hypercube Sampling) optimized by some heuristic algorithm (simulated annealing [3], genetic algorithms [4], etc.). The aim of optimization is to maximize or minimize the selected criterion, thereby the optimality with respect to this criterion is ensured.

For certain optimization algorithms the knowledge of the lower bound is crucial. As Audze-Eglājs (AE) criterion is said to prioritize uniform space-filling [5, 6] and its lower bound for arbitrary N_s is not known, the authors investigate deterministic designs that fill the unit hypercube uniformly, in order to estimate the lower bound of the criterion for stochastic designs.

AE Criterion

The AE criterion is based on the analogy with system of mass points interacting by repulsive forces. It is defined [5] using the distances between all pairs of points $L_{i,j}$ as

$$E^{\mathrm{AE}} = \sum_{i=1}^{N_\mathrm{s}} \sum_{j=i+1}^{N_\mathrm{s}} \frac{1}{L_{ij}^2} \,. \tag{1}$$

Investigated deterministic designs

In order to estimate the lower bound of AE, we test two different types of design (arrangement of points in N_v-dimensional unit hypercube). The two types of design are the full factorial design (FFD) and a new type of design called regular triangular design (RTD).

FFD. This design places $N_\mathrm{s} = N^{N_\mathrm{v}}$ points in an N_v-dimensional hypercube arranged in a perfect orthogonal grid (N is a natural integer here selected identical for all marginal variables). The computation of AE criterion may become very time-consuming for large N_s, therefore we present an analysis of distances between all pairs of points. This combinatorial analysis allows for fast evaluation of AE criterion using closed form expressions.

RTD. The other type of design – regular triangular grid – arranges the points into repeated units formed by triangles ($N_\mathrm{v} = 2$), tetrahedrons ($N_\mathrm{v} = 3$) etc. in N_v-dimensional space while fulfilling the requirement of periodicity. We present an algorithm for construction of such a design, limited to $N_\mathrm{s} = N^{N_\mathrm{v}}$ and the analysis of lengths among all pairs of points and AE criterion.

These two designs are compared with respect to the histograms of lengths between points and also their AE criteria. It is believed that these perfect arrangements lead to lower bounds of the AE criterion.

Acknowledgement: The authors acknowledge financial support provided by the Czech Ministry of Education, Youth and Sports under Specific University Research project No. FAST-J-13-1922, and also support provided by the Czech Science Foundation under projects Nos. GC13-19416J and GA14-10930S (SPADD).

References

[1] G. Box, The exploration and exploitation of response surfaces: Some general considerations and examples, Biometrix, 10 (1954) 16–60.

[2] C. G. Bucher, U. Bourgund, A fast and efficient response surface approach for structural reliability problems, Structural Safety, 7 (1990) 57–66.

[3] M. Vořechovský, D. Novák, Correlation control in small sample Monte Carlo type simulations I: A Simulated Annealing approach, Probabilistic Engineering Mechanics, 24 (2009) 452–462.

[4] L. D. Davis, Handbook of Genetic Algorithms, Van Nostrand Reinhold, 1st ed., 1991.

[5] P. Audze, V. Eglājs, New approach for planning out of experiments: Problems of Dynamics and Strengths, 35 (1977) 104–107. (in Russian).

[6] B. G. Husslage, G. Rennen, E. R. van Dam, D. den Hertog, Space-filling latin hypercube designs for computer experiments, Optimization and Engineering, 12 (2011) 611–630.

21st International Conference **ENGINEERING MECHANICS 2015**
Svratka, Czech Republic, May 11 –14, 2015
Paper **#018, pp. 286–287**

Forced Vibration Analysis of Timoshenko Beam with Discontinuities by Means of Distributions

Jiří Sobotka

67550 Dukovany, Czech Republic

jiri.sobotka.@cez.cz

Keywords: Timoshenko beam, vibration, discontinuities distribution, Dirac-delta

Abstract: The general equations of motion for forced vibration of Timoshenko beam have been used since they were derived assuming there were not any discontinuities in the shear force, the bending moment, the cross-section rotation and the deflection of the beam. However in practice, computing harmonic response of the beam, we encounter concentrated loading, concentrated supports, hinges connecting beam segments, concentrated masses or concentrated moments of inertia all of which may be situated between ends of the beam. The definition of the distributional derivative is chosen in order that all the cases causing jump discontinuities in the shear force or the bending moment or the cross-section rotation can be incorporated. As a result of this approach, more general equations of motion for forced vibration of Timoshenko beam implying all jump discontinuities mentioned are presented in this paper. An analytic closed-form solution to the system of equations is found with integration constants in the form of initial parameters. Making use of this approach, we can find exact expression for the harmonic steady-state response of the uniform beam without summing infinite series and without doing a modal analysis of the beam.

Introduction

Classical analytical method of calculating the harmonic steady-state response of the uniform beam is based on the following main steps [1, 2]. Firstly, we obtain a frequency equation for specific support conditions of the beam. Secondly, we solve the frequency equation for natural frequencies. Thirdly, we find orthogonal mode shapes corresponding to the natural frequencies of the beam. Finally, applying modal analysis, we express the response as a linear combination of the mode shapes by finding corresponding modal participation coefficients.

In this paper, a new analytical method is presented. Applying distributions, it is not necessary for natural frequencies, mode shapes and modal participation coefficients to be computed in analyzing the harmonic steady-state response of the uniform beam.

The model for forced vibration of Timoshenko beam with discontinuities

In practice, computing harmonic response of the beam, we encounter concentrated loading, concentrated supports, hinges connecting beam segments, concentrated masses or concentrated moments of inertia situated between ends of the beam causing jump discontinuities.

We can apply the Schwartz-Sobolev theory of distributions [3] in order to express jump discontinuities in a quantity, which is to be differentiated. The first-order distributional derivative of a function with a jump discontinuity contains a continuous part and a distributional one which is the product of a magnitude of the jump and the Dirac-delta distribution moved to the point of the jump.

The right-hand side of Eq. 1 is the distributional derivative of the shear force $Q(x,t)$ with $n_1+n_2+n_3$ jump discontinuities. The beam may be supported also between its ends at n_1 concentrated supports with reaction forces of r_i, may carry n_2 concentrated masses of m_i, and may also be subjected to n_3 concentrated transverse forces of f_i and to a distributed transverse loading of $f(x,t)$.

The right-hand side of Eq. 2 is the distributional derivative of the bending moment *M(x,t)* with n_4+n_5 jump discontinuities. The beam may carry n_4 concentrated mass moments of inertia of j_i, and may be subjected to n_5 concentrated force pairs of s_i situated between ends of the beam.

The right-hand side of Eq. 3 is the distributional derivative of the cross-section rotation *φ(x,t)* with n_6 jump discontinuities of ψ_i. The beam may contain n_6 internal hinges connecting beam segments.

The right-hand side of Eq. 4 is the classical derivative of the deflection *w(x,t)* covering the effects of bending and shear deformations [2].

$$\frac{\partial Q}{\partial x} = \rho A(x)\frac{\partial^2 w}{\partial t^2} + \sum_{i=1}^{n_1} r_i \delta(x-\xi_i) + \sum_{i=1}^{n_2} m_i \frac{\partial^2 w(x=\eta_i)}{\partial t^2}\delta(x-\eta_i) - \sum_{i=1}^{n_3} f_i \delta(x-\zeta_i) - f(x,t) \tag{1}$$

$$\frac{\partial M}{\partial x} = Q - \rho J(x)\frac{\partial^2 \varphi}{\partial t^2} - \sum_{i=1}^{n_4} j_i \frac{\partial^2 \varphi(x=\gamma_i)}{\partial t^2}\delta(x-\gamma_i) + \sum_{i=1}^{n_5} s_i \delta(x-\varepsilon_i)\ , \tag{2}$$

$$\frac{\partial \varphi}{\partial x} = -\frac{M}{EJ(x)} + \sum_{i=1}^{n_6} \psi_i \delta(x-\lambda_i)\ , \tag{3}$$

$$\frac{\partial w}{\partial x} = \varphi + \frac{Q}{kGA(x)} \tag{4}$$

Conclusions

Having applied distributions, we present Eqs. 1 to 4 for forced vibration of the Timoshenko beam implying jump discontinuities in the shear force, the bending moment and the cross-section rotation. An analytic closed-form solution to the system of Eqs. 1 to 4 for harmonic steady-state response of the uniform beam is found with integration constants in the form of initial parameters. Making use of this approach, we can find exact expression for the harmonic steady-state response of the beam without summing infinite series and without doing a modal analysis.

References

[1] S.M. Han, H. Benaroya, T. Wei, Dynamics of transversely vibrating beams using four engineering theories, Journal of Sound and Vibration 225 (1999) 935-988.

[2] S. S. Rao, Vibration of Continuous Systems, Wiley, New Jersey, 2007.

[3] R. P. Kanwal, Generalized Functions, Birkhäuser, Boston, 2004.

21st International Conference **ENGINEERING MECHANICS 2015**
Svratka, Czech Republic, May 11 –14, 2015
Paper **#138, pp. 288–289**

Analytical Solution of Hydrostatic Pocket Tilting

Eduard Stach[a] *, Jiří Falta[b], Matěj Sulitka[c]

Research Center for Manufacturing Technology, Czech Technical University, Horská 3, Prague 2

[a]e.stach@rcmt.cvut.cz, [b]j.falta@rcmt.cvut.cz, [c]m.sulitka@rcmt.cvut.cz

Keywords: hydrostatic; pocket; tilt; guideway; bearing

Abstract: Tilting (parallelism error) of guiding surfaces may cause reduction of load capacity of hydrostatic (HS) guideways and bearings in machine tools (MT). Using coupled finite element (FE) computational models of MT structures, it is nowadays possible to determine the extent of guiding surfaces deformation caused by thermal effects, gravitational force, cutting forces and inertia effects. Assessment of maximum allowable tilt has so far been based merely on experience. The paper presents a detailed model developed for description of the impact of HS bearing tilt on the load capacity characteristics of HS guideways. The model allows an evaluation of the tilt influence on the change of the characteristics as well as determination of the limit values of allowable tilt in interaction with compliant machine tool structure. The proposed model is based on the model of flow over the land of the HS pocket under extended Navier-Stokes equation. The model is verified using an experimental test rig.

Introduction.

Hydrostatic (HS) guideways are considered as one of the fundamental types of sliding guideways in the machine tool industry. HS guideways are used for its low friction, high precision, load capacity, stiffness and damping. HS guideways consist of two sliding surfaces. One of the sliding surfaces is fitted with HS pockets, designed as cavities bounded by land. The cavities are connected to regulators and pressurized oil supply. Throttling of the pressurized cavity oil occurs between the land and the other sliding surface. This results in the creation of a thin oil film, which provides fluid friction between sliding surfaces.

A parallelism error (tilting) of guiding surfaces causes a change in the hydraulic resistance of an HS pocket and a corresponding reduction in the reaction force in the guideways. It is the aim of this paper to propose a detailed model of load capacity characteristics of HS guideways taking into account tilting without the demand for a numerical solution of the problem. This model can be used in an iterative approach to optimize the entire design process for HS machine tool guideways, combining a finite element (FE) model of a compliant MT structure coupled with nonlinear characteristics of HS guideway and multiparametric, multi-criterion optimization [1].

Analytical solution.

Pressure distribution on the land is generally described by the Reynolds equation. Under certain conditions, this equation can be solved exactly, for example tilted bearing of infinite length solved by Beek and Ostayen [2]. The presented calculations use the perturbation theory to simplify the Reynolds equation and boundary conditions describing a real HS pocket. The pressure boundary condition on the inner inlet into the land takes into account the Bernoulli effect as it may cause a significant pressure drop if kinetic energy of a fluid volume element is comparable with its pressure energy. The influence of HS pocket tilt on hydraulic resistance R of HS pocket is shown in Eq.1, where a and b are inner dimensions of the cavity, D is width of the land, μ is dynamic viscosity of hydraulic oil, Δ_a and Δ_b describe the tilt around x and y axis of the HS pocket, ρ is density of hydraulic oil, p_T is pressure inside pocket.

$$R \approx \frac{3\mu D}{H_S^3(a+b)}\left[1-\frac{a+3b}{a+b}\Delta_a^2-\frac{3a+b}{a+b}\Delta_b^2+\frac{\rho H_S^4 p_T}{240\mu^2 D^2}\right]. \quad (1)$$

The influence of the HS pocket tilt on the hydraulic resistance of the HS pocket is also illustrated in Fig. 1 on the left. The tilt ratio Δ is plotted on the X axis and the pocket surface to pocket land surface ratio Ψ is plotted on the Y axis. For a pocket with $\Psi = 0.5$, three tilt ratios have been selected. Their influence on the load capacity F with respect to the height of the throttling gap in the center of the pocket h_{centre} is shown in Fig. 1 on the right.

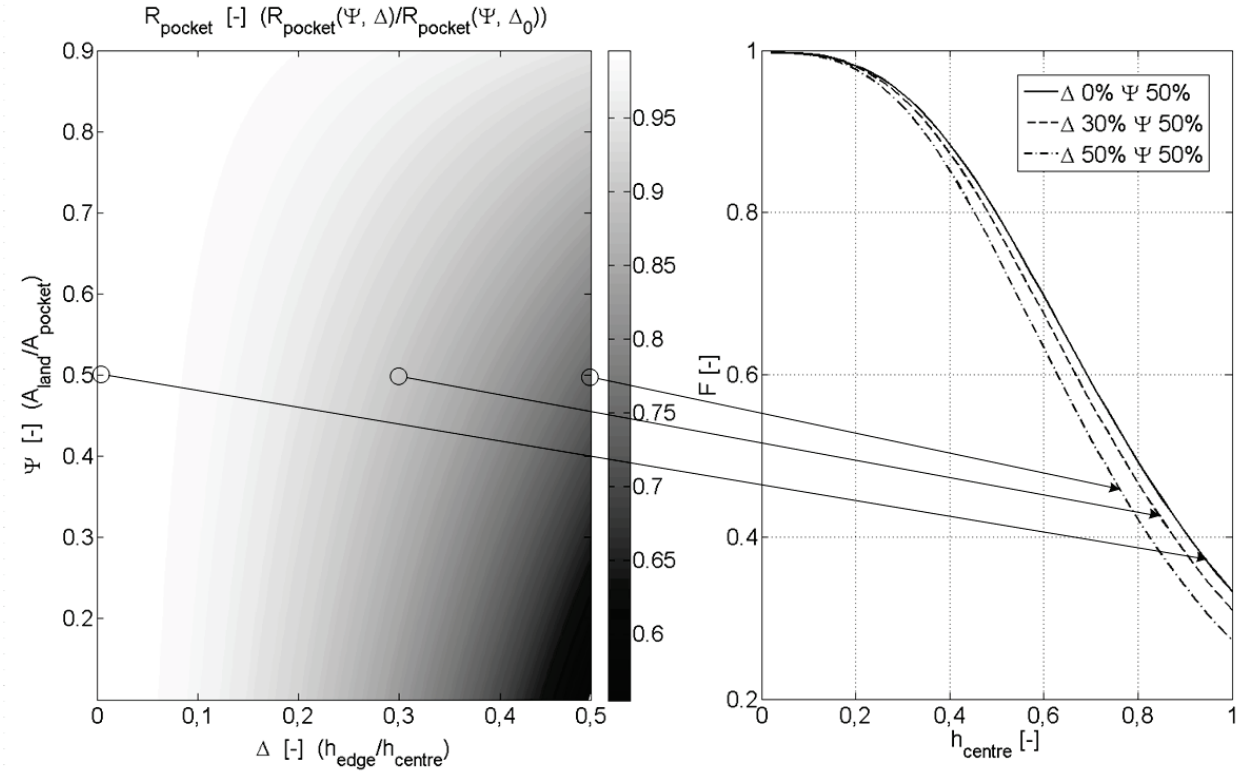

Fig. 1: Influence of tilt ratio Δ and pocket surface to pocket land surface ratio Ψ on hydraulic resistance R and on load capacity F of HS guideways

Verification

The presented calculations were verified on laboratory test rig STD21 used for experiments with high speed HS. The test rig also allows tilt and throttling gap change of HS pockets. The influence of tilt on oil flow rate and pressure in the HS pocket cavity was measured and compared with the values based on the hydraulic resistance calculation (Eq. 1). The experimental results are in good agreement with the calculated values.

Summary

Coupling a FE model of a compliant MT structure with the presented detailed model of nonlinear load capacity of HS guideways allows us to include the influence of tilt on load capacity directly in the calculation, instead of sequential evaluation of tilt at each pocket and comparison with allowable values given by experience.

Acknowledgement: This research has been supported by the Competence Center - Manufacturing Technology project TE01020075 funded by the Technology Agency of the Czech Republic.

References

[1] M. Mares, E. Stach, T. Holkup, Applied Method for Design Optimization of Hydrostatic Bearing on Real Machine Tool, in: EM2012 Conference Proceedings, 18 (2012) 857-868.

[2] A. van Beek, R.A.J. van Ostayen, Analytical solution for tilted hydrostatic multi-pad thrust bearings of infinite length, Tribology International, 30 (1997) 33-39.

21st International Conference **ENGINEERING MECHANICS 2015**
Svratka, Czech Republic, May 11 –14, 2015
Paper **#222, pp. 290–291**

Estimation of Pressure Vessel Lower Head Impact Force

Petr Štemberk[a] *, Michaela Vaitová[b], Martin Petřík[c]

Czech Technical University, Thákurova 7, 166 29 Prague 6, Czech Republic

[a]stemberk@fsv.cvut.cz, [b]michaela.vaitova@fsv.cvut.cz, [c]martin.petrik@fsv.cvut.cz

Keywords: corium-concrete interaction, pressure vessel lower head, corium configuration, impact force

Abstract: This paper presents a method of estimation of the concrete basement slab ablation acceleration during the nuclear severe accident. The molten fuel creates the corium pool in the lower part of the reactor pressure vessel. The stratification of the corium causes the focusing effect which leads to the rupture of the lower head of the pressure vessel. The impact of the lower head filled with the corium affects the subsequent corium-concrete interaction. The method of estimation of the impact load on the concrete basement slab and the related determination of the depth of the crushed concrete layer are presented.

Introduction

Three Miles Island, Chernobyl and Fukushima–Daichi nuclear power plants confirmed that most severe accidents are possible. Although each of these cases happened under different conditions, human errors and natural disasters seem to be the most common causes of accidents in nuclear power plants. Nuclear safety management has to be aware and ready for this type of accident when the reactor cannot be cooled and the overheating leads to melting of the fuel, Fig. 1, and possibly to melting of the reactor vessel itself. The molten materials (corium) create a pool inside lower head of the pressure vessel.

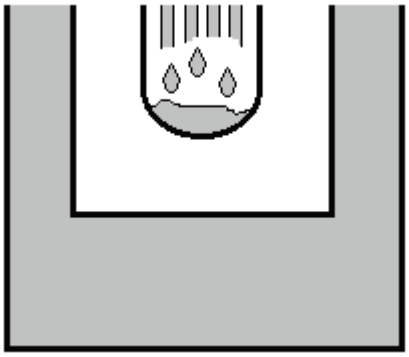

Fig. 1: Pressure vessel lower head with melting fuel

Impact force estimation

The corium pool inside the vessel is stratified due to the difference in material densities. Two layers within the pool are created by oxides and metals. The oxidic layer is heavier, thus located at the bottom of the pool, and generates the decay heat. The metallic layer has much higher thermal conductivity therefore conducts the heat generated in the lower layer easily towards the vessel wall. This phenomenon is called the focusing effect. The vessel wall heated by the metallic layer loses its strength. Then, the vessel wall ruptures in the anticipated area when the self weight of the lower head filled with corium exceeds its strength.

Assuming that the entire lower head is separated from the rest of the vessel, the weight of the falling mass is approximately 150 tons. The distribution of the pressure produced by the impacting corium is not considered as exactly normal to the surface of the lower head as depicted in Fig. 2a). This assumption results from high viscosity of corium and the nature of the impact loading.

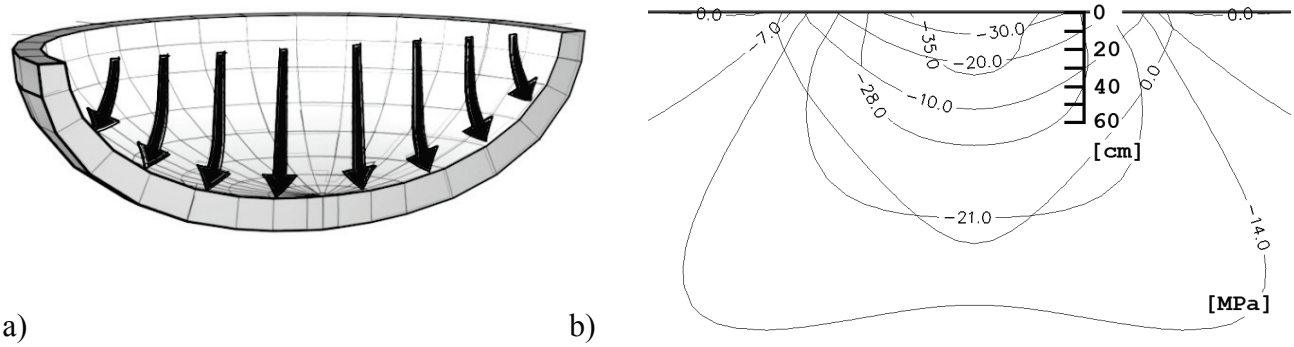

a) b)

Fig. 2: a) Distribution of pressure on lower head caused by impacting corium, b) Resulting stress distribution in concrete basement slab

The aim is to obtain the peak value of the force which is necessary for determination of concrete crushing of the basement slab. The finite element model of the lower head was created for the purposes of a nonlinear static analysis which provided a force-displacement curve of the lower head. Then an iteration process based on determination of the total height of fall is performed. The distribution of the peak force is related to the deformed shape of the lower head. A two-dimensional plane strain analysis was performed in order to get the resulting stress in the concrete basement slab, see Fig. 2b). The results show the estimated extent of damage for the peak force of intensity around 30 MN. It is supposable that the impact area of the concrete basement slab is significantly crushed in the depth of 40 cm.

Acknowledgements: This work was financially supported by the Czech Science Foundation, project P104/15-11753S, which are gratefully acknowledged.

References

[1] M. Cranga, et al., Simulation of corium concrete interaction in 2D geometry. Progress in Nuclear Energy. 52 (2010) 76–83.

[2] M. Vaitová, P. Štemberk, Numerical Model of Corium-concrete Interaction. In: Mechanika 2014 - Proceedings of the 19th International Conference, pp. 277–280. Kauno technologijos universitetas, Kaunas (2014).

[3] International Atomic Energy Agency. Thermophysical properties database of materials for light water reactors and heavy water reactors [online]. Vienna: International Atomic Energy Agency, 2006. Available: http://www.pub.iaea.org/MTCD/publications/PDF/te_1496_web.pdf

[4] P. Tusheva, et al., Investigations on in-vessel melt retention by external cooling for a generic VVER-1000 reactor. Annals of Nuclear Energy. 75 (2015) 249–260.

21st International Conference **ENGINEERING MECHANICS 2015**
Svratka, Czech Republic, May 11 –14, 2015
Paper **#145, pp. 292–293**

Dynamic Analysis of Mechatronic System with Ball Screw

Jakub Stetina[a] *, Tomas Brezina[b], Zdenek Hadas[c]

Brno University of Technology, Faculty of Mechanical Engineering,
Technicka 2896/2, 616 69, Brno, Czech Republic

[a] stetina.j@fme.vutbr.cz, [b] brezina@fme.vutbr.cz, [c] hadas@fme.vutbr.cz

Keywords: dynamics, multibody system, ball screw, flexible parts

Abstract: This paper deals with dynamic modelling and analysis of a ball screw system for accurate machine tools. Ball screws are basic mechatronic subassemblies of accurate machine tools in the present time. Various mechanical parameters of ball screw affect dynamics of the whole mechatronic system and effects of individual parameters will be investigated. The screw of the ball screw system has flexible behaviour and it affects behaviour of the whole machine tool. There is length of the flexible screw determines natural frequency and it determine maximal speed of movement. The design of modern ball screw systems is focused on speed increasing of movement. The speed increasing of the ball screw systems is main aim of our development and the dynamic analysis of this system are presented in this paper.

Introduction

The main issue of machine tools are compensation of thermal influence for accuracy, machining technology and especially dynamic properties. The movement during machining and especially temporary rapid movement can cause significant vibrations. Increasing the speed is important to increase effectivity of production. Machining speed can be increased by definition of the correct machining technology and the most of production time is wasted during temporary rapid movements. Machine tool use linear actuators and ball screws. The linear actuators are very expensive and therefore the ball screws are commonly used in machine tools. The ball screw dynamic analyses and limitations are presented in this paper. Some methods of extending of ball screw operation range are mentioned.

This paper analyses the rapid moving of machine tools especially its modelling and control possibilities. The design of the screw, kinematic joints and the whole system assembly affects critical revolution of the ball screw; it means maximal revolutions without significant mechanical oscillation [1]. Diameter, length and material properties of ball screw determinate the critical revolution. Initial dynamic model of simple unbalanced mass-spring-damper model of ball screw is shown in Fig. 1a) and thereafter the FEM model will be analyzed – Fig. 1b). The basic dynamic analyses are presented.

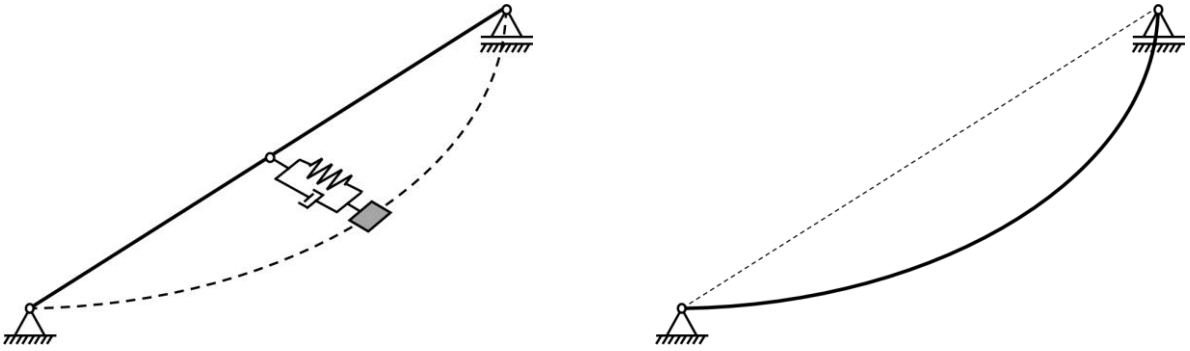

a) mass-spring-damper model b) FEM model

Fig. 1: Dynamic models of rotating ball screw

Results

The recommended operation of ball screw and generally the shaft is under the critical revolutions [1]. The value of critical revolution depends on design parameters and it is shown in Fig. 2.

The value of critical revolutions for shafts with circular cross section is calculated from motion equation. The derived motion equation describes maximal revolutions per minute which depends on diameter and length of the ball screw.

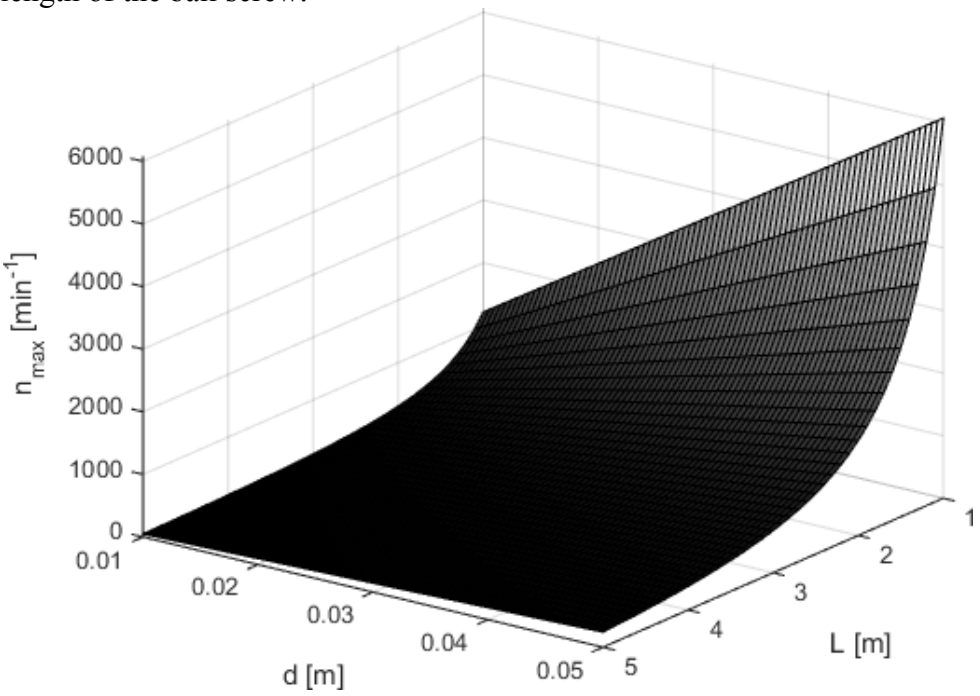

Fig. 2: Critical revolutions of ball screw depending on diameter and length

Summary

The main aim of this paper are dynamic analyses of ball screw simplified and FEM models, which will be used for design of new ball screws with high critical revolutions and control methods for avoiding of mechanical oscillation at critical revolutions.

Models of the dynamics systems are realized in MSC.Adams environment and these models can be co-simulated with Matlab control models [2]. It can provide very useful simulation tool for development of new mechatronic systems like adaptronic ball screws.

Acknowledgement: The presented results of this paper were created under the project NETME CENTRE PLUS (LO1202) with financial support from the Ministry of Education, Youth and Sports under the „National Sustainability Programme I".

References

[1] H. Zhu, H. Fujimoto, Mechanical Deformation Analysis and High-Precision Control for Ball-Screw-Driven Stages. IEEE/ASME Transactions on Mechatronics, 20 (2015) 956-966.

[2] Z. Hadas, T. Brezina, O. Andrs, J. Vetiska, L. Brezina, Simulation modelling of mechatronic system with flexible parts. In: 15th International Power Electronics and Motion Control Conference and Exposition, EPE-PEMC 2012 ECCE Europe. 1. Novi Sad, Serbia: EPEPEMC Council 2012. p. LS2e.1-1 (LS2e.1-7 p.)

21st International Conference **ENGINEERING MECHANICS 2015**
Svratka, Czech Republic, May 11 –14, 2015
Paper **#019, pp. 294–295**

Influence of the Radial Gap Under the Stator Blade on Flow Around the Hub-End of the Rotor

Petr Straka[a*], Martin Němec[b]

Výzkumný a zkušební letecký ústav, a.s., Beranových 130, 199 05 Praha-Letňany, Czech Republic

[a]straka@vzlu.cz, [b]nemec@vzlu.cz

Keywords: turbomachinery, axial turbine stage, drum-type rotor, secondary flow

Abstract: The contribution deals with experimental and numerical investigation of flow-field in an axial turbine stage with prismatic blades which are not equipped with a shroud. Main attention is paid to the influence of the radial clearance under the stator blade on generating of the secondary flow structure which dramatically affect flow-field in the hub part of the rotor blade. Results of the numerical simulation are compared with the experimental data. Both numerical and experimental data point to a significant drop in efficiency of the stage due to interaction of the rotor blades with the secondary vortices generated behind the radial clearance under the stator blade.

Introduction

The axial steam turbines of low power (around hundreds kilowatts to units megawatts) are typically designed with the drum-type rotor as shown in Fig. 1 (left). For reduction of a production cost the shroud-less stator and rotor wheels are still in use. In this configuration it is necessary to maintain the radial clearance under the hub-end of the stator blades and above the tip-end of the rotor blades. However, flow through the radial clearance generates large secondary flow structures which has negative influence on the efficiency.

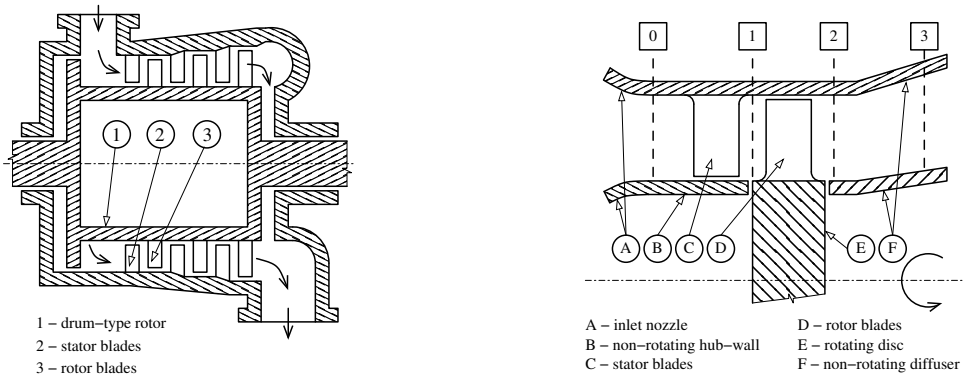

Fig. 1: Simplified scheme of axial turbine with drum-type rotor (left). Scheme of experimental stage (right).

The effect of the radial clearances is investigated experimentally and numerically on the testing stage which is schematically shown in Fig. 1 (right). Tested regimes are defined by total/static pressure ratio in range $1.4 \leq p_{T0}/p_{S2} \leq 1.9$ and velocity ratio in range $0.35 \leq u/c_{2is} \leq 0.65$, where p_{T0} is the total pressure in plane 0, p_{S2} is the static pressure in plane 2, u is the circumferential velocity at the middle diameter and c_{2is} is the isentropic velocity in plane 2. Planes 0 and 2 are defined in Fig. 1.

The test rig (see. [1, 2]) is a part of the high-speed closed-loop wind tunnel allowing independent setting of the Mach and Reynolds numbers. Testing stage is loaded by hydraulic dynamometer. A concept of the rotatable stator was used in consequence of linear probe manipulators. Fast response pressure probes were also used in order to study the unsteady flow field at the outlet of the rotor. The mass flow rate is measured using the orifice plate.

The in-house CFD code (see. [3, 4]) is used for simulation of the unsteady, compressible, viscous, turbulent flow of the perfect gas in testing stage. The CFD code is based on the finite volume method for discretization of the RANS equations closed by $k - \omega$ turbulence model. Multi-block structured mesh of hexahedral elements is used for discretization of the computational domain which is bounded by planes 0 and 3 (as shown in Fig. 1) and contains periodical repeated section containing five stator and six rotor blades. Interface between stator part and rotating rotor part of the computational domain is implemented via the sliding mesh technique.

Results and discussions

Left part of Fig. 2 shows secondary vortices generated behind the radial clearance under the hub-end of the stator blades. These vortices are drifted on the higher diameter along the suction side of the rotor blades, which leads to decreasing of the efficiency at lower forty percent of the span as shown in Fig 2 right. The efficiency drop at lower forty percent of the span is of about ten percent. The efficiency at upper twenty percent of the span is negatively influenced by secondary vortices generated behind the radial clearance above the tip-end of the rotor blades.

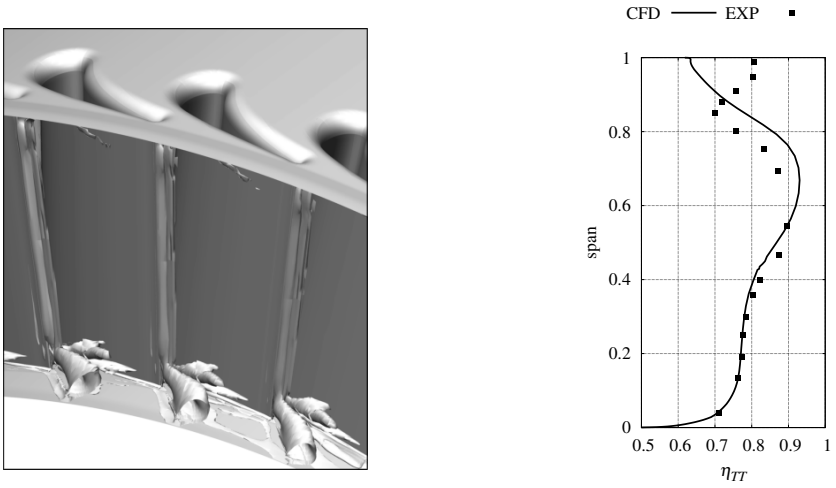

Fig. 2: Vortices generated behind the hub-end of the stator blades (left), span-wise distribution of the total-total efficiency (right).

Acknowledgments: This work was supported by the grant project TA02021336 of the Technology Agency of the Czech Republic.

References

[1] T. Jelíınek, M. Němec, The axial turbine stage test rig, Turbomachinery 2010, Plzeň, (2010) (in Czech).

[2] M. Němec, T. Jelínek, J. Benetka, Test turbine VZLÚ integral characteristics measurement, VZLU report R-4939, Prague, (2010) (in Czech).

[3] P. Straka, Simulation of a 3D unsteady flow in an axial turbine stage, in: Proc. Conf. Exp. Fluid Mech. 979-987, (2011).

[4] P. Straka, Calculation of 3D unsteady inviscid flow in turbine stage ST6, VZLÚ Report R-4910, Prague, (2010) (in Czech).

21st International Conference **ENGINEERING MECHANICS 2015**
Svratka, Czech Republic, May 11 –14, 2015
Paper **#107, pp. 296–297**

Stochastic Wang Tiles Generation Using the Discrete Element Method

Jan Stránský[a], Martin Doškář[b]

Faculty of Civil Engineering, Czech Technical University in Prague,
Thákurova 7/2077, 166 29 Prague, Czech Republic

[a]jan.stransky@fsv.cvut.cz, [b]martin.doskar@fsv.cvut.cz

Keywords: discrete element method, Wang tiling, dense packing, microsctructure reconstruction

Abstract: An algorithm for generation of 2D and 3D stochastic Wang tiles is presented in this contribution. The algorithm is based on the discrete element method (DEM) and is therefore applicable for matrix-based structures with separate inclusions. Moreover, the approach is designed for dense packings. An open-source free DEM code YADE was used for all the computations. The method is illustrated on a 2D exemplary realization of Wang tiling and its statistical comparison with periodic tiling.

Introduction

In comparison to the up-to-date scheme based on Periodic Unit Cell (PUC), stochastic Wang tilings bring wider diversity in microstructure representation. This concept allows to represent non-periodic material microstructure using limited number of basic tiles [1]. The tiles are boundary-compatible such that during the tiling process, i.e. consecutive placing the tiles side by side to cover up a portion of a plane, there always exist at least two possible tiles to place with boundaries compatible with the previously placed tiles. The random choice results in stochastic realizations of the compressed microstructure.

An algorithm for a design of Wang tiles morphology based on the discrete element method (DEM) [2] is presented in this paper. The algorithm is based on periodic contact detection and proper determination of particles interaction. The method is applicable for representation and reconstruction of random inclusion-matrix microstructures. Apart from the microstructure generation, the approach can also be used to prepare initial positions of particles for DEM itself. This step of DEM simulations is very important in certain applications and might take significant amount of time [3]. With the tiling concept, DEM sample of arbitrary size can be prepared (almost) instantaneously once the tiles are pre-generated. The presented algorithm results in random isotropic dense packings.

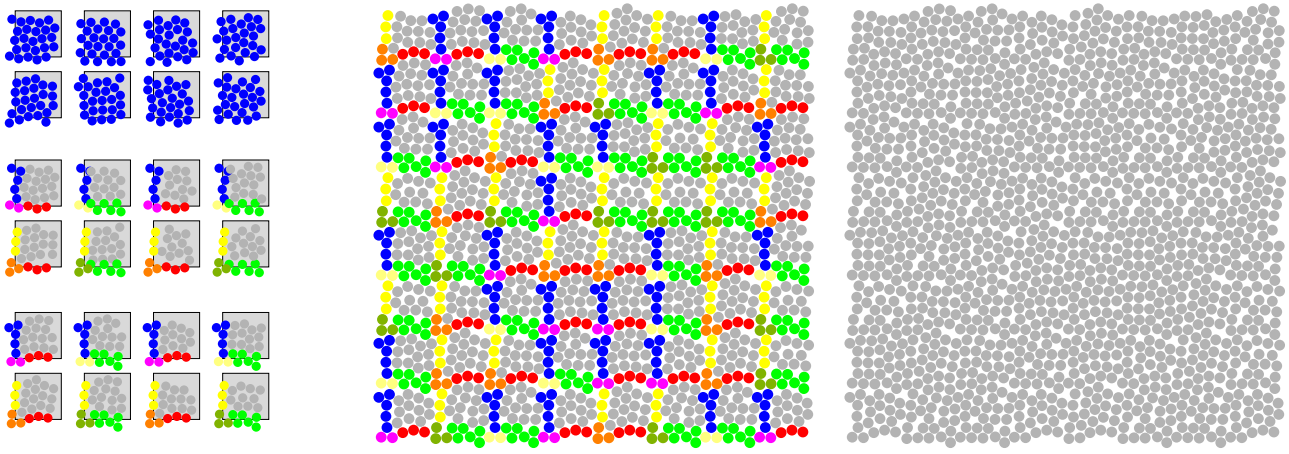

Fig. 1: Illustration of the method (left) and resulting tiling (right)

Algorithm

The approach will be described in detail with an illustrative example (see Fig. 1). For the sake of brevity, 2D case will be presented. However, the concept can be straightforwardly extended to 3D as well as to incorporate different particle shapes. Some implementation details and advantages of free open source YADE software [4] will be addressed.

Results

Two applications, the microstructure generation and a simple DEM simulation, will be outlined together with advantages of the approach (in terms of simple statistical descriptors). Fig. 2 shows comparison between periodic tiling (PUC) and Wang tiling in terms of two point probability function.

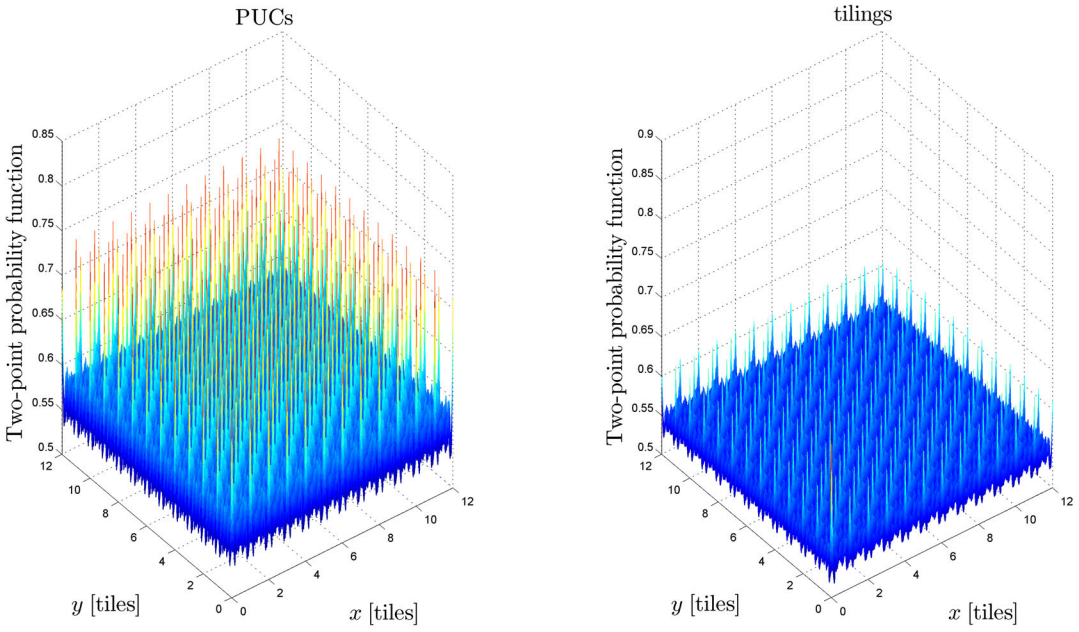

Fig. 2: Comparison of PUC (left) and Wang tiling (right)

References

[1] M. Doškář, J. Novák, J. Zeman, Aperiodic compression and reconstruction of real-world material systems based on Wang tiles, Physical Review E. 90 (2014).

[2] P.A. Cundall, O.D.L. Strack, A discrete numerical model for granular assemblies, Géotechnique. 29 (1979) 47–65.

[3] J.-F. Jerier, V. Richefeu, D. Imbault, F.-V. Donzé, Packing spherical discrete elements for large scale simulations, Comput. Method. Appl. M. 199 (2010) 1668–1676.

[4] V. Šmilauer, E. Catalano, B. Chareyre, S. Dorofeenko,J. Duriez, A. Gladky, J. Kozicki, C. Modenese, L. Scholtès, L. Sibille, J. Stránský, K. Thoeni, Yade Documentation (V. Šmilauer, ed.). 1st ed. [online]. The Yade Project, 2010 [cited 2015-03-09]. Available from: http://yadedem.org/doc/.

21st International Conference **ENGINEERING MECHANICS 2015**
Svratka, Czech Republic, May 11 –14, 2015
Paper **#102, pp. 298–299**

Determination of the Turning Knife Thermal Stress during Longitudinal Turning

Marek Stránský

Brno University of Technology, Faculty of Mechanical Engineering, Heat Transfer and Fluid Flow Laboratory, Technická 2896/2, 616 69 Brno, Czech Republic
stransky@LPTaP.fme.vutbr.cz

Keywords: temperature, thermo vision, thermocouple, machining, emissivity

Abstract: A turning knife enters a work piece during turning. Due to friction, heat is produced proportionate to the turning speed. The resulting temperature influences the quality of the machined surface and wear of the knife. Thus, new machine tools must be developed which minimize the production of unwanted heat. To accomplish this task, a new experimental device has been prepared, where thermocouples were built into the knife and surface thermocouples were welded onto its surface. The measurement process was supplemented by thermovision. Heat flux and surface temperatures were computed from the subsurface data using a one-dimensional inverse task. A detailed temperature distribution on the surface of the turning knife was determined using a combination of these methods.

Introduction

An understanding of turning tool thermal stress is very important due to its influence on surface quality and tool wear, but more importantly for the development of better cutting tools. Currently, there are a number of contact and non-contact methods using various instruments to measure this stress. For this study, shell thermocouples, thermocouple wires and a thermal imaging camera were used. To determine the surface temperature and heat flux at the point of heat generation (the contact-point of the work piece and a tool), a one-dimensional inverse task was used.

Experimental measurements

The experiment was performed using a Radeco side turning tool. Firstly, 20 mm deep and 0,6 mm wide holes were created 1 mm under the surface and 2 mm from the tool tip using electro-erosion, and then were fitted with 0,5 mm shell thermocouples. Secondly, thermocouple wires were welded to the blade surface to record the surface temperature - see Fig. 1 and 2. Finally, a detailed view of the temperature field of the tip of the tool was obtained using a ThermaCAM SC 2000 thermal imager. Three experiments with different cutting speeds were performed [1].

Fig. 1: Tool with thermocouples,

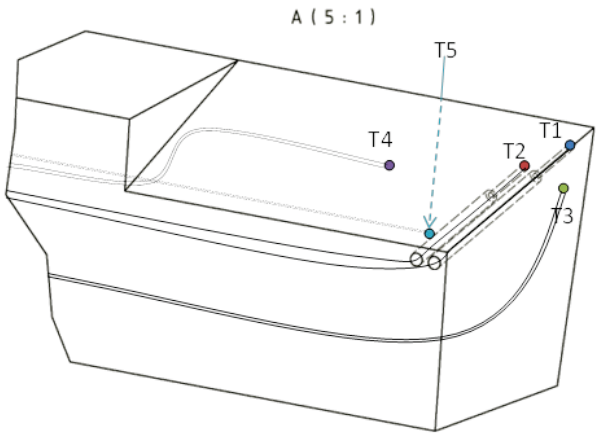

Fig. 2: Position and indication termocouple

Results

The thermogram in Fig. 3 shows the areas where the temperature record was recorded - T1 and T2 stand for the subsurface shell thermocouples, points 1 and 2 are the areas where the data from the thermal imager was evaluated. Fig. 4 shows the evolution of temperature over time. The maximum measured temperature was 140°C at a cutting speed of 26 m/min.

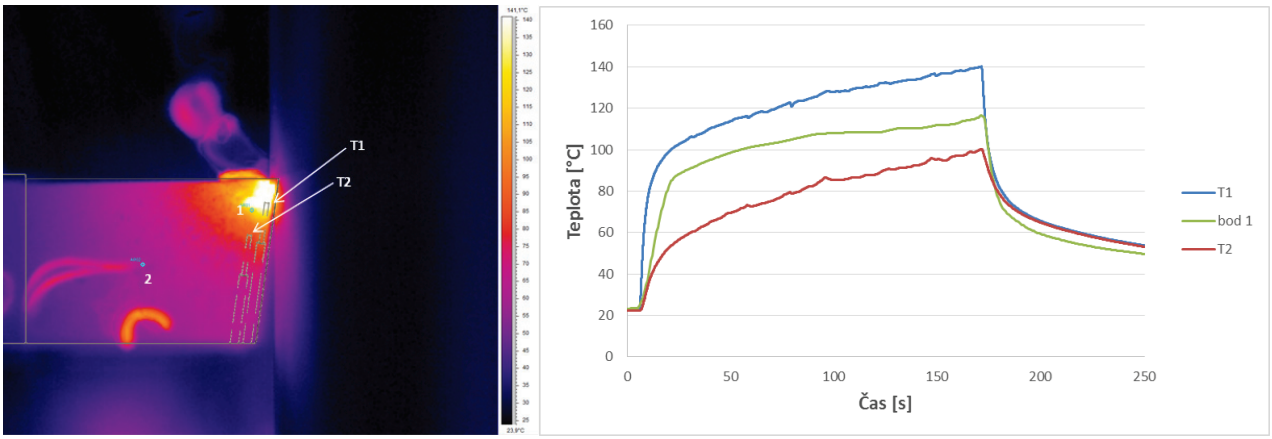

Fig. 3: The thermogram showing points for evaluation, Fig. 4: The comparison of T1 and T2 thermocouples and point 1 data from the thermocamera at cutting speed 26.14 m/min

The data from the T1 and T2 thermocouples was used for input values in a one-dimensional inverse task to calculate the surface temperatures on the head of the turning tool. The outcome values are shown in Fig. 5.

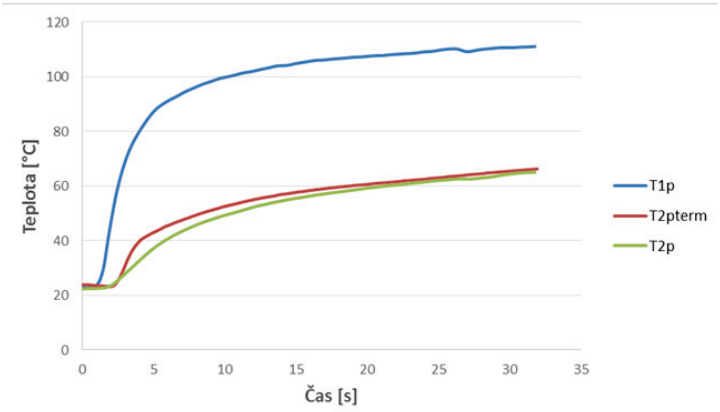

Fig. 5: Comparison of the calculated surface temperatures of T1P and T2P with the surface temperature measured by the thermocamera at a cutting speed 26.14 m/min

Conclusion

A 10 m/min cutting speed increase can increase the temperature in tens of degrees Celsius. The advantage of using this method is that it can obtain temperatures for places where a surface thermocouple or thermal imager cannot be used, as well as under standard machining conditions (using coolant).

Acknowledgement This work is an output of research and scientific activities of this project LO1202 and the project No. CZ.1.07/2.3.00/20.0188, HEATEAM - Multidisciplinary Team for Research and Development of Heat Processes with financial support of the MEYS under the programme NPU I.

References

[1] M. Stránský, Měření povrchových teplot ve strojírenství, thesis, VUT, Brno 2014.

21st International Conference **ENGINEERING MECHANICS 2015**
Svratka, Czech Republic, May 11 –14, 2015
Paper **#089, pp. 300–301**

Comparison of Energy Efficiency of the Redundant Actuation of Positioning Axes

Kamil Šubrt[a] *, Radek Knoflíček[b], Pavel Houška[c]

Faculty of Mechanical Engineering, Brno University of Technology,
Technická 2896/2, 616 69 Brno, Czech Republic

[a] subrt@fme.vutbr.cz, [b] knoflicek@fme.vutbr.cz, [c] houska.p@fme.vutbr.cz

Keywords: redundant actuation, Ecodesign, energy efficiency, linear axis, master-slave

Abstract: Presently, production machines and mainly contemporary machining centers are subjected to ever increasing pressure to enhance energy efficiency, both from the side of customers and also in terms of legislative regulations. A selection of drives for the individual axes is primarily a compromise between achievable dynamics, precision and price. The electrical efficiency and energy consumption is not usually taken into consideration during the design of the axis. In this paper, the electricity consumption of single drive axis actuator and redundant actuation through two drives is compared under various operating conditions. The measurement results are used to assess the benefits of redundant actuation of positioning axes with emphasis on energy efficiency, which is consistent with the current trend of the so-called Ecodesign.

Introduction

Increasing energy efficiency of the production machines is a very topical and live issue among the development teams of leading manufacturers and customers. Reducing energy costs with maintaining the technical and operational characteristics requires knowledge of the energy consumption characteristic of the machine. Case studies or statistical data of production facilities are usually the base of these characteristics, which are then used for potential increase in energy efficiency. During this process, a methodology of various test procedures is also derived [1, 2, 3].

A power consumption measurement itself is a partial task. Generally, there are two methods of how to approach this task; to measure torque and speed on the electric motor shaft, or to measure the total electrical power supplied to the motor [4]. Each of these two methods is appropriate for different goals. This article is devoted to the measurement of electrical power delivered to the motor.

However, when exploring the opportunities for increasing the energy efficiency of already manufactured production equipment, i.e. the one physically existing, it is not possible to significantly affect its conception, hence the structure or the drive unit topology. The measured data of the drive properties in terms of energy consumption are not always available during the design phase of the machine; therefore it is necessary to rely on theoretical knowledge and measurement methodologies. Enhancement of energy efficiency in the design phase therefore requires knowledge of new energy-efficient topology and the use of adequate products [5].

The aim of this research is to experimentally compare the energy consumption of one linear axis with ball screw, when designed with one drive and with redundant actuation with two drives from each side of the screw driven in master-slave mode. While carrying out all parts of the experiment, it was necessary to maintain the same operating parameters, including the same climatic conditions that correspond to typical conditions of production workplaces. This research is related to the theoretical knowledge of the authors [6], who refer to potential energy savings when using the redundant actuation under certain operating conditions. The entire experimental stand is shown in Fig. 1.

Fig. 1: Experimental stand for testing of linear axis with ball screw

Results and summary

The experiment results demonstrate the potential energy savings of ca. 7% for the drive solution by redundant actuators. These savings were achieved under specific operating conditions, particularly at lower values of acceleration and higher speeds; this confirms theoretical assumptions [6]. These savings for one motion axis are undoubtedly interesting. However, during the operation of the machine, its operating conditions can change; therefore these results cannot be considered the final energy savings of one linear axis. More *feasible* savings will be verified in the future using the known trajectory reconstruction obtained during the machining of specific component.

Acknowledgement: The research leading to these results has received funding from the Ministry of Education, Youth and Sports under the National Sustainability Programme I (Project LO1202).

References

[1] S. Hu, F. Liu, Y. He, T. Hu, An on-line approach for energy efficiency monitoring of machine tools, J. Clean. Prod., 27 (2012) 133–140.

[2] T. Behrendt, A. Zein, S. Min, Development of an energy consumption monitoring procedure for machine tools, CIRP Ann. - Manuf. Technol., 61 (2012) 43–46.

[3] A. Vijayaraghavan, D. Dornfeld, Automated energy monitoring of machine tools, CIRP Ann. - Manuf. Technol., 59 (2010) 21–24.

[4] S. Hu, F. Liu, Y. He, T. Hu, An on-line approach for energy efficiency monitoring of machine tools, J. Clean. Prod., 27 (2012) 133–140.

[5] J. Böhner, M. Hamacher, A. Reger, R. Steinhilper, Derivation of measures for energy efficient machine design by evaluating energy consumption data, Procedia CIRP, 15 (2014) 437–442.

[6] R. Huzlík, M. Holub, F. Bradáč, P. Blecha, Simulation of linear axis withball screw and permanent magnet synchronous machine. 2012.

[7] R. Huzlík, P. Blecha, A. Vašíček, P. Houška, M. Holub, Device for Measuring of Active Power and Energy at Machine Tools, in Mechatronics 2013, 2013, pp 503–509.

21st International Conference **ENGINEERING MECHANICS 2015**
Svratka, Czech Republic, May 11 –14, 2015
Paper **#106, pp. 302–303**

Frequency Analysis of Torsion Vibration of Hard Rubbers under Finite Deformations

Petr Šulc[a*], Luděk Pešek[b], Vítězslav Bula[c], Jan Cibulka[d], Jan Košina[e]

Institute of Thermomechanics AS CR, v. v. i., Dolejškova 1402/5 , 182 00 Praha 8 , Czech Republic

[a]sulc@it.cas.cz, [b]pesek@it.cas.cz, [c]bula@it.cas.cz, [d]cibulka@it.cas.cz, [e]kosina@it.cas.cz

Keywords: hard rubber, torsion vibration, large deformation, rheology, parameter identification

Abstract: The paper deals with experimental analysis of hard rubber dynamic tests under finite torsion deformations. The experimental test rig based on controlled servo-motor was proposed and built for torsion straining of the rubbers under defined amplitudes and frequencies and temperature of angle vibration. The paper brings results of the tests for different excitation frequencies under different levels of torsion deformations. The mathematical rheological model of rubber is also presented for phenomenological description and parametric identification of hard rubbers.

Introduction

Contrary to the most standard construction materials, the time variable material behavior of hard rubbers occurs during their dynamic loading due to deformation level, creep, temperature and aging [1]. Therefore, we have been dealing with the thermo-mechanical behavior of hard rubbers in our dynamic laboratory. Recently we investigated behavior of rubbers under small deformations and latest we start to deal with their behavior under larger finite deformation (up to 10%) [2].

Experimental set-up for torsional tests

For finite deformations, an experimental set-up for torsional dynamic tests of rubber samples of circular cross-section has been designed and assembled. Furthermore methodology and programs for evaluation rubber material constants from the measured force and response signals of the test rig depending on frequency, amplitude and temperature were developed, too. Excitation is directly controlled by the control unit of the engine. The control unit provides one analogue output signal, either position or speed. Analogue signals were digitized A/D converter NI PCI-6035 and processed by DAQ toolbox and numerical programs in the environment Matlab 2007 b.

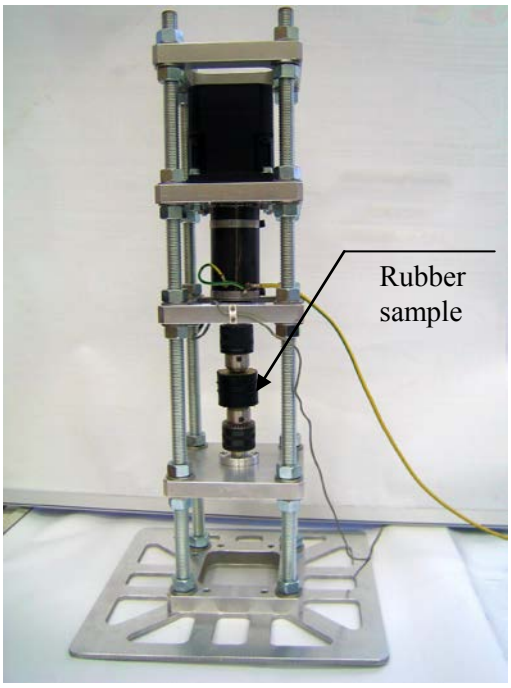

Fig. 1: Test rig for torsional tests of hard rubbers

The rheological model of hard rubber

Mathematical rheological model was proposed for phenomenological description of rubber behaviour under torsional straining. Parameters of the model are to be identified from the

comparison of the analytical and experimental hysteresis curves. The type of rheological model was designed to fit the experimental results of hysteresis of the rubber at finite (up to 10%) straining.

Total inner force of the rheological model as a sum of forces acting in its parallel branches is expressed

$$F_{cel} = k_0 \cdot \varphi + F_{mt\alpha} + F_{t0} \cdot \frac{2}{\pi} \cdot arctg(\alpha \cdot \dot{\varphi}) \tag{1}$$

where the first member equation (1) represents the stiffness force, $F_{mt\alpha}$ is force of differential equations obtained from force equilibrium of the Maxwell member

$$\dot{F}_{mt\alpha}(t) + \frac{F_{mt\alpha}(t)}{\tau_\alpha} = k_\alpha \cdot \dot{\varphi}(t) \tag{2}$$

and the third member of equation (1) is a friction force of the rheological model. After substituting the inner force in the equation of torsion motion we get

$$I_0 \ddot{\varphi} + k_0 \cdot \varphi + F_{mt\alpha} + F_{t0} \cdot \frac{2}{\pi} \cdot arctg(\alpha \cdot \dot{\varphi}) = M \cdot \sin(\omega \cdot t) \quad , \tag{3}$$

where an external excitation is realized by harmonic torque moment M with excitation frequency ω.

The equation of motion (3) and equation (2) were transferred into the system of differential equations of the first order for numerical solution by Runge-Kutta method.

Sumary

This paper brings first results of evaluation of hard rubber material constants (Fig.2) from the torsion tests. The material characteristics show higher dependence on the level of straining than on the frequency. Since the loss factor is ratio of the dissipation and deformation energy at a given strain it leads to the conclusion that the dissipation energy of hard rubbers under larger strains is related to the deformation energy by multiplication constant similarly as at the dissipation by small strains.

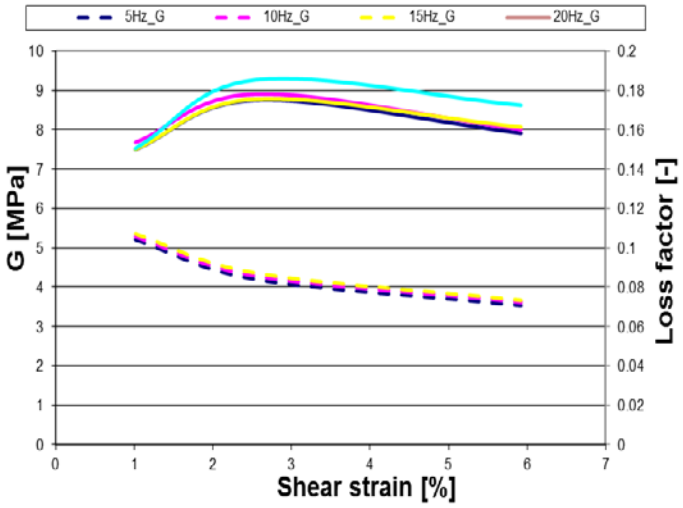

Fig. 2: Characteristics of the shear modulus (dashed) and loss factor (solid lines) on strains at different excitation frequencies (5, 10, 15, 20)Hz

References

[1] David 1. G. Jones, Viscoelastic Vibration Damping. John Wiley and Sons Ltd, Chichester, 1988.

[2] P. Šulc, L. Pešek, V. Bula, J. Cibulka, J. Košina, Experimentální analýza torzních kmitů tvrdých pryží při velkých deformacích, Colloquim Dymamesi (2014) 73-80.

21st International Conference **ENGINEERING MECHANICS 2015**
Svratka, Czech Republic, May 11 –14, 2015
Paper **#101, pp. 304–305**

On the Finite Element Method Application for Approximation of Free-Surface Flows with Surface Tension

Petr Sváček

Czech Technical University, Faculty of Mechanical Engineering, Dep. of Technical Mathematics,
Karlovo nám. 13, Praha 2, Czech Republic

Petr.Svacek@fs.cvut.cz

Keywords: finite element method, surface tension, contact angle

Abstract: This paper focuses on the mathematical modelling and the numerical approximation of the flow of two immiscible incompressible fluids. The surface tension effects are taken into account and mixed boundary conditions are used. The weak formulation is introduced, discretized in time, and the finite element method is applied. The free surface motion is treated with the aid of the level set method. The numerical results are shown.

Introduction

The mathematical modelling of two-phase flows with the consideration of the free surface motion influenced by the surface tension is addressed in various scientific as well as technical applications. Such a problem is important both from the mathematical modelling point of view and also from the technical practice. Particularly, its numerical approximation is very challenging task, see among others [1], [2] or [3]. The approximation of the surface tension or the contact angle naturally can play a key role here.

In this paper, we consider the two-dimensional flow of two immiscible fluids, the problem is mathematically described and the variational formulation is introduced. For the discretization the finite element(FE) method is used. The free surface motion is realized using the level set method, cf. [7] or [5]. In the case of high surface tension, a modification of the standard FE method is required to avoid the spurious currents, see [6] or [1]. For the verification of the implemented method a benchmark problem is solved, cf. [3].

Mathematical description

Let us consider the computational domain $\Omega \subset \mathbb{R}^2$ with the Lipschitz continuous boundary $\partial\Omega$ with its mutually disjoint parts Γ_W, Γ_S, Γ_O. The domain is occupied at time t by two immiscible fluids, i.e. $\Omega = \Omega^A_{(t)} \cup \Omega^B_{(t)}$. Let us denote the Heaviside function $H(x,t)$ as $H(x,t) = 1$ for $x \in \Omega^A_{(t)}$, $H(x,t) = 0$ for $x \in \Omega^B_{(t)} \cup \hat{\Gamma}_t$. The density and the viscosity functions are then defined by $\rho(x,t) = \rho^A H(x,t) + (1 - H(x,t))\rho^B$ and $\mu(x,t) = \mu^A H(x,t) + (1 - H(x,t))\mu^B$, respectively. Then the twophase flow is governed by the equation

$$\rho \frac{\partial \boldsymbol{u}}{\partial t} + \rho(\boldsymbol{u} \cdot \nabla)\boldsymbol{u} - \nabla \cdot \boldsymbol{\sigma} = \rho \boldsymbol{f} + \gamma \kappa \boldsymbol{n} \delta_{\hat{\Gamma}_t}, \tag{1}$$

which in the weak form reads

$$\int_\Omega \rho \left(\frac{\partial \boldsymbol{u}}{\partial t} + (\boldsymbol{u} \cdot \nabla)\boldsymbol{u} \right) \cdot \boldsymbol{v} + \boldsymbol{\sigma} \cdot (\nabla \boldsymbol{v}) \, \mathrm{d}x = \int_{\hat{\Gamma}_t} \gamma \kappa \boldsymbol{n} \cdot \boldsymbol{v} \, \mathrm{d}S + \int_\Omega \rho \boldsymbol{f} \cdot \boldsymbol{v} \, \mathrm{d}x, \tag{2}$$

where $\boldsymbol{\sigma}$ is the Cauchy stress tensor given by $\boldsymbol{\sigma} = -pI + \mu(\nabla \boldsymbol{u} + \nabla^T \boldsymbol{u})$.

In order to treat the surface tension term, the Laplace-Beltrami operator $\triangle_\Gamma = \nabla_\Gamma \cdot \nabla_\Gamma$ is used, where ∇_Γ denotes the tangent derivative with respect to the surface. Now, using the relation $\kappa \boldsymbol{n} = \triangle_\Gamma \boldsymbol{x}$ and applying the integration by parts on $\hat{\Gamma}_t$ we get

$$\int_{\hat{\Gamma}_t} \gamma \kappa \boldsymbol{n} \cdot \boldsymbol{v} \, \mathrm{d}S = - \int_{\hat{\Gamma}_t} \gamma (\nabla_\Gamma \boldsymbol{x}) \cdot (\nabla_\Gamma \boldsymbol{v}) \, \mathrm{d}S, \tag{3}$$

where for the sake of simplicity it was assumed that $\hat{\Gamma}_t$ is a closed curve.

Furthermore, to treat the motion of the free surface $\hat{\Gamma}_t$ the *level set* method is applied. First, the initial condition for the level set function $\phi = \phi(x,t)$ is prescribed by $\phi(x,0) = \mathrm{dist}(x, \hat{\Gamma}_0) > 0$ for $x \in \Omega^A_{(0)}$, $\phi(x,0) = -\mathrm{dist}(x, \hat{\Gamma}_0) < 0$ for $x \in \Omega^B_{(0)}$, and $\phi(x,0) = 0$ for $x \in \hat{\Gamma}_0$. The motion of the interface $\hat{\Gamma}_t$ is then realized by forcing the function ϕ to solve the equation

$$\frac{\partial \phi}{\partial t} + \boldsymbol{u} \cdot \nabla \phi = 0. \tag{4}$$

Numerical approximation

The presented problem is approximated in time using the backward difference formula and then the problem is spatially discretized by the FE subspaces defined over an admissible triangulation $\mathcal{T}_h$. For the approximation the well-known Taylor-Hood FE are used. In order to treat the discontinuity, the extended finite element method XFEM is used. The XFEM enlarges the original FE pressure space using the localization of an enrichment function, which in this case is the discontinuous Heaviside function.

Acknowledgements: This work was supported by grant No. 13-00522S of the Czech Science Foundation.

References

[1] J.W. Barrett, H. Garcke, R. Nürnberg, Eliminating spurious velocities with a stable approximation of viscous incompressible two-phase Stokes flow. Computer Methods in Applied Mechanics and Engineering, 267 (2013) 511–530.

[2] C.W. Hirt, B.D. Nichols, Volume of fluid (VOF) method for the dynamics of free boundaries. Journal of Computational Physics, 39 (1981) 201–225.

[3] S. Hysing, et al., Quantitative benchmark computations of two-dimensional bubble dynamics. International Journal for Numerical Methods in Fluids, 60 (2009) 1259–1288.

[4] D. Kuzmin, On the design of general-purpose flux limiters for finite element schemes. I. Scalar convection. Journal of Computational Physics, 219 (2) 2006, 513–531.

[5] S.R. Ransau, Solution methods for incompressible viscous free surface flows: A literature review. Tech. Rep. 3/2002, Norwegian University of Science and Technology, Trondheim, 2002.

[6] H. Sauerland, T.P. Fries, The stable XFEM for two-phase flows. Computers & Fluids, 87 (2013) 41–49.

[7] J.A. Sethian, Level Set Methods and Fast Marching Methods. Cambridge Monograph on Applied and Computational Mathematics, Cambridge University Press, Cambridge, U.K., 1999, 2nd edn.

21st International Conference **ENGINEERING MECHANICS 2015**
Svratka, Czech Republic, May 11 –14, 2015
Paper **#132, pp. 306–307**

Comparing the Use of Compressible and Incompressible Flow in the FE Model of Human Vocal Folds Self-Oscillation

Pavel Švancara[1,2,a]*, Jaromír Horáček[2,b], Petr Hájek[1,c], Michal Matug[1,d], Jan G. Švec[3,e]

[1]Institute of Solid Mechanics, Mechatronics and Biomechanics, Brno University of Technology, Technická 2896/2, 616 69, Brno, Czech Republic

[2]Institute of Thermomechanics, Academy of Sciences of the Czech Republic, Dolejškova 1402/5; 182 00, Prague; Czech Republic

[3]Department of Biophysics, Palacky University Olomouc, 17. listopadu 12, 771 46, Olomouc; Czech Republic

[a]svancara@fme.vutbr.cz, [b]jaromirh@it.cas.cz, [c]y126528@stud.fme.vutbr.cz, [d]ymatug01@stud.fme.vutbr.cz, [e]svecjang@gmail.com

Keywords: biomechanics of voice, fluid-structure-acoustic interaction, finite element method, Navier-Stokes equations

Abstract: In this study a three-dimensional (3D) finite element (FE) model of the flow-induced self-oscillation of the human vocal folds in interaction with air in a simplified vocal tract model is presented. The 3D vocal tract model of the acoustic spaces for Czech vowel [a:] was created by converting the data from the magnetic resonance images (MRI). The developed FE model includes fluid-structure interaction, morphing the fluid mesh according to the vocal-fold motion, unsteady viscous compressible/incompressible airflow described by the Navier-Stokes equations, airflow separation during the glottis closure, large deformations of the vocal-fold tissue and vocal-fold contact. The aim of this work is to analyze the effect of compressible and incompressible flow model on produced air pressure fluctuations and on vibrations of the vocal folds using the identical FE mesh and boundary conditions.

Introduction

Voice production should be modelled as a complex fluid-structure-acoustic interaction problem. Computational models of human voice production published in literature can be divided into three groups: reduced-order models, models of flow and finite element models. In previous works of the authors [1,2] FE model of flow-induced oscillations of the vocal folds in interaction with acoustic spaces of the vocal tract was developed. In this study a new FE model of phonation was constructed using four-layers vocal fold structure and in literature widely used M5 geometry of the vocal folds. The 3D FE model was developed using the program system ANSYS 15.0 (see Fig. 1.).

Results and discussion

Example of computed fluid pressure in point located 3 cm above the vocal folds for incompressible and compressible flow model is shown in Fig. 2. From the results we can see that for incompressible flow model vocal folds oscillating with higher fundamental frequency and after the vocal folds opening there is only one negative peak of fluid pressure. Whereas for compressible flow model fluid pressure oscillates several times from positive to negative values after the vocal folds opening. For compressible flow model we can see in the power spectral density spectrum of the pressure near the lips (see Fig. 2.), that some harmonics are enhanced by the resonant frequencies of the vocal tract and producing so called “formants”. For incompressible flow model we can in the resulting spectrum observe only peaks of fundamental frequency and its harmonics.

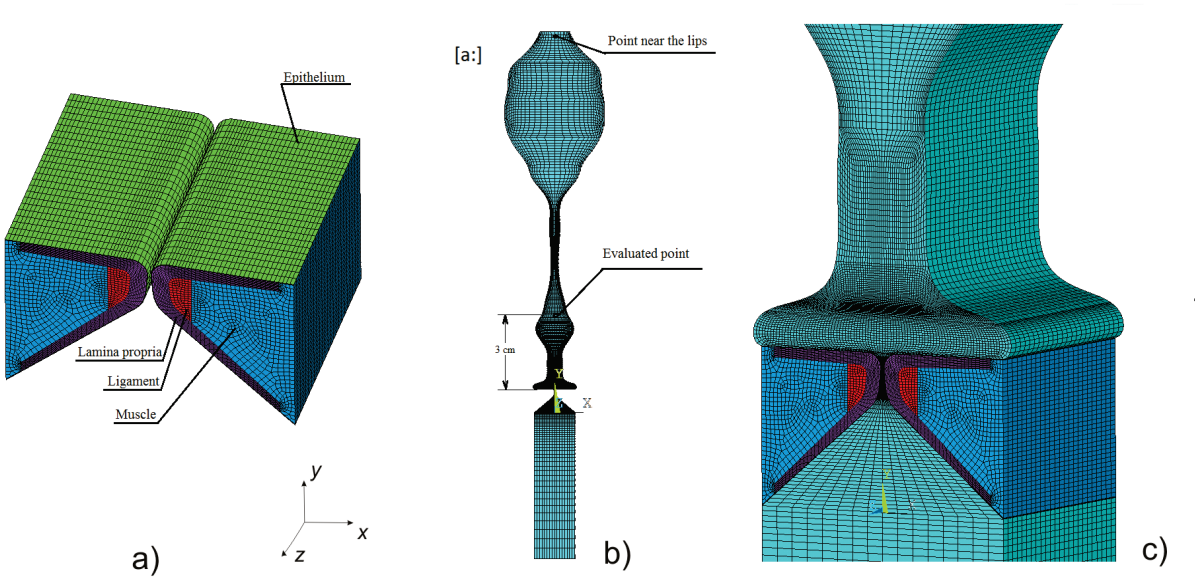

Fig. 1: a) FE model of the four layered tissue of the vocal folds b) FE model of the acoustic spaces of the trachea and the vocal tract for Czech vowel [a:] c) detail of the complete FE model of the vocal folds together with a part of the model of the vocal tract.

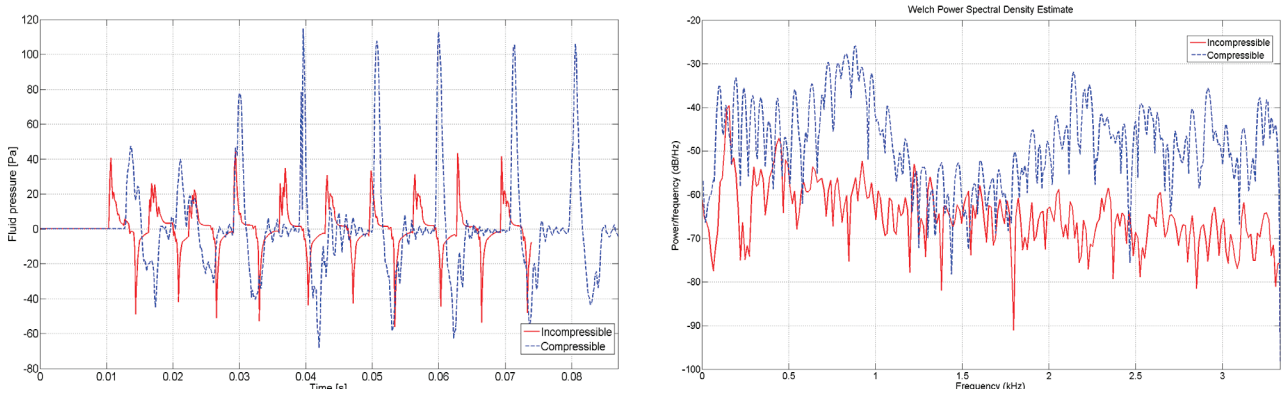

Fig. 2: Computed fluid pressure in point located 3 cm above the vocal folds (left) and power spectral density spectrum of the pressure near the lips (right) for incompressible and compressible flow model.

Summary

The developed model can be utilized to analyze the differences between use of compressible or incompressible flow model and to better understand the mechanisms of sound creation during phonation process.

Acknowledgement: This work was supported by the Grant Agency of the Czech Republic by the project No P101/12/1306.

References

[1] P. Švancara, J. Horáček, V. Hrůza, FE modelling of the fluid-structure-acoustic interaction for the vocal folds self-oscillation, in: Vibration Problems ICOVP 2011, Springer, Berlin (2011), pp. 801-807.

[2] P. Švancara, J. Horáček, J. G. Švec, Numerical Simulation of the self-oscillations of the vocal folds and of the resulting acoustic phenomena in the vocal tract, in: Advances in Mechanisms Design, Springer, Dordrecht (2012), pp. 357-363.

21st International Conference **ENGINEERING MECHANICS 2015**
Svratka, Czech Republic, May 11 –14, 2015
Paper **#031, pp. 308–309**

Impact of Landslide on Blasting in the Quarry Dobkovičky

Bohumil Svoboda[a]*, Jan Svoboda, Radim Kašpar

Geodyn spol. s r.o. Bajkonurská 736, Prague 11, Czech Republic

[a]geodyn@email.cz

Keywords: landslides, slope stability

Abstract. The day before the landslide took place the author visited and photographically documented the open cracks found near the offices and weight of the quarry Dobkovičky. The second day after the landslide again there were documented all damages and also a video of the moving soil was taken. On the basis of the Geofond documentation was realized the static and dynamic calculation of stability in time before and during the landslide as well as during the blast works in the quarry. Each blast is carefully monitored on 5 posts by vibrographs (by the official standard machines) near the quarry with the focus on fixed points before and after the blast. The results clearly show that the blast has no influence on stability conditions.

Fig. 1: Aereal picture of the mutual position of the quarry Dobkovičky and landslide.

Fig. 2: The landslide area, smashed railway and burried motorway

Fig. 3: Open cracks at the offices of the quarry Dobkovičky on the day before landslide

21st International Conference **ENGINEERING MECHANICS 2015**
Svratka, Czech Republic, May 11 –14, 2015
Paper **#223, pp. 310–311**

Kinematic Excitation of the Rotor

David Svoboda

Technical University of Liberec, Studentská 1402/2 461 17 Liberec 1, CZ

david.svoboda1@tul.cz

Keywords: rotor dynamics, kinematic excitation, finite element method

Abstract: Dynamic response of rotor with kinematically excited support is investigated. The finite element method model was set up and results were validated using MSC.Adams software.

Introduction

The work deals with rotor dynamics problem. Dynamic response of rotor with kinematically excited support is investigated. The studied case can represent for example a turbocharger that is component of an engine. Vibration of the engine is transported to the rotor of turbocharger through bearings. The finite element method model was prepared and results were validated using the MSC.Adams software. The finite element method describes the shaft [1], the disc is assumed to be rigid. The complete model of rotor with discs and bearings is studied, including modal analysis and simulation of motion [2]. All computation is performed using the math software Scilab [3].

The current work concentrates on problems which arise when body rotates. Therefore, the physical model considers internal material damping and gyroscopic effect. The most important phenomenon in rotor dynamics is the non-constant critical speed and area of instability.

Model of rotor

The rotor is described using the finite element method in Scilab. Only beam elements are used. The obtained results were compared with those of solid FEM model in NASTRAN software. During this tuning stage, only static analysis was performed. Simulation in Scilab was preceded by such tuning procedure.

Our contribution divides into three parts:

- The first part of work describes finite element model of rotor.
- Next, the natural frequencies and stability of rotor are studied.
- The last part is devoted to the simulation of motion and comparing all results.

The basic equation of motion which describes the rotor system can be schematically written as:

$$\mathbf{M}\ddot{\mathbf{q}} + (\mathbf{B_E} + \mathbf{B_I} + \omega_0\mathbf{G})\dot{\mathbf{q}} + (\mathbf{K} + \omega_0\mathbf{K_I})\mathbf{q} = \mathbf{F}(t) \tag{1}$$

In Eq. 1 is denoted: matrix of mass $\mathbf{M}$, matrix of external damping $\mathbf{B_E}$, matrix of gyroscopic effect $\mathbf{G}$ and matrix of stiffness $\mathbf{K}$, vector of displacements $\mathbf{q}$ and vector of kinematical excitation $\mathbf{F}(t)$. Physical model considers internal damping. This effect is described by matrix of internal damping $\mathbf{B_I}$ and circular matrix $\mathbf{K_I}$. In rotor dynamics, the physical model depends on the rotor speed ω_0. Maximal speed of experimental rotor is 318 rps, but in the numerical experiments the speed range from 0 to 500 rps was considered. The frequency of kinematic excitation can be arbitrary, but only the range from 0 to 500 Hz was studied.

Results

The transfer function of disc 1 in radial displacement for varying rotor speed and different frequency vibration of support is displayed in Fig. 1. The area of resonance is white and the area of antiresonance is black. Resonance and antiresonance are next to each other somewhere and it is very interesting result. Resonance can be like forward precession (FP) or backward precession (BP). The value of displacement is in logarithmic value, "A" is amplitude of motion of disc, "A_{ref}" is amplitude of kinematic excitation. MSC.Adams confirmed the results in simulation experiment. This research shows us safe areas and danger areas of using rotor.

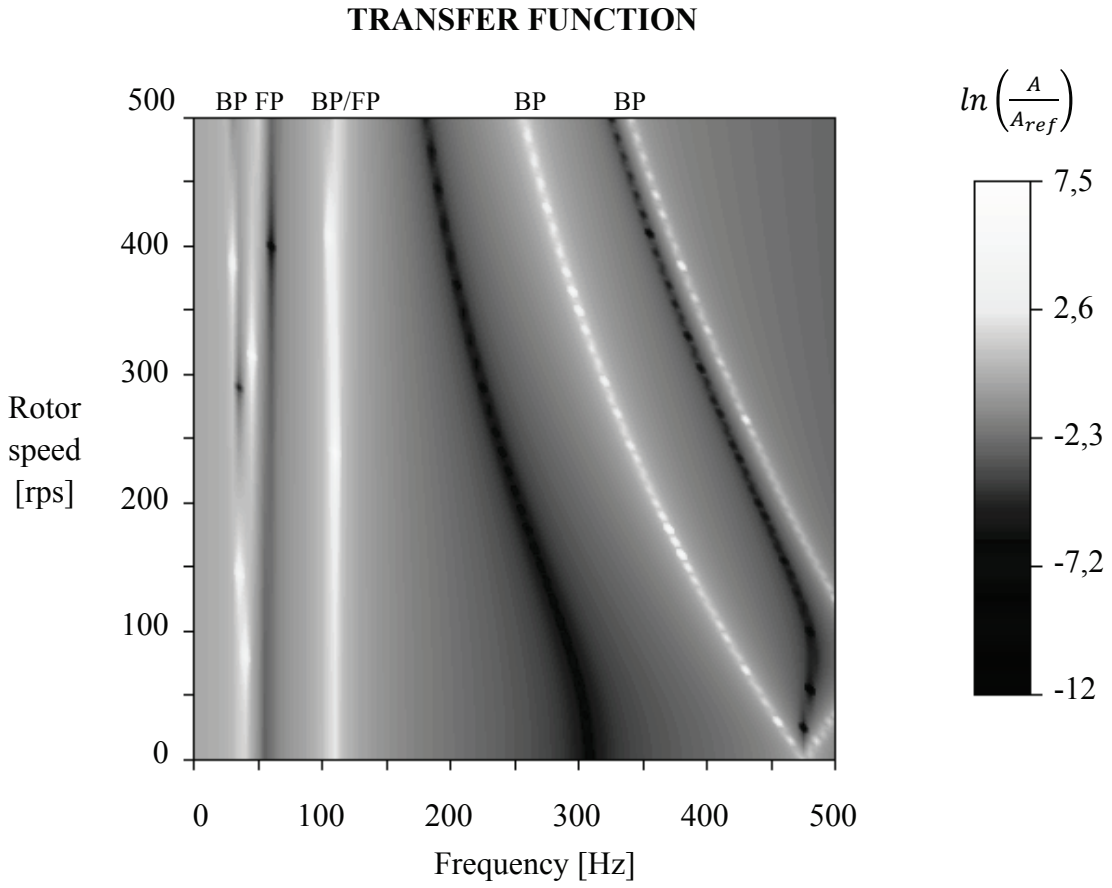

Fig.1: Response of system

Acknowledgement: This work was supported by national financial resources of Ministry of Education Youth and Sports of Czech Republic for specific university research.

References

[1] J. Slavík, V. Stejskal, V. Zeman, Základy dynamiky strojů. ČVUT, Praha 1997.

[2] M. Byrtus, M. Hajžman, V. Zeman, Dynamika rotujících soustav. ZČU, Plzeň 2010.

[3] Information on http://www.scilab.org/ (cited in March 2015)

21st International Conference **ENGINEERING MECHANICS 2015**
Svratka, Czech Republic, May 11 –14, 2015
Paper **#033, pp. 312–313**

Influence of Textile Membrane on Stability of Supporting Steel Arch

Ondrej Svoboda[a]*, Josef Machacek[b]

Czech Technical University in Prague, Faculty of Civil Engineering
Thakurova 7, 166 29 Prague, Czech Republic

[a]ondrej.svoboda.4@fsv.cvut.cz, [b]machacek@fsv.cvut.cz

Keywords: arch stability, experimental testing, membrane structure, nonlinear analysis, parametrical study, supporting structure, textile membrane

Abstract: In the last few decades, the membrane textile surface structures became popular not only because of their visual attractiveness, but also as a light fully-load carrying systems. In comparison with use of a traditional roof decking these structures are much more economical and attractive. However, the complex analysis and computational design methods are demanding and still not codified. The real physical model of a membrane structure supported by two inner steel arches and covering a concert stage was constructed and tested in laboratory of CTU in Prague. The membrane used was the Précontraint 702S Ferrari [1] prestressed textile membrane with PVC coating. The arches were hot-formed in a workshop from Grade S355J0 steel. The full paper presents experimental results for: i) isolated inner arch, ii) complex structure of the membrane with supporting arches, both under symmetrical and asymmetrical loading. Furthermore the numerical nonlinear FEM model created in SOFiSTiK software package and its validation for the above structural configurations and loading is presented. Subsequent parametrical studies cover various levels of the membrane prestressing to show its significance for nonlinear behaviour and stability of the inner arch. Finally some recommendations concerning numerical modelling are presented.

Introduction

A rapid improvements and novelties of materials used in lightweight structures such as textile membranes, plastic foils, high strength steels, cables and rods, led in last decades to their huge expansion. Membrane structures with subtle supporting steelwork require demanding nonlinear analyses. Simplified separate modeling of membranes and supporting structures is usually unacceptable and can lead to incorrect results or even a collapse of the entire system. In general, the complex analysis of membrane surface and supporting structure is necessary [2,3]. Herein the complex analysis concentrates on stabilization effect of a membrane to the supporting steel arch.

Tests and numerical investigation

A model of real concert stage was constructed and investigated in laboratory of the FCE CTU in Prague. The main size *L*x*B*x*H* of the model is roughly 4500x2250x1200 [mm], inner and outer tubes of steel grade S355J0 Ø 26.9x3.2 [mm] and Ø 88.9x3.2 [mm], respectively. Loading points were defined along the arch and both symmetrical and asymmetrical loading was applied to two configurations: i) isolated arch alone; ii) complex membrane-arch assembly. Careful monitoring of deflections and strains at the required positions were performed during the given loading steps.

The SOFiSTiK software using geometrically and materially nonlinear analysis with imperfections (GMNIA) was used to model complex (entire) membrane-arch system. The deformed geometry obtained from measurement in laboratory and precise values of loading increments were introduced into analysis. Due to non-uniform membrane pretension in the tests and difficult measurements of the resulting membrane stress on the textile surface, various values of the membrane uniform prestress were analyzed.

Comparison of experimental results and results obtained from numerical analysis

First the isolated arch build-in in the supports (otherwise free) was analyzed. Numerical and test deflections at various points confirm excellent agreement (e.g. the in-plane vertical one in Fig. 1).

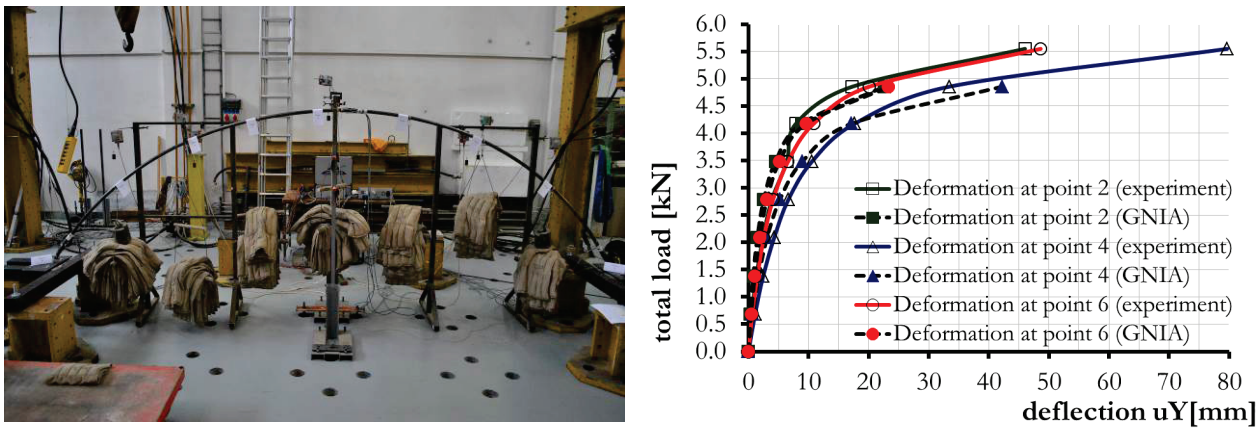

Fig. 1: Isolated arch under symmetrical loading (left); Comparison of experimental and numerical (SOFiSTiK) vertical deflections (uY) under symmetrical loading (right)

In the membrane-arch assembly the level of the membrane prestressing proved to be the most important parameter and rather low numerical prestressing gives corresponding results, Fig. 2.

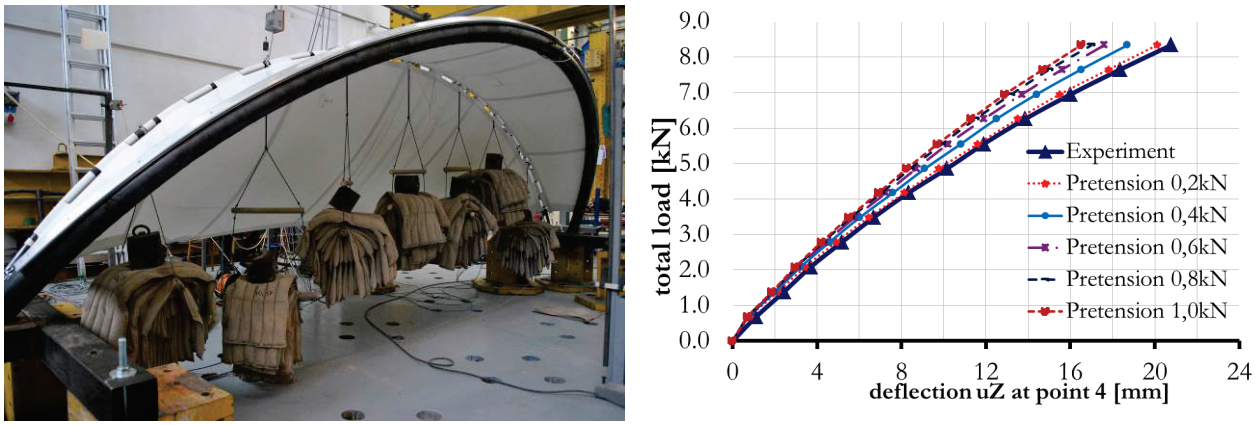

Fig. 2: Symmetrical loading of complex structure (left); Comparison of experimental horizontal deflections and numerical (SOFiSTiK) ones with various prestressing (right)

Conclusion

The stabilization effect of a membrane on supporting steelwork is enormous and membrane as a load bearing and stabilizing element must be included into the analysis to ensure safe and correct design. Real reasonable value of uniform directionless prestress was assessed as 0.4 kN/m'.

Acknowledgement: The support of the GACR grant No. 103/13/25781S is gratefully acknowledged.

References

[1] Serge Ferrari, http://www.sergeferrari.com/

[2] Technet GmbH Berlin-Stuttgart, http://www.technet-gmbh.com.

[3] J. Uhlemann, N. Stranghöner, K. Saxe, Stiffness parameters for architectural fabrics: An analysis of two determination procedures. Structural Engineering International. 25 (2015) 9-19.

21st International Conference **ENGINEERING MECHANICS 2015**
Svratka, Czech Republic, May 11 –14, 2015
Paper **#005, pp. 314–315**

Study of Scale Effect in a Starved Elastohydrodynamically Lubricated Contact

Petr Svoboda[a]*, David Kostal[b], Ivan Křupka[c]

Brno University of Technology, Faculty of Mechanical Engineering, Institute of Machine and Industrial Design, Technicka 2896/2, 616 69 Brno, Czech Republic

[a]svoboda.pe@fme.vutbr.cz, [b]kostal@fme.vutbr.cz, [c]krupka@fme.vutb.cz

Keywords: EHD lubrication, grease, starvation, scale effect

Abstract: One of the most important parameters determining the performance and life of machine parts is a lubrication film thickness and its distribution. Current experimental and numerical studies are mostly connected with oil lubrication. However greases are used in more than 80 % of all rolling bearings where the starvation phenomenon occurs most frequently. The question is whether the results obtained from the laboratory scaled contact test device are transferable to real operating conditions of full scale bearings. The aim of this work is to compare these two approaches to measuring film thickness of different greases. The use of multiple contacts optical test rig based on thin film colorimetric interferometry for film thickness measurement has enables to obtain film thickness of starved contact and the film distribution. The experimental observation of full-scale model of bearing will help to understand better the behavior of real bearing.

Introduction

In the rolling bearing there is always a slight slippage between the rolling elements and bearing ring. The rolling element is separated by a lubricant in the bearing ring, which greatly reduces the pressure, friction, wear and bearing life. Lots of articles dealing with the study of greases and influence of operation conditions on film thickness were already published. In subsequent studies it was found that the replenishment significantly affects not only the operating, but also bearing design, such as presence of a cage or spin of the balls bearings.

Cann further experimented with the relationship between the film thicknesses [1], the properties of the lubricant and variable parameters: oil volume, speed, load and viscosity. The thickness of the lubricant film in contact with non-conformal friction surfaces can be affected by a number of operational factors. It is essential to know how bearing works under the starved regime. The fully flooded regime is characterized by a film thickness, which increases with increasing speed, in accordance with the Hamrock–Dowson rules [2]. Interesting results in [1] were obtained when examining the effect of the ball spin. The spin motion helps to transfer the lubricant to the track after contact.

The effect of cage design on replenishment was also studied. With grease lubrication, the presence of a cage can have a significant effect upon film thickness. The onset of starvation is delayed until far higher speeds with the closely conforming cage. The cage appeared to work by redistributing the grease in the cage/ball contact [3]. In most of articles measurements was made on single contact ball-on-disc bearing simulator. One exception is a study [4] where a relationship between full-scale bearing test and laboratory simulation is described on the case of friction. These experiments have shown that friction is reduced for semi-starved contacts but increases dramatically for starved conditions.

Experimental measurement

Ball-on-disc device with single bearing contact (Fig. 1a) was used to establish the behavior of the film thickness with a range of speed conditions. For full-scale measurement two series of test were conducted. In the first series axial bearing with a full number of 16 balls (Fig. 1b) was used. In another series of tests dimensionally identical axial bearing with 8 balls were used.

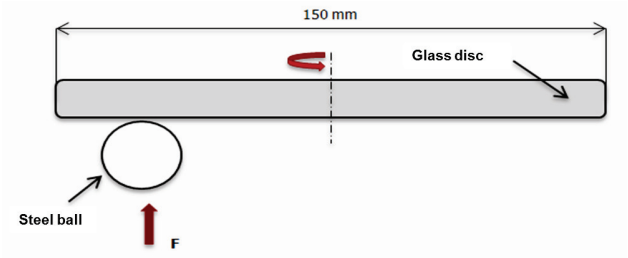

Fig. 1a: Single contact (ball-on-disc) device

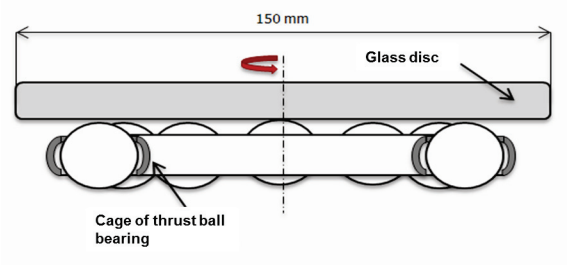

Fig. 1b: Full scale test device

If the gap between the cage and the ball is too small, the lubricant is wipe out by the cages and contact is starving. It is also necessary to consider the material selection of bearing cage. A metal cage is a potential source of wear particles that can act as a catalyst for oxidation and degradation of the grease. The early aging of lubricant may result in a reduction in the ability self-regeneration of lubricant in elastohydrodynamic contact and it can leads to surface contact and consequently to bearings damage.

Acknowledgments: Outputs of this project LO1202 were created with financial support from the MEYS under the National Sustainability Programme I, in cooperation with Czech Science Foundation under project no.: 13-30879P and CZ.1.07/2.3.00/30.0005 – "Support for the creation of excellent interdisciplinary research teams at Brno University of Technology".

References

[1] P.M.E. Cann, A A Lubrecht, Bearing performance limits with grease lubrication: the interaction of bearing design, operating conditions and grease properties. Journal of Physics D: Applied Physics. 2007-09-21, 40 (2007) 5446-5451.

[2] B.J. Hamrock, D. Dowson, Isothermal Elastohydrodynamic Lubrication of Point Contacts: Part III—Fully Flooded Results. Journal of Lubrication Technology. 99 (1977) 264-275.

[3] B. Damiens, A. A. Lubrecht, P. M. Cann, Influence of cage clearance on bearing lubrication. Tribology Transactions. 47 (2004) 2-6.

[4] H. Baly, G. Poll, P. M. Cann, A. A. Lubrecht, Correlation between Model Test Devices and Full Bearing Tests under Grease Lubricated Conditions: the interaction of bearing design, operating conditions and grease properties. IUTAM Symposium on Elastohydrodynamics and Micro-elastohydrodynamics. Springer Netherlands, 40 (2006) 229.

21st International Conference **ENGINEERING MECHANICS 2015**
Svratka, Czech Republic, May 11 –14, 2015
Paper **#182, pp. 316–317**

Crash Test of Carbon Composite

Martina Syrovátková[b], Michal Petrů[b]*, Martina Novotná[c]

Institute for Nanomaterials, Advanced Technologies and Innovation,
Technical University of Liberec, Studentská 2, Liberec, Czech Republic

[a]martina.syrovatkova@tul.cz, [b]michal.petru@tul.cz, [c]martina.ernest.novotna@tul.cz

Keywords: composite, carbon fiber, mechanical properties, crash test

Abstract: Composite structures are now increasingly used for their properties in all areas of industrial production where high specific strength is demanded. They gradually replace metal parts and components not only because they are lighter, but above all for their comparable and in many ways even better mechanical properties. Knowledge of behavior of simple synergies between the fibres and the matrix allows the prediction of behavior of complex components and their application in practice [1,2]. The subject of this article is a description of an experiment and numerical model that compares the mechanical properties of carbon fiber composite with the values obtained using analytical models as is Chamis model and Halpin-Tsai model. Carbon composite samples were studied in laboratory conditions through Barrier test (ie. Crash test).

Materials and methods

Measurement and FEM modeling

Samples of the carbon prepreg are double-layered, the layers relative to one another oriented at an angle of 90°. After our previous experiences with similar tests (for examples: tension test, ball-drop test, Charpy test) was the crash test selected as a test of endurance of a composite barrier against penetration. Impactor, which is part of the hydraulic cylinder, encounters at a certain speed a sample of carbon composite and passes through it. The whole process records the speed-camera, other experimental data are registered at the same time. The complete setup is shown in Fig. 1.

Results and Summary

Measured values of the mechanical properties of the tested samples were compared. The force distribution measured during the experiment for given high speed hydraulic cylinder is plotted in (Fig. 2). The distribution of deformation is influenced by composition and angle of fiber layer orientation in the composite. Comparison of FEM simulation models and measurement results are shown (Fig. 3).

Conclusions and acknowledgements

The results of this project LO1201 were obtained through the financial support of the Ministry of Education, Youth and Sports in the framework of the targeted support of the "National Programme for Sustainability I" and the OPR&DI project Centre for Nanomaterials, Advanced Technologies and Innovation CZ.1.05/2.1.00/01.0005.

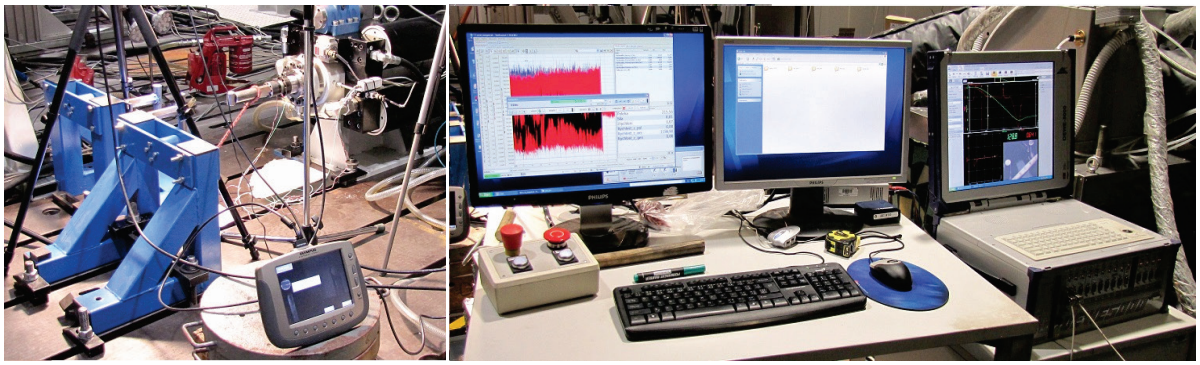

Fig. 1: Experimental device and measurement

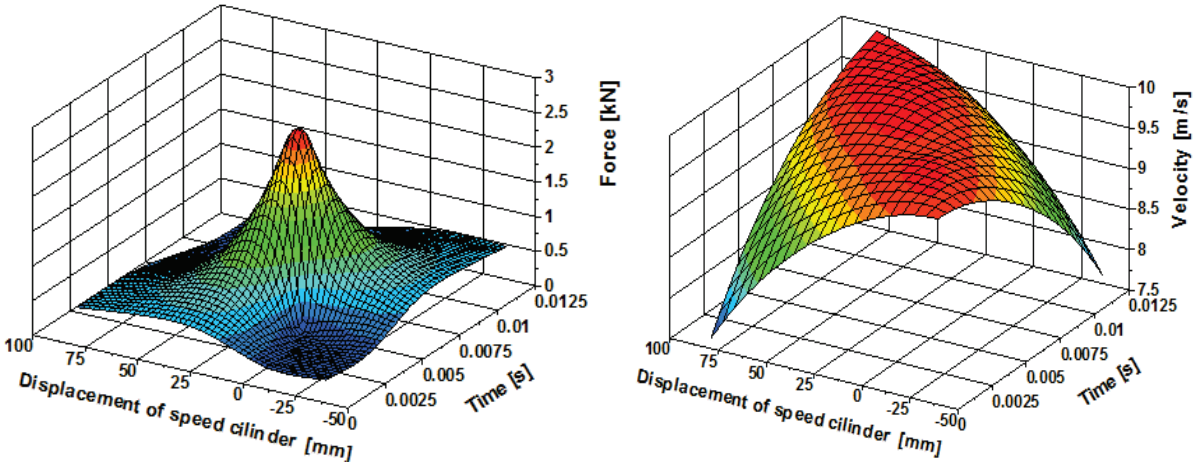

Fig. 2: a) 3D dependency graph of displacement speed cylinder/force/time, b) 3D dependency graph of displacement of speed cylinder/velocity/time

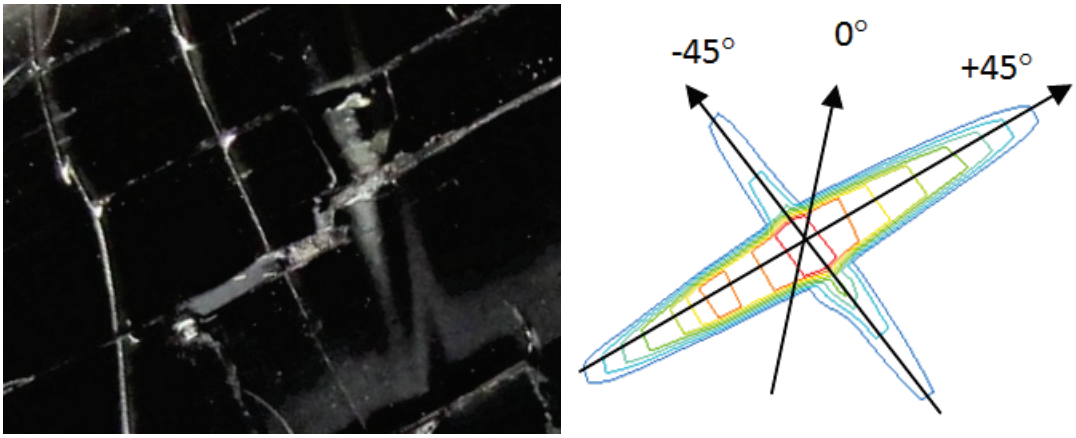

Fig. 3: Strain of the real sample (left), Distribution of stress in FEM model (right).

References

[1] M. Petru, M. Syrovatkova, T. Martinec, P. Lepsik, Analysis of changes in the surface quality of a UD prepregs composite due to mechanical loading, Mat.Sci.Forum, 2015, In Print

[2] M. Petru, J. Broncek, P. Lepsik, O. Novak, Experimental and numerical analysis of crack propagation in light composite materials under dynamic fracturing, Komunikacie, 16 (3A) 82-89.

21st International Conference **ENGINEERING MECHANICS 2015**
Svratka, Czech Republic, May 11 –14, 2015
Paper **#111, pp. 318–319**

Influence of Vertebral Compression Fractures on the Deformation in Thoracolumbar Spine

Klaudia Szkoda[a] *, Celina Pezowicz[b]

[1]Department of Biomedical Engineering, Mechatronics and Theory of Mechanisms, Wroclaw University of Technology, ul. Łukasiewicza 7/9, 50-371 Wrocław, Poland

[a]klaudia.szkoda@pwr.wroc.pl, [b]celina.pezowicz@pwr.wroc.pl

Keywords: thoracolumbar spine, mechanical properties, finite element modeling.

Abstract: The aim of this study is to create a numerical model of the thoracolumbar spine. The model was built on the basis of diagnostic computed tomography. The simulations were performed on a physiological model, with a vertebral compression fracture and model with transpedicular fixation system. The knowledge about the mechanical properties obtained from numerical simulations would allow explain influence of vertebral compression fracture on the deformation thoracolumbar spine and the biomechanical aspects in the treatment of spine injury.

Introduction

Spine, as the main organ of movement, is subjected to variable loads and overloads often lead to injuries and mechanical damage. Treatment of the damaged spine segment is a very complicated process, consisting mainly from a complex construction and the occurrence of multiple connections of joints and ligaments. It is usually based on the use of technical aids to improve the stability in the form of implants. Thoracic and lumbar spine differ from each other both in movements as well as in structure. This affects the complicated structure of the transition between them, thereby increasing the instability of the connection [1,2].

Material and methods

The numerical model of the thoracolumbar spine was built on the basis of diagnostic CT. The motion segment (Th11-Th12-L1) was developed in several stages using programs such as: Mimics, MeshLab, AutoMesher and Ansys. The physiological model was constructed with solid elements (more than 2 million tetrahedral 10-nodes elements), divided into several structures with different tissues; the isotropic material properties are shown in the Fig.1. Numerical simulations were performed for three cases: physiological condition , condition with a vertebral compression fracture and model with transpedicular fixation system. The vertebral compression fracture in the motion segment was simulated as a fissure of thickness 2mm comprising two-thirds of the volume L1 vertebra. The analysis was carried out under the influence of axial compression force equal to 600N for each case.

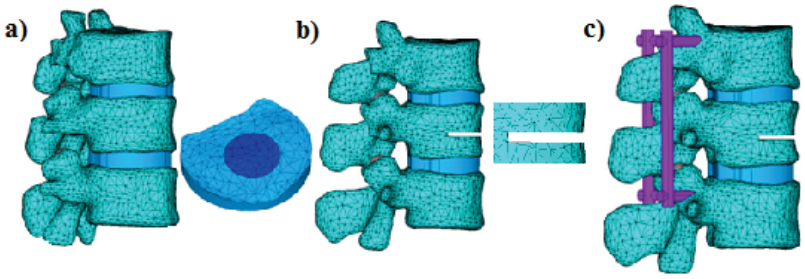

Component name	E [MPa]	υ [-]
Cortical bone	12 000	0,3
Cancellous bone	100	0,2
Annulus fibrosus	8,4	0,4
Nucleus pulposus	1	0,499
Articular cartilage	33	0,3
Titanium alloy Ti-6Al-4V (stabilization)	110 000	0,36

Fig. 1: The numerical model of the spine segment: a) physiological, b) with a vertebral compression fracture, c) with transpedicular fixation system and their material properties [3,4]

Results

Analysis was performed to show the impact of stabilization on the state of displacement of the damaged segment of the thoracolumbar spine. The computed displacements for all three cases considered models are shown in the chart (Fig.2). It can be concluded that the transpedicular fixation system increases stiffness of the spine motion segment and prevents the excessive deformation caused by the compressive load. Considering the distribution of computed displacements (right hand side of Fig. 2) the differences between the physiological model and the model with transpedicular fixation system is easily distinguishable. Additionally, it can be seen that the fracture in front of the vertebral body (L1) contributes to the compression mechanism connected with the bending.

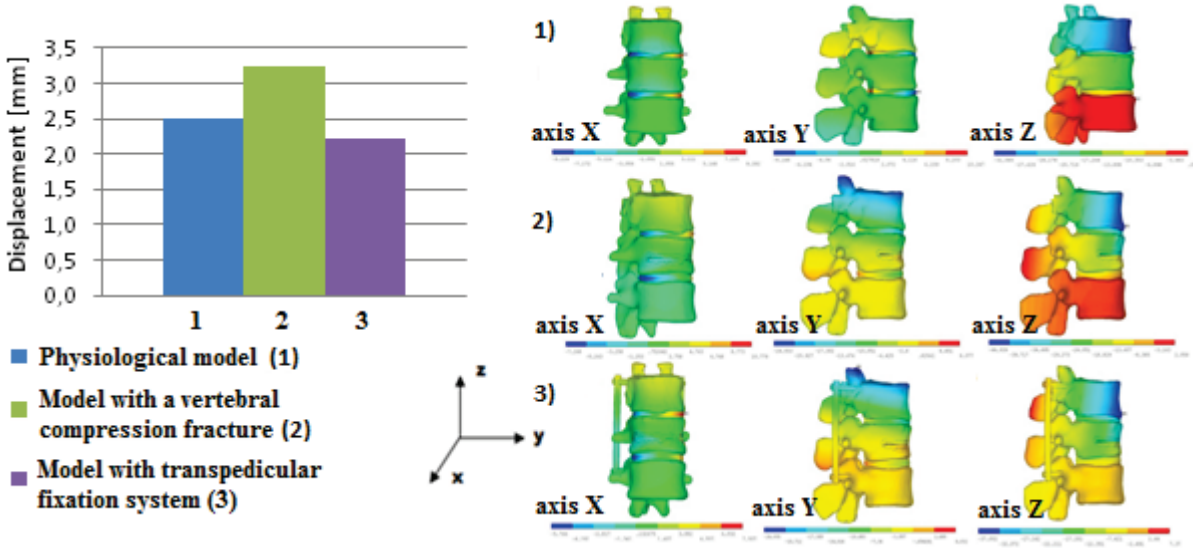

Fig. 2: Complete displacement case considered models under the influence of the loading force equal to 600N

Summary

The analysis showed that the transpedicular stabilization of vertebral fracture in the thoracolumbar segment does not provide enough stability in case of compressive load, causing bending of the motion segment. This could justify the fact that the two-segment spine stabilization is not able to completely prevent displacement of the region damaged vertebra. Therefore, in clinical practice thoracolumbar spine fractures are often stabilized in four segments constructs [4]. It should be also noted that the transpedicular stabilization of thoracolumbar segment with the vertebral fracture gives the opportunity to improve the stability and stiffness of the case.

References

[1] C. Pezowicz, Biomechanika krążka międzykręgowego - ocena przeciążeń oraz skutków wprowadzenia implantów. Oficyna Wydawnicza Politechniki Wrocławskiej, Wrocław, 2008.

[2] R. Będziński, A. Wall, Wybrane zagadnienia biomechaniki kręgosłupa w aspekcie stabilizacji, Uniwersalny system korekcyjno-stabilizujący DERO do operacyjnego leczenia kręgosłupa, LfC, Zielona Góra, 1995.

[3] T.H. Smit, A. Odgaard, E. Schneider, Structure and function of vertebral trabecular bone, Spine, 22 (1997) 2823-2833.

[4] T.X. Qiu, K.W. Tan, V.S. Lee, E.C. Teo. Investigation of thoracolumbar T12–L1 burst fracture mechanism using finite element method. Medical engineering & physics, 28 (2006) 656-664.

21st International Conference **ENGINEERING MECHANICS 2015**
Svratka, Czech Republic, May 11 –14, 2015
Paper **#169, pp. 320–321**

The Influence of Facet Joint Load Transmission in the Spine Column on the Mechanical Properties of the Intervertebral Disc in Finite Element Modeling

Klaudia Szkoda[a] *, Celina Pezowicz[b], Małgorzata Żak[c]

Department of Biomedical Engineering, Mechatronics and Theory of Mechanisms,
Wroclaw University of Technology, ul. Łukasiewicza 7/9, 50-371 Wrocław, Poland

[a]klaudia.szkoda@pwr.wroc.pl, [b]celina.pezowicz@pwr.wroc.pl, [c]malgorzata.a.zak@pwr.wroc.pl

Keywords: intervertebral disc, mechanical properties, finite element modeling

Abstract: This study is aimed to determine the impact support of the spine motion segments on mechanical properties of the intervertebral disc (IVD). In the simulations, the combinations of flexion-extension movements in spine motion segments were modeled. The analysis of the mechanics of the intervertebral disc clearly indicates a wide differentiation between anterior/posterior anatomical locations in the annulus fibrosus.

Introduction

The intervertebral disc is a highly-specialized element of the spine then provides flexibility and adsorbing capacities. Additionally, the disc separates adjacent vertebra and acts as a shock absorber, dissipating energy between them under loading. When mechanical loads are transmitted along the spine, the IVD mainly supports compression and flexion stresses. This results in excessive hydrostatic pressure in the nucleus pulposus and generates circumferential tensile stresses in the surrounding annulus fibrosus [1,2]. The aims of the present study are to develop a finite element model of a thoracic motion segment which allows the simulation of different movements in segment and their influence on the layer structure of the annulus fibrosus of IVD.

Material and methods

Simplified numerical model of the thoracic spine segment was built on the basis of diagnostic CT. The motion segment (Th11-Th12) is divided into several structures with different tissues material properties, which are shown in Table 1. Model contained 6 layers of fibers inclined alternatively at an angle of 30º to the horizontal plane embedded in a homogeneous ground substance. Annulus fibers and 3 different ligaments were modeled as non-linear links elements. Two cases of spine motion segment are examined: intact segments and acutely injured segments with anterior column only. Both cases are modeled using tetrahedral 10-node elements for the endplates and rigid elements to simulate the bone behavior. These segments models were used to predict load transmission in axial compression (using force 650 N), flexion and extension (gradient force 650 N causing bending moment) on the behavior of the IVD.

Table 1: Material properties of the motion segment components [3,4]

Link component name	E [MPa]	υ [-]	Θ [mm^2]	Solid component name	E [MPa]	υ [-]
Annulus fiber 6 layer	550÷360	0,45	0,2	Cortical bone	12 000	0,3
Anterior longitudial ligaments	20	0,3	64	Cancellous bone	100	0,2
				Endplata	25	0,1
Posterior longitudial ligaments	50	0,3	20	Nucleus pulposus	1	0,49
				Annulus ground substance	4.2	0,45
Interspinous ligaments	12	0,3	40	Articular cartilage	33	0,3

Results

The changes of the height in individual layers of the structure of the annulus fibrosus in anterior and posterior location of the IVD of both models are shown in Fig. 1. The loads acting on the annulus fibers layer change the IVD height and thus are causing the bulge in accordance with the generally known mechanism. This is caused by the fact that the collagen fibers of the annulus fibrosus under the influence of the load decrease the angle of inclination relative to the surface of vertebral bodies.

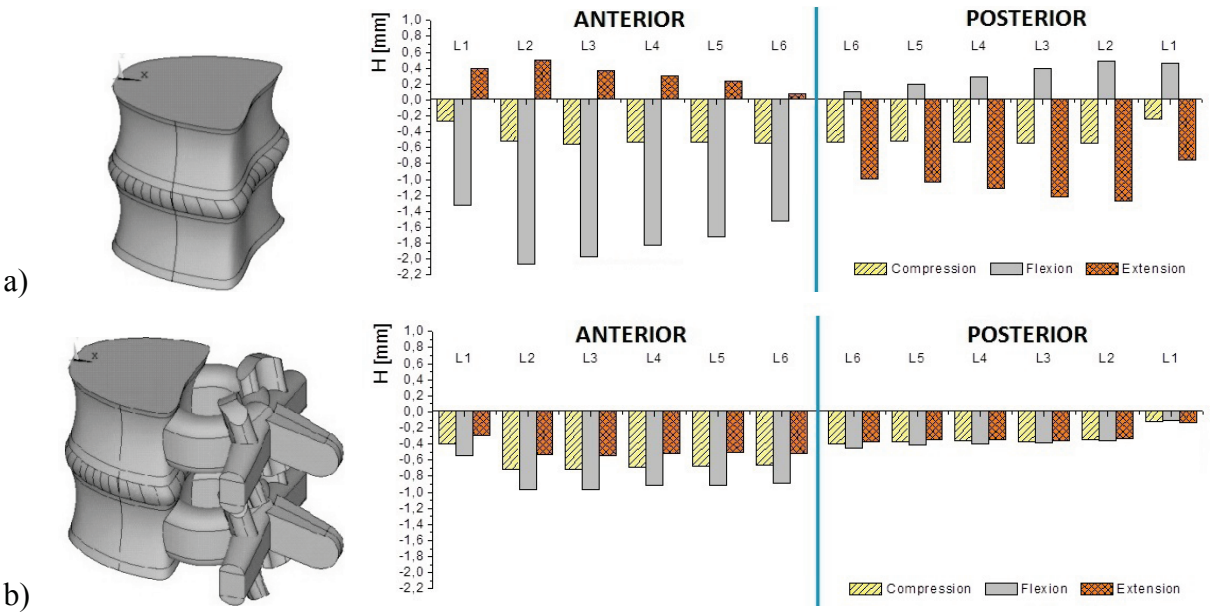

Fig. 1: The value of the height difference (H) layers in anterior and posterior location of the IVD for the three load incidents in the model: a) intact segments; b) acutely injured segments

Analyzing these results for both models it can be noted that posterior column undertakes a significant role in the transfer of loads through the spine. The posterior column constitutes an additional support for the spinal column, especially during flexion and extension. This effect significantly levels tension of the annulus fibrosus in the anterior or posterior region, depending on the acting load.

Summary

The facet joints included in the three-point support of the spin motion segment allow to compensate a large loads acting on the IVD as indicated by the results of the above research.

References

[1] A. Shirazi-Adl., Strain in fibers of a lumbar disc. Analysis of the role of lifting in producing disc prolapse. Spine, 14 (1989) 96–103.

[2] C.A. Pezowicz, P.A. Robertson, N.D. Broom, Intralamellar relationships within the collagenous architecture of the annulus fibrosus imaged in its fully hydrated state. Journal of Anatomy, 207 (2005) 299–312.

[3] T.H. Smit, A. Odgaard, E. Schneider, Structure and function of vertebral trabecular bone, Spine, 22 (1997) 2823-2833.

[4] T. Pitzen, F.H. Geisler, D. Matthis, H. Müller-Storz, K. Pederson, W.- I. Steudel, The influence of cancellous bone density on load sharing in human lumbar spine: a comparison between an intact and a surgically altered motion segment, European Spine Journal, 10 (2001) 23-29.

21st International Conference **ENGINEERING MECHANICS 2015**
Svratka, Czech Republic, May 11 –14, 2015
Paper **#062, pp. 322–323**

Aeroelastic Response of Slender Full Sky Telescope

Alexander Tesar

Institute of Construction and Architecture, Slovak Academy of Sciences,
Dubravska cesta 9, 845 03 Bratislava 45, Slovak Republic

usarate@savba.sk

Keywords: aeroelastic stability, wind tunnel measurement

Abstract: The paper deals with advanced approach for aeroelastic assessment of slender full sky telescope (see Fig. 1) for astronomical observation of the star-sky [1]. The telescope will be positioned outside in high geographical locations with dominant action of the wind. Functional requirements in such locations have resulted in a daring structural design of the telescope. The reliability of such device cannot be estimated unless ultimate aeroelastic response is considered. Telescope is equipped with two side sheets which can be opened in order to allow the full view function. The telescope is subjected to tuned vibration control in order to face extreme wind velocities in territories of its application for the case with open side sheets. The main question to be answered was the value of maximal wind velocity allowable for the case with slightly or full open size sheets. The measurements were made on actual telescope in the wind canal. The wind velocity varied in scope from 0 until 52 m/sec. Measured were the influences of laminar air flow, with consideration of turbulences in the boundary layer in proximity of the experimental set-up (see Fig. 2).

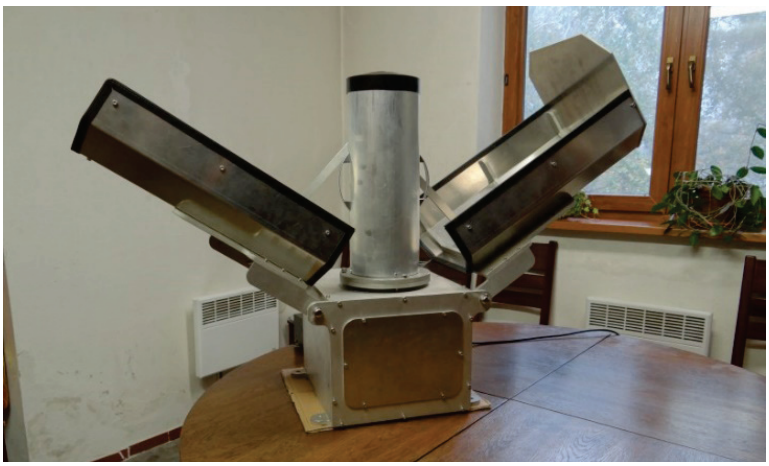

Fig. 1: Telescope in open configuration

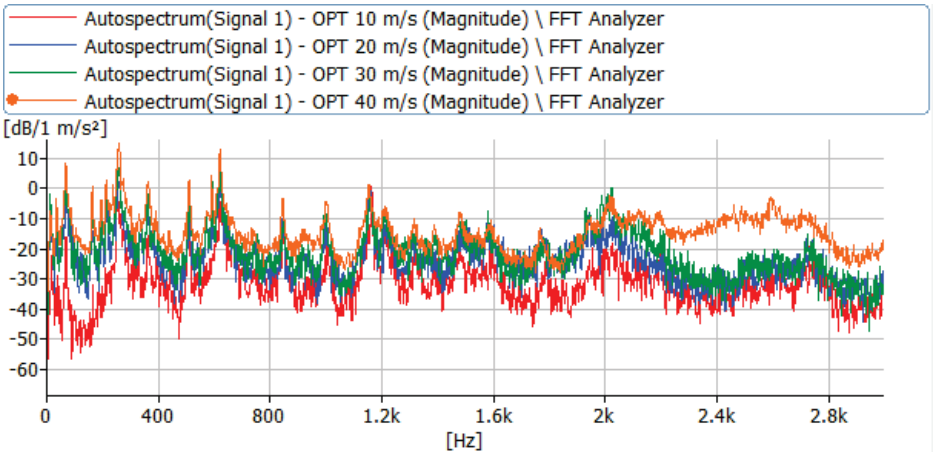

Fig. 2: Some measured RMS spectra

The measurements were made on actual telescope in the wind canal of Institute of Construction and Architecture, Slovak Academy of Sciences, Bratislava, Slovak Republic. Used was the wind canal modul with cross-section 1200 x 1200 mm and length 6000 mm. The wind velocity varied in

scope from 0 until 52 m/sec. Measured were the influences of laminar air flow, with consideration of turbulences in the boundary layer in proximity of the experimental set-up. Measurements were made by the system Bruel-Kjaer, incorporated into research facilities of the wind tunnel. The experimental set-up was positioned on circular platform rotating the telescope in various directions to the wind flow.

The accelerations, velocities and deformations were registered in three points – point 1 located midspan in the face of left side sheet, point 2 located midspan in the face of right side sheet and point 3 located midspan on the top of the experimental set-up studied. The measurements were made for seven structural configurations specified below. Measured were the root mean squares (RMS spectra of vibrations) as statistical measures of accelerations studied. The accelerations were calculated and measured for series of discrete values of continuously varying functions. They were specified as square roots of the mean of squares of the values of laminar and turbulent waveforms appearing in the boundary layer.

Structural configuration:

CL – closed camera – basic position
CLR – closed camera – rotation by 45 degrees
CLQ – closed camera – rotation by 90 degrees
CLS – closed camera – rotation by 180 degrees
OP – slightly open camera – basic position
OPT – totally open camera – basic position
OPTR – totally open camera – rotation by 45 degrees

The evaluation of the results has specified the following final conclusions:

1. Closed configuration of the all sky camera studied is aerodynamically stable and reliable in whole scope of wind velocities studied (from 0 until 0 until 52 m/sec).
2. The configuration with open side fins of the camera is aerodynamically stable in scope of wind velocities from 0 until 32 m/sec.
3. The reliability of the camera at wind velocities above 32 m/sec is not available and camera must be put into closed configuration.
4. Critical wind velocity for the camera with open side fins is 32 m/sec.

The results obtained were put into the databasis adopted for tuned vibration control of the telescope.

Conclusions

Theory and numerical as well as experimental verification results sampled up in present paper submit some image on aeroelastic response of of outside located astronomy telescopes. The wave analysis adopting the FETM-approach and experiments in the wind canal were closely connected, verified and evaluated. The application was made on actual structure of the full sky telescope. The results obtained were used in the assessment of ultimate aeroelastic behaviour, aerodynamic stability as well as in tuned vibration control of the telescope studied.

References

[1] A. Tesar, J. Petrzala, Aeroelastic assessment of special telescope in aerodynamic canal. Research Report, Inst. of Construction and Architecture, Slovak Academy of Sciences, Bratislava, 2014

[2] A. Tesar, Aeroelasticity of Slender Structures. EDIS – Zilina Universiy Publisher, 2014

[3] E.C. Teleman, R/ Silion, E. Axinte, R. Pescaru, Turbulence scales simulations in atmospheric boundary layer wind tunnels. Bulletinul Institutului Polytehnic din Iasi, Publicat de Universitatea Tehnica “Gheorghe Asachi” din Iasi, Tomul LIV (LVIII), Fasc. 2, 2008, pp. 7-14

Acknowledgements: The author is indebted to the Slovak Grant Agencies VEGA and APVV for supporting the research reported.

21st International Conference **ENGINEERING MECHANICS 2015**
Svratka, Czech Republic, May 11 –14, 2015
Paper **#026, pp. 324–325**

Fluidic Relaxation Oscillators for Microbubble Generation

Václav Tesař
Institute of Thermomechanics Academy of Sciences of the Czech Republic v.v.i.
Prague, Czech Republic
tesar@it.cas.cz

Keywords: fluidics, oscillators, relaxation

Abstract: Paper discusses low-frequency oscillators based on the unusual relaxation principle. In the fluidic version, the oscillator is suitable for supplying CO_2 to cultivated unicellular algae.

Introduction

There is a demand for fluidic oscillators making possible generation of sub-millimetre microbubbles in water – while simple, non-oscillated aerator air flows tend to generate bubbles larger by a decimal order of magnitude. Even with the oscillator the microbubble generation task is by no means easy. Initial development was misguided, being led to operation at very high frequencies by the idea of fragmentation of the larger bubbles. Found only recently [1] was the proper approach, requiring low frequency and return of newly generated microbubble into aerator exit channel for the rest of the period to protect it from growth by conjunctions. Standard fluidic oscillator designs are not suitable for the task and it is desirable to investigate new approaches.

Relaxation oscillators

One of the promising approaches is offered by oscillators based on the idea of initially storing the energy-carrying fluid and discharging it when the storage reaches a level at which the active element meets its load-switching level. Though by far not a direct analogy, the basic idea of this relaxation principle has been already developed in 1921 in the electronic oscillator of Pearson and Anson [2] – Fig.1. In fact, there is a little known Patent by Zalmanzon [3] who developed a fluidic version of relaxation oscillator (Fig. 2) in 1960. His design would not work at the low frequencies.

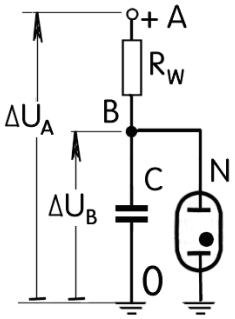

Fig. 1: (*Left*) The electronic relaxation oscillation phenomenon, discovered in 1921 by S. O. Pearson and H.S. Anson [2], is a periodic variation of the voltage ΔU_B across a capacitor C, the latter connected in parallel with neon bulb N. When charged through the working resistor R_w from the source of constant DC voltage ΔU_A, the voltage ΔU_B slowly increases until the breakdown value is reached at which the neon gas inside N ionises.

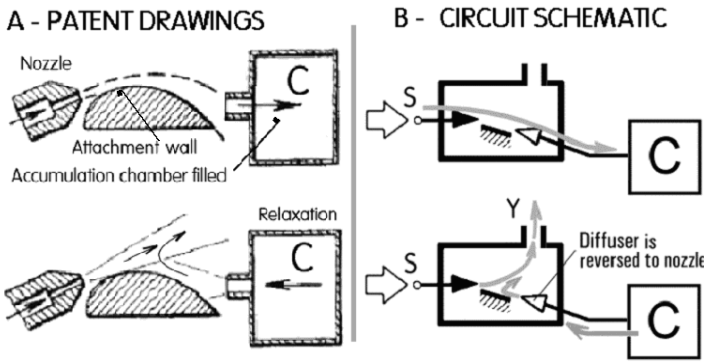

Fig. 2: (*Right*) Zalmanzon's 1960 fluidic relaxation-type oscillator [3]. The compressibility-type capacitance C is small (pressure grows rapidly with accumulated amount of air), making this oscillator suitable for high frequencies.

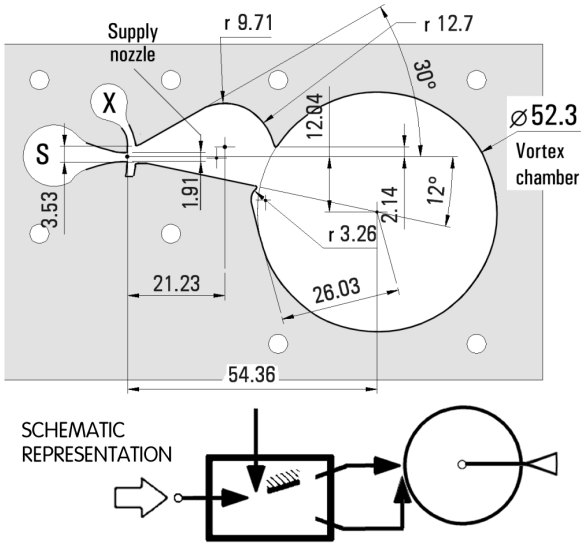

Fig. 3: (*Above*) Author's relaxation type fluidic oscillator. Essential novelty is the charged accumulating element replaced by the vortex-type restrictor, with the time delay effect caused by the spin-up (and spin-down) period in the vortex chamber. Presence of the control terminal X in this picture is misleading: it was simply open to atmosphere.

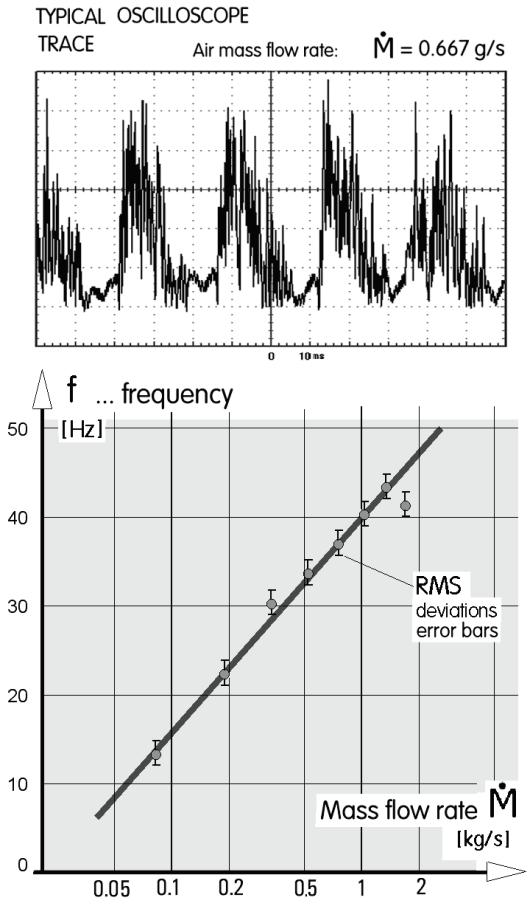

Fig. 4: (*Right*) Measured performance results.

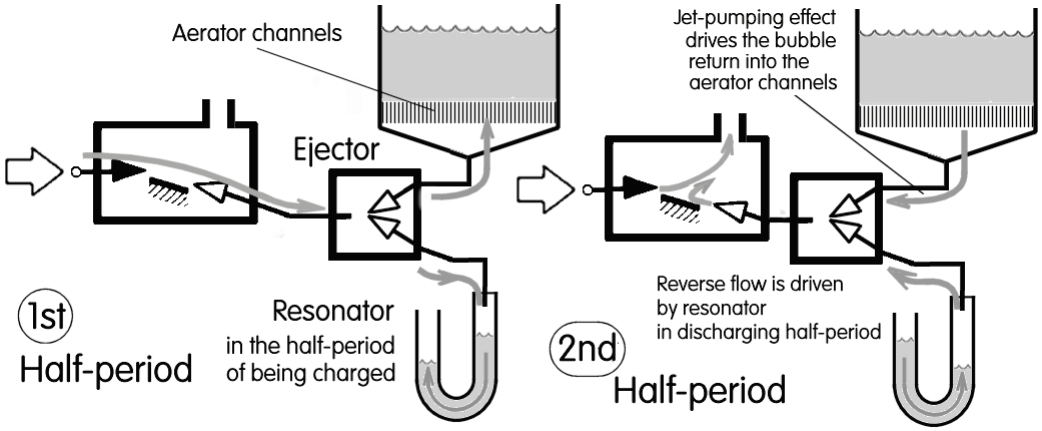

Fig. 5: Another author's relaxation oscillator with the jet pump ("Ejector") that generates the flow reversal using the energy temporarily stored in the resonator (here in the form of U-tube). The dominant low natural frequency of the resonator also suppresses the high-frequency noise.

Acknowledgements: Support by GAČR grants Nos. 23046S and 14-08888S as well as institutional support RVO: 61388998 are gratefully acknowledged.

References

[1] V. Tesař, Mechanisms of fluidic microbubble generation, Part II: Suppressing the conjunctions, Chemical Engineering Science 116 (2014) 849.

[2] S. O. Pearson, H. St. G. Anson, Demonstration of some electrical properties of neon-filled lamps, Proc. of the Physics Soc. of London, 34 (1921) 175.

[3] L. A. Zalmanzon, Method of automatically controlling pneumatic or hydraulic elements of instruments and other devices, US Patent 3,295,543 filed Feb 1960.

21st International Conference **ENGINEERING MECHANICS 2015**
Svratka, Czech Republic, May 11 –14, 2015
Paper **#206, pp. 326–327**

Fluidic Oscillators with Active Devices Operating in Anti-Parallel

Václav Tesař
Institute of Thermomechanics, Academy of Sciences of the Czech Republic v.v.i.
Prague, Czech Republic
tesar@it.cas.cz

Keywords: fluidics, oscillators, anti-parallel operation

Abstract: Paper discusses a low-frequency fluidic oscillator consisting of a pair, A and B, of monostable Coanda-effect diverter amplifiers, each with load restrictor of vortex type with variable entrance flow direction. The pair operates in anti-parallel: OPEN regime in A is concurrent with CLOSED regime in B.

Introduction

Development of devices for generation air microbubbles in water became recently of importance especially because of the potential role in production of renewable automobile liquid fuels [1] from unicellular organisms producing biomass by photosynthesis using CO_2 from the supplied air bubbles. An efficient approach eliminating the difficulties of the bubbles being too large was found in pulsating the air supply into the aerator by a fluidic oscillator. The initially small microbubbles nevertheless tended to increase their size by repeated conjunctions while they were still at the aerator exit. A solution was found in retracting each of the newly formed microbubble back into the aerator exit channel for the subsequent part of the cycle [2] – and these complicated bubble and liquid column motions required a lower than originally expected oscillation frequency.

The novel oscillator

Standard design of fluidic oscillators with a jet-deflection amplifier and feedback loop(s) exhibits in this case of low oscillation frequency a number of drawbacks and had to be replaced by a different oscillation generation principle. This paper discusses an oscillator based on the idea of two units — each with an active element and its load restrictor — having their control terminals interconnected so that e.g. the OPEN regime in one active element forces the other element to switch into also the OPEN state, but this generates a control effect reversing the regimes into the CLOSED one.

This is a fluidic version of the electronic *multivibrateur* invented by Abrahan & Bloch in 1919. The vacuum valves of their electronic device [3] is in the discussed new fluidic oscillator [4] replaced by the Coanda-effect jet-deflection diverter amplifiers, Figs. 1 to 3. Instead of charging an accumulation chamber (which would be the direct correspondent to the electric capacitor in [3], the necessary time delay (reversing the phases) is provided by the spin-up of the vortex in vortex-type superquadratic fluidic resistors. Another new and unusual feature of this design is the pre-chamber between the amplifiers and the resistors. In the stable regime, the jet issuing from the supply nozzle of the amplifier is guided into the vortex chamber radially (Fig. 3), passing through it with very low hydraulic resistance. When the jet is deflected by the control flow to other Coanda-attachment wall, its trajectory is bent and entering the chamber tangentially (Fig. 2). The bending increases the resistance and even more effective resistance increase is then provided by the centrifugal acceleration the fluid flow has to overcome so as to get to the exit opening located in the centre of the vortex.

The sequence of schematic representation of flows in Fig. 4 shows at the time instant 1 spinning up taking place in the vortex chamber A concurrent with slowing down in chamber B. At the time 2 the vortex in chamber A blocks the flow there while the chamber B is in the OPEN regime. In the next instant 3 the flow in chamber A is slowing down while in B the rotation rate increases. Finally, in A there is the low-loss radial flow and rotation in B.

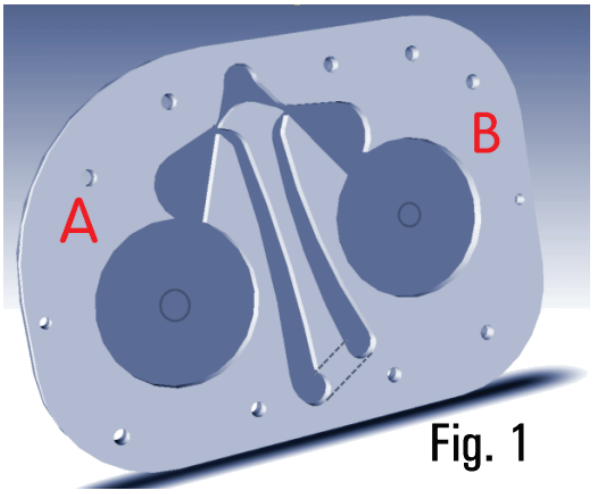

Fig. 1

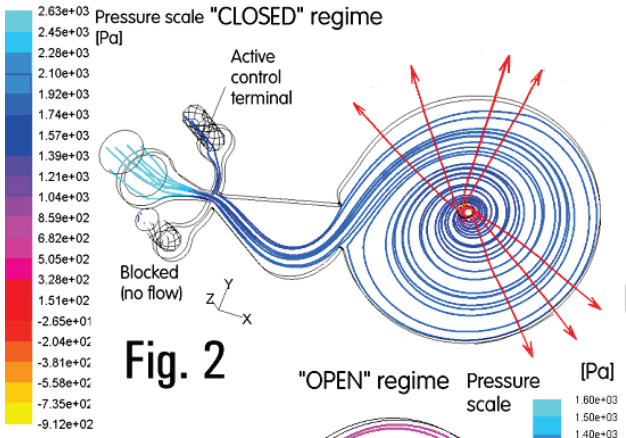

Fig. 2

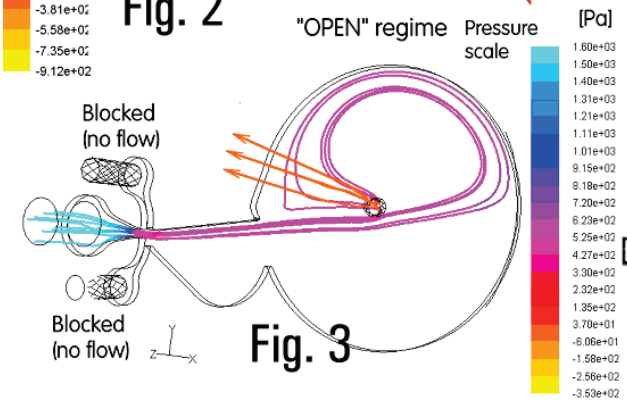

Fig. 3

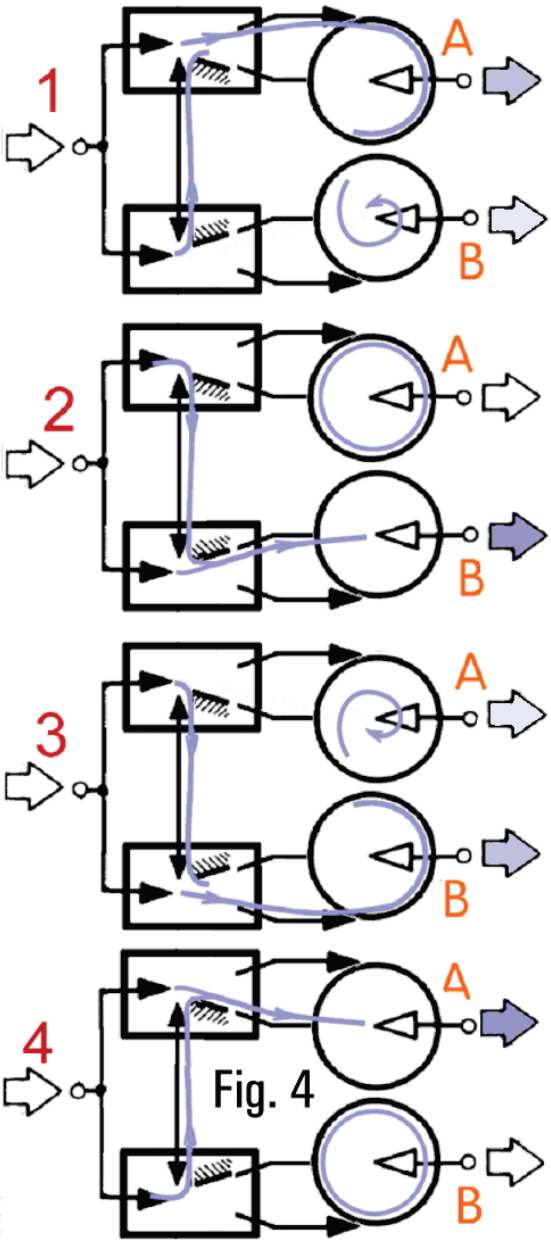

Fig. 4

Fig.1: *(Top left)* Vie of the cavities of two Coanda-switched diverters with vortex restrictors operating in anti-parallel. Fig. 2: *(Middle left)* Computed flow in CLOSED regime. Fig. 3: *(Bottom left)* Flowfield in the OPEN regime. Fig 4: *(Right-hand side):* Phases of the anti-parallel operation: OPEN regime in A concurrent with CLOSED regime in B.

Acknowledgements: Support by GAČR grants Nos. 23046S and14-08888S as well as institutional support RVO" 61388998 are gratefully acknowledged.

References

[1] Biofuel from algae, A. Padney, D.-J. Lee, Y. Chisti, C. R. Soccol. (Eds), Elsevier, 2014

[2] V. Tesař, Mechanisms of fluidic microbubble generation, Part II: Suppressing the conjunctions, Chemical Engineering Science 116 (2014) 849

[3] H. Abraham, E. Bloch E, Mesure en valeur absolue des périodes des oscillations électriques de haute fréquence, Annales de Physique 9 (1919). 237

[4] V. Tesař, Unit of a generator of gas bubbles in a liquid, Czech Rep. Patent No. 304314 and European Patent No.2735362

21st International Conference **ENGINEERING MECHANICS 2015**
Svratka, Czech Republic, May 11 –14, 2015
Paper **#255, pp. 328–329**

Repair Formulations for Fine-Grained Stone Arte-Facts

Renata Tišlová[a]*, Adéla Novotná

University of Pardubice, Faculty of restoration, Jiráskova 3, 570 01 Litomyšl, Czech Republic

[a]renata.tislova@upce.cz

Keywords: repair mortar, biodetritic limestone, mudstone, compatibility

Abstract: Stone restoration practice continuously deals with the problem of the selection of suitable repair materials. In establishing the requirements that guide their specification, the fundamental aim should always be to achieve the best compatibility between the substrate and the repair. When dealing with the restoration of stone, several aspects must be taken into consideration: not only the way in which compatibility influences the durability and structural and environmental resistance of the repair, but also the properties of the stone substrate itself must be considered. Compatibility is a highly complex problem but when considering the above-mentioned aspects, *functional* compatibility – the compliance between physical and mechanical characteristics of the materials – is the most critical in prolonging the sustainability of the repair.

In this work two examples of restoration projects dealing with the development of the repair compounds for two inland stones commonly used as materials for making carvings or sculptures and/or construction building material have been conducted. The first project deals with the restoration of Kutná Hora limestone on sculptures in front of the Jesuit College in Kutná Hora, Czech Republic; the second is aimed at the repointing of the defects and missing parts on the spongolite, the construction material of the main portico entrance pillars to the Liechtenstein crypt at St. Virgin Mary Church in Vranov near Brno. In both restoration projects inorganic "mortar" binders were used for repairs and filling defects, this being the most common repair materials in current stone restoration practice. The material selection of components and composition of the repair mortars were selected in accordance with determined stone mineralogical composition and properties. Kutná Hora limestone can be classified as organodetritic middle to coarse grained limestone whose homogeneity and properties depend on the site and stratigraphic level of the quarry; the original stones of the statues were rather homogenous with a high total porosity determined by mercury intrusion porosimetry of about 18 % (per volume) and bimodal pore size distribution composed of capillary pores varying from 0.1-5 mm and larger macropores. The compressive strength of such limestones may vary from 30-84 MPa. The spongolite stone (in Czech "opuka", and in literature also referred to as a "mudstone") of the pillars in Vranov, comes from local sources and represents Upper Cretaceous sediment of the Czech Cretaceous basin. The rock can be classified as sedimentary, siliceous and fine grained, often fossiliferous, containing traces of carbonate and clay. The deterioration also observed on pillars often takes the form of disintegration, delamination or fragmentation. The pillar stone can be described as highly porous with a total porosity of some 20.8 vol.% , the porous structure consists of capillary pores of 0.2-2 mm in diameter and macropores in a region over 0.3 mm. Although the stone is highly porous it possesses extremely high compressive strength with values varying from 59.0-94.0 MPa. The strength values of both stones used on-site was impossible to determine as only limited sampling was possible. However, the ultrasonic pulse velocity method was used instead which is rapid and easy to use directly on-site or on small samples. Complete characterization of the stone composition and its characteristics help to develop a basis for the repair mortar compounds which were first developed in the laboratory and, after assessment, the best was applied on-site for compatibility assessment in natural atmospheric conditions. Eight mortar mixtures were prepared in the laboratory for the limestone repairs, with aerial lime or hydraulic binders as a binder. The mortar

mixtures were of a home-made formulation as well as premixed commercial binders also used by restorers containing a quite similar spectrum of binders. The binders were mixtures of areal lime, NHL2 and 3.5. For comparison, a mixture with white Portland cement was also prepared. The aggregate and b/a ratio was similar for all mixtures; crushed Kutná Hora stone was used as an aggregate with particle size D‹2 mm, mortars were produced at a volumetric binder to aggregate ratio of 2:1. Such mortar recipes possess good performance properties and workability. All mortars were produced to a constant flow of about 15 cm to ensure similar performance properties. The mortars used for spongolite repair were only of hydraulic origin, as these binders suit the properties of the original stone properties better, especially as regards high strength and porosity. Mixtures of Roman cement, Natural hydraulic lime (NHL5) and areal lime were mixed with standardized sand in a volumetric ratio of 2:1 and applied directly on-site and left for almost one year to harden and age naturally in external atmospheric conditions. After that time the mortars were cut away from the stone substrate and tested in the laboratory. The general focus of this work was to discuss the compatibility of the mortars as regards their compliance from the point of view of selected physical and mechanical properties. These two model examples also help to define the importance of particular physical and mechanical parameters for the assessment of compatibility between the original substrate and repairs, and based on that, help to make a ranking of the importance of a particular property (characteristic). It was found that just a narrow range of critical properties such as water transmittance properties together with the characterization of the pore structure by means of mercury intrusion porosimetry, modulus of elasticity/deformability and ultrasound velocity was found to provide reliable information in order to a make a general choice of safe repair material and provide general instructions for each substitution project. This is a highly positive finding, especially in cases when dealing with cultural heritage properties where only minimum sampling is possible and/or compatibility assessment should be often done directly on-site.

Acknowledgement: The authors gratefully acknowledge support from the Czech Ministry of Culture NAKI Project DF12P01OVV018 entitled "*Conditions and requirements of compatible care of the historical inorganic porous materials*", "Podmínky a požadavky kompatibilní péče o historické anorganické porézní materiály".

21st International Conference **ENGINEERING MECHANICS 2015**
Svratka, Czech Republic, May 11 –14, 2015
Paper **#023, pp. 330–331**

Influence of the Natural Frequency Mistuning and the Damping and Kinematic Properties of Blades on Subsonic Flutter Stability of Blading

Volodymyr A. Tsymbalyuk

G.S. Pisarenko Institute for Problems of Strength, Nat. Ac. Sci. of Ukraine,
01014, 2, Timiryazevskaya str., Kiev, Ukraine

Keywords: mistuned blade assembly, subsonic flutter, aeroelastic stability prediction

Abstract. The investigations of the subsonic flutter conditions in alternately mistuned blading, the blades of which differ in both the natural frequencies and the mechanical damping and vibration modes, are presented. The experimental aerodynamic influence coefficients for various attack angles are used for the stability calculations.

Introduction

It is known that one of the means to increase the stability of blading against self-excited vibration is its mistuning, which can be implemented by various ways:
– the mounting of blades with different geometric, elastic and damping properties;
– the use of dissimilar blade-to-disc interlocking joints;
– the introduction of changes of the flow in individual blade passages, e.g., by way of changing the blade spacing or angles of incidence.

Up to now, the effect of the differences in the natural frequencies of blades on the dynamic stability of blading has been studied most extensively. In this paper, the influence of the differences in the mechanical damping and vibration modes of the blades of the blade assembly is studied together with the frequency mistuning.

In case of alternating mistuning, the blade assembly can be considered as consisting of identical packets, and the packet blades differ from one another in the natural frequencies, vibration mode and mechanical damping, as shown in Fig.1 (the blades with different mechanical properties are denoted by different colors, whereas the identical packets of the blades are encircled).

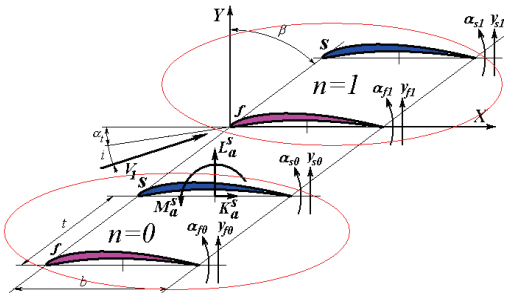

Fig. 1: Schematic of the blade assembly for alternating mistuning (i is the attack angle)

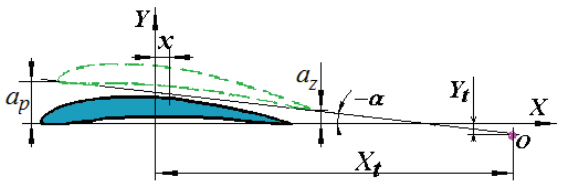

Fig. 2: Schematic motion of the blade tip section for the first vibration mode of the blade

Mathematical model

To calculate the flutter stability for the alternating distribution of mistuning, the following computational model of the blade assembly was adopted:
- there is no mechanical coupling between the blades;
- the inertial and elastic forces of the blade far exceed the aerodynamic forces;

- each blade has one degree of freedom, while the blade assembly consisting of 2N blades has 2N degrees of freedom and comprises N identical packets consisting of two blades that differ from one another in the elastic inertial and dissipative properties, etc.

We denote these blades by "*f*" and "*s*", their mechanical logarithmic decrements by δ_{fm} and δ_{sm}, the natural frequencies by Ω_f and Ω_s, and the detuning of the natural frequencies by $\gamma = \Omega_f / \Omega_s$.

The displacements of the cross-sections of the blades "f" and "s" in the first vibration mode will be considered as the angular displacements relative to the axes located at the distance X_{ft} and X_{st} from the center of the profile, as shown in Fig 2.

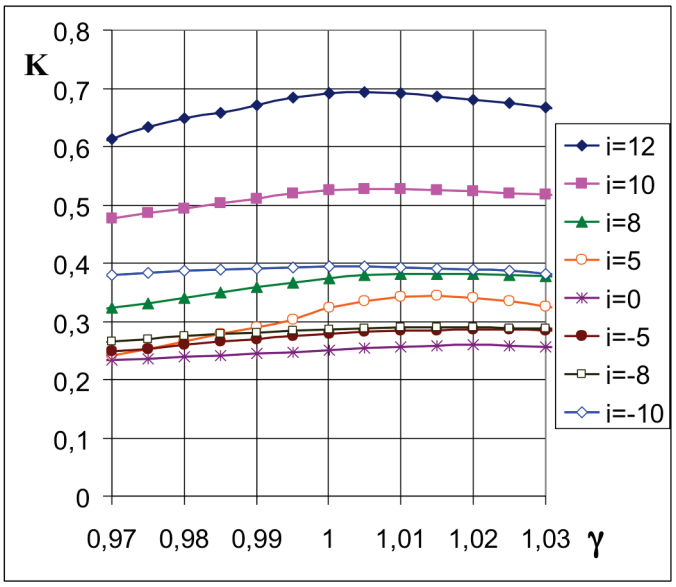

Fig. 3: Subsonic flutter stability boundaries for the first mode of vibration of the blade assembly

The aerodynamic force and moment influence coefficients $m_{n\alpha}, m_{ny}, l_{n\alpha}, l_{ny}$ obtained in the experiment make it possible to define the unsteady aerodynamic moments on the oscillating blades for an arbitrary value of X_t.

Substituting the unsteady aerodynamic moments into the equations of blade vibration, we find the eigenvalues. Next, we determine the flutter boundary of the mistuned blade assembly (the critical reduced vibration frequencies K_{cr} at which its stability is neutral). In-flow vibration of the blade assembly will be stable if its reduced frequency is higher than the critical one ($K > K_{cr}$).

Results

The stability boundaries of the first vibration mode of the blade assembly against subsonic flutter depending on the frequency detuning γ for different values for the position of the rotation axis of adjacent blade sections ($\overline{X}_{ft} = 1{,}79$; $\overline{X}_{st} = 2{,}29$) and different values of their mechanical logarithmic decrement ($\delta_{fm} = 0{,}003$; $\delta_{sm} = 0{,}03$) are illustrated in Fig. 3 for different angles of attack i. It is seen that the stability boundaries shown are non-symmetrical relative to $\gamma = 1$.

It can be concluded that with a simultaneous introduction of the alternating distribution of the natural frequencies, the position of the rotation axis of the blade tip sections and the mechanical logarithmic decrement, the effect of the joint variation in these parameters depending on their combination can be enhanced or diminished. For example, the blade assembly, whose blades with higher natural frequencies have a more distant position of the rotation axis of the sections and a higher mechanical damping, is more stable against subsonic flutter. That is, a blade assembly is more stable if $\Omega_f < \Omega_s$, $\overline{X}_{ft} < \overline{X}_{st}$, $\delta_{fm} < \delta_{sm}$.

Acknowledgement: This study was performed within the framework of the joint research project between the G.S.Pisarenko Institute for Problems of Strength of the NAS of Ukraine and Institute of Thermomechanics AS CR for conducting investigations on „Interaction of Elastic Bodies with Air Flow".

21st International Conference **ENGINEERING MECHANICS 2015**
Svratka, Czech Republic, May 11 –14, 2015
Paper **#124, pp. 332–333**

Modeling of Nonlinear Behavior of Textile Composites

Soňa Urbanová[a], Jan Vorel[b], Michal Šejnoha[c]

Faculty of Civil Engineering, CTU in Prague, Thákurova 7, 166 29, Prague, CZ

[a]sona.urbanova@fsv.cvut.cz, [b]jan.vorel@fsv.cvut.cz, [c]sejnom@fsv.cvut.cz

Keywords: textile composites, periodic unit cell, periodic boundary conditions, homogenization, damage, Hashin-type criterions

Abstract: This paper deals with the analysis of composite systems reinforced by plain weave textile fabric with attention accorded to the modeling of damage. Solution of this problem requires complex and time demanding preparation consisting of several steps such as formulation of the periodic unit cell exploiting computational microtomography to determine the actual 3D porous structure, meshing the computational model equipped with appropriate boundary conditions and finally evaluating the effective properties of yarns using, e.g. the Mori-Tanaka micromechanical model. Assessing the damage evolution of such systems then requires the solution of the first-order homogenization problem of a periodic unit cell assuming non-liner response of individual phases. Herein an approach based on Hashin-type failure criteria combined with an appropriate damage evolution law is examined.

Formulation of SEPUC

The crucial part of the analysis is the determination of geometrical and material model of statistically equivalent periodic unit cell (SEPUC), see e.g. [1], involving all the technological imperfections developed during the production of the composite including non-uniform layer width and tow undulation, inter-layer shift and nesting, a relatively high-intrinsic porosity as well as disordered arrangement of fibers within the yarn cross-section, which distinctly influences the macroscopic response of the final composite [2]. Therein, the porous phase plays the most important role when predicting the effective properties of the composite. Its volume fraction is obtained from μ-CT measurements. This phase is considerably influenced by the curing temperature as can be seen when comparing its actual distribution plotted in Fig. 1(a) – 9% and Fig. 1(b) – 9.2%. On the other hand, it appears that other imperfections do not evolve much as a function of curing temperature. A scheme of implementation of porous phase to the model of SEPUC is displayed in the Fig. 1(a-c). Figs. 1(c,d) further show the assumed two-level modeling approach.

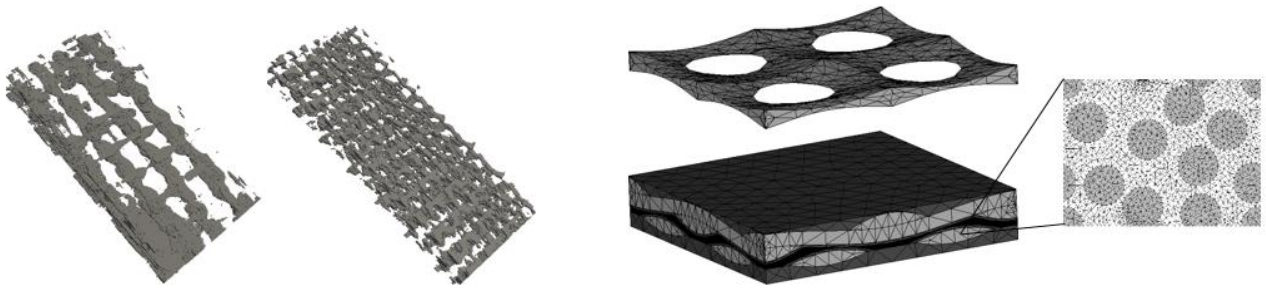

(a) (b) (c) (d)

Fig. 1: (a) porous phase of the sample cured at 200°C in 3D, (b) porous phase of the sample cured at 800°C in 3D, (c) meshed two-layer SEPUC with porous phase (separately shown above) – meso-scale, (d) mesh of yarn – micro-scale

Computational procedure

To assess the damage evolution of micromechanical model of SEPUC a model based on Hashin-type failure criteria reflecting three typical damage mechanisms (transverse matrix cracking, fiber-matrix shearing debond and longitudinal fiber breakage) is introduced. Herein, an improved damage evolution model introduced by Fang et al. [3] is applied. When using this model the tensile and compressive strength of yarn in each direction and full damage equivalent displacement of the examined failure mode are required [3,4]. They are, however, difficult to obtain experimentally. On the contrary, these can be estimated from virtual computational experiments performed at the level of yarns, where properties of individual phases are typically known. In this regard the damage model originally proposed for yarns can be used for the fiber phase on the micro-scale, see Fig. 1(d). A simple maximum stress based criterion is employed for the matrix phase on both scales. This approach falls within the category of uncoupled multi-scale modeling strategies.

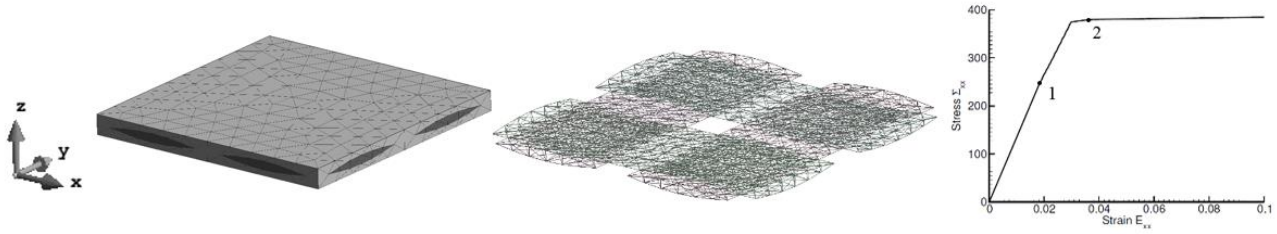

(a) (b) (c)

Fig. 2: (a) one-layer SEPUC, (b) example of yarn mesh, (c) tensile stress-strain curve: point 1 - damage initiation, point 2 – full damage of yarns

Example and summary

To validate the implementation of the damage model a one layer SEPUC of textile polymer matrix based composite reinforced by plain weave basalt fabric is considered, see Fig. 2(a,b). The unit cell is subjected to macroscopic tensile stress Σ_{xx}. For the sake of simplicity the porous phase is omitted and only yarns are allowed to undergo progressive damage, whereas the matrix phase is assumed to be elastic. The necessary material parameters are taken from [4]. The resulting macroscopic stress-strain curve is displayed in Fig. 2(c). As expected, upon complete yarn failure the composite stiffness is controlled by the stiffness of the matrix.

At present the research effort is devoted to the determination of meso-scale strength parameters from macro-scale simulations. This will allow us to properly address the effect of curing temperature (effect of the evolving porous phase) on the macro-scale response of the composite.

Acknowledgement: The research project by the Grant Agency of the Czech Technical University in Prague grant no. SGS15/031/OHK1/1T/11 is gratefully acknowledged.

References

[1] Šejnoha M, Zeman J, Micromechanics in Practice. WIT Press, Southampton, Boston, 2013

[2] Vorel J, Grippon E, Šejnoha M, Effective Thermoelastic Properties of Polysiloxane Matrix Based Plain Weave Textile Composites. International Journal for Multiscale Computational Engineering, 2015, 13(3):181-200

[3] Fang GD, Liang J, Wang BL, Progressive damage and nonlinear analysis of 3D four-directional braided composites under unidirectional tension. Compos Struct 2009;89:126-33

[4] Zhou Y, Lu Z, Yang Z, Progressive damage analysis and strength prediction of 2D plain weave composites, Composites: Part B 2013, 220-229

21st International Conference **ENGINEERING MECHANICS 2015**
Svratka, Czech Republic, May 11 –14, 2015
Paper **#188, pp. 334–335**

Wind Tunnel Experimental Study of Coupled Rocking-Swivelling Model of Guyed Mast Shaft

Shota Urushadze[a] *, Miroš Pirner[b], Ondřej Fischer[c]

ITAM ASCR, v.v.i., Prosecká 76, 190 00 Praha 9, Czech Republic

[a]urushadze@itam.cas.cz, [b]pirner@itam.cas.cz, [c]fischero@itam.cas.cz

Keywords: Dynamics of guyed masts, dynamic response, swivelling of the shaft, wind tunnel, aerodynamic model

Abstract: Systematic monitoring of torsion (swivelling) of guyed mast shafts has been performed in ITAM since 2005. The occurrence of this phenomenon is conditioned by the fact that the guy ropes are attached to the surface of the shaft, i.e. out of its axis. The simple static calculation model serves for making the proof of the occurrence of the moment, affecting the shaft, which is guyed by three ropes. The exact theoretical solution of the real phenomenon assumes the introduction of dynamics of guy ropes, which vibrate in 3D shapes during the shaft's movement along the orbit and it´s torsion (swivelling).

Introduction

The theoretical analysis of the mast should always be corrected on the basis of monitoring of the real structure. From the measuring of the dynamic response of masts or of their models it was known that the resulting movement of the shaft in ground plan appears as an ellipse, whose major axis forms an angle smaller than 90° with the direction of the wind. Usually low intensity of turbulence and smooth surface of the shaft are conditions for the regularity and intensity of the vortex shedding. High intensity of turbulence disturbs the regularity of the shedding and thus also the cross-wind direction excitation and then the ellipse becomes more a circle.

Torsion or swivelling of the mast shaft

The shifting from zero position will result in changes of the forces in the ropes and moments in the points of connection to the shaft, which are out of the axis of the shaft. If the shaft is guyed by three ropes, there are 6 points on the elliptical track, in which the sum of the moments from the eccentric connection of the ropes is zero, and thus also the swivelling is zero (see Fig. 1). Theses points delimit the domains with positive or negative rotation of the shaft. The zero points may lie close to each other; in such a case the domains prevail with their size at the apexes of the ellipse. If the ellipse degenerates into a line, there are two domains of rotation which differ in the plus/minus sign.

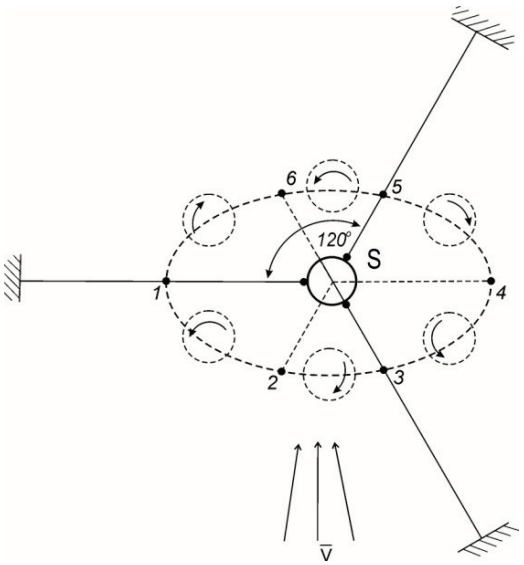

Fig. 1: Rotation of the shaft owing to the eccentricity of the ropes

The frequency of torsion or swivelling of the shaft depends on the position of the zero points on the ellipse (Fig. 1): if the zero points are far enough from each other, the torsion of the shaft is governed by the 6 domains of moments and the frequency of swivelling f_{tor} is

$$f_{tor} = 3 f_b \tag{1}$$

If points (see Fig. 1) 2 and 3 merge into one, and so do points 5 and 6, then:

$$f_{tor} = f_b \tag{2}$$

Monitoring of swivelling on the model

In more detail and more stable aerodynamic conditions was the phenomenon of swivelling of the mast shaft examined on a simple model. The shaft was a tube of hardened PVC, of an outer diameter of 75 mm, supported by a point at the bottom and guyed by three wires in one level.

The flexural rigidity of the shaft is not modelled; the bending is substituted by the tilting. That is why there are no higher shapes of tilting and the orbit is always close to ellipse.

The torsion was verified in a wind tunnel and by deformations were determined. The experiments has been performed in the new aerodynamic tunnel (ITAM – Telč). Wind tunnel section size enabled experiment with model shaft up to 1500 mm high, anchored by three ropes at a height of 1000 mm. The top end of the shaft was equipped with a horizontal arm with two accelerometers attached on its ends; the distance between the accelerometers is 380 mm - see Figure 2. Accelerometers 1 and 2 sense the motion in the direction perpendicular to the horizontal arm. Besides the two accelerometers on the horizontal arm there is also the third accelerometer at the upper end of the shaft, which senses the motions perpendicular to the direction of the above pair of accelerometers.

The mast model was adjusted within the admissible limits by means of stressing of the wires and increasing of the mass concentrated on the top of the shaft. Fig. 3 shows the records of the orbit and swivelling of the shaft relative to it.

Fig. 2: The model of the guyed mast

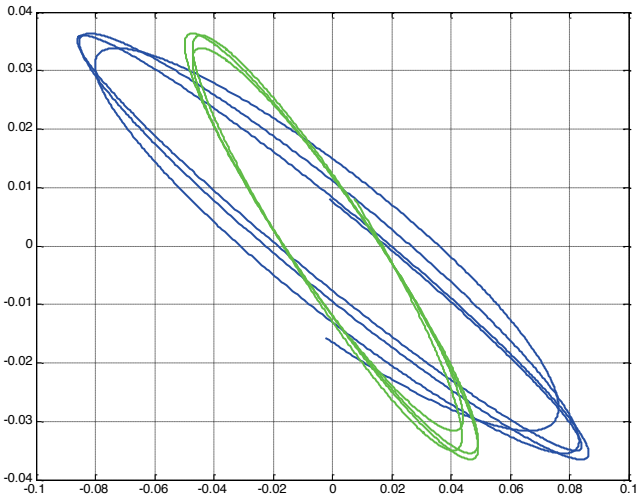

Fig. 3: Examples of the superposition of the shaft motions.
The green (less inclined) line is the orbit and the blue line is the swivel according to the parallel sensors.

The existence of torsion (swivelling) takes short time in which orbit of the shafts the shape is near the ellipse. The curve which intersects the ellipse in several points formulates shaft rotation of the positions place of the sensors.

Acknowledgments: The kind support of the Czech Science Foundation Project No. GC13-34405J and of the RVO 68378297 institutional support are gratefully acknowledged.

21st International Conference **ENGINEERING MECHANICS 2015**
Svratka, Czech Republic, May 11 –14, 2015
Paper **#211, pp. 336–337**

Assessment of Vibrations in Museum's Environment

Jaroslav Valach[1,a]*, Benjamin Wolf[1,b], Eva Paulová[2,c], Shota Urushadze[1,d]

[1]Institute of Theoretical and Applied Mechanics of AS CR, v.v.i.,
Prosecká 76, 190 00 Prague 9, Czech Republic

[2]Czech Museum of Music, Karmelitská 2, 118 00 Prague 1, Czech Republic

[a]valach@itam.cas.cz, [b]wolf@itam.cas.cz, [c]eva.paulova@nm.cz, [d]urushadze@itam.cas.cz

Keywords: museum collections, transport induced vibrations, cultural heritage, damaging process, monitoring

Abstract: This paper deals with measurement of mechanical vibrations and accelerations threatening objects in museum collections. Two case studies are presented. The first case analyses situation in museum exhibitions strongly influenced by street traffic in its close proximity. It compares results obtained by sensitive professional measurement system to the custom-built user device for acceleration recording. The second case analyzes object's accelerations during transport based on measurement by the custom-built device.

Introduction

The project "Unified modular system of remote on-line monitoring of environmental parameters of depositories and expositions" deals mainly with monitoring of parameters of internal environment in museums [1]. Among parameters like temperature, humidity and light intensity, also mechanical vibrations play important role in protection of collections objects. In order to protect the irreplaceable historical objects, sources of vibrations in museum have to be studied and if exceed safe level, also eliminated. As there is still an incomplete knowledge relating scale of mechanical load due to vibrations and their damaging effects on various object types, it is interesting experimental task to measure the true extent of vibrations and accelerations found in the museum environment [2]. Secondly, collections are shipped to different locations and the transport represents substantial impact on object's life. To properly assess the extent of loads during transport, mobile monitoring device accompanies it and records the events occurring during transport.

Case one - vibrations in museum

The Czech Museum of Music is situated in 19th century building located on street with a heavy traffic including trams. Each vehicle passing the building induces vibrations into the exposition, especially those due to trams are severe. The measurement performed in the museum had two major goals: quantify influence of traffic on vibrations of displayed objects and use the simultaneous measurement of the vibrations for comparison and "calibration" of custom made acceleration recording device. Satisfactory agreement between the two measurements was obtained, therefore the custom-built device was used with reasonable degree of confidence also in another experiments.

The measurement yielded the following findings: Comparing dynamical response to loads caused by street traffic between the two adjacent exhibition rooms suggests that the floor that shakes more is more compliant. Second finding confirms observations known from literature: humans are very sensitive detectors of vibrations, they get alarmed on levels of load that are two orders of magnitude lower prior any damage to objects can happen [2]. But the most important result is a proof that vibrations due to traffic are much smaller than those produced by visitors walking in the room.

Case two – dynamical loading during transport

The custom built device was used to analyze accelerations to which the transported object is subjected to. Dummy object playing role of a "precious artefact" was placed into padded suitcase typically used as transport box. Then the box was sent from Prague to Vienna and back with other true objects in exhibition exchange. Upon its arrival, the custom built device was retrieved and recorded data were downloaded into computer and processed. It was observed that the most severe forces arise from handling operation, when the box is handled – Fig. 1.

The innovative part of the device is its capacity to record simultaneously accelerations of the transport box and object using detachable sensor. This way quality of object's protection from external forces can be assessed. The device can be therefore also used to optimize transport boxes and improve their protection properties. The true dynamic analysis of box-object interaction can reveal the necessity to relate compliance of interior padding to inertia of the protected object itself.

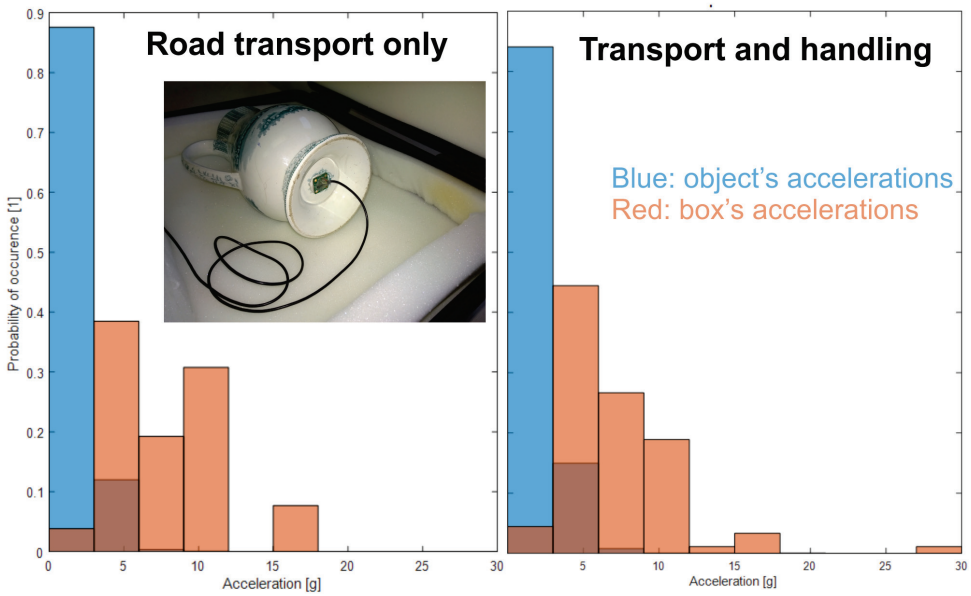

Fig. 1: Histograms representing distribution of accelerations measured on the transport box and on the object during transport only and also including handling. Significantly reduced portion of high acceleration events for object in comparison to transport box indicates that the object was properly protected.

Summary

Presented results cast interesting light on possibilities of experimental measurement of dynamical variables in environment distant from typical engineering practice.

Acknowledgement: The project is supported by the program of applied research and development of national and cultural identity (NAKI) of the Ministry of Culture – grant No. DF12P01OVV27.

References

[1] P. Štefcová, J. Valach, K. Juliš, Modular system of Sensors for Monitoring of Museum Internal Environment, International Journal of Heritage in the Digital Era 1 (2012) 39-42. ISSN: 2047-4970, DOI: 10.1260/2047-4970.1.0.39.

[2] D. Thickett, Vibration damage levels for museum objects, in: ICOM Committee for Conservation, ICOM-CC: 13th Triennial Meeting, Rio de Janeiro, 22-27 September 2002. ICOM-CC; James & James, London, 90-95, 2002.

21st International Conference **ENGINEERING MECHANICS 2015**
Svratka, Czech Republic, May 11 –14, 2015
Paper **#130, pp. 338–339**

Numerical Simulation of Interaction of Fluid Flow and Elastic Structure Modelling Vocal Fold

Jan Valášek[1,a], Petr Sváček[1,b], Jaromír Horáček[2,c]

[1]Department of Technical Mathematics, Faculty of Mechanical Engineering, Czech Technical University in Prague, Karlovo nám. 13, Praha 2, 121 35, Czech Republic

[2]Institute of Thermomechanics, Czech Academy of Sciences, Dolejškova 5, 182 00 Praha 8, CZ

[a]Jan.Valasek1@fs.cvut.cz, [b]Petr.Svacek@fs.cvut.cz, [c]Jaromirh@it.cas.cz

Keywords: finite element method, 2D Navier-Stokes equations, vocal folds, aeroelasticity

Abstract: This paper deals with an interaction between the fluid flow and an elastic body. A simplified model of the human vocal fold is considered. In order to capture deformation of the elastic body the arbitrary Lagrangian-Euler method (ALE) is used. The viscous incompressible fluid flow and linear elasticity models are considered. The problem is solved by the developed finite element method (FEM) based solver. Particularly, for the flow approximation the crossgrid elements are used, whereas for the elastic structure the piecewise linear elements are employed. Results of numerical experiments are shown.

Mathematical model

For the sake of simplicity our study is restricted to a 2D model problem. A scheme of the used model is shown in Figure 1, where Ω^s_{ref} is the reference representation of the structure and Ω^f_{ref} denotes the domain of the fluid.

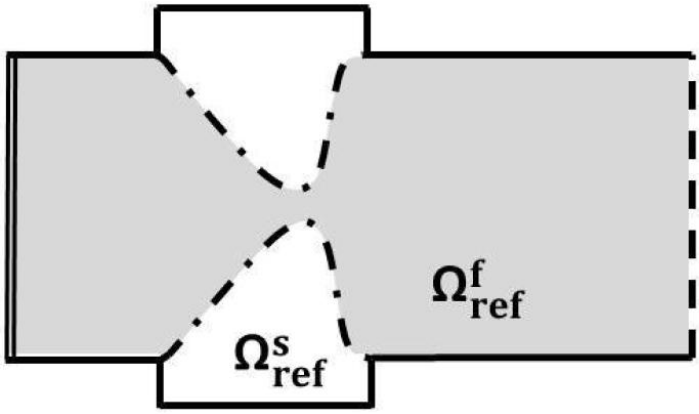

Fig. 1: Schema of vocal folds model in undistorted shape.

The deformation of the structure is then described by the equations (see [1])

$$\rho^s \frac{\partial^2 \mathbf{u}}{\partial t^2} - \frac{\partial \tau^s_{ij}(\mathbf{u})}{\partial x_j} = \mathbf{f^s} \quad \text{in } \Omega^s_{ref} \times (0, \mathrm{T}), \tag{1}$$

where ρ^s is the structure density, $\mathbf{u}$ is the sought deformation, τ^s_{ij} denotes the Cauchy stress tensor and the vector $\mathbf{f^s}$ is the volume density of an acting force. Under the assumption of small displacements and with the help of Hook's law the stress tensor τ^s_{ij} of an isotropic body can be expressed as

$$\tau^s_{ij} = \lambda^s \mathrm{div}\, \mathbf{u} + 2\mu^s e^s_{ij}, \tag{2}$$

where λ^s, μ^s are Lame constants and $e^s_{ij} = \frac{1}{2}(\frac{\partial u_i}{\partial x_j} + \frac{\partial u_j}{\partial x_i})$.

The motion of the viscous incompressible fluid in the time dependent domain Ω_t^f is modelled by the Navier-Stokes equations in the ALE form (see [2], [3])

$$\frac{D^A\mathbf{v}}{Dt} + ((\mathbf{v} - \mathbf{w}_D) \cdot \nabla)\mathbf{v} - \nu^f \Delta\mathbf{v} + \nabla p = \mathbf{g}^f, \qquad \text{div } \mathbf{v} = 0 \quad \text{in } \Omega_t^f, \tag{3}$$

where $\mathbf{v}$ is vector of the fluid velocity and p denotes the kinematic pressure, $\mathbf{w}_D$ is the domain velocity of the deformation defined by the ALE mapping, ν^f is the kinematic viscosity of the fluid and $\mathbf{g}^f$ is vector of volume forces. Eq. 1 and 3 are considered with respective initial and boundary conditions, see article [4].

The flow and structure models are coupled with the aid of boundary conditions prescribed on the common interface $\Gamma_{\mathrm{W_t}}$. First, the kinematic boundary condition reads

$$v(x,t) = w_D(x,t) \quad \text{for } x \in \Gamma_{\mathrm{W_t}}. \tag{4}$$

Further, the dynamic boundary condition is given by

$$\sum_{j=1}^{2} \tau_{ij}^s(X)\, n_j^s(X) = \sum_{j=1}^{2} \sigma_{ij}^f(x)\, n_j^s(x), \quad i = 1,2, \quad x \in \Gamma_{\mathrm{W_t}},\ X \in \Gamma_{\mathrm{W_{ref}}}, \tag{5}$$

where σ_{ij}^f is the stress tensor of fluid, $n_j^s(X)$ denotes the components of the unit outward normal to the interface $\Gamma_{\mathrm{W_{t=0}}}$ pointing into Ω_{ref}^f.

Numerical approximation

The both model equations are discretized with constant time step. In the case of structure the space discretization by FEM piecewise linear elements are performed and then the system of ordinary differential equations of second order is approximated by the Newmark method.

On the other hand Eq. 3 is discretized in time with help of BDF2 scheme and then for space discretization so called cross-grid P1 elements are used. The acquired nonlinear equations are lineared by Oseen linearization and iterative solution is seeked with the support of mathematical library UMFPACK.

Acknowledgements: The financial support for the presented work was partly provided by the Czech Science Foundation under the Grant No. 101/11/0207 and project SGS 13/174/OHK2/3T/12.

References

[1] M. Brdička, L. Samek, B. Sopko, Mechanika kontinua. Academia, Praha, 2000. [in Czech]

[2] M. Feistauer, et al., Numerical Simulation of Fluid-Structure Interaction Problems with Applications to Flow in Vocal Folds, In: Fluid-Structure Interaction and Biomedical Applications, edited by Bodnár, T., Galdi, G. P., Nečasová, S., Series: Advances in Mathematical Fluid Mechanics, XIV, pp. 312–393, Birkhauser, 2014. [Book chapter]

[3] T. Nomura, T.J.R. Hughes, An arbitrary Lagrangian-Eulerian finite element method for interaction of fluid and a rigid body. Computer Methods in Applied Mechanics and Engineering, 95 (1992) 115–138.

[4] Valášek, et al., On Numerical Approximation of Fluid-Structure Interactions of Air Flow with a Model of Vocal Folds, In: Topical problems of Fluid Mechanics 2015, edited by D. Šimurda, T. Bodnár, pp. 245–254, 2015.

21st International Conference **ENGINEERING MECHANICS 2015**
Svratka, Czech Republic, May 11 –14, 2015
Paper **#080, pp. 340–341**

Numerical Simulation of the Speaker's Formant for Different Geometric Configuration of the Human Vocal Tract

Tomáš Vampola[1,a*], Jaromír Horáček[2,b]

[1]CTU in Prague, Dept. of Mechanics, Biomechanics and Mechatronics,
Technická 4, 166 07 Prague 6, Czech Republic

[2]Institute of Thermomechanics, Academy of Science of the Czech Republic,
Dolejškova 5, 182 00, Prague 8, Czech Republic

[a]Tomas.Vampola@fs.cvut.cz, [b]jaromirh@it.cas.cz

Keywords: numerical simulation of phonation, voice quality, biomechanics of voice

Abstract: Various side branches of the human vocal tract exhibit antiresonances and resonances in the human voice frequency spectrum which influence the voice quality. This study investigates the possibility how these specific resonances can contribute to the speaker's formant cluster around 3-5 kHz. A reduced finite element (FE) models were created which allows numerical simulation of the effects of changing the parallel cavities volume on the acoustic resonance and antiresonance characteristics of the vocal tract. These simplified models, created from accurate three-dimensional (3D) FE models of the human vocal tract for vowel [a:,i:,u:], are computationally effective and allow parametric changes of the parallel cavities continuously within the human physiologic range. These changes are expected to play also a role in voice exercising, voice therapy and operatic singing.

Introduction

While the influence of the geometric configuration of the main channel of the vocal tract on the vocal output has been studied rather extensively, the influence of side cavities of human vocal tract, has received less attention. Generally, these cavities have been reported to cause antiresonances in the resulting vocal spectrum, i.e., largely decreasing radiation of some of the spectral frequencies out of the mouth, particularly those around 4–5 kHz [1,2,3,4,5]. As such, their role for the resulting vocal intensity may be considered undesirable, since it contradicts the general goal of enhancing vocal output with the smallest vocal effort. However, newest studies with perceptual evaluation of sound produced using 3D mathematical and physical models of the singers' vocal tracts revealed that the voice quality is perceived as being better when side branches are present.. Furthermore, spectral analysis of singers indicates that the formant structure around 3–5 kHz is more complex than usually expected. A more detailed analysis shows that besides the antiresonances there are also new resonances which occur because of these side cavities.

Computational models

The sophisticated accurate 3D FE models of the vocal tract for vowels [a:,i:,u:,] were created from the CT images. Their usage for investigating the effect of vocal tract shape modifications on the changes in acoustic resonance properties is time consuming. Therefore the reduced FE models were created including all the dominant parallel cavities and their resonance and antiresonance frequencies were tuned to correspond to those of the full FE model. These reduced models were then used for analyzing the antiresonances, resonances and the pressure transfer function of the vocal tract. The accuracy of the results obtained using the reduced models were examined by comparing these to the results obtained by the full 3D FE model.

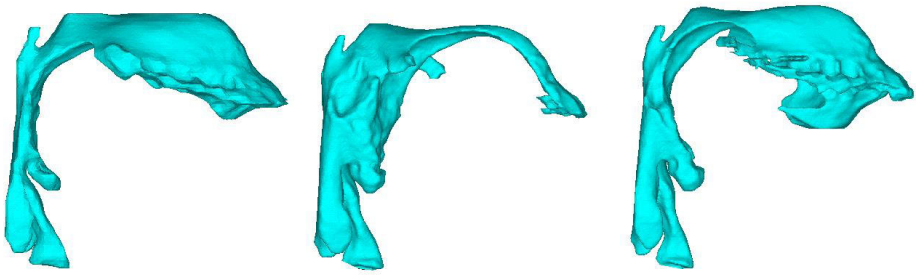

Fig. 1: The geometric configuration of the vocal tract cavities for vowels [a:,i:,u:]

The influence of geometric configurations of the human vocal tract on the generated acoustic pressure was simulated by the reduced FE model shown in Fig. 2.

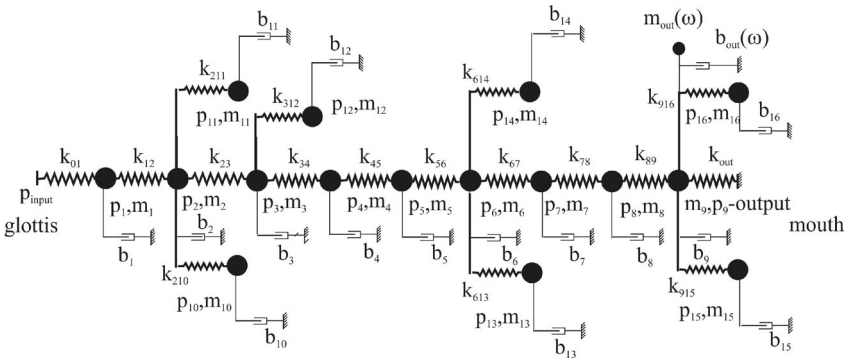

Fig. 2: The simplified reduced model for vowel [i:]

Summary

Based on the numerical analyzes can be concluded that the parallel cavities influence the voice quality for the vowels [a:,i:,u:] by different mechanism. For the vowels [a:,u:] the most important is the increase of the parallel cavities near the human vocal folds. On the contrary for vowel [i:] the phonation characteristics are influenced mostly by the parallel cavities near the tonsils.

Acknowledgement: The research has been supported by the grant GAČR No. P101/12/1306 Biomechanical modeling of human voice production - a way to artificial vocal folds.

References

[1] J. Dang, K. Honda, Acoustic characteristics of the piriform fossa in models and humans. Journal of the Acoustical Society of America 101 (1997) 456–465.

[2] K. Motoki, Three-dimensional acoustic field in vocal tract. Acoustical Science and Technology 23 (2002) 207–212.

[3] S. Fujita, K. Honda: An experimental study of acoustic characteristics of hypopharyngeal cavities using vocal tract solid models. Acoustical Science and Technology 26 (2005) 353–357.

[4] H. Takemoto, S. Adach, T. Kitamura, P.Mokhtari, K.Honda, Acoustic roles of the laryngeal cavity in vocal tract resonance. Journal of the Acoustical Society of America 120 (2006) 2228–2238.

[5] P. Mokhtari, H. Takemoto, T. Kitamura, Single matrix formulation of a time domain acoustic model of the vocal tract with side branches. Speech Communication 50 (2008) 179–190.

21st International Conference **ENGINEERING MECHANICS 2015**
Svratka, Czech Republic, May 11 –14, 2015
Paper **#040, pp. 342–343**

Computer-Aided Plastic Limit Analysis of Plates

Vladimír Vančík[a], Milan Jirásek[b]

Department of Mechanics, Faculty of Civil Engineering, Czech Technical University in Prague, Thákurova 7, 166 27, Prague; CZ

[a]Vladimir.Vancik@fsv.cvut.cz, [b]Milan.Jirasek@fsv.cvut.cz

Abstract: This paper aims to explore the potential of using the yield line theory for design of reinforced concrete plates. The primary focus is development of a computer program able to solve arbitrary yield line systems. The program will include a GUI, which will allow for quick and intuitive input and analysis of yield line systems regardless of the complexity of their analytical solution. Furthermore, optimization of orthotropic reinforcement will be implemented. Possibility of use of the program for design compliant with Eurocode 2 will be discussed.

Introduction

It has been shown e.g. in [1, 2] that design of reinforced concrete plates based on plastic limit analysis (specifically the yield-line theory) can lead to a significant reduction in reinforcement volume as opposed to the elastic approach mostly employed in engineering practice. The yield-line theory gives an upper bound of the limit load and it is therefore important to find the right collapse mechanism which gives the lowest limit load. The solution is also influenced by the ultimate bending moment, which for orthotropically reinforced concrete plates can depend on the angle between a plate cross section (i.e. a yield-line) and the main reinforcement direction.

Optimizing collapse mechanisms has been extensively covered in [3, 4], but optimization of reinforcement proportion[1] has not received much attention. This paper aims at providing a user friendly computer program for the analysis of yield-line mechanisms, allowing both geometry and reinforcement optimization.

Both [1, 2] offer an extensive validation of computations obtained by the yield-line theory by experiments. It is always assumed, however, that the reinforcement ductility is sufficient due to the plates being lightly reinforced. Therefore we investigate whether some still feasible reinforcement ratios and proportions can occur for which the optimal collapse mechanism is not able to develop.

The program

The program was developed in Python 2.7 environment using the Enthought TraitsUI package for the graphical interface. A general yield-line mechanism is defined through so-called 'plate segments' (henceforth refered to as 'segments'), which in turn consist of nodes. The whole object structure is evident from the tree view in Fig.1. The segments represent the rigid, mutually rotated parts of a yield-line mechanism. A node in general has three coordinates (two coordinates in plane and one deflection coordinate) of which some may be unknown. A well-defined mechanism must be unambiguous (must not be under-determined) and must be geometrically compatible (must not be over-determined). The basic unknowns of every mechanism are three parameters per segment and with more complex mechanisms some nodal coordinates may have to be unknowns as well in order to assure the geometrical compatibility.

[1] Assuming a plate reinforced in two mutually perpendicular directions, we will refer to the ratio of reinforcement area to concrete area in both directions as reinforcement ratio, as opposed to the ratio of the two reinforcement areas, which we will call reinforcement proportion.

Input data specific to optimization are managed by the Parametric Study object. There are two categories - node data specify node coordinates and plate data specify plate attributes (in practice mostly reinforcement ratios, but any attribute may be chosen). Both data types then specify an optimization parameter on which they depend. That enables the user to set the conditions precisely and also save computation time, as more values can depend on one parameter. Optimization parameters are kept separately and may have their bounds specified. The limit load must be minimal according to node positions but at the same time maximal according to plate attributes. The optimization itself is performed by the SciPy package optimize library - two function calls, one encapsulated in the other, are used to fulfil both the minimizing and the maximizing criteria.

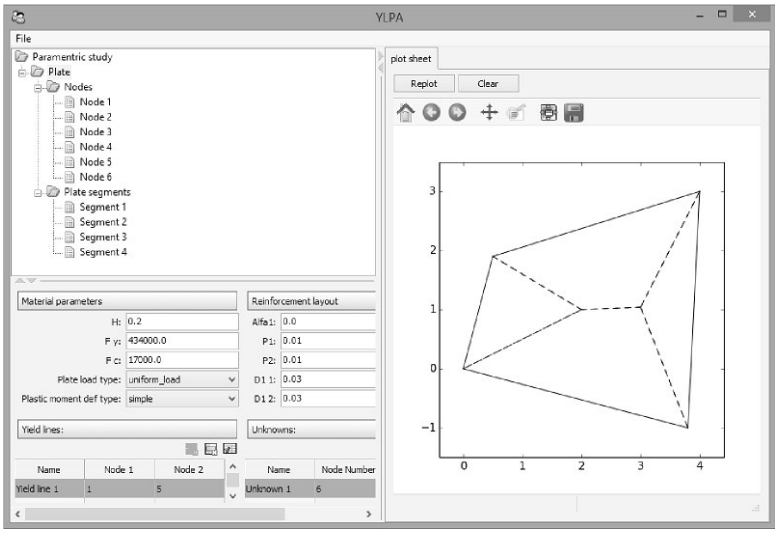

Fig. 1: The user interface

Ductility of collapse mechanisms

As has been stated, we want to go beyond the simple assumption of lightly reinforced plates. Our program contains a routine for checking rotational capacity across all yield-lines. That allows us to easily discover cases where a seemingly optimal collapse mechanism cannot develop due to insufficient ductility. As it is unclear how to define a moment-curvature relation in a general cross section of a plate, we work with an equivalent reinforcement ratio based on the angle of a section with the main reinforcement direction. For concrete, the stress-strain law for nonlinear calculations according to [6] has been utilized.

References

[1] K.W.Johansen, Yield-line Theory,Cement and Concrete Association, 1962.

[2] R.Park, W.L.Gamble, Reinforced Concrete Slabs, John Wiley & Sons, 1980.

[3] A. Thavalingam, A. Jennings, J.J. McKeown, D. Sloan, A computerised method for rigid-plastic yield-line analysis of slabs,Computers and Structures 68 (1998) 601–612.

[4] A. Thavalingam, A. Jennings, D. Sloan, J.J. McKeown, Computer-assisted generation of yield-line patterns for uniformly loaded isotropic slabs using an optimisation strategy, Engineering Structures 21 (1999) 488–496.

[5] A. Jennings, On the identification of yield-line collapse mechanisms,Engineering Structures, 18 (1996) 332-337.

[6] EN 1992-1-1:2004 + AC:2010, (CEN, 2010)

21st International Conference **ENGINEERING MECHANICS 2015**
Svratka, Czech Republic, May 11 –14, 2015
Paper **#116, pp. 344–345**

Multidisciplinary Multi-Body Modeling of Machine Tools

Jan Vetiska[1,a]*, Zdenek Hadas[2,b], Michal Holub[1,c]

[1]Institute of Production Machines, Systems and Robotics, Faculty of Mechanical Engineering, Brno University of Technology, Technicka 2896/2; 619 69, Brno; CZ

[2]Institute of Solid Mechanics, Mechatronics and Biomechanics, Faculty of Mechanical Engineering, Brno University of Technology, Technicka 2896/2; 619 69, Brno; CZ

[a]vetiska@fme.vutbr.cz, [b]hadas@fme.vutbr.cz, [c]holub@fme.vutbr.cz

Keywords: multi-body model, machine tool, actuator, control, mechatronics

Abstract: This paper deals with a multi-body modeling of machine tools with actuators. The aim of this paper is demonstration of a multibody dynamics during design process of the machine tool and choice of an optimal actuator. The modern machine tool is a mechatronic system and usage of simulation modeling is a necessary step in the development process. The model-based design of the several modern machine tool assemblies is presented in this paper. This modeling technique can be used to determine the force of interactions of individual machine parts, dimensional drives, modal and harmonic analysis, etc.

Introduction

This abstract presents a modelling and a mechatronic development process in branch of machine tools. The modern machine tool is complex mechatronic system with integrated adaptronic systems. The development process of modern machine tools uses several modeling techniques and tools for design (CAD environment), multi-body dynamic analyses, finite element method computations, thermal analyses and electronics design techniques. The main aim is prediction of behavior of the developed machine tool and its optimal design with respect to customer requirements. A virtual prototype of machine tool is useful tool [1] for specification of its performance before it is built up. The accuracy of the prediction depends on complexity of the virtual prototype model.

The presented development process is based on multi-body model in MSC.ADAMS environment. The multi-body model represents mechanical parts of the machine tool assembly. This model allows to introduce connections to other multidisciplinary actuator system or adaptronic model and co-simulation of both models in other simulation environment like Simulink. The presented assembly of machine tool is created with rigid and flexible bodies of the machine tool. The analyses of this model are very useful for choice of actuators and for development of active damping systems.

The mechanical model is created in several development steps. The initial mechanical model with rigid parts is used for dynamic analyses of force interaction. As a next step, the CAD models are created and used for finite element analyses. The results of reduced finite element analyses are imported to the model and the improved mechanical model with flexible parts is used for static, harmonic and transient analyses. Furthermore, the model of mechatronic actuator or other developed adaptronic system is included [2]. The presented approach will be shown for a spindle, which is the key element of several types of machine tools.

Task formulation and spindle model

The spindle is very important part of machine tool and its operation affects quality of a workpiece and lifetime of tools. The spindle design has to respect accuracy and performance requirements; it means high the static and dynamic stiffness and stable thermal properties. The spindle stiffness characteristics are usually determined using finite element method with calculated or predicted boundary conditions.

The presented model use multi-body model of the spindle, where the flexible parts are used for direct calculation of the spindle stiffness characteristic, the results compared with measurements. The model is useful for choice of suitable actuator for high performance cutting and complex dynamic analyses. The verified model will be used for design of an active damping system for high performance cutting process.

The spindle model is shown in Fig. 1. This model was developed in several steps [3] and was compared with real measurement. The complex multi-body model consists of flexible mechanical parts which were created from CAD models on the basis of Craig-Bampton reduction. These parts are placed in models of bearings with radial and axial stiffness and damping. The mechanical parts are connected with an actuator. The model includes preloads of actuator and bearing assemblies. A cutting force is applied to the tool; it provides the real model of cutting process. The cutting velocity is assumed during simulation, the displacement of the spindle is observed for static and dynamic analyses of the spindle behavior. The simulation results together with measurements are shown in Fig. 1. The left graph plots the dependence of displacement of the spindle on applied force, whereas the right graphs shows the same plot for stiffness of the spindle. .

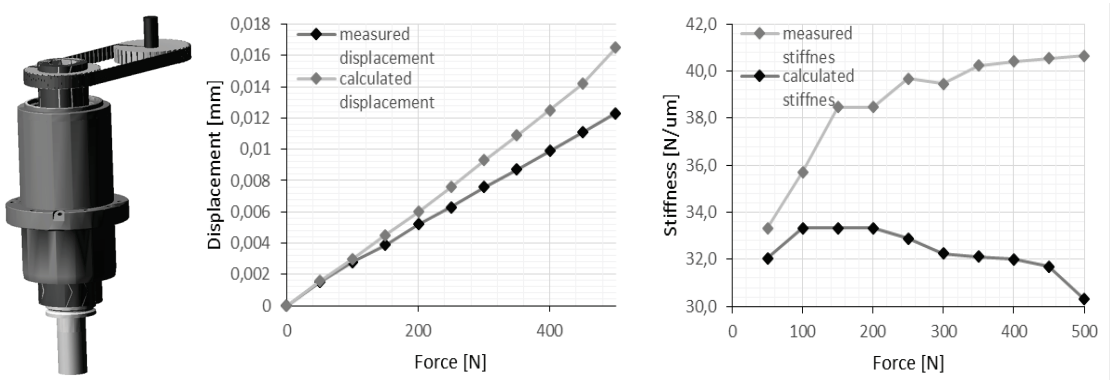

Fig. 1: Spindle model and verified static analyses of displacement and stiffness

Summary

The presented verified mechatronic model of the spindle provides a useful tool for actuator optimization study and the development of active adaptronic system for increasing of the cutting performance of a machine tool. The full paper contains more detail results and analyses.

Acknowledgement: The presented results of this paper were created under the project NETME CENTRE PLUS (LO1202) with the financial support from the Ministry of Education, Youth and Sports under the „National Sustainability Programme I"**.**

References

[1] Y. Altintas, C. Brecher, M. Weck, S. Witt, Virtual Machine Tool, CIRP Ann. - Manuf. Technol., 54 (2005) 115–138.

[2] Z. Hadas, T. Brezina, O. Andrs, J. Vetiska, L. Brezina, Simulation modelling of mechatronic system with flexible parts, in: 15th Int. Power Electron. Motion Control Conf., pp. LS2e.1–1–LS2e.1–7, Sep. 2012.

[3] VDI - Association of German Engineers, VDI 2206 - Design methodology for mechatronic systems, Design. p. 118, 2004.

21st International Conference **ENGINEERING MECHANICS 2015**
Svratka, Czech Republic, May 11 –14, 2015
Paper **#226, pp. 346–347**

Properties of Ultrafine-Grained Tungsten Prepared by Ball Milling and Spark Plasma Sintering

Monika Vilémová[1,a], Barbara Nevrlá[1,b] *, Zdenek Pala[1,c], Marek Janata[1,d], Jiří Matějíček[1,e], Dana Tonarová[2,f]

[1]Institute of Plasma Physics, ASCR, v.v.i., Za Slovankou 3, 182 00, Prague 8, Czech Republic

[2]Czech Technical University in Prague, Faculty of Nuclear Sciences and Physical Engineering, Trojanova 13, Prague 2, 120 00, Czech Republic

[a]vilemova@ipp.cas.cz, [b]nevrla@ipp.cas.cz, [c]pala@ipp.cas.cz, [d]janata@ipp.cas.cz, [e]jmatejic@ipp.cas.cz, [f]tonarovadana@gmail.com

Keywords: ultrafine-grained tungsten, planetary ball milling, spark plasma sintering

Abstract: This work studies preparation and properties of fine-grained tungsten which is thought to be more resistant to the harsh conditions inside a nuclear fusion device than standard coarse-grained tungsten. Three types of tungsten were prepared, two of them from ultrafine-grained tungsten prepared in a planetary ball mill. Flexural strength, microhardness and thermal conductivity are studied. In this paper, preliminary results are introduced.

Introduction

Tungsten is currently considered as a most suitable plasma facing material for nuclear fusion reactor. The so-called first wall will be subjected to harsh conditions that will gradually deteriorate properties of the wall material. For example, irradiation by neutrons and ions and subsequent forming of He bubbles in the material cause a substantial degradation of mechanical and thermal properties [1]. Some studies point out that fine-grained tungsten could be more resistant to radiation than coarse-grained tungsten [2]. Tailoring of tungsten microstructure is very laborious. Due to its high melting point, tungsten is very often processed mechanically and subsequently sintered into a compact body.

In this study, preparation of ultrafine-grained tungsten by mechanical processing in a planetary ball mill was examined. Three types of tungsten were compared. One was made from micron-size tungsten powder consolidated by spark plasma sintering (SPS). Other two samples (pure tungsten and tungsten with addition of Y_2O_3) were prepared from the powder processed in a planetary ball mill. After ball milling the powders were consolidated by SPS, i.e. fast sintering process that allows preserving fine-grained structure of the powder material. Properties of the samples such as microhardness and thermal conductivity were examined and correlated with the grain size.

Experimental

The ultrafine-grained tungsten was prepared using planetary ball mill PULVERISETTE 5 (FRITSCH GmbH, Germany) from a tungsten powder with initial average size of particles of 2 microns. The milling was performed in a tungsten carbide vial with tungsten carbide balls under argon atmosphere. Milling velocity was 240 rpm and the total milling time 25 h.

Powders were consolidated by SPS 10-4 (Thermal Technology, USA) under 1800 °C, 70 MPa and hold time of 2 min. The samples prepared from the milled powder are referred as W_M (tungsten only) and W_{MY} (tungsten with addition of Y_2O_3). Samples prepared from the initial powder are referred as W_0 and serve as reference for properties of W_M and W_{MY} samples.

Thermal diffusivity was measured by the xenon-flash method using Anter FL-3000 (Anter, Pittsburgh, PA, USA) under a nitrogen atmosphere.

Results and discussion

Ball milling under specified conditions led to a significant decrease of particle size of the initial powder, i.e. from median value around 1,2 micron prior milling (number distribution of the particle sizes in the measured powder) to median value around 250 nm after milling. The crystallite size determined by X-ray diffraction of the milled powder batches was less than 15 nm and remained within hundreds of nanometers after sintering into compact bodies.

Microstructure of the prepared samples is presented in Fig. 1. Fine grains surrounded by Y_2O_3 particles (dark spots) are fairly visible in the case of W_{MY} sample.

The influence of powder processing as well as the yttria particle reinforcement on hardness of the prepared materials is quite significant (Fig.2). More important are the results of thermal conductivity where a major increase for the W_M sample was observed (Fig.3).

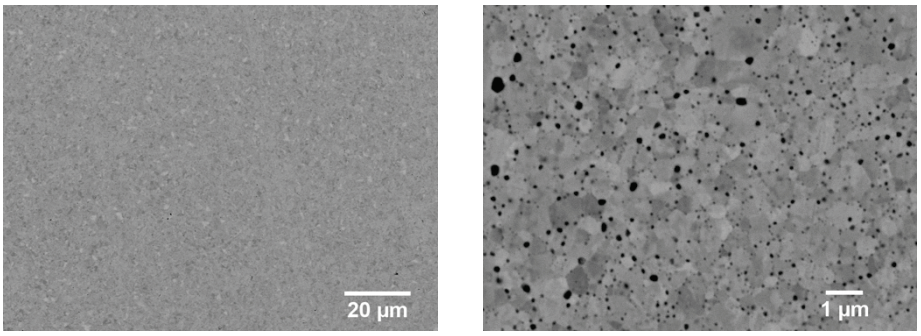

Fig. 1: Microstructure of W_M (left) and W_{MY} (right) sample

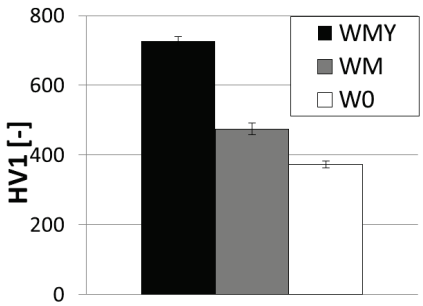

Fig. 2: Hardness of the tungsten samples

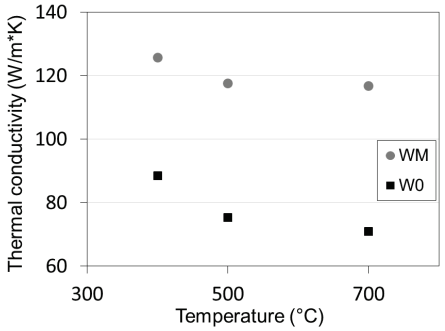

Fig. 3: Thermal conductivity of the tungsten samples

Conclusion

Powder processing in a planetary ball mill has a significant effect on the properties of prepared tungsten samples. Especially increase in the thermal conductivity will have a positive effect on the behavior under fusion like condition.

Acknowledgements: This work was supported by the Czech Science Foundation through grant no. 14-12837S.

References

[1] N. Yoshida, H. Iwakiri, K. Tokunaga, T. Baba, Impact of low energy helium irradiation on plasma facing metals, J. Nucl. Mater. 337 (2005) 946–950.

[2] M. Efe, O. El-Atwani, Y. Guo, D.R. Klenosky, Microstructure refinement of tungsten by surface deformation for irradiation damage resistance, Scripta Mater. 70 (2014) 31–34.

21st International Conference **ENGINEERING MECHANICS 2015**
Svratka, Czech Republic, May 11 –14, 2015
Paper **#183, pp. 348–349**

Assessment of Carotid Stenoses by the Principle of Fractional Flow Reserve Derived from CT

Jan Vimmr[1,a], Alena Jonášová[2,b], Ondřej Bublík[2,c]

[1]Department of Mechanics, University of West Bohemia,
Univerzitní 8, CZ-306 14 Pilsen, Czech Republic

[2]NTIS – New Technologies for the Information Society, University of West Bohemia,
Univerzitní 8, CZ-306 14 Pilsen, Czech Republic

[a]jvimmr@kme.zcu.cz, [b]jonasova@ntis.zcu.cz, [c]obublik@ntis.zcu.cz

Keywords: patient-specific model, complete carotid bifurcations, hemodynamics, fractional flow reserve, non-Newtonian fluid

Abstract: The content of the study is focused on multiscale modelling of pulsatile non-Newtonian blood flow in patient-specific models of complete carotid bifurcations. The modelled flow parameters, especially those of outlet Windkessel models, are tuned on the basis of in-vivo measurements provided by the courtesy of the University Hospital Pilsen. The process of tuning is carried out by utilising corresponding 1D models of the carotid bifurcations. To assess the physiological significance of atherosclerotic lesions present in the models, a novel non-invasive variant of the fractional flow reserve method known as FFR_{CT} is used.

Introduction

The use of computer-aided imaging methods such as the computed tomography (CT) angiography has opened up new possibilities in the detection and assessment of hemodynamically significant carotid stenoses, which are often the primary cause of brain stroke in the European population. Although the use of CT enables a direct visualisation of the damaged arterial segment, this noninvasive imaging technique is not always reliable as it shows a tendency to overestimate the stenosis severity and its hemodynamical significance [1]. To avoid the inaccuracy and to use the full potential of CT, a novel noninvasive technique known as the fractional flow reserve derived from CT (FFR_{CT}) has been developed and successfully tested for the assessment of lesion-specific coronary ischemia [1, 2]. Basically, the noninvasive assessment of stenosis severity based on FFR_{CT} is also applicable to peripheral arteries including the carotid ones, where the knowledge of flow field distribution provided by the tools of computational fluid dynamics (CFD) in combination with anatomic image data shows the potential to improve the difficult diagnosis of stenoses of intermediate severity (40 – 70% lumen reduction).

Following the idea of FFR_{CT} described in detail, e.g., in [2], the present study is focused on the development of a CFD-based tool that would be able to perform multiscale patient-specific simulations of carotid artery fluid dynamics and provide a better insight into the hemodynamical significance of stenoses identified in patient-specific models of complete carotid bifurcations.

Multiscale modelling

For the purpose of the study, several different patient-specific models of stenosed carotid bifurcations (Fig. 1a) are obtained with the help of the in-house segmentation/meshing software DICOM2FEM [3]. Considering the complexity of the flow problem, the numerical simulations of pulsatile non- Newtonian blood flow are carried out on the basis of several simplifications such as the assumption of inelastic model walls and blood's non-Newtonian rheology described by the shear-dependent Carreau-Yasuda model [4]. The mathematical model given by the non-linear system of incompressible Navier-Stokes equations is numerically solved using in-house software based on a stabilised variant of the

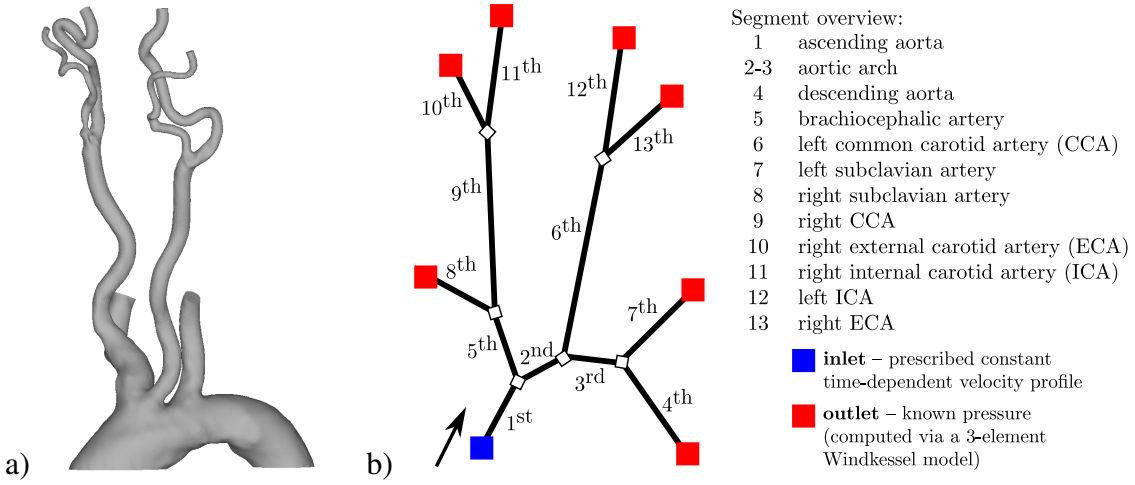

Fig. 1: (a) 3D and (b) 1D representations of a patient-specific model of carotid bifurcation.

projection method in combination with the cell-centred finite volume method formulated for hybrid unstructured tetrahedral grids. For the details, see [5].

Similarly to other flow problems, the quality and accuracy of computed results can be influenced by the inlet and outlet values prescribed at corresponding boundaries of the computational domain. As the clinical determination of physiological pressure at relevant parts of the cardiovascular system is difficult to perform, this study approaches this problem by adding a 0D model (*three-element Windkessel model*) to each arterial model outlet, where it can simulate the flow resistance of a real downstream vascular bed and provide a physiological pressure value. The Windkessel parameters are estimated in an iterative manner on the basis of in-vivo measurements provided by the courtesy of the University Hospital Pilsen. To achieve a flexible and computationally efficient estimation process, the 3D arterial models (Fig. 1a) are substituted with their 1D representatives (Fig. 1b) in accordance with the approach described and tested in [6].

The analysis and discussion of obtained numerical results, including the assessment of relevant carotid stenoses, is carried out with the help of two well-known hemodynamical wall parameters (the cycle-averaged wall shear stress, WSS, and the oscillatory shear index, OSI) and the already mentioned $\mathrm{FFR_{CT}}$, principle of which is similar to that of its invasive counterpart (FFR). In other words, the hemodynamical significance of a stenosis is determined on the basis of pressure difference before and after the arterial narrowing ($\mathrm{FFR_{CT}} \leq 0.8$ indicates ischemia [1]).

Acknowledgement: This study was supported by ERDF, project ”NTIS – New Technologies for the Information Society”, European Centre of Excellence, CZ.1.05/1.1.00/02.0090 and by the internal student grant project SGS-2013-036 of the University of West Bohemia.

References

[1] R. Nakazato, H.B. Park, D.S. Berman et al., Circ.-Cardiovasc. Imaging 6 (2013) 881–889.

[2] C.A. Taylor, T.A. Fonte, J.K. Min, J. Am. Coll. Cardiol. 61 (2013) 2233–2241.

[3] V. Lukeš, DICOM2FEM, http://sfepy.org/dicom2fem .

[4] Y.I. Cho, K.R. Kensey, Biorheology 28 (1991) 241–262.

[5] J. Vimmr, A. Jonášová, O. Bublík, Int. J. Numer. Meth. Biomed. Vol. 29 (2013) 1057–1081.

[6] A. Jonášová, O. Bublík, J. Vimmr, App. Comp. Mech. 8 (2014) 177–186.

21st International Conference **ENGINEERING MECHANICS 2015**
Svratka, Czech Republic, May 11 –14, 2015
Paper **#204, pp. 350–351**

Experimental Investigation of the Flutter Incidence Range for Subsonic Flow Mach Numbers

V. Vlček[1,a], M. Štěpán[2,b], I. Zolotarev[1,c]*, J. Kozánek[1,d]

[1]Institute of Thermomechanics, v.v.i., AS CR, Dolejškova 5, 182 00, Prague 8, Czech Republic

[2]Technical University of Liberec,Studentská 1402, 640 01 Liberec 1, Czech Republic

[a]vlcek@it.cas.cz, [b]martin.stepan@tul.cz, [c]igor@it.cas.cz, [d]kozanek@it.cas.cz

Keywords: aeroelasticity, flutter, interferometry, subsonic flow

Abstract: For the grant of the Grant Agency of the Czech Republic „Subsonic flutter analysis of elastically supported airfoils using interferometry and CFD“ new airfoil model NACA0015 was constructed and manufactured. Profile is divided in five parts and inside is the replaceable elastic element, which enable the pitch angle changes. Inside the body there is also pitch angle sensor and four semiconductor pressure sensors. The second degree of freedom is allowed by the plunge of the structure with the airfoil and centered its position by two feathers with position detected with the magnetic sensor. The whole arrangement of the experiment was described with all details in [2].

Introduction

The experimental device was constructed with idea to generate self-excited motion of the airfoil in subsonic air flow with possibility to change the elasticity of both degrees of freedom and simultaneously enable the optic, mainly interferometric measurements. As a result experiments were made, which verify that the arrangement as a whole is suitable for flutter experiments in subsonic Mach number range. During the experiments, the diapason of both support elasticity parameters was determined, where flutter occurs. The total scheme of the experiment arrangements presented in [2], the view of the test section with an older airfoil model is in [3].

Experimental set-up

The airfoil model with a chord length of 59 mm, thickness 8.85 mm and width of 76.6 mm was divided into five parts, as we can see in Fig.1. The reason of such solution was easy to arrange the relatively complicated system of elastic element and set of sensors, which must be supported on roll bearings, because the lowest damping of the rotational degree of freedom was required. The negligible attenuation of the translational motion was achieved by fixation of the frame with the airfoil on the thin blades.

The photography of the profile taken apart is in Fig. 1. There are two variations of tested springs; one use more elastic winding spring, the other is a torsion spring. The part devoted to the non-contact method of the pitch-angle is described in detail in [1]. It was used the sensor RM08, which is located in a case 3 mm long and with diameter 8 mm. For the pressure measurement on the profile surface four semiconductor absolute pressure sensors MPXH6115A6U - FREESCALE SEMICONDUCTOR with size 7x7x3 mm were used. Sensors are situated on the back-side of airfoil parts always in couples, as we can see in Fig. 1. These sensors will serve for correction of interferometric measurements, which evaluation assumes isentropic flow. For the registration of the plunge of the rotation center of the profile, the contactless magnetic linear sensor LM13TCD40CB10A05 was used; the accuracy of the measurement is 5μ, the length of the plunge detection is not limited

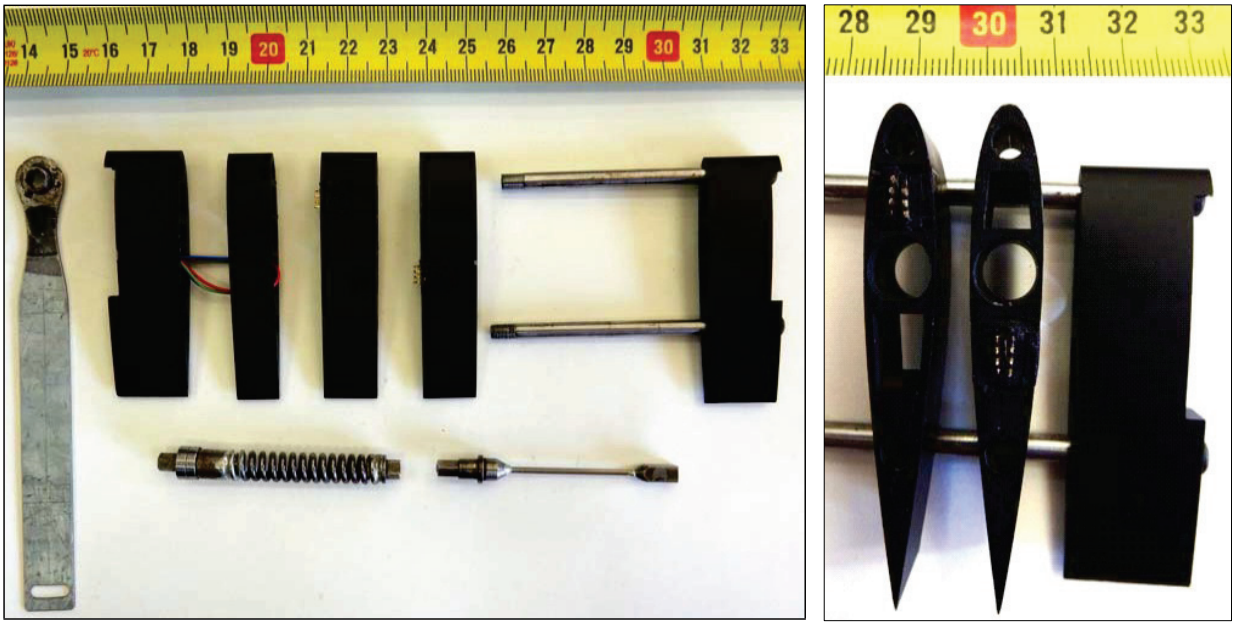

Fig. 1: Details and components of the measured profile: profile weight = 40.5/34 g (with the different axis); the axis of profile rotation is situated in 1/3 of the chord, measured from the leading edge; the instrument situated in the left part of the picture is used for zero position setting of the angle of attack.

Summary

After some corrections realized in the experimental setup construction a study verified, where the aim of the grant was achieved and enhanced stand has main properties suitable for detailed research of the flutter with profile which has pitch and plug degrees of freedom. The main interval of Mach numbers, where flutter occurs, was M = 0.2 – 0.4.

Acknowledgement: The authors gratefully acknowledge the Grant Agency of the Czech Republic for supporting this work under Grant No. 13-10527S „Subsonic flutter analysis of elastically supported airfoils using interferometry and CFD“.

References

[1] M. Štěpán, Měření náklonu profilu při flutteru (Measurement of pitch on a fluttering profile), DYMAMESI 2014 - Proceedings, Prague, November 25-26, 2014, pp. 67-72.

[2] V. Vlček, J. Kozánek, I. Zolotarev, Použití interferometrických měření pro výpočet sil a momentů působících na samobuzeně kmitající profil (The calculation of the forces and moments acting on the fluttering profile using interferometric measurements), Interaction and Feedbacks 2012. Prague 2012, pp. 137-142.

[3] J. Kozánek, V. Bula, I. Zolotarev, Matematický model uložení zkušebního aerodynamického profile (Mathematical model of the support of experimental aerodynamical profile), Interaction and Feedbacks 2010 - Proceedings. Prague 2010, pp. 57-64.

21st International Conference **ENGINEERING MECHANICS 2015**
Svratka, Czech Republic, May 11 –14, 2015
Paper **#079, pp. 352–353**

The Influence of Parameters of Interface Contact Elements of the LSB48 Blade's Computational Model on the Resonant Frequencies of the Bladed Disc

Josef Voldřich[a]*, Jan Lazar[b]

New Technologies – Research Centre, University of West Bohemia, Plzeň, Czech Republic

[a]voldrich@ntc.zcu.cz, [b]jlazar@ntc.zcu.cz

Keywords: contact stiffness, bladed disc, cyclic symmetry, natural frequency

Abstract: To perform the nonlinear vibration analysis of a bladed disc with contacts between blades, the properties of the interface contact elements of the computational model used must be set correctly. In this study, the numerical method is proposed for calculation of the resonant frequencies of the computational model of the bladed disc in case that the so-called "contact stiffnesses" are given. The method is demonstrated for the case of the bladed disc provided with LSB48 blades that comprise two integral contact elements, one in the middle and the second one on the tip of the blade. The values of contact stiffnesses are fitted to get the calculated values of resonant frequencies in accord with the measured ones. The method utilizes the cyclic symmetry properties of the bladed disc.

Introduction

In the works of Petrov and Ewins [1,2], the effective computational method is proposed for the nonlinear vibration analysis of the bladed disc. It utilizes the cyclicity of the mechanical assembly and allows for the modelling of the frictional dampers between blades via dry Coulomb friction model. One of the parameters of the friction model is the so-called "contact stiffness". This is rather a misleading naming since this parameter is not related solely to the physical properties of the contact. It also captures the numerical approximation of the frequency response function of one sector of the bladed disc with all the contact elements omitted, which is pointed out in the work [3]. In the following, we present the method of calculation of natural frequencies of the bladed disc with all contact elements stuck, i.e., in the linear situation with no macroscopic slip, using (i) the values of natural frequencies, (ii) mode shapes and (iii) the values of contact stiffnesses. All the input parameters are the outputs of the model with no contact elements employed.

Mathematical background

Let $\omega_{k,i}$ and $\boldsymbol{w}_{k,i}$ be the i-th natural frequency and the respective mode shape with k nodal diameters of the (cyclically symmetric) bladed disc provided with the N blades with no contact elements. Making use of the cylindrical coordinate system we can write $\boldsymbol{w}_{k,i} = \frac{1}{\sqrt{N}} [1, \mathrm{e}^{\mathrm{j}k\sigma}, \cdots, \mathrm{e}^{\mathrm{j}(N-1)k\sigma}]^T \otimes \boldsymbol{v}_{k,i}$, where $\sigma = -2\pi/N$, $\boldsymbol{v}_{k,i}$ denotes the restriction ("imprint") of the eigenvector $\boldsymbol{w}_{k,i}$ to the reference sector, i.e., to the section of the bladed disc embracing the first blade and the corresponding part of the disc. The $\otimes$ symbol stands for the Kronecker product. The quantities $\omega_{k,i}$ and $\boldsymbol{v}_{k,i}$ are obtained performing the modal analysis of the reference sector

$$-\omega^2 \boldsymbol{M}\boldsymbol{v} + \left(\boldsymbol{K}_0 + \boldsymbol{K}_1 \mathrm{e}^{\mathrm{j}k\sigma} + \boldsymbol{K}_{N-1} \mathrm{e}^{-\mathrm{j}k\sigma}\right) \boldsymbol{v} = \boldsymbol{0}\,. \tag{1}$$

Using this notation, the mass matrix of the entire bladed disc is $\boldsymbol{I}_N \otimes \boldsymbol{M}$ and its stiffness matrix is $\boldsymbol{I}_N \otimes \boldsymbol{K}_0 + \boldsymbol{P}_N \otimes \boldsymbol{K}_1 + \boldsymbol{P}_N^{\mathrm{T}} \otimes \boldsymbol{K}_{N-1}$. Here, $\boldsymbol{I}_N$ stands for the identity matrix and $\boldsymbol{P}_N = [\delta_{i,j-1}]_{i,j=1,\cdots,N}$ ($\delta_{i,0} = \delta_{i,\mathrm{N}}$), for the permutation matrix of the same order N. Note that $\boldsymbol{K}_{N-1} = \boldsymbol{K}_1^{\mathrm{T}}$. Let the contact stiffnesses in the normal and the tangential directions of the α-th contact be denoted as $k_{\mathrm{N},\alpha}$, $k_{\mathrm{T1},\alpha}$ and $k_{\mathrm{T2},\alpha}$, which are the parameters of the computational model [3]. If

there is no slip in the contacts, the model is linear. In such a case, the objective is to calculate the natural frequencies $\omega_{\mathrm{S},k,r}$ and (restricted) mode shapes $\boldsymbol{v}_{\mathrm{S},k,r}$, given the corresponding quantities $\omega_{k,i}$ and $\boldsymbol{v}_{k,i}$ of the system with omitted contact elements. The mode shapes are of the form $\boldsymbol{v}_{\mathrm{S},k,r} = x_{r,1}\,\boldsymbol{v}_{k,1} + \cdots + x_{r,m}\,\boldsymbol{v}_{k,m}$, where the multipliers $x_{r,i}$ and the natural frequencies $\omega_{\mathrm{S},k,r}$ are the solution of the eigenvalue problem

$$\left(-\omega^2 \boldsymbol{I}_m + \left[\omega_{k,i}^2 \delta_{i,j} + h_{k,i,j}\right]_{i,j=1,\cdots,m}\right) \begin{bmatrix} x_1 \\ \vdots \\ x_m \end{bmatrix} = \boldsymbol{0} \tag{2}$$

with

$$h_{k,i,j} = \sum_{\alpha=1}^{2} \boldsymbol{v}_i^{\mathrm{H}}|_\alpha \left(\begin{bmatrix} -1 & \mathrm{e}^{-\mathrm{j}k\sigma} \\ \mathrm{e}^{\mathrm{j}k\sigma} & -1 \end{bmatrix} \otimes \mathrm{L}_\alpha^{-1} \begin{bmatrix} k_{\mathrm{N},\alpha} & 0 & 0 \\ 0 & k_{\mathrm{T1},\alpha} & 0 \\ 0 & 0 & k_{\mathrm{T2},\alpha} \end{bmatrix} \mathrm{L}_\alpha \right) \boldsymbol{v}_j|_\alpha. \tag{3}$$

Here, the matrix L_α transforms the cylindrical coordinate axes to the local coordinate system of the contact α and the $|_\alpha$ symbol indicates the restriction of the vector to the one containing the degrees of freedom of the contact element only.

Results for the LSB48 blade - example

Consider the case that the contact in the middle of the LSB48 blade (tie-boss) is stuck and the tip contact (shroud) is free. For such a configuration, the dependency of the normalized first natural frequency with $k = 0$ and $k_{\mathrm{N},2} = 5 \times 10^4$ N/mm on the value of $k_{\mathrm{T1},2} = k_{\mathrm{T2},2}$ is plotted in Fig. 1. In Fig. 2 the same is plotted for $k_{\mathrm{N},1} = 10^4$ N/mm, $k_{\mathrm{T1},2} = k_{\mathrm{T2},2} = 6.5 \times 10^4$ N/mm and both contacts stuck. Moreover, the impact of the number, m, of the mode shapes employed on the values of calculated natural frequencies is depicted in the figures.

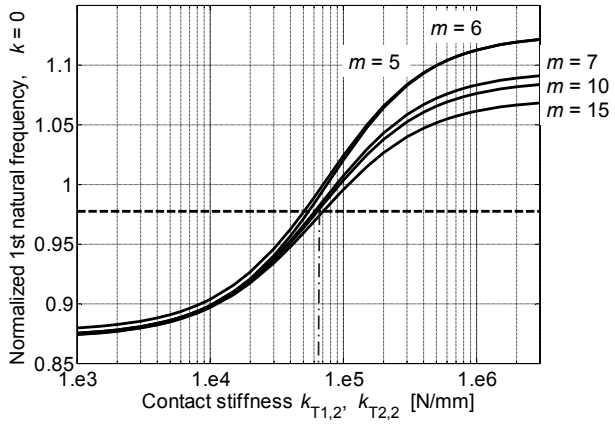

Fig. 1: Normalized first natural frequency, $k_{\mathrm{N},2} = 5 \times 10^4$ N/mm.

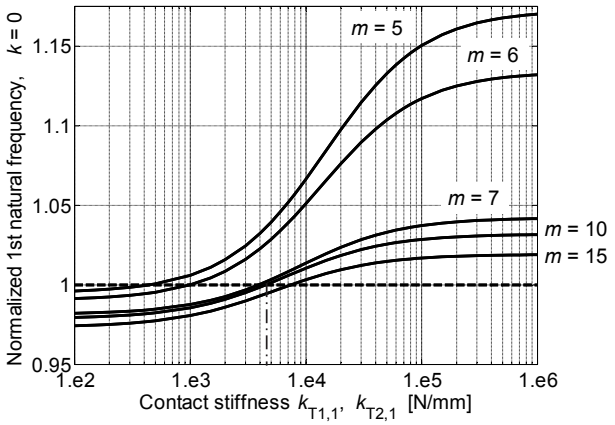

Fig. 2: Normalized first natural frequency, $k_{\mathrm{N},1} = 10^4$ N/mm, $k_{\mathrm{T1},2} = k_{\mathrm{T2},2} = 6.5 \times 10^4$ N/mm.

Acknowledgement: The work originated in framework of solution of the "Centres of Competence" program of the Technology Agency of the Czech Republic, project number TE01020068.

References

[1] E.P. Petrov, A method for use of cyclic symmetry properties in analysis of nonlinear multiharmonic vibrations of bladed disks. ASME J. Turbomachinery 126 (2004) 175–183.

[2] E.P. Petrov, D. Ewins, Analytical formulation of friction interface elements for analysis of nonlinear multiharmonic vibrations of bladed disks. ASME J. Turbomachinery 125 (2003) 364–371.

[3] J. Voldřich, P. Polach, J. Lazar, T. Míšek, Use of cyclic symmetry properties in vibration analysis of bladed disk with friction contact between blades. Procedia Engineering 96 (2014) 500–509.

21st International Conference **ENGINEERING MECHANICS 2015**
Svratka, Czech Republic, May 11 –14, 2015
Paper **#135, pp. 354–355**

Study of Water Jets Collision of High Pressure Flat Jet Nozzles for Hydraulic Descaling

H. Votavová[a], M. Pohanka[b]

Heat Transfer and Fluid Flow Laboratory, Faculty of Mechanical Engineering,
Brno University of Technology (BUT), Technická 2896/2; 616 69, Brno; CZ

[a]votavova@lptap.fme.vutbr.cz, [b]pohanka@fme.vutbr.cz

Keywords: descaling, hydraulic hot rolling, scales, pressure distribution, erosion, measurement, surface quality

Abstract: One of the most effective methods for descaling hot-rolled steel products is performed using high pressure flat jet nozzles. These descaling nozzles are arranged in rows in hot rolling mills and are set in such a way that each adjoining pair of nozzles creates an overlapping area of water jet streams. Good homogeneity of the pressure distribution over the width of the hot-rolled plate is often used as an indicator of quality of the homogeneity of descaling. The presented laboratory measurements examine one pair of adjoining nozzles with a particular focus on the pressure distribution in the overlapping area. This paper deals with one particular setting of a pair of descaling nozzles with zero offset angles for the jet streams. A measured pressure distribution and an outcome of an erosion test on an aluminum plate are presented and discussed. The erosion test shows that spots with higher pressures do not necessarily result in a higher amount of taken material during an erosion test. The erosion test differs from the expected outcome in such a way as to warrant a detailed discussion of this phenomenon with possible explanations outlined.

Introduction

Steel production is indivisible from very hot surfaces in many cases. Hot steel reacts with oxygen in the surrounding atmosphere and unwanted scales are formed on the surface. Hydraulic descaling using high pressure flat jet nozzles is very effective for removing these scales. A row of nozzles must be used for larger products. This paper explores the overlapping area where water from two adjoining nozzles interacts due to the zero offset angles. Tested configuration was as follows: EVERLOY DNM04835 nozzle type, 55 mm spray height, 43 mm nozzle pitch, 40 MPa water pressure, 15° inclination angle, 0° offset angle. The pressure distribution measurement and erosion test are commonly used for descaling nozzle efficiency studies. However, it was found that the pressure distribution may not be in accordance with erosion tests.

A pressure distribution measurement was performed on a flat test plate equipped with a pressure sensor with 1 mm in diameter. The sensor moves in the X/Y direction under spraying nozzles and measures the position-dependent pressure. The measured data is slightly blurred due to the nonzero size of the sensor. The outcomes of the pressure experiments are presented in Fig. 1. It includes the pressure distribution for nozzles measured separately, together and with the algebraic sum from single sprays.

An erosion test was performed on an aluminum plate (A1050). The plate was exposed to the water jet streams for 10 seconds. Part of the aluminum was sprayed away and a hole in the plate was created due to the high impact of water. A 3D scan was done to obtain a computer model of the excavated hole. The maximum depth of the hole was taken in the dimension perpendicular to the length. A similar maximum was taken for the pressure distribution. Both maxima are compared in Fig. 2.

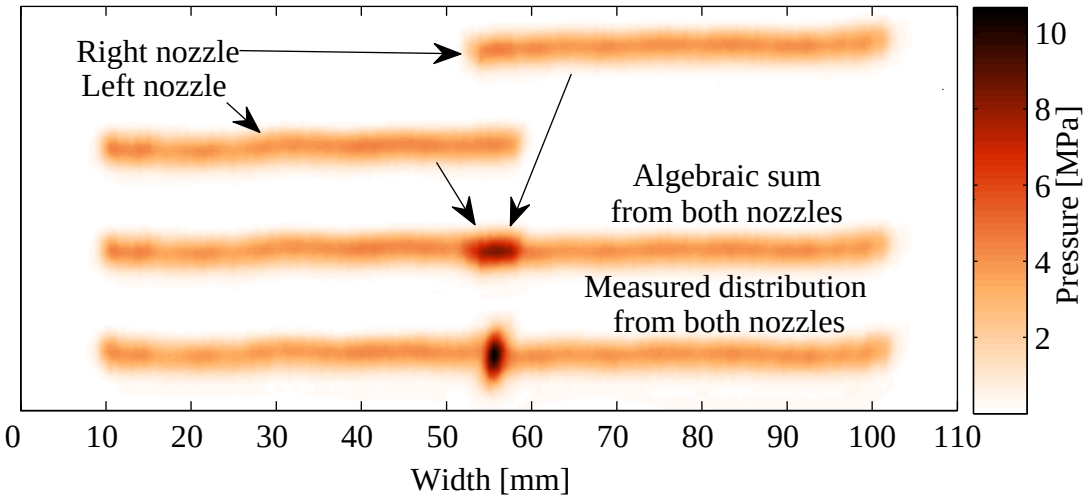

Fig. 1: Pressure distributions of the nozzles

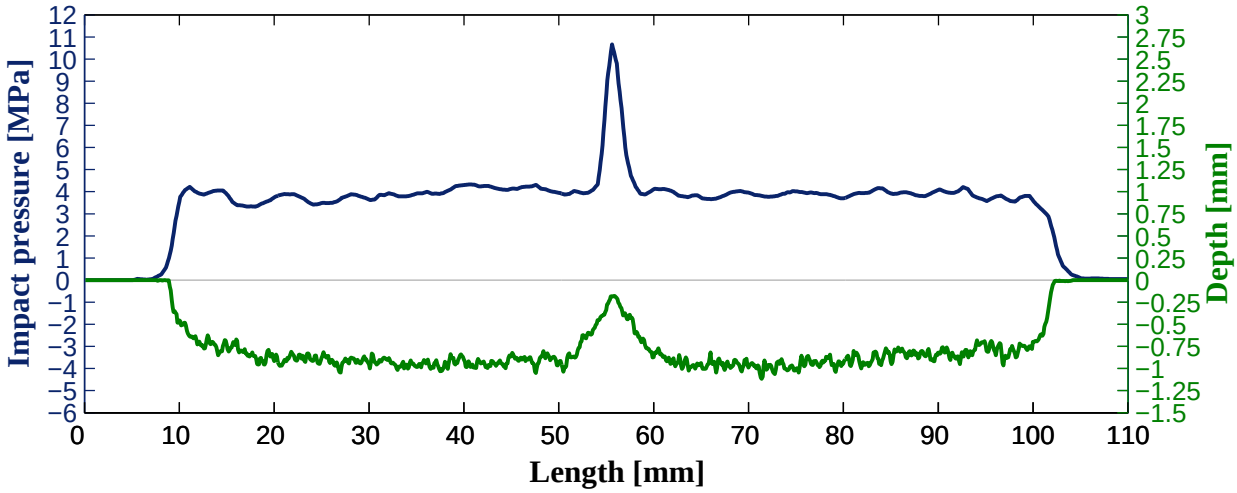

Fig. 2: Pressure distribution vs. erosion test

Conclusion

The pressure distribution change in the overlapping area is evident. Impacting water creates higher pressure in the middle of the overlapping area than what could be expected just from the algebraic sum from single sprays. Whereas the maximum pressure of the algebraic sum is 8.4 MPa, the maximum pressure of the adjoining configuration is 10.66 MPa. Although the pressure in the overlapping area reaches its maximum, the erosion for the same position is minimal. An important observation is that the erosion test reflects only the mechanical effect of the descaling and does not say anything about the thermal effects on the scales. This indicates a substantial change of the character of the stream and supports the statement in [1] that "pressure is not a measure of descaling effectiveness".

Acknowledgement: This work is an output of research and scientific activities of this project LO1202 and the internal grant of the Brno University of Technology focused on specific research and development No. FSI-S-14-2437 with financial support of the MEYS under the programme NPU I.

References

[1] D. Blazevic, Hot strip mill operation. Vol. VI: Descaling, Sun Lakes, Arizona, U.S.A., 2008.

21st International Conference **ENGINEERING MECHANICS 2015**
Svratka, Czech Republic, May 11 –14, 2015
Paper **#098, pp. 356–357**

Acoustic Emission Localization in the Dynamic Fatigue Testing of a Composite Wing

Martin Weis, Jakub Cejpek, Jaroslav Juračka

Institute of Aerospace Engineering, Faculty of Mechanical Engineering,
Brno University of Technology, Brno, Czech Republic

Keywords: Acoustic emission localization, nondestructive testing, monitoring, acoustic emission detection.

Abstract: Acoustic emission (AE) is current trend of non-destructive monitoring methods. It suits perfectly for supporting of fatigue tests. Method is also applicable in monitoring of quasi-static tests. AE helps the engineers to understand the degradation process in the tested object and also keep track of the failures. Article offers an insight into the practical experience with acoustic emission. Tests of three different composite structures (wing, fuselage and hull panel) were chosen to illustrate the application of AE monitoring system during fatigue and quasi-static tests. These tests have shown that accuracy of localization is sufficient to identify damaged areas. Moreover the system may offer an early warning of upcoming failure.

Method used and described in this article is the *"passive acoustic emission detection"*. This means, that the sensors, attached to the tested structure, were "listening" to the emissions produced (emitted) by component due to the external loading. This external force builds the level of elastic energy in the structure, which is released afterwards as the sound and heat energy. The released energy travels through the structure with certain speed, specific to each material.

Gain the experiences

The most important aspect of using acoustic emission for monitoring is about experience. Using AE for different test, conducted at the Institute of Aerospace Engineering (IAE), led to different applications. Important steps prior each test is to measure the speed of sound (speed of wave propagation), damping characteristics and accuracy. Choosing the type of localizations is important decision. For some tests the linear localization is sufficient, some tests will benefit from planar localization. The type of localization depends on the experience and requested results. In fatigue tests, linear localization is used for preliminary measuring and identifying the most critical areas. These critical areas can be monitored in more detail by additional sensors (both types of localization are possible: denser linear, or planar).

Clearly, the luxury of identifying the critical areas belongs to fatigue tests only. Considering static strength tests is different case.

Quasi - static test

Acoustic emission analysis has been used for a quasi-static test of the in-house built VLA category airplane, the VUT 061 Turbo. In this case, the results were huge success, because the AE identified the same problematic area as the finite element analysis has predicted. Acoustic emission analysis has proven to be really accurate in identifying the areas, where the foam core collapsed. Moreover it discovered the exact point of the final failure initiation and linked this event with the loading level.

Fatigue test

Fatigue tests are recognized by international authorities as a proof, that the tested product ensures either safe life or provides time to discover any problems without endangering the user. The object of these tests can be whole assemblies, such as wings or fuselage, or just single parts or representation of parts (laboratory samples).

A total of four wing segments were tested at the IAE since 2008. These tests were an inspiration for using the acoustic emission analysis for monitoring of the test process. There was a hope that it would be possible to predict and track failures in the composite structural parts.

The acoustic emission is easily applicable on the composite wing under fatigue tests. It offers quite accurate structural-health monitoring. The drawbacks are mostly in the need for experienced personnel and – in case of long fatigue tests – huge data storage and computer processing capacity.

As it turned out, it takes a very experience engineer to immediately recognize the upcoming failure. Some indications of upcoming failure are easily hidden in the amount of data. Other failures, like loosened bolts are very easily detectible even for a novice.

The series of four wings fatigue tests was preceded by a series of 5 static tests as a part of airworthiness certification (first in 2004). First fatigue test (specimen #6) ran in period from September 2007 till April 2008. As it was the first fatigue test of its kind at the institution, all parameters had to be defined and the experience to be gained. After two segments were tested, other changes in the design were made and sample #8 has been tested under static loading in February 2010 (sample #8 was a full scale wing). AE has been involved in this static test; however the results were inconclusive for unpredicted area of failure.

Since January 2013 until august 2014, wing segment #9 has been tested. This test will be discussed further in this article.

21st International Conference **ENGINEERING MECHANICS 2015**
Svratka, Czech Republic, May 11 –14, 2015
Paper **#235, pp. 358–359**

Determining the Distribution of Forces in Reinforcing Bars in Slab-Column Connections of Reinforced Concrete Structures

Barbara Wieczorek

Department of Theory of Building Structures, Faculty of Civil Engineering,
Silesian University of Technology, Akademicka 5 st.,44-100 Gliwice, Poland

barbara.wieczorek@polsl.pl

Keywords: reinforced concrete structure, slab-column connections, experimental research, theoretical model of calculation

Abstract: The behaviour of reinforced concrete slab-column structures under the impact of accidental loading is very significant due to safety reasons. The failure of the support zone by punching and lack of proper structural integrity reinforcement can lead to a progressive collapse. However, the instructions on how to prevent such situations are not very detailed. According to the guidelines of standard EC2, the structural integrity reinforcement should be continuous throughout the length and consist of at least two bars above the column in each perpendicular direction. The article presents a theoretical model of calculation that permits a more detailed analysis of internal forces in reinforcing bars located directly above the column. Adopting a solution in the form of exact equations makes it possible to take into account the influence of a non-linear change of the bar rigidity and considerable deflections. The calculation model is based on the results of the experimental investigations.

Introduction

The designing of slab-column connections in reinforced concrete structures requires the application of proper reinforcement in the support zone. In case of the failure of this zone by punching the upper reinforcement is detached off the slab, causing it to fall down. One of the options to counteract this kind of situation is introducing an additional bottom reinforcement in the form of bars passing directly above the column. The primary aim is to counteract the possibility of a progressive collapse in case of a local damage of the structure. Current standards do not directly state any guidelines in this issue, pointing only at the necessity of using this type of reinforcement.

In order to investigate the problem in more detail, a research was conducted including a detailed analysis of phenomena occurring in connections of this type. The research included full-scale models constituting a part of the reinforced concrete structure [1].The numerical analysis of this range was presented in [2].

Description of the problem

During the research [1] an actuator was used to impose a load of the force P in the middle of the span of the bar L. After that the induced vertical deflections f of the bar were measured. The deflections depend not only on the dimensions of the bar, the material properties, the way of mounting the ends of the bar and the value of the load. As a result of deflection, the centre line of the bar becomes elongated. For this reason the value of deflection f depends also on the value of force N, causing the tensioning of the bar. In case of considerable deflections the value of force N is significant and cannot be neglected in the calculations.

The conducted experimental investigations primarily revealed the necessity of modifying axial forces and bending stiffness of the bars. This is a problem of considerable importance. Such detailed analysis of the changes in internal forces in the bar in the course of its deformation is possible only in theoretical methods and numerical calculations.

Description of the method

The observation of the behaviour of the reinforcing bar during the experimental investigations was the basis adopting a substitute static scheme (Fig.1). The differential equation of the deformed axis of the bar subjected to tension with force N and the transverse load P has the form Eq. 1. The solution of Eq. 1 taking into account the boundary conditions is presented in Eq. 2. Assuming the load of value P corresponds to a deflection of value f, the dependence Eq. 2 is the basis for obtaining Eq. 3. The value a obtained from this Eq. 3 allows to determine the axial force $N=EI\,a^2$ in a deflected bar.

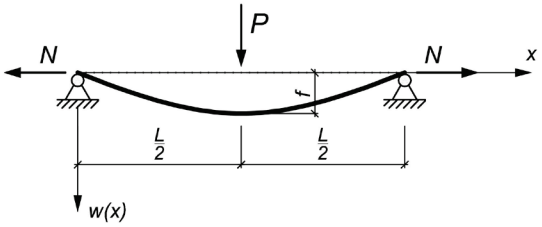

Fig. 1: Static scheme

$$EI\frac{d^4w}{dx^4} = N\frac{d^{42}w}{dx^2} \tag{1}$$

$$w(x) = \frac{P}{2EI\,a^2}\left(x - \frac{1}{a}\frac{sinh(ax)}{cosh(aL/2)}\right), \quad a = \sqrt{\frac{P}{EI}} \tag{2}$$

$$\frac{4EI\,f}{P\,L}a^3 - a + \frac{2}{L}tanh(aL/2) = 0 \tag{3}$$

Calculation

The calculations were conducted on the basis of the introduced dependences (2) and (3) for a bar with the diameter 16 mm and length of L=2.4 m. The dependence between the applied load P and the deflection f corresponding to it (Fig.2) was adopted in accordance with the results of the experimental investigations [1]. Additionally, each stage of the calculations incorporates a non-linear change in stiffness EI in accordance with the material tests [2] (Fig.3). The graph illustrating the changes in the value of the force N at each level of the load is presented in Fig.4.

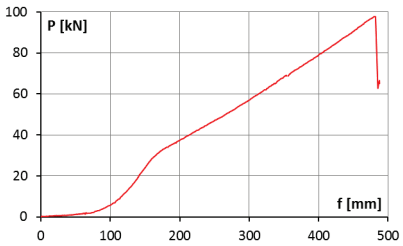

Fig. 2: Dependence P-f [1]

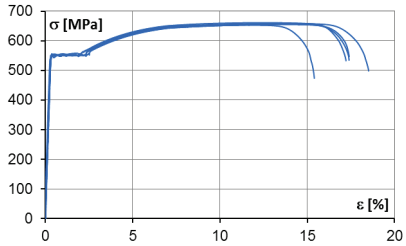

Fig. 3: Dependence σ–ε [2]

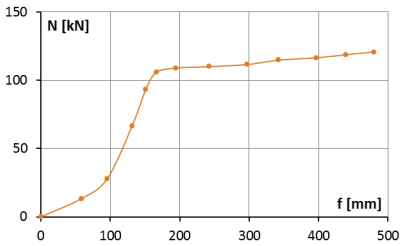

Fig. 4: Dependence N-f

Summary

The developed method of theoretical determination of distribution of internal forces in a reinforcing bar in the course of its loading leads to the results presented in the form of equations. In the case of considerable deflections an additional tensile force N associated with the elongation of the bar is present. This force should be taken into account in the calculations. The presented solution permits to directly calculate the sought force N. Moreover, the solution takes into account a non-linear change in the bending stiffness of the bar which has a significant impact on the value of the force N, especially in the case of minor spans of the bar. The conducted calculations suggest a correlation between the imposed load P and the tensile force N.

References

[1] B. Wieczorek, Idea of a simplified model to determination of the load capacity of and inner slab-column connection after its punching, Procedia Engineering, 65 (2013) 126–134.

[2] B. Wieczorek, Load-bearing capacity of reinforcing bars in the zone of the slab-column connection determined experimentally and in the result of numerical calculations, Procedia Engineering, 65 (2013) 149–157.

21st International Conference **ENGINEERING MECHANICS 2015**
Svratka, Czech Republic, May 11 –14, 2015
Paper **#236, pp. 360–361**

Numerical Model on the Example of Experimental Investigations of a Punching in the Central Connection of the Slab with the Column Situated Eccentrically

Barbara Wieczorek

Department of Theory of Building Structures, Faculty of Civil Engineering,
Silesian University of Technology, Akademicka 5 st.,44-100 Gliwice, Poland

barbara.wieczorek@polsl.pl

Keywords: reinforced concrete structure, punching, slab-column connections, experimental research, numerical modelling

Abstract: The topics of punching in slab-column connections of reinforced concrete structures are particularly important due to the safety of their exploit. The paper presents a spatial numerical model of connection between the slab and the column, where the column is situated eccentrically to the surface of the slab. The geometric and material parameters adapted in the numerical model were the same as in the experimental model. The numerical model bases on predefined material models of steel and concrete, taking into account non-linear dependences of the strength of these materials. The obtained results of calculations based on a numerical model have been compared with results of experimental investigations.

Introduction

In the light of previous studies, the design principles of support zones of the slab-column structures have been developed. However, the work of this type of structures in the range of loads close to destructive loads needs to be precisely understood due to their consequences for the safety of people. The primary aim is to prevent the possibility of progressive collapse in the event of a local damage of structure. Some suggested solutions in this scope have been mentioned only in Model Code 2010, ACI 318 and CSA A23.3.

The current development of computer methods aided the calculations using finite-element method and allows a more precise determination of internal forces in the support zone, where bending moments and shear forces are concentrated. In order to determine the value of the load capacity of the support zones to puncture, the numerical model of the slab and column connection was developed. Apart from the two parallel reinforcing meshes at the upper and bottom surface of the slab, additional bottom reinforcing bars crossing directly over the column have been used, according to recommendations [1].

Description of the numerical model

The numerical model has been developed on the basis of experimental research [2] concerning the central slab-column connection in which an extra recommended reinforcement securing the structure against a failure has been installed. The test model (Fig.1) consisted of a 20 cm thick square slab with the dimensions 2.65×2.65 m and 50 cm high bottom square-section column with the dimensions 40×40 cm. The reinforcement of the model consisted of the two parallel reinforcing meshes at the upper and bottom surface of the slab. A detailed description of the model and the test stand along with the test course description can be found in paper [2].

The numerical analysis was conducted using the *ANSYS* system. The numerical simulation of the slab-column connection has been conducted using Solid65, 8-node 3D finite elements. In the conducted analysis the behaviour of concrete was described using a multi-parameter material model Concrete. The model of slab reinforcement has been developed in a discrete way using 2-node bars Beam188. In order to reflect the behaviour of reinforcing steel a non-elastic model

with isotropic reinforcement has been applied. The parameters of the model have been described using von Misses criteria. The analysis assumes a full cooperation between linear reinforcement elements and 3D concrete elements by assuming the compatibility of the displacement of the nodes. The parameters of concrete and steel models have been applied on the basis of material tests which can be found in [2], [3].

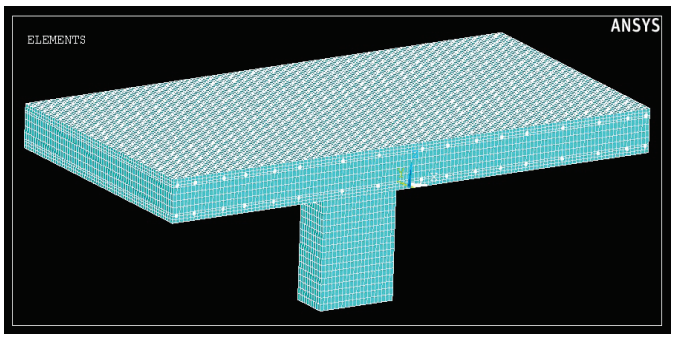

Fig. 1: View of the cross section in the numerical model – ½ of the model

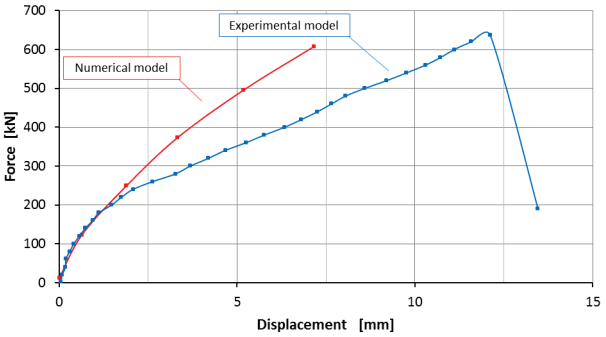

Fig. 2: Values of vertical displacements in the centre of slab in the function of the load

Synthesis of the results

The numerical simulations reflecting the laboratory tests of the model presented in paper [2] allowed to obtain, e.g., a comparison of values of the vertical displacement of the upper surface. Fig. 2 presents the comparison of the load-displacement relationship obtained through a numerical simulation with an experimental curve. It can be observed that theoretical prediction of the limit load of 607.7 kN is fairly consistent with experimental results where the punching force was 637.2 kN.

Summary

Despite small differences obtained during experimental research and numerical analysis it can be stated that numerical simulation allows to represent the existing knowledge about punching. The obtained quantitative results are similar to previous strength analyses. The 4.6% difference between values of the forces can arise from the lack of a perfect mapping of mechanical parameters of concrete and steel. The numerical simulation represents a considerably higher stiffness than in the real experimental model. Therefore depending on the level of load values, the significant differences in the value of displacements for both models were obtained.

References

[1] ACI-ASCE Committee 352, Recommendations for design of slab-column connections in monolithic reinforced concrete structures, 1988.

[2] B. Wieczorek, Influence of the location of the column on the load capacity of a slab-column connection for the inner column after punching, Procedia Engineering, 57 (2013) 1251–1259.

[3] B. Wieczorek, Numerical model and the geometrical and material imperfection of the test model on the example of experimental investigations of a punching in the central connection of the slab with the column, in: 12th International Conference ”New Trends in Statics and Dynamics of Buildings”, Bratislava, Slovakia, October 16-17, 2014.

21st International Conference **ENGINEERING MECHANICS 2015**
Svratka, Czech Republic, May 11 –14, 2015
Paper **#237, pp. 362–363**

Attempt of Numerical Mapping of a Real Model of Slab-Beam Connection Using the Simplified Shell Model

Miroslaw Wieczorek

Department of Building Structures, Faculty of Civil Engineering,
Silesian University of Technology, Akademicka 5 st.,44-100 Gliwice, Poland

miroslaw.wieczorek@polsl.pl

Keywords: reinforced concrete structure, slab-beam-column connections, numerical modelling.

Abstract: A great advantage of computer calculations is the opportunity to map the whole floor, including the supporting beams, columns and walls, in one model, with the elements fully cooperating with one another. In this way the need for a strenuous compiling of the loads on supporting elements and independent searching for extreme values becomes eliminated. As a separate part of a floor, in this case a beam is appears occasionally. Beam mapping in a model can have various forms. The paper presents a comparison of the influence of the way in which a rib is modelled on the results of statistical calculations. As a reference point for substitute shell models a solid spatial model was adopted.

Introduction

In order to determine the most adequate way of modelling the behaviour of a beam element in a beam-and-slab floor, several different spatial floor models have been developed in a computer programme. The exemplary dimensions of a spatial model are visible in Fig. 1. The models were prepared with 8-node solid elements with the dimensions 2.0×2.0×2.0 cm. Simplified models were prepared using shell and bar elements. During the analysis the following substitute models were proposed:

1. The floor was modelled with shell elements only (Fig. 2a).
2. The floor slab was cut off the beam on the edge of the horizontal contact beneath the slab surface and connected using rigid elements fastened in the axis of the slab (modelled with shell elements) and the axis of the cut-off beam (also modelled with shell elements). It was assumed that cross dimensions if each such rigid element are 1.0×1.0 m^2 (Fig. 2b).
3. The floor slab was cut off the beam on the edge of the horizontal contact beneath the slab surface and connected using rigid elements fastened in the axis of the slab and the axis of the cut off beam, as in point no.2; however, instead of the beam modelled with shell elements, at the end of the stiff bars a bar was placed with the dimensions $\boldsymbol{b_w}$×$\boldsymbol{h}$. It was assumed that cross dimensions of each such rigid element are 1.0×1.0 m^2 (Fig. 2c).
4. Along the rib axis, a bar was inserted in the slab with stiffness calculated according to the standard guideline for T-shaped cross-sections – (actual height of the rib, the cooperating slab b_{eff} width consistent with standard guidelines) (Fig. 2d).
5. The slab in the spot of the rib was thickened to $\boldsymbol{h'}$, so that it its stiffness corresponds to the stiffness calculated for the rib in point no.4 (Fig. 2e).
6. The slab was thickened in the spot of the rib in accordance with the real height of the rib (Fig. 2f).
7. The thickening was adopted as in point no.6 with the change of the material parameters, so that the flexural and torsional stiffness of the beam were compliant with the standard guidelines of the model, as in point no.4 (Fig. 2g).

During the simulation the analysis of the following parameters was conducted: the length $\boldsymbol{l}$ of the beam, the spacing $\boldsymbol{a}$ of the beams, the thickness $\boldsymbol{h_p}$ of the slab, and the height $\boldsymbol{h_b}$ of the beam.

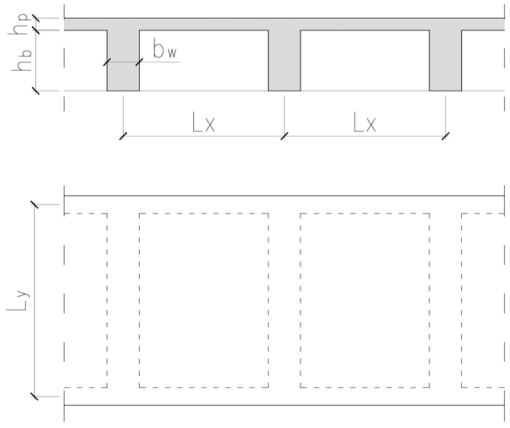

Fig.1: View of the plan and cross section in the numerical model

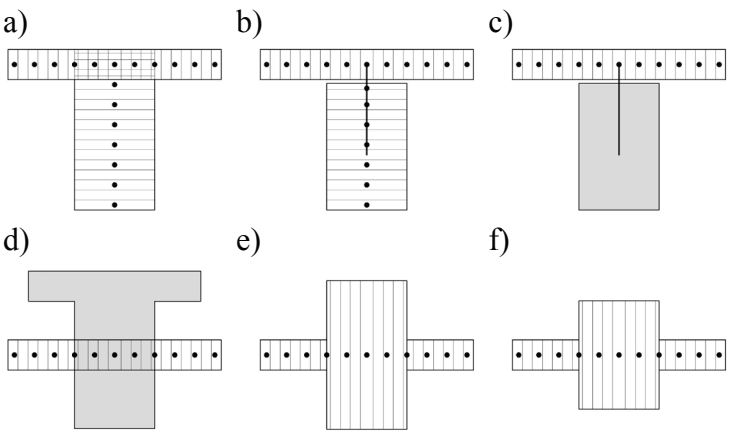

Fig. 2: Suggested simplified models

Synthesis of the results

The shell model (Fig. 2a) is a rather faithful mapping of the actual situation. What is inconsistent about the model, apart from adopting the isotropy and the linear elasticity of the material, is reciprocal overlapping of horizontal and vertical shell elements that occurs on a certain length. Due to a considerable width of the cooperating slab this impact is minor and usually neglected in calculations. The obvious advantage of approximating the beam using a bar (Fig. 2d) in the 2D floor model is faithfulness to the standard guidelines concerning the stiffness of the beam. Simultaneously, the disadvantage of this type of modelling is the impossibility to calculate the loading of the construction with its dead weight on the basis of the construction volume, as well as difficulties with taking into account the increased stiffness of the slab on the beam area. The advantage of thickening the slab to the beam dimensions (Fig. 2f) is the opportunity to directly determine the dead weight of the construction and direct stiffening of the slab above the beam. The indisputable disadvantage lies in a simultaneous decrease of the flexural and torsional stiffness in relation to the reference model which is a solid model.

Summary

Numerical modelling of buildings is always a compromise between the accuracy of mapping, the opportunities offered by a particular programme, the time of calculations, and the expected results. Modelling using volumetric elements always constitutes a far better source of results than shell or shell-bar models. The conducted calculations confirm the argument stating that modelling of internal floor beams that work unidirectionally is not connected with a significant error in calculation of the bending moments, as the beams are treated as local thicker elements of the floor and their value is consistent with the actual height of the beams. The obtained conclusions apply only to models with traditional proportions of slab and beam dimensions.

References

[1] W. Starosolski, Computer modeling of concrete structures engineering, Publishing house of Silesian University of Technology, Gliwice, 2013. (in Polish)

21st International Conference **ENGINEERING MECHANICS 2015**
Svratka, Czech Republic, May 11 –14, 2015
Paper **#238, pp. 364–365**

Proposed Way of Calculating the Value of the Failure Load in the Span Zone of Slab-Column Structures

Miroslaw Wieczorek

Department of Building Structures, Faculty of Civil Engineering,
Silesian University of Technology, Akademicka 5 st.,44-100 Gliwice, Poland

miroslaw.wieczorek@polsl.pl

Keywords: reinforced concrete structure, slab-column connections, slab-column construction

Abstract: In a properly designed slab-column structure the failure of the floor should be signalled by scratches and significant and visible deflections of the floor in the spans. The paper presents two proposed ways of calculating a uniform loading causing the destruction of the central field of a typical slab-column structure. The values obtained in the ultimate state were compared with the value of the load obtained during the experimental research.

Introduction

One of the main factors causing the failure of the slab-column structures is the phenomenon of punching. The threat of such failure can occur in the case of a support zone lacking a transverse reinforcement. The stronger reinforcement over the support is, the higher becomes the threat of a brittle destruction. To be able to utilize the load capacity of the slab reinforcement, the construction must have a guaranteed protection of the structure against a brittle destruction by punching among the columns. In order to determine the limit of the load capacity of a flat slab, two mechanisms of its destruction have to be considered. The first assumes that the destruction of the area of the floor slab can occur in the course of unidirectional fracture (Fig. 1a). In the second mechanism it is assumed that individual slabs can be destroyed independently (Fig. 1b). The first destruction model (Fig. 1a) assumes the following conditions of equilibrium:

$$0{,}125 \cdot q \cdot l_y \cdot \left(l_x - c_x\right)^2 \le f_{yd}\left(A_{s,prz} \cdot z_{prz} + 0{,}5 \cdot A^P_{s,pod} \cdot z^P_{pod} + 0{,}5 \cdot A^L_{s,pod} \cdot z^L_{pod}\right) \tag{1}$$

c_x, c_y – the width of the support,

$A_{s,prz}$ – the cross section area of the bottom reinforcement of the central part of the span along its width;

$A^P_{s,pod}, A^L_{s,pod}$ – the cross section area of the upper reinforcement above the left and right support;

$z_{prz}, z^P_{pod}, z^L_{pod}$ – the arm of internal forces in the centre of the span, and above the right and left support.

The second destruction model (Fig. 1b) assumes the following conditions of equilibrium:

$$\frac{q \cdot l_x \cdot l_y}{8}\left(\frac{l_x + l_y}{2} - 2c + \frac{4}{3}\frac{c^3}{l_x \cdot l_y}\right) \le \frac{f_{yd}}{2}\left(z_{prz} \cdot \left(A_{s,prz,x} + A_{s,prz,y}\right) + \left(A_{s,pod,x} + A_{s,pod,y}\right) \cdot z^P_{pod}\right) \tag{2}$$

$A_{s,prz,x}, A_{s,prz,y}$ – the cross section area of the bottom span reinforcement in the central part of the span, working in directions x and y and summarized from the entire width of the span;

$A_{s,pod,x}, A_{s,pod,y}$ – the cross section area of the average upper support reinforcement of two supports for directions x and y and summarized from the entire width of the span;

z_{prz}, z_{pod} – average arm of internal forces for the span and support respectively.

Description of the experimental model

In order to verify the presented formulas the laboratory research of the central part of a slab-column floor with the dimensions 3000×3000×100 mm has been conducted (Fig. 2). The model loading was induced with a set of hydraulic actuators of the load range up to 4.0 T. The substitute value of the uniform variable load was 69.76 kN/m^2 above the dead load of the investigated element. In the initial phase of the conducted research two distinct directions of scratches in the bottom surface of the investigated element were observed:

- latitudinal scratches propagating in the form of concentric circles relative to the centre of the model,
- meridional scratches propagating in the form of straights lines beginning in the centre of the model.

From the value of load equal to ca. 60% of the maximum load on the lower and upper surface of the model an image of a scratch consistent with Fig. 1b started to emerge.

Fig. 1: Patterns of destruction of the internal area of a continuous slab (described in the text)

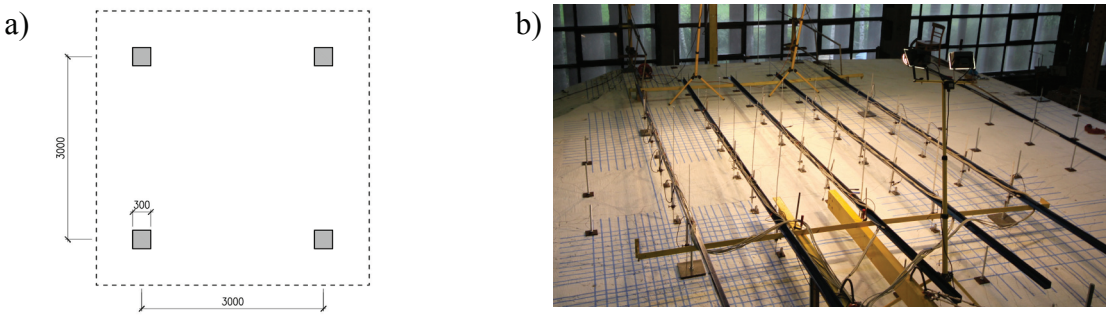

Fig. 2: Test model: a) the dimensions of the model, b) view of the model

Summary

Reinforced concrete slab-column structures are very often used in municipal, industrial and service buildings. Their improper utilization or improper way of building can lead to their destruction through the emergence of punching in support zones or rupturing of the reinforcing bars in the centre of the slab. The value obtained in the course of the loading was significantly higher than the value of loading obtained on the basis of the presented formulas. Such considerable difference results from the change of the behaviour of the test element. At zero or a small deflection of the central area of the tested element in cross-section only bending moment occurs (flexural work of element). With the increase of deflection in cross-section an additional membrane forces also appear (tension work of element).

References

[1] M. Wieczorek, Influence of amount and arrangement of reinforcement on the mechanism of destruction of the corner part of a slab-column structure, Procedia Engineering, 57 (2013) 1260–1268.

[2] J. Kobiak, W. Stachurski, Concrete construction, fifth ed., Arkady, Warszawa, 1987.

21st International Conference **ENGINEERING MECHANICS 2015**
Svratka, Czech Republic, May 11 –14, 2015
Paper **#068, pp. 366–367**

Numerical Simulation of Aerodynamic Forces Which Have an Impact on the Pantograph

Paweł Wątroba

Silesian University of Technology, Faculty of Mechanical Engineering, Department of Theoretical and Applied Mechanics, 44-100 Gliwice, Konarskiego 18A, Poland

pawel.watroba@polsl.pl

Keywords: pantograph, numerical simulation, aerodynamics, fluid mechanics, ANSYS CFX

Abstract: The paper presents the process of creation of a numerical model, designed for determination of the aerodynamic forces which have an impact on the pantograph. Numerical analyses were carried out in ANSYS CFX environment. The object of the study was the author's original concept model of pantograph. The values of aerodynamic forces have been computed for different velocities and heights of pantograph elevation. Furthermore, the model allowed to specify percentage of the individual elements of the pantograph on the total drag force. The values were determined by a special algorithm, which was implemented in a dynamic model of the pantograph.

Introduction

Nowadays, the development of high-speed rail causes the maximum speed increase. At the moment, the speed record of conventional high-speed train is 574.8 km/h. The record was established by the French train TGV. This is an impressive result, but the majority of high-speed railways in Europe is designed for speeds between 200-300 km/h. The railway which can reach the speed above 300 km/h appears only in Spain and France.

Developing such a high speed by trains, which receive electricity from overhead catenary traction causes a number of problems associated with the current reception. The aerodynamic force has strong impact on the proper work of pantograph and disturb the flow current. Definition of the aerodynamic force is necessary when the interaction between pantograph and catenary is modeled.

Research facility

The pantograph is a multibody construction, which changes height of elevation depending on working conditions. Changing the elevation of the pantograph also affects the change of the cross section and the drag coefficient in the pantograph.

This behaviour requires the calculation of the aerodynamic force for different elevations of the pantograph and to determine the coefficient of drag for these values. Numerical analyses were carried on the author's original concept model of pantograph. (Fig. 1.).

Fig. 1: The author's original concept model of pantograph

Results

Numerical analyses were carried out in ANSYS CFX environment for three heights of elevation: 1000 mm, 2000 mm, and 3000 mm. The results are presented in Fig. 2.

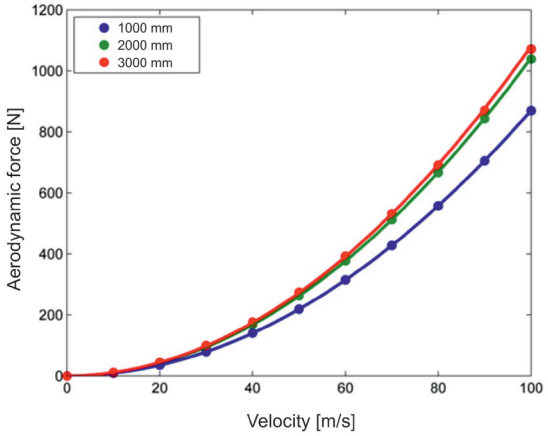

Fig. 2: Values of the aerodynamic force acting on pantograph

The aerodynamic force which acts on pantograph depends on heights of elevation of the pantograph. This dependence is non-linear and it is associated with the change of the surface which the force acts.

In addition to the determination of total aerodynamic force, the influence of the air flow on the individual components of the pantograph is summarized in Table 1 as percentage of the total force.

Tab. 1: Percentage of the total aerodynamic force for selected items

Heights of elevation pantograph [mm]	Pantograph Head	Lower Arm	Upper Arm
	Percentage of total aerodynamic force		
1000	83%	19%	6%
2000	62%	24%	4%
3000	57%	32%	10%

Summary

- The study showed that the increased height of elevation of pantograph increases the value of the aerodynamic force acting on pantograph. This change is non-linear.
- The percentage of total aerodynamic force depend on height of elevation of pantograph.
- The drag coefficient at height of elevation 3000mm is about 118% greater than that corresponding to the height of elevation 1000 mm.

References

[1] J. Skibicki, Pojazdy elektryczne cz. 2. Gdańsk: Wydawnictwo Politechniki Gdańskiej, 2012.

[2] Y. Lee, Aerodynamic Characteristics of High Speed Train Pantograph with the Optimized Panhead Shape. Proceedings of the 7th IASME/WSEAS International Conference on Fluid Mechanics and Aerodynamics, 2009, p. 84-88.

21st International Conference **ENGINEERING MECHANICS 2015**
Svratka, Czech Republic, May 11 –14, 2015
Paper **#052, pp. 368–369**

Issues with Determination of Mean Time to Dangerous Failure and Diagnostic Coverage in Safety Functions of Machine Tools

Jiří Zahálka[a]*, František Bradáč[b], Jiří Tůma[c] , Miloš Synek[d]

Brno University of Technology, Technická 2896/2, 616 69 Brno, Czech Republic

[a]zahalka@fme.vutbr.cz, [b]bradac@fme.vutbr.cz, [c]tuma.j@fme.vutbr.cz, [c]synek@fme.vutbr.cz

Keywords: functional safety, mean time to dangerous failure, diagnostic coverage

Abstract: Safety is currently a widely discussed topic in the design and construction of machine tools. Similarly important is the area of functional safety. This article focuses on determining the mean time to dangerous failure and diagnostic coverage in safety function of machine tools. Legislative requirements (2006/42/EC [1]) and requirements of current standards (EN ISO 13849-1 [2], EN 62061 [3]) are discussed. The current state of calculating the mean time to dangerous failure and diagnostic coverage and the shortcomings of current approach is presented. A new methodology for determining of mean time to dangerous failure and diagnostic coverage is outlined.

Introduction

The functional safety is part of the overall safety that depends on the electrical, electronic and programmable electronic systems. The area of functional safety is important from the perspective of protection of worker's health, the environment and property protection and we are also committed to comply with the valid EU legislation. Legislative documents and technical standards provide support and guidance for manufacturers of machine tools how to ensure and assess functional safety. However as shown below, neither of these technical documents can provide a hundred percent support; when solving these issues there appear to be gaps in their interpretation. This article is devoted to these gaps and suggests guidelines how these issues can be solved.

Formulation of the issue with determining of $MTTF_d$ and DC in safety function

As already indicated in the introduction, in functional safety standards the deficiencies can be found; these lead to different results of analyses of functional safety. Let us consider the following specific case. We will evaluate a safety emergency stop function in category 3, according to ISO 13849-1 [2] and from the analysis we will obtain the values $MTTF_d$=24 years and DC_{avg}=62 %. The required parameter PLr (Required Performance Level) will be "d" for this safety function. If we use the PL table 7 of ISO 13849-1 [2] for evaluation, we obtain PLc; the requirement PLr is not satisfied and the safety function would have to be further improved. If the same standard ISO 13849-1 [2] is used with the table in Annex K.1, it can be seen that the PLd is reached using the same input parameters. To evaluate the results of the functional safety analysis of the machine's equipment, e.g. SISTEMA software can also be used. In this case, PLd is provided in SISTEMA software; i.e. the PLr value is also satisfied. However with other parameters completely opposite results can be achieved. Another important problem in the current methodology for determining the level of functional safety is counting of cycles of individual components, which are also active in a number of safety functions. In the construction of the current machine tools, we nearly always find the components that carry out more of these functions at a time; i.e. one component performs e.g. 3200 cycles per year in one particular safety function. A reliability level of this safety function is therefore calculated on the basis of this number of operating cycles. Calculation is carried out as if there was only this particular safety function on the machine. However, the same component can also be found in another safety function, which performs e.g. 6400 cycles per year. This is again calculated only with the number of cycles concerning the particular function. The fact that these functions can interact is not included at all. It is obvious that these numbers of operating cycles

must be added up since one particular component performs in these three functions in total 9600 operating cycles per year. The mean time to dangerous failure is therefore shortened (equation C.1 in [2]), and so is the mean time to dangerous failure of all three safety functions, in which the component occurs. This reduction of total $MTTF_d$ is not insignificant. In practice, the average of the summation of operating cycles leads to a reduction of $MTTF_d$ by 20 years. Similarly to $MTTF_d$, these issues also affect the calculation of diagnostic coverage (DC), which can be calculated according to formula E.1 in [2].

Summary

The above text refers to and describes two different issues that have a significant impact on the accuracy and consistency of evaluation of the level of functional safety of safety functions implemented in machine tools. The first problem is the quantity and inconsistency of methods which could be used to evaluate the resulting level of functional safety. Thus, the manufacturers can virtually choose their own method of final evaluation, which will ensure that the implemented safety function will meet legislative requirements. These different approaches are four in total. EN ISO 13849-1 standard [2] offers three approaches (Fig. 5, Tab. 7 and Tab. K. 1); the fourth approach is provided by SISTEMA software, which, according to its developers, offers "*refined analysis method for the performance level*" [4].

Another problem described in this article touches upon the actual determination of $MTTF_d$ for each safety function as one of the important parameters for obtaining the final PL. Here the current legislation is "benevolent" and allows the evaluation of each safety function separately. It also, among others, allows achieving of significantly better results of the respective analyses. How to deal with this ambiguity is proposed in the following solutions. At the beginning of each analysis of functional safety of the machine tool it is necessary to perform an inventory of all the components implementing safety functions. This is followed by the selection of all components that perform simultaneously more functions and the sum of their working cycles from all safety functions is calculated. It is supposed that only this method can ensure a correct determination of PL.

Acknowledgement: This work has been supported by Brno University of Technology, FME, Czech Republic (Grant No. FSI-S-14-2401).

References

[1] Directive 2006/42/EC of the European Parliament and of the Council of 17 May 2006 on machinery, and amending Directive 95/16/EC (recast). http://eur-lex.europa.eu/LexUriServ/LexUriServ.do?uri=OJ:L:2006:157:0024:0086:cs:PDF

[2] EN ISO 13849-1, Safety of machinery – Safety-related parts of control systems – Part 1: General principles for design

[3] EN 62061, Safety of machinery – Functional safety of safety-related electrical, electronic and programmable electronic control systems

[4] M. Huelke, M. Hauke, J. Pilger, SISTEMA: a Tool for the Easy Application of the Control Standard EN ISO 13849-1. [online]. 2008. http://www.dguv.de/medien/ifa/en/pra/softwa/sistema/paper_e.pdf

21st International Conference **ENGINEERING MECHANICS 2015**
Svratka, Czech Republic, May 11 –14, 2015
Paper **#047, pp. 370–371**

Modelling of Textile Structures

Josef Žák

VÚTS, a.s., Svárovská 619, Liberec XI, Czech Republic
josef.zak@vuts.cz

Keywords: textile structures, fabric modelling

Abstract: In our work we tried to find a simple and reliable method to determine geometric properties of a textile structure with the main respect to the woven fabrics. We were using primarily means of classical mechanics and we tried to avoid as much as possible the use of computer resource demanding tools. Also we were concerned by the as large as possible applicability of results in design of our weaving machines.

Introduction

By modelling textile structures such as a woven fabrics, double or triple twisted threads or knitted structures one soon realizes that a mathematical model is needed to describe their form or properties. There are several methods to do it, most of them using a geometric interpretation of the structure without taking into account the mechanic properties of the constituting yarns (Pierce's model). Some methods are using them, e.g. Oloffson for woven fabrics, but neither those latter ones do cover completely the characteristics of the structures. There exist some methods said modern, although the term trendy or popular should be more appropriate, that use the instruments of classic mechanics to determine the properties of textile structure. Here come mainly methods based on finite elements. Their drawbacks lie primarily in requirements on computational resources, secondly, the method necessarily requires a complete set of physical constants to enter in the computation - and to be determined by a cost demanding experiment - and thirdly, its versatility is - for a given input - only limited.

Principles of method

The presented method uses a combination of geometric methods with the principle of minimization of energy of a system. As design variables it takes such parameters which characterize the shape of a geometric model. The minimum of energy is then found in terms of those parameters. Unlike the classical variational methods this method does not determine the unknown shape, for example by searching a weak solution of differential equation.

Examples of use

In this section we give some examples of use of the method applied on different textile structures.
Double twisted yarn. It consists of two identical simple yarns which are twisted together. The sense of twist is most commonly opposite to the spinning twist. Each yarn is modelled by using helical model as presented in [1].

Cross section of such a structure is shown in Fig.1. In this case only one design variable, common to both yarns and determining unequivocally the shape is used. Energy to be minimized consists of energy of elongation of individual yarns due to the twisting and of energy of deformation of their cross section, see [1]. By expressing this energy in terms of design variable we can find easily its minimum. In Fig. 2 we can see the resulting shape of twisted yarn, either in model and in reality.
Fabric binding point. Another, more practical example is the guess of shape of one binding point in plain weave. Unlike the previous example we must use here several design variables, it is to say one per yarn (weft or warp) and one variable common to both. This said we are taken to solve a system of

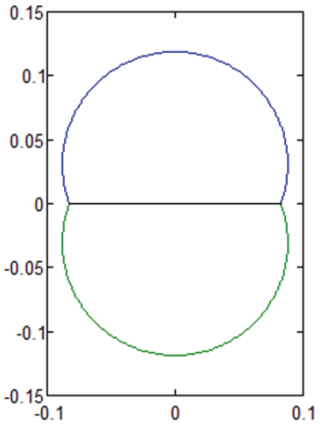

Fig. 1: Cross section

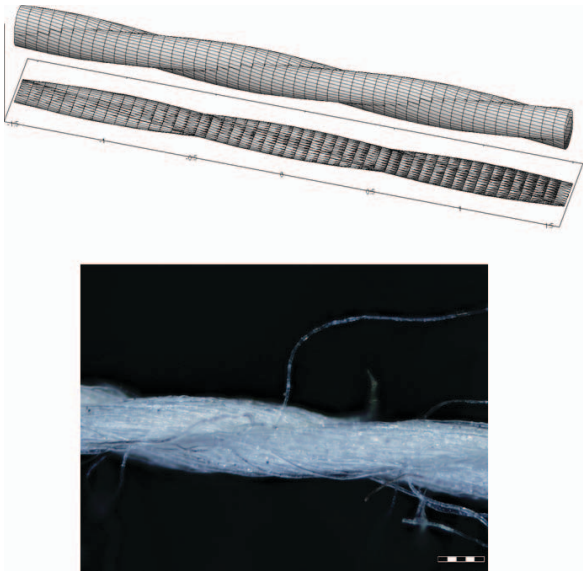

Fig. 2: 3D representation and real yarn

three non-linear algebraic equations. Using e.g. Newton - Raphson's method we obtain three values characterising the resulting shape.

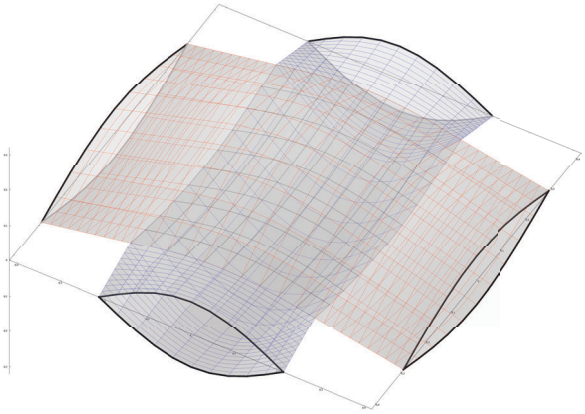

Fig. 3: Model of binding point

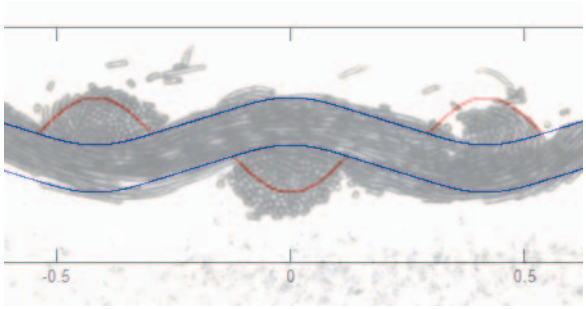

Fig. 4: Comparison of model and real shape

In Fig. 3 the model of one binding point in plain weave is represented and in Fig. 4 we can see a comparison of calculated shape with a section of corresponding real fabric.

Summary

Using methods of classical mechanics we have succeeded in determination of the shape of various textile products. Although this method has its own drawbacks it offers a good tool to predict the behaviour of such textile structures.

References

[1] J. Žák, Mechanische Eigenschaften des Garns, in: 14. Chemnitzer Textiltechnik-Tagung '14, (2014) pp. 183-190.

Investigations of Transient Oscillations of Rotors Supported by Magnetorheological Squeeze Film Dampers Using Bilinear Material to Model the Lubricant

Jaroslav Zapoměl[1,2,a] *, Jan Kozánek[3,b], Petr Ferfecki[4,c]

[1]Institute of Thermomechanics ASCR, Dolejškova 5, Praha 8, Czech Republic

[2]Department of Applied Mechanics, VSB-Technical University of Ostrava, Ostrava, Czech Republic

[3]Institute of Thermomechanics ASCR, Dolejškova 5, Praha 8, Czech Republic

[4]IT4Innovations, VSB-Technical University of Ostrava, Ostrava, Czech Republic

[a]jaroslav.zapomel@vsb.cz, [b] kozanek@it.cas.cz, [c] petr.ferfecki@vsb.cz

Keywords: magnetorheological squeeze film damper, magnetorheological oil, bilinear material, transient phenomena, rotordynamics

Abstract: Magnetorheological squeeze film dampers are added to the rotor supports to reduce lateral vibrations of rotating machines with the possibility to control the damping effect. In mathematical models magnetorheological oils are usually represented by Bingham or Herschel-Bulkley theoretical materials. Here the magnetorheological oil is modelled by bilinear material with the yielding shear stress depending on magnetic induction. Its flow curve is continuous which contributes to reducing nonlinear character of the motion equations. The new mathematical model was applied to investigate several operating regimes of rotating machines.

Introduction

The main parts of magnetorheological squeeze film dampers for rotordynamic applications are two concentric rings between which there is a layer of magnetorheological oil. The rings are coupled with the damper casing, the outer one directly, the inner one by a squirrel spring and with the shaft through a rolling element bearing. The damping device is equipped with an electric coil generating magnetic flux passing through the lubricating oil. As resistance against its flow depends on magnetic induction, changing the applied current makes it possible to control the damping force.

In mathematical models magnetorheological liquids are usually represented by Bingham or Herschel-Bulkley theoretical materials characterized by a discontinuous flow curve. In this paper a mathematical model of a short magnetorheological squeeze film damper based on bilinear material is reported and applied for investigation of transient phenomena occurring during several operating regimes of rotating machines. Its main advantage is a continuous flow curve of bilinear material.

Determination of the damping force

The developed mathematical model of a short magnetorheological squeeze film damper is based on assumptions of the classical theory of lubrication accept those for the lubricant. Derivation of the governing equation for the pressure distribution in the thin film of lubricating oil starts from the equation of equilibrium of an infinitesimal element specified in the oil layer, the equation of continuity and from the constitutive relationship referred to bilinear material. After performing a series of manipulations one obtains the Reynolds equation modified for bilinear material. In areas where the core extends up to the rings surfaces the pressure is governed by a classical Reynolds equation referred to Newtonian fluid. In regions where the thickness of the damper gap rises with time a cavitation is assumed. In cavitated areas pressure of the medium remains constant. The components of the damping forces are calculated by integration of the pressure distribution around the circumference and along the length of the damper. More details on determination of the yielding shear stress in dependence on the applied current can be found in [1].

Results of the computational simulations

The investigated rotor is rigid. It consists of a shaft carrying one disc and at each its end it is supported by one magnetorheological squeeze film damper. The rotor is loaded by its weight and by the disc unbalance. The system can be considered as symmetric relative to the disc middle plane perpendicular to the shaft centre line. In the computational model the rotor is represented by an absolutely rigid body and the dampers by springs and force couplings.

Because of the symmetry vibration of the system is governed by a set of two nonlinear motion equations. For their solving a step by step Adams-Moulton integration method was applied.

In the first operating regime the rotor rotates at constant angular speed of 80 rad/s and at the moment of time of 0.5 s it starts to accelerate for the period of 0.2 s. The time history of the rotor vibrations in the horizontal direction can be seen in Fig. 1a. No current was applied.

In the second operating regime the rotor turns at constant angular velocity of 80 rad/s. At the point of time of 0.5 s the current feeding the magnetorheological dampers is switched on (its rising from 0.0 to 0.5 A lasts for 0.1 s). The corresponding response is evident from Fig. 1b. Application of the currect reduces amplitude of the oscillations significantly.

In the last operating regime the dampers are fed by the current of 0.5 A. At the moment of time of 0.2 s the rotor starts to accelarate to increase its angular velocity from 80 rad/s to 160 rad/s during the time interval of 0.2 s. Comparing Fig. 1a and 1c the applied current incereases the damping effect which arrives at increased reduction of the oscillations amplitude.

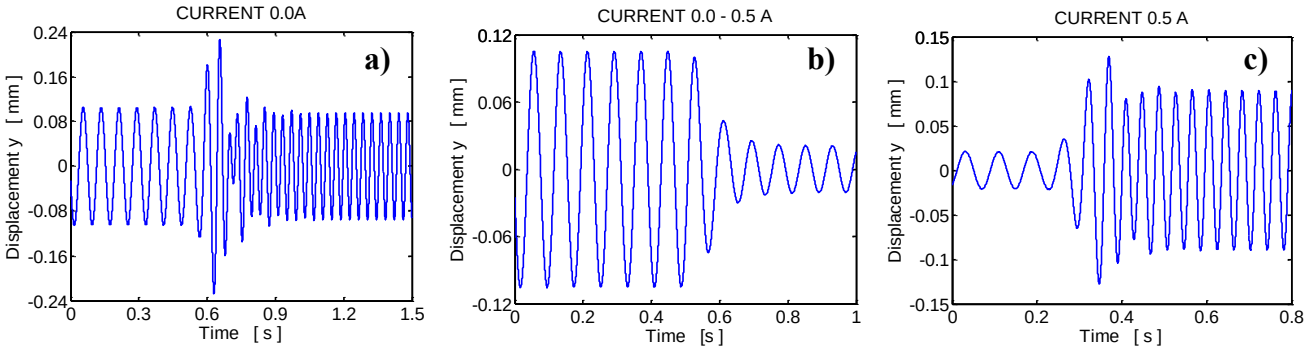

Fig. 1: Rotor center displacement in the horizontal direction.
a) rotor acceleration, 0.0 A b) constant speed, 0.0 – 0.5A c) rotor acceleration, 0.5 A

Summary

The principal contribution of the presented paper consists in development of a new mathematical model of a short squeeze film damper for the rotordynamic applications. The magnetorheological oil is represented by bilinear material whose yielding shear stress depends on magnetic induction. Its behaviour is described by a continuous flow curve which reduces nonlinear character of the governing equations and thus increases computational stability of the calculations. The developed mathematical model and consequently, the carried out computational simulations enabled to learn more about the vibrations attenuation of rigid rotors damped by controllable magnetorheological squeeze film dampers.

Acknowledgement: This work has been supported by the Czech Science Foundation 15-06621S and by the European Regional Development Fund CZ.1.05/1.1.00/02.0070.

References

[1] J. Zapomel J., P. Ferfecki, P. Forte, A computational investigation of the transient response of an unbalanced rigid rotor flexibly supported and damped by short magnetorheological squeeze film dampers, Smart Materials and Structures 21(2012), 1–12.

21st International Conference **ENGINEERING MECHANICS 2015**
Svratka, Czech Republic, May 11 –14, 2015
Paper **#038, pp. 374–375**

Prediction of the Nuclear Fuel Rod Abrasion in the Probability Sense

Vladimír Zeman[a], Zdeněk Hlaváč[b]

Faculty of Applied Sciences, University of West Bohemia, Univerzitní 22, 306 14, Plzeň, Czech Republic

[a]zemanv@kme.zcu.cz, [b]hlavac@kme.zcu.cz

Keywords: nuclear fuel assembly, flexural vibration, friction work, fretting wear, random parameters, sensitivity

Abstract: The paper deals with the upper and lower limits estimation of the friction work and fretting wear in the contact of nuclear fuel rods with fuel assembly (FA) spacer grid cells. The friction work is deciding factor for the prediction of the fuel rod cladding abrasion caused by FA vibration. Design and operational parameters of the FA components are understood as random variables defined by mean values and standard deviations. The gradient and three sigma criterion approach is applied to the calculation of the upper and lower limits of the friction work and fretting wear in particular contact surfaces between the fuel rod cladding and some of spacer grid cells.

Introduction

The friction forces in the contact of nuclear fuel rods with FA spacer grid cells, caused by flexural vibration of fuel rods (FR), produce the FR cladding abrasion. The goal of this contribution, in direct sequence at deterministic interpretation of FR abrasion [1,2], is a presentation of the probabilistic method [3] for the estimation of the upper and lower limits of the work of friction forces and fretting wear of the FR cladding in the contact surfaces. The chosen fuel rod (Fig. 1) is surrounded by three spacer grid cells (Fig. 2) on every level of spacer grid g. Elastic properties of cells can be expressed by three springs with identical stiffnesses k between cell centres and contact points [2].

The dynamic contact forces $F_{i,g},\ i = 1, 2, 3$ between fuel rod and cells at the level of spacer grid g in the course of FA vibration can be expressed by means of cell centres displacements $x_{i,g}, y_{i,g}$, $(i = 1, 2, 3)$ and lateral displacements ξ_g, η_g of the chosen FR. Fuel rod lateral displacements are generalized displacements of the FA global mathematical model presented in [2]. The *total contact*

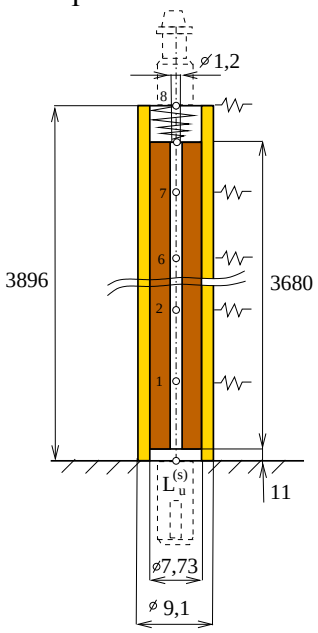

Fig. 1: Model of the fuel rod

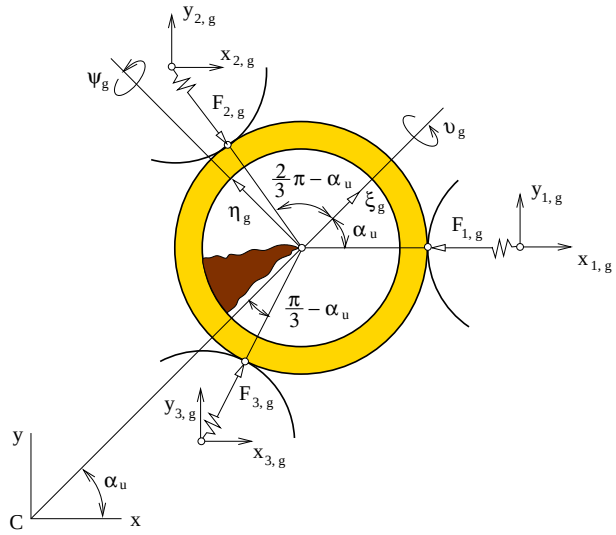

Fig. 2: Section of the fuel rod at the level of spacer grid g

forces between fuel rod and the spacer grid cells at the level $g = 1, \ldots, G$ are determined by the sum of the static contact force F_{st} after fuel rods installation into the load-bearing skeleton with spacer grids and the dynamic contact forces caused by vibration $N_{i,g}(t) = [F_{st}+F_{i,g}(t)]H(F_{st}+F_{i,g}(t)), i = 1, 2, 3$. H is Heaviside function (for $F_{st} + F_{i,g}(t) < 0$, when contact is interrupted, $H = 0$).

Estimation of works of friction forces

The criterion of the FR cladding fretting wear can be expressed using the work of friction forces during the representative time interval $t \in \langle t_1, t_2 \rangle$ in contact surfaces as

$$W_{i,g} = \int_{t_1}^{t_2} f_0 \, |N_{i,g}(t)\dot{z}_{i,g}(t)| \, \mathrm{d}t \, , \; i = 1, 2, 3 \, , \; g = 1, \ldots, G \tag{1}$$

where f_0 is the computational friction coefficient and $\dot{z}_{i,g}$ are vertical sliding velocities. Let us assume dependence of FA mathematical model on stochastical independent random design parameters $\boldsymbol{p}_d = [p_j] \in R^s$ defined by mean values $\overline{p}_j$ and diagonal covariance matrix $\Sigma_{\boldsymbol{p}_d} = \mathrm{diag}[\sigma_j^2] \in R^{s,s}$. Using the gradient method and on condition that standard deviations σ_j are relatively small we can write [3] the approximate relation for the covariance matrix of the works of friction forces (further *friction works*) in all contact surfaces in the form

$$\Sigma_W \doteq \left[\frac{\partial \boldsymbol{w}(\boldsymbol{p}_d)}{\partial \boldsymbol{p}_d^T}\right]_{\boldsymbol{p}_d=\overline{\boldsymbol{p}}_d} \Sigma_{p_d} \left[\frac{\partial \boldsymbol{w}(\boldsymbol{p}_d)}{\partial \boldsymbol{p}_d^T}\right]^T_{\boldsymbol{p}_d=\overline{\boldsymbol{p}}_d} . \tag{2}$$

Friction works are compiled in the vector $\boldsymbol{w}(\boldsymbol{p}_d) = [\ldots, W_{i,g}(\boldsymbol{p}_d), \ldots], i = 1, 2, 3 \, , \; g = 1, \ldots, G$ of dimension $3G$. Diagonal elements $\sigma^2_{W_{i,g}}$ of the covariance matrix Σ_W can be used for the upper and lower limits calculation of the friction works in all contact surfaces. Similarly to friction works limits, the limits of fretting wear of the FR cladding are calculated using experimentally obtained loss of FR cladding mass in contact surface generated by the friction work $W = 1$[J] and friction coefficient [4].

Summary

As described analytical-numerical method enables to investigate the limits of the friction work and fretting wear of the nuclear Zr FR cladding in contact surfaces with FA spacer grid cells. The FA vibration is caused by spatial motion of the fuel assembly support plates investigated on the global reactor model. FA design and operational parameters are understood as random variables defined by mean values and standard deviations or relative ranges of values. The presented method was applied on the Russian TVSA-T fuel assembly in the VVER 1000 type reactor in NPP Temelín.

Acknowledgement: This work was supported by the European Regional Development Fund (ERDF), project "NTIS", European Centre of Excellence, CZ.1.05/1.1.00/02.0090 within the research project "Fuel cycle of NPP" coordinated by NRI Řež plc.

References

[1] V. Zeman, Z. Hlaváč, Prediction of the nuclear fuel rod abrasion, Applied and Computational Mechanics, 7 (2013) 235-250.

[2] Z. Hlaváč, V. Zeman, Vibration of Nuclear Fuel Assemblies, Lap Lambert Academic Publishing, Saarbrücken, 2013.

[3] M. Kleiber, T. D. Hien, The Stochastic Finite Method, John Wiley & Sons, London, 1992.

[4] L. Pečínka, J. Svoboda, V. Zeman, Fretting wear of the Zr fuel rod cladding, in: Proceedings of the 22nd International Conference of Nuclear Engineering ICONE 22, 2014, Prague.

21st International Conference **ENGINEERING MECHANICS 2015**
Svratka, Czech Republic, May 11 –14, 2015
Paper **#015, pp. 376–377**

Influence of Elastic Characteristics of Regular System on the Vibrodiagnostic Parameter Due to the Presence of a Breathing Crack

A.P. Zinkovskii[a] *, V.A. Kruts[b], E.A. Sinenko[c], I.G. Tokar' [d]

G.S. Pisarenko Institute for Problems of Strength, Nat. Ac. Sci. of Ukraine,
01014, 2, Timiryazevskaya str., Kiev, Ukraine

[a] zinkovskii@ipp.kiev.ua, [b] kruzvadim@gmail.com, [c] gen6ok@gmail.com, [d] tokar@ipp.kiev.ua

Keywords: regular system, breathing crack, elastic coupling, vibrodiagnostic parameter

Abstract: The paper presents the results of computational experiments on determination of the influence of the coefficient of elastic coupling between the discrete model elements (rods) of regular system on the value of vibrodiagnostic parameter due to the presence of a breathing crack. It is shown that due to elastic coupling between the elements the chosen parameter is evident not only within the damaged subsystem, but also within the undamaged one.

Introduction

During operation many structural elements of machines, in particular turbine rotor blades, are subjected to a wide spectrum of mechanical and temperature loads resulting in the occurrence of closing or the so-called "breathing" fatigue cracks. They give rise to a significant change in the elastic characteristics during the cycle of deformation being the cause of the nonlinearity of vibrations of the object under investigation.

Recently, a great attention has been paid to studying vibrations of the objects of engineering with a crack in question and search for reliable vibrodiagnostic criteria of its presence.

In view of the presence of various constraints between components of machine assemblies, which is typical of them, separate consideration of a structural element does not allow one to describe its dynamic state with sufficient accuracy. This is only possible by taking into consideration its interaction with other elements of the system under investigation. Therefore, in the theory of vibrations, increasingly greater attention is being paid to studying complex mechanical systems, among which regular systems involving series of parallel connection of equitype elements (subsystems) occupy a special place. Among such systems are primarily the set of blades and blade assembly as a special type of regular systems with rotation symmetry.

Considering the above-said, the purpose of the present paper is the calculated determination of the influence of the coefficient of elastic coupling between subsystems $\gamma = k_s/k$ on the value of vibrodiagnostic parameter due to the presence of a breathing crack of a discrete model of the simplest regular system presented in Fig. 1.

Computational experiments on determination of the vibrodiagnostic parameter at the subharmonic mode of vibrations of order ½ have been performed using the method presented in [1]. The ratio of the amplitudes $æ_1 = A^{(1)}/A^{(2)}$ of the first $A^{(1)}$ and second $A^{(2)}$ harmonics of vibrations is chosen as a specified parameter.

From the results of computational experiments the dependences of the vibrodiagnostic parameter on the damage parameter $\alpha = (k - k_o)/k$ have been obtained for damaged and undamaged subsystems of discrete model of regular system as well as for damaged subsystem in an isolated state ($\gamma = 0$).

Their analysis shows that the value of vibrodiagnostic parameter for damaged subsystem in an isolated state is higher than that one for subsystems of the model of regular system, which makes its use for the diagnostics of damage under investigation as a fatigue crack for such systems more difficult. Moreover, with an increase of the coefficient of elastic coupling γ of the model of regular

system the value of vibrodiagnostic parameter decreases for damaged subsystem, whereas it increases for undamaged subsystem.

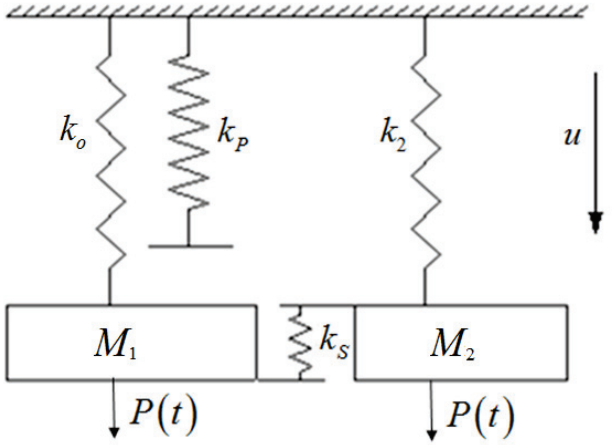

Fig. 1: Discrete model of the simplest regular system with a closing crack

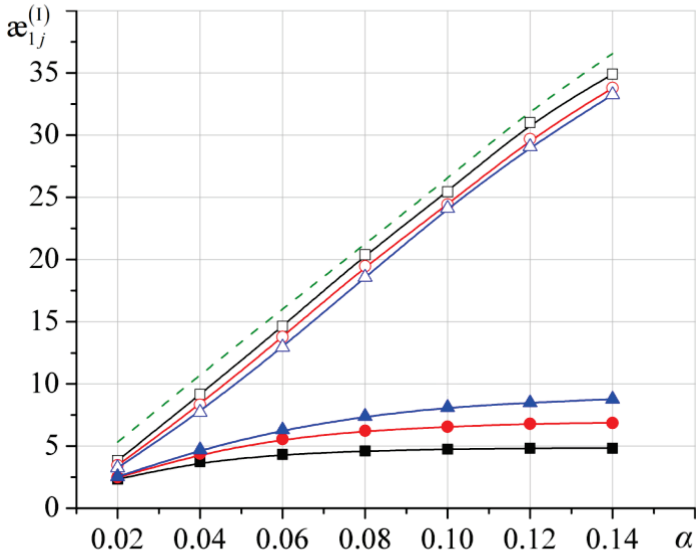

Fig. 2: Dependence of the vibrodiagnostic parameter on the damage parameter for damaged (open symbols) and undamaged (filled symbols) subsystems at the subharmonic resonance for h = 0.0008 sec^{-1} and the coefficient of elastic coupling γ equals to 0.01 (■,□), 0.015 (●,○), 0.02 (▲,Δ). Dashed line is the damaged subsystem in an isolated state.

References

[1] V. A. Kruts, , A. P. Zinkovskii, E. A. Synenko, Influence of a fatigue crack on the vibrations of the simplest regular elastic system, Strength of Materials. 45(2013) 308-315.

21st International Conference **ENGINEERING MECHANICS 2015**
Svratka, Czech Republic, May 11 –14, 2015
Paper **#009, pp. 378–379**

Influence of the Conditions for Coupling of the Shrouds on the Static Stress State of Blade Rings

A.P. Zinkovskii[a]*, K.V. Savchenko[b], Ya.D. Kruglii[c]

G.S. Pisarenko Institute for Problems of Strength, Nat. Ac. Sci. of Ukraine,
01014, 2, Timiryazevskaya str., Kiev, Ukraine

[a] zinkovskii@ipp.kiev.ua, [b] c.savchenko@hotmail.com, [c] yanademuz@gmail.com

Keywords: turbine blade, shroud coupling, orientation of contact surfaces, static stress state

Abstract: The paper presents results of computational experiments on the determination of the influence of the contact surface orientation for two types of shrouds on the static stress state characteristics of the turbine rotor blades.

1. Introduction

Flange shrouding of rotor wheels, being an efficient design and manufacturing solution for reducing the level of resonant vibrations in rotor blades, is widely used in current turbomachinery structures to improve their reliability and serviceability. This is achieved by integration of blades into a system or packages that are closed to a circle.

The analysis of the investigations involving the determination of the influence of design and manufacturing, as well as operational, factors on the characteristics of the stress-strain state of turbine rotor blades with different types of shrouds shows that at present, there are no generalizing regularities in the influence of their parameter, such as the orientation of the contact surfaces, that is defined by the angle of their inclination α to the rotor wheel plane of rotation, as illustrated in Fig. 1 where N is the resultant of the normal forces acting on the contact surfaces.

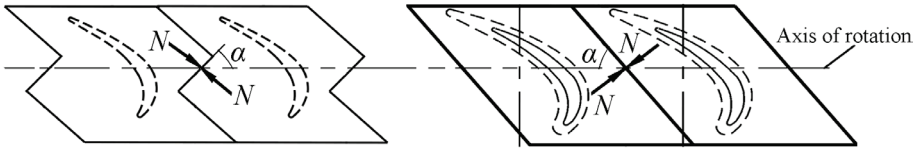

Fig. 1: Schematic of the interaction of Z-shaped (a) and straight (b) shrouds

In view of the above, the aim of the present work is the computational determination of the influence of the angle of inclination α of the contact surfaces of specific types of shrouds on the static stress state of rotor blades.

2. Object of investigation and its simulation

Two blade rings, the blades of which have Z-shaped and straight shrouds, were selected to perform the computational experiments.

The considered blade rings are the systems with a cyclic symmetry, in which the coupling of blades is due to their contact interaction along the shrouds. In this case, in performing the computational experiments, we can confine ourselves to the consideration of one cycle of the blade row with the appropriate boundary conditions [1].

To generate the finite element (FE) model of the blade, the 8-node finite element SOLID 45 was used exhibiting a satisfactory accuracy and high calculation speed [2].

The simulation of the contact interaction along the shrouds was carried out using the procedure the main provisions of which are described in [2]. The rigid attachment of the blade root in the disk groove was taken as the boundary conditions.

3. Results of the computational experiments

A comprehensive set of computational experiments has been performed involving the determination of the influence of the angle of inclination α (in the range of its variation from 45 to 60°) of the shroud contact surfaces on the static stress state characteristics, for which the contact pressure P_{max} along the shrouds and the stress intensity σ_i in the shroud and blade airfoil portion determined using the below formula were selected:

$$\sigma_i = \sqrt{\sigma_1^2 + \sigma_2^2 + \sigma_3^2 - \sigma_1\sigma_2 - \sigma_2\sigma_3 - \sigma_3\sigma_1}\,, \tag{1}$$

where σ_i (i = 1, 2, 3) are the principal stresses.

Based on the obtained results of calculations, the diagram of the maximum values of the selected characteristics *vs*. the value of the angle of inclination α of contact surfaces was plotted as illustrated in Fig. 2.

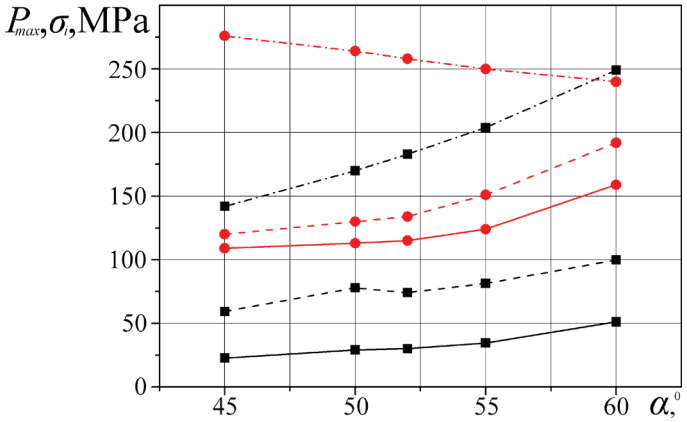

Fig. 2: Diagram of the maximum values of the contact pressures (solid line) and the stress intensity in the shroud (dashed line) and the blade airfoil portion (dot-and-dashed line) versus the value of the angle of inclination α of the contact surfaces to the rotor wheel plane of rotation for blade rings with a Z-shaped (•) and a straight (■) shrouds

Based on the analysis of the presented results of calculations, the following conclusions can be drawn:

1. Irrespective of the type of the shroud coupling, the values of the contact pressure and the stress intensity in the shroud increase in the whole range of variation of the angle of inclination α of the contact surfaces.

2. In the blade airfoil portion with a straight shroud, the values of the stress intensity increase, whereas in that with a Z-shaped shroud, they decrease with increasing angle of inclination of their contact surfaces.

3. As a whole, a Z-shaped shroud is responsible for the increase in the static intensity of blades as compared to that in the blades with a straight shroud.

References

[1] V. P. Ivanov, Vibration of Turbomachine Rotor Wheels [in Russian], Mashinostroenie, Moscow, 1983.

[2] A. P. Zinkovskii, Ya. D. Kruglii, Effect of identity violations of contact interaction between shrouds on the static and dynamic stress state characteristics of blade rings, Strength of Materials, 44 (2012) 144–156.

21st International Conference **ENGINEERING MECHANICS 2015**
Svratka, Czech Republic, May 11 –14, 2015
Paper **#212, pp. 380–381**

Testing of Energy Absorption Capability of Sandwich Structures Based on Metal Foams for Design of Protective Helmets

Petr Zlámal[1,a], Tomáš Fíla[2,b], Vlastimil Králík[3,c]

[1]Faculty of Transportation Sciences, CTU in Prague, Konviktská 20, 110 00 Prague 1, CZ

[2]Institute of Theoretical and Applied Mechanics AS CR, v.v.i., Prosecká 76, 190 00 Prague 9, CZ

[3]Faculty of Civil Engineering, CTU in Prague, Thákurova 7, 166 29 Prague 6, CZ
[a]xzlamal@fd.cvut.cz, [b]fila@itam.cas.cz, [c]vlastimil.kralik@fsv.cvut.cz

Keywords: Alporas, Aluhab, EPS, sandwich structure, impact test, metal foam, HIC

Abstract: Purpose of this study is investigation of energy absorption capability of the sandwich structures composed of combination of polystyrene and metal foam element. Two types of the metal foams were experimentally tested: Alporas (Shinko Wire Ltd., Japan) and Aluhab (Aluinvent Plc., Hungary). Samples of the sandwich structure are composed of two layers: bottom expanded polystyrene (EPS 200S) layer and upper metal foam layer which are glued together. Prepared samples are tested using a drop tower experiment to measure sample response (acceleration, reaction force) at different strain rates and energies. From acceleration/time history the Head Injury Criterion (HIC) is calculated. Measured and derived characteristics are compared with EPS samples.

Introduction

Nowadays, expanded PolyStyrene (EPS) is the most common liner material used in protective helmets as energy absorbing element [1]. It is cheap to manufacture, light, easy machinable and has suitable crush characteristics. EPS represents crushable foams structures where the cell walls crush on impact and slow the head gradually. This deformation behaviour is ideal for helmets optimised for one hard impact. However, the protective effect depends on the portion of the impact energy which the structure is capable to absorb. If this rate is exceeded the rest of the impact energy is transferred to the head. Closed-cell metal foams as polystyrene also represent the crushable foam structures but in contrast with EPS the stiffness is significantly higher (with low specific weights) and thus are able to absorb more impact energy. In this study two sandwich structure composed from EPS and metal foam layer are tested and their extended energy absorption capability of the material is analysed.

Materials and Methods

All samples were machined using CNC device to obtain samples that perfectly fit on the headform impactor. Three types of structures were prepared: (i) Alporas sandwich (EPS layer thickness: 10 mm, Alporas layer thickness: 25 mm), (ii) Aluhab sandwich (EPS: 10 mm, Aluhab: 25 mm) and (iii) pure EPS (EPS: 35 mm). EPS and metal foam layers In in sandwich structure were together bonded by glue (UHU Por, UHU GmbH & Co. KG, Germany). Prepared samples were tested using a drop tower experiment to measure of the sample response at different strain rates and energies. The headform impactor was equipped with a triaxial accelerometer (EGCS3, Measurement Specialties, USA) with $\pm$ 1000 g measuring range and a bottom platen of the drop tower was equipped with an impact quartz force sensor (200C20, PCB Piezotronics, Inc., USA). Both sensors were time synchronised and analog input module (NI 9234, National instruments, USA) with 51.2 kSs^{-1} maximum sampling rate was used for fast read out of measured data. Acceleration/time history was used for Head Injury Criterion (HIC) [2] calculation:

$$HIC_{15} = \left\{ \left[\frac{1}{t_2 - t_1} \int_{t_1}^{t_2} a(t)dt \right]^{2.5} (t_2 - t_1) \right\}_{\max} \tag{1}$$

where t_1 and t_2 define time interval (limited to 15 ms) during which HIC attains a maximum value and a is acceleration in g.

Results and Discussion

Measured acceleration for pure EPS, Aluhab and Alporas sandwich samples is shown in Fig. 1. As can be seen in this figures Alporas is not good material for design of protective helmets because acceleration and HIC values are very high (e.g. HIC=1000 means 18% probability of a severe head injury, a 55% probability of a serious injury and a 90% probability of a moderate head injury). On the other hand with increasing impact energy the HIC value and the peak acceleration is progressively decreasing. This behaviour shows that Alporas takes effect for higher impact energy where protection

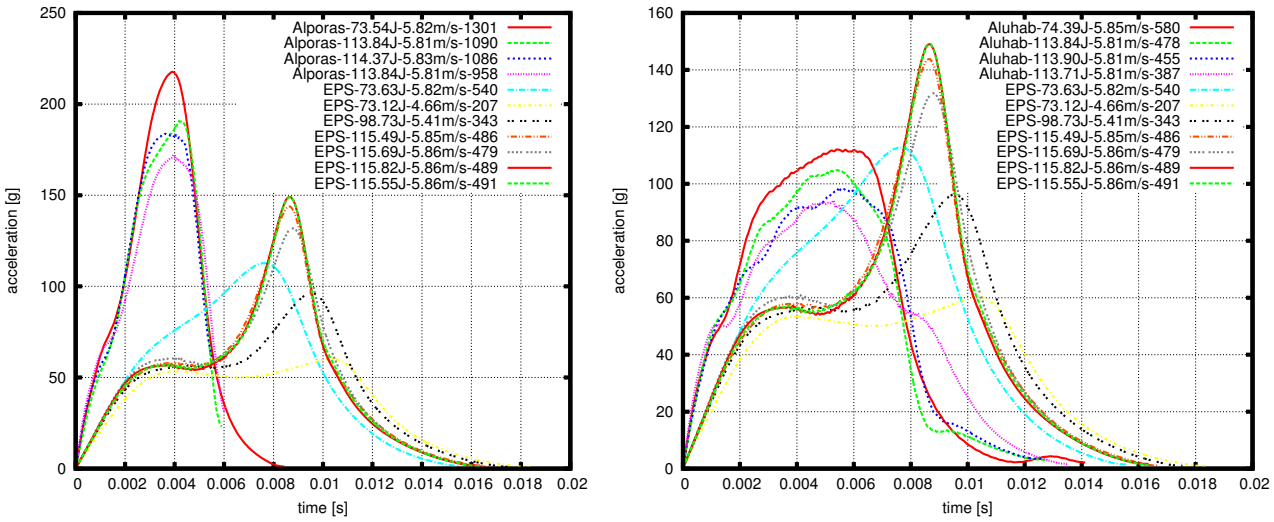

Fig. 1: Measured acceleration curves for Alporas (left) and Aluhab (right) compared with EPS (in legend: impact energy - impact velocity - HIC value)

ability is significantly increasing. The same trend was observed with Aluhab sandwich but in comparison to the Alporas the overal stiffness of the structure is lower and HIC and acceleration values are even comparable with values of the pure EPS. Moreover Aluhab sandwich can potentially absorb the significantly higher portion of the impact energy in comparison with EPS. As conclusion the Aluhab sandwich can be considered promising structure how to improve current protective materials in helmets however further optimisation of the structure properties (thickness, number of the layers, etc.) will be necessary.

Acknowledgment: The research was supported by the Grant Agency of the Czech Technical University in Prague (SGS14/121/OHK1/2T/11), Czech Science Foundation (research project No. 15-15480S) and by the institutional support of RVO: 68378297.

References

[1] F.A.O Fernandes, R.J. Alves De Sousa, Accident Analysis and Prevention 56 (2013) 1–21.

[2] H.W.Henn, Teaching mathematics and its application 17 (1998) 162–170.

21st International Conference **ENGINEERING MECHANICS 2015**
Svratka, Czech Republic, May 11 –14, 2015
Paper **#160, pp. 382–383**

Artificial Neural Network in Approximation of Solution for Short-Cylinder-Shaped Inclusion Problem

Lukáš Zrůbek[a], Anna Kučerová[b], Jan Novák[c]

Czech Technical University in Prague, Faculty of Civil Engineering, Department of Mechanics, Thákurova 7, 166 29, Praha 6, Czech Republic

[a]lukas.zrubek@fsv.cvut.cz, [b]anicka@cml.fsv.cvut.cz, [c]novakj@cml.fsv.cvut.cz

Keywords: Micromechanics, Artificial Neural Network, Short-cylinder-shaped Inclusions, Finite Element Method

Abstract: Mechanical fields like strains, stresses or displacements inside isotropic infinite body with ellipsoidal-like inclusions, can be obtained easily by analytical solution given by J. D. Eshelby in 1957. Unfortunately for inclusions in form of short cylinders (e.g. steel fibers in steel-fiber-reinforced concrete) is Eshelby's solution not applicable and finite element analysis is quite time consuming. By means of artificial neural network trained on sufficiently large set of reference solutions to predict desired mechanical fields one can achieve considerable speedup at the cost of approximate solution.

Introduction

The main aim of this paper is to present our preliminary work which will allow us better understanding of materials behavior. We will apply the proposed approach to obtain mechanical response of materials consisting of short-cylinder-shaped inclusions and isotropic matrix.

In 1957 J. D. Eshelby [1] presented in his fundamental work an analytical solution for isotropic ellipsoidal inclusion. Solution can be found for any ellipsoid with arbitrary sizes of three semi-axes, even for ellipsoid with one semi-axis set to infinity which gives us an infinite cylinder. However for inclusions with shape of short cylinders the Eshelby's solution is not applicable. One of possible options is the use of finite element method (FEM), but it could be quite time consuming depending on fineness of the element mesh.

Artificial neural network

Therefore, we propose to use FEM to obtain a set of reference solutions which will be used to train an artificial neural network (ANN) [2, 3] for predicting of material response.

ANNs are computational models based on central nervous systems, especially on brain. These models are capable of machine learning and recognizing of patterns in given data. ANN consists of many simple processing nodes – so called neurons – interconnected into systems that can change their structure during the training (learning) phase. An adaptive value representing synaptic weight is assigned to each connection between two neurons. Based on given data and respective results used as an external information flowing through the system, these weights are balanced in a way that the output of ANN corresponds to the actual results. For our purposes we will use software called RegNeN [4] with implemented most widely used type of ANN called multi-layer perceptron with the sigmoid transfer function and so called backpropagation learning algorithm.

Reference solutions

First step in the whole process is creating a sufficiently large set of FEM solutions for inclusions depending on varying dimensions, material properties and load. In order to create these variable inputs in a way that the resulting set of reference solutions will evenly cover the space of possible input combinations we will generate them through software called SPERM [5] which utilizes the method of Latin Hypercube Sampling (LHS). One simulation is performed by FEM software called OOFEM [6] for each generated sample and then used for the ANN training phase.

Creating of ANN and results prediction

During the training process the actual architecture of neurons is created. Number of neurons in the input layer is equal to the number of variables in samples. Next layer - so called hidden - consists of *n* neurons, where *n* is determined automatically within the training process by testing the over-training of ANN based on the cross-validation error. The number of neurons in the last layer is equal to the number of results. To predict results for desired inclusion the parameters of relevant inclusion should be used as ANN inputs and after the simple evaluation the results are obtained.

Summary

Because the accuracy of results predicted by ANN depends on the training phase [7], creating a set of reference solutions, that provides sufficient quantity and variety of samples, is one of the essential steps in this approach. Nevertheless, certain error will always be part of the predicted results since we obtain only an approximate solution. But if the error is adequately small and we can afford to neglect it, the results are predicted many times faster than with standard FEM calculation and in case of large amounts of desired results it is possible to achieve considerable speedup.

Acknowledgment: This work was supported by the Czech Science Foundation, through projects No. 13-24027S (L. Zrůbek, A. Kučerová, J. Novák) and by Grant Agency of Czech Technical University in Prague through project No. SGS15/030/OHK1/1T/11 (L. Zrůbek, A. Kučerová, J. Novák).

References

[1] J. D. Eshelby, The determination of the elastic field of an ellipsoidal inclusion, and related problems, Proceedings of the Royal Society A: Mathematical, Physical and Engineering Sciences. 241 (1957) 376-396. Available from: doi: 10.1098/rspa.1957.0133

[2] K. Gurney, An introduction to neural networks, Boca Raton: CRC Press, (1997), xi, p. 234, ISBN 978-1-85728-503-4

[3] S. S. Haykin, et al., Neural networks and learning machines, 3rd ed. Upper Saddle River, N.J.: Pearson, (2009), p. 934, ISBN 01-312-9376-1

[4] T. Mareš, A. Kučerová, RegNeN 2012 [online], Faculty of Civil Engineering, Czech Technical University in Prague, (2012) [cited 2015-03-01] Available from: http://klobouk.fsv.cvut.cz/anicka/regnen/regnen.html

[5] J. Novák, Generator of optimal LHS designs SPERM v. 2.0, Centre for Integrated Design of Advanced Structures (CIDEAS), Czech Technical University in Prague, (2011)

[6] B. Patzák, OOFEM - an object-oriented simulation tool for advanced modeling of materials and structures, Acta Polytechnica, 52 (2012) 59-66, (2012)

[7] T. Mareš, E. Janouchová, A. Kučerová, Different approaches to calibration of nonlinear mechanical models using artificial neural networks, (2015), submitted for publication, e-print: arXiv:1502.01380

Author index

Items are referred in the form: SECTION-page number, #paper number

G

H

I

J

K

L

M

N

P

R

S

T

U

V

W

Z

ISBN 978-80-86246-42-0
ISSN 1805-8248